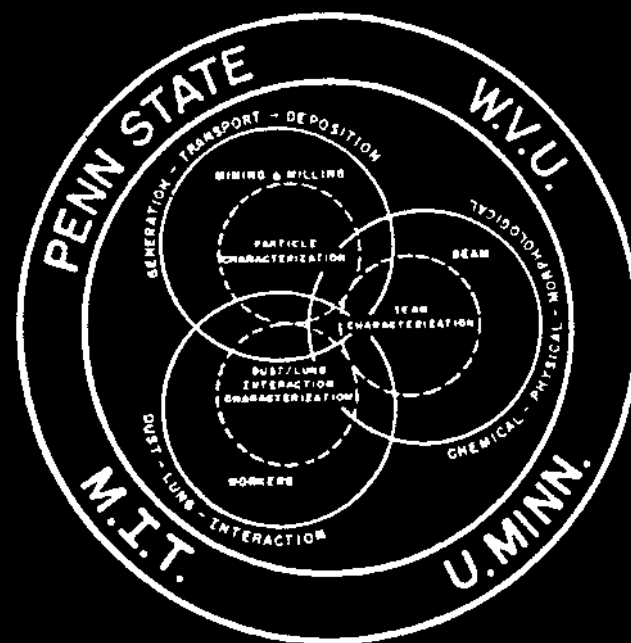


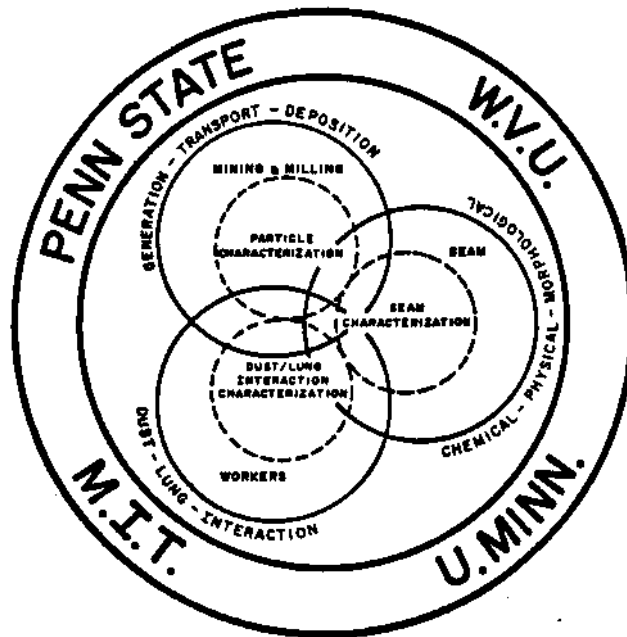
# PUBLICATIONS 1986

Edited by  
**ROBERT L. FRANTZ**  
and  
**RAJA V. RAMANI**



**GENERIC MINERAL  
TECHNOLOGY CENTER  
FOR RESPIRABLE DUST**

# PUBLICATIONS 1986



## GENERIC MINERAL TECHNOLOGY CENTER FOR RESPIRABLE DUST

The Pennsylvania State University  
West Virginia University  
University of Minnesota  
Massachusetts Institute of Technology  
Michigan Technological University

Submitted To  
Office of Mineral Institutes  
U.S. Bureau of Mines  
Washington, D.C.

March 1989

] ] ]

**The views and conclusions contained in this document are those of the authors and should not be interpreted as necessarily representing the official policies or recommendations of the Interior Department's Bureau of Mines, the U.S. Government or of the Generic Mineral Technology Center for Respirable Dust. Reference to specific brands, equipment or trade names in this report is made to facilitate understanding and does not imply endorsement by the Bureau of Mines or the Dust Center.**

---

# **PUBLICATIONS**

PRODUCED IN

## **THE GENERIC MINERAL TECHNOLOGY CENTER FOR RESPIRABLE DUST**

IN THE YEAR

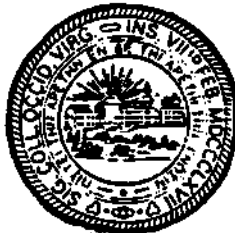
**1986**

Edited by  
Robert L. Frantz  
Raja V. Ramani

# PENNSSTATE



# WEST VIRGINIA UNIVERSITY





## **Volumes of the Respirable Dust Center**

<b>VOLUME 1</b>	<b>Status Report, 1984-1988</b>
<b>VOLUME 2</b>	<b>Report to the Committee on Mining and Mineral Resources Research, 1987</b>
<b>VOLUME 3</b>	<b>Publications, 1984</b>
<b>VOLUME 4</b>	<b>Publications, 1985</b>
<b>VOLUME 5</b>	<b>Publications, 1986</b>
<b>VOLUME 6</b>	<b>Publications, 1987</b>
<b>VOLUME 7</b>	<b>Respirable Dust Center Research Program Review</b>
<b>CONFERENCE PROCEEDINGS</b>	<b>Coal Mine Dust Conference West Virginia University Morgantown, West Virginia October 1984</b>
<b>CONFERENCE PROCEEDINGS</b>	<b>Respirable Dust in the Mineral Industries: Health Effects, Characterization and Control The Pennsylvania State University University Park, Pennsylvania October 1986</b>

# CONTENTS

	Page
Foreword	xi
National Plan	xii
Advisory Council Members	xiii
<b>I. Control of Dust and Particulate Matter Generation</b>	<b>1</b>
<b>1. Mixed Mode Testing for Fracture Toughness of Coal Based on Critical-Energy-Density</b>	<b>3</b>
<i>R. Karl Zipf, Jr. and Z. T. Bieniawski, Department of Mineral Engineering, The Pennsylvania State University, University Park, PA 16802. Presented at the 27th U.S. Symposium on Rock Mechanics, The University of Alabama, June 23-25, 1986. (PS-1)</i>	
<b>2. Fracture Mode and Loading Rate Influence on the Formation of Respirable Size Fragments on New Fracture Surfaces</b>	<b>11</b>
<i>R. Karl Zipf, Jr. and Z. T. Bieniawski, Department of Mineral Engineering, The Pennsylvania State University, University Park, PA 16802. Presented at the International Symposium on Respirable Dust, The Pennsylvania State University, University Park, PA 16802, October 14-16, 1986. (PS-1)</i>	
<b>3. An Analysis of Respirable Dust Generation by Continuous Miner</b>	<b>18</b>
<i>A. Wahab Khair and N. P. Reddy, Department of Mining Engineering, West Virginia University, Morgantown, WV 26506. Presented at the Engineering Health and Safety in Coal Mining SME Annual Meeting Symposium, New Orleans, LA, March 2-6, 1986. (WV-1)</i>	
<b>4. Characterization of Coal Breakage as a Function of Operating Parameters</b>	<b>42</b>
<i>A. Wahab Khair and N. P. Reddy, Department of Mining Engineering, West Virginia University, Morgantown, WV 26506. Presented at the Proceedings of the International Symposium on Applications of Rock Characterization Techniques in Mine Design, Annual Meeting, SME-AIME, New Orleans, LA, March 1986. (WV-1)</i>	
<b>II. Dilution, Dispersion and Collection of Dust</b>	<b>53</b>
<b>5. Experimental Studies on Dust Dispersion in Mine Airways</b>	<b>55</b>
<i>R. Bhaskar and R. V. Ramani, Department of Mineral Engineering, The Pennsylvania State University, University Park, PA 16802 and R. A. Jankowski, U.S. Bureau of Mines, Pittsburgh, PA 15236. Presented at SME-AIME Annual Meeting, New Orleans, LA, March 2-6, 1986. (PS-2)</i>	

	<b>Page</b>
<b>6. Theoretical and Experimental Studies on Dust Transport in Mine Airways: A Comparative Analysis</b>	<b>61</b>
<i>R. V. Ramani and R. Bhaskar, Department of Mineral Engineering, The Pennsylvania State University, University Park, PA 16802. Presented at the Conference on Respirable Dust in the Mineral Industries, September 1986, University Park, PA 16802. Published in Respirable Dust in the Mineral Industries: Health Effects, Characterization, and Control, Ed: R. L. Frantz and R. V. Ramani, American Conference of Governmental Industrial Hygienists, Cincinnati, Ohio. (PS-2)</i>	
<b>7. Air Velocity Distribution Measurements on Four Mechanized Longwall Coal Faces</b>	<b>72</b>
<i>S. S. Peng and H. S. Chiang, Department of Mining Engineering, West Virginia University, Morgantown, West Virginia 26506. Published in the International Journal of Mining and Geological Engineering, 4 (1986), pgs. 235-246. (WV-3)</i>	
<b>8. Simulation of Dust Dispersion for a Coal Mine Face Using a Scale Model</b>	<b>82</b>
<i>T. H. Ueng, S. D. Thompson and Y. J. Wang, Department of Mining Engineering, West Virginia University, Morgantown, WV 26506. Presented at the Proceedings of the International Symposium on Respirable Dust, The Pennsylvania State University, University Park, PA 16802, October 14-16, 1986. (WV-2)</i>	
<b>9. Size Distribution of the Airborne Dust in Longwall Coal Faces</b>	<b>85</b>
<i>H. S. Chiang, S. S. Peng and Y. Luo, Department of Mining Engineering, West Virginia University, Morgantown, WV 26506. Presented at the Proceedings of the International Symposium on Respirable Dust, The Pennsylvania State University, University Park, PA 16802, October 14-16, 1986. (WV-11)</i>	
<b>10. Application of a Particle Dispersion System for Obtaining the Size Distribution of Particles Collected on Filter Samples</b>	<b>109</b>
<i>K. L. Rubow and V. A. Marple, Particle Technology Laboratory, Mechanical Engineering Department, University of Minnesota, Minneapolis, MN, 55455. Published in Aerosols: Formation and Reactivity, 2nd International Aerosol Conference, Berlin, 1986, Pergamon Journals Ltd. Printed in Great Britain. (MN-1)</i>	
<b>11. Numerical Technique for Calculating the Equivalent Aerodynamic Diameter of Particles</b>	<b>113</b>
<i>V. A. Marple, Z. Zhigun and B. Y. H. Liu, Particle Technology Laboratory, Mechanical Engineering Department, University of Minnesota, Minneapolis, MN 55455. Presented at the International Symposium on Respirable Dust in the Mineral Industries, University Park, PA, October 14-16, 1986. Particle Technology Laboratory Publication No. 629. (MN-1)</i>	

TABLE OF CONTENTS

	Page
<b>III. Characterization of Dust Particles</b>	<b>121</b>
<b>12. Wetting Characteristics and Their Significance in Dust Abatement</b>	<b>123</b>
<i>S. Chander, B. R. Mohal and F. F. Aplan, Mineral Processing Section, The Pennsylvania State University, University Park, PA 16802. Presented at the International Symposium on Respirable Dust, The Pennsylvania State University, University Park, PA 16802, October 14-16, 1986. (PS-8)</i>	
<b>13. Wetting Behavior of Coal in the Presence of Some Nonionic Surfactants</b>	<b>129</b>
<i>S. Chander, B. R. Mohal and F. F. Aplan, Mineral Processing Section, Department of Mineral Engineering, The Pennsylvania State University, University Park, PA 16802. Presented at the 191st National Meeting of the American Chemical Society, New York, April 13-18, 1986. Printed in Colloids and Surfaces, 26 (1986), Elsevier Science Publishers, B.V., Amsterdam - Printed in The Netherlands, pp. 193-203. (PS-8)</i>	
<b>14. A New Technique to Determine Wettability of Powders-Imbibition Time Measurements</b>	<b>139</b>
<i>B. R. Mohal and S. Chander, Mineral Processing Section, Department of Mineral Engineering, The Pennsylvania State University, University Park, PA 16802. Printed in Colloids and Surfaces, 21 (1986), Elsevier Science Publishers, B. V., Amsterdam - Printed in The Netherlands, pp. 193-203. (PS-8)</i>	
<b>15. Estimation of Particle Size Distributions Using Pipet-Withdrawal Centrifuges</b>	<b>148</b>
<i>T. F. Dumm and R. Hogg, Mineral Processing Section, Department of Mineral Engineering, The Pennsylvania State University, University Park, PA 16802. Printed in Particle Characterization, 3 (1986), pp. 122-128. (PS-3)</i>	
<b>16. Standard Respirable Dusts</b>	<b>155</b>
<i>T. F. Dumm and R. Hogg, Mineral Processing Section, Department of Mineral Engineering, The Pennsylvania State University, University Park, PA 16802. Presented at the International Symposium on Respirable Dust, The Pennsylvania State University, University Park, PA 16802, October 14-16, 1986. (PS-3)</i>	
<b>17. A Procedure for Extensive Characterization of Coal Mine Dust Collected Using a Modified Personal Sampler</b>	<b>186</b>
<i>T. F. Dumm and R. Hogg, Mineral Processing Section, Department of Mineral Engineering, The Pennsylvania State University, University Park, PA 16802. Presented at the International Symposium on Respirable Dust, The Pennsylvania State University, University Park, PA 16802, October 14-16, 1986. (PS-3)</i>	

	Page
<p><b>18. Electron Spin Resonance Detection of Reactive Free Radicals in Fresh Coal Dust and Quartz Dust and Its Implications to Pneumoconiosis and Silicosis</b></p> <p><i>N. S. Dalal, M. M. Suryan, B. Jafari and X. Shi, Chemistry Department, West Virginia University, Morgantown, WV 26506 and V. Vallyathan and F. H. Y. Green, National Institute of Occupational Safety and Health, Morgantown, WV 26505. Presented at the International Symposium on Respirable Dust, The Pennsylvania State University, University Park, PA 16802, October 14-16, 1986. (WV-10)</i></p>	194
<p><b>19. Detection of Organic Free Radicals in Coal-dust Exposed Lung Tissue and Correlations with Their Histopathological Parameters</b></p> <p><i>B. Jafari and N. S. Dalal, Chemistry Department, West Virginia University, Morgantown, WV 26506 and V. Vallyathan and F. Y. H. Green, National Institute of Occupational Safety and Health, Morgantown, WV 26505. Presented at the International Symposium on Respirable Dust, The Pennsylvania State University, University Park, PA 16802, October 14-16, 1986. (WV-10)</i></p>	200
<p><b>20. Cascade Impactor Sampling and Data Analysis - Chapter (4) Theory and Design Guidelines</b></p> <p><i>Virgil A. Marple and Kenneth L. Rubow, Mechanical Engineering Department, University of Minnesota, Minneapolis, MN 55455. Copyright - American Industrial Hygiene Association 475 Wolf Ledges Parkway, Akron, Ohio, pp. 79-101. (MN-2)</i></p>	204
<p><b>21. Cascade Impactor Sampling and Data Analysis - Chapter (5) Low-Pressure and Micro-orifice Impactors</b></p> <p><i>Susanne V. Hering, Department of Chemical Engineering, University of California, Los Angeles, CA 90024 and Virgil A. Marple, Mechanical Engineering Department, University of Minnesota, Minneapolis, MN 55455. Copyright - American Industrial Hygiene Association, 475 Wolf Ledges Parkway, Akron, Ohio, pp. 103-127. (MN-2)</i></p>	224
<p><b>22. Micro-orifice Uniform Deposit Impactor</b></p> <p><i>Virgil A. Marple, Kenneth L. Rubow, G. Ananth, University of Minnesota, Minneapolis, MN 55455 and H. J. Fissan, University of Duisburg, D 4100 Duisburg, F. R. G. Printed in <u>Journal of Aerosol Science</u>, Vol. 17, No. 3, pp. 489-494. (MN-2)</i></p>	244
<p><b>23. A Hypothesis on the Possible Contribution of Coal Cleats to CWP</b></p> <p><i>Thomas P. Meloy, West Virginia University, Morgantown, WV 26505. Presented at the International Symposium on Respirable Dust, The Pennsylvania State University, University Park, PA 16802, October 14-16, 1986. (WV-12)</i></p>	249
<p><b>24. A Working Hypothesis on How Silica and Silica Surface May Cause Silicosis and CWP</b></p> <p><i>Thomas P. Meloy, West Virginia University, Morgantown, WV 26505. Presented at the International Symposium on Respirable Dust, The Pennsylvania State University, University Park, PA 16802, October 14-16, 1986. (WV-12)</i></p>	251

TABLE OF CONTENTS

	Page
<b>IV. Interaction of Dust and Lungs</b>	<b>255</b>
<b>25. Measurement of Superoxide Release From Single Pulmonary Alveolar Macrophages</b>	<b>257</b>
<i>K. A. DiGregorio, E. V. Cilento, and R. C. Lantz, Departments of Chemical Engineering and Anatomy, West Virginia University, Morgantown, WV 26506-6302. Presented at the International Symposium on Respirable Dust, The Pennsylvania State University, University Park, PA, October 14-16, 1986. (WV-9)</i>	
<b>26. The Effect of Lecithin Surfactant and Phospholipase Enzyme Treatment on Some Cytotoxic Properties of Respirable Quartz and Kaolin Dusts</b>	<b>261</b>
<i>W. E. Wallace, Engineering Sciences, West Virginia University, Morgantown, WV 26506 and M. J. Keane, V. Vallyathan, F. Saus, V. Castranova, D. Bates and C. A. Hill, Appalachian Laboratory for Occupational Safety and Health, Division of Respirable Disease Studies, National Institute for Occupational Safety and Health, Presented at the International Symposium on Respirable Dust, The Pennsylvania State University, University Park, PA 16802, October 14-16, 1986. (WV-2)</i>	
<b>27. Effects of Coal Dust and Alveolar Macrophages on Growth of Lung Fibroblasts</b>	<b>274</b>
<i>G. L. Bartlett and Ann B. Pedersen, Department of Pathology, The Milton S. Hershey Medical Center, The Pennsylvania State University, Hershey, PA 17033. Presented at the International Symposium on Respirable Dust in Mineral Industries, The Pennsylvania State University, University Park, PA, October 14-16, 1986. (PS-4)</i>	
<b>28. The Effects of Coal Mine Dust Particles on the Metabolism of Arachidonic Acid By Pulmonary Alveolar Macrophages</b>	<b>282</b>
<i>L. M. Demers, R. E. Edelson, M. P. Rose and D. T. Superdock, Department of Pathology, The Milton S. Hershey Medical Center, The Pennsylvania State University, 500 University Drive, Hershey, PA 17033. Presented at the International Symposium on Respirable Dust, The Pennsylvania State University, University Park, PA 16802, October 14-16, 1986. (PS-9)</i>	
<b>29. Development of Alterations in the Lung Induced by Inhaled Silica: a Morphometric Study</b>	<b>289</b>
<i>R. Clark Lantz<sup>1</sup>, Charles Stanley<sup>2</sup> and David E. Hinton<sup>1</sup>, <sup>1</sup>Department of Anatomy, West Virginia University, Morgantown, WV 46505 and <sup>2</sup>Department of Mechanical Engineering, West Virginia University, Morgantown, WV 46505. Presented at the International Symposium on Respirable Dust, The Pennsylvania State University, University Park, PA 16802, October 14-16, 1986. (WV-5)</i>	

	Page
<b>V. Relationship of Mine Environment, Geology and Seam Characteristics to Dust Generation and Mobility</b>	<b>293</b>
<b>30. A Strategy for Coal Mine Respirable Dust Sampling Using Multi-Stage Impactors for Characterization Purposes</b>	<b>285</b>
<i>C. Lee and J. M. Mutmansky, Department of Mineral Engineering, The Pennsylvania State University, University Park, PA 16802. Presented at the Engineering Health and Safety in Coal Mining--SME Annual Meeting Symposium, New Orleans, LA, March 2-6, 1986. (PS-5)</i>	
<b>31. Statistical Analysis of the Elemental Characteristics of Airborne Coal Mine Dust</b>	<b>306</b>
<i>C. Lee and J. M. Mutmansky, Department of Mineral Engineering, The Pennsylvania State University, University Park, PA 16802. Presented at the International Symposium on Respirable Dust in the Mineral Industries, October 14-16, 1986, The Pennsylvania State University, University Park, PA. (PS-5)</i>	
<b>32. Variation in Mineral and Elemental Composition of Respirable Coal Mine Dusts by Worker Location and Coal Seam</b>	<b>319</b>
<i>R. A. Andre, West Virginia Geological Survey, T. Simonyi, and R. L. Grayson, West Virginia University, Morgantown, WV 26506. Presented at the International Symposium on Respirable Dust, The Pennsylvania State University, University Park, PA, October 14-16, 1986. (WV-6A)</i>	
<b>33. Characterization of Respirable Dust on a Longwall Panel--A Case Study</b>	<b>328</b>
<i>R. L. Grayson and S. S. Peng, Department of Mining Engineering, College of Earth and Mineral Resources, West Virginia University, Morgantown, WV 26506. Presented at the SME Annual Meeting Symposium, New Orleans, LA, March 2-6, 1986. Published in Health and Safety in Coal Mining, Chapter 9, pp. 95-117. (WV-6A)</i>	
<b>34. A Methodology for Determining the Mineral Content and Particle Size Distribution of Airborne Coal Mine Dust</b>	<b>346</b>
<i>T. J. Stobbe, R. W. Plummer, H. Kim, Department of Industrial Engineering, West Virginia University, and W. G. Jones, Division of Respiratory Disease Studies, National Institute for Occupational Safety and Health. Published in Applied Industrial Hygiene, Volume 1, No. 2, July 1986. (WV-6A)</i>	
<b>35. Characterization of Coal Mine Dust</b>	<b>352</b>
<i>Terrence J. Stobbe, Ralph W. Plummer, H. Kim, and J. M. Dower, Department of Industrial Engineering, West Virginia University, Morgantown, WV 26506. Printed in the <u>American Conference of Governmental Industrial Hygienists</u>, Vol. 14, 1986, pp. 689-696. (WV-6B)</i>	

TABLE OF CONTENTS

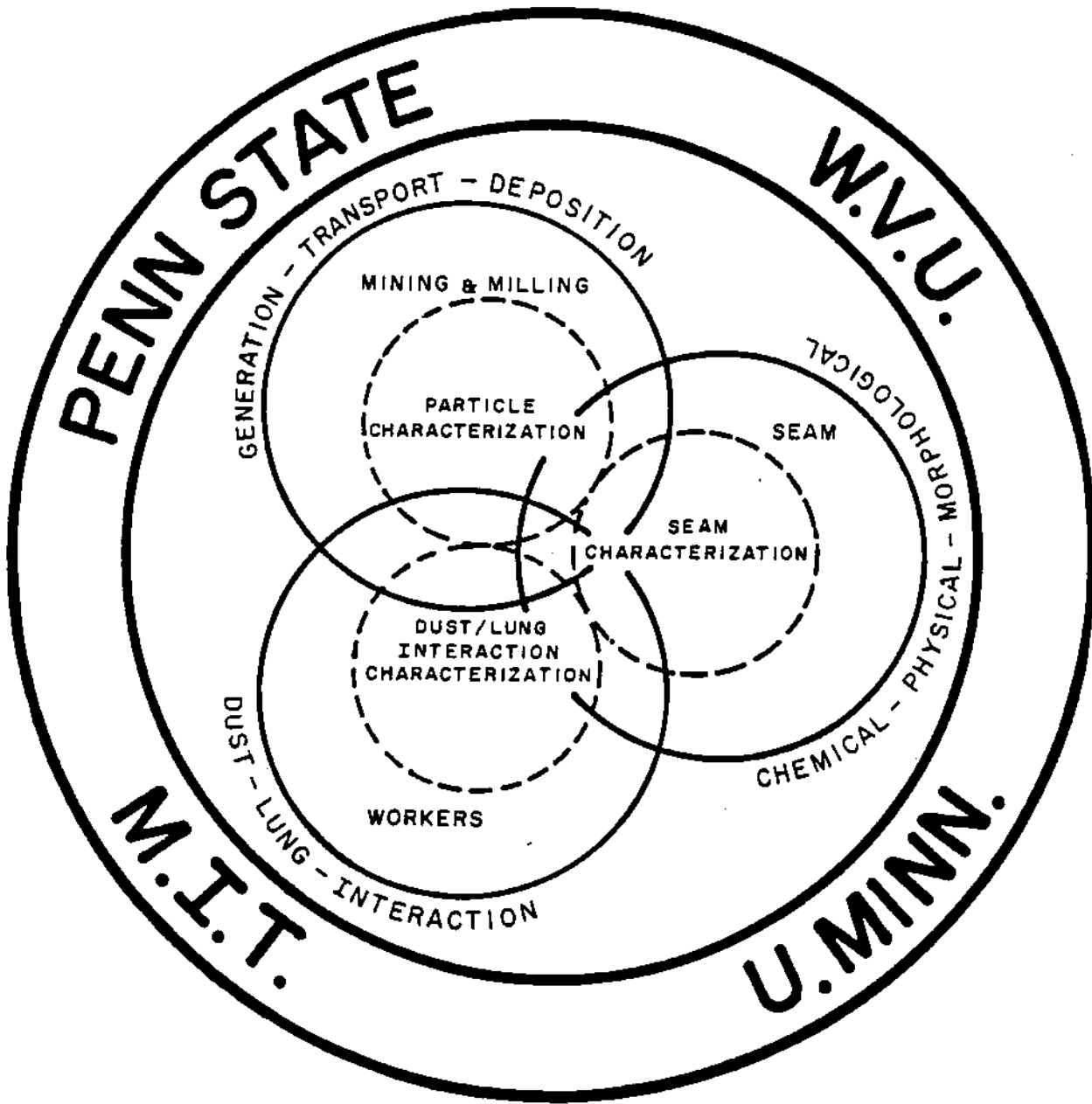
	<b>Page</b>
<b>VI. Coordination</b>	<b>359</b>
<b>36. A Review of the Programs and Activities of the Generic Mineral Technology Center for Respirable Dust</b>	<b>361</b>
<i>R. L. Frantz and R. V. Ramani, Department of Mineral Engineering, The Pennsylvania State University, University Park, PA 16802. Presented at the SME-AIME Annual Meeting, New Orleans, Louisiana, March 2-6, 1986. (PS-6)</i>	

**INDEX**

<b>Cumulative Author Index</b>	<b>369</b>
<b>Cumulative Subject Index</b>	<b>371</b>



THE RESPIRABLE DUST CENTER



**The Respirable Dust Center**

## FOREWORD

This volume contains publications resulting from respirable dust research performed in the Generic Mineral Technology Center for Respirable Dust by faculty, staff and graduate students at The Pennsylvania State University, West Virginia University, University of Minnesota, and Massachusetts Institute of Technology. These publications have appeared in scientific journals, proceedings of the national and international symposiums and meetings. Complete citations of the publications can be found in the text. The Generic Mineral Technology Center for Respirable Dust is funded by the U.S. Bureau of Mines through the Mining and Mineral Resources Research Institute Program. The opinions and conclusions expressed in the papers are those of the authors alone and do not represent the opinions of the Generic Mineral Technology Center for Respirable Dust, the Mining and Mineral Resources Research Institute Program or the U.S. Bureau of Mines. Citation of manufacturers' names in the papers were made for general information purposes, and do not imply endorsement of the products by the authors.

All of the publications in this volume are on research that has been supported by the Department of the Interior's Mineral Institute program administered by the Bureau of Mines through the Generic Mineral Technology Center for Respirable Dust under allotment grant number G1135142 or G1175142.

In addition to these papers, a dust conference was organized by the Center and held at The Pennsylvania State University in October 1986. The conference was co-sponsored by ACGIH, MSHA, NIOSH and USEM. Proceedings from this conference are available from ACGIH. The generic center maintains a reference center that serves as a clearinghouse for technical information for the generic area and supplies reports on generic center accomplishments.

The support from the United States Congress for the Generic Mineral Technology Center for Respirable Dust is gratefully acknowledged. We also acknowledge and appreciate the support and inputs from USEM, NIOSH, MSHA, the Research Advisory Council, and the Committee on Mining and Mineral Resources Research which have significantly contributed to the activities of the Generic Mineral Technology Center for Respirable Dust.

Respectfully submitted,

**Robert L. Frantz**  
Co-Director, Generic Mineral  
Technology Center for Respirable Dust  
Co-Editor

**R. V. Ramani**  
Co-Director, Generic Mineral  
Technology Center for Respirable Dust  
Co-Editor

THE RESPIRABLE DUST CENTER

Excerpted From The  
1988 UPDATE TO THE NATIONAL PLAN  
FOR  
RESEARCH IN MINING AND MINERAL RESEARCH

Report to:

December 15, 1987

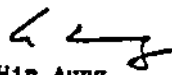
The Secretary of the Interior  
The President of the United States  
The President of the Senate  
The Speaker of the House of Representatives

Section 9(e) of Public Law 98-409 of August 29, 1984, (98 Stat. 1536 et seq.) mandates that the Committee on Mining and Mineral Resources Research submit an annual update to the National Plan for Research in Mining and Mineral Resources: "Improving Research and Education in Mineral Science and Technology through Government-(Federal, State and Local), Industry, and University Cooperation."

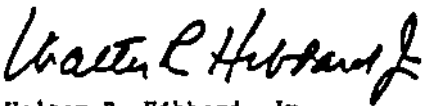
Respirable Dust (centered at Pennsylvania State U. and West Virginia U., with affiliates at U. of Minnesota and Massachusetts Institute of Technology): brings together experts concerned with particles causing potentially disabling or fatal diseases, including pneumoconiosis ("black lung"), silicosis, and asbestosis, the latter of deep concern not just to workers in the mineral sector of the economy but also to the general populace.

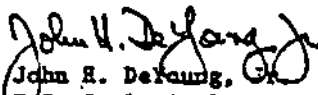
SIGNED:

  
Carl V. Randolph  
Mining Industry


  
Win Aung  
National Science  
Foundation


  
Don L. Warner  
University Administrator

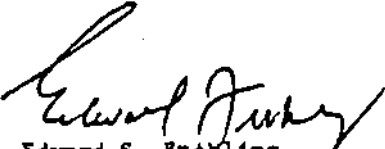
  
Walter R. Hibbard, Jr.  
National Academy of  
Sciences

  
John R. DeYoung, Jr.  
U.S. Geological  
Survey

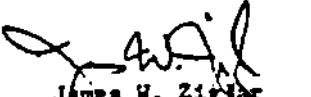
  
Joseph N. Crowley  
University Administrator

  
John C. Calhoun, Jr.  
National Academy of Engineering

  
John D. Morgan  
Bureau of Mines

  
Edward S. Frothingham  
Mining Industry

  
Orme Lewis, Jr.  
Conservation Community  
COCHAIR

  
James W. Ziegler  
Assoc. Secretary-  
Water & Science  
U.S. Department of

**THE RESPIRABLE DUST CENTER**

**Generic Mineral Technology Center For Respirable Dust**

**RESEARCH ADVISORY COUNCIL MEMBERS**

Dr. John A. Breslin  
Senior Staff Physical Scientist  
U.S. Bureau of Mines  
2401 E Street, N.W.  
Columbia Plaza  
Washington, D.C. 20241  
(202) 634-1220

Dr. Ronald Munson  
Director, Office of Mineral  
Institutes - MS 1020  
U.S. Department of the Interior  
2401 E Street, N.W.  
Washington, D.C. 20241  
(202) 634-1328

Dr. Lewis Wade  
Research Director  
Twin Cities Research Center  
U.S. Bureau of Mines  
5629 Minnehaha Avenue, S.  
Minneapolis, MN 55417  
(612-725-4610

Dr. John A. Campbell  
Director, Engineering and  
Technology Support  
Kerr-McGee Corporation  
P.O. Box 25861  
Oklahoma City, OK 73125  
(405) 270-3778

Mr. John Murphy  
Research Director  
Pittsburgh Research Center  
U.S. Bureau of Mines  
P.O. Box 18070  
Pittsburgh, PA 15236  
(412-675-6601

Dr. James L. Weeks, C.I.H.  
Deputy Administrator for  
Occupational Health  
United Mine Workers of  
America  
900 15th Street, N.W.  
Washington, D.C. 20005  
(202) 842-7300

Mr. Robert E. Glenn  
Director, Division of Respiratory  
Disease Studies - NIOSH  
944 Chestnut Ridge Road  
Morgantown, WV 26505  
(304) 459-5978

Dr. Kandiah Sivarajah  
State Toxicologist  
Room 825--Health and Welfare  
Building  
Harrisburg, PA 17108  
(717) 787-1708

Dr. Jerome Kleiner  
Department of Pathology  
Cleveland Met. General Hospital  
3395 Scranton Road  
Cleveland, OH 44109  
(216) 459-5978

Dr. Pramod Thakur  
Research Group Leader  
CONOCO, Inc.  
R & D Division  
Route #1, Box 119  
Morgantown, WV 26505  
(304) 983-2251

**PAST RESEARCH ADVISORY COUNCIL MEMBERS**

Mr. Darrel Auch  
Senior Vice President  
Northern West Virginia Region  
Consolidation Coal Company  
P.O. Box 1314  
Morgantown, WV 26507  
(304) 296-3461

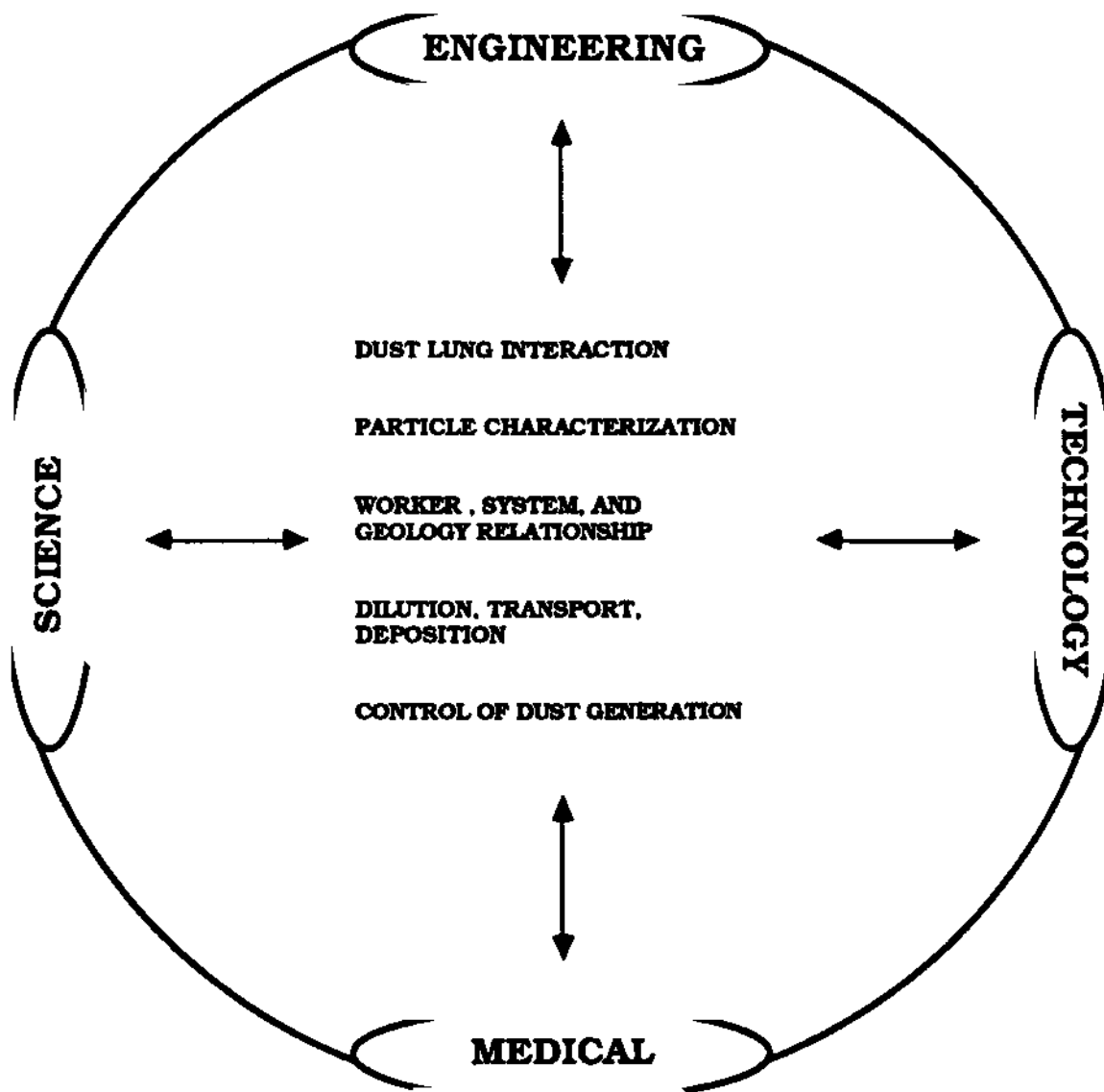
Dr. Thomas Falkie  
President  
Berwind Natural Resources  
Company  
Centre Square West  
1500 Market Street  
Philadelphia, PA 19102  
(215) 563-2800

Mr. C. Wesley McDonald  
Senior Vice President  
(Mining)  
Northern West Virginia  
Region  
Consolidation Coal Company  
P.O. Box 1314  
Morgantown, WV 26505  
(304) 296-3461

Dr. J. Harrison Daniel  
Program Manager, Mining  
Research  
Health and Safety  
2401 E Street, N.W.  
Washington, D.C. 20241  
(202) 634-1253

Dr. Fred Kissell  
Research Supervisor  
Pittsburgh Safety Research Center  
U.S. Bureau of Mines  
4800 Forbes Avenue  
Pittsburgh, PA 15213  
(412) 675-6679

Dr. Donald Reid  
Deputy Secretary for Public  
Health Programs  
Department of Health  
Health and Welfare Building  
P.O. Box 90  
Harrisburg, PA 17108  
(717) 783-8804



**Standardized protocols for Respirable Dust Research  
in scientific, engineering, and medical areas.**

RESEARCH



CONTROL OF GENERATION

- Amount
- Fracture

DILUTION,  
TRANSPORT  
AND  
DEPOSITION

- Concentration
- Size Consist
- Modeling

MINE WORKER,  
MINING SYSTEM,  
SEAM GEOLOGY

- Seam Sections
- Silica
- Trace Elements
- System Configuration
- Worker Location



- Coal Data Bank
- Mine Samples

SUITE OF  
GENERATED  
RESPIRABLE  
DUSTS

- Anthracite
- Medium Volatile Bituminous
- High Volatile Bituminous
- Silica
- Fireclay
- Rock Dust



CHARACTERIZATION

- Size/Shape/Composition
- Surface/Functional Groups
- Particle Interaction

DUST LUNG  
INTERACTION

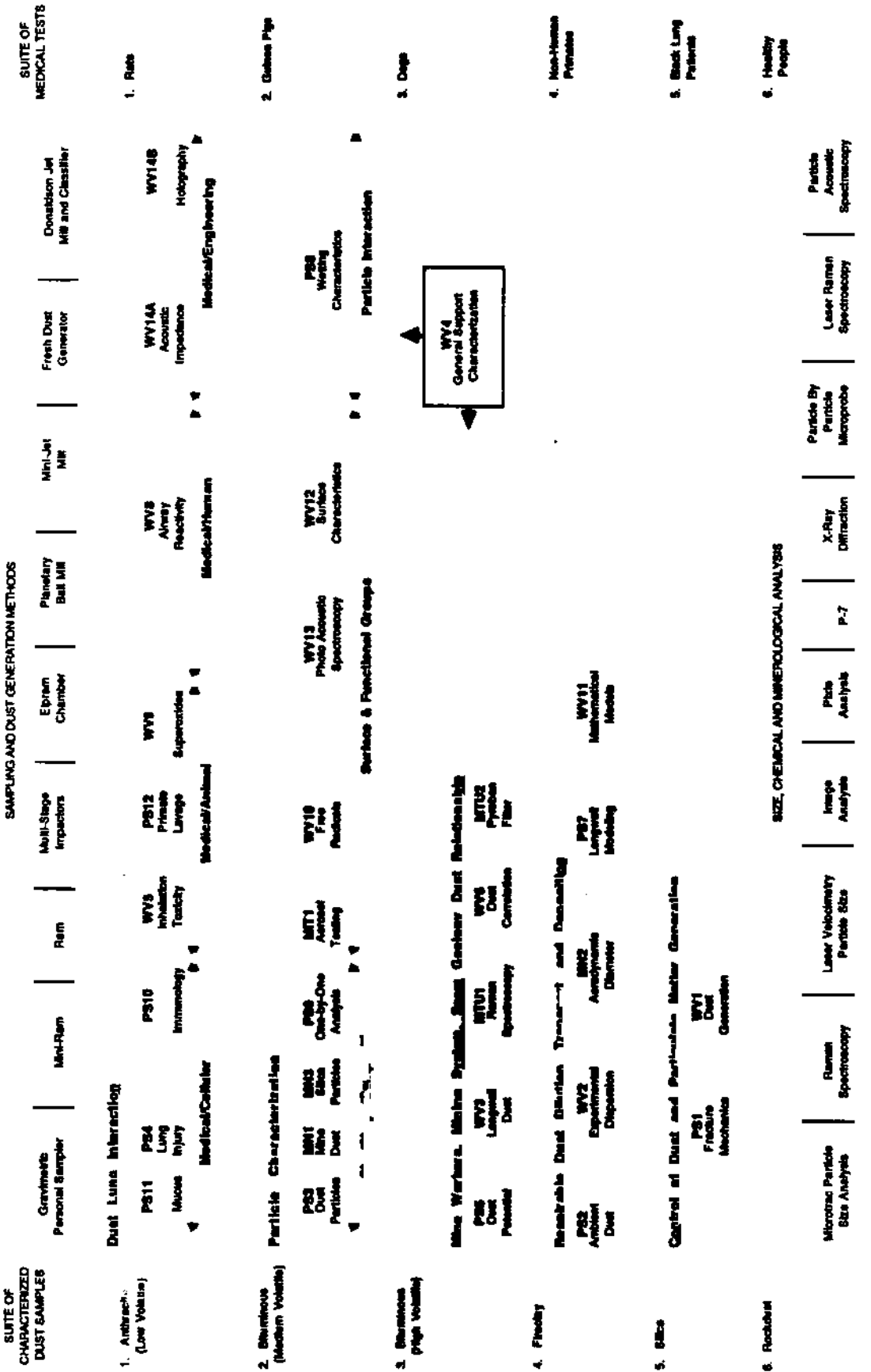
- Medical/Cellular
- Medical/Animal
- Medical/Human
- Medical/Engineering



TRAINING

Train engineers, scientists, medical personnel, graduate students and undergraduate students in the interdisciplinary aspects of respirable dust.

1986



The integration of scientific, engineering, and medical research findings into on-going projects.

# THE RESPIRABLE DUST CENTER

## The Generic Mineral Technology Center for Respirable Dust

<b>SUITE OF CHARACTERIZED DUST SAMPLES</b>	<b>SAMPLING AND DUST GENERATION METHODS</b>	<b>SUITE OF MEDICAL TESTS</b>
1. Anthracite (Low Volatile)	Dust/Lung Interaction	1. Rats
2. Bituminous (Medium Volatile)	Particle Characterization	2. Guinea Pigs
3. Bituminous (High Volatile)	Mine Workers Mining System Seam Geology Dust Relationship	3. Dogs
4. Fireclay	Respirable Dust Dilution, Transport and Deposition	4. Non-Human Primates
5. Silica	Control of Dust Generation	5. Black Lung Patients
6. Rockdust		6. Healthy People

**SIZE, CHEMICAL AND  
MINEROLOGICAL ANALYSIS**

### STATEMENT OF GOAL

The primary goal of the Generic Mineral Technology Center for Respirable Dust is to reduce the incidence and severity of respirable dust disease through advancing the fundamental understanding of all aspects of respirable dust associated with mining and milling and the interaction of dust and lungs.

**The holistic approach to standardized protocols and procedures.**



**I**

**Control of Dust and  
Particulate Matter Generation**

# Mixed Mode Testing for Fracture Toughness of Coal Based on Critical-Energy-Density

R. Karl Zipf, Jr. and Z. T. Bieniawski

Department of Mineral Engineering, The Pennsylvania State University

**Abstract.** Based on the premise that understanding the fundamental mechanics of fine fragment formation in coal will lead to reducing coal dust problems in mines, a thorough study of the mechanics of crack propagation in coal was undertaken. Two approaches were considered in an attempt to understand and quantify the fracture process as it relates to fine fragment formation.

In one approach, theoretical models are used which describe the size of the fracture process zone which may relate to the amount of structural damage and fine fragment formation on the new crack surface. The other approach is based on the relationship between crack tip stress intensity and new surface appearance for mixed mode crack propagation. Preliminary observations with a scanning electron microscope support the premise that fine fragment formation is related to fracture surface appearance and fracture initiation conditions.

An experimental program designed to supply the input parameters for these approaches is presently underway. The experimentation features mixed mode fracture toughness testing, using a special mixed mode testing rig, and fracture velocity measurements with a crack propagation gage. The interpretation of this data via the approaches discussed will provide further understanding of the mechanics of fine fragment formation in coal.

## INTRODUCTION

As part of a larger effort to reduce the incidence of coal workers pneumoconiosis (black lung) in coal miners, researchers at The Pennsylvania State University are engaged in a project to understand the fundamental mechanics of fine fragment formation in coal. This project is part of a comprehensive research effort within the Generic Mineral Technology Center for Respirable Dust which is jointly administered by The Pennsylvania State University and West Virginia University. The human and direct dollar cost of dust induced illnesses in coal miners is very large. By one account (Roepke et al., 1983) the Federal Government paid out almost \$12 billion to some 500,000 coal miners and their beneficiaries

from 1970 to 1980. Since then, the present liability of the Federal disability trust funds approaches \$20 billion per year. There are other hidden costs of coal dust as well, mostly in the form of increased equipment wear and decreased operator productivity both of which are due to the poor environment. Quantifying these costs is difficult; however, they are certainly in the same range as the present pneumoconiosis costs. Thus, the need for long-term research efforts to remedy or prevent this costly situation arises.

The principal source of the coal dust in underground mining is the cutting operation. The USBM has conducted investigations into the mechanics of coal cutting for many years. Roepke (1984) summarized the principals of proper coal cutting to minimize dust formation by recommending to "cut at maximum depth (maximum advance rate) at all times, at minimum RPM, with the fewest possible bits, having the lowest possible included tip angle." Most coal in the U.S. is mined with the continuous mining machine which inherently cannot meet these design recommendations (Roepke and Hanson, 1979).

It is known that respirable size dust particles are formed and/or liberated by the fracture process. One of the first investigations conducted by the USBM determined the amount of respirable dust of 0.9 to 10 micrometer size adhering to the surfaces of various bituminous coals (Chen and Zukovich, 1973). They found that the number of particles ranged from  $10^{11}$  to  $10^{12}$  particles per pound. Fortunately, much less than 1% of the respirable particles ever become airborne (Streibig and Zeller, 1975). In a recent study sponsored by the National Academy of Sciences (Cook, 1982) these observations raised certain key questions regarding the mechanical events occurring immediately after particles are produced and the quantity of particles that actually become airborne. Moreover, one should know the nature of the particles that become airborne versus those that remain behind on the new fracture surface.

Our present knowledge of the fundamental mechanisms of coal dust generation and entrainment is not sufficient to clarify let alone

control the processes involved. When a cutting tool interacts with coal, it causes numerous cracks to propagate through the intact material. Numerous larger fragments are broken free, but another quantity of undesirable fine fragments are also created. The formation of these fine fragments is a direct result of the crack propagation process; hence, a thorough understanding of the mechanics of crack propagation is required to minimize the production of unwanted fine fragments.

The aim of the research reported in this paper was to provide accurate measurements of fracture toughness in coal as a parameter controlling the unstable crack growth and to study the fracture velocity in coal. This last aspect is a novel concept based on the observation that crack bifurcation occurs above some critical velocity. This leads to the hypothesis that when crack bifurcation does occur, fine fragments of coal material are generated which leads to increased dust formation. Figure 1 shows a propagating crack in glass as the crack bifurcates and leads to fine fragment formation (Bieniawski, 1968).



Figure 1. Crack Bifurcation in Glass (Bieniawski, 1968).

The present investigation was concerned with: (1) the fracture process zone and its influence on fine fragment formation; (2) fracture surface characterization with the scanning electron microscope; (3) development of mixed mode testing procedures for coal.

In conjunction with the fracture toughness testing, determination of related coal material properties is essential. These properties include the unconfined compressive strength, the tensile strength from Brazilian tests, the point load index, the Young's modulus and the Poisson's ratio. Sonic velocity measurements will provide compressional and shear wave velocities from which calculation of dynamic moduli is possible. Determination of these coal material properties should enable more complete characterization of the various coals and also provide useful cross checks and correlations for the fracture mechanics properties. Recent work by Nelson et al.

(1985) has demonstrated a strong correlation between the critical energy release rate  $G$  (which relates to fracture toughness  $K$ ) and the performance characteristics of a tunnel boring machine. By direct analogy, there is a reason to believe that a similar relationship exists between  $G$  and  $K$  and the performance of a continuous mining machine or a longwall shearer. Determination of these correlations between fracture toughness, other mechanical properties and cutting machine performance will provide additional insight into the dust generation potential of various coals.

ENERGY DISSIPATION, CRACK PROPAGATION AND FINE FRAGMENT FORMATION

Studies in many materials, including coal, show that when a crack propagates through a material, it rarely produces a smooth, clear, well-defined surface. Microcracks are opened up all along the newly created surfaces and successful or unsuccessful attempts at crack bifurcation may occur. The material on either side of the new crack surface is affected by the "fracture process zone" (FPZ) which surrounds the propagating crack tip. Energy supplied to the crack tip by various external loads is largely dissipated in the FPZ and relatively little is consumed as free surface energy. When loading conditions are such that the crack tip is provided with excess energy for crack propagation, it responds by dissipating that energy through additional microcracking and crack bifurcation within the FPZ. As a result, new fracture surfaces may exhibit rougher appearances and increased structural damage which in turn may correlate with an increased tendency to produce unwanted fine fragments. Two approaches are considered in these attempts to understand and quantify the fracture process as it relates to fine fragment formation: one is based on theoretical models of the size of the fracture process zone; and the other is based on relationships between crack tip stress intensity and new fracture surface appearance as seen under a scanning electron microscope.

THE FRACTURE PROCESS ZONE AND FINE FRAGMENT FORMATION

In this approach, theoretical models are considered which describe the size of the microcrack zone or FPZ. It is postulated that the size of the process zone relates to the amount of material damage expected on the new crack surface which may characterize the propensity of the coal to generate unwanted fine fragments. Two alternative models exist which describe the size of the FPZ. One is based on a maximum stress criterion and the other is based on the strain energy density theory.

With the maximum stress criterion, different analysis approaches exist and all lead to similar results. The approaches are based on analyses of the plastic zone surrounding the crack tip originally developed for metals by Irwin and Dugdale (Broek, 1974). In recent work, Labuz

## MIXED MODE TESTING

(1985) uses a Dugdale approach to develop the concept of an effective crack length which is essentially the sum of the actual crack length plus the length of the FPZ. Schmidt (1980) begins with the Irwin approach in the development of a microcrack zone model. For purposes of this work, the latter approach is preferred because of its ready ability to incorporate effects of hydrostatic compression and anisotropic stress on the size and shape of the microcrack zone or the FPZ. The radius  $r$  of the FPZ as a function of angle  $\phi$  from the crack plane is:

$$r(\phi) = \frac{1}{2\pi} \left[ \cos \frac{\phi}{2} \left( 1 + \sin \frac{\phi}{2} \right) \right]^2 \left( \frac{K_{Ic}}{\sigma_t} \right)^2$$

where  $K_{Ic}$  is the Mode I fracture toughness and  $\sigma_t$  is the uniaxial tensile strength of the intact material. Plane strain conditions are assumed.

The alternative description of the size of the fracture process zone is the radius of the "core region" in the strain energy density theory (Gdoutos, 1984). The radius  $r$  is given by

$$r = \frac{S}{\left( \frac{dW}{dV} \right)}$$

The strain energy density factor  $S$  is given by

$$S = a_{11}K_I^2 + 2a_{12}K_I K_{II} + a_{22}K_{II}^2$$

where  $K_I$  and  $K_{II}$  are the Mode I and Mode II stress intensity factors and  $a_{ij}$  are geometry functions given in full by Gdoutos (1984). Also  $(dW/dV)$  is the strain energy density at a point found as

$$\frac{dW}{dV} = \frac{1}{2E} (\sigma_1^2 + \sigma_2^2 + \sigma_3^2) - \frac{\nu}{E} (\sigma_1\sigma_2 + \sigma_2\sigma_3 + \sigma_3\sigma_1)$$

Both alternative fracture process zone descriptions require similar laboratory data; however, in the latter approach based on the strain energy density theory, mixed mode test conditions can be accommodated.

### FRACTURE SURFACE CHARACTERIZATION WITH THE SCANNING ELECTRON MICROSCOPE

The other approach to characterizing the potential of a coal to produce unwanted fine fragments is based on the relationship between crack tip stress intensity and fracture velocity and their effect on new fracture surface appearance for mixed mode crack propagation. When a crack propagates through a material, post-mortem examination of the new fracture surfaces typically reveals a mirror, mist or hackle type of surface appearance. These surface appearances are seen in a wide variety of materials ranging from metals, ceramics, glass and polymers as illustrated by Ravi-Chander and Knauss (1984), Broek (1974), and Abdel-Latif, Bradt and Tressler (1981). However, such materials are homogeneous and this kind of surface character is not as well developed or as readily visible with inhomogeneous materials like rock (Forseka, Murrell and Barnes, 1985) or in coal. However, different degrees of structural damage on new fracture surfaces are readily seen.

It is postulated that the appearance of these new surfaces may correlate with the propensity of a coal to produce unwanted fine fragments on the new fractures. The appearance of these new surfaces depends largely on the amount of energy dissipation occurring in the passing fracture process zone. Experimentation with ideal materials by Ravi-Chander and Knauss demonstrated a useful relationship between crack tip stress intensity, fracture velocity and fracture surface appearance or degree of surface damage. The nature of the relationship is sketched in Figure 2. In the experiments mentioned, specimens of Homalite 100 were loaded almost instantaneously by various crack pressures. The higher loading pressures (hence higher loading rates) resulted in higher crack propagation velocities.

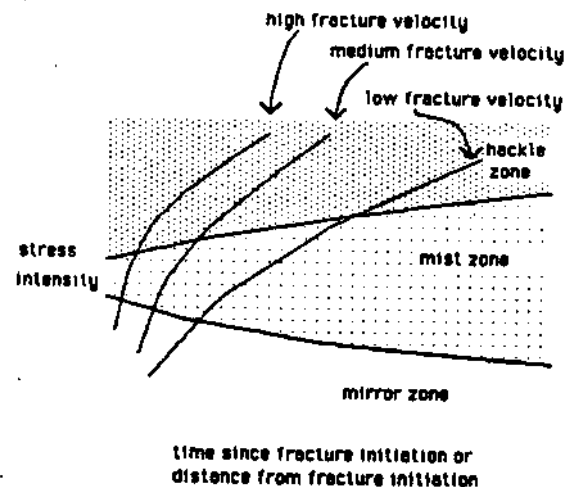


Figure 2. Schematic of Crack Tip Stress Intensity, Fracture Velocity, Surface Appearance Relationship (after Ravi-Chandar and Knauss, 1984).

Generally, crack velocity remained almost constant during the fracture event. Crack bifurcation occurs only in the so-called hackle zone or those areas with high degree of fracture surface damage.

A similar relationship is believed to exist for various coals and it may serve as a basis for: (1) ranking coals according to their tendency to form unwanted fine fragments; (2) directly relating surface appearance to the fracture initiation conditions such as crack tip stress intensity and loading conditions.

The latter relation may in turn suggest means to control the fracture process so that the production of unwanted fine fragments is minimized.

# THE RESPIRABLE DUST CENTER

## Experimental Studies

In order to make a preliminary assessment of this concept, a number of small notched cubes of Pittsburgh coal were failed by dominately Mode I or dominately Mode II loading conditions at both slow and fast loading rates. Fracture was also propagated in various directions either parallel to the bedding planes, the face cleat or the butt cleat. Next, the newly created fracture surfaces were examined under the SEM.

Four pairs of comparative SEM micrographs are shown in Figure 3 for the face cleat. The pairs are for (1) Mode I cracks under slow loading conditions; (2) Mode I cracks under fast loading conditions; (3) Mode II cracks under slow loading conditions; and (4) Mode II cracks under fast loading conditions. In each pair, the right image is at 100X and the left image is at 1000X. On the bottom of the right image is a scale bar which represents 100 microns in the right image and 10 microns on the left image.

In comparing these sets of images, we make the following observations:

- (1) The least amount of structural damage and fine fragment generation occurs under slow loading conditions in Mode I.
- (2) Increasing the loading rate in Mode I appears to increase the structural damage and fine fragment generation on the new fracture surface.

- (3) Changing the loading condition from Mode I to Mode II at slow loading rates increases the structural damage and fine fragment generation on the new fracture surface.
- (4) Increasing the loading rate from slow to fast in Mode II or changing the mode from I to II under fast loading conditions does not appear to change the fracture surface character in any readily apparent way; however, there is increased structural damage and fine fragment generation in fast loading conditions in Mode II versus slow loading conditions in Mode I.

These preliminary observations provide further impetus for developing means to generate and control mixed mode loading conditions in coal specimens.

## MODE I FRACTURE TOUGHNESS TEST DATA FOR COAL

Relative to other materials, few studies exist on the fracture toughness of rock (Bieniawski, 1981) and even less on coal. Considerable controversy remains regarding test procedures and the fracture strength for various coals. Table 1 presents a compilation of existing measurements of the Mode I fracture toughness of coal. These measurements were completed by researchers in the U.S. Canada, and Australia. This table shows that the fracture toughness can range over an order of magnitude for different coals and that the standard deviation of the mean for these

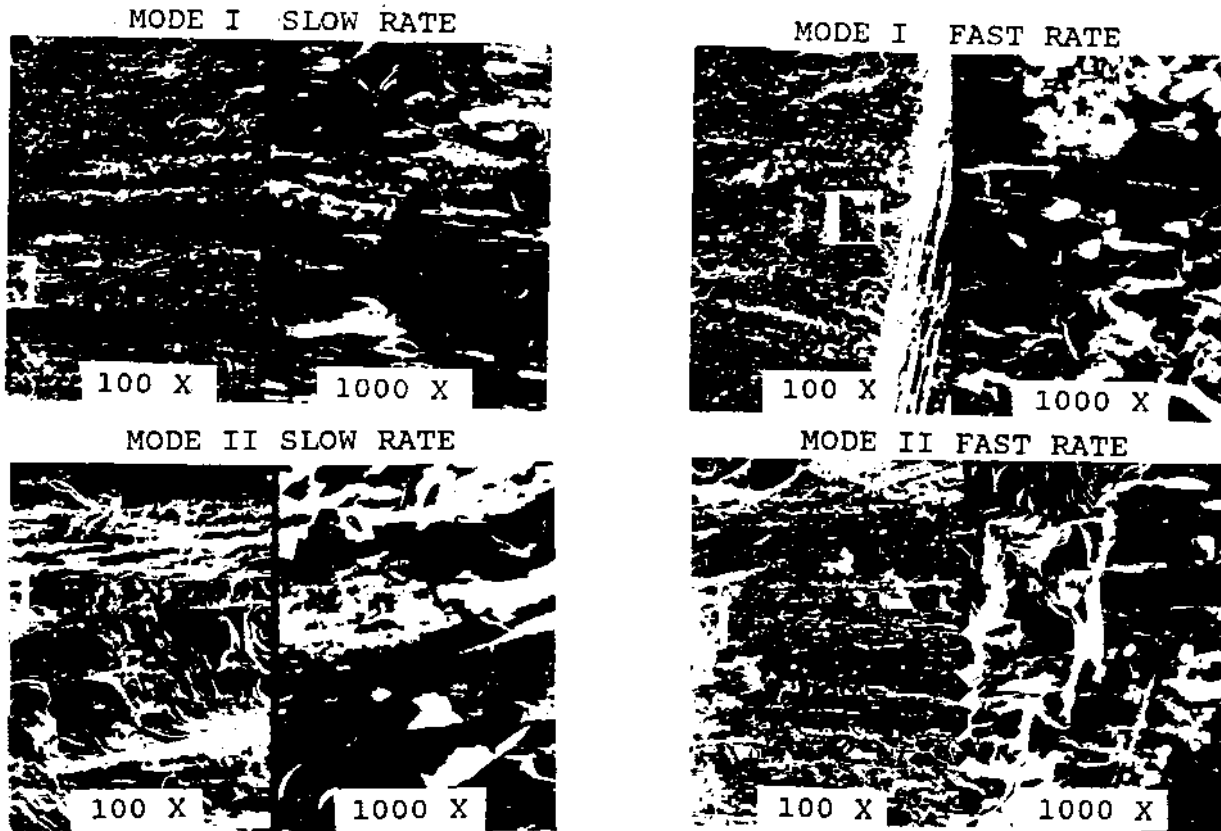


Figure 3. SEM Micrographs of Coal Fracture Surfaces Along the Face Cleat Scale Bar in 100 X Photo - 100 microns in right image and 10 microns in left image.

# MIXED MODE TESTING

TABLE 1. Summary of Coal Fracture Toughness Test Results

Source	Coal	Specimen Type	Specimen Size	$K_{Ic}$ MPa $\sqrt{m}$	Standard Deviation of Mean	No. of Tests
Advani et al. 1978	Pittsburgh	SEND-3PB	15 cm x 3.8 cm	0.0281	86%	2
	Waynesburg	SEND-3PB	x 1.9 cm	0.156	36%	3
	Redstone	SEND-3PB		0.0348	60%	6
Powell et al. 1981	Pittsburgh	SEND-3PB	15 cm x 3.8 cm	0.0629	37%	15
	Pittsburgh	SEND-3PB	x 1.9 cm	0.0472	34%	25
Bhagat, 1981	Lower Freeport	SEND-3PB	20 cm x 3.8 cm	0.0283	35%	10
	Redstone	SEND-3PB	x 1.9 cm	0.0474	72%	20
	Waynesburg	SEND-3PB		0.121	48%	5
	Sewickley	SEND-3PB		0.267	19%	9
Szendi-Horvath, 1982	Black Coking Coal	DMC	1.6 to 3.8 cm	0.219	13%	12
	Black Steaming "	DMC		0.435	12%	6
	Semi-Anthracite	DMC		0.132	11%	6
	Black Coking "	SEND-3PB	4 to 7 cm	0.321	11%	12
Bassin and Hau, 1982	Coal A	SEND-3PB	up to 8 cm	0.020 to 0.225	-	11
Klepaczko, et al. 1984	Coal A	WLCT	3.8 x 3.8 cm	0.154	25%	4
	Coal B	WLCT	x 3.2 cm	0.181	3%	3
	Coal A	WLCT-dynamic		2.014	11%	4
Bieniawski and Mark, 1984	Bone Coal	DMC	1.6 cm	0.220	25%	11
	Kitt Mine	SEND-4PB	up to 3 cm long	0.346	17%	3
	Coal	DMC	1.6 cm	0.150	19%	4
	Kitt Mine					
	Anthracite	DMC	1.6 cm	0.296	32%	11
Rushton Mine		SEND-4PB	up to 3 cm long	0.172	42%	4
		DMC	1.6 cm	0.032		2

TABLE 2. Fracture Toughness for Rock and Other Materials (Bieniawski, 1981)

Material	$K_{Ic}$ (MPa $\sqrt{m}$ )
Quartzite	0.721
Chelmsford Granite	0.592-0.636
Indiana Limestone	0.990
Coarse Sandstone	0.57-1.46
Texas Limestone	0.37-0.58
Berea Sandstone	0.23
Tennessee Sandstone	0.454
Carrara Marble	0.644
Westerley Granite	2.6

---

Concrete	0.6-0.8
Fused Silica	0.753
Aluminum Alloy	31.1
Steel	92-146

TABLE 3. Stress Intensity Factors for Mixed Mode Test Specimens

	Richard's Equation Original Geometry	Numerical Analysis of New Specimen
	$K_I$ MPa $\sqrt{m}$	
0° (Mode I)	0.190	0.183
30°	0.165	0.092
60°	0.095	0.011
90° (Mode II)	0.000	0.000

---

	$K_{II}$ MPa $\sqrt{m}$	
0° (Mode I)	0.000	0.000
30°	0.047	0.014
60°	0.082	0.043
90° (Mode II)	0.094	0.099

## THE RESPIRABLE DUST CENTER

tests is quite high, typically 30 to 50%. To put the magnitude of these fracture toughness values into perspective, typical fracture toughness values for other materials are given in Table 2.

The primary reason for this variability is the highly anisotropic, nonhomogeneous and discontinuous character of all coals. Many of these studies encountered problems with sample collection, preservation and preparation because of the weak, friable and moisture sensitive nature of coal. Because of its nature, only the strongest, most durable coal samples are ever tested which tends to produce very suspect fracture toughness test data.

Recognizing the difficulties in preparing and testing coal samples for mechanical properties, Bieniawski and Mark (1984) performed additional fracture toughness tests on several Appalachian coals. Those test results, also included in Table 1, show fracture toughness values in the same range as the other results; however, the standard deviation about the mean for those tests is somewhat better than many published results. This testing utilized the Diametral Compression (DMC) specimen, originally developed by Szendi-Horvath, and the SENB-4PB specimen. The work relied on the use of small specimens in order to minimize the effect of the innumerable macroscopic flaws in the coal.

One of the major problems in working with coal is obtaining properly sized and representative specimens for testing in a suitable test rig. Basic fracture mechanics theory sets minimum size requirements on test specimens so that the stress field in the immediate vicinity of the notch tip is unaffected by the specimen boundaries thus assuring that the loads are in effect at "infinity." If indeed the standards apply to rock, then the minimum crack length must meet the condition

$$a > 2.5 \left( \frac{K_{Ic}}{\sigma_t} \right)^2$$

where  $K_{Ic}$  is the Mode I fracture toughness and  $\sigma_t$  is the tensile strength. This condition implies that the "yielded" material in the fracture process zone surrounding the crack tip is contained by at least 40 diameters of test material. Recently, Bhagat (1985) found the following empirical relation for a variety of Appalachian Region coals.

$$K_{Ic} = 0.00187 \sigma_t + 0.00479$$

where  $K_{Ic}$  is in MPa  $\sqrt{m}$  and  $\sigma_t$  is in MPa. Using this relation implies that the minimum crack length should exceed about 0.2 m. Such a crack length requires a minimum specimen size of at least 0.4 m for cube like test specimens and 1.6 m for beam like test specimens. Such specimen sizes are not generally feasible in the laboratory due to limitations of available preparation and testing equipment. For practicality then, a

0.05 m crack length in a 0.10 m cubical specimen is used whenever possible and subsequent equipment designs and specifications are based on this decision. With such a specimen size, the theoretical containment on the crack tip process zone decreases from 40 down to 10. Such a specimen size does match the scale of fracture occurring in the vicinity of a coal cutting tool so it is reasonable to accept this specimen size even though it is theoretically subsize.

Successful preparation of these specimens requires use of delicate, 'low energy' preparation equipment. The laboratory at Penn State has acquired a horizontal bandsaw, diamond bandsaw and a belt/disc sander for this purpose. In addition, fresh coal is stored in a chamber at 100% relative humidity at all times to prevent drying and shrinkage cracking.

### DESIGN OF MIXED MODE FRACTURE TOUGHNESS TESTS FOR COAL

To study realistically the mechanics of fine fragment formation in coal requires a mixed mode test procedure since the actual crack propagation in the vicinity of the coal cutting tool is almost certainly under mixed mode loading conditions. From a general review of the rock mechanics literature, relatively little test work has been completed under mixed mode conditions (Ouchterlony, 1982) and only relatively recently has such testing become important in other materials such as metals and ceramics. Ingraffea (1977, 1981) completed the most recent studies with rock under mixed mode loading conditions using limestone and granite. The specimen used in those experiments is a variant of a single edge notch beam in four point bending.

Central to the fracture toughness measurement efforts is a special mixed mode testing rig that can accept a 0.1 m cubical test specimen. Drawings of this rig which is under fabrication at the time of this paper writing are shown in Figure 4. The rig design is modified from concepts originally developed by Richard (1984) for testing metals and plastics under mixed mode conditions.

Richard (1984) presented equations relating the stress intensity factors  $K_I$  and  $K_{II}$  for loading conditions on a similar specimen as a function of specimen width, specimen thickness, crack length and applied force. Because the loading method is considerably different from Richard's original concept, re-analysis of the specimen geometry and loading conditions is required. Program ANSYS\*, which has a crack tip element, was utilized in the numerical work. The mesh is shown in Figure 5. Convergence studies demonstrated that a mesh with 588 elements provided sufficiently accurate numerical results for an estimate of the K factors as a function of loading conditions. These factors are presented in Table 3. Actually, they compare reasonably

\*ANSYS is developed by Swanson Analysis Systems, Inc. Houston, Pa.

# MIXED MODE TESTING

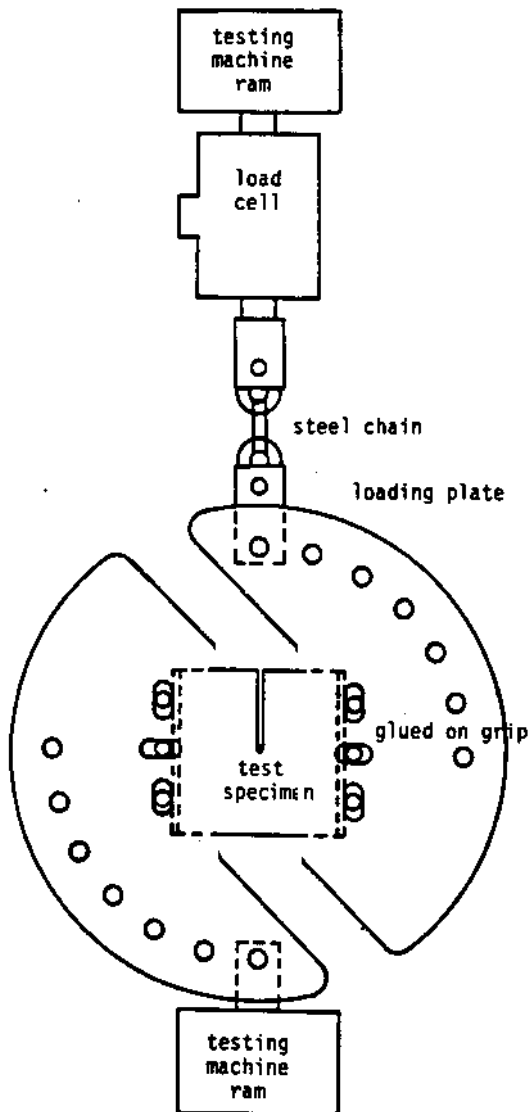
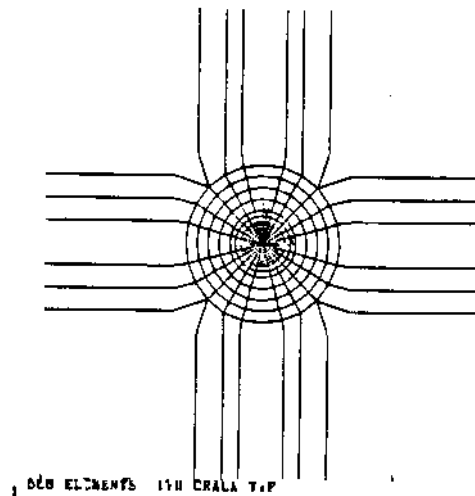


Figure 4. Mixed Mode Fracture Toughness Test Fixture.

well with the factors originally developed by Richard for a somewhat different loading geometry; thus, they are used hereafter with confidence.

## CONCLUSION

A scientific rationale and an approach to investigating the fundamental mechanics of fine fragment formation in coal has been developed. When a crack tip is supplied with excess energy, it responds by dissipating the energy through increased structural damage to the new fracture surface and crack bifurcation which leads to larger amounts of fine fragment formation. Preliminary scanning electron microscope studies



ANSYS 4.2  
JAN 5 1988  
11:26:06  
PLOT NO. 1  
POST1 ELEMENTS  
ORIG SCALING  
ZV=1  
DIST=2.31  
ZF=.5

Figure 5. Finite Element Mesh for Analysis of Mixed Mode Test Specimen.

demonstrated that different loading rates and fracture modes induce qualitative differences in the amount of structural damage and fine fragment formation on the new fracture surfaces. To study these differences, a mixed mode fracture toughness testing rig is under development.

Two theoretical approaches were proposed for quantifying these differences. One approach is based on mathematical descriptions of the size of the fracture process zone. Two models exist: one based on a maximum stress criterion and the other based on the strain energy density theory. The other approach is based on relationships between crack tip stress intensity and new fracture surface appearance as seen under an SEM. It is believed that these approaches may lead to an index or procedure for ranking coals according to their tendency to produce unwanted fine fragments and relating new fracture surface appearance to the fracture initiation conditions such as crack tip stress intensity or loading conditions. In the long term, the objective is to understand better the mechanics of fine fragment formation which may lead to decreased coal dust formation with the resulting human health benefits.

## ACKNOWLEDGMENT

This paper was supported under the Mineral Institutes Program by Grant No. G1135142, #4201-PS1 from the Bureau of Mines, U. S. Department of the Interior, as part of the Generic Mineral Technology Center for Respirable Dust.

## REFERENCES

- Abdel-Latif, A. I. A., Bradt, R. C. and Tressler, R. E. (1981) "Multiple-Mist Regions on Glass Fracture Surfaces," *Fractography and Materials Science*, ASTM STP 733 pp. 259-270.



## THE RESPIRABLE DUST CENTER

- Advani, S. H., Lin, Y. T., Gmeindl, F. D. and Powell, W. R. (1978) "Coupled Roof Fracture Response and Surface Subsidence Evaluations Related to Underground Coal Gasification," Proc. 4th Underground Coal Conversion, pp. 507-514.
- Bassim, M. N. and Hsu, T. R. (1982) "Fracture Behavior of Coa," Fifth Canadian Fracture Conference, Winnipeg, Pergamon Press, pp. 239-247.
- Bhagat, R. M. (1981) "Fracture Toughness of Coal: Variability Between Seams and Correlation with its Grindability and Chemical Characteristics," M.S. Thesis, West Virginia Univ. 55 pp.
- Bhagat, R. M. (1985) "Mode I Fracture Toughness of Coal," Int. Journal of Mining Engineering, Vol. 3, 1985, pp. 229-236.
- Bieniawski, Z. T. (1968) "An Application of High Speed Photography to the Determination of Fracture Velocity in Rock," Proc. 8th Int. Cong. on High Speed Photography, Almqvist and Wiksell, Stockholm, pp. 440-443.
- Bieniawski, Z. T. (1981) "Rock Materials Under Mixed Mode Fracture," Proc. U.S.-Greece Symp. on Fracture, Athens, Greece, Sijthoff and Noordhoff, Rockville, MD, 1981, pp. 333-347.
- Bieniawski, Z. T. and Mark, C. (1984) "A Fracture Mechanics Study of Crack Propagation Mechanisms in Coal." First Annual Report, Grant No. G1135142, The Pennsylvania State University, October, 70 p.
- Broek, D. (1974) Elementary Engineering Fracture Mechanics, Martinus Nijhoff Publishers, Boston, 453 p.
- Cheng, L. and Zukovich, P. P. (1973) Respirable Dust Adhering to Run-of-Face Bituminous Coals, USBM RI 7765, 10 pp.
- Cook, N. G. W., et al. (1980) Measurement and Control of Respirable Dust in Mines, National Academy of Sciences, Washington, DC, 1980, 405 pp.
- Fonseka, G. M., Murrell, S. A. F., Barner, P., (1985) "Scanning Electron Microscope and Acoustic Emission Studies of Crack Development in Rocks," Int. J. of Rock Mech. and Min. Sci. and Geomech. Abstr., Vol. 22, No. 5, October, pp. 273-289.
- Gdoutos, E. E. (1984) Engineering Application of Fracture Mechanics, VII, Problems of Mixed Mode Crack Propagation, Martinus Nijhoff Publishers, Boston, 204 pp.
- Ingraffea, A. R., Heuze, F. E., Ko, H. Y., Gerstle, K. (1977) "An Analysis of Discrete Fracture Propagation in Rock Loaded in Compression," Proc. 18th U. S. Symp. on Rock Mechanics, CSM Press, Golden, Co., pp. 2A4-1 to 2A4-7.
- Ingraffea, A. R. (1981) "Mixed-Mode Fracture Initiation in Indiana Limestone and Westerly Granite," Proc. 22nd U.S. Symp. on Rock Mechanics, MIT Press, Cambridge, pp. 199-204.
- Klepaczko, J. R., Bassim, M. N., and Hsu, T. R. (1984) "Fracture Toughness of Coal Under Quasi-Static and Impact Loading," Eng. Fracture Mechanics, Vol. 19, No. 2, pp. 305-316.
- Labuz, J. F., Shah, S. P. and Dowding, C. H. (1985) "Experimental Analysis of Crack Propagation in Granite," Int. J. Rock Mech. Min Sci. & Geomech. Abstr., Vol. 22, No. 2, pp. 85-98.
- Nelson, P. P., Ingraffea, A. R. and O'Rourke, T., (1985) "TBM Performance Prediction Using Rock Fracture Parameters," Int. J. Rock Mech. Min. Sci. & Geomech. Abstracts, Vol. 22, No. 3, pp. 189-192.
- Ouchterlony, F. (1982) "Review of Fracture Toughness Testing of Rock," Solid Mechanics Archives, Vol. 7, pp. 131-211.
- Powell, W. R., Khan, S., Ramsey, D. G., and Gmeindl, F. (1981) "Fracture Mechanics Model for Pittsburgh Coal," Paper 81-Pet-16, American Society of Mechanical Engineers, Petroleum Division.
- Ravi-Chander, K. and Knauss, W. G. (1984) "An Experimental Investigation into Dynamic Fracture: II. Microstructural Aspects," Int. J. of Fracture, Vol. 26, pp. 65-80.
- Richard, H. A., (1984) "Some Theoretical and Experimental Aspects of Mixed Mode Fractures," Proc. 6th Int. Conf. on Fracture, Pergamon Press, New York, pp. 3337 to 3344.
- Roepke, W. W. and Hanson, B. D. (1979) "New Cutting Concepts for Continuous Miners," Coal Mining and Processing, Vol. 16, No. 10, October, pp. 62-67.
- Roepke, W. W., Wingquist, C. F., Olson, R. C., Hanson, B. D. (1983) Bureau of Mines Coal Cutting Technology Facilities at the Twin Cities Research Center, USBM IC 8951, 26 pp.
- Roepke, W. W. (1984) "General Methods of Primary Dust Control During Cutting," Mining Engineering, Vol. 26, No. 6, June, pp. 636-644.
- Schmidt, R. A. (1980) "A Microcrack Model and Its Significance to Hydraulic Fracturing and Fracture Toughness Testing," Proc. 21st U. S. Symp. on Rock Mechanics, pp. 581-590.
- Streibig, K. C. and Zeller, H. W. (1975) Effect of Depth of Cut and Bit Type on the Generation of Respirable Dust, USBM RI 8042, 15 pp.
- Szendi-Horvath, G. (1982) "On the Fracture Toughness of Coal," Australian J. of Coal Mining and Technology and Research, No. 2, pp. 51-57.

# Fracture Mode and Loading Rate Influence on the Formation of Respirable Size Fragments on New Fracture Surfaces

R. Karl Zipf, Jr. and Z. T. Bieniawski

Department of Mineral Engineering, The Pennsylvania State University

Researchers at The Pennsylvania State University are engaged in a project to understand the mechanics of respirable size fragment formation in coal. The project is based on the premise that a thorough understanding of the fundamental mechanics of fine fragment formation may lead to techniques for reduction and better control of coal dust problems in mines. Presently, it is believed that the mode of fracture propagation which can range from pure tensile to pure shear or any mixed mode in between and the loading or displacement rate can influence the amount of respirable size fragments that are generated on new fracture surfaces during the fracture propagation process. The essence of any coal cutting process is one of mixed mode fracture propagation. To study the crack propagation process, a unique mixed mode testing rig was designed and fabricated. This rig is capable of applying loads to a prenotched test specimen that range from pure Mode I (tensile mode) to nearly pure Mode II (shear mode) or many mixed mode loading combinations. It is also possible to apply different loading or displacement rates to the test specimen. With this rig, it is possible to create new fracture surfaces via the different fracture modes and under various loading conditions.

These new fracture surfaces are examined with a scanning electron microscope (SEM) to characterize the amount of structural damage and respirable size fragment formation that occurs during the fracture process. Initial observations suggest that the amount of fine fragment formation and the new fracture surface appearance is related to the fracture initiation conditions, particularly the fracture mode and the loading rate. Mode II loading and higher loading rates seem to generate more structural damage and respirable size fragment formation than Mode I loading at slower rates.

With the mixed mode test rig, the mechanics of fracture initiation for a single crack can be controlled to better understand its influence on respirable size fragment formation. Such understanding may lead to methods which characterize the tendency of specific coal seams to produce undesirable fine fragments during the fracture process, or it may lead to rational recommendations and design guidelines or coal mining machines which inherently produce less dust.

## Introduction

As part of a larger effort to reduce the incidence of coal workers pneumoconiosis (black lung) in coal miners, researchers at The Pennsylvania State University are engaged in a project to understand the fundamental mechanics of fine fragment formation in coal. This project is part of a comprehensive research effort within the Generic Mineral Technology Center for Respirable Dust which is jointly administered by The Pennsylvania State University and West Virginia University.

The principal source of the coal dust in underground mining is the cutting operation. The U.S. Bureau of Mines (USBM) and various European research organizations have conducted investigations into the mechanics of coal cutting for many years. These studies of airborne respirable dust (ARD) formation have concentrated on empirical studies of the various cutting parameters and their effect on ARD formation. The parameters study include depth of cut, cutting speed and bit spacing.<sup>(1,2)</sup> Other studies investigated the effect of symmetric and asymmetric bit wear and various bit geometries and designs.<sup>(3-5)</sup> Roepke<sup>(6)</sup> summarized the principals of proper coal cutting to minimize dust formation by recommending to "cut at maximum depth (maximum advance rate) at all times, at minimum RPM, with the fewest possible bits, having the lowest possible included tip angle." Most coal in the U.S. is mined with the continuous mining machine which inherently cannot meet these design recommendations.<sup>(3)</sup>

It is recognized that respirable size dust particles are formed and/or liberated by a fracture process. One extremely interesting and useful study performed very early in the USBM dust research effort determined the amount of respirable dust of 0.9 to 10 micrometer size adhering to the surfaces of various coals.<sup>(7)</sup> They found that the number of particles ranged from  $10^{11}$  to  $10^{12}$  particles per pound or from 20 to  $60 \times 10^6$  particles per square centimeter of fracture surface. These numbers are evidently independent of the average fragment size. Fortunately, much less than one percent of the respirable particles formed ever become airborne.<sup>(1)</sup>

In a recent study sponsored by the National Academy of Sciences (NAS)<sup>(8)</sup> these observations and empirical correla-

tions raised certain key questions regarding the mechanical events that occur immediately after particles are produced and the quantity of particles that actually become airborne. Moreover, one should know the nature of the particles that become airborne versus those that remain behind on the new fracture surface. A further question raised by the NAS study is whether the majority of the dust is liberated from the crush zone near the bit tip, from the newly created surfaces during

finite element program that simulates mixed mode crack propagation based on linear elastic fracture mechanics. The problem analyzed is shown in Figure 1. This model is identical to one used by the USBM for coal cutting.<sup>(6)</sup> The cutter moves across the rock where a chip was previously removed until it engages the rock ahead of it. A new crack is propagated under mixed mode loading conditions until a new chip is removed.

The cutting model used by the USBM and analyzed by Saouma and Kleinosky<sup>(11)</sup> serves as a basis for postulates of fundamental mechanisms for ARD production. The basis for these postulates is recent work by researchers at the Southwest Research Institute<sup>(10)</sup> and additional modifications at The Pennsylvania State University. The fundamental mechanisms for dust production may include:

1. Crushing, grinding and scraping by the tool tip.
2. Energy dissipation in the fracture process zone.
3. Explosive disintegration during chip formation caused by violent release of stored elastic strain energy.
4. Preferential detachment of impurity particles during fracture due to their differing elastic moduli.

In addition to the production mechanisms, further mechanisms have been proposed for subsequent entrainment of the dust particles, but they will not be discussed here.

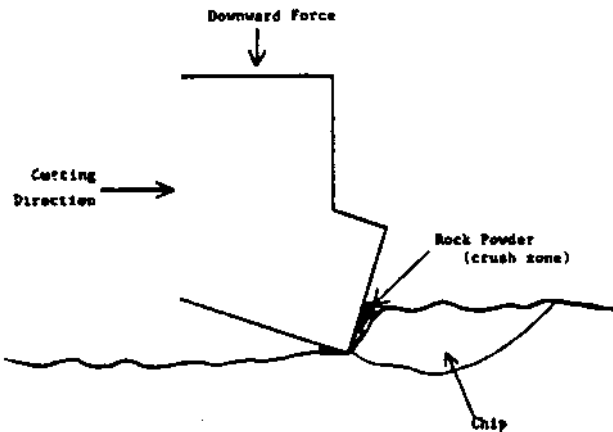


FIGURE 1. Basic coal cutting model.<sup>(11)</sup>

fracture, or from the new surface because of falling. Little work has been done on these fundamental problems.

### Coal Cutting Models and Dust Formation Mechanics

Several rock cutting and rock failure theories have been proposed in the past, but it is only very recently that fracture mechanics concepts have been successfully applied to the study of rock cutting mechanics. All of these cutting models seek to predict the cutting forces and the cutter geometry necessary to cause rock breakage and chip formation given some fundamental mechanical properties of the rock. The models have wide applications in drilling, tunnel boring and mining problems.

The indentation type of models<sup>(9)</sup> consider a rock loaded by a wedge. A crushed zone is postulated around the wedge tip and interfacial friction between the bit and the rock is included. Failure or chip formation occurs when the unconfined compressive strength of the rock is exceeded. The analysis is based on plasticity theory and the size of the chip formed is determined by the size of the plastic zone around the wedge tip. In another indentation type model, a Mohr-Coulomb failure criteria is applied along an assumed failure path.<sup>(10)</sup> The cutting force is determined when the failure criteria is exceeded.

Only one model successfully analyzes rock cutting using fracture mechanics concepts. Saouma and Kleinosky,<sup>(11)</sup> model the action of a drag bit cutter with a special purpose

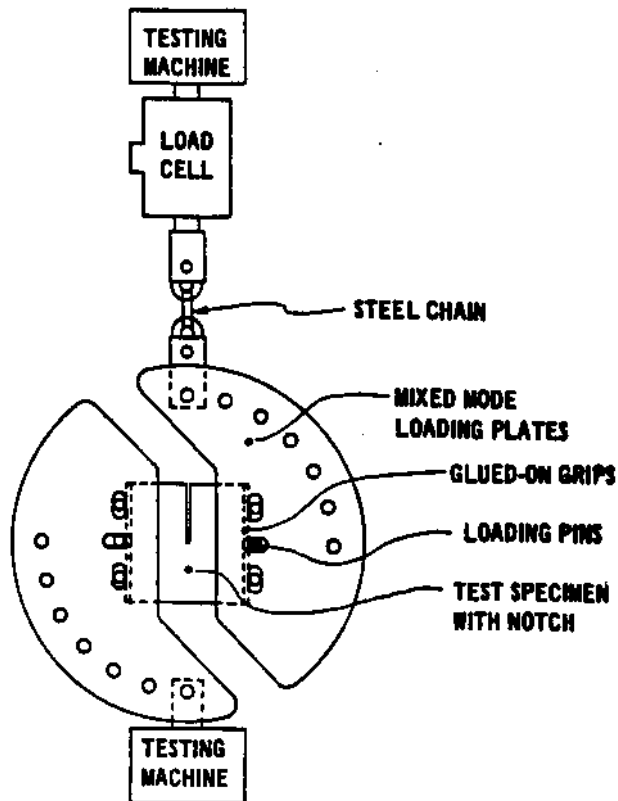


FIGURE 2. Mixed mode fracture toughness test fixture.

## FRACTURE MODE AND LOADING RATE INFLUENCES

The relative importance of the above mechanisms and the factors which influence their relative importance are not well understood. Many regard the crushing mechanism as most important although experimental evidence for this contention is conflicting and sparse. For instance, the decrease in specific ARD with deep cutting is supportive of the contention since presumably, the size of the crush zone and the amount of grinding and scraping are not greatly affected by increased depth. On the contrary, it is known that using dull and worn bits does not effect the specific ARD. Assuming that dull and worn bits increase the amount of crushing, grinding and scraping, one should expect higher specific ARD.

Our present research thus focuses on the energy dissipation mechanisms that occur in the fracture process zone during a crack propagation event and the various mechanical properties that influence the amount of energy dissipation and the resulting fine fragment formation. It is known that when a crack propagates through a material including coal, it rarely produces a smooth, clear, well-defined surface. Microcracks are opened up all along the newly created surfaces and successful or unsuccessful attempts at crack bifurcation may occur. The material on either side of the new crack surface is affected by the "fracture process zone"

(FPZ) which surrounds the propagating crack tip. Energy supplied to the crack tip by various external loads is largely dissipated in the FPZ and relatively little is consumed as free surface energy. When loading conditions are such that the crack tip is provided with excess energy for crack propagation, it responds by dissipating that energy through additional microcracking and crack bifurcation within the FPZ. As a result, new fracture surfaces may exhibit rougher appearances and increased structural damage which in turn may correlate with an increased tendency to produce unwanted fine fragments. Two approaches have been advanced to understand and quantify the fracture process as it relates to fine fragment formation: one is based on theoretical models of the size of the FPZ; and the other is based on relationships between crack tip stress intensity and new fracture surface appearance as seen under a scanning electron microscope.<sup>(12)</sup>

### Experimental Methods

The present experimental work aims to provide the necessary mechanical properties data to quantify the energy dissipation processes that occur during coal cutting and which may lead to unwanted ARD production. Of central impor-

**TABLE I**  
**Summary of Coal Fracture Toughness Test Results**

Source	Coal	Specimen Type	Specimen Size	KICMPa m	Deviation of Mean	Standard No. of Tests
Advani et al <sup>(15)</sup>	Pittsburgh	SEND-3PB	15 cm x 3.8 cm	0.0281	86%	2
	Waynesburg	SEND-3PB	x 1.9 cm	0.156	36%	3
	Bedstone	SEND-3PB		0.0348	60%	6
Powell et al <sup>(16)</sup>	Pittsburgh	SEND-3PB	15 cm x 3.8 cm	0.0629	37%	15
	Pittsburgh	SEND-3PB	x 1.9 cm	0.0472	34%	25
Bhagat <sup>(17)</sup>	Lower Freeport	SEND-3PB	20 cm x 3.8 cm	0.0283	35%	10
	Redstone	SEND-3PB	x 1.9 cm	0.0474	72%	20
	Waynesburg	SEND-3PB		0.121	48%	5
	Sewickley	SEND-3PB		0.267	19%	9
Szendi-Horvath <sup>(18)</sup>	Black Coking Coal	DMC	1.6 to 3.8 cm	0.219	13%	12
	Black Steaming Coal	DMC		0.435	12%	6
	Semi-Anthracite	DMC		0.132	11%	6
	Black Coking Coal	SEND-3PB	4 to 7 cm	0.321	11%	12
Bassim and Hsu <sup>(19)</sup>	Coal A	SEND-3PB	up to 8 cm	0.020 to 0.225	—	11
Klepaczko et al <sup>(20)</sup>	Coal A	WLCT	3.8 x 3.8 cm	0.154	25%	4
	Coal B	WLCT	x 3.2 cm	0.181	3%	3
	Coal A	WLCT-dynamic		2.014	11%	4
Bieniawski and Mark <sup>(13)</sup>	Bone Coal	DMC	1.6 cm	0.220	25%	11
	Kitt Mine	SEND-4PB	up to 3 cm long	0.346	17%	3
	Coal	DMC	1.6 cm	0.150	19%	4
	Kitt Mine					
	Anthracite	DMC	1.6 cm	0.296	32%	11
Rushton Mine		SEND-4PB	up to 3 cm long	0.172	42%	4
		DMC	1.6 cm	0.032		2

fracture toughness measurements in coal as a parameter controlling unstable crack growth and fracture velocity measurements. The last aspect is a novel concept based on the observation that crack bifurcation occurs above some critical velocity. This leads to the hypothesis that when crack bifurcation does occur, fine fragments of coal material are generated which leads to increased dust formation.

Relative to other materials, few studies exist, on the fracture toughness of rock<sup>(13)</sup> and even less on coal. Considerable controversy remains regarding test procedures and the fracture strength for various coals. Table I<sup>(12)</sup> presents a compilation of the existing Mode I fracture toughness measurements of coal by various researchers in the U.S., Canada, Australia, and at Penn State. The fracture toughness for coal can range over an order of magnitude for different coals and the standard deviation for individual coals can reach 30 to 50 percent. The primary reason for the variability is the highly anisotropic, non-homogeneous, and discontinuous nature of coal. Because of its nature, only the strongest, most durable coal samples are ever tested which tends to produce very suspect fracture toughness test data.

Existing data for the fracture toughness of coal is for Mode I only. From a general review of the rock mechanics literature, relatively little test work has been completed under mixed mode conditions<sup>(14)</sup> and only relatively recently has such testing become important in other materials such as metals and ceramics. Since the coal cutting mechanism is indeed one of mixed mode crack growth, it was necessary to design, analyze, and calibrate a special mixed mode testing rig in order to study the crack growth mechanism and its ef-

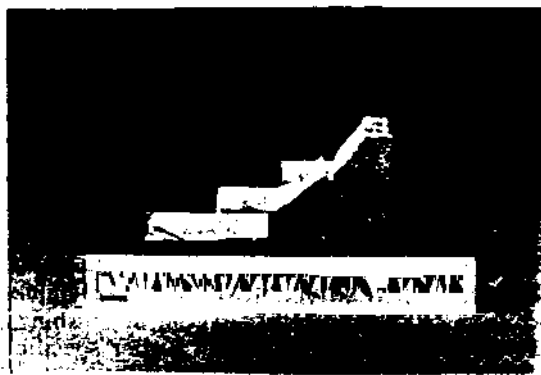


FIGURE 3. Calibration specimens fractures by mixed mode test rig. A schematic of the test fixture is shown in Figure 2. It can subject a 0.1 meter, pre-notched test specimen to pure mode I loading, a nearly pure mode II loading or various mixed mode loadings. Figure 3 shows three plaster of paris test specimens that were fractured in the test rig for calibration purposes. The specimen in the front was fractured by a mode I loading, the hardness, the NCB indenter hardness and the Young's Modulus and Poisson's Ratio. Determination of these coal material properties enables more complete characterization of the various coals and also provides useful cross checks and correlations for the fracture mechanics properties.

Table II shows the design of the mechanical properties test program presently underway. The program is basically designed to supply input data to the models of fracture

TABLE II  
Mechanical Properties Tests for Each Coal Seam

Test Type	Perpendicular to Bedding Planes	Perpendicular to Face Cleat	Perpendicular to Butt Cleat	Total
<b>Mixed Mode Fracture Toughness Tests</b>				
slow load rate	7			21
middle load rate	7			21
fast load rate	7			21
<b>Tensile Strength Tests</b>	5			15
<b>Unconfined Compressive Strength Tests</b>	5			15
<b>Dynamic Moduli Tests</b>	10			30
<b>Point Load Index Tests</b>	10			30
<b>Schmidt Hardness Tests</b>	10			30
<b>NCB Indenter Tests</b>	10			30

# FRACTURE MODE AND LOADING RATE INFLUENCES

## MODE I - SLOW RATE



## MODE I - FAST RATE



## MODE II - SLOW RATE



## MODE II - FAST RATE



FIGURE 4. SEM micrographs of coal fracture surfaces along the face cleat at 1000x — Scale 0.820 Cm = 10 micros.

process zone size and the relationship between crack tip stress intensity and new fracture surface appearance as seen with the scanning electron microscope. Tests are conducted under various mixed mode loading conditions at different one in the rear by a mode II loading, and the one in the middle by a mixed mode loading. The increasing angle of crack growth observed as the amount of mode II loading is increased is as expected from theoretical considerations.

In conjunction with the fracture toughness testing, determination of related coal material properties is essential. The properties include the unconfined compressive strength, the direct tensile strength, the point load index, the Schmidt loading rates and at different orientations relative to the natural structure of coal.

Successful preparation of these specimens required use of delicate, low energy preparation equipment. The laboratory at Penn State has acquired a horizontal bandsaw, diamond bandsaw, and a belt/disc sander for this purpose. In addition, fresh coal is stored in a chamber at 100 percent relative humidity at all times to prevent drying and shrinkage cracking. Preparation of specimens has been extremely successful. In order to obtain better, more meaningful cross correlations between tests, specimens for a mixed mode test, compressive strength test, tensile strength test, and the other tests are cut from the same lump of raw coal. With the existing preparation equipment, sample preparation has been extremely reliable. It is estimated that it has been possible to successfully prepare fracture toughness test specimens from over 75 percent of the coal lumps collected in the field. This leads to laboratory fracture toughness data that is indeed more representative of the *in situ* coal.

To demonstrate the effect of fracture mode and loading rate on the formation of respirable size fragments on new fracture surfaces, a small number of pre-notched cubes of Pittsburgh coal were fractured by dominantly Mode I or dominantly Mode II loading conditions at both slow and fast loading rates. Fracture was also propagated in various directions either parallel to the bedding planes, the face cleat or the butt cleat. The newly created fracture surfaces are then examined under the scanning electron microscope at 1000X magnification.

Under the SEM, respirable size fragments on the fracture surfaces appear quite readily as lighter areas or white spots. This contrast is due to charging by the electron beam because the particles are detached. Four SEM micrographs are shown in Figure 4 for

1. Mode I cracks under slow loading conditions.
2. Mode I cracks under fast loading conditions.
3. Mode II cracks under slow loading conditions.
4. Mode II cracks under fast loading conditions.

In comparing these images, we make the following observations:

1. The least amount of structural damage and fine fragment formations occurs under slow loading conditions in Mode I.

2. Increasing the loading rate or changing the loading condition from mode I to Mode II can increase the structural damage and fine fragment formation.

## Conclusion

A scientific rationale and an approach to investigating the fundamental mechanics of fine fragment formation in coal has been developed. When a crack tip is supplied with excess energy, it responds by dissipating the energy through increased structural damage to the new fracture surface and crack bifurcation which leads to larger amounts of fine fragment formation. Since the coal cutting process is best considered as a mixed mode crack propagation problem, a special mixed mode test rig was constructed to study crack growth in coal under mixed mode loading conditions and to determine its influence on fine fragment formation. A thorough mechanical testing program is well underway to determine fracture toughness and other related mechanical properties for several coals under different fracture mode and loading conditions and at different orientations relative to the natural structure of coal. Preliminary SEM studies show that higher loading rates and different fracture modes induce differences in the amount of structural damage and fine fragment formation on the new fracture surfaces.

## Acknowledgment

This research has been supported by the Department of the Interior's Mineral Institute program administered by the Bureau of Mines through the Generic Mineral Technology Center for Respirable Dust under grant number G1135142

## References

1. Strebig, K.C. and H.W. Zeller: *Effect of Depth of Cut and Bit Type on the Generation of Respirable Dust*. USBM RI 8042, 15 pp. (1975).
2. Roepke, W.W., D.P. Lindroth and T.A. Myren: *Reduction of Dust and Energy During Coal Cutting Using Point-Attack Bits*. USBM RI 8185, 53 pp. (1976).
3. Roepke, W.W. and B.D. Hanson: *Effect of Symmetric Bit Wear and Attack Angle on Airborne Respirable Dust and Energy Consumption*. USBM RI 8395, 24 pp. (1979).
4. Roepke, W.W. and B.D. Hanson: *Effect of Asymmetric Wear of Point Attack Bits on Coal-Cutting Parameters and Primary Dust Generation*. USBM RI 8761, 16 pp. (1983).
5. Roepke, W.W. and B.D. Hanson: *Testing Modified Coal-Cutting Bit Designs for Reduced Energy, Dust, and Incentivity*. USBM RI 8801, 31 pp. (1983).
6. Roepke, W.W.: *General Methods of Primary Dust Control During Cutting*. *Mining Engineering* 26(6):636-644 (June 1984).

## FRACTURE MODE AND LOADING RATE INFLUENCES

7. Cheng, L. and P.P. Zukovich: *Respirable Dust Adhering to Run-of-Face Bituminous Coals*. USBM RI 7765, 10 pp. (1973).
8. Cook, N.G.W. et al: *Measurement and Control of Respirable Dust in Mines*, 405 pp. National Academy of Sciences, Washington, DC (1980).
9. Pariseau, W.G. and C. Fairhurst: The Force-Penetration Characteristic for Wedge Penetration into Rock. *Int. J. Rock Mech. Min. Sci.* 4:165-180 (1967).
10. Stecklein, G., R. Branstetter, R. Arrowood et al: *Basic Research on Coal Fragmentation and Dust Entrainment*. USBM Contract No. J0215009, 121 pp. South West Research Institute (May 1982).
11. Sauma, V.E. and M.J. Kleinosky: Finite Element Simulation of Rock Cutting; a Fracture Mechanics Approach. 25th U.S. Symposium on Rock Mechanics. Evanston, Illinois. (1984).
12. Zipf, R.K. and Z.T. Bieniawski: Mixed Mode Testing for Fracture Toughness of Coal Based on Critical-Energy-Density. *27th U.S. Symposium on Rock Mechanics*, pp. 16-23. Tuscaloosa, Alabama (1986).
13. Bieniawski, Z.T. and C. Mark: A Fracture Mechanics Study of Crack Propagation Mechanism in Coal. *First Annual Report*, Grant No. G1135142, 70 p. The Pennsylvania State University (October, 1984).
14. Ouchterlony, F.: Review of Fracture Toughness Testing of Rock. *Solid Mechanics Archives* 7:131-211 (1982).
15. Advani, S.H., Y.T. Lin, F.D. Gmeindl and W.R. Powell: Coupled Roof Fracture Response and Surface Subsidence Evaluations Elated to Underground Coal Gasification. *Proceedings of the 4th Underground Coal Conversion*, pp. 507-514. (1978).
16. Powell, W.R., S. Khan, D.G. Remsey and F. Gmeindl: Fracture Mechanics Model for Pittsburgh Coal. *Paper 81-Pet-16*. American Society of Mechanical Engineers, Petroleum Division. (1981).
17. Bhagat, R.M.: *Fracture Toughness of Coal: Variability Between Seams and Correlation with its Grindability and Chemical Characteristics*. M.S. Thesis, 55 pp. West Virginia University (1981).
18. Szendi-Horvath, G.: On the Fracture Toughness of Coal. *Australian J. Coal Mining and Technology and Research* 2:51-57 (1982).
19. Bassim, M.N. and T.R. Hsu: Fracture Behavior of Coal. *Fifth Canadian Fracture Conference*, pp. 239-247. Winnipeg, Pergamon Press (1982).
20. Klepaczko, J.R., M.N. Bassim and T.R. Hsu: Fracture Toughness of Coal Under Quasi-Static and Impact Loading. *Eng. Fracture Mechanics* 19(2):305-316 (1984).



# An Analysis of Respirable Dust Generation by Continuous Miner

A. Wahab Khair and N. P. Reddy  
Department of Mining Engineering, West  
Virginia University

## INTRODUCTION

The continuous mining machines which were introduced in the 1950's now account for more than half the production of coal from underground mines. Unfortunately, these continuous miners which were designed for increased productivity have also increased the concentration of respirable dust in mines. Inhalation of this respirable dust by miners causes the Coal Worker's Pneumoconiosis (CWP). Concern for CWP increased in the United States following a 1963-65 survey that showed definite x-ray evidence of CWP in 9.8 percent of working miners and in 18.2 percent of nonworking miners in the Appalachian bituminous coal region (Breslin and Niewiadomski, 1982).

One of the major objectives of the Federal Coal Mine Health and Safety Act of 1969 was the prevention of CWP. This law initially limited the daily average exposure of coal miners to  $3 \text{ mg/m}^3$  of respirable dust. However, following the results of a probabilistic model developed by Jacobsen, et. al. in 1971, the limit was reduced to a mass concentration of  $2 \text{ mg/m}^3$  unless quartz content exceeds 5 percent, a rare occurrence in mines. Based on x-ray categorization prior to death it is believed that the mass concentration in the respirable fraction is a parameter of primary interest for hygienic

evaluation of dust exposure. Morgan, Burgess and Jacobson (1973) suggested that the quantity of inhaled dust, although influential is not the only aspect of exposure which is significant in producing CWP. Miners working in higher rank coal (anthracite) mines are more susceptible to CWP (Morgan, Burgess and Jacobson, 1973). This also confirms the findings of the British (Bennett, Dick and Kaplan, 1979 and Hurley, et. al., 1979) and Germany (Reisner and Rubock, 1977). Based on the cytotoxicological evidence Reisner and Rubock (1979) suggested that when coal properties are similar, increasing quartz and mineral content increases toxicity. David, Octery and Le Roux (1975) examined that as the severity of the CWP increased the retention of the coal dust content in the pulmonary region remained the same, while that of quartz content increased significantly. Leiteritz, Baur and Bruckman (1971) studied the various components of coal dust and showed that coal particles comprised a smaller fraction of the mass of fine dust than did particles of quartz and minerals. It is ironic that quartz and mineral matter both comprise smaller fractions of the higher rank coal dust (Dodgson, et. al., 1971 and Dwiggin, 1981). Results of a recent research revealed that quartz or any other mineral examined had no strong or consistent effect on the incidence or progress of CWP (Attfield,

# ANALYSIS OF RESPIRABLE DUST GENERATION

1984) while Dodgson, et. al., (1971) concluded that high exposures to minerals such as illite, kaolinite and mica will retard the progress of CWP. Size and shape characteristics are believed to be important in the relationship between mineral particles and health effects (Shedd, Virta and Wylie, 1982).

The above inconsistencies in the coal mine respirable dust research certainly suggests that, more research is needed to study the physical and chemical properties of coal mine dust and the dependence of those properties on fragmentation and particle size and shape. This paper, in particular deals with the analysis of dust generation due to the action of a continuous miner under different operating parameters using two types of coal. Underground coal cutting by a drum type continuous miner was simulated in the laboratory using a specially designed unique automated rotary coal cutting simulator (ARCCS). All the fragments of the cut product were collected after each experiment and sized to as small as -10 microns. The analysis in this study consists of three size ranges which are 1.885 cm (0.742 in) to -0.0038 cm (-0.0015 in) or -400 mesh (-37 microns), 37 microns to -10 microns and 10 microns to 0.6 microns.

## STUDY PROGRAM

### Laboratory Equipment and Instrumentation

Review of the literature on coal cutting technology and the basic parameters that effect this technology revealed that most of the existing coal cutting machinery is of the rotary type and that the parameters that effect the fragmentation of coal in such cuttings depend on the following (Terry, 1959; Pomeroy and Foote, 1960; Pomeroy, 1963, 1964; Evans and Pomeroy, 1966; Pomeroy, 1968; Bower, 1970; Warner, 1970; Hurt, 1980; Ford and Friedman, 1983; Friedman and Ford, 1983; Fuh, 1983, Evans, 1984; Khair and Quinn, 1985; Khair and Reddy, 1985):

$$\text{Coal fragmentation} = f(C_p, I_c, I_p)$$

where  $C_p$  is the mechanical properties of coal,  $I_c$  is the in-situ conditions (vertical and horizontal stresses), and  $O_p$  is the operating parameters. Based on this premise a unique automated rotary coal cutting simulator (ARCCS) (Fig. 1) was designed and fabricated in the Mining Engineering Department at West Virginia University (Khair, 1984). This design incorporates the capability to study the different machine and in-situ parameters that influence the fragmentation of coal. It operates under the simulated mining conditions with equivalent in-situ stresses (horizontal and vertical stresses) being applied to a coal block of 45.7 cm x 38.1 cm x 15.2 cm (18 in. x 15 in. x 6 in.) located in a suitably designed confining chamber. The cutting drum with a maximum tip to tip diameter (varies with the bit angle) of 48.3 cm (19 in.) has the capability of rotating from 1 to 50 rpm. The drum can be stopped any time after a predetermined number of revolutions. Tests can be performed with four different bit angles 15, 30, 45 and 60 degrees. A maximum of seven bits can be mounted on the drum in an echelon pattern. The ARCCS can be operated and controlled manually or automatically, and the operating parameters can be preset with a series of hydraulic valves and could be recorded in analog/digital or in both forms.

Test and monitoring facilities can be seen in Fig. 1, ARCCS (Fig. 1a), programmable control and monitoring unit (Fig. 1b), sonic testing unit (Fig. 1c), acoustic emission (A.E.) monitoring unit (Fig. 1d), microscope and attached camera unit (Fig. 1e), cascade impactors (Fig. 1f), hood and air generating unit (Fig. 1g) and data acquisition and recording unit (Fig. 1h). In addition to this, linear variable differential transformers (LVDTs), pressure transducers, flow meters, flow controls and drum rpm indicator were some of the other monitoring devices. LVDTs were used to monitor the displacement of the coal block as well as the depth of cut. Pressure transducers were used to

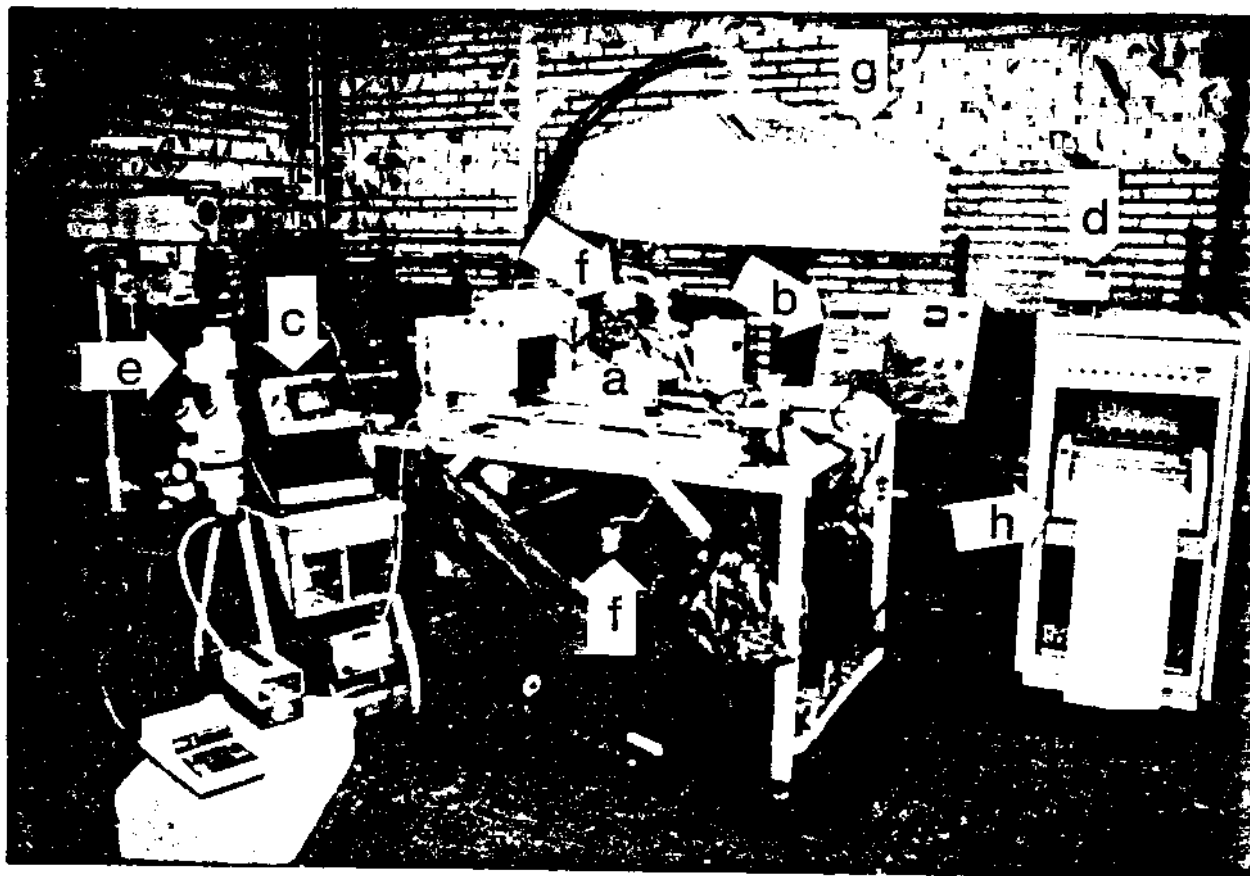


Fig. 1. Test and monitoring equipment facilities (a) automated rotary coal cutting simulator, (b) programmable control and monitoring unit, (c) sonic testing unit, (d) acoustic emission monitoring unit, (e) microscope and the attached camera unit, (f) cascade impactors, (g) hood and air current generating unit and (h) data acquisition and recording unit.

monitor the changes in pressure both due to the thrust and due to the intermittent cutting nature of the rotary cutting. Flow controls were used to run the drum at a particular rpm between 1 and 50 and to provide a specific rate of advance.

U.S. Sieve Series/ASTM Specification E-11-61 was used in conjunction with the Ro-Tap Testing Sieve Shaker to size the fragments from 1.885 cm (0.742 in.) to -0.0038 cm (-0.0015 in.) or -400 mesh (-37 microns). Allen Bradley Sonic Sifter, model L3P, Series A was used to size the product from 37 microns to -10 microns. The sizing of the total respirable dust was accomplished by using the model

296, 6-stage cascade impactors, manufactured by Anderson Samplers, Incorporated in conjunction with the DuPont 2500 personal sampling pump. The cut points of this impactor were 10, 6, 3.5, 2, 1 and 0.6 microns at 2 lpm constant flow rate of the sampling pump.

#### Specimen Preparation

Most of the coal samples were obtained from a surface mine. Coal blocks so obtained were then cut in the laboratory to an approximate dimension of 43.2 cm x 33 cm x 15.2 cm (17 in. x 13 in. x 6 in.). A typical specimen with cutting face as face/butt cleat was then placed in a wooden box of

## ANALYSIS OF RESPIRABLE DUST GENERATION

45.7 cm x 35.6 cm x 15.2 cm (18 in. x 15 in. x 6 in.) in dimension. Plaster of paris was then poured in the box to fill all the remaining space other than that occupied by the coal block. This process gives a perfect dimension of 45.7 cm x 35.6 cm x 15.2 cm (18 in. x 15 in. x 6 in.) which is very essential to avoid stress concentration in the specimen when confining pressure is applied. After a week the molded coal samples were removed from the box to test.

### Experimental Procedure

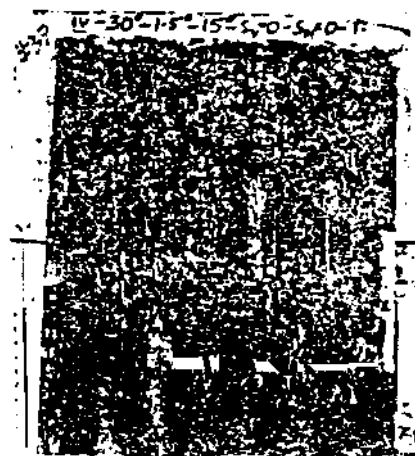
During a typical experiment the molded specimen was placed in the confining chamber, the test conditions were set, and the in-situ equivalent pressure and operating parameters were marked on the top mold layer of the sample. A series of experiments for this study were done without any significant confining pressure. An insignificant amount of confining pressure was applied in order to keep the specimen in the confining chamber during the cutting process. A 2.54 cm (1.0 in.) thick steel plate was positioned between the sample and hydraulic jacks in order to distribute the pressure uniformly over the whole surface of the specimen. Each set of hydraulic jacks were connected in parallel to a hand pump. Before the test, the operating parameters such as velocity of the cutting drum and rate of advancement were adjusted to predetermined values. Then seven bit blocks of 30 degree attack angles were mounted on the cutting drum in an echelon pattern at 3.81 cm (1.5 in.) spacing. Since from the earlier tests it was observed that the resultant force necessary to cut coal is the least for a 30 degree attack angle, while it increases for less than or greater than 30 degree attack angle (Khair and Quinn, 1985), all the tests for this study were conducted at 30 degree attack angles. Bits of specific make and type were inserted into the bit block slots and were kept in position by a screw in such a way so as to allow bit rotation inside the block which prevents non-symmetric bit wear. Six-stage cascade impactors were prepared for respirable

dust sampling. Model C-290-MY mylar media filters, 34 mm in diameter were greased by Model 290IGS Impaction Grease Sprayer using a Model C-290-IGT impaction grease plate. Preparation was done in accordance with the instruction manual provided by Anderson Samplers, Inc. Filters were left for 24 hours to dry before weighing. Weighing was done both before and after sampling to the nearest 0.01 mg by a Sartorius, type 2462, semi automatic, electronic analytical balance with digital readout. A set of four impactors were then mounted on the specially designed arms at fixed positions with respect to the rotating drum. The canvas was then hooked to the main frame of the machine and a plastic sheet was spread on it to collect the coal fragments after each experiment. The number of rotations by the cutting head was set in the counter unit in the control module and then the machine was started to execute the program in a continuous or counter mode. The counting of the number of rotations starts when the hydraulic pressure is increased, due to the cutting process, or when the cutting head has traveled to a preset distance measured mechanically and by the LVDT. After the execution of the predetermined number of rotations, the cutting head retreats and stops. Test conditions were marked on each specimen as well as on the recorded data. The nomenclature in Fig. 2b reads as follows: #42-test number, IV-bit type, 30°-bit attack angle, 1.5"-bit spacing, 25-cutting head rpm,  $S_v$  and  $S_h$ -vertical and horizontal confining pressures, F-face cleat, II-coal type. After each experiment the canvas is unhooked and the coal fragments are collected in the ziploc bags and the vacuum bag with the help of a vacuum cleaner. This product is then sieved into different sizes using sieves manufactured by the Fisher Scientific Company according to ASTM Specification E-11-61. However, a slight modification was made in this procedure. In general two dips appear in the size distribution curves. These are due to the type of screens used in the analysis. A standard  $\sqrt{2}$  series was used from 1.885 cm (0.742 in.) to 0.475 cm (0.187 in.), then the screens

were used alternatively, meaning that the previous screen size was divided by  $\sqrt{2}$  to get the net size. From 0.475 cm (0.187 in.) to 0.0074 cm (0.0029 in.) the screens were used alternately, or a 2 series where the previous screen size was divided by 2. The -0.015 cm (-0.0059 in.) sizes are screened with the  $\sqrt{2}$  series again. This method was adopted to reduce the number of screens, thus reducing dust loss, and also distributing irregularities at both ends of the size range. The dips occur because the screens that start the change in a series receives twice the amount of material it would have in a straight series. The bump occurring at the 0.0038 cm (0.0015 in.) or 400 mesh size was natural and is characteristic of the tested material but not related to the screening. This idea was substantiated by using a -0.0013 cm (-0.0001 in.) screen tested against another screen with similar results. The length of the sieving time was 2 minutes for sizing 1.685 cm (0.742 in.), 1.334 cm (0.525 in.) and 0.942 cm (0.371 in.) while it was 20 minutes for sizing from 0.64 cm (0.25 in.) to -0.0038 cm (-0.0015 in.) or -400 mesh (-37 microns). Ro Tap Testing Sieve Shaker, built for handling 20.3 cm (8 in.) diameter testing sieves which reproduces the circular and tapping motion given to testing sieves in hand-sieving, but with a uniform, mechanical action, assuring accurate and dependable results, was used in sizing the fragments. The sizing from 400 mesh (37 microns) to -10 microns was done by the Sonic Sifter. A 10 minute sieving time was adequate during this sizing. All the sized products were then weighed up to 0.1 gm by Sartorius, Type 2351, mechanical balance with analog readout and the percent weights retained were then calculated.

RESULTS AND DISCUSSION

Most of the coal used in the experimental study is part of the Waynesburg coal seam. Presently, only one test has been completed on the Pittsburgh coal seam. The physical and mechanical



a



b

Fig. 2. Typical specimens cut against face cleat, (a) Waynesburg coal, and (b) Pittsburgh coal.

properties of the Waynesburg coal were determined in the laboratory and are given in Tables 1 and 2. The properties for the Pittsburgh seam are now being determined and hence are not available at the present time.

A study of forty-three experiments has been completed analyzing both the

## ANALYSIS OF RESPIRABLE DUST GENERATION

Table 1. Physical Properties of Waynesburg Coal

Moisture %	Ash %	Sulfur %	Rank	HGI*	Sp.Gr.
0.0-1.5	13.5-13.7	2.03-2.06	hVbB**	50.43	1.42

\*Hardgrove Grinability

\*\*High Volatile B Bituminous

Table 2. Mechanical Properties of Waynesburg Coal

Cleat/Bedding Plane Orientation	Compressive Strength psi (KPa)	Young's Modulus psi (KPa)	Poisson's Ratio	Indirect Tensile Strength psi (KPa)	Direct Shear Strength psi (KPa)
Face Cleat	3289 (473.6)	$5.1 \times 10^5$ ( $7.3 \times 10^4$ )	0.25	154 (22.2)	204 (29.4)
Butt Cleat	3459 (498.1)	$4.7 \times 10^5$ ( $6.8 \times 10^4$ )	0.31	205 (29.5)	180 (25.9)
Bedding Plane	4912 (707.4)	$4.6 \times 10^5$ ( $6.6 \times 10^4$ )	0.32	146 (21.0)	80 (11.5)

mechanisms of respirable dust generation and the effects of operating, in-situ and geologic parameters on the fragmentation of coal. The parameters involved during these tests were bit spacing, drum velocity, depth of cut, confining pressure, coal cleat direction, angle of attack and types of bit. Despite the limited number of tests, a large volume of data was collected of which only a part involving the parametric study of cutting drum velocity, bit type, coal cleat orientation and type of coal, under unconfined and 30 degree attack angle will be presented for discussion.

Mechanism of respirable dust generation in continuous mining is complex. It is a function of the fragmentation process and machine bit coal interaction. An analysis of the fracture surface, fragmentation process, and machine bit coal interaction was presented elsewhere (Khair and Quinn, 1985).

Before presenting the results of this study it is necessary to define size limits used in this paper. Large

fragments are defined as fragments between 1.885 cm (0.742 cm) and 0.238 cm (0.0937 in.); fine fragments between -0.238 cm (-0.0937 in.) and 0.0038 cm (0.0015 in.) or 400 mesh while dust is defined as -37 microns (-400 mesh). Airborne respirable dust is defined as -10 micron size. The size distribution up to 10 microns in size is a product of the settled fragments and particles while the airborne respirable dust from 10 microns to 0.6 micron size was sampled by the cascade impactors. It should be mentioned that efforts to sample the dust around the cutting head for mapping purposes were futile as the respirable mass collected was insufficient or inconsistent. Hence only the mass fractions collected on the bottom impactors were presented here for discussion.

To evaluate the effects of bit configuration and carbide tip shape and size, a series of experiments were conducted after the necessary test modifications were made to eliminate the influence of the other parameters affecting fragmentation. Four specimens

of Waynesburg coal were tested against face cleat. Parameters used were attack angle, 30 degrees; cutting head speed, 25 rpm; depth of cut per revolution, 0.079 cm (0.0313 in.); total depth of cut, 8.89 cm (3.5 in.); and confining pressure, insignificant. The four cutting bits used were pencil bit, type II; plumbob bit with a large carbide tip, type III; slender/sharp bit with fins, type IV; and plumbob bit with regular carbide tip, type V (Fig. 3). Size distribution for the four experiments is shown in Figs. 4a and 4b.

Results indicated that the blunt bit type, type III, produced less large and more fine material than the slender/sharp, type IV, bit. Pencil, type II, bit produced the highest amount of large fragments and lowest amount of fine fragments when compared to any of the other three bits. This could be imputed to the fact that the gap between the bit body and the carbide tip in a pencil bit is relatively less due to a better alignment between the two. Results of the -400 mesh (-37 microns) sizing show that the plumbob bit, type V, produces more respirable size

(-10 microns) mass than any other bit while the slender/sharp bit, type IV, produces the lowest respirable size (-10 microns) mass (Fig. 4b).

Effects of the cutting head speed was evaluated by a series of five experiments, three against face cleat cutting and two against butt cleat cutting. Parameters used were slender/sharp bit, type IV; attack angle, 30 degrees; depth of cut per revolution 0.079 cm (0.0313 in.); total depth of cut, 8.89 cm (3.5 in.) and confining pressure, insignificant.

Increasing rpm of the cutting head increased the required resultant force to cut the coal. Under high speed cutting most of the energy imposed on the coal was utilized during dynamic loading (fracturing) and less energy was utilized during quasi static loading (grading). Hence, more large and deep fractures were induced into coal and consequently more large fragments than fine were produced. Size distribution characteristics in Figs. 5 and 6 indicate that large size fragments are directly proportional to

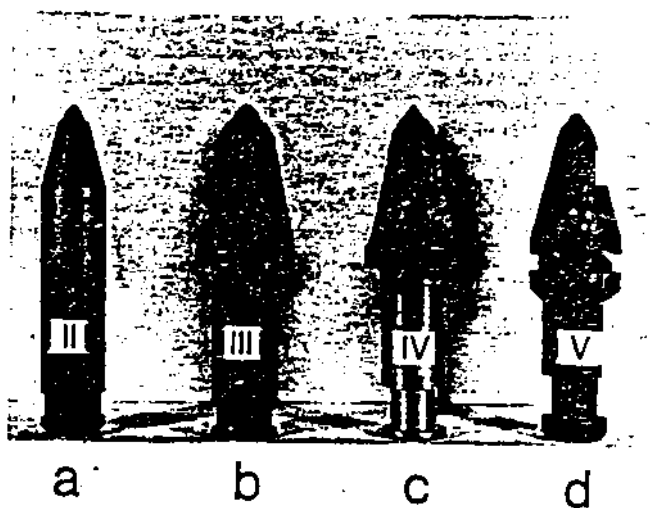


Fig. 3. Four bits used in the study, (a) pencil bit, type II; (b) plumbob bit with a large carbide tip, type III; (c) slender/sharp bit with fins, type IV; and (d) plumbob bit with a regular carbide tip, type V.

## ANALYSIS OF RESPIRABLE DUST GENERATION

cutting head speed while the fine size are inversely proportional to cutting head speed. Generally, the percent of dust size particles retained was proportional to cutting head speed. However, the inconsistency with the cutting head speed of 35 rpm (Fig. 5a) has to be clarified with additional tests at a later time. Also, generally, the production of finer fragments and the dust size particles is more for the butt cleat than for the face cleat (Fig. 6a and 6b). Figure 5b illustrates that an increase in the respirable size (-10 microns) mass is inversely proportional to the increase in the drum speed. This may be due to the fact that higher velocity of the cutting head increases the kinetic energy of the particles which then increases entrainment. Observations of the experiments verified this. Higher entrainment does not necessarily mean higher airborne particles but in this case it did increase the magnitude of airborne particles at the expense of the settled material. Similar trend was observed with tests against butt cleat (Fig. 6b).

Finally, the size distribution for the two coals (Fig. 7a) tested under the same parameters, except at a constant cutting head speed of 35 rpm with cutting against face cleat shows that the Pittsburgh coal produces less fragments and more fines when compared to the Waynesburg coal. But the percent of dust size particles was observed to be higher with Waynesburg coal than Pittsburgh coal. However, the trend was again reversed for the respirable size (-10 microns) mass (Fig. 7b).

Particle size distribution of the entrained dust sampled by 6 stage cascade impactors was plotted on the log-probability graphs (Figs. 8 to 11). Most distribution functions like this require two parameters, one that identifies the location or center of the distribution and the other that characterizes the width or spread of the distribution. Location or center of the distribution here is identified by mass median diameter (MMD). MMD is defined as the diameter for which half the mass is contributed by particles

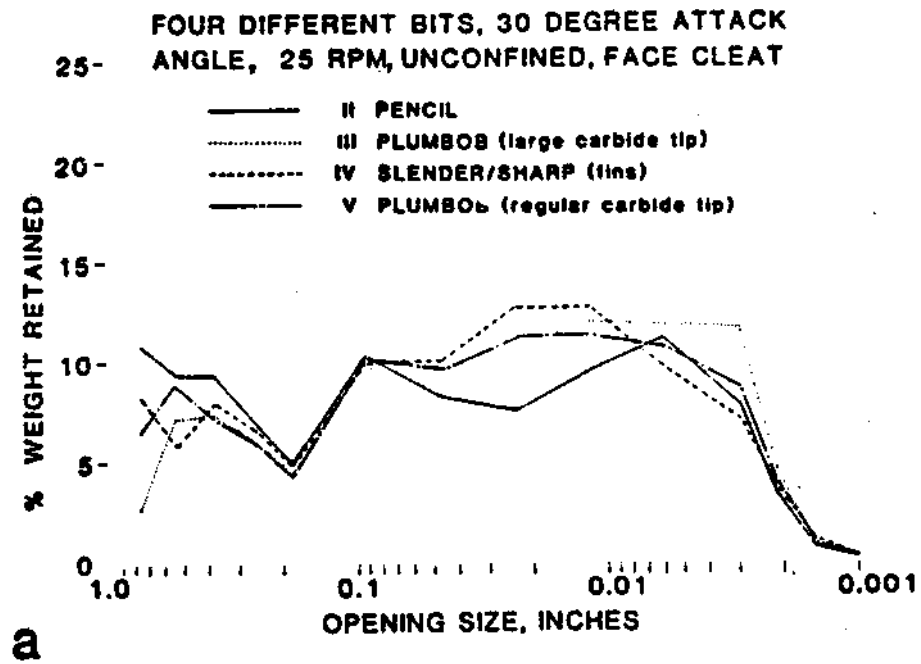
larger than the MMD and half by particles smaller than the MMD. The geometric standard deviation (GSD) is a measure of the spread of the particle size distribution. It is defined as the ratio of MMD and the particle size at 16 percentile. If  $GSD = 1$ , all the particles are of the same size, i.e., the entrained dust is "monodisperse" (Hinds, 1982).

The MMD and the GSD for each test plotted can be seen in Figs. 8 to 11. MMD and GSD for a plumbob bit, type V, are 5.4 and 3.55, respectively. They are considerably different when compared to the bit types III and IV for which the MMDs and the GSDs are consistent between 9.2 and 9.4 and 2.16 and 2.38, respectively. Table 3 shows the weight and percent of respirable size mass divided into 10.0 x 6.0 microns and 6.0 x 0.6 microns. This table confirms with the MMDs and GSDs where in the bit type V produces 76.3 percent of the mass in the 6.0 x 0.6 micron size range while the other bits produce only 58.0 and 56.7 percent in the same size range. The MMDs were observed to be consistent in the evaluation of the effects of cutting head speed (Fig. 9), cleat orientation (Fig. 10), and two coal types (Fig. 11) while the spread of the particle size varies from 2.16 to 2.79. However, the actual weights of the respirable size mass divided into 10.0 x 6.0 microns and 6.0 x 0.6 microns in Tables 4, 5 and 6 show some differences even though not very significant. Additional experiments are in progress which may aid us in a more authentic evaluation by placing statistical confidence limits.

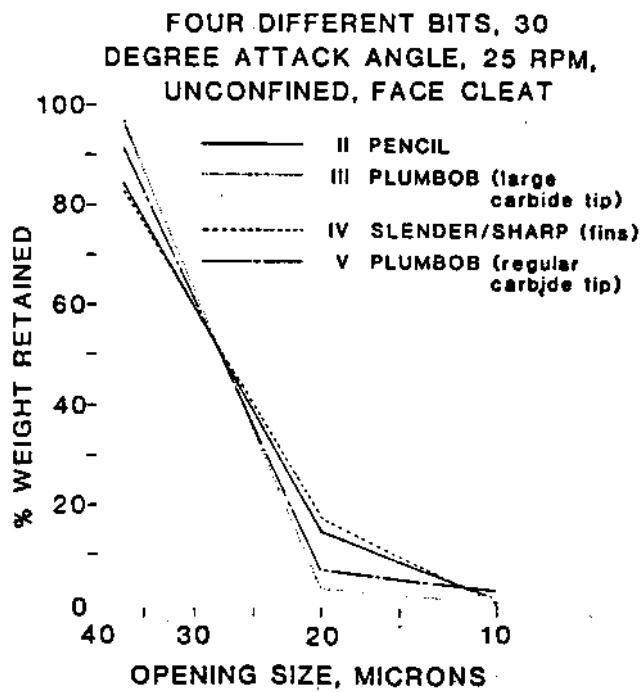
### CONCLUSIONS

The results presented in this paper must be considered of a preliminary nature since they are based on a limited number of tests on two specific coals. Nevertheless, some parameters do appear to have considerable effect on dust generation. Bit type V produces significantly large amount of respirable dust in the size range of 6.0 x 0.6 microns when compared to



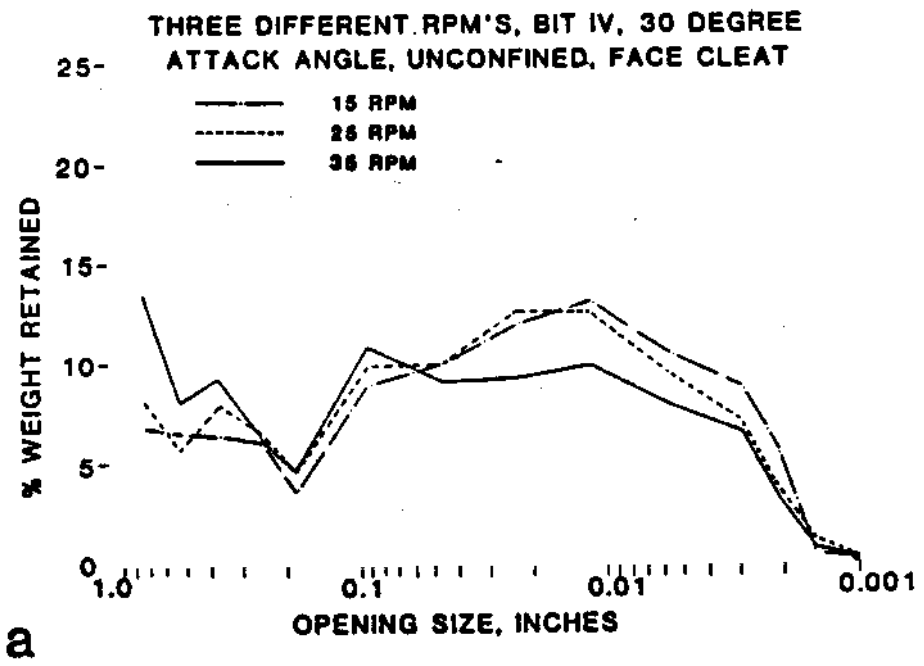


# ANALYSIS OF RESPIRABLE DUST GENERATION

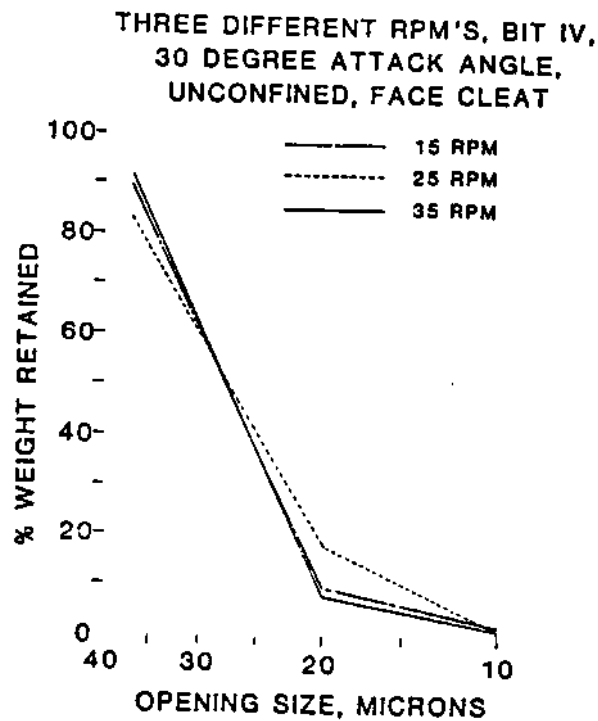


b

Fig. 4. Mesh size versus percent of weight retained as a function of bit type, (a) fragment size distribution from 1.885 cm (0.742 in.) to 0.0038 cm (0.0015 in.) or 400 mesh and (b) dust size distribution from 37 microns (400 mesh) to -10 microns.

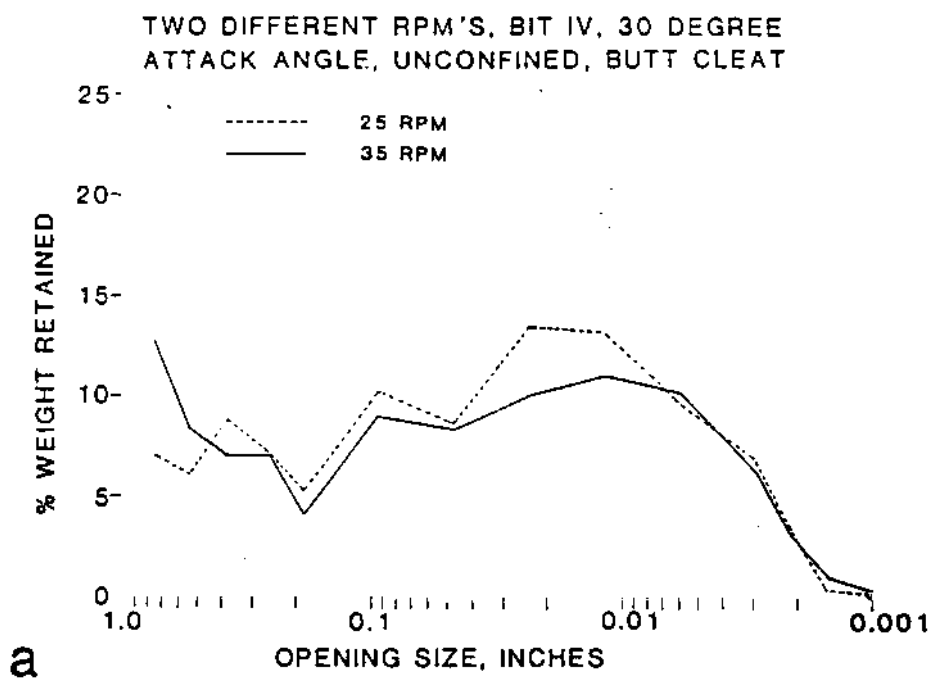


# ANALYSIS OF RESPIRABLE DUST GENERATION



**b**

Fig. 5. Mesh size versus percent of weight retained as a function of cutting head speed (rpm) for face cleat orientation, (a) fragment size distribution from 1.885 cm (0.742 in.) to 0.0038 cm (0.0015 in.) or 400 mesh and (b) dust size distribution from 37 microns (400 mesh) to -10 microns.



# ANALYSIS OF RESPIRABLE DUST GENERATION

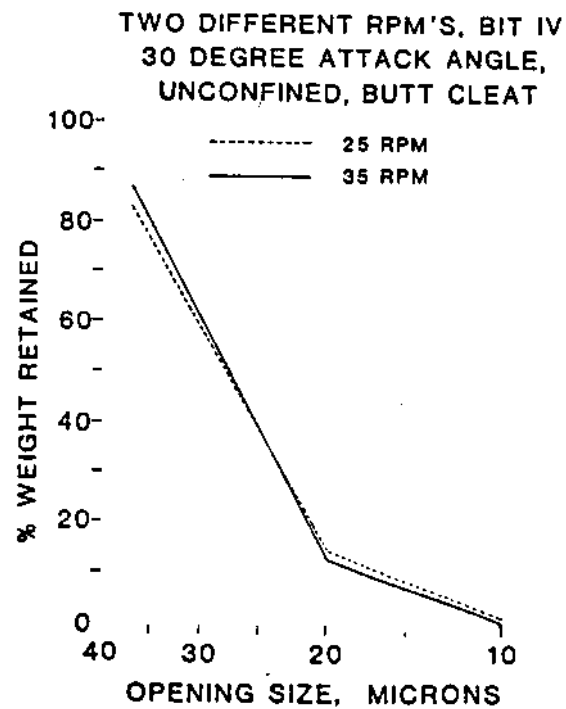
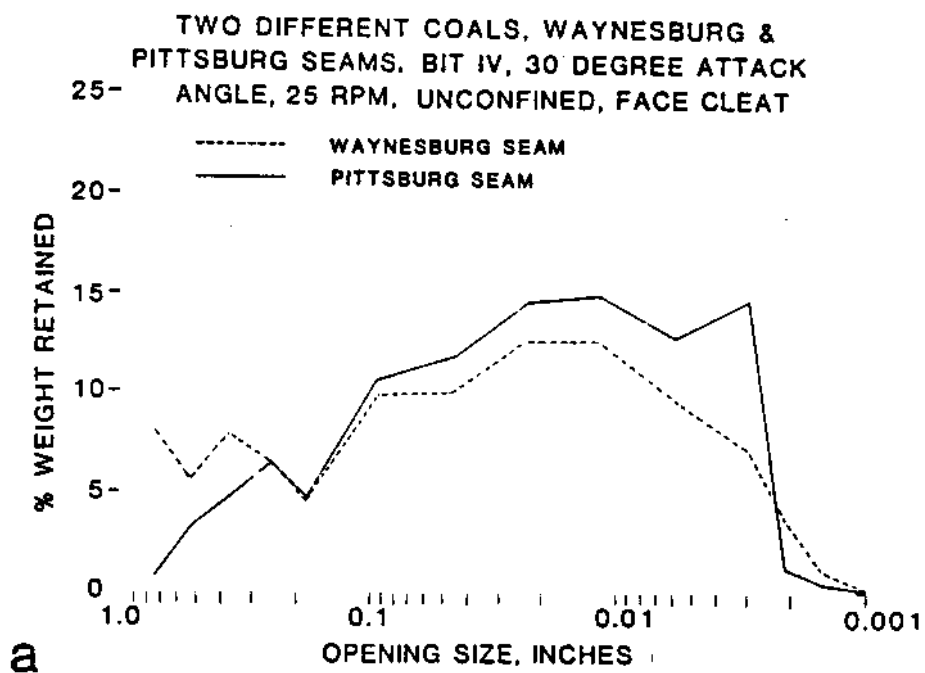


Fig. 6. Mesh size versus percent of weight retained as a function of cutting head speed (rpm) for butt cleat orientation, (a) fragment size distribution from 1.885 cm (0.742 in.) to 0.0038 cm (0.0015 in.) or 400 mesh and (b) dust size distribution from 37 microns (400 mesh) to -10 microns.



ANALYSIS OF RESPIRABLE DUST GENERATION

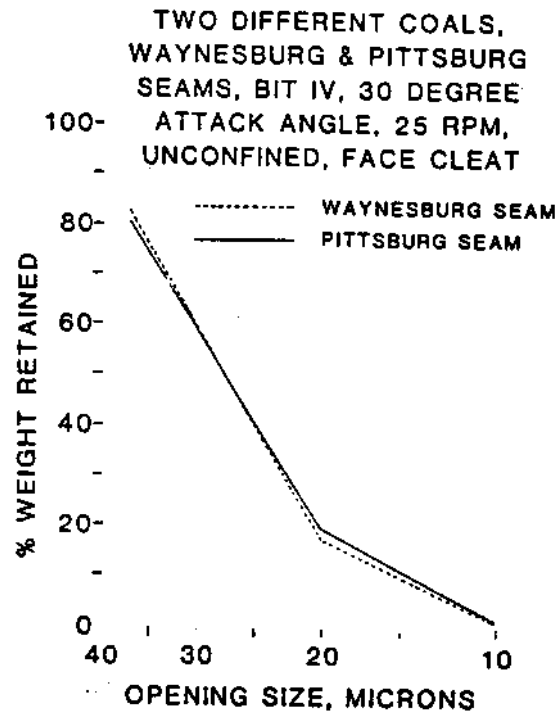


Fig. 7. Mesh size versus percent of weight retained as a function of coal type (a) fragment size distribution from 1.885 cm (0.742 in.) to 0.0038 cm (0.0015 in.) or 400 mesh and (b) dust size distribution from 37 microns (400 mesh) to -10 microns.



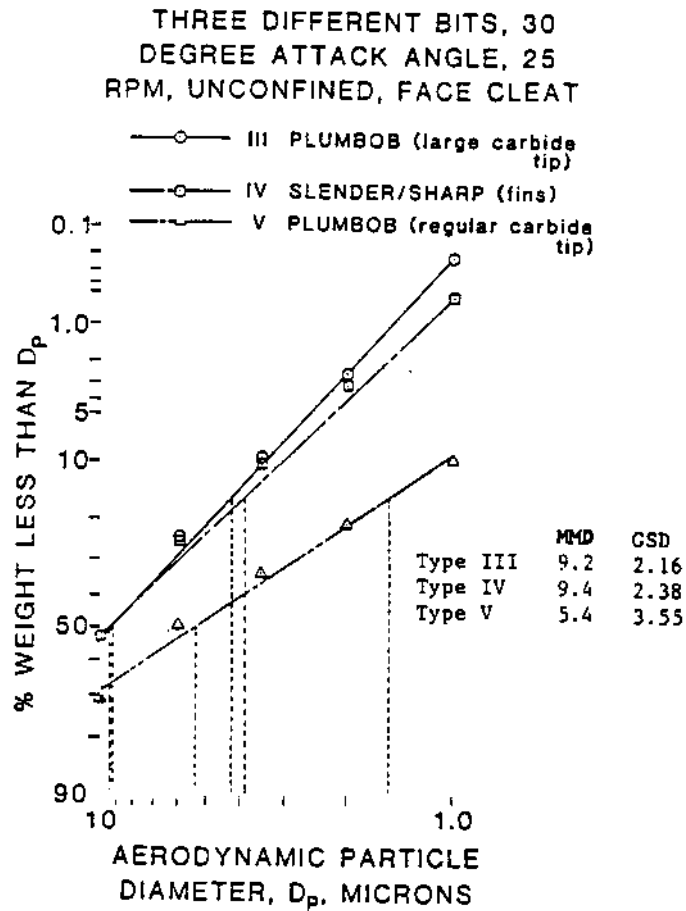


Fig. 8. Particle size distribution of the respirable coal dust sampled by cascade impactors, while cutting coal with different types of bits.

# ANALYSIS OF RESPIRABLE DUST GENERATION

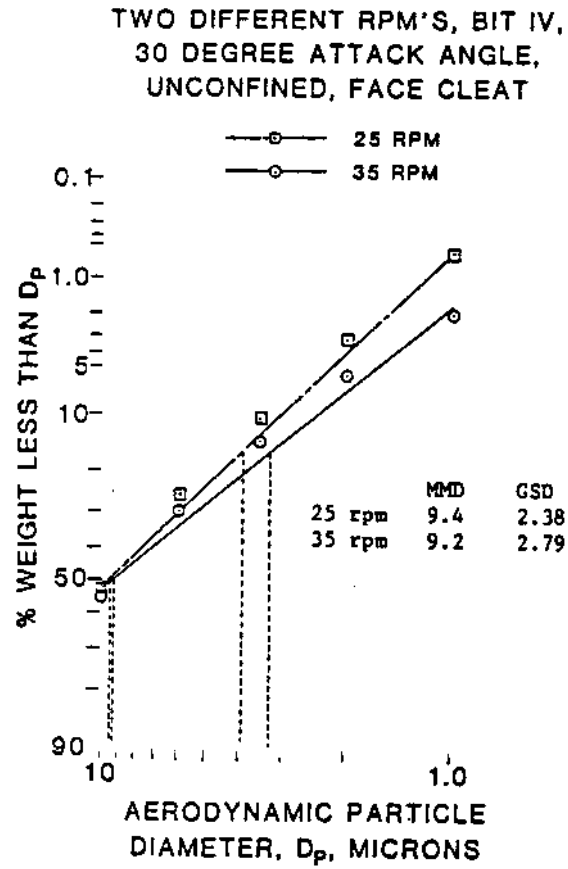


Fig. 9. Particle size distribution of respirable coal dust sampled by cascade impactors while cutting coal with different cutting head speeds (rpm).

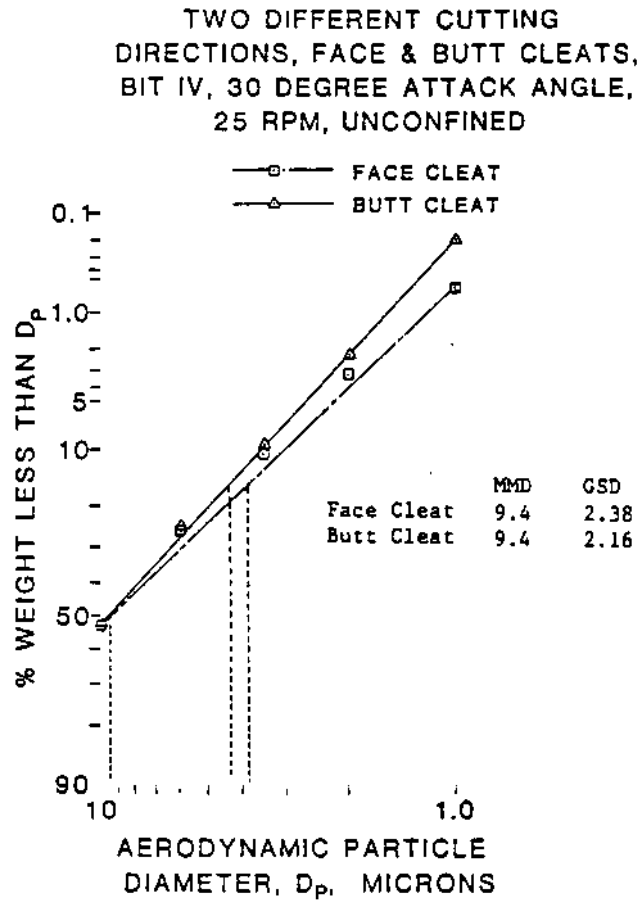


Fig. 10. Particle size distribution of respirable coal dust sampled by cascade impactors while cutting coal with different cleat orientations.

TWO DIFFERENT COALS,  
WAYNESBURG & PITTSBURG SEAMS,  
BIT IV, 30 DEGREE ATTACK ANGLE,  
25 RPM, UNCONFINED, FACE CLEAT

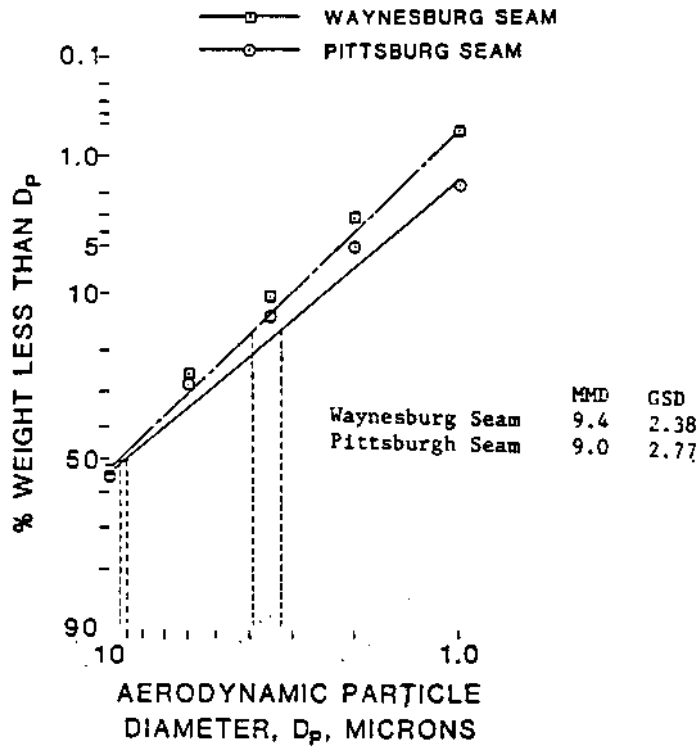


Fig. 11. Particle size distribution of respirable coal dust sampled by cascade impactors while cutting two different coals.

**THE RESPIRABLE DUST CENTER**

Table 3. Respirable Mass Fraction Sampled by Impactors While Cutting with Different Bit Types (Face Cleat)

Bit Type	Concentration	Particle Size (um)	
		10.0 x 6.0	6.0 x 0.6
III	A. Weight* (mg)	7.69	10.61
	N. Weight <sup>+</sup> (mg)	8.35	11.53
	Percent	42.00	58.00
IV	A. Weight* (mg)	8.61	11.28
	N. Weight <sup>+</sup> (mg)	8.61	11.28
	Percent	43.30	56.70
V	A. Weight* (mg)	2.95	9.45
	N. Weight <sup>+</sup> (mg)	4.72	15.17
	Percent	23.70	76.30

Table 4. Respirable Mass Fraction Sampled by Impactors While Cutting at Different Drum Speeds (Face Cleat)

Drum RPM	Concentration	Particle Size (um)	
		10.0 x 6.0	6.0 x 0.6
25	A. Weight* (mg)	8.61	11.28
	N. Weight <sup>+</sup> (mg)	8.76	11.47
	Percent	43.30	56.70
35	A. Weight* (mg)	8.99	11.24
	N. Weight <sup>+</sup> (mg)	8.99	11.24
	Percent	44.40	55.60

\*Actual weight sampled

<sup>+</sup>Normalized with the highest weight in series

# ANALYSIS OF RESPIRABLE DUST GENERATION

Table 5. Respirable Mass Fraction Sampled by Impactors when Cutting Against Face/Butt Cleat Orientations at 25 rpm.

Cleat Orientation	Concentration	Particle Size ( $\mu\text{m}$ )	
		10.0 x 6.0	6.0 x 0.6
Butt Cleat	A. Weight* (mg)	13.02	15.64
	N. Weight <sup>+</sup> (mg)	13.02	15.64
	Percent	45.40	54.60
Face Cleat	A. Weight* (mg)	8.61	11.28
	N. Weight <sup>+</sup> (mg)	12.40	16.25
	Percent	43.30	56.70

Table 6. Respirable Mass Fraction Sampled by Impactors While Cutting Different Types of Coals (Face Cleat)

Coal Type	Concentration	Particle Size ( $\mu\text{m}$ )	
		10.0 x 6.0	6.0 x 0.6
Waynesburg	A. Weight* (mg)	8.61	11.28
	N. Weight <sup>+</sup> (mg)	11.12	14.57
	Percent	43.30	56.70
Pittsburgh	A. Weight* (mg)	9.83	15.86
	N. Weight <sup>+</sup> (mg)	9.83	15.86
	Percent	38.30	61.70

\*Actual weight sampled

<sup>+</sup>Normalized with the highest weight in series

type III and IV (Table 3). Comparison of the dust levels in the size range of 6.0 x 0.6 microns show that bit V produces about 35 percent more than bit IV and about 31 percent more than bit III. Bits III and IV produce 77 percent and 82 percent more, respectively, in the size range of 10.0 x 0.6 microns when compared to bit V. From Table 4 we can observe that a drum speed of 25 rpm produces 2 percent more respirable dust in the size range of 6.0 x 0.6 microns and about 3 percent less in the size range of 10.0 x 6.0 micron size when compared to a drum speed of 35 rpm. According to Table 5, cutting against the face cleat produces about 4 percent more in the size range of 6.0 x 0.6 microns and about 5 percent less in the size range of 10.0 x 6.0

microns when compared to cutting against butt cleat. Similarly, the Pittsburgh coal produces about 9 percent more respirable dust in the size range of 6.0 x 0.6 microns and about 13 percent less in the size range of 10.0 x 6.0 microns when compared to the Waynesburg coal.

Based on these preliminary results we can say that bit type, coal type, cleat orientation and drum speed listed in the order of their importance affect the dust generation.

### ACKNOWLEDGMENTS

The authors acknowledge the assistance of Marilyn Noah, Technician in

## THE RESPIRABLE DUST CENTER

the Analytical Laboratory, College of Mineral and Energy Resources. The assistance of S. Jung and R. Chaffins, graduate students in the Mining Engineering Department is also appreciated. This project was funded by the Generic Center for Respirable Dust Research sponsored by the U. S. Bureau of Mines under Grant No. G1135142.

### REFERENCES

- Attfield, M. D., 1984, "Recent Results and Forthcoming Studies in Epidemiology of Coal Workers' Pneumoconiosis in Underground Miners," Proceedings Coal Mine Dust Conference, West Virginia University, Morgantown, pp. 156-162.
- Bennett, J. G., Dick, J. A., Kaplan, Y. S., et. al., 1979, "The Relationship Between Coal Rank and the Prevalence of Coal Workers Pneumoconiosis," *British J. Ind. Med.*, 36, pp. 206-210.
- Breslin, J. A. and Niewiadomski, G. E., 1982, "Improving Dust Control Technology for U. S. Mines," a Bureau of Mines Impact Report, U. S. Government Printing Office, Washington, DC, pp. 1-2.
- Christian, R. T. and Nelson, J., 1978, "Coal: Response of Cultured Mammalian Cells Corresponds to the Incidence of Coal Workers' Pneumoconiosis," *Environmental Research*, 15, pp. 232-241.
- Christian, R. T., Nelson, J. B., Cody, T. E., Larson, E., and Bingham, 1979, "Coal Workers' Pneumoconiosis: In Vitro Study of the Chemical Corporation and Particle Size as Causes of the Toxic Effects of Coal," *Environmental Research*, 20, pp. 358-365.
- Dalal, N. S., et. al., 1985, "Detection of Reactive Free Radicals in Fresh Coal Mine Dust and Its Implications on Pneumoconiosis," paper presented at the 6th International Conference on Inhaled Particles, Cambridge University, England, 6 pp.
- Davis, J. M. G., Ottery, J. and Le Roux, A., 1975, "The Effect of Quartz and Other Non-coal Dusts in Coal Workers' Pneumoconiosis, Part II, Lung Autopsy Study," *Inhaled Particles IV*, Walton, W. H., ed., Unwin Brothers, Old Working, Surrey, pp. 691-702.
- Dodgson, J., Hadden, G. G., Jones, C. O., et. al., 1971, "Characteristics of the Airborne Dust in British Coal Mines," *Inhaled Particles III*, Walton, W. H., ed., Unwin Brothers, Old Working, Surrey, pp. 757-782.
- Dwiggins, G. A., 1981, "Variations in the Properties of Coal Dusts, Their Significance to the Health of Occupationally Exposed Workers, and Their Relationships to Patent Material Characteristics," Ph.D. Dissertation, University of North Carolina, Chapel Hill, 111 pp.
- Evans, I. and Pomeroy, C. D., 1966, *Strength, Fracture, and Workability of Coal*, Pergamon Press.
- Ford, L. M. and Friedman, M., 1983, "Optimization of Rock-Cutting Tools Used in Coal Mining," *Proc. 24th U. S. Symposium on Rock Mechanics*, June, pp. 703-711.
- Friedman, M. and Ford, L. M., 1983, "Analysis of Rock Deformation and Fractures Induced by Rock Cutting Tools Used in Coal Mining," *Proc., 24th U. S. Symposium on Rock Mechanics*, June, pp. 713-723.
- Fuh, G. F., 1983, "On the Determination of Cutter Bit Spacing for Optimum Coal Mining," *Proc. 24th U. S. Symposium on Rock Mechanics*, June, pp. 703-711.
- Hatch, G. E., Gardner, D. E. and Menzel, D. B., 1980, "Stimulation of Oxidant Production in Alveolar Macrophages by Pollutant and Letex Particles," *Environmental Research*, 23, pp. 121-136.
- Hinds, C. W., 1982, "Particle Size Statistics," Chapter 4, *Aerosol Technology, Properties, Behavior*,

## ANALYSIS OF RESPIRABLE DUST GENERATION

- and Measurement of Airborne Particles, John Wiley and Sons, pp. 69-103.
- Hurley, J. F., et. al., 1979, "Simple Pneumoconiosis and Exposure to Respirable Dust: Relationships from Twenty Five Years' Research at Ten British Coal Mines," Institute of Occupational Medicine Report No. TM/79/13.
- Hurt, K. G., 1980, "Rock Cutting Experiments with Point Attack Tools," Colliery Guardian Coal International, April, pp. 47-50.
- Jacobson, M., Rae, S., Walton, W. H. and Rogan, J. M., 1971, "The Relation Between Pneumoconiosis and Dust Exposure in British Coal Mines," Inhaled Particles III, Walton, W. H., ed., Unwin Brothers, Old Working, Surrey, pp. 903-917.
- Khair, A. W., 1984, "Design and Fabrication of a Rotary Coal Cutting Simulator," Proceedings of the Coal Mine Dust Conference, October, pp. 190-197.
- Khair, A. W. and Quinn, Mark K., 1985, "Mechanisms of Respirable Dust Generation by Continuous Miner," presented at the SME-AIME Fall Meeting, Albuquerque, October, 14 pp.
- Khair, A. W. and Reddy, P. N., 1986, "Characterization of Coal Breakage as a Function of Operating Parameters," to be presented at the International Symposium on Application of Rock Characterization Techniques in Mine Design, Annual Meeting, SME-AIME, New Orleans, March, 12 pp.
- Leiteriz, H., Baur, D. and Bruckman, E., 1971, "Mineralogical Characteristics of Airbone Dust in Coal Mines of Western Germany and Their Relations to Pulmonary Changes in Coal Hewers," Inhaled Particles III, Walton, W. H., ed., Unwin Brothers, Old Working, Surrey, pp. 729-743.
- Morgan, W. K. C., Burgess, D. B., Jacobson, G., et. al., 1973, "The Prevalence of Coal Workers' Pneumoconiosis in U.S. Coal Miners," Archives of Environmental Health, 27, pp. 221-226.
- Pomeroy, C. D. and Foote, P., 1960, "A Laboratory Investigation of the Relation Between Ploughability and Mechanical Properties of Coal," Colliery Engineering, April, pp. 146-154.
- Pomeroy, C. D., 1963, "The Breakage of Coal by Wedge Action, Factors Influencing Breakage by Any Given Shape of Tool-1," Colliery Guardian, November, pp. 642-677.
- Pomeroy, C. D., 1964, "Breakage of Coal by Wedge Action, Factors Affecting Tool Design-2," Colliery Guardian, July, pp. 115-121.
- Pomeroy, C. D., 1968, "Mining Applications of the Deep Cut Principle," Mining Engineer, June, pp. 506-517.
- Reisner, M. T. R. and Rubock, K., 1977, "Results of Epidemiological, Mineralogical and Cytotoxicological Studies on the Pathogenicity of Coal Mine Dusts, Inhaled Particles IV," Walton, W. H., ed., Unwin Brothers, Old Working, Surrey, pp. 703-715.
- Shedd, K. B., Virta, R. L. and Wylie, A. G., 1982, "Size and Shape Characterization of Fibrous Leolites by Electron Microscopy," USBM, RI 8674, 20 pp.
- Terry, N. B., 1959, "The Dependence of the Elastic Behavior of Coal on the Microcrack Structure," Fuel, London, 38, pp. 125-146.
- Walton, W. H., Dodgson, J., Hadden, G. G., et. al., 1975, "The Effect of Quartz and Other Non-coal Dusts in Coal Workers' Pneumoconiosis. Part I: Epidemiological Studies," Inhaled Particles IV, Walton, W. H., Walton, ed., Unwin Brothers, Old Working, Surrey, pp. 669-690.
- Warner, E. M., 1970, "Machine and Cutting Element Design," Mining Congress Journal, August, pp. 35-43.



# Characterization of Coal Breakage as a Function of Operating Parameters

A. Wahab Khair and N. P. Reddy  
Department of Mining Engineering, West  
Virginia University

**Abstract.** This paper attempts to characterize coal breakage due to the action of a continuous miner. Coal blocks with an approximate dimension of 45.7 cm x 38.1 cm x 15.2 cm (18 in. x 15 in. x 6 in.) were first subjected to confining pressures equivalent to in-situ conditions. Then the blocks were cut along the face/butt cleat direction by the cutting head of a specially designed unique automated rotary coal cutting simulator (ARCCS), simulating the action of the continuous miner in underground coal mining. During the tests under a particular set of in-situ and operating parameters a number of other parameters such as 1) penetration of bit into coal, 2) penetration resistance (thrust and cutting pressures), 3) rotating velocity of cutting head, and 4) acoustic emission activity in the coal block were monitored. After each cutting cycle the fractured surfaces were photographed and a velocity survey was conducted by using a sonic technique. At the end of each experiment, the coal fragments were collected in bags using a vacuum cleaner. These fragments were then sieved for size distribution analysis.

## INTRODUCTION

The Federal Coal Mine Health and Safety Act of 1969 was enacted to emphasize to coal operators that the airborne respirable dust should not exceed  $2 \text{ mg/m}^3$ , thus reducing the incidence of coal workers pneumoconiosis.

Dust control techniques such as conventional water sprays and dust collectors are only partially effective and require additional equipment expenditures. A more authentic approach would be to reduce respirable dust at the source, the continuous mining machine cutting head, where the fragmentation process occurs. Improving the fragmentation process by characterizing the coal breakage will not only reduce respirable dust at the face, but it will also decrease the amount of respirable dust that is liberated during the secondary handling.

Fragmentation of coal can be expressed as a function of three major groups of parameters;

namely, 1) coal properties, 2) in-situ conditions and 3) operating parameters. This paper deals with the characterization of coal breakage along both face/butt cleat direction as a function of machine operating parameters such as rate of advance, angle of attack, bit configuration, bit lacing (spacing and pattern) and bit speed at various equivalent in-situ pressures.

## STUDY PROGRAM

### Laboratory Equipment and Instrumentation

Review of the literature on coal cutting technology and the basic parameters that effect this technology revealed that most of the existing coal cutting machinery is of the rotary type and that the parameters that effect the fragmentation of coal in such cuttings depend on the following (Terry, 1959; Pomeroy and Foote, 1960; Pomeroy, 1963, 1964; Evans and Pomeroy, 1966; Pomeroy, 1968; Bower, 1970; Warner, 1970; Hurt, 1980; Ford and Friedman, 1983; Friedman and Ford, 1983; Fuh, 1983; Evans, 1984):

$$\text{Coal fragmentation} = f(C_p, I_c, O_p)$$

where  $C_p$  is the mechanical properties of coal,  $I_c$  is the in-situ conditions (vertical and horizontal stresses), and  $O_p$  is the operating parameters.

Based on this premise a unique automated rotary coal cutting simulator (ARCCS) (Figure 1) was designed and fabricated in the Mining Engineering Department at West Virginia University (Khair, 1984). This design incorporates the capability to study the different machine and in-situ parameters that influence the fragmentation of coal. It operates under the simulated mining conditions with in-situ stresses (horizontal and vertical stresses) being applied to a coal block of 45.7 cm x 38.1 cm x 15.2 cm (18 in. x 15 in. x 6 in.) located in a suitably designed confining chamber. The cutting drum with a maximum tip to tip diameter (varies with the bit angle) of 19 inches has the capability of rotating from 1 to 50 rpm. The drum can be stopped any time after a predetermined number of revolutions. Tests can be performed with four different bit angles,

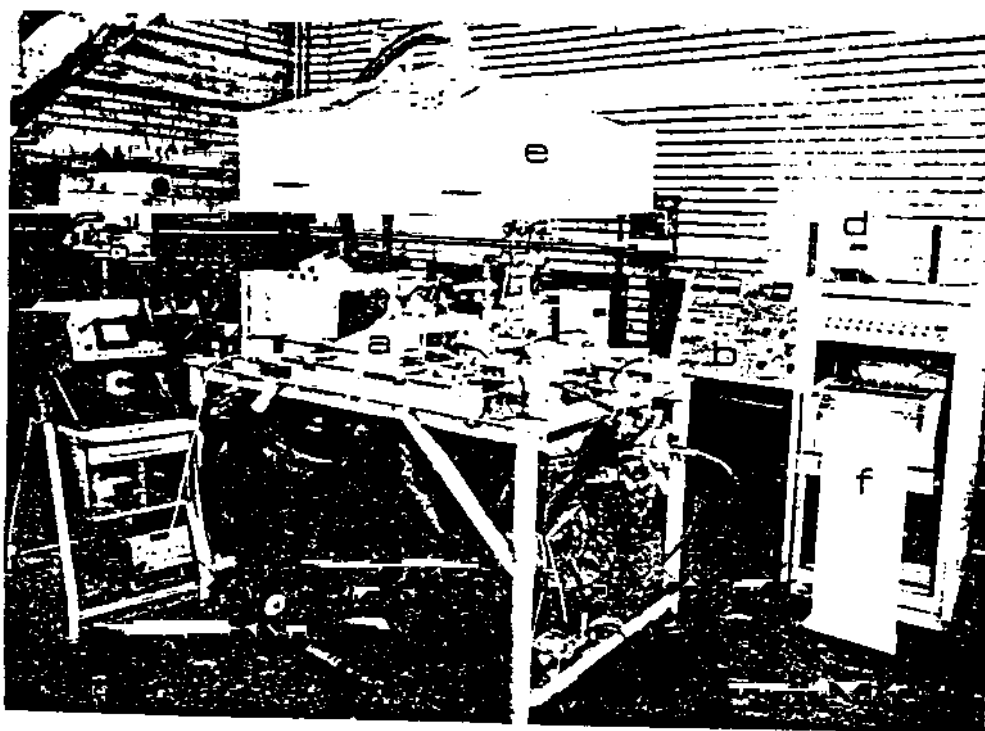


Figure 1. Test and monitoring equipment facilities (a) automated rotary coal cutting simulator, (b) programmable control and monitoring unit, (c) sonic testing unit, (d) acoustic emission (A.E. monitoring unit), (e) hood and air-current generating unit and (f) data acquisition and recording unit.

15, 30, 45 and 60 degrees. A maximum of seven bits can be mounted on the drum in an echelon pattern. The ARCCS can be operated and controlled manually or automatically, and the operating parameters can be preset with a series of hydraulic valves and could be recorded in analog/digital or in both forms.

Test and monitoring facilities can be seen in Figure 1, ARCCS (Figure 1a), programmable control and monitoring unit (Figure 1b), sonic testing unit (Figure 1c), A.E. monitoring unit (Figure 1d), hood and air current generating unit (Figure 1e) and data acquisition and recording unit (Figure 1f). In addition to this, linear variable transformers, pressure transducers, flow meters, flow controls and drum rpm were some of the other monitoring devices. LVDT's are used to monitor the displacement of the coal block as well as the depth of cut. Pressure transducers are used to monitor the changes in pressure, both due to the thrust and due to the intermittent cutting nature of the rotary cutting. Flow controls are used to run the drum at a particular rpm between 1 and 50 and to provide a different rate of advance. All of the above mentioned devices are operated and monitored by a fully automated control system. The fracture size, shape and intensity is characterized, a) by monitoring the acoustic emission and b) by monitoring the sonic signal in the coal block located in the confining chamber with the help of

sonic transducers, signal generator, and an oscilloscope.

#### Specimen Preparation

Large blocks of coal were obtained from a surface mine. These blocks were then cut in the laboratory to an approximate dimension of 43.2 cm x 33.0 cm x 15.2 cm (17 in. x 13 in. x 6 in.). A typical specimen with cutting face as face cleat was then placed in a wooden box of 45.7 cm x 35.6 cm x 15.2 cm (18 in. x 15 in. x 6 in.) in dimension. Two blocks of wood 3.2 cm x 3.8 cm x 12.7 cm (1.25 in. x 1.5 in. x 5 in.) were wedged between the coal sample and the wooden box. Plaster of paris was then poured in the box to fill all the remaining space other than that occupied by the coal block. This process gives a perfect dimension of 45.7 cm x 35.6 cm x 15.2 cm (18 in. x 15 in. x 6 in.) which is very essential to avoid stress concentration in the specimen when confining pressure is applied. After a week the molded coal samples were removed from the box and the wooden blocks that were wedged before pouring the mold were dislodged from the sample carefully, thus creating room to house the sonic transducers. A typical specimen ready to be cut is shown in Figure 2.

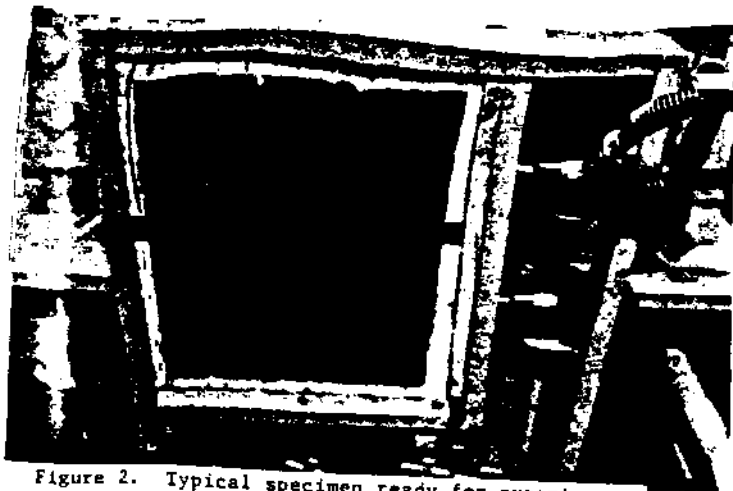


Figure 2. Typical specimen ready for experiment.

Experimental Procedure

During a typical experiment the molded specimen was placed in the confining chamber, the test conditions were set, and the in-situ and operating parameters were marked on the top mold layer of the sample. A sonic test was done by which the stress wave travel time through the coal sample and the amplitude of the signal was measured and recorded. Equivalent in-situ stresses were then applied to the specimen using two sets of hydraulic jacks (two for horizontal and two for vertical). A 2.54 cm (1 in.) thick steel plate was positioned between the sample and hydraulic jacks in order to distribute the pressure uniformly over the whole surface of the specimen. Each set of hydraulic jacks were connected in parallel to a hand pump. After the confining pressure was applied another sonic test was made and the corresponding stress wave travel time and amplitude was measured and recorded. Before the test, the operating parameters such as velocity of the cutting drum and rate of advancement were adjusted to predetermined values. Then bit blocks of specific attack angle (15, 30, 45 and 60 degrees) were mounted on the cutting drum at a particular spacing (Figure 3a-b), i.e., 3.8 cm to 7.6 cm (1.5 in. to 3.0 in.) and pattern. Bits of specific make and type were inserted into the bit block slots and were kept in position by a screw in such a way so as to allow bit rotation inside the lock which prevents non-symmetric bit wear. The number of rotations by the cutting head was set in the counter unit in the control module and then the machine was started to execute the program in a continuous or counter mode. The counting of the number of rotations starts when the hydraulic pressure is increased, due to the cutting process, or when the cutting head has traveled to a preset distance measured mechanically and by LVDT. After the execution of the predetermined number of rotations the cutting head retreats and stops. After each cutting cycle, the samples were photographed and a sonic test was done. During the test a number of parameters were recorded (Figure 4). Test conditions were marked on each specimen as well as on the recorded data (i.e., 1-bit type; 1.5"-bit spacing; 5-number of bits; 15°-bit attack angles; 1/8"-depth of cut; 15-drum rpm; F-face cleat;  $S_v$ ,  $S_h$  - vertical and horizontal confining pressures).

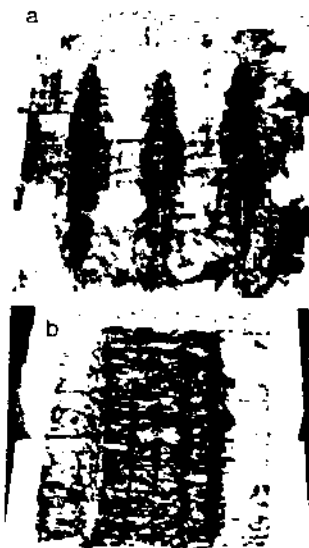


Figure 3. Coal blocks cut with different bit spacing (a) 7.62 cm (3 in.) spacing and (b) 3.81 cm (1.5 in.) spacing (face cleat direction).

RESULTS AND DISCUSSION

The coal used in the experimental study is part of the Waynesburg coal seam. Prior to the experiments the physical and mechanical properties of this coal were determined in the laboratory. The physical and mechanical properties can be seen in Table 1.

A study of thirty experiments have been completed so far and more are being done to study the effects of operating and geologic parameters on the fragmentation of coal in detail. The parameters observed were spacing, effect of velocity, depth of cut, confining pressure and angle of attack. Despite a limited number of tests, enormous data was collected of which only a part will be presented here for discussion.

Using a 7.62 cm (3 in.) and 3 bits mounted in an echelon pattern, a cut of up to 6.35 cm to 7.62 cm (2.5 to 3 in.) depth was made without breaking the boundary walls between the bit paths (Figure 3a). These series of tests with 7.62 cm (3 in.) spacing were done for 15, 30, 45 and 60 degree attack angles.

C  
T  
C  
  
Pl.  
Fac  
But  
Bed  
  
mou  
the  
wer  
deg  
pai  
  
tes  
  
stat  
rest  
rest  
func  
face  
resu  
bit

# COAL BREAKAGE AS A FUNCTION OF OPERATING PARAMETERS

CUTTING PRESSURE,  $C_c$ : 7011 LBS(3187KG)FS  
 THRUST PRESSURE,  $T_p$ : 14416 LBS(6563KG)FS  
 DEPTH OF CUT  $D_c$ : 2" IN.(5.08CM)FS

#71-1.5°-5-15°-1/8°-15-F-S<sub>v</sub>: 0-S<sub>h</sub>: 0  
 DRUM RPM: 50RPM FS  
 AE: 10 VOLTS FS 999 COUNTS,  
 70 Db AT 0.25sec

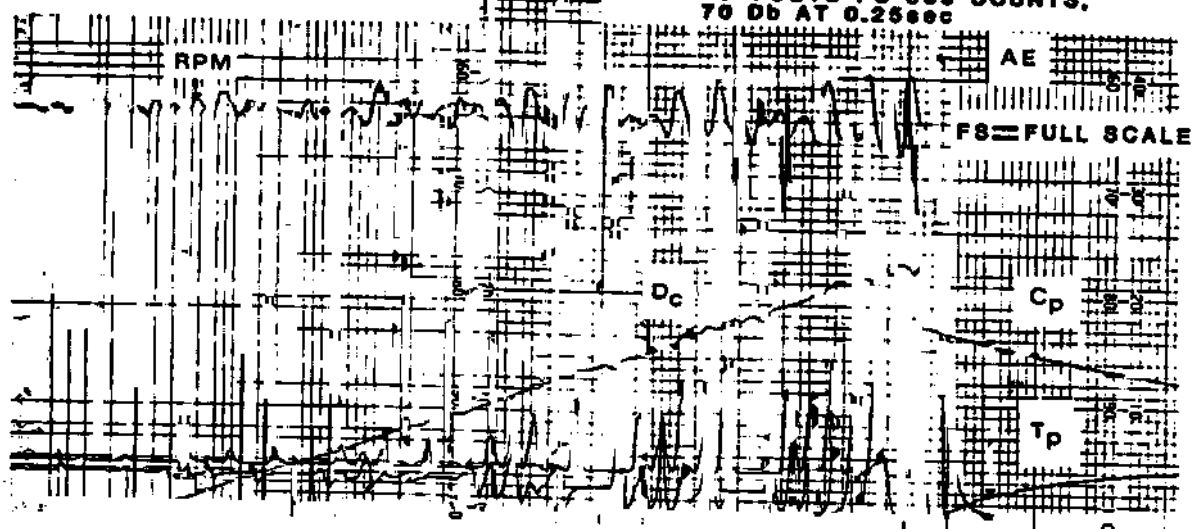


Figure 4. Typical chart on which the different parameters such as the A.E., cutting pressure, thrust pressure, drum rpm and depth of cut are recorded for a particular set of operating parameters under zero confining pressure.

Table 1. Physical and Mechanical Properties of Waynesburg Coal

Cleat/Bedding Plane Orientation	Compressive Strength KPa (psi)	Young's Modulus KPa (psi)	Poisson's Ratio	Indirect Tensile Strength KPa (psi)	Direct Shear Strength KPa (psi)	Sp. Gr.
Face Cleat	473.6 (3289)	$7.3 \times 10^4$ ( $5.1 \times 10^5$ )	0.25	22.2 (154)	29.4 (204)	1.42
Butt Cleat	498.1 (3459)	$6.8 \times 10^4$ ( $4.7 \times 10^5$ )	0.31	29.5 (205)	25.9 (180)	
Bedding Plane	707.4 (4912)	$6.6 \times 10^4$ ( $4.6 \times 10^5$ )	0.32	21.0 (146)	11.5 (80)	

With 3.81 cm (1.5 in.) spacing and 5 bits mounted in an echelon pattern, the side walls of the bit paths were broken. These series of tests were done for attack angles of 15, 30, 45 and 60 degrees and at 0, 43.2 and 64.8 KPa (0, 300 and 450 psi) vertical and corresponding horizontal pressures.

The preliminary findings resulting from these tests are:

**Force.** Due to the enormous amount of data, a statistical analysis was done to calculate the resultant force. Figures 5 through 8 show the resultant force necessary to cut coal as a function of the various parameters along the face cleat direction. Figure 5 shows that the resultant force necessary to cut increases as the bit attack angle increases from 30 to 60 degrees.

However, the force required with a 15 degree attack angle is much higher. This could be attributed to the fact that with a 15-degree attack angle the bit rubs along the cutting path more than the other angles and hence requires high thrust and cutting pressure. A similar trend was observed with confining pressures of 43.2 KPa (300 psi) and 14.4 KPa (100 psi), vertical and horizontal, respectively, except that the rate of increase of the resultant force is higher as the depth of cut increases (Fig. 6). Using a 45 degree attack angle, it was observed that as the equivalent in-situ confining pressure increases the required resultant force increases (Fig. 7). Also the rate of increase gets higher as the vertical and horizontal confining pressures increase from 0 to 57.6 KPa (400 psi) and 0 to 19.15 KPa (133 psi), respectively. Figure 8 shows that for a

# THE RESPIRABLE DUST CENTER

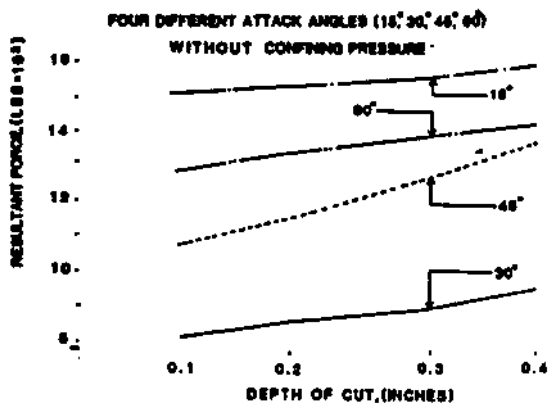


Figure 5. Resultant force vs. depth of cut as a function of bit attack angle (face cleat direction) (1 lb = 0.45 kg; 1 in = 2.54 cm)

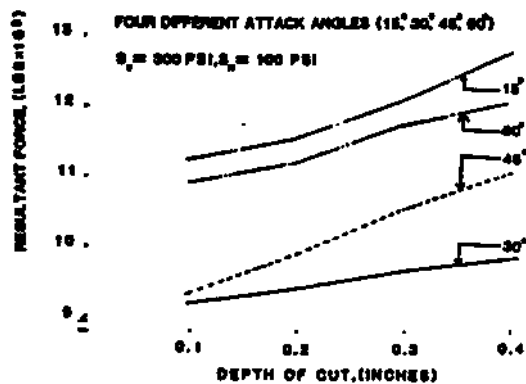


Figure 6. Resultant force vs. depth of cut as a function of bit attack angle and equivalent in-situ pressures (face cleat direction).

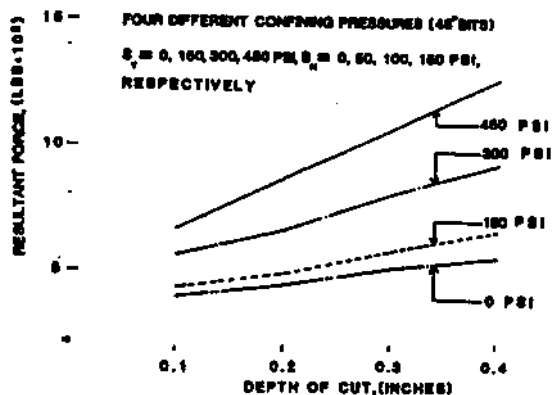


Figure 7. Resultant force vs. depth of cut as a function of equivalent in-situ pressures (face cleat direction). (1 psi = 0.144 KPa)

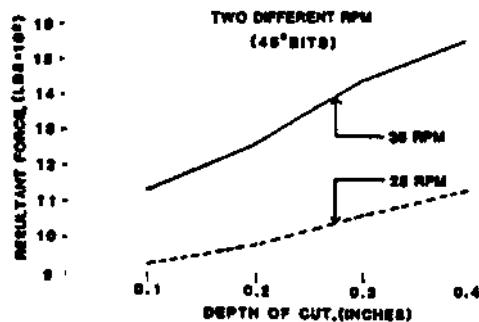


Figure 8. Resultant force vs. depth of cut as a function of rpm (face cleat direction).

45 degree attack angle as the rpm increases the resultant force increases. Also the rate of increase is higher. Figure 9 shows the high rate of increase of the force necessary when the spacing is increased. This could be due to the fact that there is no free space available when there is a cut with a 7.62 cm (3 in.) spacing, where the walls between the two bits were cut when using a 3.81 cm (1.5 in.) bit spacing.

Testing coal blocks along the butt cleat produced similar results to blocks tested along the face cleat direction (Figures 10-12). The

magnitude of forces (both thrust and cutting) were higher when coal blocks were tested along the butt cleat as shown by the resultant forces. The main difference here is that the lowest resultant force to cut coal is achieved by using a 15° attack angle and this increases as the attack angle increases (Figure 10). The walls between the cutting path of the bits remained partially unbroken (Figure 13). These two different failure characteristics were due to the higher compressive strength of coal along the butt cleat than the face cleat. Table 1 indicates that the compressive strength of tested coal is 5.2% higher

# COAL BREAKAGE AS A FUNCTION OF OPERATING PARAMETERS

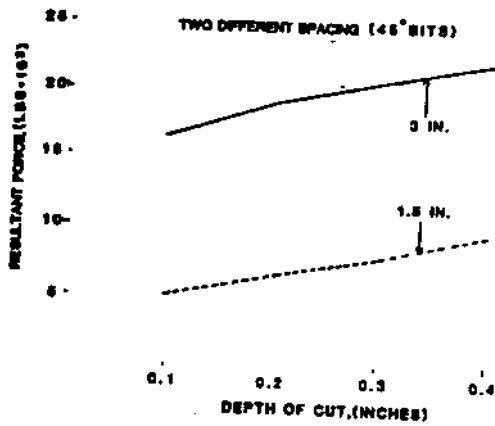


Figure 9. Resultant force vs. depth of cut as a function of bit spacing (face cleat direction).

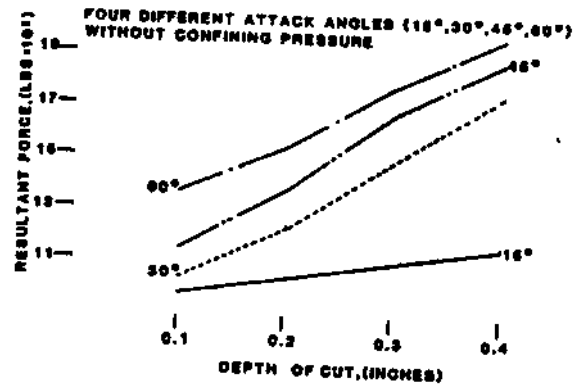


Figure 10. Resultant force vs. depth of cut as a function of bit attack angle (butt cleat direction).

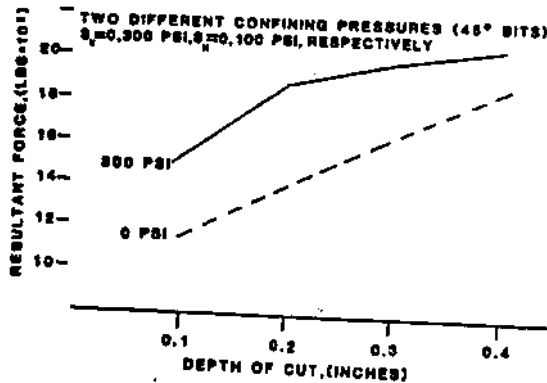


Figure 11. Resultant force vs. depth of cut as a function of equivalent in-situ pressures (butt cleat direction).

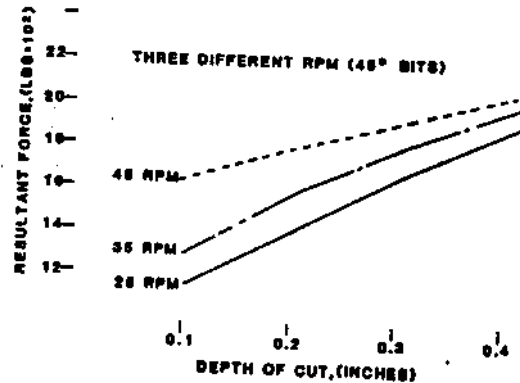


Figure 12. Resultant force vs. depth of cut as a function of rpm (butt cleat direction).

in the butt cleat direction than in the face cleat direction.

**Size Distribution.** A statistical analysis was done to fit the curves for the size distribution. The curves are plotted on the semi log graph. Figures 14 through 18 show the mesh size versus the percent of weight retained as a function of various parameters for coal tested along the face cleat direction. Figure 14 indicates that the percent weight decreases as the opening size decreases for all angles. However, the percent weight is the highest for all angles at 0.25 cm (0.1 in.) opening size. The percent weight for the 30 degree attack angle is larger below 0.25 cm (0.1 in.) than for the other angles. With confining pressures of 43.2 KPa (300 psi) and 14.4 KPa (100 psi), vertical and horizontal, respectively, a similar trend was observed except that the percent weight for the 60 degree attack

angle is more under 0.25 cm (0.1 in.) than at the higher size (Figure 15). Using a 45 degree attack angle, it was observed that as the confining pressure increases the weight percent increases in the finer range and decreases in the larger range (Figure 16). Figure 17 shows that the percent weight of the fragments larger than 0.25 cm (0.1 in.) are higher with 35 rpm while the percent weight of the fragments smaller than 0.25 cm (0.1 in.) are more with 25 rpm. The weight percent of fragments larger than 0.76 cm (0.3 in.) are more for 3.8 cm (1.5 in.) spacing while the weight percent of fragments less than 0.76 cm (0.3 in.) are higher for 7.6 cm (3 in.) spacing (Figure 18). This could be imputed to the fact that the walls of the bit cut paths do not break for the 7.6 cm (3 in.) spacing while they break with 3.8 cm (1.5 in.) spacing (Figure 3a-b).



Figure 13. Typical cut surface for coal block tested along the butt cleat direction.

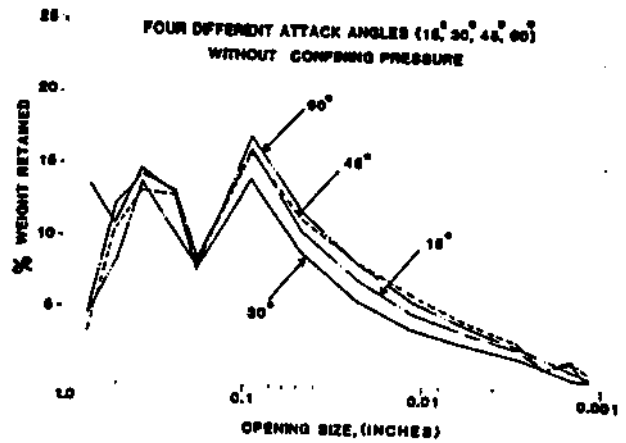


Figure 14. Mesh size vs. percent of weight retained as a function of bit attack angle (face cleat direction).

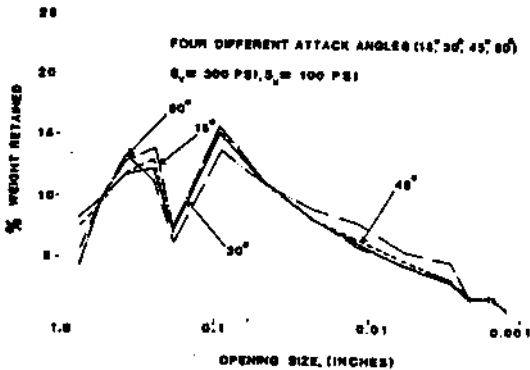


Figure 15. Mesh size vs. percent of weight retained as a function of bit attack angle and equivalent in-situ pressures (face cleat direction).

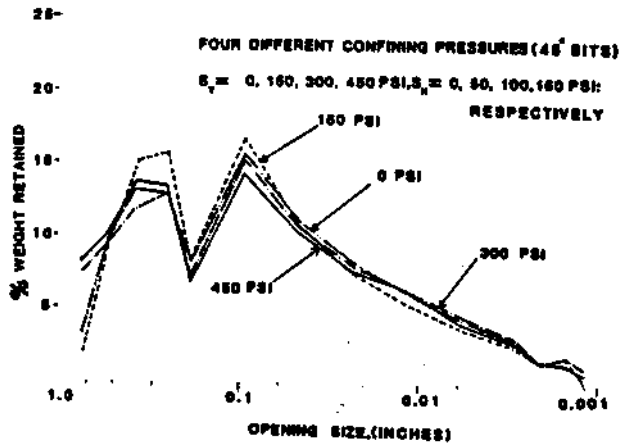


Figure 16. Mesh size vs. percent of weight retained as a function of equivalent in-situ pressures (face cleat direction).

Results of tests along the butt cleat direction were similar to the results obtained when the tests were carried out along the face cleat direction, except that the magnitude of fine particles were higher when the coal blocks were cut along the butt cleat direction. The results are presented in Figures 19-21. More airborne dust was liberated during the cutting of coal along the butt cleat as it was observed during the experiments.

**Fracture Extension.** Before and after applying the confining pressure, but before the first cut was made, the time that a stress wave takes to pass across the width of the coal sample and the amplitude and attenuation of this wave was measured, and the photograph was taken with a

camera attached to an oscilloscope. Using this data, the velocity of this wave and the dynamic Young's modulus of the coal sample were calculated. A similar procedure was followed to calculate the velocity and the dynamic Young's modulus after every cut (Figure 22). Results indicated that the application of confining pressure increases the dynamic Young's modulus of coal as evidenced in Figure 22. During cutting the fracture(s) extended from the cut surface through the block. The magnitude and the length of extension of these cracks depend on the original condition of the block (pre-existence of cracks), the operating parameters such as velocity of the cutting drum, depth of cut, angle of attack, magnitude of the dynamic shock produced and magnitude of the confining pressure. At lower or zero confining

# COAL BREAKAGE AS A FUNCTION OF OPERATING PARAMETERS

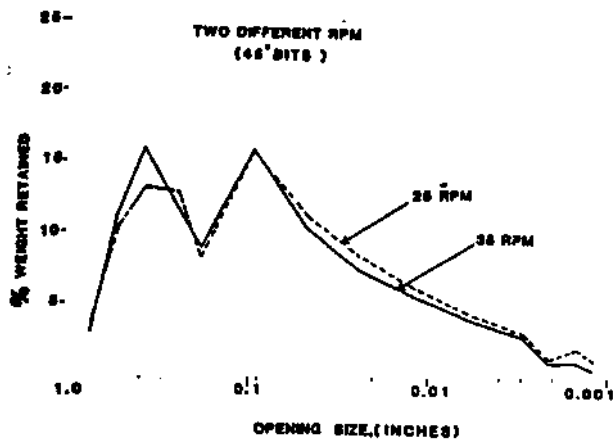


Figure 17. Mesh size vs. percent of weight retained as a function of rpm (face cleat direction).

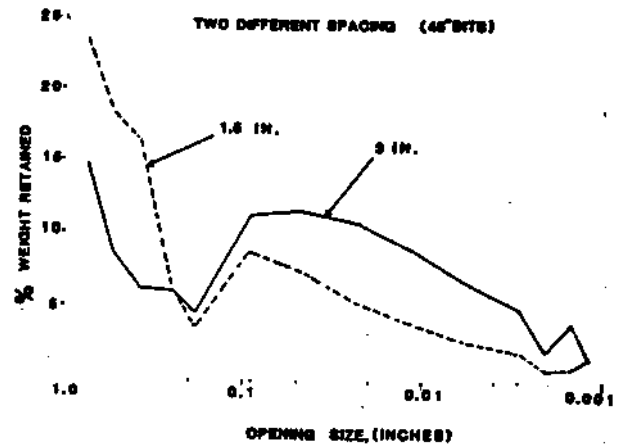


Figure 18. Mesh size vs. percent of weight retained as a function of bit spacing (face cleat direction).

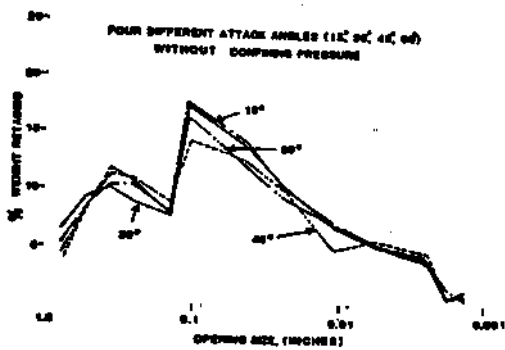


Figure 19. Mesh size vs. percent of weight retained as a function of bit attack angle (butt cleat direction).

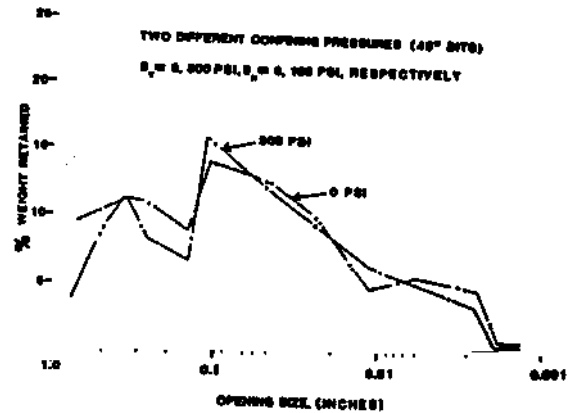


Figure 20. Mesh size vs. percent of weight retained as a function of equivalent in-situ pressures (butt cleat direction).

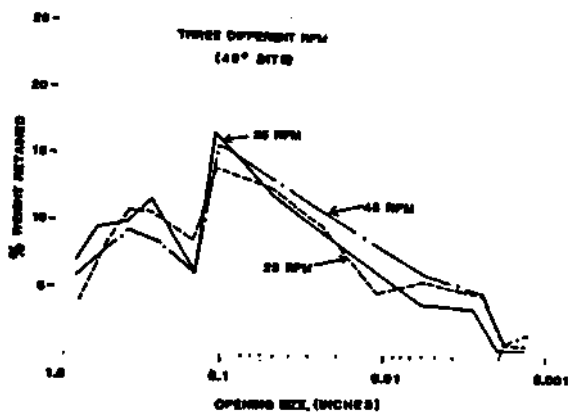


Figure 21. Mesh size vs. percent of weight retained as a function of rpm (butt cleat direction).



pressures, the shock due to the impact of the bits fractures the coal block after one or two cycles of cutting and the fractures thus formed remain open as depicted by the diminishing rate of acoustic emission (A.E. hereafter)(Figure 23). However, under higher confining pressures, the magnitude and extension of the fractures is less, and furthermore, the fractures developed during the cutting tend to close due to the confining pressure. Figure 24 illustrates the continued A.E. activity even after cutting is over. This is an indication of the fracture closure. The high rate of A.E. during the application of confining pressure can also be seen in this figure at location a. Apart from this, the other recorded data such as cutting pressure, thrust pressure, rpm of the drum and depth of cut can also be seen in Figures 23 and 24. The fluctuation in the depth of cut and rpm curves in Figure 24 in contrast to Figures 4 and 23 is due to the higher depth of cut than the anticipated 0.64 cm (1/4 in.). This was due to the higher temperature of the hydraulic oil.

The results of sonic tests when the coal block was cut along the butt cleat were inconclusive. Perhaps because in such cases the sonic test had to be performed along the face cleat direction which had distinct discontinuous features along the cleat plane, consequently the stress wave produced by the signal generating unit attenuated significantly while passing through the cleat discontinuities.

CONCLUSIONS

Although the results presented in this paper must be considered of a preliminary nature since they are based on a limited number of tests on a specific coal, nevertheless a number of significant points appear evident. These include the following:

- (1) The resultant force necessary to cut the coal is the least for 30 degree attack angle while it increases for lesser than or greater than 30 degree attack angles.
- (2) In general the resultant force necessary to cut the coal increases with the increasing compressive strength of coal and equivalent in-situ pressure.
- (3) The higher the drum rpm the greater is the force required to cut thus producing more airborne dust.
- (4) The 30 degree attack angle produces more larger fragments than any other attack angle.
- (5) The higher the equivalent in-situ pressure the finer are the coal fragments.
- (6) The finer fragments increase with the increasing compressive strength of coal.
- (7) The optimum spacing needed to break the boundary walls between the bit paths in the face

CUTTING PRESSURE,  $C_p = 6273$  LBS(2851 KG) FS  
 THRUST PRESSURE,  $T_p = 12898$  LBS(5863 KG) FS  
 DEPTH OF CUT,  $D_c = 2$  IN.(5.08CM) FS  
 DRUM RPM = 50RPM FS  
 AE=10 VOLTS FS 999 COUNTS, 70 Db AT 0.25 sec  
 $\pm 10$  1-1.5" -5-60°-1/4" -25-F-8, 0-S, 0

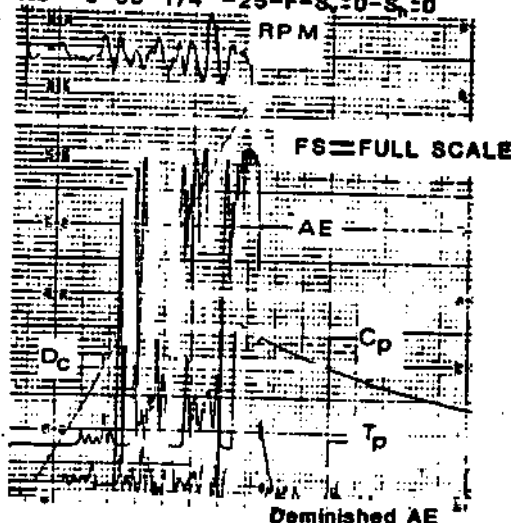


Figure 23. Typical chart on which the different parameters such as A.E., cutting pressure, thrust pressure, drum rpm and depth of cut are recorded for a particular set of parameters. Angle, depth of cut and rpm are different from that of Figures 24 and 4.

cleat direction (medium compressive strength) was found to be 3.81 cm (1.5 in.). However less spacing is required for butt cleat direction (high compressive strength).

(8) Irregular breakage of the cutting face (wall between the bit path) causes excessive abrasion of the bit and bit-blocks, consequently producing more airborne dust.

ACKNOWLEDGMENTS

The authors acknowledge the assistance of M. Quinn, R. Begley, G. Begley and S. Jung, graduate students in the Mining Engineering Department, in preparing this paper. This project was funded by the Generic Center for Respirable Dust Research sponsored by the United States Bureau of Mines under Grant Number G1135142.

REFERENCES

Bower, Jr., A. B., 1970, "Bit Design: Key to Coal Cutting," *Coal Age*, July, pp. 70-75.  
 Evans, I., 1984, "A Theory of the Cutting Force for Point-Attack Picks," Technical Note, *International Journal of Mining Engineering*, pp. 63-71.

COAL BREAKAGE AS A FUNCTION OF OPERATING PARAMETERS

TEST #17 I-1.5"-5-45°-1/4"-25-S<sub>v</sub>=150-S<sub>h</sub>=50-F

DEPTH OF CUT 0.0"  
 VEL 8156 1/s  
 Vmax 0.20 v  
 Ed 1.08 E06 psi  
 50mV/DIV  
 0.1ms/DIV



INITIAL-UNCONFINED



THIRD

DEPTH OF CUT 0.0"  
 VEL 8156 1/s  
 Vmax 0.25 v  
 Ed 1.08 E06 psi  
 50mV/DIV  
 0.1ms/DIV



INITIAL-CONFINED



FOURTH

DEPTH OF CUT 0.62"  
 VEL 8390 1/s  
 Vmax 0.28 v  
 Ed 1.12 E06 psi  
 50mV/DIV  
 0.1ms/DIV



FIRST



FOURTH-UNCONFINED

DEPTH OF CUT 1.48"  
 VEL 8232 1/s  
 Vmax 0.22 v  
 Ed 1.08 E06 psi  
 50mV/DIV  
 0.1ms/DIV



SECOND

TEST #7 I-1.5"-5-15°-1/8"-15-S<sub>v</sub>=0-S<sub>h</sub>=0-F

DEPTH OF CUT 0.0"  
 VEL 7581 1/s  
 Vmax 0.16 v  
 Ed 8.17 E05 psi  
 20mV/DIV  
 0.1ms/DIV



INITIAL



THIRD

DEPTH OF CUT 0.46"  
 VEL 7819 1/s  
 Vmax 0.08 v  
 Ed 8.00 E05 psi  
 20mV/DIV  
 0.1ms/DIV



FIRST



FOURTH

DEPTH OF CUT 0.68"  
 VEL 7449 1/s  
 Vmax 0.08 v  
 Ed 8.83 E05 psi  
 20mV/DIV  
 0.1ms/DIV



SECOND

b

Figure 22. Sonic stress wave patterns at different stages of the experiment under a particular set of parameters (a) without any confining pressure (b) with confining pressure.

a

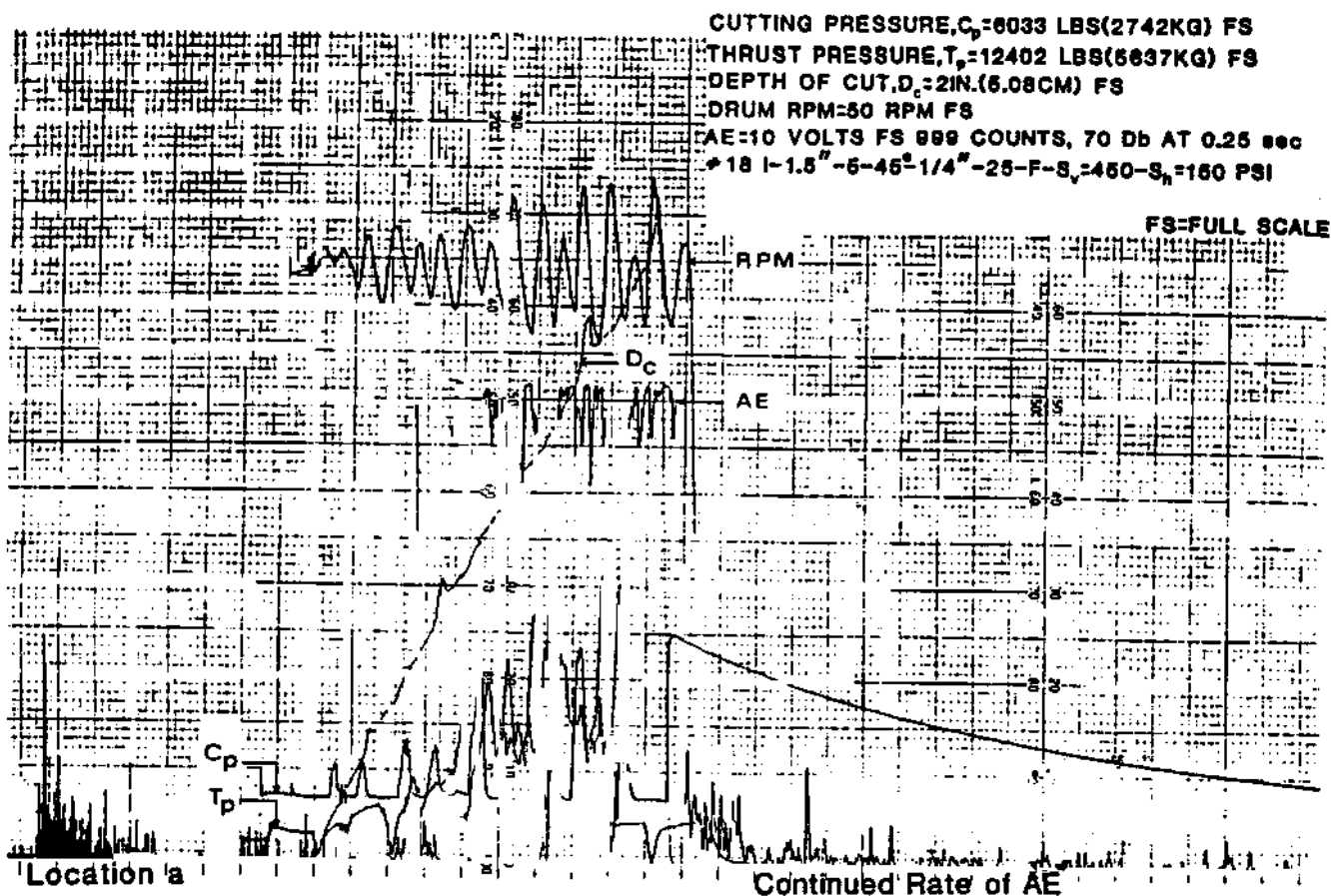


Figure 24. Typical chart on which the different parameters such as the A.E., cutting pressure, thrust pressure, drum rpm and depth of cut are recorded for a particular set of parameters under vertical and horizontal confining pressures of 64.8 and 21.6 KPa (450 and 150 psi), respectively.

Evans, I. and Pomeroy, C. D., 1966, Strength, Fracture, and Workability of Coal, Pergamon Press.

Ford, L. M. and Friedman, M., 1983, "Optimization of Rock-Cutting Tools Used in Coal Mining," Proc. 24th U. S. Symposium on Rock Mechanics, June, pp. 703-711.

Friedman, M. and Ford, L. M., 1983, "Analysis of Rock Deformation and Fractures Induced by Rock Cutting Tools Used in Coal Mining," Proc., 24th U. S. Symposium on Rock Mechanics, June, pp. 713-723.

Fuh, G. F., 1983, "On the Determination of Cutter Bit Spacing for Optimum Coal Mining," Proc., 24th U. S. Symposium on Rock Mechanics, June, pp. 703-711.

Hurt, K. G., 1980, "Rock Cutting Experiments with Point Attack Tools," Colliery Guardian Coal International, April, pp. 47-50.

Khair, A. W., 1984, "Design and Fabrication of a Rotary Coal Cutting Simulator," Proceedings of the Coal Mine Dust Conference, October, pp. 190-197.

Pomeroy, C. D., 1963, "The Breakage of Coal by Wedge Action, Factors Influencing Breakage by Any Given Shape of Tool-1," Colliery Guardian, November, pp. 642-677.

Pomeroy, C. D., 1964, "Breakage of Coal by Wedge Action, Factors Affecting Tool Design-2," Colliery Guardian, July, pp. 115-121.

Pomeroy, C. D., 1968, "Mining Applications of the Deep Cut Principle," Mining Engineer, June, pp. 506-517.

Pomeroy, C. D. and Foote, F., 1960, "A Laboratory Investigation of the Relation Between Ploughability and Mechanical Properties of Coal," Colliery Engineering, April, pp. 146-154.

Terry, N. B., 1959, "The Dependence of the Elastic Behavior of Coal on the Microcrack Structure," Fuel, London, 38, pp. 125-146.

Warner, E. M., 1970, "Machine and Cutting Element Design," Mining Congress Journal, August, pp. 35-43.

**II**

**Dilution, Dispersion,  
and Collection of Dust**

o  
l  
e  
c  
t  
t  
r  
c  
c  
c

I

e:  
() B  
F  
m  
u:  
sp  
di  
as  
ar  
or  
ai  
te  
ur  
Se  
ps  
ov  
ra  
ini  
op  
of  
Re

# Experimental Studies on Dust Dispersion in Mine Airways

R. Bhaskar and R. V. Ramani

Department of Mining Engineering, The Pennsylvania State University

**Abstract** – *The spatial distribution of airborne dusts, deposition of dust in the airway, as well as the effect of airflow velocity and particle density on dust behavior in mine airways were studied in a set of experiments performed in a mine airway under controlled conditions. Considerable deposition of dust near the source was indicated. Pronounced effects due to velocity were observed in ambient dust concentration and deposition along the mine airway, both in the respirable and the total size ranges. Cross-sectional concentration measurements indicate an increase in concentration from the roof to the floor. The average cross-sectional concentration is about 75% of the concentration in the center of the airway.*

## Introduction

A number of studies have been performed since the early 1950s on the behavior of dust in mine air (Bradshaw and Godbert, 1954; Dawes and Slack, 1954; Bradshaw et al., 1954; Hall, 1955-56; Reinhardt, 1971; Ford, 1971; Courtney et al., 1982). While the experimental data available from these studies are indeed useful in understanding dust cloud behavior in a specific situation, no generalized conclusions can be drawn because of the lack of data on parameters such as flow velocity, size distribution of the source dust, and particle density. These change from mine to mine or even within the same mine. The present study is aimed at providing a better understanding of the temporal and spatial behavior of dust particles in underground mine airways (National Academy of Sciences, 1980). The characteristics studied encompassed airborne concentrations and floor depositions over the entire size range as well as the respirable size range. The experimental results in this paper are intended to complement a mathematical model developed to predict ambient concentration and deposition of airborne dust in mine airways (Bhaskar and Ramani, 1986).

## Experimental design

The experiments were designed to simulate dust transportation and deposition in mines. They were performed in the D-drift at the Lake Lynn Laboratory of the US Bureau of Mines. Comprehensive description of this experimental mine can be found in Mattes et al. (1983). The drift has a cross section of 2.1 × 6.1 m (7 × 20 ft) and a length of 507 m (1663 ft). About 400 m (1312 ft) of the drift was used in the experiment. In all, six experiments were conducted, with each experiment differing from the others either in the type of dust dispersed or in the velocity of the air in the drift. The experiments are coded as follows:

	Dust Type	Velocity, m/s
Experiment 1	Semianthracite	0.838
Experiment 2	Bituminous	0.838
Experiment 3	Semianthracite	1.855
Experiment 4	Bituminous	1.855
Experiment 5	Semianthracite	1.525
Experiment 6	Bituminous	1.525

For each experiment, 10 to 13 measuring stations were set up, each 30.5 m (100 ft) apart (Fig. 1). The spacing between measuring stations was selected to utilize the maximum possible length of the drift for the

R. Bhaskar and R.V. Ramani, members SME, are research associate and professor of mining engineering, respectively, Department of Mineral Engineering, The Pennsylvania State University, University Park, PA. R.A. Jankowski, member SME, is a physical scientist with the US Bureau of Mines, Pittsburgh, PA. SME preprint 86-140, SME-AIME Annual Meeting, New Orleans, LA, March 1986. Manuscript March 1986. Discussion of this paper must be submitted, in duplicate, prior to May 31, 1988.

experiment. The experiments were designed to provide data for studying:

- variations in ambient concentration (both total and respirable size range) along the length of a typical airway,
- variations in deposition of the dust (both total and respirable size range) along the airway,
- changes in the size distribution of the airborne dust as the cloud travels along the length of the airway,
- variations in dust concentration at various cross sections of an airway, and
- relationship between the average cross-sectional concentration and that in the center of the airway.

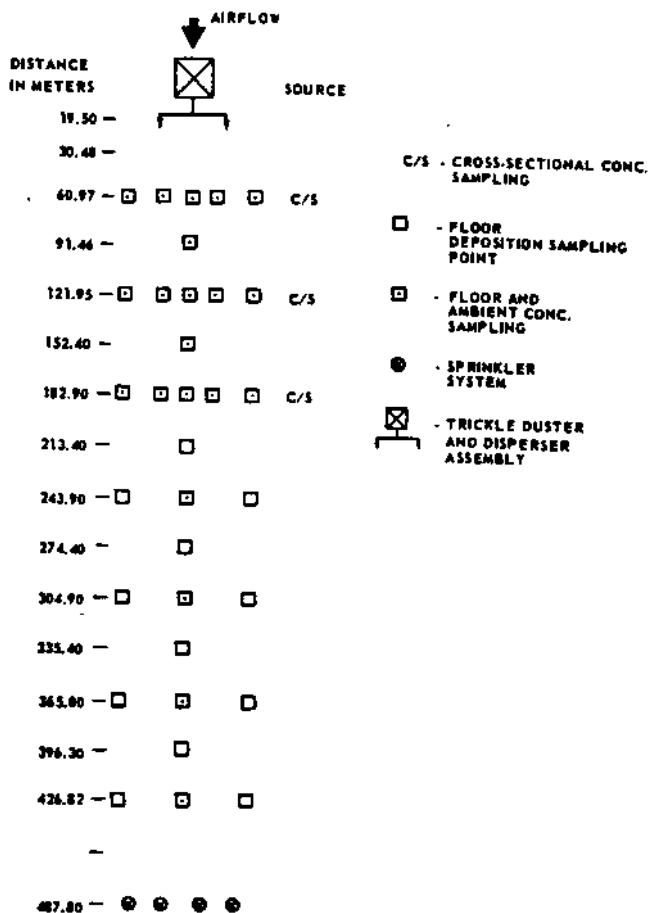


Fig. 1 — Schematic of the airway showing locations of the sampling points (experiment 6)

**Sampling procedures**

Sampling procedures were developed for collecting airborne concentration and floor deposition data.

**Ambient concentration sampling**

Two types of ambient concentration sampling were performed: sampling of air at the center of the airway and cross-sectional sampling. In each experiment,

three measuring stations were selected for detailed cross-sectional sampling. At each cross section, 12 points following the equal area representation method were delineated, and personal gravimetric samplers were set up at these points (Fig. 2). These 12 sampling points were in addition to the sampling point in the center of the cross section.

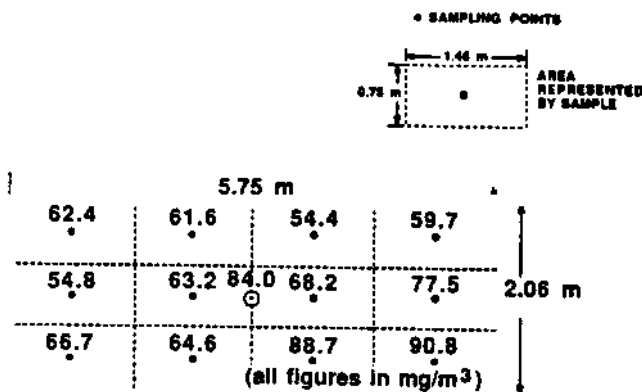


Fig. 2 — Cross-sectional ambient concentration sampling plan

**Isokinetic sampling:** To ensure isokinetic sampling under experimental conditions, specially shaped sharp-edged nozzles were designed and fabricated for use with conventional two-piece personal sampling units to reduce disturbance to the airflow at the point of sampling. By adjusting the pumping rate of the sampling unit, the velocity of the air through the nozzle was matched with the velocity in the airway. This procedure ensures that a representative sample of the mine air concentration is obtained in the cassette. Analysis of the data obtained from the experiments with the Belyeav and Levin (1974) corrections for isokinetic sampling indicated very little correction of gravimetric data for the size distribution of the dusts used in these experiments. If the experiments were performed in calm air, considerable correction would have been required.

To reduce the amount of dust deposited on the inner surface of the tube connecting the nozzle to the cassette, the tube was kept as short as possible. However, the tube was long enough to keep the sampling assembly from interfering with the airflow at the nozzle. The amount of dust deposited on the inner surface of the connector tube was determined and added to the filter weights.

**Filters:** For this study, Nuclepore® filters were considered most suitable for sampling purposes, as the deposited dust would be subjected to gravimetric and size analyses. Compared to conventional filters, Nuclepore filters have a smooth surface, good control of pore sizes, and are nonhygroscopic. These filters also have a lower and more uniform weight but similar flow rate/pressure drop characteristics.

**Pumps:** Constant-volume flow pumps (MSA Fixt Flo and DuPont 2500 series) were used to ensure that pumping rate did not vary with filter loading.

\*The use of specific brand names of products is for illustrative purposes only. This does not imply endorsement by the US Bureau of Mines or The Pennsylvania State University.

# DUST DISPERSION IN MINE AIRWAYS

## Deposition

Deposition plates were placed at the measuring stations along the airway. To ensure that the amount deposited was comparable to that on the floor, flat plates without any lips were used. The absence of lips reduces the formation of eddies near the deposition sampling area. The flat plates were covered with "sharkskin" filter papers, which do not tear easily during sample handling. The rough texture and extremely light weight of the paper (about 2 g, or 0.07 oz, for a 29-cm, or 11-in., diam paper) make it ideally suited for gravimetric analysis.

## Dust source

### Dust generation

The dust was dispersed by a fluidized bed-type trickle duster through a specially designed system of 25-mm (1-in.) diam plastic tubes to four release points in a cross section. The location of the source in the airway (Fig. 1) was dictated by the need to ensure that at the point of release, the airflow is uniform, and that there is good mixing of dust with the air in the drift before the first sampling point.

### Source dust

Two types of dusts (semianthracite and bituminous) were used in the experiments. The size distributions of the two source dusts (Table 1) show a significant proportion of respirable dust. The densities of the semianthracite and bituminous dusts were 1.567 and 1.4 g/m<sup>3</sup>, respectively.

Table 1 — Cumulative Size Distribution of Source Dust

Size* (microns)	Semianthracite (% finer)	Bituminous (% finer)
29.85	100.0	100.0
21.1	100.0	98.0
14.92	94.8	86.0
10.55	86.2	84.0
7.46	73.0	45.6
5.27	53.6	31.6
3.73	36.1	20.5
2.63	21.8	12.7
1.69	12.1	7.4
1.01	5.7	3.5
0.66	2.0	1.3
0.43	0.8	0.2
0.34	0.2	0.0

\* Size analyses performed on Microtrac SPA.

## Sample analysis

The cassettes from the personal gravimetric samplers and the deposition plates were processed at the dust laboratory at The Pennsylvania State University. The mass of dust was measured using a Mettler electronic microbalance. All size distributions were

determined using an X-ray diffraction device (Microtrac small particle analyzer) capable of measuring dust in the 42.21- to 0.17-micron range.

## Results

Several analyses were performed on the experimental data. The results of the following analyses are presented:

- ambient concentration characteristics of the dust cloud in the drift,
- deposition decay curves of the dust cloud,
- effect of velocity on ambient concentration and deposition patterns,
- cross-sectional sampling results, and
- variation in size distribution as the dust cloud traverses the drift and the relation between the velocity of airflow and size distribution of the dust at any point.

### Ambient concentration

The ambient total concentration and ambient respirable concentration of dust along the length of the airway for experiments 1 and 6 are shown in Fig. 3. The respirable concentration is obtained from a size analysis of the total concentration dust. Particles less than 5.27  $\mu\text{m}$  in projected area diameter are taken as respirable. This translates to slightly less than 5  $\mu\text{m}$  aerodynamic diameter. In all the six experiments, ambient total concentrations decrease with distance faster than respirable concentrations, indicating longer residence times in the airflow for smaller particles. The rates of decrease in the concentrations, both total and respirable, are higher in the first 60 m (197 ft) than at greater distances from the source. Also, with distance, the total concentration curves tend toward the respirable concentration curves, showing that most of the larger particles are deposited in the initial portions of the airway.

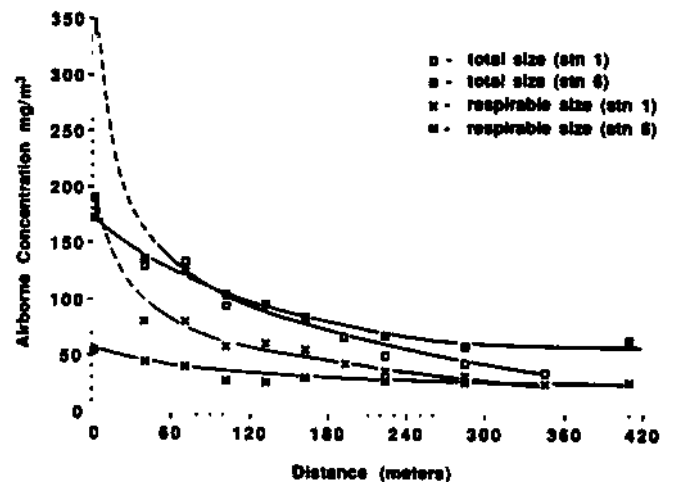


Fig. 3 — Concentration of airborne dust along airway



**Deposition**

Depositions as a function of distance from the source for experiments 1 and 6 are shown in Fig. 4. As one moves away from the source, the total deposition curve approaches the respirable deposition curve, indicating a high proportion of respirable dust in the ambient air. At stations further from the source, both the curves assume an asymptotic form, indicating little change in deposition.

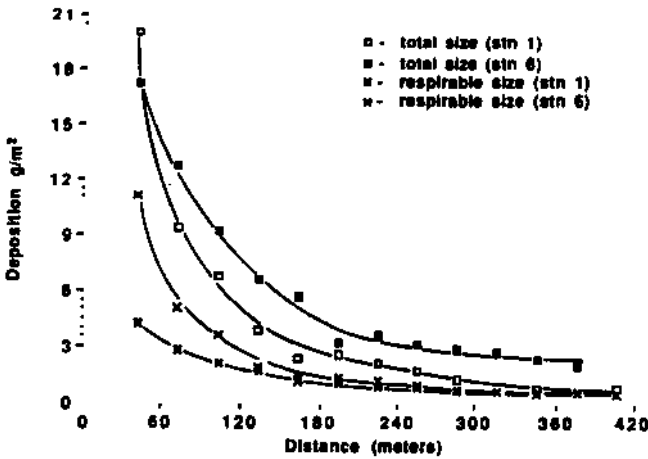


Fig. 4 — Deposition of airborne dust along airway

**Effect of velocity on concentration and deposition patterns**

The concentration and deposition results from experiments 2, 4, and 6 (bituminous dust at three different velocities) are presented in Figs. 5 and 6. The concentration data were normalized with respective concentrations at the first point and expressed as a fraction of those at the first point. With the increase in velocity, the ambient concentration of total dust (Fig. 5) is more even along the airway, a trend that is also seen in the respirable size range (Fig. 6). At velocities of 1.525 and 1.855 m/s (5 and 6.1 fps), concentration curves approach a limit value after some distance from the source, indicating little deposition after that distance. In Figs. 5 and 6, this distance is about 290 m (950 ft). The effect of velocity on total and respirable dust deposition is shown in Figs. 7 and 8, respectively. Again, the curves tend to be flatter at higher velocities though the effects of velocity on depositions is not as dramatic as on ambient concentrations.

**Cross-sectional sampling**

Data from 18 cross-sectional concentration sampling setups (three cross-sectional sampling stations per experiment and six experiments) show that the average concentration across the cross section is 75% of the concentration at the center of the airway, with all the points in the cross section given equal weight. However, the concentration increases as one moves down from the roof to the floor. Specifically, for the consolidated data, the top third of the airway has a concen-

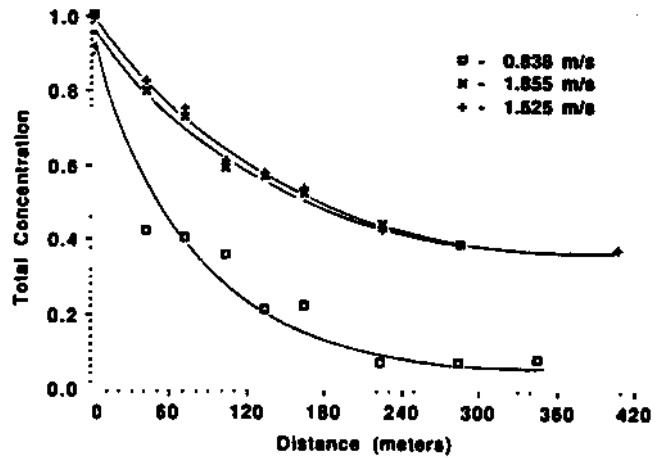


Fig. 5 — Effect of velocity on total airborne concentration (concentration normalized with respect to source concentration)

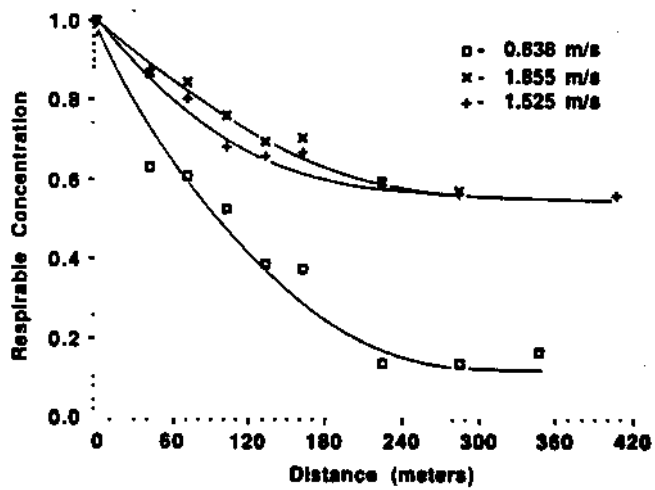


Fig. 6 — Effect of velocity on respirable airborne concentration (concentration normalized with respect to source concentration)

tration 72% of that in the lower third. The concentration in the middle third of the airway is 89% of that in the lower third. An example of the cross-section data is shown in Fig. 2.

**Variation in size distribution**

The change in size distribution of the dust cloud as it traverses the airway is shown in Fig. 9. The data is from experiment 1. Similar analyses were performed for all the experiments. A distinct decrease in the larger-sized particles is indicated by a corresponding shift in the peaks for the 61-, 244-, and 366-m (200-, 800-, and 1200-ft) station ambient concentrations. The change in the shape of the curves in the smaller size range is less compared to that for the larger size. This complements the ambient concentration and deposition data, which show that smaller particles (respirable range) have a reduced rate of deposition.

Total Deposition

Fig. 4

Respirable Deposition

Fig. 5

2

1

1

% Fraction

Fig. 6

dista

# DUST DISPERSION IN MINE AIRWAYS

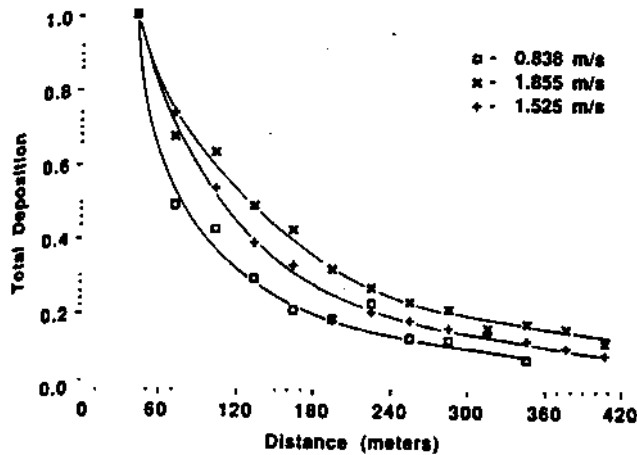


Fig. 7 — Effect of velocity on deposition (total size) (deposition normalized with respect to first sampling station)

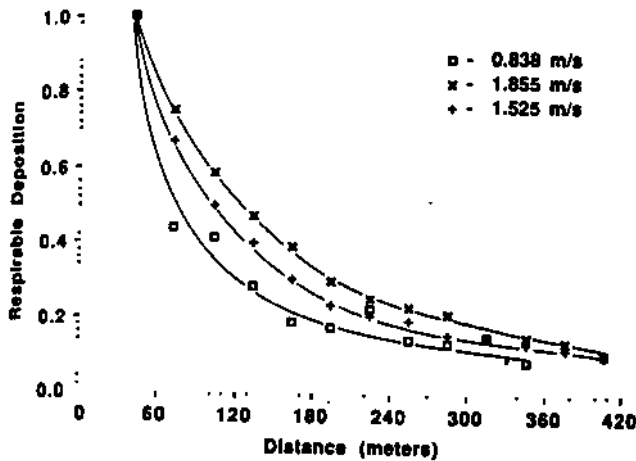


Fig. 8 — Effect of velocity on deposition (respirable size) (deposition normalized with respect to first sampling station)

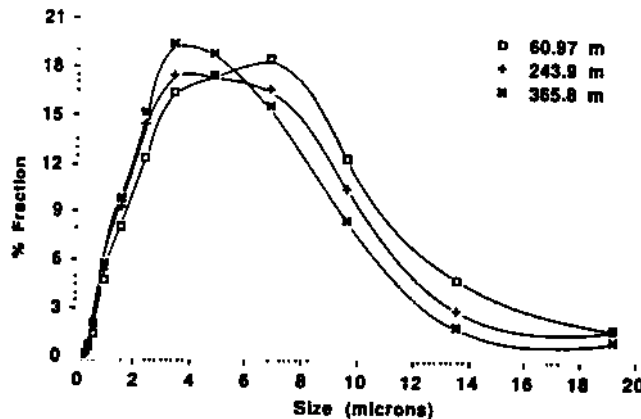


Fig. 9 — Change in size distribution of airborne dust with distance from source (experiment 1)

The size distributions of the dust clouds for 0.838, 1.855, and 1.525 m/s (2.75, 6, and 5 fpe) measured at the 366-m (1200-ft) station are shown in Fig. 10. The data here is also from experiment 1. At the lower velocities, a comparatively less amount of large-sized particles is found. As the velocity increases, larger particles are carried longer distances and, therefore, contribute to a higher concentration of large-sized particles downstream. Therefore, the peaks of the distributions tend to be flatter at high velocities. Again, the effect of velocity on the distribution for the smaller sizes is less noticeable.

## Discussion

The data from the ambient concentration-deposition experiments have enabled quantification of the spatial behavior of airborne dust clouds in mine airways — the decay patterns for ambient total concentration, ambient respirable concentration, and deposition. Experimental studies such as the one presented here are not without problems. For example, some deposition of extremely fine particles was noted on the sides of the airway. In some deposition plates, small pieces of falling roof rock caused distortion in values. Considering the fact that a large number of deposition data were collected, no systematic error contribution from the falling particles was noticed.

Errors in the ambient concentration data can result from variations in pump rate during the experiment as well as calibration, deviation from isokinetic sampling principles, and static charge effect during weighing. Pumps calibration errors of  $\pm 10\%$  may occur. During the correction of concentration data for non-isokineticity, a correction of  $+8\%$  to  $-11\%$  was necessary for a few samples. However, no major errors were found in the concentration data, lending credence to the validity of the experimental design, sampling procedures, and sample analyses techniques. ■

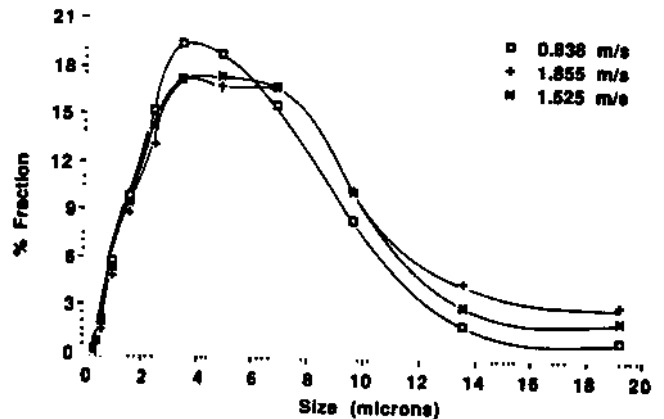


Fig. 10 — Size distribution at 365.8-m station at different velocities (experiment 1)

**Acknowledgments**

The cooperation of the staff of the Ventilation Group, Pittsburgh Research Center, US Bureau of Mines, the staff at the Lake Lynn Laboratory, and the Department of Mineral Engineering is gratefully acknowledged.

The research reported in this paper was supported under the Mineral Institutes Program by Grant No. G1185142 from the Bureau of Mines, US Department of the Interior, as part of the Generic Mineral Technology Center for Respirable Dust at The Pennsylvania State University.

**References**

Belyaev, S.P., and Levin, L.M., 1974, "Techniques for Collection of Representative Aerosol Samples," *Journal of Aerosol Sciences*, Vol. 5, No. 4, pp. 325-338.  
 Bhaskar, R., and Ramani, R.V., 1966, "Behavior of Dust Clouds in Mine Airways," *Trans. SME-AIME*, Vol. 260, pp. 2051-2059

Bradshaw, F., and Godbert, A.L., 1954, "The Deposition of Dust in Return Airways," Research Report No. 92, SMRE, p. 37.  
 Bradshaw, F., Godbert, A.L., and Leach, E., 1954, "The Deposition of Dust Conveyor Roads," Research Report No. 106, SMRE, p. 82.  
 Courtney, W.G., Koel, J., and Colinet, J., 1962, "Dust Deposition in Coal Mine Airways," Technical Progress Report 118, US Bureau of Mines.  
 Dawes, J.G., and Slack, A., 1954, "Deposition of Airborne Dust in a Wind Tunnel," (Interim Report) Research Report No. 105, SMRE.  
 Ford, V.H.W., 1971, "Experimental Investigations into the Dispersion and Transport of Respirable Dust in Mechanised Coal Mining," PhD Thesis, University of Newcastle Upon Tyne, June.  
 Hall, D.A., 1955-56, "Factors Affecting Airborne Dust Concentrations with Special Reference to the Effect of Ventilation," *Trans. Institution of Mining Engineers*, Vol. 115, pp. 245-269.  
 Mattes, R.H., Bacho, A., and Wade, L.W., 1963, "Lake Lynn Laboratory: Construction, Physical Description, Air Capability," BuMines I.C. 6011, p. 40.  
 National Academy of Sciences, 1960, "Measurement and Control of Respirable Dust in Mines," Report of the Committee on Measurement and Control of Respirable Dust, NMAB 363, p. 405.  
 Reinhardt, M., 1971, "Untersuchungen in Strecken über das Verhalten von Staub in Grubenwettern," *Glückauf-Forschungshefte*, Vol. 33, No. 1, pp. 19-32 ("Studies in Mine Roads on the Behavior of Dust in Air Currents," NCB Translation, A.2945/AL).

re:  
pli  
de  
wa

# Theoretical and Experimental Studies on Dust Transport in Mine Airways: A Comparative Analysis

R. V. Ramani and R. Bhaskar

Department of Mining Engineering, The Pennsylvania State University

## Introduction

The behavior of dust clouds in mine atmospheres has been a subject of longstanding interest due to both health and safety reasons. Pioneering studies in Germany and SMRE focussed on ambient dust concentration, principally aimed at determining optimum velocities for effective dilution. A summary of studies related to this area is provided by Hall.<sup>(1)</sup> Efforts to understand dust deposition from the explosion hazard point of view led to experiments in return airways<sup>(2-4)</sup> followed by experiments in longwalls.<sup>(5)</sup> Concerted efforts, either experimental or theoretical, were not made until recently to relate ambient concentration with dust deposition in mines. In 1974 Hwang *et al.*<sup>(6)</sup> developed a computer model to predict dust concentration which considered deposition-concentration relationships. Also, experimental studies involving concurrent dust deposition and ambient concentration were conducted in the U.S. by Courtney *et al.*<sup>(7)</sup> in operating mines. Efforts to relate theory with experimental results have been made by Owen<sup>(8)</sup> and Hwang *et al.*<sup>(6)</sup> for dust deposition. There has been limited work, however, to determine the application of the theories and assumptions from aerosol sciences for modeling dust flows in mine atmospheres.<sup>(9)</sup> This is the objective of the work currently underway in the Generic Technology Center on Respirable Dust since 1983 under a project titled, "Prediction of Ambient Dust Concentration in Mine Atmospheres." The scope of the project activities include:

1. Development of a mathematical model to predict dust deposition and concentration in mine atmospheres.
2. Experimental studies on dust transport and deposition in mine airways.
3. Comparison of the model results with the experimental data.

The specific objective of this paper is to present the results of the comparative analysis and to examine the applicability of the various mechanisms used in the model to describe particle behavior with respect to flow in mine airways.

## Mathematical Modeling

In the first phase of the project, a mathematical model was developed for studying the behavior of dust clouds in mine airways (Figure 1). The model was designed to predict

1. Dust deposition along the length of an airway.
2. Ambient concentration at various points in a mine airway.
3. Size distribution of dust at various points in the airway.

The model takes into account a number of factors affecting dust transport, including source dust characteristics (amount, size distribution, density), airway characteristics (size, shape, length, friction factor), airflow characteristics (velocity, viscosity, temperature, dispersion) and coagulation of dust in mine airways.<sup>(10)</sup>

Since the size-dependent behavior of dust in mine airways is the major difference between dust flows and gas flows, considerable attention was focussed on those mechanisms which are size-dependent. In fact, the principal part of modeling was devoted to modeling the dust deposition phenomenon. The three major mechanisms of particle deposition in turbulent flow that were modeled are Brownian and eddy diffusion, and sedimentation. While all three mechanisms were used to predict deposition on the floor, Brownian and eddy diffusion were considered for the roof and sides of the airway. Coagulation was considered as a mechanism that affects the size distribution and hence deposition rate. The transfer of dust in turbulent air flow was described using a dispersion coefficient developed by Skubunov.<sup>(11)</sup> A step type function describes the dust emission from the source as a function of its operating duty cycle. The concentration is determined from the numerical solution of a convection-diffusion population balance equation.

A computer program was developed to solve the equation for various size classes with applicable size-dependent relationships for each class. The overall behavior of the dust cloud is obtained as the sum effect of the individual size classes. The ambient concentration was calculated from a mass-

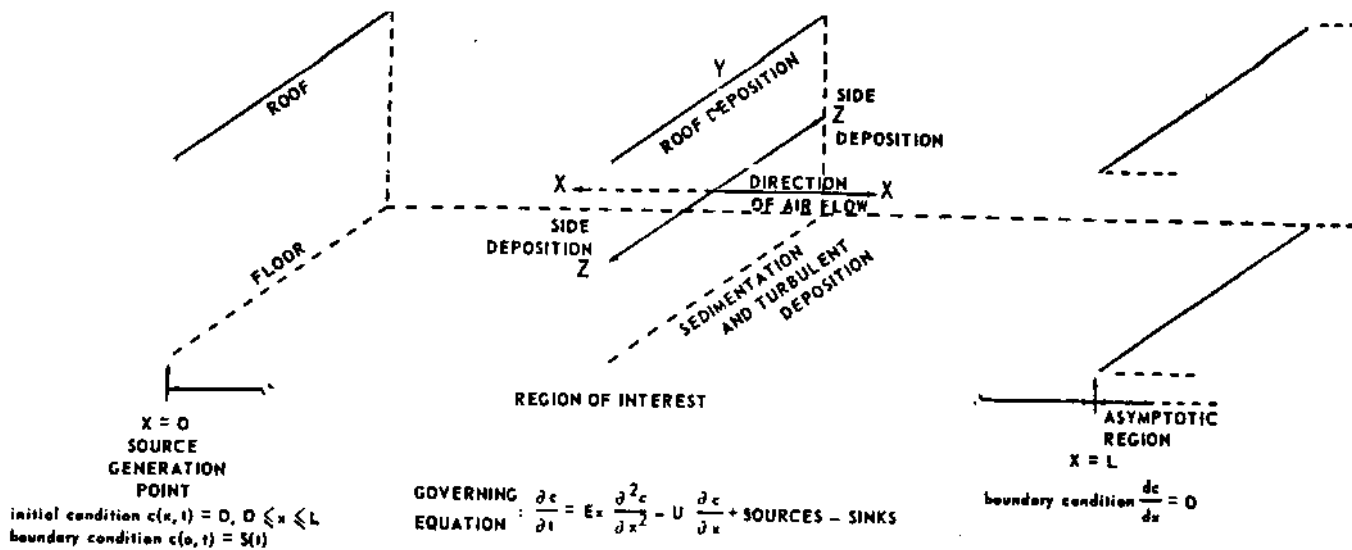


FIGURE 1. Schematic of dust flow in a mine airway.

balance of the convection-diffusion equation describing the concentration change. Sensitivity analysis of the model parameters was performed to identify the relative importance of various factors in the model.

**Experimental Work**

To complement the theoretical work and to compare the model prediction with actual behavior, a set of experiments were conducted at the Lake Lynn Laboratory Mine of the U.S. Bureau of Mines (Figures 2 and 3). Six tests using two types of dust at three different velocities for each coal type were performed (Table I).<sup>(10)</sup>

Ambient concentration and floor deposition of dust were measured for the period dust was dispersed. The experimental data were analyzed to yield the following information: 1) variations in ambient concentration (both total and respirable size range) along the length of the airway, 2) variations in deposition of the dust (both total and respirable size range) along the length of the airway, 3) changes in the size distribution of the airborne dust as the cloud travels in the airway, 4) variations in dust concentration across the airway at three different stations, 5) variations in dust deposition across the airway at different stations, 6) relationship between the average cross-sectional concentration and the concentration in the center of the airway, and 7) relationship between the average deposition in an airway cross section and the deposition in the center.

**Comparative Analysis**

The experimental data and results provided not only a better understanding of spatial and temporal behavior of dust in mine airways but also a comprehensive set for evaluation of the mathematical model of dust flows.

For the purposes of the comparative analyses, the model is used to predict the ambient concentration and dust

deposition along the airway. The inputs to the model were derived from the experimental conditions and included source dust characteristics, mine airway characteristics, and mine airflow characteristics.

*Source Dust Characteristics*

The description of the source dust involved determining the maximum, minimum, median size, and standard deviation of the source dust, as well as its density, release rate, and time duration of dust release. Due to the relatively high concentration of dust released at the source, some of the dust

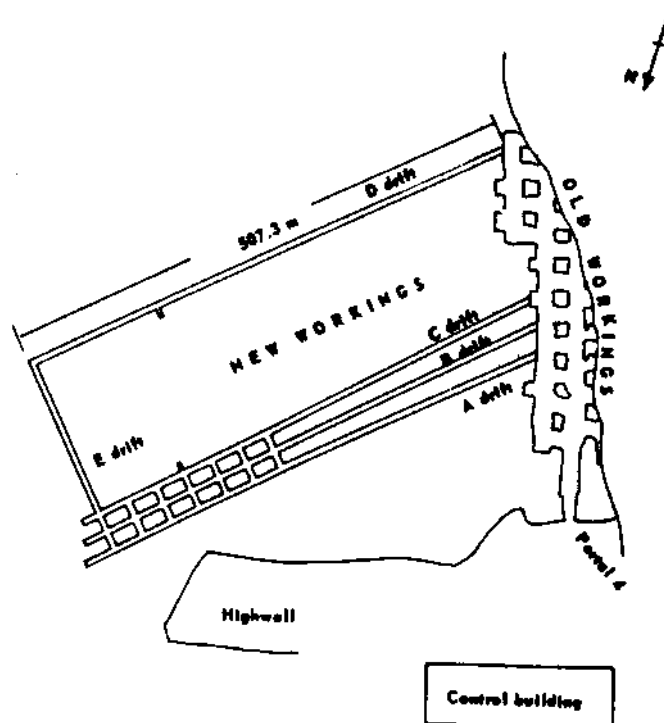


FIGURE 2. Plan view of Lake Lynn Laboratory underground workings.

# DUST TRANSPORT IN MINE AIRWAYS

TABLE I  
Salient Details of Controlled Experiments

Experiment	Dust Type	Velocity, m/s
Experiment 1	Semi-anthracite	0.838
Experiment 2	Bituminous	0.838
Experiment 3	Semi-anthracite	1.855
Experiment 4	Bituminous	1.855
Experiment 5	Semi-anthracite	1.525
Experiment 6	Bituminous	1.525

failed to get mixed in the air and settled just beneath the source. Approximately eighteen percent of the dust released by the dispenser did not get airborne. This is taken into account when determining model source input.

### Mine Airway Characteristics

The mine parameters input to the model are the dimensions and the friction coefficient. The friction coefficient was determined using an altimeter survey. The dispersion coefficient used in the model is obtained from the work of Skubunov<sup>(11)</sup> The dispersion coefficient assumes that particulate transfer in airflow is independent of particle size.

### Mine Airflow Characteristics

The flow conditions were represented by the average flow velocity, air temperature and viscosity of air.

### Observations on Experimental Results

The experiments revealed several findings which are significant for comparing model results with experimental results.

1. The cross-sectional data indicated that the average concentration in the mine airway was approximately 75 percent of the concentration in the center of the airway. The model assumes thorough mixing and equal concentration across the airway. This difference is taken into account by multiplying centerline concentration obtained from experiments by a factor of 0.75.
2. Similarly, floor deposition data showed an increased deposition in the center of the airway than at the sides. Experiment and station specific factors were used to relate centerline to average readings. At stations where such factors could not be determined because only one deposition plate was used, the factor used was the average of those of the station preceding and the station following.
3. While every effort was made to ensure isokinetic sampling of dust, deviation from isokinetic sampling occurred for some experiments and stations. All the ambient concentration data were adjusted to account for deviations from isokinetic sampling using procedures described by Belyaev and Levin.<sup>(12)</sup>

4. In the experiments, dust was dispersed at four points, each in the center of a quadrant in the airway cross section. This resulted in less than complete mixing for some distance from the source. Therefore, for comparative purposes, emphasis is placed on data collected at stations farther from the source.

## Results

The ambient concentration and dust deposition along the length of the airway as observed in experiments were compared with the model predictions. The comparisons were made for both the total and respirable size ranges.

### Ambient Total Concentration

The experimental data and corresponding model output for ambient concentration ( $\text{mg}/\text{m}^3$ ) are shown respectively for the six experiments in Figures 4 through 9. Experiments 1 and 2 were performed at 0.838 m/s, 3 and 4 at 1.855 m/s, and 5 and 6 at 1.525 m/s. The model output in Figures 4, 5, 7, and 9 are, in general, in agreement with the experimental data for total dust except for the first two stations. Thereafter one notices an exponential decline in model output, tracking the experimental data points to approximately 300 meters. Thereafter, the experimental points tend to be flat while the model output continues its decline. Comparison of model output and experimental data for experiments 3 and 5 shows the experimental data to be consistently lower than model predicted values.

### Ambient Respirable Concentration

In the model, respirable dust is assumed to be made up of particles less than or equal to 5  $\mu$ . Therefore, for comparative purposes, the amount of dust in the 5  $\mu$  and below ranges in the total dust from the experiment is considered respirable dust. The respirable concentrations are also shown in Figures 4 through 9. The experimental results and model outputs are in better agreement closer to the source than away from the source. In fact, in all the experiments, the respirable concentration becomes asymptotic whereas the model continues to show a decline in concentration. Also, the observed respirable concentrations are higher than the predicted concentration.

### Deposition (Total and Respirable)

The experimental results and model outputs for total and respirable deposition and shown in Figures 10 through 15. In general, good agreement is obtained between model output and experimental data testifying to the appropriateness of the deposition equations used in the model. Deposition data in the respirable range is also in close agreement with model output, barring the first two points.

## Discussion

Several points with respect to the model and experimental results are to be stressed. The model uses a single dispersion coefficient for all particles sizes. This may not necessarily be the case since smaller particles tend to follow the airstream more closely than larger particles and hence

# THE RESPIRABLE DUST CENTER

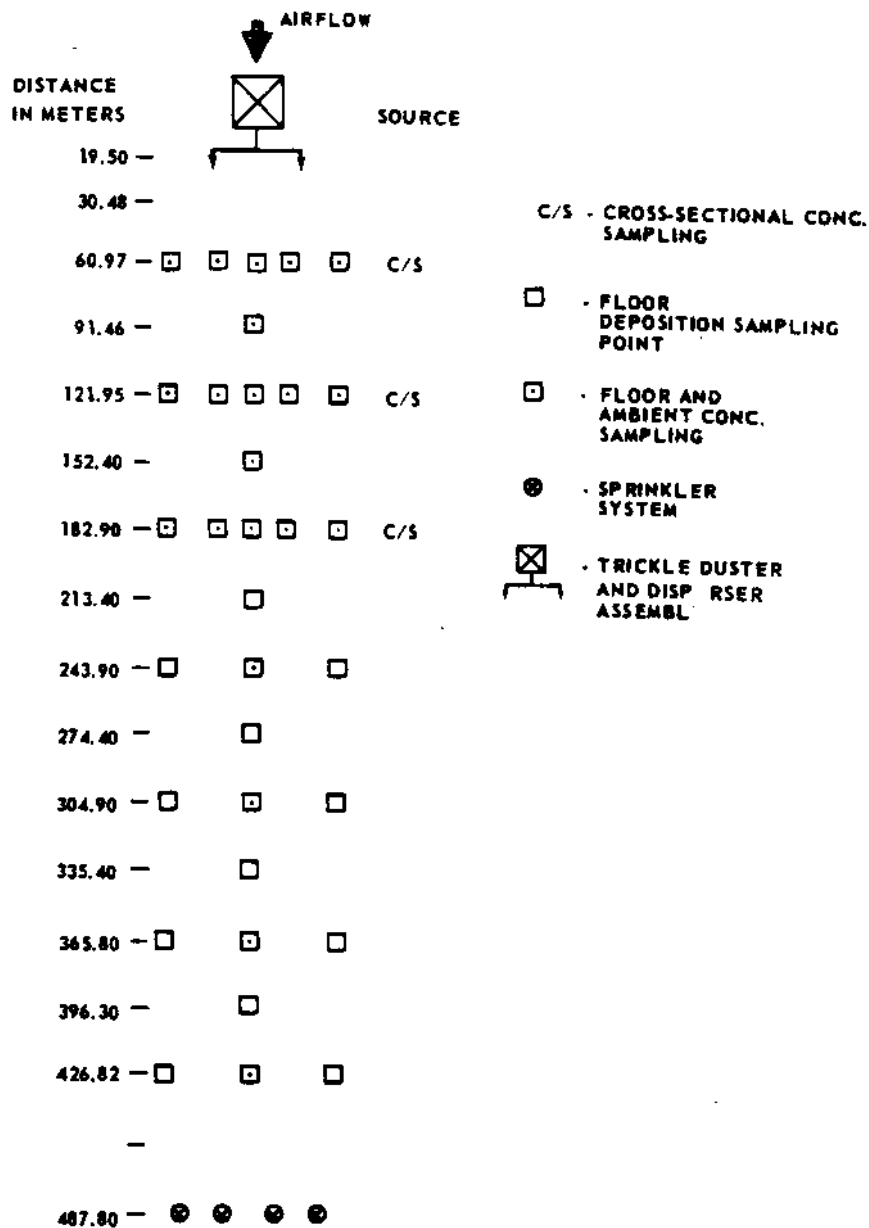


FIGURE 3. Schematic of the airway showing the location of the sampling points (Experiment 6).

are carried longer distances. This may result in higher concentration of fine dust downstream than predicted by the model. But, large particles have greater inertia and will tend to be less affected by flow fluctuations. Hodgkinson and Leach<sup>(13)</sup> present data that show considerable difference between theoretically predicted dispersion coefficients and values determined from experimental data. Research is needed on determining the influence of density and size of particulate matter on dispersion.

The deposition data collection and analysis procedures ensure more accurate results than those used for ambient concentration data. The latter is influenced by several factors such as pumping rate, cross-section concentration variation and flow velocity fluctuation. In practice, high coefficients of variation have been reported. In addition, the

model uses the deposition data and predicts the concentration at the following station using mass-balance whereas the experimental data will include any reentrainment which may occur between two stations. Since the forces required to entrain a deposited particle back into the airstream is dependent on particle size, smaller particles will have a higher propensity to enter the airstream thereby resulting in higher levels of ambient respirable concentration, especially at higher velocities. Also, re-entrainment from the sides and roof may be higher primarily because of the noninfluence and positive influence of gravity respectively in dislodging the adhering particles.

A preliminary examination of the ambient concentration and deposition data reveals that for each size class as measured by the Microtrac Small Particle Analyzer, the

# DUST TRANSPORT IN MINE AIRWAYS

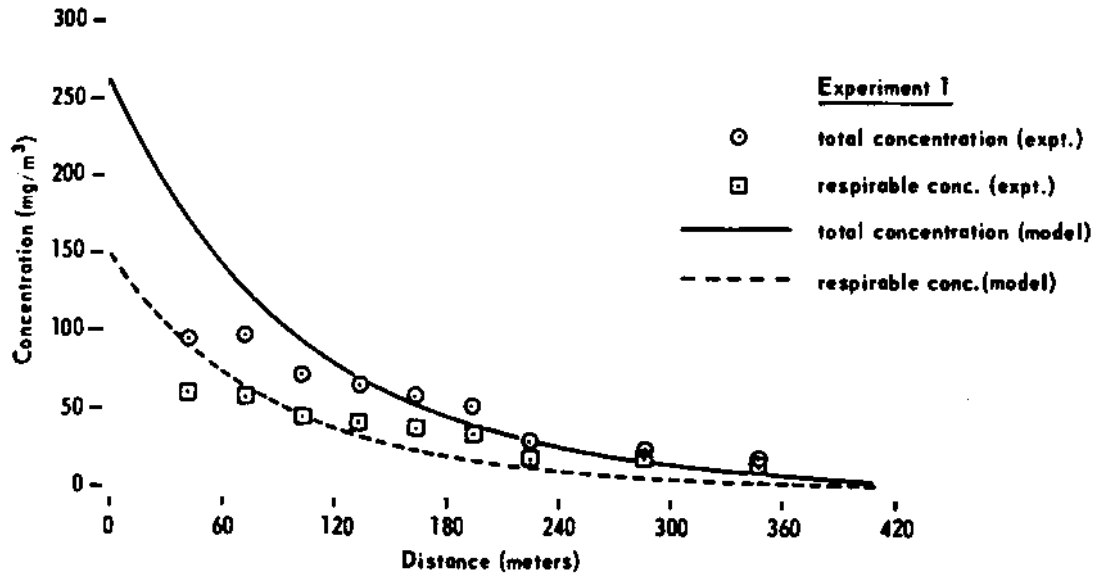


FIGURE 4. Comparison of model predicted ambient concentration with experimental data (Experiment 1).

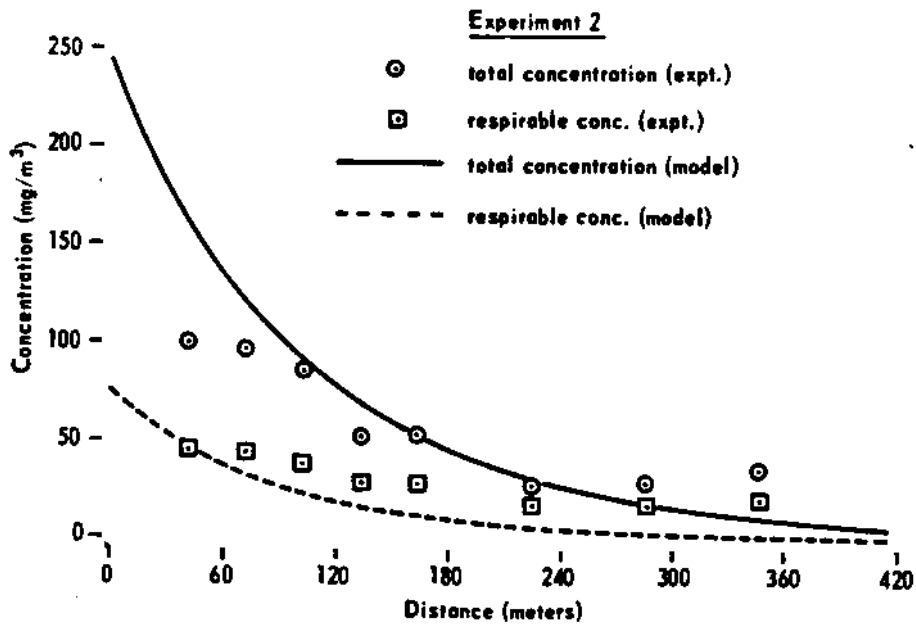


FIGURE 5. Comparison of model predicted ambient concentration with experimental data (Experiment 2).



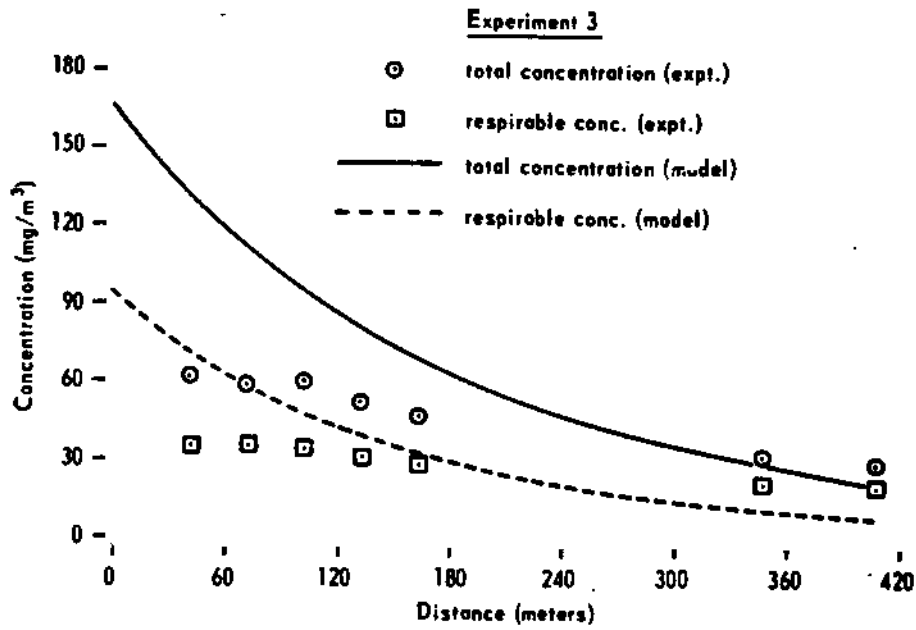


FIGURE 6. Comparison of model predicted ambient concentration with experimental data (Experiment 3).

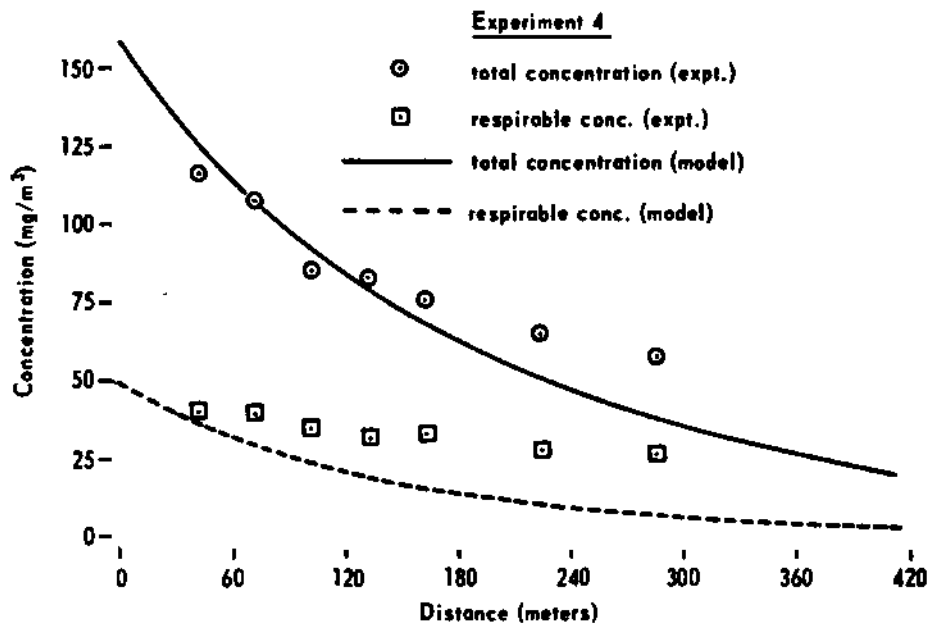


FIGURE 7. Comparison of model predicted ambient concentration with experimental data (Experiment 4).

## DUST TRANSPORT IN MINE AIRWAYS

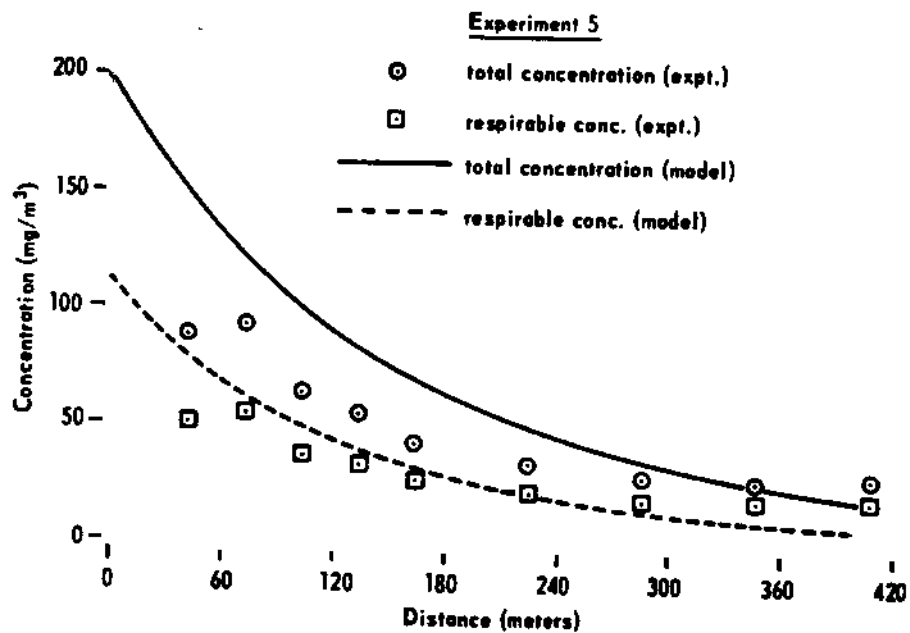


FIGURE 8. Comparison of model predicted ambient concentration with experimental data (Experiment 5).

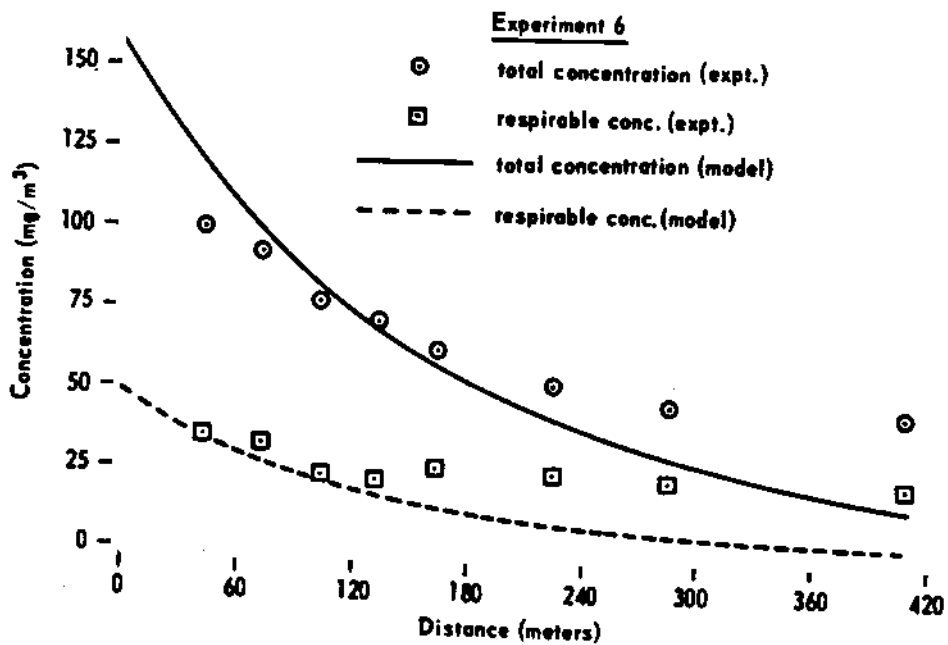


FIGURE 9. Comparison of model predicted ambient concentration with experimental data (Experiment 6).

# THE RESPIRABLE DUST CENTER

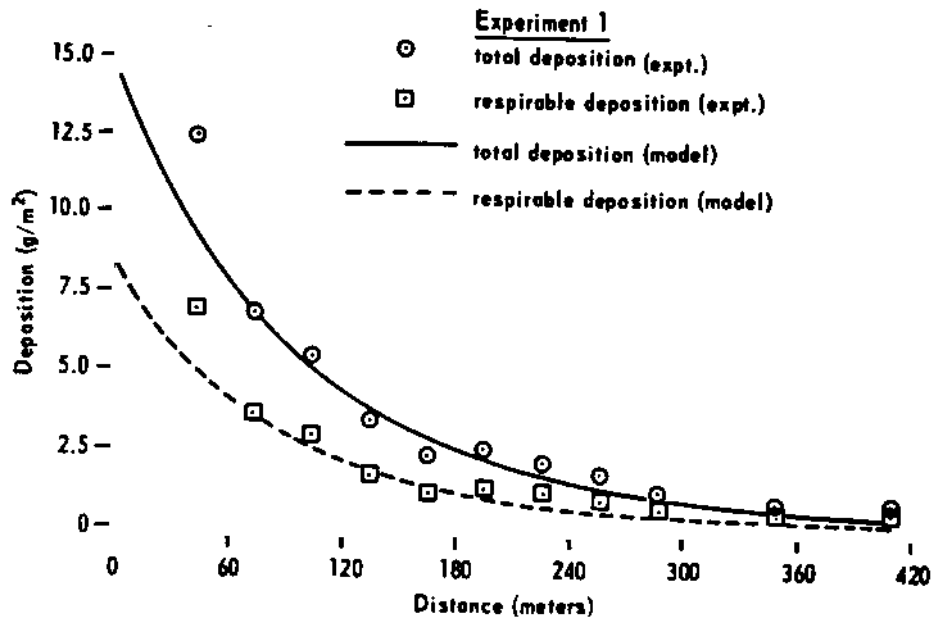


FIGURE 10. Comparison of model predicted floor deposition with experimental data (Experiment 1).

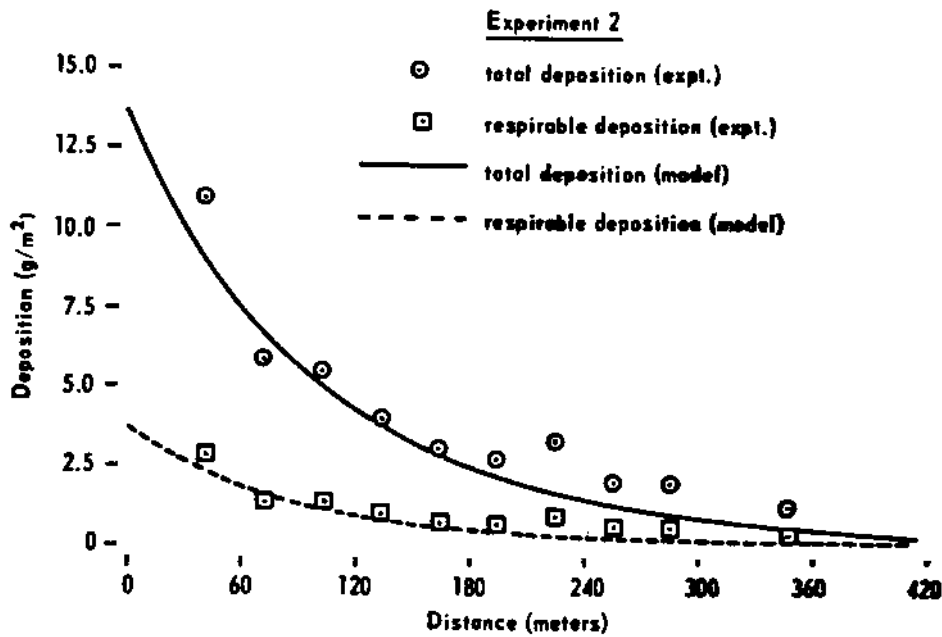


FIGURE 11. Comparison of model predicted floor deposition with experimental data (Experiment 2).

# DUST TRANSPORT IN MINE AIRWAYS

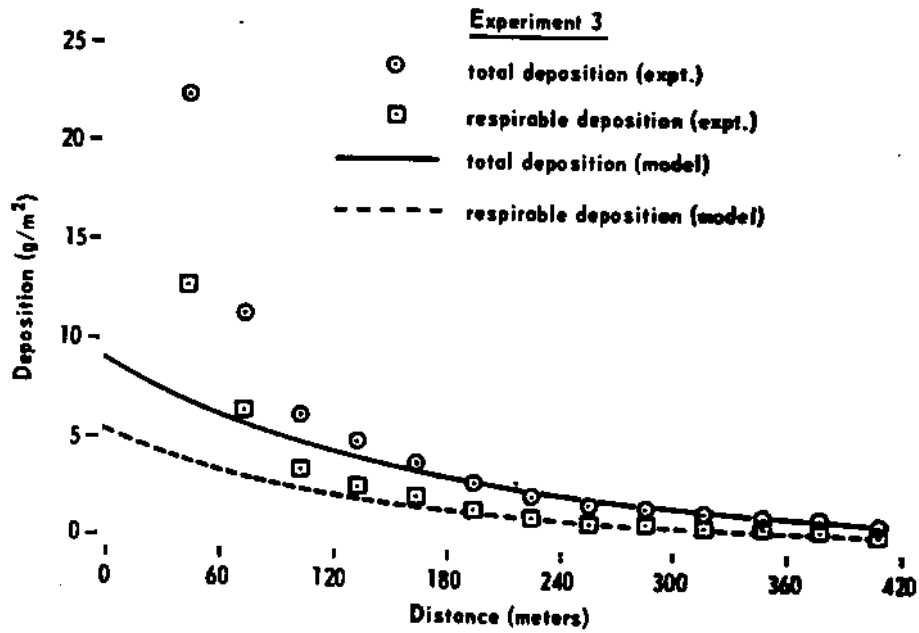


FIGURE 12. Comparison of model predicted floor deposition with experimental data (Experiment 3).

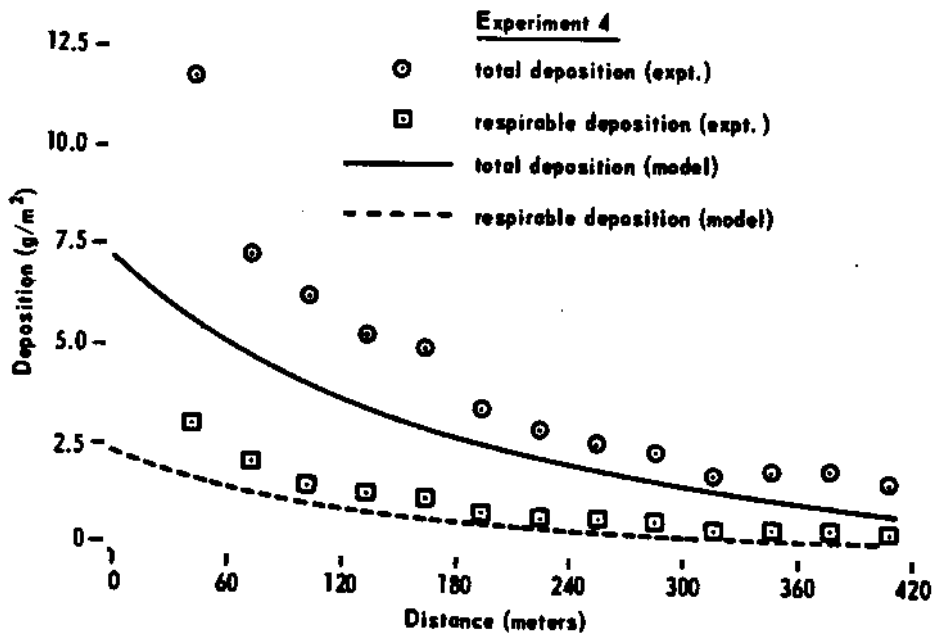


FIGURE 13. Comparison of model predicted floor deposition with experimental data (Experiment 4).

THE RESPIRABLE DUST CENTER

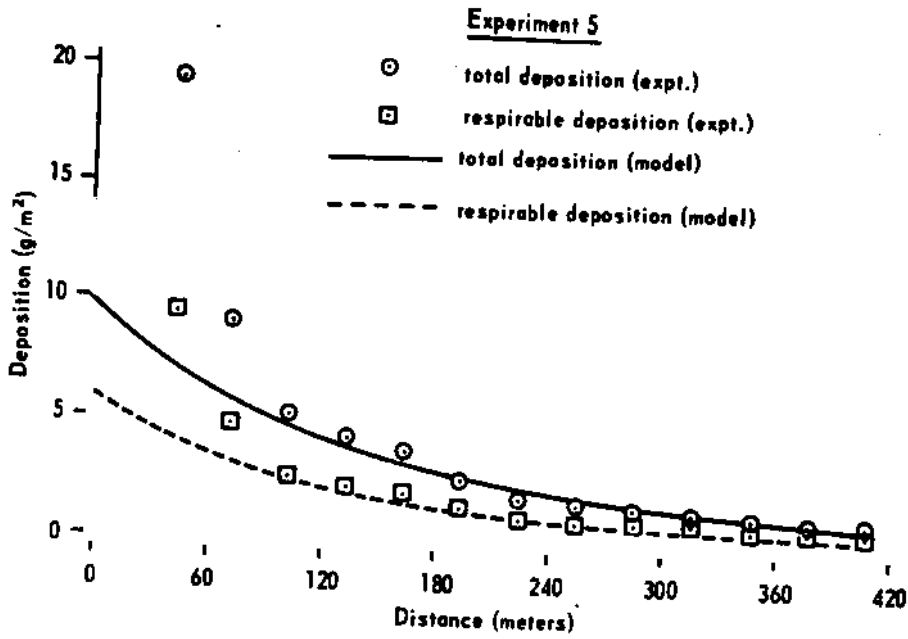


FIGURE 14. Comparison of model predicted floor deposition with experimental data (Experiment 5).

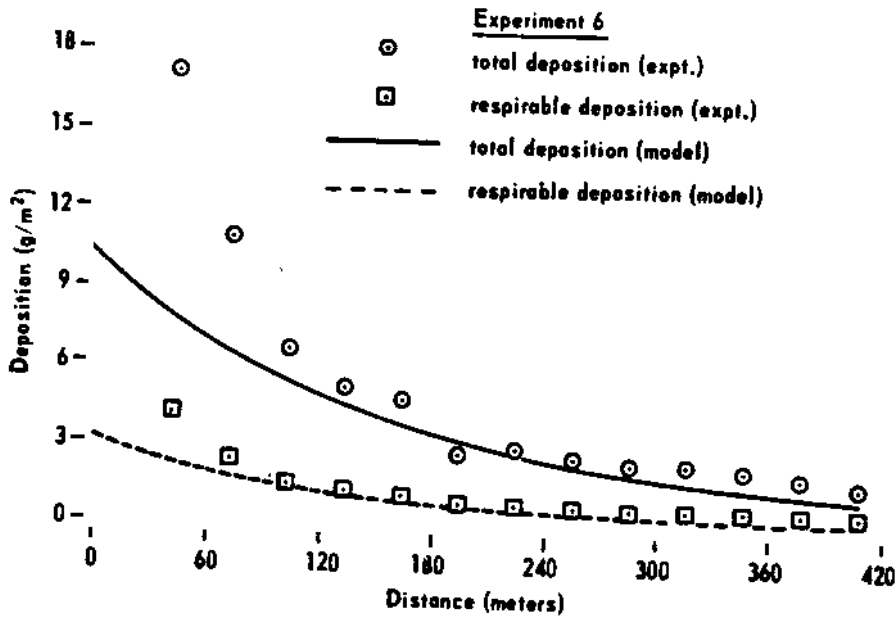


FIGURE 15. Comparison of model predicted floor deposition with experimental data (Experiment 6).

deposition rate, i.e., deposition ( $\text{mg}/\text{m}^2/\text{sec}$ ) to ambient concentration ( $\text{mg}/\text{m}^3$ ), for all sizes is highest at the first station and decreases nonlinearly with decreasing concentration. In the model, deposition rate for a particular size is assumed a constant for a set of experimental parameters.

### Summary and Conclusions

This paper has presented the results of a study into the spatial and temporal behavior of dust in mine airways using both theoretical and experimental studies. A mathematical model was developed to predict the ambient concentration and deposition in a mine airway as a function of the characteristics of the dust source mine airway and airflow. Six experiments were designed and conducted in a mine airway to study dust transport and deposition phenomena as well as to generate data to examine the conceptual and computational aspects of the model.

The results of the comparative analysis are as follows:

1. The model predicted deposition is in good agreement with experimental data in both the respirable and total size range.
2. The model appears to predict total concentrations better at lower velocities of flow.
3. At distances farther from the source the prediction is better for the total size range than for the respirable size range.
4. The model appears to predict respirable concentration closer to the source better than at distances farther from it.

The experimental data reveals that the deposition rate may be a function of concentration and that recirculation may be contributing to the ambient dust concentration. The effect of these mechanisms, as well as others, on particle behavior in mine airways, particularly in the respirable size range, needs to be further examined.

### Acknowledgments

The cooperation of the staff of the Ventilation Group, Pittsburgh Research Center, U.S. Bureau of Mines, the staff at the Lake Lynn Laboratory, and the Department of Mineral Engineering is gratefully acknowledged.

The research reported in this paper was supported under the Mineral Institutes Program by Grant No. G1135142 from the Bureau of Mines, U.S. Department of the Interior, as part of the Generic Mineral Technology Center for Respirable Dust.

### References

1. Hall, D.A.: Factor Affecting Airborne Dust Concentrations, with Special Reference to the Effect of Ventilation. *Trans. Inst. Min. Eng.* 115:245-269 (1955-56).

2. Bradshaw, F. and A.L. Godbert: The Deposition of Dust in Return Airways. *Research Report No. 92*, SMRE:37 (1954).
3. Bradshaw, F., A.L. Godbert and E. Leach: The Deposition of Dust on Conveyor Roads. *Research Report No. 106*, SMRE:62 (1954).
4. Dawes, J.G. and A. Slack: Deposition of Airborne Dust in a Wind Tunnel (Interim Report). *Research Report No. 105*, SMRE:41 (1954).
5. Ford, V.H.W.: Experimental Investigations Into the Dispersion and Transport of Respirable Dust in Mechanized Coal Mining, Ph.D. Thesis, University of Newcastle upon Tyne, pp. 227 (June 1971).
6. Hwang, C.C., G.E. Geiger and P. Radulovic: *Dust Concentration Simulator for Mine Ventilation Systems for Coal Mines*, pp. 186-238. NTIS PB 213833 (1972).
7. Courtney, W.G., J. Kost and J. Collinet: Dust Deposition in Coal Mine Airway. *Technical Progress Report 116:15*. U.S. Bureau of Mines (1982).
8. Owen, P.R.: *Dust Deposition from a Turbulent Airstream. Aerodynamic Capture of Particles*, pp. 3-24. E.G. Richardson, Ed. Pergamon (1960).
9. Bhaskar, R. and R.V. Ramani: Behavior of Dust Clouds in Mine Airways. *SME Preprint 85-154*, accepted for publication in *SME Trans:10* (1985).
10. Bhaskar, R., R.V. Ramani and R.A. Jankowski: Experimental Studies on Dust Dispersion in Mine Atmospheres. *SME Preprint 11:86-140* (1986).
11. Skubunov, V.V.: Turbulent Transport Coefficients for Mine Workings and Tunnels. *Soviet Mining Science* 9:402-412 (1973).
12. Belyaev, S.P. and L.M. Levin: Techniques for Collection of Representative Aerosol Samples. *Aerosol Sci.* 5:325-338 (1974).
13. Hodgkinson, J.R. and S.J. Leach: The Longitudinal Dispersion of Pulses of Respirable Dust on Gas in Ventilated Mine Workings, studied by a Radioactive Tracer Technique. *Trans. Inst. Min. Eng.* 117:683-702 (1957-58).

# Air Velocity Distribution Measurements on Four Mechanized Longwall Coal Faces

S. S. Peng and H.S. Chiang

Department of Mining Engineering, West Virginia University

## Summary

Air velocity distribution surveys on four mechanized longwall faces are presented and discussed. Although there are discernible patterns in the velocity distribution, there are wide differences in distribution in the cases examined. This can be attributed to differences in mining and face geometry. An important factor is air leakage into the goaf.

*Keywords:* Longwall mining; airborne dust; air velocity distribution; mine ventilation.

## Introduction

Over the past two years several intensive air velocity surveys have been carried out in West Virginia coal mines as part of a programme aimed at understanding dust transport mechanisms on mechanized longwall faces. These are presented here and some of the patterns of velocity distribution are discussed.

## Ventilation survey methodology

The air velocity vector consists of three mutually perpendicular subvectors; the vertical subvector is directed toward the roof, one of the horizontal subvectors is parallel to the coal face and the other pointing to the gob. The air velocity which was measured in this paper is the horizontal subvector parallel to the coal face.

To record the velocity distributions at the longwall faces, the surveying stations and the surveying points were established as follows.

(1) The first station usually was set at the third support from the headentry T-junction. Within the first few supports, the air coming from the intake airway encounters a sharp right-angle turn at the T-junction, and forms a turbulent region close to the coal face. The intake air in this region is also influenced by the motors that drive the face conveyer. But when the air reaches the different. But for the same face the number was the same. The main air-travelling area was divided into six to 12 equally sized sub-areas, and each surveying point was situated approximately at the centre of the sub-area.

The velocity survey was carried out by two persons, one reading the meter and the other taking down the readings. A complete survey at one station took about 5–8 min. Usually, the dimension of the cross-sectional area was measured during that time.

A third person used the smoke tubes to observe the following: (1) the air movement patterns at different locations; (2) the extent and the direction of the air leakage; and (3) the machines'

## AIR VELOCITY DISTRIBUTION MEASUREMENTS

influence on the main airflow. At the same time he observed and recorded the roof conditions and the compactness of the roof-caving in the gob.

### Ventilation survey - results and analysis

Two steps of data reduction were carried out. The first step was to convert the velocity readings into air quantity:

$$Q = V_m A \quad (1)$$

where:  $Q$  = air quantity

$A$  = equivalent ventilation area,

$V_m$  = average air velocity which is defined as

$$V_m = \frac{1}{N} \sum_{i=1}^N V_i \quad (2)$$

$N$  = number of survey points at one station,

$V_i$  = velocity reading at the  $i$ th point.

The equivalent ventilation area was obtained by plotting the face cross-sectional profile on a grid paper, counting the number of the squares covered by the travelling space and multiplying the number by the area of the unit square. The area behind the front legs and before the caving shields was discounted since this region was partially occupied by pipes, tubes and gauges, and since the velocity of the air flowing in this region was much slower than that in the main ventilation area.

The air quantities along each face are plotted in Fig. 2. The plots show that although there are variations between rounds and between faces, some general trends exist. For convenience, the face line is the X-axis with the headentry T-junction as the origin, and the unit is expressed by the number of supports. The analyses of air quantity distribution in the longwall face area are based on the initial air quantity measured at the first survey station, i.e. the third support. Usually, the air quantity at the third support was approximately 75–90% of the total initial air quantity measured outby the headentry T-junction.

### Detailed observations for each face

*Panel No. 1.* The Eagle seam was 1.5–1.8 m thick. The immediate roof consisted of sandy shale and gray shale about 0.6–0.9 m thick. It appeared to be sufficiently stable with the roof beam third support, its direction has almost turned parallel to the coal face. Thus from this point on, the air flow becomes normal.

(2) The second station was set at the eleventh support and the subsequent stations at every other tenth support. The requirements for the survey accuracy and the time needed to accomplish a complete survey were taken into consideration in the selection of station location.

(3) The last station was usually set at the third support from the tailentry T-junction.

(4) Six to 12 surveying points at each station were arranged on the cross-section perpendicular to the coal face (Fig. 1). For different faces, the numbers of surveying points were overhanging about 0.9 m–1.5 m in the gob. However, the immediate roof fell periodically with a short delay after the support advance. Before the immediate roof caved, there was a free-opening about 1–15 m wide between the support caving shields and the caved rock piles.

After a short delay, the immediate roof caved just behind the supports and formed a new free-opening above the caved rock piles. All the free-openings in the goaf appeared to be interconnected from the headentry to the tailentry. Consequently, a small branch of the intake air flowed through the free-opening in the goaf parallel to the main branch of the intake airflow in the longwall face. The main flow in the face area (Fig. 2a) totalled about 75% of the incoming flow (about  $10\,000 \text{ l s}^{-1}$ ) surveyed in the headentry T-junction. The quantity of the main air flow in the face area was relatively stable with a change of less than  $2500 \text{ l s}^{-1}$ .



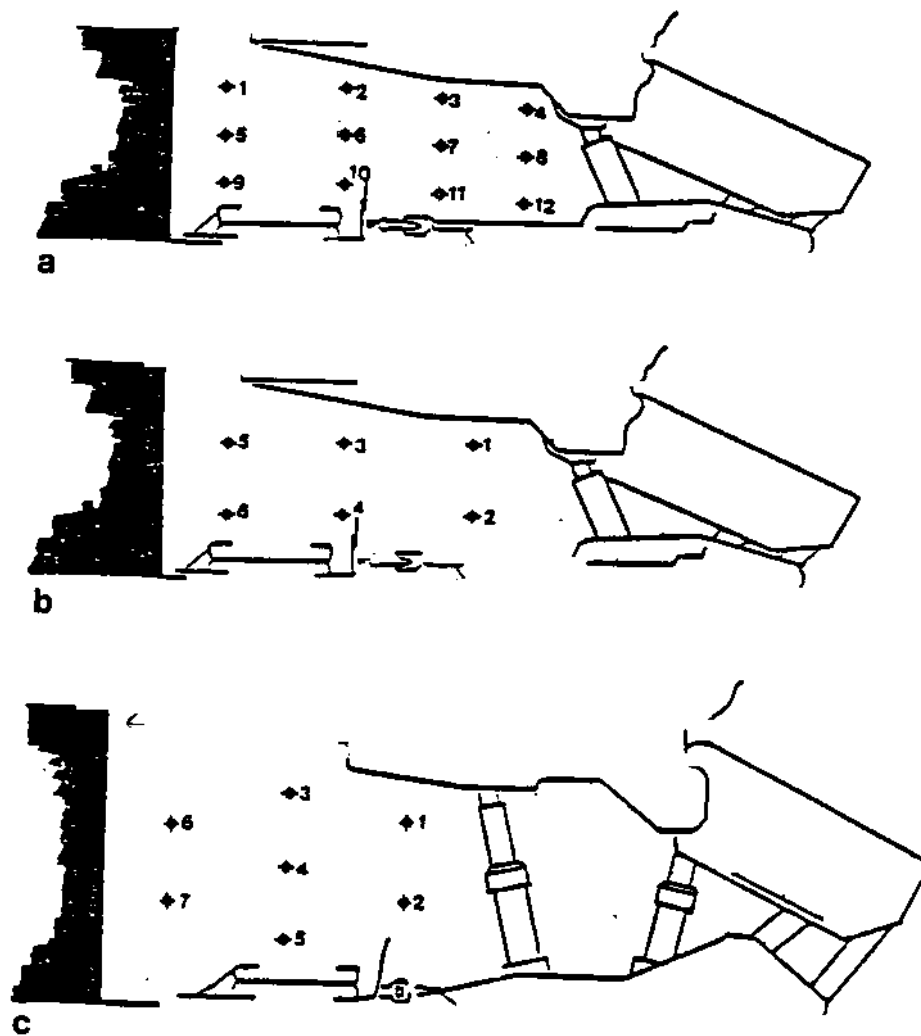
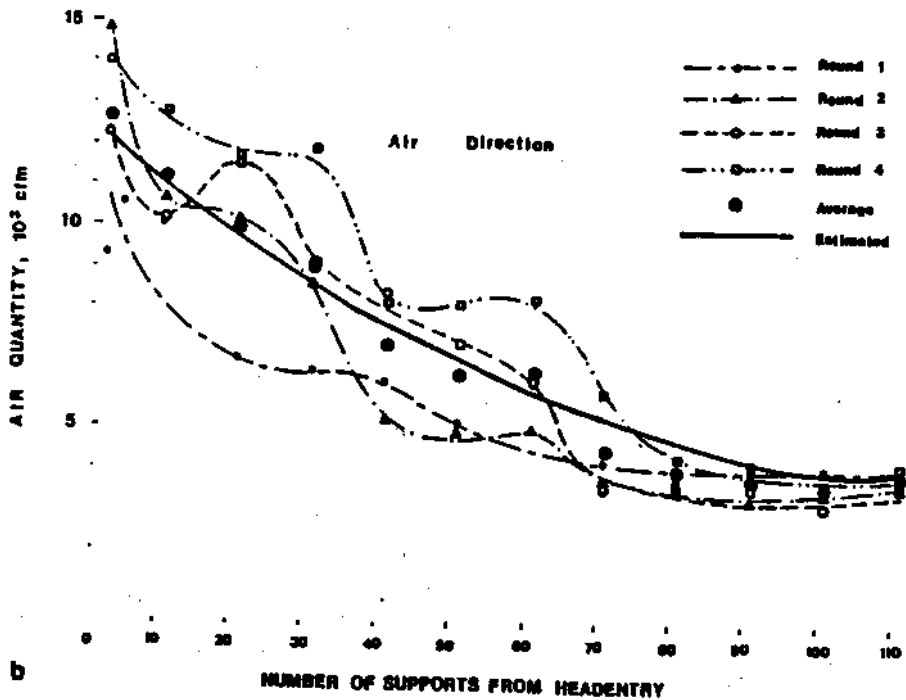
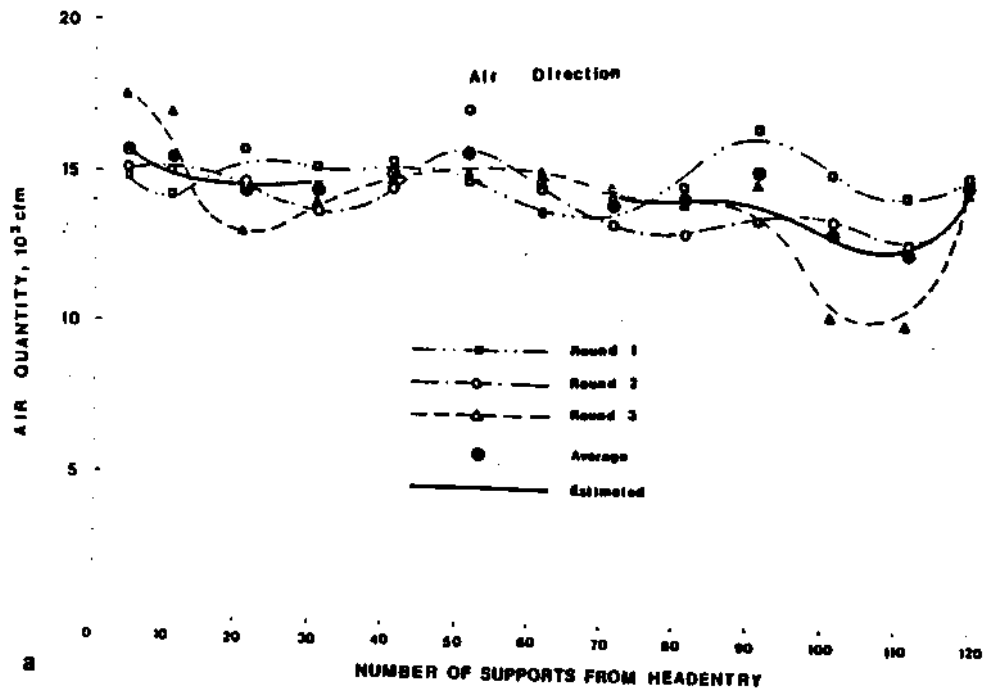


Fig. 1. Arrangement of survey points. (a) Panel No. 1 and Panel No. 3. (b) Panel No. 2. (c) Panel No. 4.

*Panel No. 2.* The longwall face in this panel mined the same coal seam as in Panel No. 1 but the immediate roof was relatively broken throughout the whole face during the survey period. There were numerous fractures that were parallel to the faceline. A fracture located at the intersection of the front and extension canopies near the panel centre was about 200 mm wide by 600 mm deep and spanned across four supports (i.e. 6 m). In addition, there were many fractures up to 0.5 m deep. In this case, the roof caving line moved toward the face at one third of the canopy length from the rear edge of the canopy. At both ends of the face, roof fractures were abundant. During the survey period of more than five days, the tailentry T-junction was blocked by fallen roof rocks and only a small space, about 0.3 m in diameter, was left to allow a small amount of the return air into the tailentry. On the other hand, the smoke tube testings and visual observations showed that the fallen immediate roof rocks in the goaf were not tightly compacted and there was a visible space above the rock pile. This allowed the leaking air to flow through the goaf to the tailend of the face. Because of the broken roof and the small opening at the tailentry T-junction, the ventilation conditions in this panel were very bad. The air quantity

# AIR VELOCITY DISTRIBUTION MEASUREMENTS

distribution pattern for this panel was determined by these factors (Fig. 2b). The general trend of the air quantity against X curve was continuously decreasing. The air quantities at the tailentry were only about 20-40% of those surveyed at the third support.



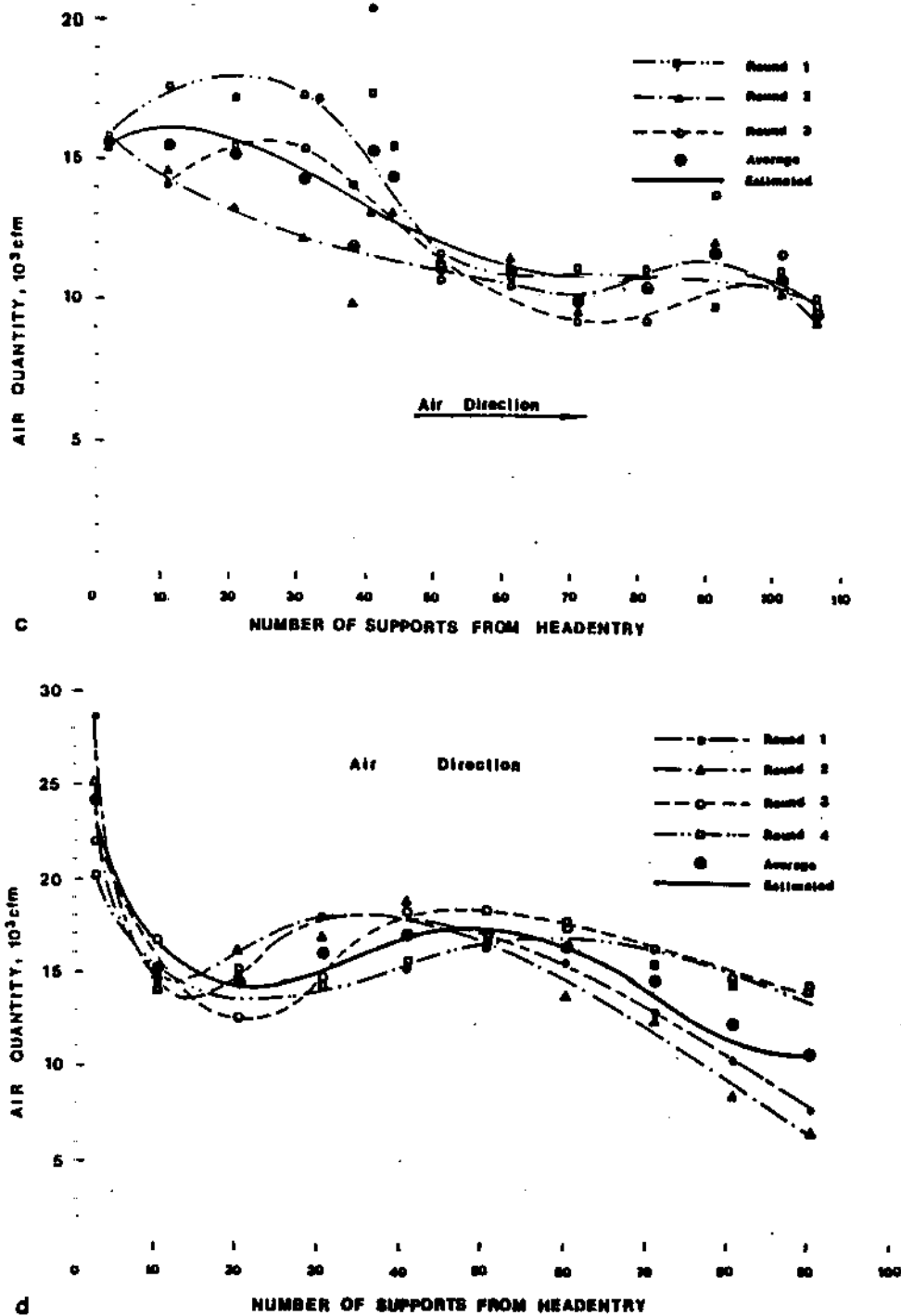


Fig. 2. Air quantity distribution along a longwall face. (a) Panel No. 1. (b) Panel No. 2. (c) Panel No. 3. (d) Panel No. 4. Note  $1 \text{ cfm} = 0.471 \text{ s}^{-1}$ . The supports are at 1.5 m centres.

**Panel No. 3.** The Pittsburgh seam was mined by this panel with the mining height ranging from 1.9–2.1 m. The immediate roof, approximately 3.9 m thick, was shale intermixed with coal and clay. It was relatively stable so that the exposed roof area and the maximum exposure time without collapses allowed unidirectional cutting to be implemented. The immediate roof caved immediately after support advance generally resulting in the caving line being near the rear edge of support canopy. The caved fragments were small in size. Due to the high frictional resistance

in the goaf caused by the compacted and small-sized caved rocks, the air leakage from the face area was not significant. The air quantity distribution pattern for this face is illustrated in Fig. 2c. Before the third or fourth support, the intake air from headentry dashed into the gob. But soon after, it returned to the face area, forming a peak region. Since the panel was near completion during the survey period, the return airflow at the tailentry was led through a cross-cut into the next parallel return airway instead of the normal tailentry immediately adjacent to the panel. Consequently, some of the air took a shortcut through the gob area to the return cross-cut, resulting in a gradual air leakage in the remaining portion of the face.

*Panel No. 4.* This panel mined the Lower Kittanning seam about 1.5–1.6 m thick. The immediate roof, consisting of sandy shale about 7.5 m thick, was relatively stable so that at both ends of the face a large area of the roof did not cave completely. The uncaved roof area ranged from 13 to 30 m (i.e. 10–20 supports) long and 6–10 m deep in the goaf, forming a large space at both ends of the face. In the middle portion of the panel, however, the immediate roof caved well right after support advancing. The caved fragments were compacted tightly in the goaf and the testing smoke flowed in this portion mainly parallel to the main airflow or, in some places, toward the face, instead of toward the goaf. The air quantity distribution pattern (Fig. 2d) shows the following characteristics.

(1) At the beginning portion of the face from the 10th to the 20th support (i.e. 15–30 m), a vast amount of air, about 30–50% of the total air measured at the first station (No. 3 support), leaked into the goaf resulting in a sharp reduction of air quantity in the face area.

(2) After the 10th–25th support, some of the leaked air returned to the longwall face forming a peak region at the middle portion of the face (usually from the 30th to the 50th support).

(3) In the remaining portion of the face, due to the poor caving conditions in the goaf at the tail portion of the face and the existence of some air shortcuts through some poorly filled cross-cuts on the goaf side, the air quantity in the longwall face decreased gradually.

### *Velocity distribution at the survey station*

The air velocity distribution in a survey station refers to the two dimensional (Y and Z directions) distribution of air velocity in the cross-section perpendicular to the face.

To understand the nature of the velocity distribution on the cross-sections, 6–12 velocity readings were taken at each surveying station in each round of the survey. Then the readings at the same location for all the rounds were averaged.

Several typical air velocity distributions in Panel No. 1 are illustrated in Fig. 3. The high velocity core usually occurs near the centre but close to the face line of the main ventilation area (i.e. between the coal face and the front leg of the support). But in normal mining conditions the core at the beginning of the face is near the line of the support front leg and at the tailend close to the coal face. The case where two high velocity cores appeared at the surveying station at Support No. 81 of Panel No. 1, is uncommon and might be attributed to the shearer influence. When the second round of the survey was conducted at the 81st support, the shearer was indeed located near the 71st support. But the magnitude and the manner of influence are still unclear. Since the space between the front legs and the caving shields is partially occupied by pipes, tubes and gauges, the quantity and the velocity of the air flowing through this area were considered insignificant.

### *Visual observations on the influence of shearer movement*

According to the principles of fluid mechanics, objects moving in a viscous fluid such as air will cause the movement and the velocity distribution of the fluid to be different from that without the moving objects. Since the air is a viscous fluid, when an object moves at certain speed whether in the same or opposing direction of the airflow, a thin layer of air adjacent to the surface of the object will flow in the same direction at almost the same speed as the object. As the distance to the surface of the moving object increases, the influence of the object on the airflow will decrease. When the distance increases the influence will no longer be strong enough to be

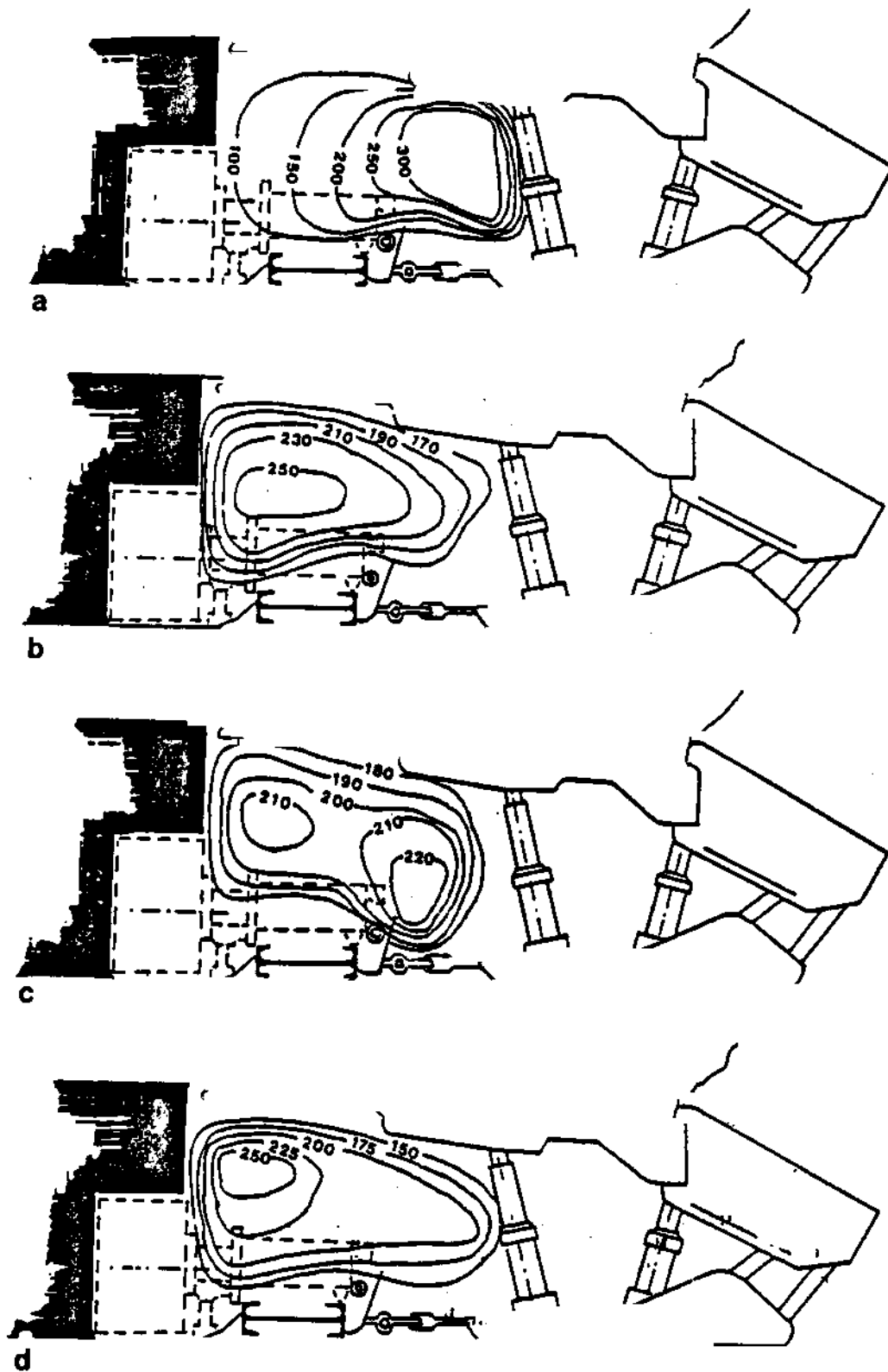


Fig. 3. Air velocity distribution contours in the machine track normal to the face line on Panel No. 1. (a) Support No. 5. (b) Support No. 41. (c) Support No. 81. (d) Support No. 116. The contours are in ft min<sup>-1</sup>; 1 ft min<sup>-1</sup> = 0.005 m s<sup>-1</sup>.

## AIR VELOCITY DISTRIBUTION MEASUREMENTS

observed. This point is called the critical point. Here, the distance from the surface of the moving object to the critical point is called the influence range. Obviously, the influence range varies with the surface roughness, the direction relative to the airflow, and the speed of the moving object.

The smoke tube tests revealed that the air flow around the shearer has the following characteristics.

(1) The air flow is controlled by the drum rotation, especially when the drums are cutting coal. The influence range can be up to 30–45 mm off the drum depending on the rotational speed.

(2) The air flow is controlled by falling coal from the drum. The closer the coal falls near the face conveyer and the bulkier the coal is, the stronger the influence will be.

(3) The air flow is controlled by spraying water. The influence range varies with the water pressure and quantity, system installation, and the main airflow direction. However, the range is usually smaller than those of the above two factors.

Two velocity surveys around the shearer were carried out at Panel No. 1 and Panel No. 3. The results are plotted in Fig. 4.

The air velocity distribution around the shearer at Panel No. 1 is shown as Figs 4a–c. The air velocity distributions are illustrated in three horizontal planes parallel to the roof and the floor: an upper layer (about 0.6 m above the shearer); a middle layer (0.15 m above the shearer); and a bottom layer (0.6 m above the floor). Under the influence of high pressure water sprays mounted on the shearer body and the ranging arms, and the rotational effects of the cutting drums, there is a high velocity core beside and/or behind the intake side drum. This is more conspicuous in the upper and middle layers. Around the return side drum, the effects are much smaller. In the bottom layer, however, the existence of the shearer does not seem to cause any significant disturbance, although there is a relatively lower velocity core behind the intake side drum. Fig. 4d shows the airflow distribution in the upper layer (about 0.3 m above the shearer and 0.3 m below the roof) around the shearer at Panel No. 3. Because a splitter arm with high pressure water sprays was mounted beside the return side (leading) drum, a high air velocity core occurred not only in front of the leading drum but also behind the trailing drum.

There are two factors which make the data for velocity distribution around the shearer unreliable. The first one is the time lapse. Each of the two surveys took about 25 min. During that time period, the shearers moved about 30 m. The other factor is the busy mining activities that frequently interrupted the surveys.

The face conveyer also disturbs the main airflow in local area. The magnitude of the influence is affected by the speed of the conveyer and the bulkiness of the moving coal. When the conveyer was empty, the range was about 75–100 mm above the conveyer. When it was fully loaded, the range could be up to 100–150 mm over the running coal.

The airflow at the ends of the face was, to some extent, disturbed by the motors that run the face conveyer. But the impact is not significant on the airborne dust distribution in the longwall face area, because there was not too much dust generated at the headentry and the dust generated at the tailentry does not affect the working space in the longwall face.

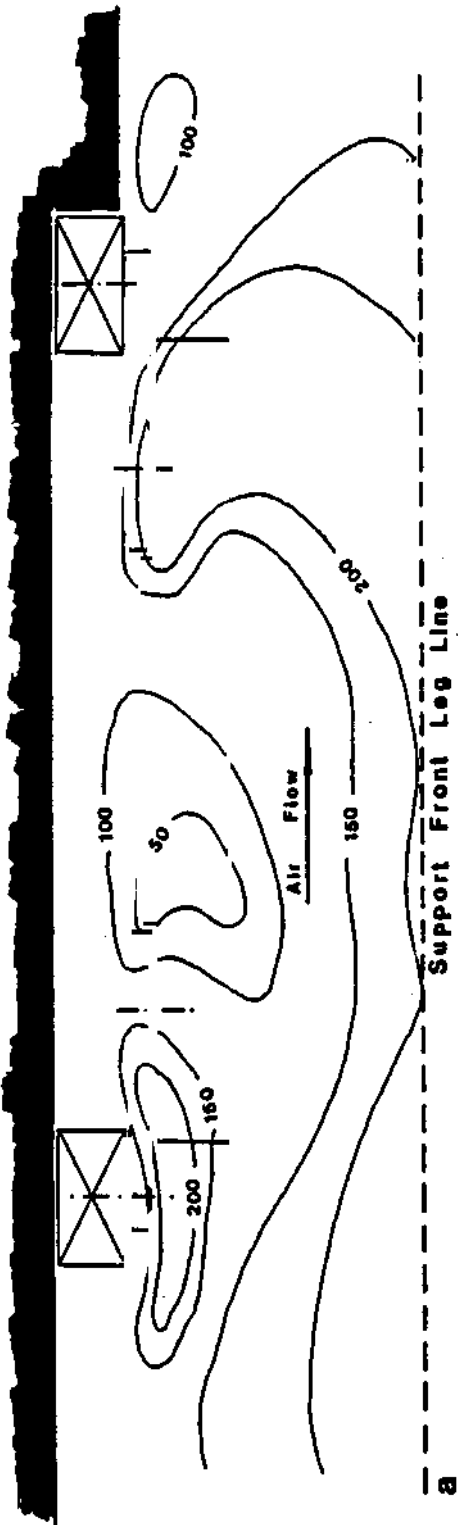
### Acknowledgement

This research was funded by the Generic Technology Research Center for Respirable Dust under the Mineral Institute Program, U.S. Bureau of Mines, Grant Number G1135142.

### References

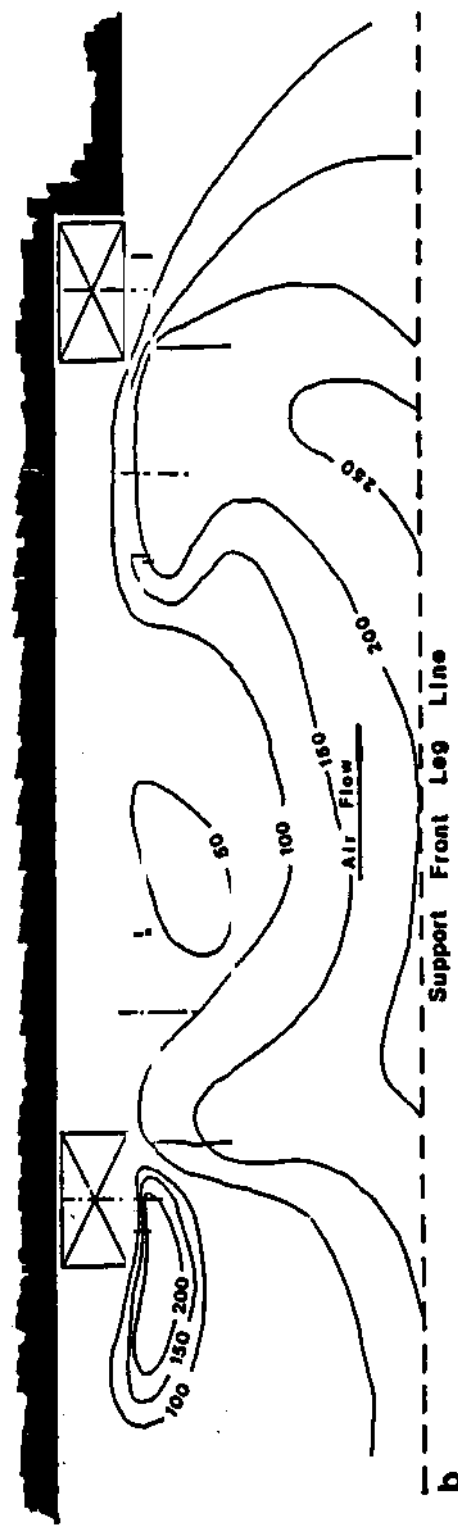
- Gottfried, B.S. (1972) *Programming with FORTRAN IV*, University of Pittsburgh, pp. 173, 212.
- Hall, C.J. (1981) *Mine Ventilation Engineering*, University of Idaho, pp. 274–282, pp. 285–290.
- Peng, S.S. and Chiang, H.S. (1985) Some Factors Influencing the Airborne Dust Distribution in Longwall Face Area, *Proceedings, Coal Mine Dust Conference*, Morgantown, West Virginia, October 8–10, pp. 206–213.

Cutting Direction



a

Cutting Direction



b

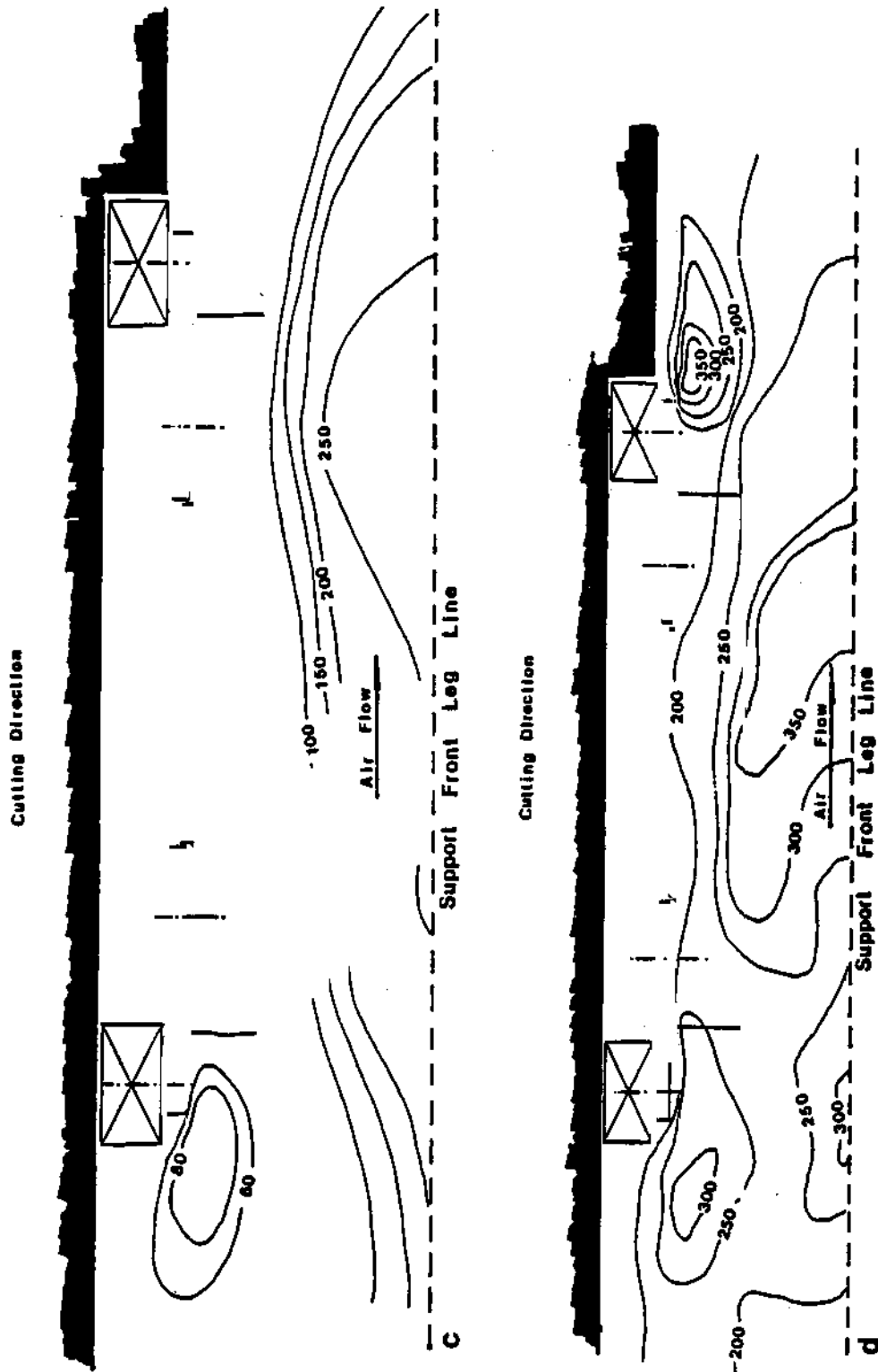


Fig. 4. Air velocity distribution around a shearer. Contours are in  $\text{ft min}^{-1}$ ;  $1 \text{ ft min}^{-1} = 0.005 \text{ m s}^{-1}$ . Panel No. 1: (a) upper layer 0.6 m above shearer; (b) middle layer 0.15 m above shearer; (c) bottom layer 0.6 m above floor. Panel No. 3 (d) 0.3 m above shearer.



# Simulations of Dust Dispersion for a Coal Mine Face Using a Scale Model

T. H. Ueng, S. D. Thompson and Y. J. Wang  
Department of Mining Engineering, West  
Virginia University

## INTRODUCTION

There is considerable interest among mining companies and government agencies in finding new ways to better control the generation and dispersion of respirable coal dust. Mine face ventilation generally has been considered the most effective tool for lowering the concentrations of respirable dust. Unfortunately, only a limited amount of research has been undertaken to determine the relationships between the various face ventilation parameters and the dust dispersion patterns. If these relationships are better understood, more efficient ways of controlling dust generation and dispersion may be evident. A practical and economical way to gain more indepth understanding of these relationships is through scale model studies. Past research (1, 2, 3) has substantiated that scale models can be successfully used in studying ventilation parameters provided that geometric, kinematic, and dynamic similitudes are maintained.

To better understand face ventilation and dust dispersion, a 1/5 scale model of a room and pillar mine face was constructed. This model was then used to conduct experimental investigation on two ventilation parameters. The parameters which were examined included the line brattice distance from the face and the air quantity. The values of these parameters were varied in numerous experiments so that their effects on dust dispersion could be measured.

The experiments of this study were unique in two ways. First, two different substances were used to simulate the respirable coal dust. Experiments were conducted with a tracer gas (methane) serving as the dust simulation substance. They were then repeated with an actual dust (Arizona Road Dust) replacing methane as the dust simulating substance. In previous scale model studies, the dust simulation substance has been limited to a tracer gas such as methane. The validity of using a tracer gas to simulate dust is not clearly known yet. The other unique thing about these experiments was the number of points measured for methane (or dust) concentration. Twenty five points in a grid arrangement were measured during each experiment of this study. The number of points measured for concentration in other studies has generally been very small (often 2 to 4). It is difficult to obtain an accurate assessment of how the ventilation parameters are effecting dust dispersion when only 2 to 4 points are measured.

# SIMULATIONS ON DUST DISPERSION

## EXPERIMENTAL APPARATUS

### Model

The 1/5 scale model used in the experiments was constructed out of prefabricated heating ducts made of sheet metal (see Fig. 1). The model is geometrically similar to a full scale mine entry of 7.5 feet by 20 feet. A 24.5 inch centrifugal fan built by Dayton Electric Manufacturing Company of Chicago, Illinois, was connected to the ducts to induce the air flow. The line brattice used to direct the airflow inside the duct work was installed 16 inches from the tight rib (see Fig. 2). This would be equivalent to a full scale distance of 6.6 feet.

The heating duct used for the dead-end face area was modified so that the dust simulation substance could be injected and measured. The end plate which covered the front of this duct had four small holes through which the dust simulation substance was injected (see Fig. 3). Twenty five holes, in a grid arrangement, were

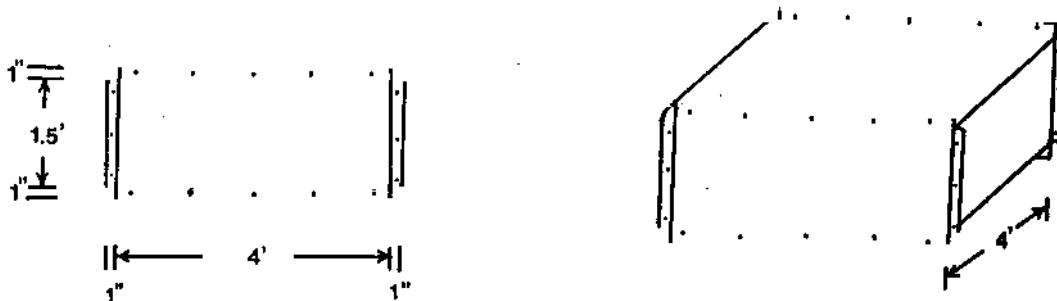


Fig. 1 Prefabricated Heating Duct

made in the top of this duct so the concentrations of the injected substance could be measured across the face area (see Fig. 4). Each of these latter holes were kept sealed unless a measurement was being taken.

The effects of the mine face machinery were not considered during these experiments. Therefore models of face machinery were not placed inside the ducts.

### Dust Generation

Both methane gas and Arizona Road Dust were used to simulate respirable coal dust in the experiments. Each substance required its own generating mechanism. Methane was injected from a pressurized cylinder. The Arizona Road Dust was injected with a Mark IX SYLCO Fine Power Feeding Apparatus. The apparatus was manufactured by Sylvester and Company of Beachwood, Ohio.

### Measuring Equipment

The methane concentrations in parts per million (ppm) were measured with a Bendix Total Hydrocarbon Analyzer (Model 8401). This instrument was built by

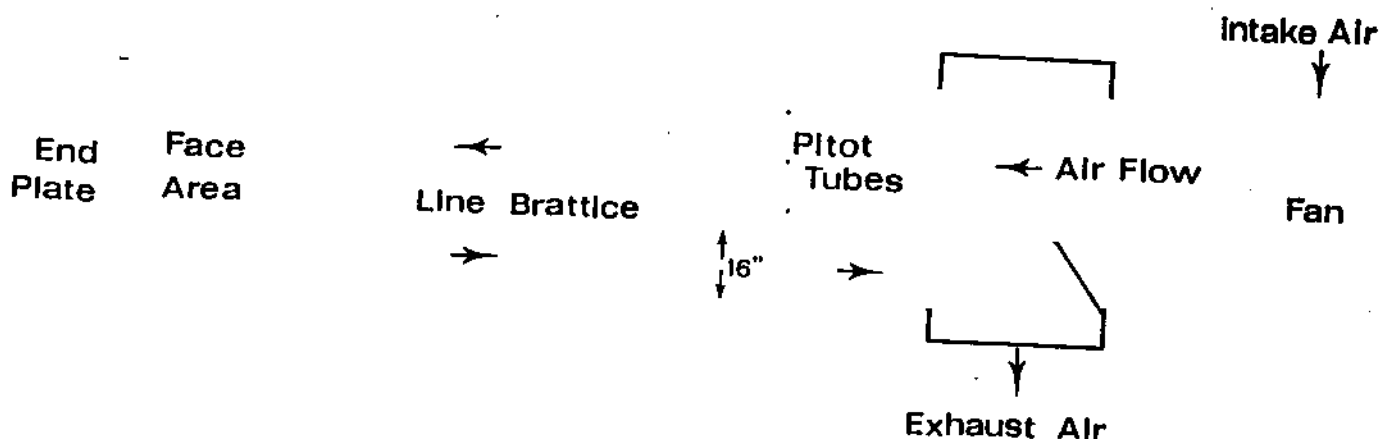


Fig. 2 Scale Model Setup

Combustion Engineering of Lewisburg, West Virginia. The analyzer was equipped with a sampling pump which operated at 6.5 psig and 35 cc/min.

Road dust concentrations in milligrams per cubic meter were measured with a Real-Time Aerosol Monitor (Ram-1). The instrument is manufactured by GCA Corporation's Technology Division of Bedford, Massachusetts.

The readings obtained from these two instruments were recorded with a strip chart recorder.

#### PROCEDURE

The 1/5 scale model was used to evaluate dust dispersion at 4 different line brattice distances (from the face). The distances examined were 4, 3, 2, and 1 feet. These correspond to full scale distances of 20, 15, 10, and 5 feet, respectively.

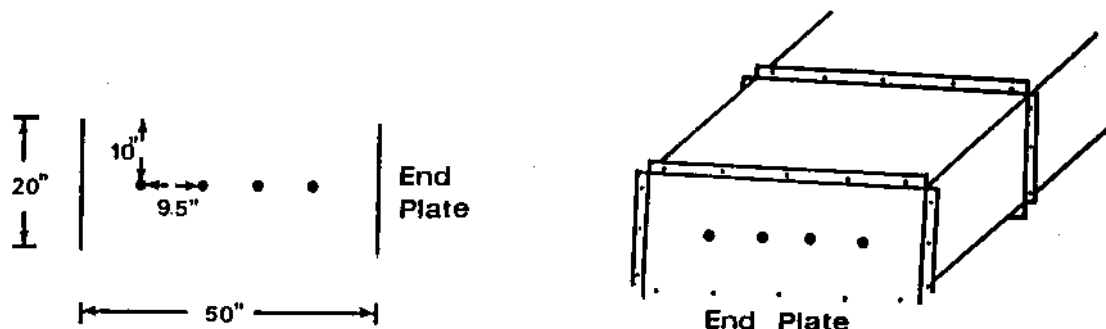
Four air quantities were studied at each brattice distance. These air quantities were selected so that dynamic similitude would be maintained. To maintain dynamic similitude, the Reynolds number for these flows must be in the range of 20,000 to 80,000 (Stein et al., 1974). This was achieved by using air quantities of 3,400, 2,400, 1,800, and 1,000 cubic feet per minute (cfm). They are roughly equivalent to full scale quantities of 17,000, 12,000, 9,000, and 5,000 cfm, respectively.

Two different substances were used to simulate the respirable dust in the experiments. The 16 combinations of air quantity and brattice distance were first studied with methane gas simulating the respirable coal dust. These same combinations were later re-examined with Arizona Road Dust serving as the respirable coal dust. The injection rates for both these substances were arbitrarily set and held constant throughout the study.

The dust dispersion for a given air quantity and brattice distance was evaluated by measuring methane (or dust) concentrations at each grid point in the dead-end face duct. The concentrations were determined from average readings obtained over a 1 minute interval with a Hydrocarbon Analyzer (or Real-Time Aerosol Monitor).

## SIMULATIONS ON DUST DISPERSION

These readings were taken at a height of 12 inches above the bottom of the duct. This would be equivalent to a full scale height of 5 feet. A one minute methane reading taken with the Hydrocarbon Analyzer was reproducible to about  $\pm 30\%$ . Dust



- Location of Methane or Road Dust Injection

Fig. 3 Injection Points

reading obtained with the Real-Time Aerosol Monitor were generally reproducible to  $\pm 40\%$ .

Once all the concentration data was collected, it was carefully summarized. For example, methane and road dust isopachs were drawn from the data obtained for each air quantity and brattice distance combination. Changes in methane (or road dust) concentrations for different air quantities and brattice distances were also calculated. This summarized information was then studied for possible trends or relationships.

### RESULTS AND DISCUSSION

Similar to previous studies (2, 3), the overall concentration of the dust simulation substance was found to decrease as the air quantity increased. The overall concentration was also found to decrease as the line brattice was extended toward the face. However, the concentration did not necessarily decrease at every grid point along the face when the air quantity was increased or the brattice was extended. This phenomenon is illustrated with Table I and Fig. 4. Notice that the concentrations at points 2, 5, 7, 14, and 18 actually increased with an increase in air quantity. Also note that the change in concentration varied from point to point. Such experimental results suggest that location and possibly other factors could be important in the relationships between air quantity, brattice distance, and dust concentration. Therefore in order to better understand these relationships, it appears that the dust dispersion behavior needs to be examined throughout the face.

To examine the dust dispersion behavior throughout the face, isopachs for substance concentrations were drawn from the data collected during the study. It was apparent from these isopachs that the changes in dust dispersion could be more thoroughly described if a low concentration zone was defined. Since methane and

Table I

Comparison of Methane Concentrations for Two Air Quantities  
(Line Brattice Distance = 3 ft)

Grid Point Number	1000 cfm Concentrations (ppm)	1800 cfm Concentrations (ppm)
1	73	< 60
2	158	424
3	3814	3134
4	4730	3016
5	3146	3734
6	1768	1708
7	2134	2238
8	451	271
9	61	< 60
10	< 60	< 60
11	< 60	< 60
12	< 60	< 60
13	85	60
14	1122	1437
15	2938	2556
16	4316	2358
17	646	1001
18	110	471
19	585	353
20	610	365
21	268	82
22	402	200
23	638	292
24	1573	695
25	3438	1447

road dust are measured differently, it was necessary to define a low concentration zone for each. The low concentration zone for the methane experiments was defined as the area of the dead-end face duct which had methane concentrations less than 250 parts per million (ppm). The low concentration zone for the road dust was the area having concentrations less than 5 milligrams per cubic meter.

The low concentration zone was found to be more prominent on the tight side of the duct. The foremost point of its boundary was generally near the end of the line brattice. While the particular dimensions of a low concentration zone was dependent on the air quantity and brattice distance, Fig. 5 roughly illustrates the general shape.

Air Quantity

As stated earlier, the study substantiated that an increase in air quantity reduces the overall face concentration of the dust simulation substance. Table II shows the effect that the indicated changes in air quantity had on the overall concentrations in the face area. Each specified air quantity change was tested at the four brattice distances. The percentages in Table II were obtained by averaging the concentration changes of the four distances.

## SIMULATIONS ON DUST DISPERSION

The overall reductions trends were the same for both the methane and road dust experiments. The smallest change in air quantity resulted in the largest decrease in concentration. The effectiveness of reducing concentrations through increased air quantity appears to depend on the range of the air quantities.

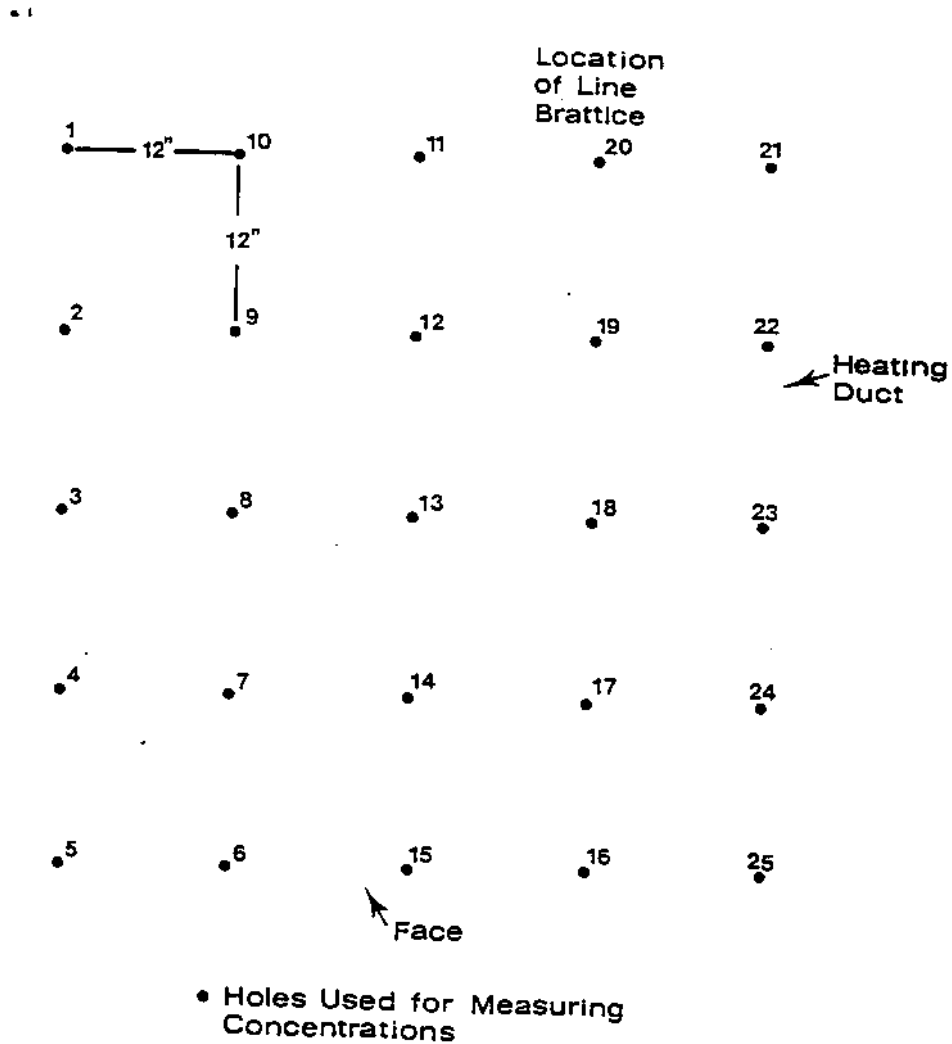


Fig. 4 Grid Arrangement for Measuring Points

Perhaps more important than overall concentration reductions, is how an increase in air quantity effects the low concentration zone. While the zone may be slightly deepen toward the face, the main effect of the increased air quantity is to widen the zone across the face. This widening is apparent if the isopachs of Figs. 6 and 7 are compared. While the widening effect is present in both the methane and road dust experiments, the margin between widening and deepening was less pronounced in the latter.

Table II

Effects of the Specific Air Quantity Change on Overall Substance Concentration

Air Quantity Change		Effect on Concentration in	
From (cfm)	To (cfm)	Methane Tests	Road Dust Tests
1000	1800	- 23%	-27%
1800	2400	- 36%	-40%
2400	3400	- 21%	-23%

Note: minus sign (-) indicates a decrease in concentration

Brattice Distance

When the end of the brattice was extended toward the face, the overall face concentrations of the dust simulation substance decreased. Table III shows the effect that the specified brattice changes had on methane and road dust concentrations. Since each specified brattice change was tested on all four air quantities, the percentages in Table III were obtained by averaging the concentration changes of the four air quantities.

The line brattice extensions mainly deepened the low concentration zone toward the face. The deepening can be seen when the isopachs of Figs. 7 and 8 are compared. The extensions also produced some widening of the zone. The margin between deepening and widening was less pronounced in the dust experiments.

Combined Effects

The combined effect of increasing the air quantity by 600-1000 cfm and extending the brattice by 1 foot was an overall reduction in substance concentration of about 50%. More specifically, the reduction averaged about 51% in the methane and 49% in the road dust experiments.

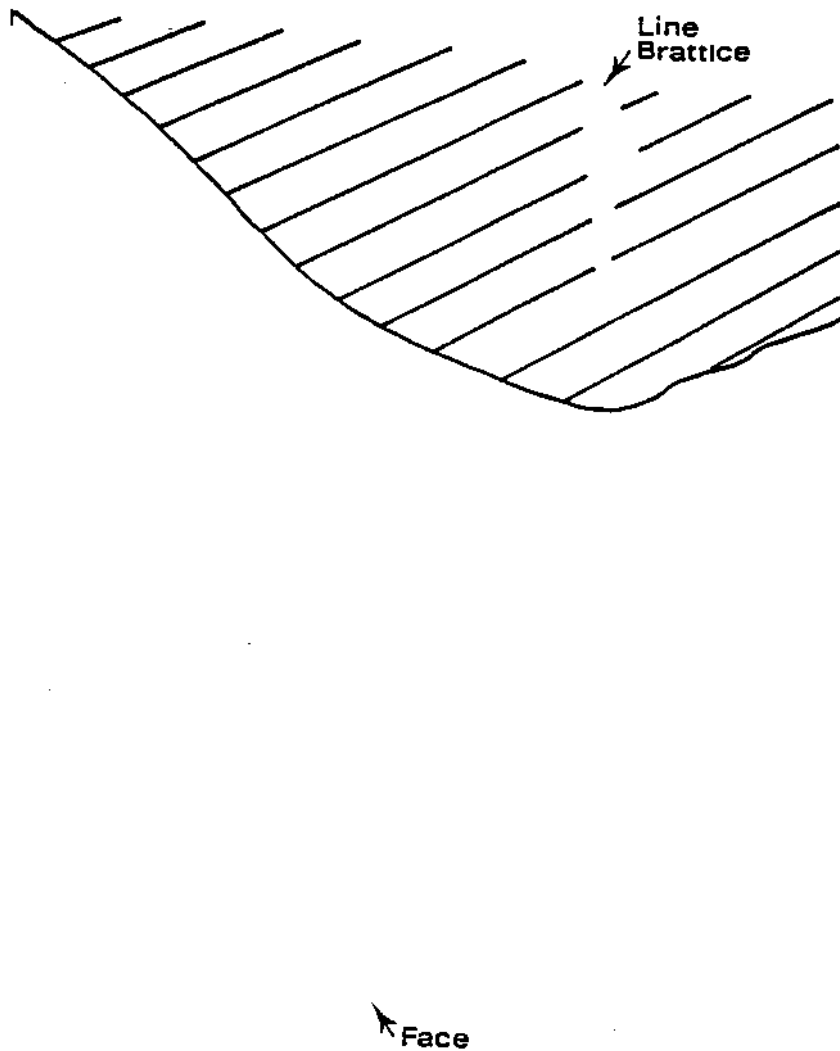
Table III

Effects of the Specific Brattice Change on Overall Substance Concentration

Brattice Change		Effect on Concentration in	
From (ft)	To (ft)	Methane Tests	Road Dust Tests
4	3	-22%	-21%
3	2	-24%	-27%
2	1	-19%	-31%

Note: minus sign (-) indicates a decrease in concentration

## SIMULATIONS ON DUST DISPERSION



 Low Concentration Zone

Fig. 5 Rough Illustration of Low Concentration

The combined effect on the low concentration zone was a widening and deepening of its dimensions. By comparing the isopachs of Figs. 9 and 10 an example of this widening and deepening can be viewed.

### Air Quantity vs. Brattice Distance

At least one study (3) has indicated that line brattice extensions are more effective in reducing dust concentrations. Because the air quantity changes were at least as effective, this study did not substantiate this claim. One possible reason for the discrepancy is that face machines were present in the earlier study, but were not considered during this study. Another possible reason is that the former researchers only measured a few points along the face. Those points were usually located near the operator compartments of the machines. This study would



substantiate that line brattice is a more effective way of deepening the low concentration zone. Therefore line brattice extensions may be a more effective way of lowering dust concentrations at some outby points such as the continuous miner operator position.

Methane vs. Road Dust

The methane and road dust experiments compared well. Basically, the same trends were evident in both sets of experiments. Therefore, this study would tend to support the premise that the respirable coal dust for scale model studies can be adequately simulated with a tracer gas. Nevertheless, one noticeable difference was observed and it should be pointed out. The methane tended to diffuse more evenly and perhaps a little farther from the injection points. This difference may be important if dust concentrations are being study at points more than 20 feet (full scale) from the face.

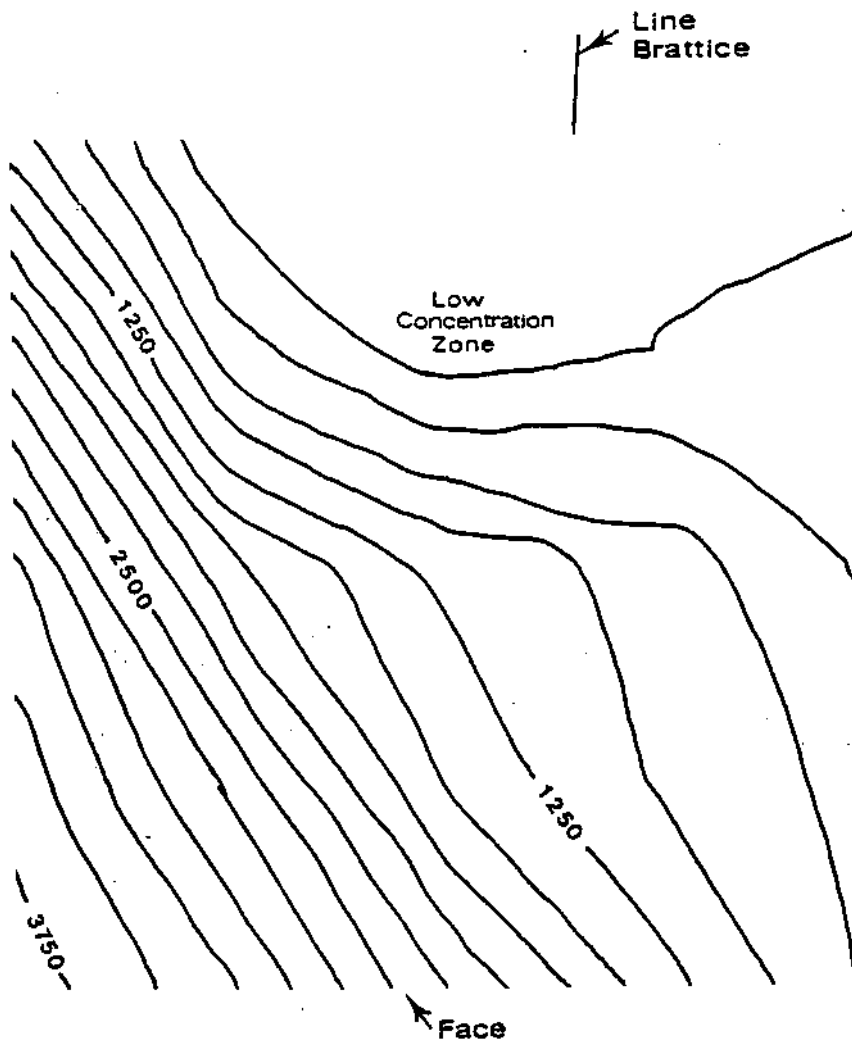


Fig. 6 Methane Concentration Isopach for Air Quantity = 2400 cfm and Brattice Distance = 4 ft

# SIMULATIONS ON DUST DISPERSION

## RECOMMENDATIONS

Either air quantity increases or line brattice extensions can be used to lower dust concentrations. Since air quantity tended to be more effective across the face and brattice extensions were more effective into it, the preferred method for reducing dust concentration could depend on the face location(s) of interest. Consequently, the current air quantity and brattice distance and also the location(s) should be carefully considered before deciding on an option.

When possible, it would be recommended that the low concentration zone be considered and used advantageously. For example, the low concentration zone was found to be most prevalent on the tight side (brattice side) of the entry. The ventilation system could be arranged so that the line brattice and the operator compartment of the continuous miner are on the same side of the entry. Another option would be to relocate the operator compartment or position to that side.

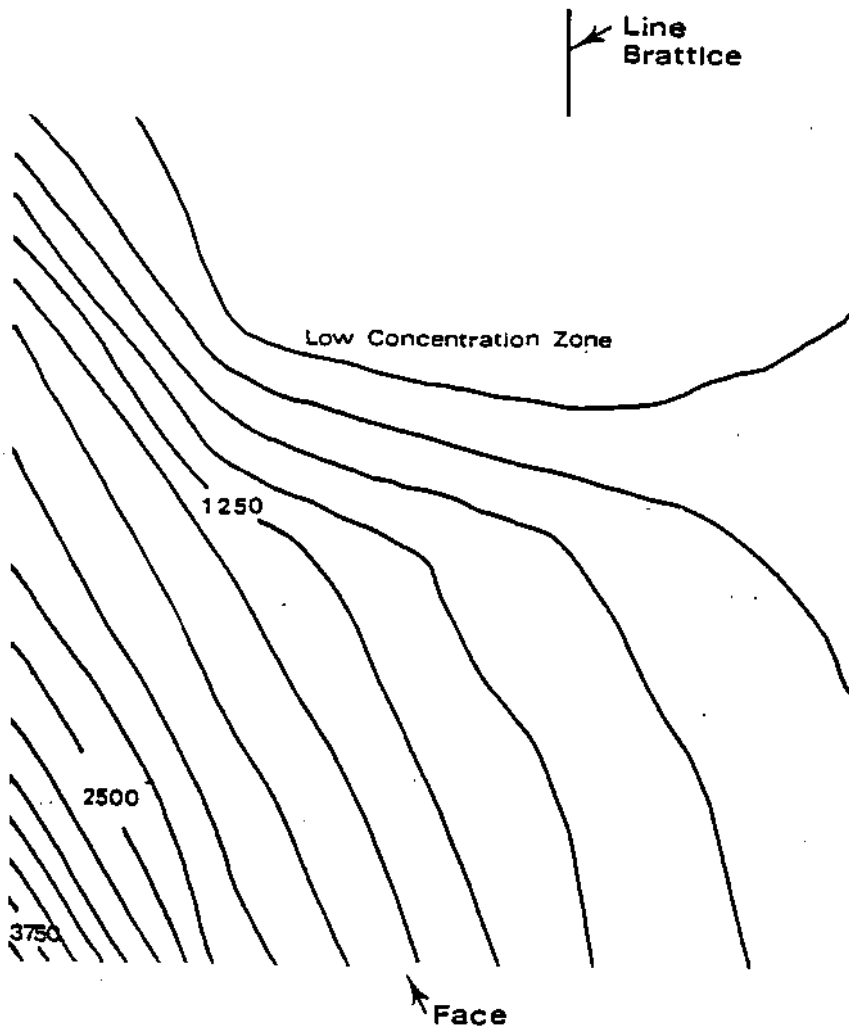


Fig. 7 Methane Concentration Isopach for  
Air Quantity = 3400 cfm and  
Brattice Distance = 4 ft

Fig. 9 Road Dust Concentration Isopach for  
Air Quantity = 1800 cfm and  
Brattice Distance = 4 ft

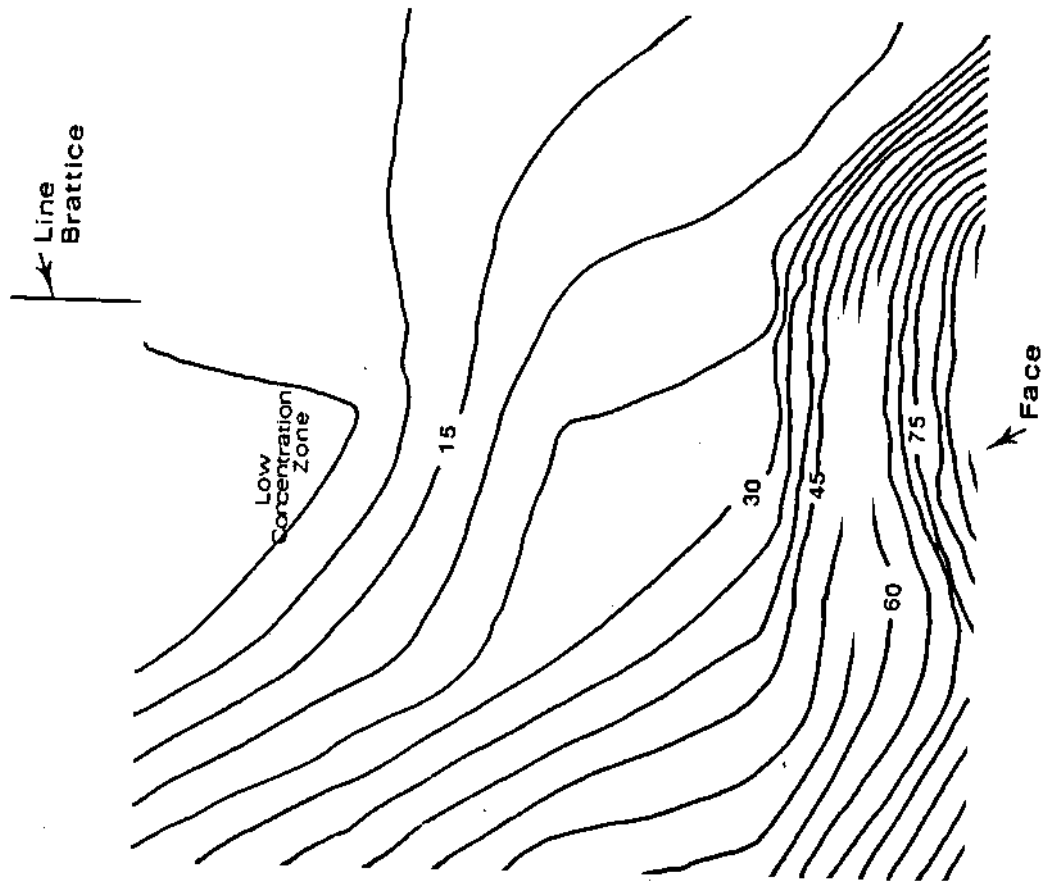
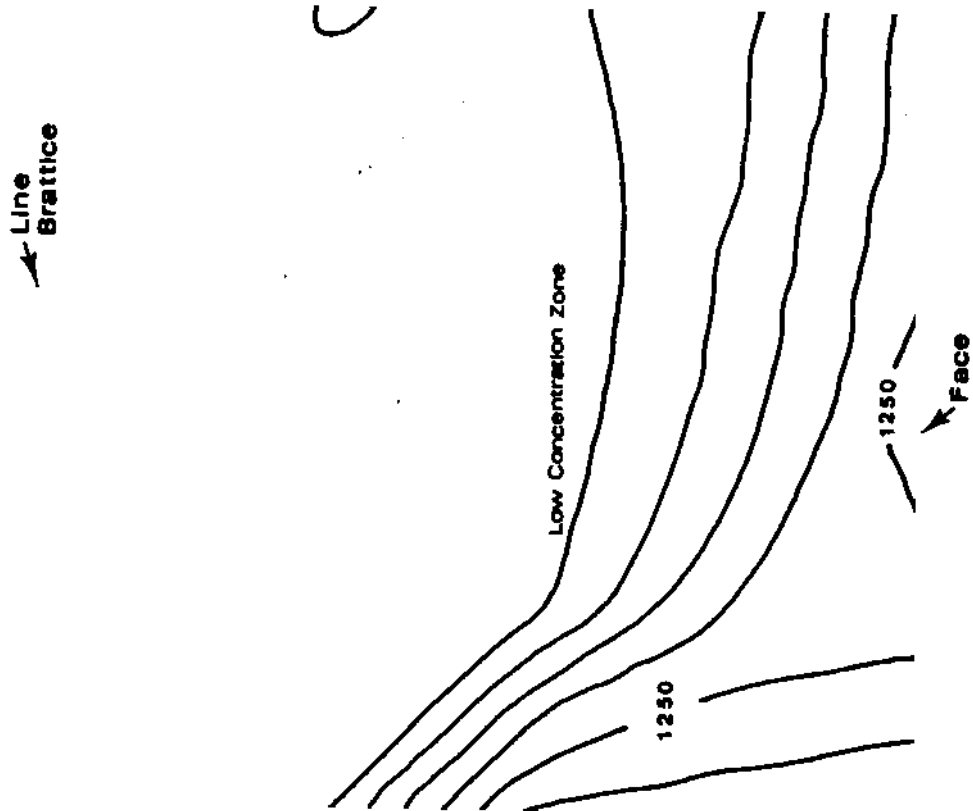


FIGURE 8. Methane concentration isopach for air quantity at 3400  
cfm and brattice distance of 4 ft.



## SIMULATIONS ON DUST DISPERSION

The final recommendation for reducing dust concentrations would be to determine the areas of the face where the air quantity and brattice extensions are least effective. Dust suppression and/or auxiliary ventilation should be emphasized to a greater extent in these locations.

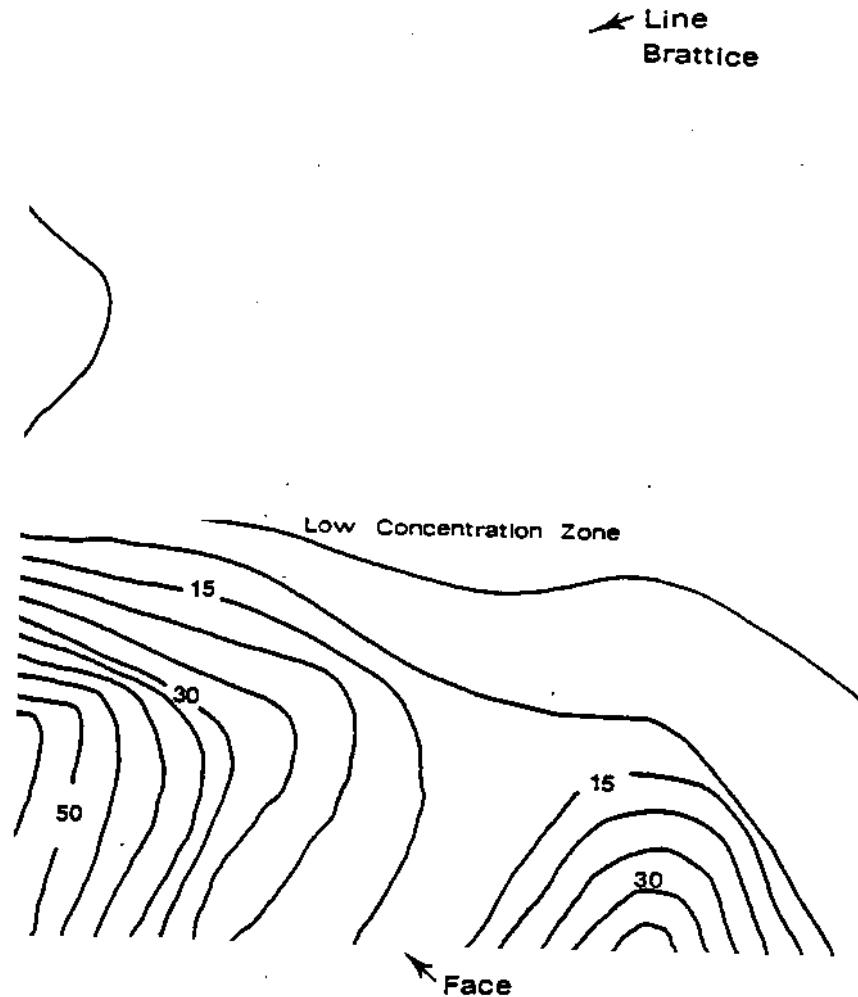


Fig.10 Road Dust Concentration Isopach for  
Air Quantity = 3400 cfm and  
Brattice Distance = 3 ft

### SUMMARY AND CONCLUSIONS

To determine the effects of brattice distance and air quantity on dust dispersion, four brattice distances and air quantities were examined during the study. The experiments utilized both a tracer gas (methane) and a dust (Arizona Road Dust) for simulating the respirable coal dust. Methane or dust concentrations were obtained at 25 grid points for each brattice distance and air quantity combination. The data were then summarized to determine the effect the various air quantities and brattice extensions had on dust dispersion. Comparisons were also made to determine if the same trends were evident in the methane and the road dust experiments.

## THE RESPIRABLE DUST CENTER

The study showed that both air quantity increases and brattice extensions are effective in reducing dust concentrations. However, these reductions were not found to be uniform throughout the face. Some points experienced greater reductions than others. In some cases, a few points actually increased in concentration.

Air quantity increases and brattice extensions tended to have somewhat different effects on dust dispersion patterns. Basically, increases in air quantity tended to be more effective in decreasing concentrations across the face. Brattice extensions were generally more effective in reducing concentrations toward the face.

Finally, the study tended to support the premise that a tracer gas can be used to simulate the respirable dust in these scale model studies. However, it is important to note that the tracer gas appeared to diffuse more evenly and further from the injection points.

### ACKNOWLEDGEMENTS

The research of this study was funded by the USBM through the Generic Technology Center for Respirable Dust. The authors are very grateful for this support under Grant Number G1135142.

The authors would also like to thank Mr. N. I. Jayaraman of the USBM and two graduate assistants, Mr. J. K. Lee and Mr. J. L. Chang, for their contributions in constructing the model.

### References

1. Gillies, A. D. S: Improvements to Coal Face Ventilation with Mining Machine Mounted Dust Scrubber System. Trans. SME-AIME 278:1982-1904 (1986).
2. Breslin, J.A. and A. J. Strazisar: Dust-Control Studies Using Scale Models of Coal Mine Entries and Mining Machines. USBM RI 8191 (1976).
3. Stein, J. A., J. A. Breslin, and A. J. Strazisar: Investigation of Dust Control by Ventilation Using A Scale Model. Am. Ind. Hyg. Assoc. J. 35:815-824 (1974).

# Size Distribution of the Airborne Dust in Longwall Coal Faces

H. S. Chiang, S. S. Peng and Y. Luo  
Department of Mining Engineering, West  
Virginia University

## Introduction

The way in which the particle sizes distribute in the airborne coal dust plays an important role in the transportation of the dust in the mine air and human respiratory systems. Though the particles of a size less than 10 microns could be inhaled, the real distractive portion of the dust is that the sizes range from 1 to 5 microns since only they can reach the lungs and be retained there. Those with an equivalent diameter larger than 5 microns will settle on the membranes of the branchial tubes<sup>(1)</sup> while those with diameter less than 1 micron can either be exhaled out of the lungs or the settled quantity is so insignificant that does very little harm to the lungs. In the transportation process, the finer dust will fly farther away from the sources than the coarser ones. Thus once the fine dust is generated and becomes airborne, it will spread out to a larger area.

In this paper, the coal samples collected from two longwall faces were analyzed statistically for size distribution. A mathematical model is proposed and the effects of different conditions on the dust size distribution were analyzed using the mathematical model.

## Sampling and Statistical Analyses

### *Sampling Instrument and Procedure*

The instrument used in the sampling were Mine Safety Appliance (MSA) personal sampling units equipped with 10-mm nylon cyclones, pre-weighed MSA PVC filters and constant-flow pumps.

Two longwall operating faces were selected for the dust sampling. The two faces were located in two coal mines extracting Pittsburgh seam. The double-ended ranging-drum shearer applying the unidirectional cutting sequence was employed. The two-leg shield supports were used for face support. The width of the two faces was about 215 meters.

In each of the two faces, four sampling stations were set up. The stations were located at the cross-cut immediately outby the headentry side, the 15th support (25 m), 65th support (107 m) and 111th support (182 m) from headentry T-

junction, and numbered as #1, #2, #3, and #4 station, respectively (Figure 1). At each sampling station, a group of three sampling units was hung at proper position. At cross-cut (#1) station, the units were hung about one foot under the roofline in the center of the cut (Figure 2a), and at the stations in the face, the units were position near the hydraulic legs and one foot below the support canopy (Figure 2b).

One complete set of 12 samples was collected for each day. The sampling were performed for five consecutive days. All the samplings were conducted in the morning shifts. The time duration of the sampling for each day was about five hours. During that time, the shearer might complete 5 to 7 mining cycles.

### *Method of Laboratory Analyses*

The samples were analyzed by Coulter Counter. In this method, the size range of the dust particles is divided into several sub-ranges with varying range widths, for example, 0.79-1.00, 1.00-1.26, 1.26-1.59, . . . , 16.01-20.17, 20.17-25.41 microns. The number of dust particles in each sub-range is counted and the total weight of those particles is determined.

### *Results of Laboratory Analyses*

Since the dust concentration at any point in the longwall faces varies with time and its relative position with shearer's cutting and support advancing, the time-weighted average dust concentration (TWADC) is more representative of the dust exposure experienced by the face crew. TWADC is the sum of the products of the instantaneous dust concentrations and its time durations divided by the total sampling time or in integral form

$$\bar{N}(x) = \frac{1}{T} \int_0^T N(x, t) dt \quad (1)$$

where:

TABLE I

Dust Sample Weight (mg) for Panel #1, Station #4

Size range (um)	Date			Average
	10/22/85	10/23/85	10/24/85	
0.79 - 1.00	0.021	0.038	0.020	0.0263
1.00 - 1.26	0.030	0.047	0.027	0.0347
1.26 - 1.59	0.045	0.065	0.042	0.0507
1.59 - 2.00	0.078	0.095	0.068	0.0803
2.00 - 2.52	0.104	0.115	0.093	0.1040
2.52 - 3.18	0.137	0.135	0.121	0.1310
3.18 - 4.01	0.127	0.112	0.112	0.1170
4.01 - 5.05	0.087	0.057	0.070	0.0713
5.05 - 6.36	0.042	0.030	0.034	0.0353
6.36 - 8.01	0.029	0.033	0.035	0.0323
8.01 - 10.09	0.017	0.017	0.010	0.0147
10.09 - 12.71	0.007	0.000	0.014	0.0070
12.71 - 16.01	0.014	0.000	0.000	0.0047
16.01 - 20.17	0.028	0.000	0.000	0.0093
20.17 - 25.41	0.000	0.006	0.000	0.0020
TOTAL	0.766	0.750	0.646	0.721

- N(x) = TWADC at the sampling station x m from headentry T-junction in the face;
- N(x,t) = instantaneous dust concentration at station x and at time t;
- T = time duration of the sampling.

The results of the size analysis for the dust samples from Station #4, Panel #1 are shown in Tables I and II. Table I shows the dust weight by size range, and Table II shows the number of dust particles in each range. It is quite obvious that there are very few dust particles larger than 20 microns (equivalent diameter).

Statistical Analyses

In order to make the analyses of the dust size distribution more accurate and meaningful, the statistical analyses go through the following three steps:

Step I: Data Transformation

The raw data are transferred into cumulative percentile data by the following equations:

A. For cumulative dust weight in percent, P<sub>w</sub>

$$P_w(D_i) = 100 \left( \sum_{j=1}^i w_j \right) / W \quad (*) \quad (2)$$

where:

- D<sub>i</sub> = upper size boundary of the ith size sub-range;
- w<sub>j</sub> = total weight of the dust particles with their size falling into jth size sub-range;
- W = total weight of the prepared samples.

The transferred cumulative dust weight percentiles for Station #4, Panel #1 are plotted against the upper boundary of each range in Figure 3. This figure shows that at the sampling station, though the size composition of each individual sample deviates from each other to some extent, the degree of the deviation is very small and the general trend is similar.

B. For cumulative number of dust particles in percent, P<sub>N</sub>,

$$P_N(D_i) = 100 \left( \sum_{j=1}^i n_j \right) / N \quad (*) \quad (3)$$

where:

- n<sub>j</sub> = number of dust particles with their size falling into the jth size sub-range;
- N = total number of the dust particles in the prepared sample.

The computed cumulative percentiles and the average values for Station #4, Panel #1 are plotted as Figure 4.

Step II: Regression

A. For cumulative dust weight, a function is proposed

$$P_w = 100 - bDe^{-cD^d} \quad (4)$$

to fit the cumulative weight percentiles. In the expression, P<sub>w</sub> is the average cumulative dust weight percentile, b, c, d are coefficients and D the equivalent diameter of the dust particles in microns.

The predicted cumulative dust weight percentile vs dust size curves for the two investigated panels are plotted in Figures 5 and 6. The good agreement between the data points and the prediction curves is evident.

B. For cumulative number of dust particles

$$P_N = 100 (1 - e^{-aD^2}) \quad (5)$$

The following regression function was proposed for the cumulative number percentiles

where:

- a = a coefficient

The prediction curves are plotted in Figures 7 and 8 for Panels #1 and #2, respectively.

# SIZE DISTRIBUTION OF AIRBORNE DUST

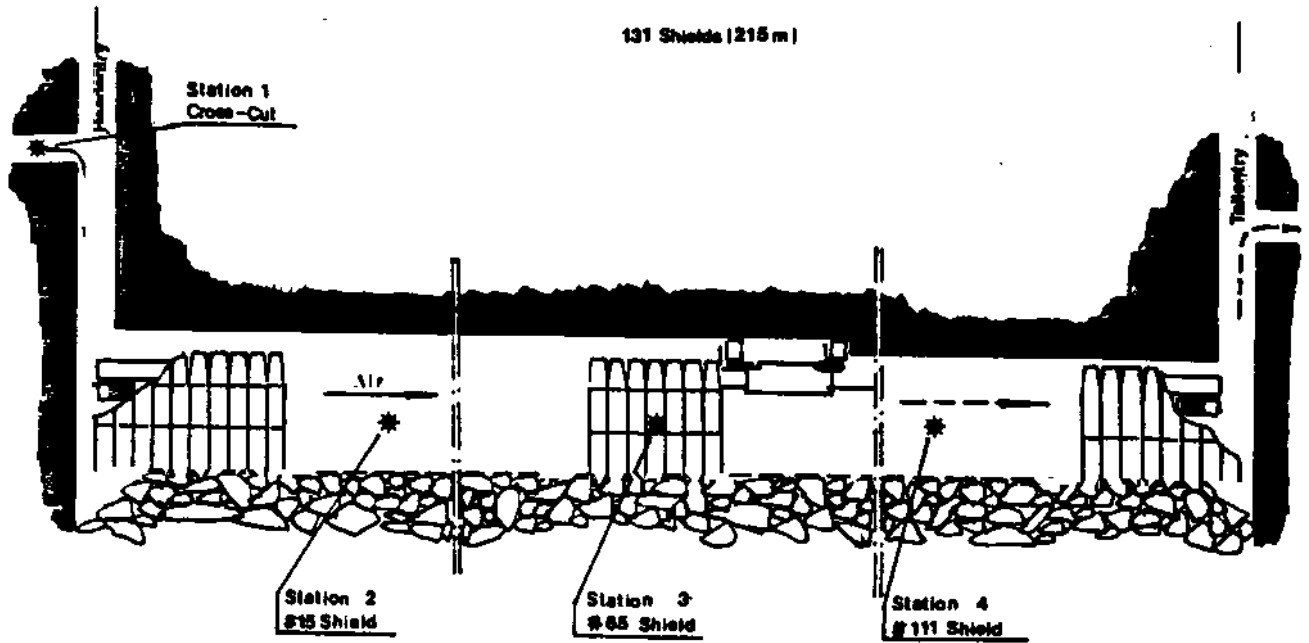


FIGURE 1. Face layout showing the location of the sampling stations.

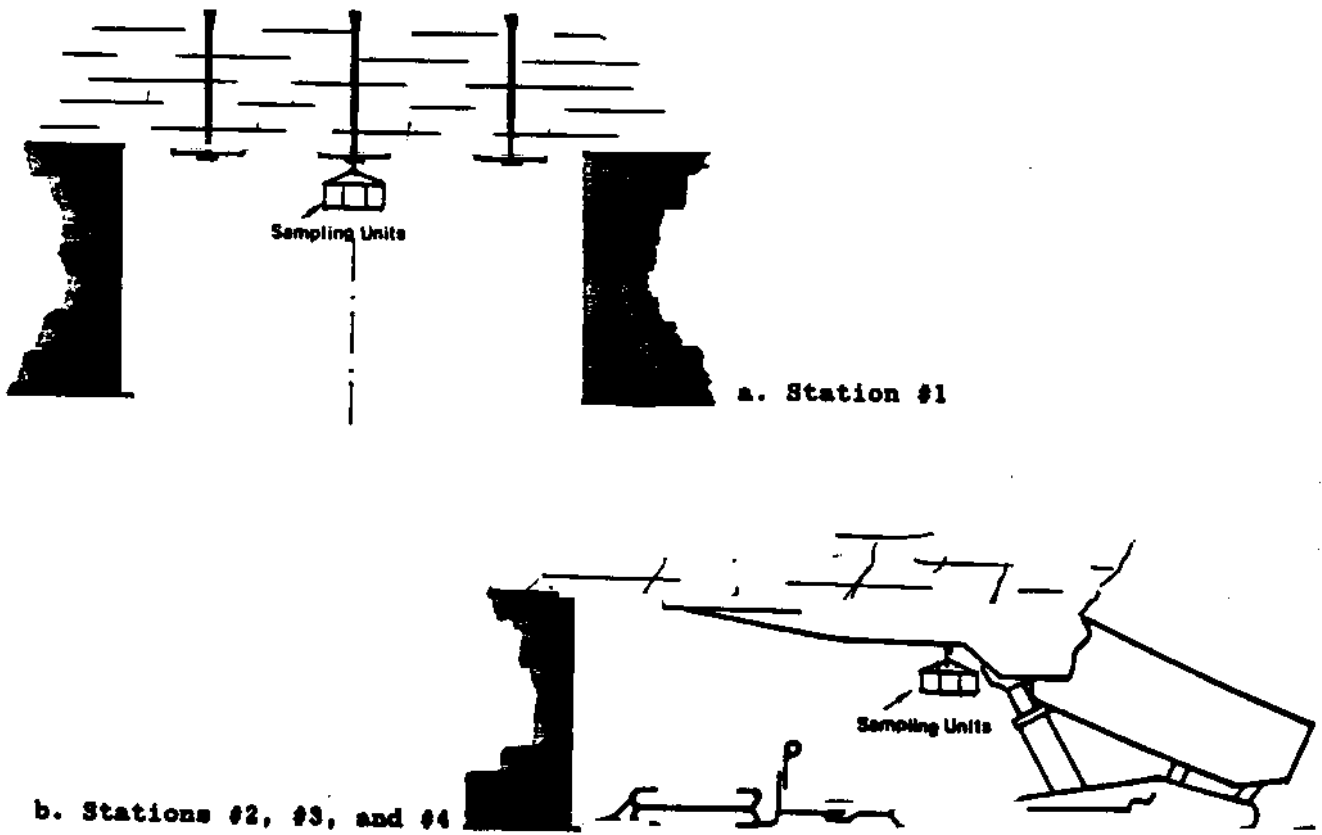


FIGURE 2. Installation methods of sampling units at various stations.



# THE RESPIRABLE DUST CENTER

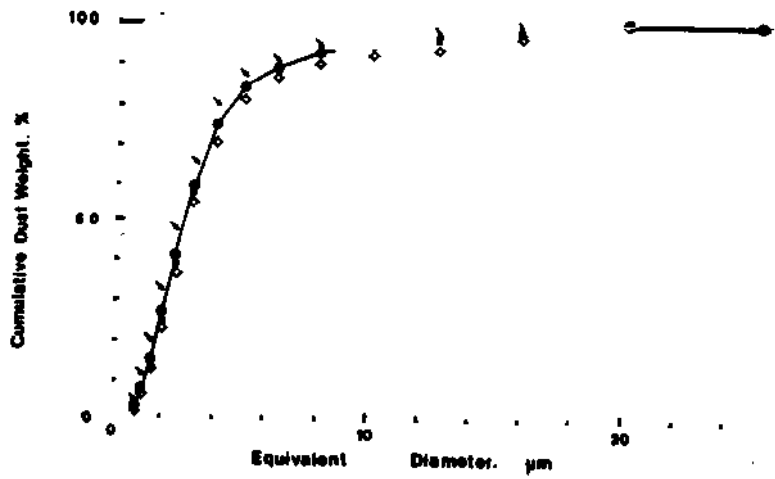


FIGURE 3. Cumulative dust weight for panel #1, station #4.

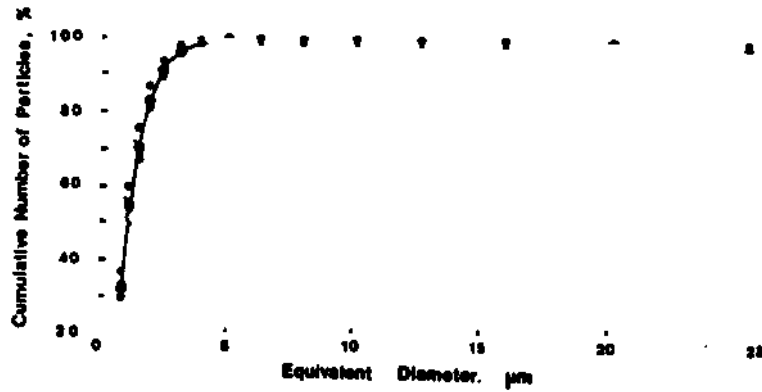


FIGURE 4. Cumulative number of particles for panel #1, station #4.

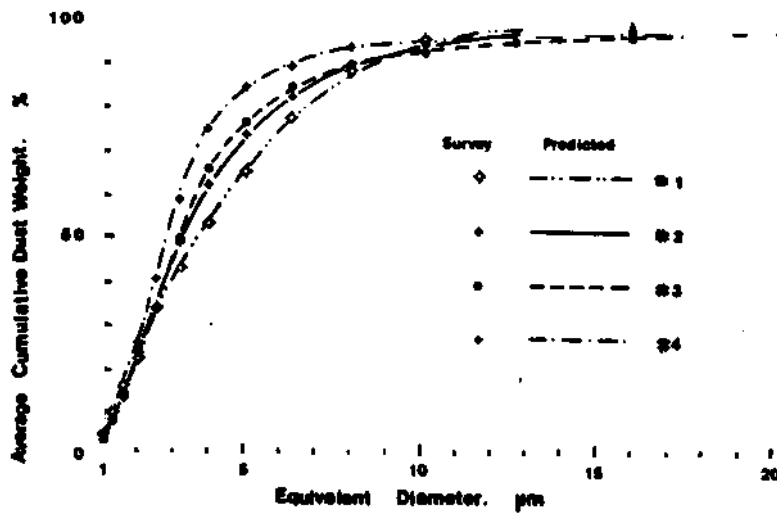


FIGURE 5. Average cumulative dust weight for panel #1.

# SIZE DISTRIBUTION OF AIRBORNE DUST

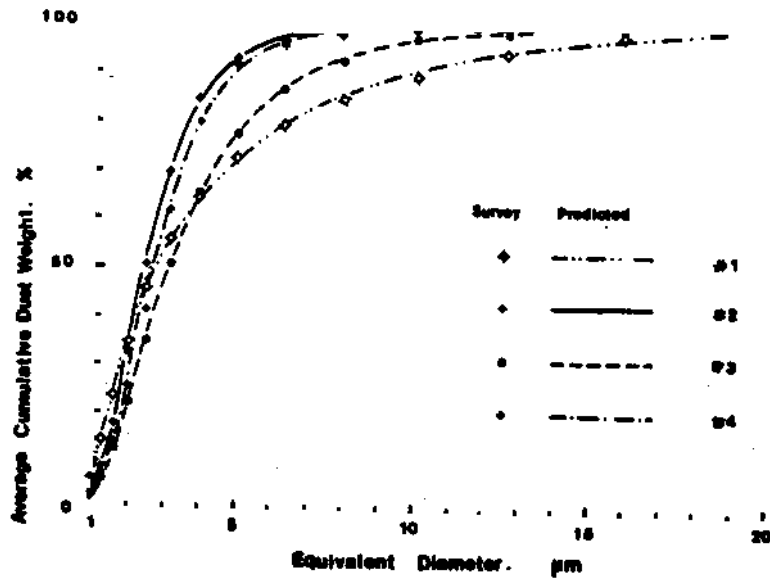


FIGURE 6. Average cumulative dust weight for panel #2.

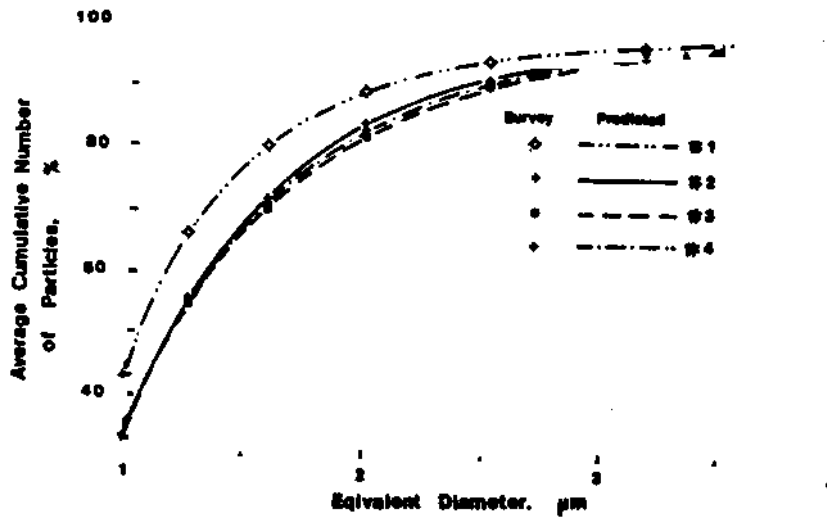


FIGURE 7. Average cumulative number of particles for panel #1.

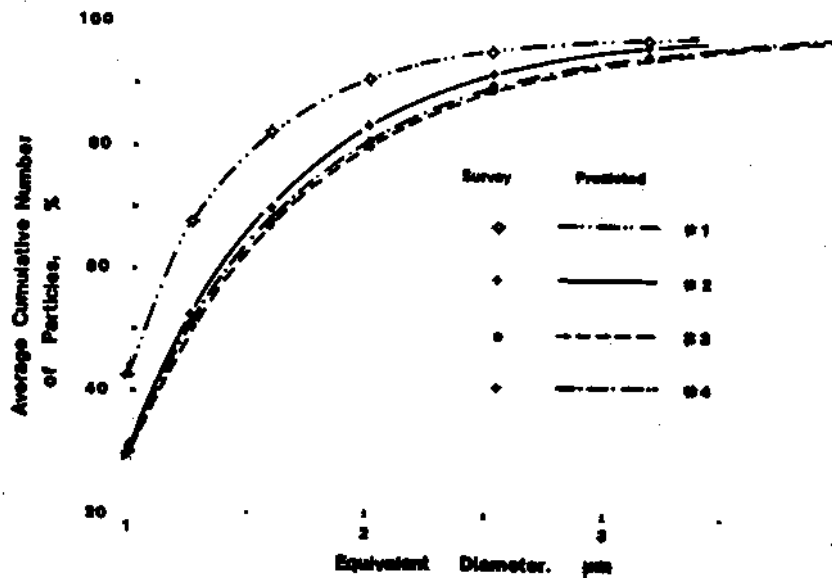


FIGURE 8. Average cumulative number of particles for panel #2.

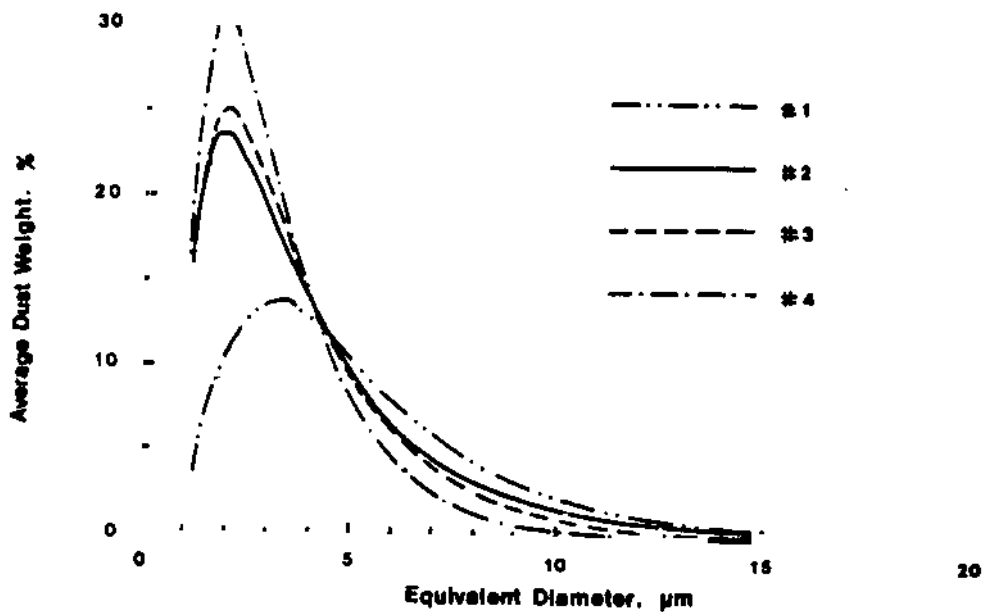


FIGURE 9a. Size distribution for Panel #1; Average dust weight.

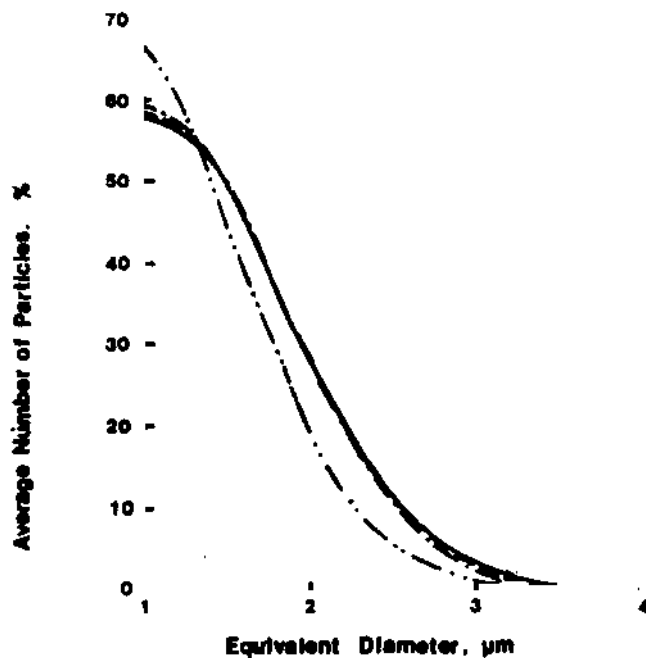


FIGURE 9b. Size distribution for Panel #1; Average number of particles.

Step III: Differentiation

By differentiating equations 4 and 5, the functions of size distribution in terms of dust weight and number of dust particles can be obtained, respectively as

$$P_w = \frac{dP}{dD} = be^{-cD^d} (cdD^{d-1} - 1) \quad (6)$$

$$P_n = \frac{dP}{dD} = 200 aD^{-aD^2} \quad (7)$$

The predicted size distribution curves for the two panels are plotted in Figures 9 and 10. It should be noted that the effective size range for equations 6 and 7 is only from 1 to 20 microns.

Figure 9a shows that at Panel #1 the dust becomes finer as the distance from headentry T-junction toward the tailentry increases; in other words, the percentage content of the fine dust (i.e., 1 to 5 microns) increases as the airborne dust travels in the face. For example, if we apply equation 4

## SIZE DISTRIBUTION OF AIRBORNE DUST

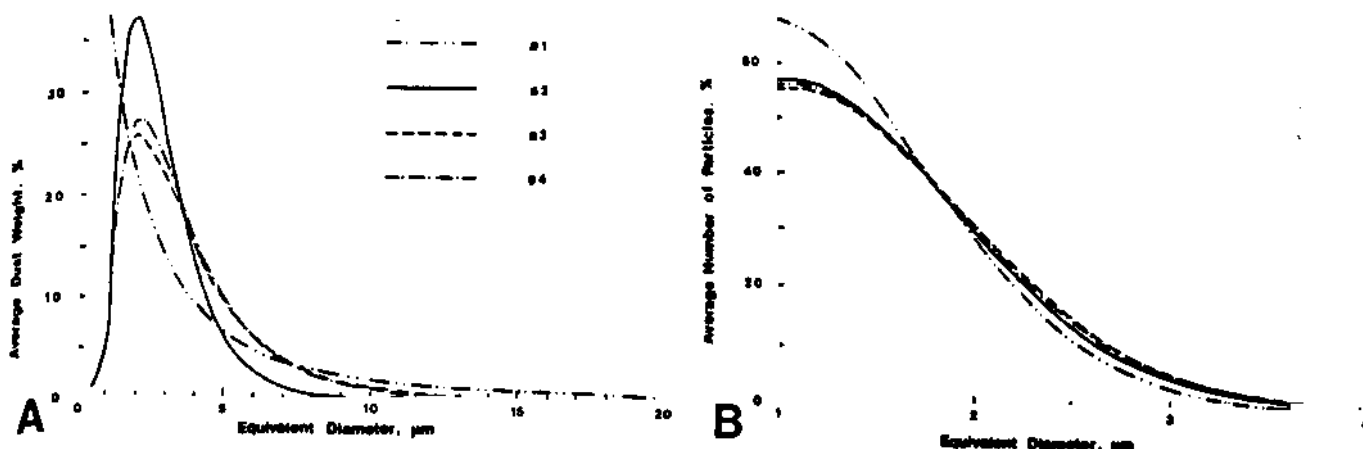


FIGURE 10. Dust size distribution for Panel #2. A. Average dust weight; B. Average number of particles.

at Stations #2, #3 and #4, the percentage contents in weight of the fine dust are 70, 72 and 80 percent respectively. However, Figure 10a indicates that in Panel #2, more fine dust exists in both the headentry side and the tailentry side of the face than that at the middle face. The weight percentage of fine dust at corresponding Stations #2, #3 and #4 are 88.5, 74 and 77 percent respectively. Another distinctive phenomenon is that the dust size distribution curve for Station #1 (cross-cut) in Panel #1 is more widely spread out while that for Panel #2 is heavily skewed toward the fine dust range. This was mainly due to the difference in air velocity in the main and panel intake entries. The air velocity measured at Station #1 and in the intake entry of Panel #1 was around 400 fpm (2.2 m/sec) while that for Panel #2 was under 300 fpm (1.64 m/sec). Thus when the ventilation air passed the airways in Panel #2, only those dust particles much finer than those at Panel #1 could reenter the airflow and stay in the air for a longer time.

In the past, some works on the size distributions of the dust samples collected in continuous mining sections<sup>(2)</sup> and the dust samples generated in laboratory<sup>(3)</sup> had been done. The size distribution curves presented in those works are somewhat different from those shown in Figures 9 and 10. The main reason might be the difference in the coal properties and experimental conditions. The size distribution curves of the coal dust in the continuous mining sections appear to have two or more modes as shown in Figure 11 instead of the single mode in Figures 9 and 10. Also, Figure 11 shows that only about 30 percent of the dust was under the size of 5 microns and the rest is between 5 and 45 microns. The discrepancy may be attributable to the following reasons:

1. In the continuous mining sections, the dust experienced at the sampling location usually comes from several major dust sources which are either fixed at certain locations or moving within a small region. They are located at various distances from the sampling location in the upstream air. As it travels to the sampling station, a larger portion of the coarse particles of the dust originated from farther source will have settled down than those from the nearer sources. Consequently, the final size distribution patterns of the dust generated and transported from various sources will be different

from the others, even if the size compositions of the source dust are the same, the superposition of the individual size distribution curves will likely define the composite size distribution curve of the mixture of the dusts from different sources and result in two or more modes.

2. During the preparation of the dust samples for Coulter Counter analysis, some rebreakage of the dust particles might have occurred. This might have made the peak region of the dust size distribution curve move toward the fine dust side to some extent. However, during the collection and analyses of the dust samples using impactor as in the continuous mining section,<sup>(2)</sup> there was no further rebreakage of the dust particles.

The size distribution patterns of the coal dust generated and collected in the laboratory are shown in Figure 12.<sup>(3)</sup> Curve A is for anthracite and Curve B is for bituminous coal. The cumulative weight percentile curves in Figure 12 could be converted into the percentile distribution curve as shown in Figure 13. The pattern of the curve for bituminous coal is

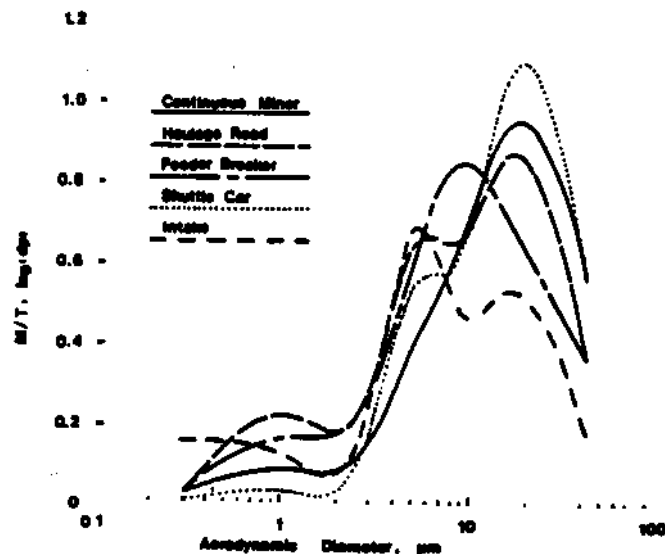


FIGURE 11. Size distribution of dust continuous mining section.<sup>(2)</sup>

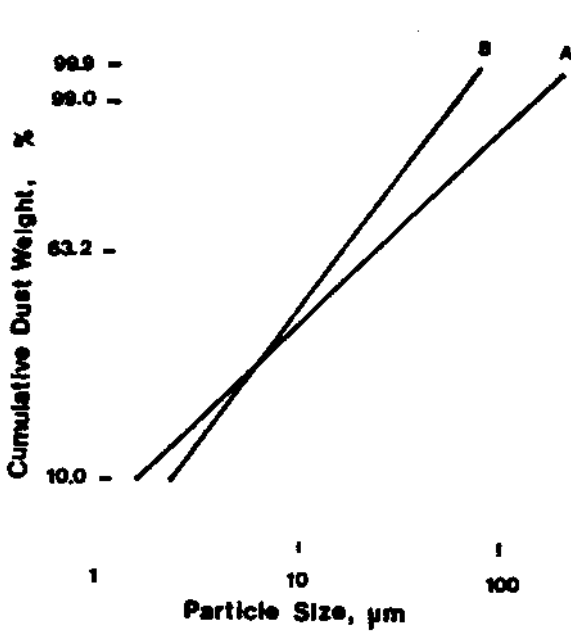


FIGURE 12. Cumulative size distribution of the coal dust generated in the laboratory A — anthracite, B — bituminous.

somewhat similar to the curves obtained in Figures 9 and 10 except that the curve is much widely spread out.

In some countries, such as Great Britain, the standards of permissible dustiness are set in term of the number of dust particles with sizes between 1.0 and 5.0 microns per unit volume of ventilation air.<sup>(4)</sup> For such countries, the studies on the size distribution in terms of number of dust particles are more important than that in terms of dust weight.

### Mathematical Modeling

#### Mathematical Development

Since the sampling time conducted for the research usually lasted as long as five hours, the dust generating sources in the longwall faces could be simplified as continuous sources. For the source emanating dust continuously, the concentration fall along a length  $dx$  on the traveling way of the dust-laden air may be regarded as proportional to the initial concentration,  $N$ ,<sup>(5)</sup> i.e.,

$$\frac{dN}{dx} = -N \quad (8)$$

The proportionality coefficient may be regarded as a function of the equivalent diameter of the dust particles  $D$ , the specific weight of dust  $\rho$ , the mean air velocity  $V_m$ , the ratio of perimeter to area of the cross-section of the ventilation space  $A$ , the acceleration due to gravity  $g$ , and the viscosity coefficient of the dust-laden air  $\mu$ , i.e.,

$$-M = \frac{A\rho D^2 g}{V_m \mu} \quad \text{or} \quad -M D^2 \quad (9)$$

where:

- $M = m (A\rho g/V_m \mu)$ ;
- $m = \text{a constant.}$

Thus the following differential equation can be set up

$$\frac{d}{dx} N(D, x) = -M D^2 N(D, x) \quad (10)$$

The particular solution to this differential equation is

$$N(D, x) = N_0(D) e^{-M D^2 x} \quad (11)$$

where:

- $N(D, x)$  = the mean concentration of the dust with equivalent diameter being  $D$  microns in the ventilation airflow on the cross-section  $x$  meters downstream from the source,
- $N_0(D)$  = the mean concentration of the dust of size  $D$  at the cross-section where the dust source originates.

Before discussing the application of equation 11, the following assumptions should be made:

1. In either the trip from headentry to tailentry or vice versa, the rate of dust generation and the size

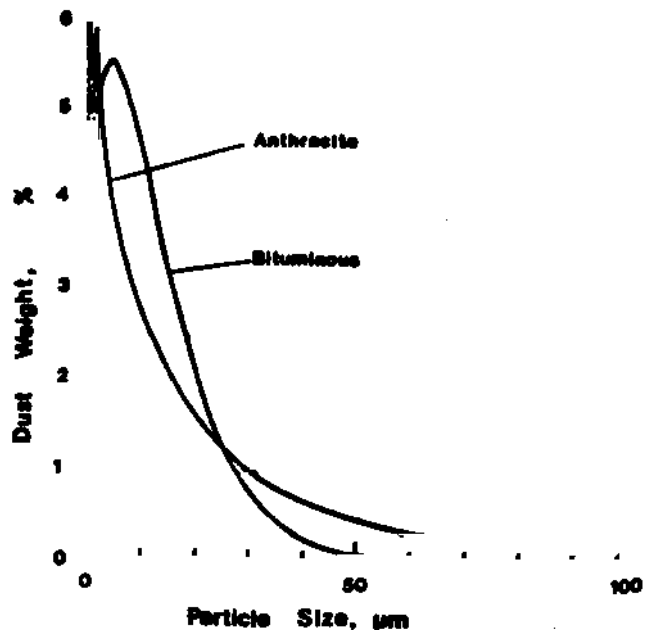


FIGURE 13. Size distribution of the coal dust generated in the laboratory.

## SIZE DISTRIBUTION OF AIRBORNE DUST

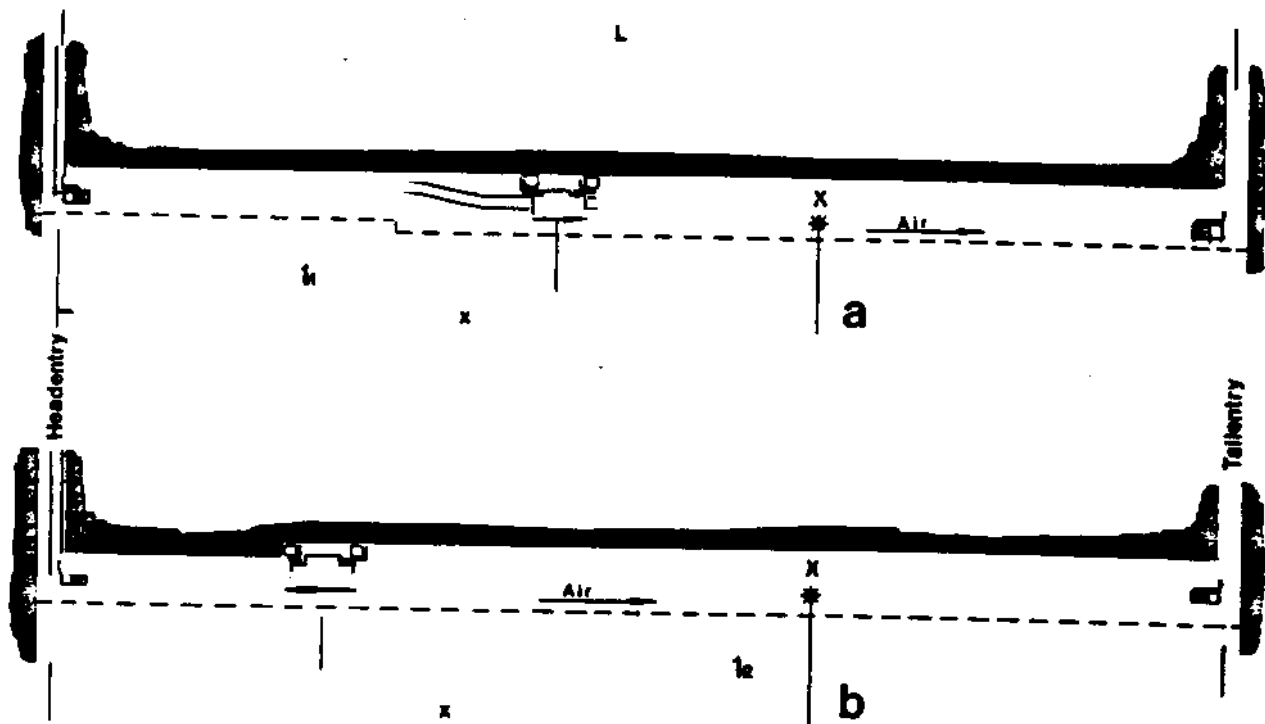


FIGURE 14. Symbols used in mathematical modeling of dust size distribution: (a) Head-to-tail; (b) tail-to-head trip.

composition of the dust generated by the shearer's operation are constant regardless of the shearer's position in the face. The size composition functions of the sources at the cross-section right behind the shearer on the return side are  $N_{01}(D)$  and  $N_{02}(D)$  for the head-to-tail trip and tail-to-head trip, respectively.

2. The haulage speed of the shearer and the rate of support advancing are synchronized, that is, when unidirectional cutting is applied, the trailing distance of the support advancing in shearer's cleaning trip is always the same. Thus in the cleaning trip, the two dust sources, i.e., support advancing and the shearer's cleaning, could be combined into a single constant continuous source.
3. As compared to the dust concentration on the return side of the shearer (mostly greater than  $1.5 \text{ mg/m}^3$ ), the dust level on the intake side of the shearer is much lower (mostly less than  $0.3 \text{ mg/m}^3$ ) and stable.<sup>(6)</sup> The dust concentration and size composition of the airborne dust on the intake side of the shearer are assumed to be constant and the same as those at headentry T-junction. The size composition function is  $N_c(D)$ .
4. The haulage speed of the shearer is constant throughout the full width of the face, or  $V_1$  for the head-to-tail and  $V_2$  for the tail-to-head trip.

Based on the above assumptions and equation 11, the mean concentration of the dust with equivalent diameter of the particles being  $D$  microns on the cross-section at the sampling location  $x$  meters from headentry T-junction could be defined as:

A. For the head-to-tail trip (Figure 14a)

$$N_1(D, x) = \begin{cases} N_{01}(D)e^{-MD^2(x-\xi_1)} & \xi_1 \leq x \\ N_c(D) & \xi_1 > x \end{cases} \quad (12)$$

B. For the tail-to-head trip (Figure 14b)

$$N_2(D, x) = \begin{cases} N_{02}(D)e^{-MD^2(\xi_2+x-L)} & \xi_2 > L - x \\ N_c(D) & \xi_2 \leq L - x \end{cases} \quad (13)$$

The integrations of the product  $N(D, x)dt$  are performed as follows:

For the time duration when the shearer is operating

$$\begin{aligned} \int_0^{L/V_1} N_1(D, x) dt &= \\ \frac{1}{V_1} \int_0^x N_{01}(D)e^{-MD^2(x-\xi_1)} d\xi_1 &+ \\ + \frac{1}{V_1} \int_x^L N_c(D) d\xi_1 & \quad (14) \\ = \frac{1}{V_1} \left[ \frac{N_{01}(D)}{MD^2} (1 - e^{-MD^2x}) + N_c(D)(L-x) \right] \end{aligned}$$

THE RESPIRABLE DUST CENTER

$$\int_0^{L/V_2} N_2(D,x) dt = \frac{1}{V_2} \int_0^{L-x} N_C(D) d\delta_2 + \frac{1}{V_2} \int_{L-x}^L N_{O2}(D) e^{-MD^2(\delta_2+x-L)} d\delta_2 \quad (15)$$

$$= \frac{1}{V_2} \left[ \frac{N_{O2}(D)}{MD^2} (1 - e^{-MD^2x}) + N_C(D)(L-x) \right]$$

If the mean idle time for a complete mining cycle is  $T_d$ , then the integration during this time is

$$\int_0^{T_d} N_C(D) dt = N_C(D) T_d \quad (16)$$

Thus the time-weighted average dust concentration (TWADC) with particle size being  $D$  microns at the sampling location  $x$  in a mining cycle, which also approximates the TWADC for the whole working shift at this location, could be calculated by

$$\bar{N}(D,x) = \frac{1}{T_c} \left[ \frac{1 - e^{-MD^2x}}{MD^2} \left( \frac{N_{O1}(D)}{V_1} + \frac{N_{O2}(D)}{V_2} \right) \right]$$

$$+ N_C(D)(L-x) \left( \frac{1}{V_1} + \frac{1}{V_2} \right) + N_C(D) T_d] \quad (17)$$

where:

$T_c$  = mean time duration of a complete mining cycle and equal to

$$T_c = L/V_1 + L/V_2 + T_d \quad (18)$$

The TWADC at the sampling location is simply an integration of equation 17 with the particle's equivalent diameter varying from 0 to the maximum possible size (i.e., 20 microns in this case). or

$$\bar{N}(x) = \int_0^{20} \bar{N}(D,x) dD \quad (19)$$

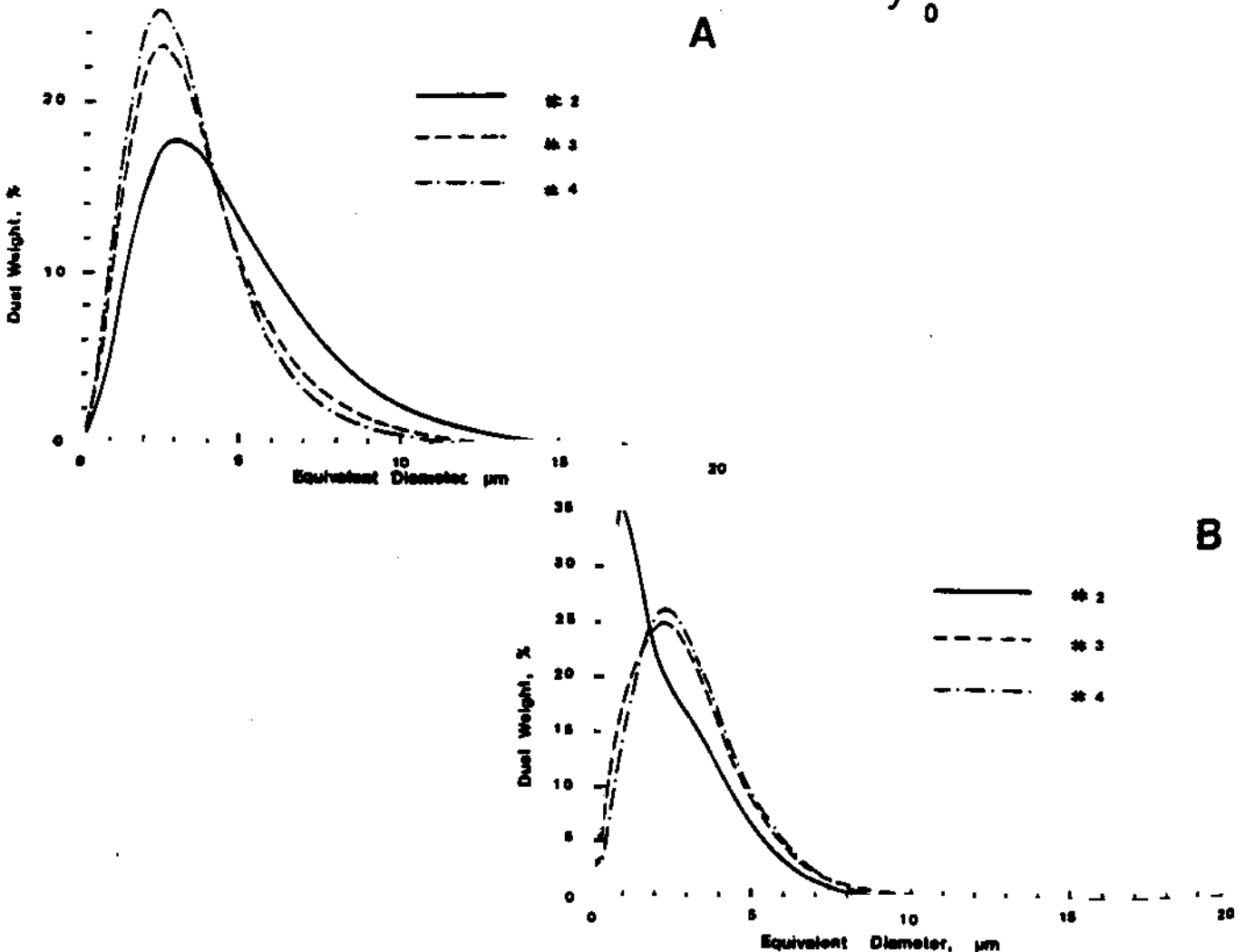


FIGURE 15. Dust size distribution as predicted by the mathematical model; A. Panel #1; B. Panel #2.

## SIZE DISTRIBUTION OF AIRBORNE DUST

The percent content of the dust with size being  $D$  microns in the dust at the sampling location  $x$  can be computed as

$$P_w(D) = 100 \bar{N}(D, x) / \bar{N}(x) \quad (20)$$

### Applications

Using equations 17, 19 and 20, the TWADC distribution and size distribution along the longwall faces can be simulated under different geological, operational and environmental conditions.

Since the integration of equation 19 cannot be performed analytically, the numerical method, Simpson's 1/3 rule, is applied. However, the process of computation is very tedious and time-consuming if done by hand. Thus a short menu-driven computer program was written to perform the task. The input information to this program is the dust size composition functions of the dust sources in the face, the size

composition function of the dust at headentry T-junction. The transporting coefficient  $m$ , shear haulage speeds  $V_1$  and  $V_2$ , mean idle time  $T_d$ , width of the longwall face  $L$ , perimeter to area ratio  $A$ , mean air velocity  $V_m$ , dust density. The output can be either one of the following two or both:

1. TWADC distribution along the face.
2. Size distribution at a specified location in the face.

### Simulation of Dust Size Distributions for the Two Panels

When running the program, the source dust size compositions  $N_{01}(D)$  and  $N_{02}(D)$  for Panel #1 are assumed to be the same functions as those at Panel #2. The  $N_c(D)$ 's for the two panels assumed the shape as obtained at the cross-cut station (Station #1). The in-mine operational conditions were used as input parameters. The mean air velocity at Panel #1 was 2.211 m/sec (404 fpm) and at Panel #2 was 1.567 m/sec (287 fpm).

The outputs were the percent contents (percentiles) in dust weight with various equivalent diameter  $D$ 's. Figure 15

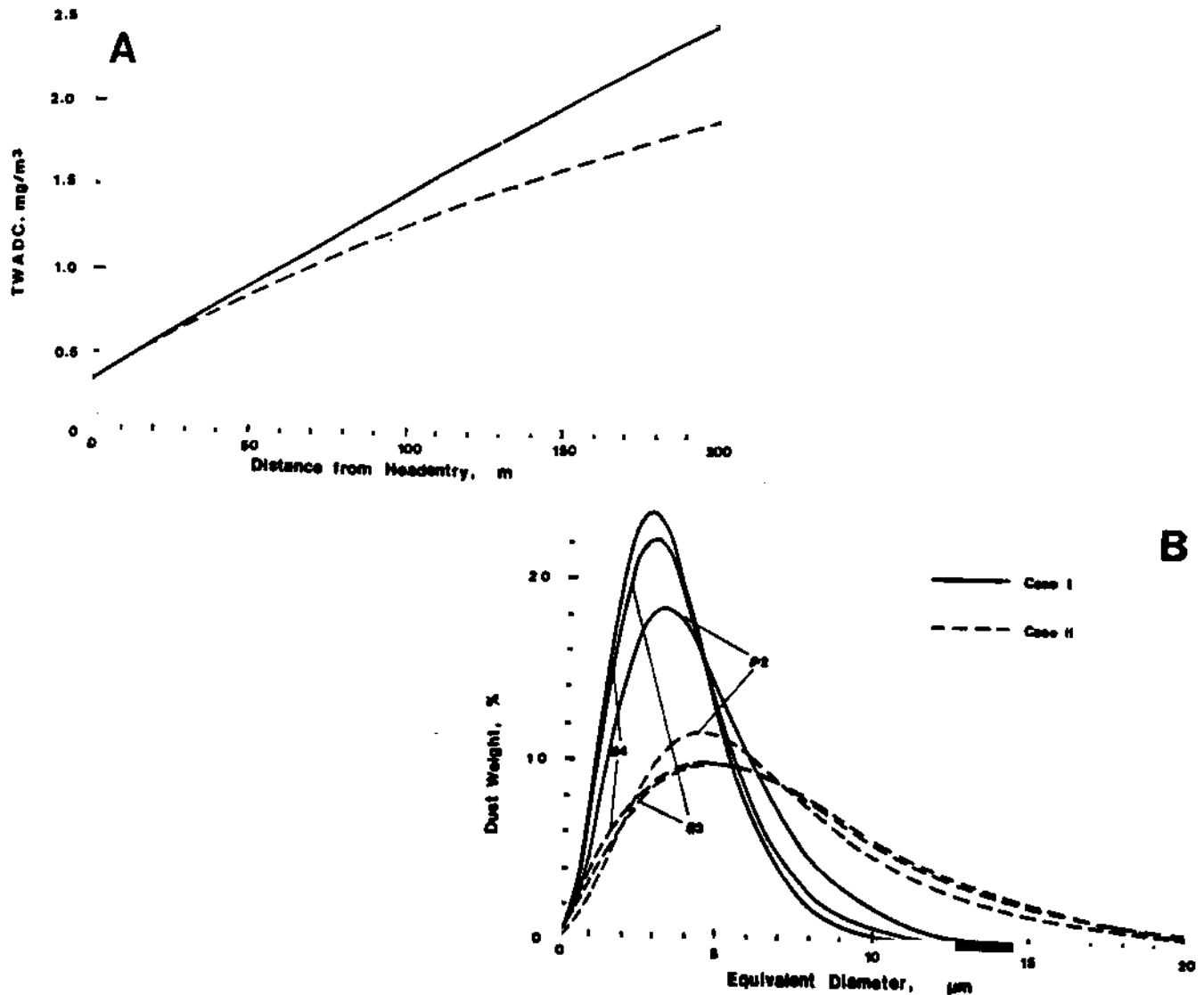


FIGURE 16. Effects of size distribution at the dust sources. A. TWADC, B. Dust weight.



shows the outputs for the two panels at locations #2, #3, and 4. Figure 15a shows the stimulated size distribution patterns for Panel #1. As compared to Figure 9a, it can be seen that though there exist some differences in magnitude ( $< 5\%$ ), the size distribution patterns are very similar. The general trend remains, i.e., more fine dust is contained in the air as the dust-laden air travels towards the tailentry. Figure 15b shows the stimulated size distribution patterns at Panel #2. The magnitude does not deviate much between the simulation and the actual survey for the sampling Stations #2, #3 and #4. The maximum difference in magnitude is only about three percent. However, the shape of the size distribution curve at Station #2 is not similar.

The preceding simulations also revealed that the size composition of the sources affects greatly the overall size distribution in the face. In order to assess the effects of some geological and operational conditions on the TWADC and size distribution in the longwall faces, the following simulations are performed using the same basic parameters as those in the simulation of Panel #1.

*Effects of Size Distribution at the Sources*

The simulation results of two cases with different size compositions in the sources are shown in Figure 16. In both cases the dust generation rate of the dust sources in the faces are the same. In Case I, the size composition functions of the dust sources are similar to those in Panel #1, and in Case II, the shapes of the size composition curves are much widely spread out, or in other words, the amount of fine dust at the sources of Case II is less than those in Case I. The simulations indicate that the TWADC at tailentry T-junction in Case II is about  $0.6 \text{ mg/m}^3$  lower than that of Case I (Figure 16a). Figure 16B shows that at all the locations in the face in Case II, the percent content of fine dust is much less than that in Case I. The significant reduction of the fine dust (1 to 5 microns in size) will surely improve the working environment of the longwall faces).

*Effects of Mean Air Velocity*

The mean air velocities 1 m/sec (183 fpm) and 4 m/sec (732 fpm) were tried on the simulation program. The results are shown in Figure 17. Since the relationship between the air velocity and the rate of dust generation at source and the dust reentrainment along the air passage is a very compli-

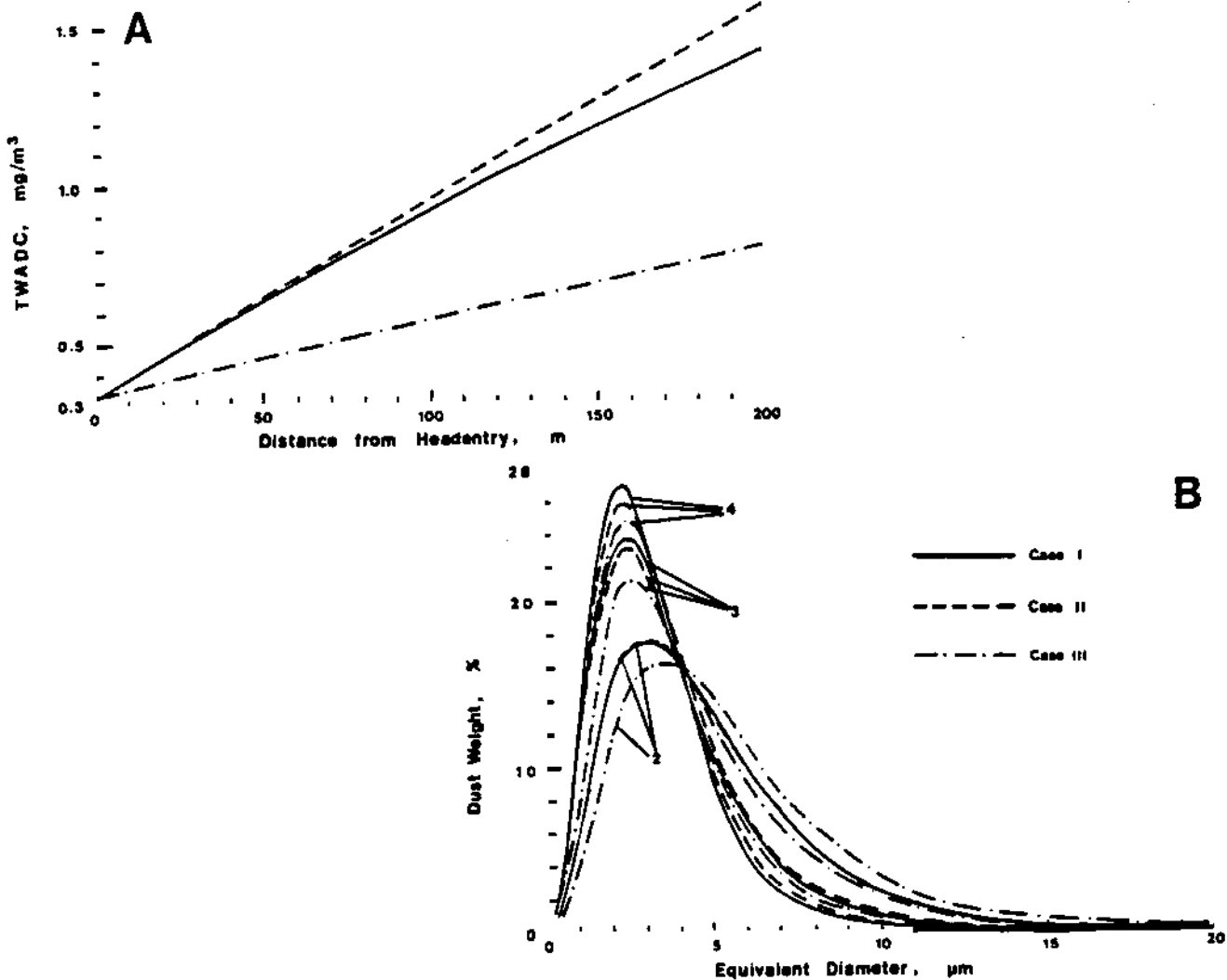


FIGURE 17. Effects of mean air velocity. A. TWADC; B. Dust weight.

## SIZE DISTRIBUTION OF AIRBORNE DUST

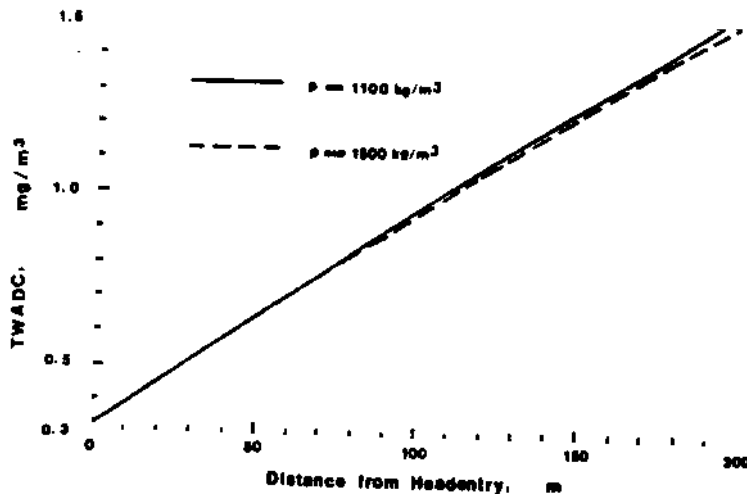


FIGURE 18. Effects of the specific weight of the dust.

cated matter, the results presented here are based on three cases of assumption:

**Case I:** The mean air velocity is 1 m/sec and the dust generation rates of the sources are  $Q_{01}$  and  $Q_{02}$ . The dust concentrations at the cross-sections where the sources originate are  $N_{01}$  and  $N_{02}$  for the head-to-tail trip and tail-to-head trips, respectively.

**Case II:** The mean air velocity is increased to 4 m/sec. However, the blowing-up effects of the fast-traveling air are so strong that the dust generation rates at the sources are increased to  $4Q_{01}$  and  $4Q_{02}$ . Thus the mean dust concentrations on the cross-sections where the sources originate remain the same as  $N_{01}$  and  $N_{02}$  for the head-to-tail and tail-to-head trips, respectively, because of the dilution of the increased ventilation air quantity. Generally speaking, this case is unlikely to happen. Here it is treated as an extreme case.

**Case III:** The mean air velocity is increased to 4 times. However, the dust generation rates of the sources are only increased to two times as those in Case I, or  $2Q_{01}$  and  $2Q_{02}$ . The mean dust concentrations become  $0.5N_{01}$  and  $0.5N_{02}$  at the cross-sections where the dust sources originate for the head-to-tail and tail-to-head trips.

Comparing the simulated results when the air velocity is 4 m/sec with those when the air velocity is 1 m/sec, the following observations are obvious:

1. In Case II, when the air velocity and the dust generation rates are increased to four times of those in Case I, the TWADC along the face increases slightly and the portion of the fine dust decreases slightly.
2. When the air velocity is increased to four times as that in Case I, but the dust generation rates are only increased to two times as those in Case I, both the TWADC and the percent content of the fine dust are reduced. The reduction of TWADC along the face is more significant. The maximum reduction is about  $0.65 \text{ mg/m}^3$  at the tailentry T-junction.

### Effects of Specific Weight of the Dust

In mining practice, there is really not much artificial control on the specific weight of the dust except the wetting of

the dust by water spraying and premining injection of water. The specific weight of the coal dust is usually taken as the specific weight of the coal. However, the specific weight of the coal differs from seam to seam, from location to location. Two cases with different specific weights of dust,  $1100 \text{ kg/m}^3$  and  $1500 \text{ kg/m}^3$ , are simulated on the program. The TWADC distribution curves along the face are shown in Figure 18. The change in specific weight of the dust from 1100 to  $1500 \text{ kg/m}^3$ , which are almost the two extremes, only results in a small reduction in TWADC. The maximum reduction in TWADC is only about  $0.1 \text{ mg/m}^3$  which occurs at the tailentry T-junction. The size distribution curves in both cases almost overlap at nearly all the locations of the face just as shown in Figure 9a.

### Assessments

Based on the computer simulations on the effects of various factors, it is found that the most effective techniques for the dust control in the longwall faces is to reduce the generation rate of fine dust at the dust sources. By this method, both the TWADC and the fine dust content decrease drastically in the faces. Past practices and experiments have demonstrated that the water-through-bit internal spray, fine particle water external spray, and water-steam spray<sup>(7)</sup> techniques can reduce the generation of the fine dust and capture the already airborne fine dust particles significantly at the sources.

The second effective method of controlling TWADC is to properly increase the air velocity in the longwall faces. For most of the longwall faces investigated in recent years,<sup>(6)</sup> the problem is how to reduce the air leakage to the gob area and improve the ventilation efficiency. For some of the faces, as much as 75 percent of the airflow measured near the headentry T-junction goes into the gob area<sup>(8)</sup> instead of going to the face working area and for the dilution of dust concentration.

### Summary

Dust samples were collected in two operating longwall faces and analyzed in the laboratory by Coulter Counter. Statistical analyses reveal that the size distribution curves at

ny location of the faces skew heavily toward the fine dust side. The amount of fine dust (1 to 5 microns) appears to be more than 70 percent in the airborne dust.

A mathematical model was developed and proven reasonably accurate. The computer simulations using the model demonstrate that the TWADC and the size composition of the dust particles are mainly governed by the size distribution at the dust sources and the air velocity in the face. These results suggest that the water-through-bit internal spray, fine particle water external spray may be the effective dust control methods. Also improvement of the ventilation efficiency in the longwall faces will lower the dust level in the faces

### Acknowledgment

This research has been supported by the Department of the Interior's Mineral Institute program administered by the Bureau of Mines through the Generic Mineral Technology Center for Respirable Dust under grant number G1135142.

### References

Peng, S.S. and H.S. Chiang: *Longwall Mining*, pp. 506, 520-521. John Wiley & Sons, Inc. (1984).

McCawley, M.A.: *Dust Sampling in the Mining Industry: Current Developments and Concerns*.

*Proceedings of the Coal Mine Dust Conference*, pp. 16-20. S.S. Peng, Ed. West Virginia University (1984).

3. Dwiggin, G.A.: *Variations in the Properties of Coal Dust*, pp. 45-53. University of North Carolina at Chapel Hill (1981).

4. Roberts, A., H.J. Bunt, J.R. Metcalf et al: *Mine Ventilation*, p. 115. Cleaver-Hume Press Ltd., London, UK (1960).

5. Radchenko, G.A.: *Ventilation for Dust Elimination in Underground Mines*, pp. 4, 20-21. Academy of Sciences, Kazakh SSR, Institute of Mining, USSR (1970).

6. Peng, S.S. and H.S. Chiang: *Measurement and Construction of Dust Distribution Maps for Longwall Faces*, pp. 65-107. Final report submitted to the Generic Mineral Technology Center for Respirable Dust, West Virginia University (1986).

7. Cheng, L., J.E. Emmerling and T.F. Tomb: *Collection of Airborne Coal Dust by Steam*, pp. 8-13. U.S. Bureau of Mines RI 7819 (1974).

8. Peng, S.S. and H.S. Chiang: *Air Flow Distribution at the Longwall Faces*, pp. 5-14. Preprint No. 85-439, SME-AIME Fall Meeting and Exhibit, Albuquerque, NM (1985).

# Application of a Particle Dispersion System for Obtaining the Size Distribution of Particles Collected on Filter Samples

K. L. Rubow and V. A. Marple

Particle Technology Laboratory  
Mechanical Engineering Department, University  
of Minnesota

KEY WORDS: PARTICLE DISPERSION, SIZE DISTRIBUTION, AERODYNAMIC PARTICLE SIZER

## Introduction

A particle dispersion system has been developed to aerosolize bulk powders or material deposited on surfaces such as filters. The size distribution of the aerosolized particles can then be obtained by sampling the particles with an aerosol sizing instrument such as a TSI aerodynamic particle sizer (APS) or a cascade impactor.

Of particular interest is the applicability of using this technique to obtain the size distribution of particles collected on filters. This system has been used to determine the size distribution of coal dust particle collected on membrane filters. The use of this device in this application is quite intriguing in that, if this technique can be shown to accurately determine the size distribution of airborne particles, one can easily collect particle samples using either personal or area particle samplers, determine the mass concentration of the collected material through gravimetric techniques and then use the particle dispersion system coupled with the APS to determine the particle size distribution. With this technique one can determine the particle size of dust in environments, such as underground mines, where it would be inconvenient or impossible to use a particle sizing instrument.

## Particle Dispersion System

A prototype particle dispersion system has been developed for aerosolizing particles. A schematic diagram of the system is shown in Figure 1. The system consists of mechanism for advancing the particle sample beneath a dust pickup tube, a venturi for deagglomerating the particles, and a instrument for analyzing the aerosolized particulate matter.

The procedure to analyze a particle sample is as follows. The particles to be aerosolized are placed on a sample plate from where the particles are picked up by an air stream flowing upward in a small capillary tube (dust pickup tube). This tube operates as a small vacuum cleaner passing over the sample plate. The air is drawn up the capillary tube at a rate of 2 L/m by a

venturi aspirator. This is accomplished by placing the outlet of the capillary tube near the throat of the venturi. The accelerated velocity of the air creates a low pressure in this region which draws flow up the capillary tube. From the outlet of the capillary tube particles are transported to the inlet of the APS where a small fraction are sampled and the aerodynamic diameter of the particles determined. The particles which are not measured by the APS are passed into a HEPA filter.

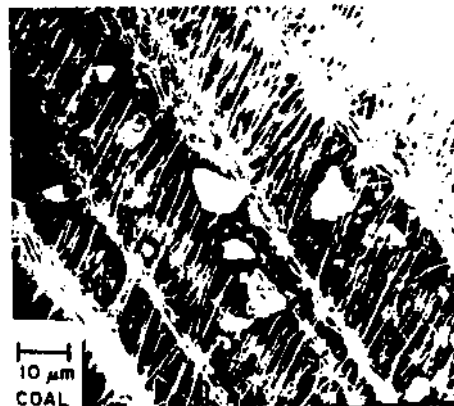
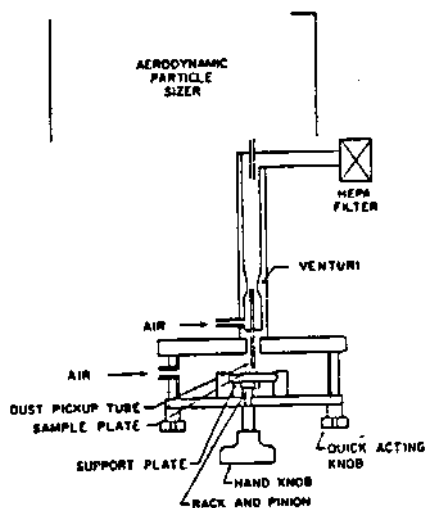


Figure 1. Schematic diagram of particle dispersion system.

Figure 2. Photomicrographs of dispersed coal dust particles.

The aerosol particles are deagglomerated in the venturi throat. This is achieved by the shear forces generated between the high velocity gas passing through the venturi and the low velocity, particle laden stream exiting from the capillary tube.

Figure 2 shows a photomicrograph of coal particles that have been dispersed in this system. The particles were dispersed from a bulk powder that had been placed on the sample plate. Note that essentially all of the particles are completely deagglomerated. Thus, the APS would be measuring the aerodynamic diameter of the individual particles.

#### Particle Dispersion from Filter Samples

The system, as shown in Figure 1, can be used to obtain the particle size distribution of bulk powder samples and, of course, the APS can be used to measure the size distribution of already airborne particles. However, the APS would be even more useful if it could measure the size distribution of airborne particles at locations where the APS cannot be taken, such as coal mines or other inaccessible industrial settings. One method to achieve this that we have found to be useful is to collect the airborne particles on filters and redisperse the particles from the filter and measure the size distribution with the APS. This has the added advantage in that the mass

## PARTICLE DISPERSION SYSTEM

concentration of particles collected on the filter can be determined before the particles are aerosolized for size distribution analysis. Thus, the mass concentration and the size distribution of the particles can be measured from one filter sample.

To investigate the redispersion of the particles from filters, the test system was configured as shown in Figure 3. A precision aerosol divider

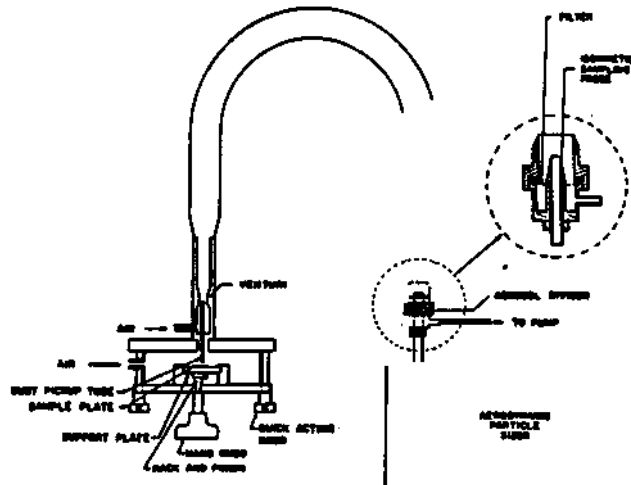


Figure 3. Schematic diagram of the particle dispersion system as setup with the precision aerosol divider.

(Marple et al, 1976) was placed on the inlet of the APS. The precision aerosol divider is essentially a filter holder with a sampling probe penetrating the center of the filter. The aerosol being sampled by the filter is then split isokinetically into two streams. One passes through the central probe to the APS. The other stream passes through the filter where the particles are collected. Since the distances between where the aerosol streams are split isokinetically to the position where the particles are collected on either the filter or sampled by the APS are very short, there are low losses in the system and an excellent split of the particles is obtained.

In this study, coal dust particles were first dispersed from the sample plate and passed through the precision aerosol divider and APS. The size distribution was measured by the APS and saved in its memory. The size distribution of this aerosol is shown in Figure 4 on both a number and mass basis. The filter was then removed from the precision aerosol divider and placed upon the sample plate. The size distribution of the particles redispersed from the filter were again measured by the APS. A comparison of this distribution to the original size distribution is shown in Figure 5 for two test runs. Note that the relative concentration of the particles in the redispersed dust was approximated 2 and 5% of the concentration of the particle in the original test. The comparison between the size distributions indicates that the size distribution of the redispersed particles is nearly the same as the that of the original particles. The variations shown in the

# THE RESPIRABLE DUST CENTER

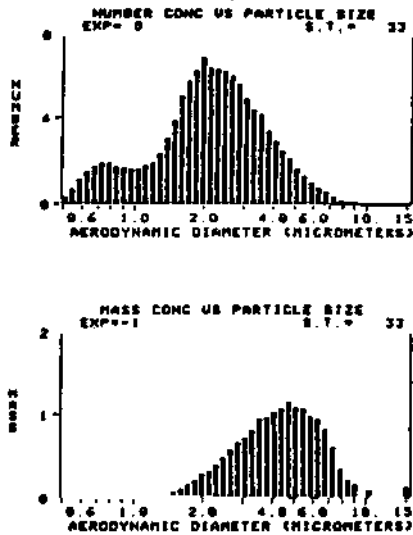


Figure 4. Size distribution of coal dust as measured with the APS.

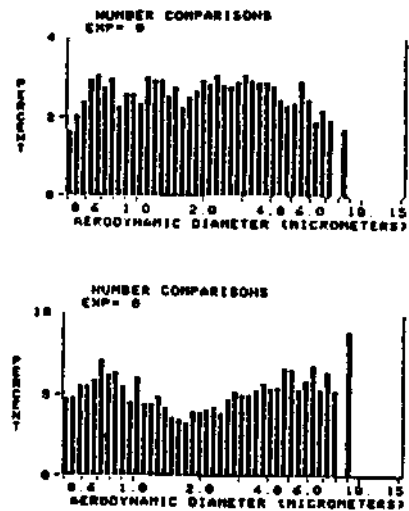


Figure 5. Comparison of the size distribution of coal dust particles redispersed from a filter to the original size distribution.

comparison graphs are, in part, due to statistical fluctuations since the number of particles in the redispersed sample were quite small.

Several different membrane filters are currently being evaluated to determine the appropriate filter to use for particle collection. Small pore size membranes are being used to maximize the particle collection of the filter surface. Furthermore, membrane filters, made of Teflon, are being used to maximize the degree of particle aerosolization. Tests are currently being performed with the Gelman TEFLO Type R2PJ and Gelman ZEFLUOR Type P5PL filters. The photomicrograph of coal particles collected on the ZEFLUOR filter, Figure 2, shows the surface collection characteristics of this filter. The small diameter of the web structure in this filter relative to the size of the coal particles also aids in the aerosolization of the particles.

## Reference

Marple, V. A., K. T. Whitby, B. R. Olson, and J. L. Wolf, "Precision Aerosol Divider", *Am. Ind. Hyg. Assoc. J.* 37:69-72.

## ACKNOWLEDGEMENTS

This research has been supported by the Department of the Interior's Mineral Institute program administered by the Bureau of Mines through the Generic Mineral Technology Center for Respirable Dust under grant number G1135142.

# Numerical Technique for Calculating the Equivalent Aerodynamic Diameter of Particles

V. A. Marple, Z. Zhiqun and B. Y. H. Liu

Particle Technology Laboratory  
Mechanical Engineering Department, University  
of Minnesota

## Introduction

It is commonly understood that aerosol particles may be injurious to human health if they are of a size that enables them to enter the respiratory tract. Coal Workers' Pneumoconiosis (CWP) is one disease known to be caused by coal mining related particles.

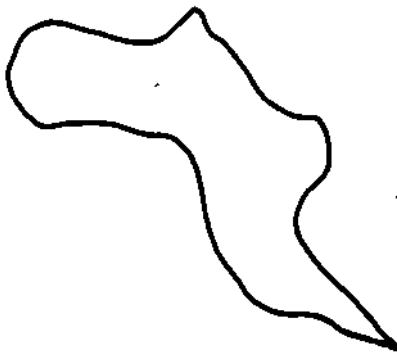


FIGURE 1. Determination of the aerodynamic diameter of an irregularly shaped particle.

The location in the respiratory tract where the particles are deposited is primarily a function of the equivalent aerodynamic diameter (EAD) of the particle. The equivalent aerodynamic diameter is the diameter of a spherical particle with a density of  $1.0 \text{ gm/cm}^3$  with the same falling speed as the particle in question. For a spherical particle the calculation is rather simple in that the equivalent aerodynamic diameter is simply the diameter of the particle in question multiplied by the square root of the density of the particle. For irregularly shaped particles, such as coal particles, there is no simple way to make the EAD calculation. For example, Figure 1 is only one of an infinite variety of particle shapes that can be found in practice and the aerodynamic size of this particle and, therefore, its deposition location in the respiratory tract would be nearly impossible to estimate accurately.

The normal method for determining the aerodynamic diameter of particles has been to experimentally measure the

size of the particles in a settling chamber or with an inertial classifier such as an impactor, cyclone or a centrifuge, since inertial classifiers have the property of classifying the particles according to their aerodynamic diameters.<sup>(1)</sup> However, these devices can only give limited information on the EAD of a single particle with a specific shape. Impactors and cyclones, for example, collect particles in size ranges and not at a specific size, so the determination of the EAD of a specific particle is not possible. A centrifuge, on the other hand, can measure the EAD of a specific particle but the equipment is costly and procedure laborious, and it may not be possible to disperse a particle of a specific shape into the centrifuge. The centrifuge can be used to determine the EAD of clusters of spheres in various arrays, but introducing particles of a specific irregular shape may not be feasible. Furthermore, the EAD is a function of the orientation of an irregularly shaped particle and the orientation of a particle in an inertial classifier is unknown. The orientation may also vary as the particle passes through the classifier.

Because of the difficulty in determining the EAD of an irregularly shaped particle, we have undertaken a program to apply theoretical numerical methods to calculate the EAD of any shape particle. In our laboratory we have, for some time, been using numerical methods to determine the flow field of air within instruments such as impactors,<sup>(2)</sup> inlets,<sup>(3)</sup> and virtual impactors.<sup>(4)</sup> Recently, this technique has been expanded into the three-dimensional regime, and the flow fields and particle motion characteristics within cyclones<sup>(5)</sup> and glove boxes have been studied. We have now begun to use these numerical three-dimensional flow programs to study the flow field around irregularly shaped particles to determine their drag coefficients, falling speed, and thus, their EAD.

Although it is quite easy to obtain answers from numerical programs, the routines may or may not be converging to a correct answer. The technique must be extensively evaluated before one has confidence in it. Therefore, the first step in our study is to use the computer techniques developed for two-dimensional flows and calculate the drag coefficients around particles of a simple shape for which the drag coefficient has been determined analytically or experimentally. If the agreement is good between the numeri-



cal solutions and the analytical or experimental solutions, the technique can be expanded into the three-dimensional regime with confidence.

This paper describes the results of the initial phase of the program, i.e., the verification that the numerical solutions in two dimensions can provide the correct drag coefficients for regular shape particles. The particles studied are those that can be generated by rotation of the coordinate system such as spheres, rods of infinite length in cross flow, disks, and chain spherical particles with axial flow along the chain.

**Numerical Analysis Technique**

Numerical analysis of the Navier-Stokes equation has been used extensively in recent years to obtain information on flow fields. Although several techniques have been used to solve the Navier-Stokes equations, they are all basically the same in that the finite difference form of the equation is expressed in terms of the stream function and vorticity, or in terms of the velocity vector components and the pressure. A grid is placed over the area of interest and the finite difference equations are solved at the node points (intersection of the grid lines) of the grid. The solution is achieved by an iterative relaxation procedure that determines the value of the stream function and vorticity or the velocity vector com-

three-dimensional solutions must be used to study irregularly shaped particles, we have chosen to use two-dimensional solutions of regular shape particles to prove the feasibility and to provide confidence in the results.

TABLE II

Comparison of Drag Force on a Cylinder in Cross Flow Calculated by Numerical Analysis  $F_{Dn}$ , and by Tomokita and Aoi<sup>(6)</sup> Solution,  $F_{DL}$

$D_p$ (um)	$F_{Dn}/F_{DL}$	Error%
10.0	1.0245	2.45%

In the past we have used numerical analysis techniques to successfully analyze the performance of aerosol instruments such as impactors,<sup>(2)</sup> virtual impactors,<sup>(4)</sup> and inlets.<sup>(3)</sup> However, in these cases the flow field within the instrument was calculated and then the particles were put into the flow field and their trajectories calculated. For these cases, the particle was much smaller than the grid spacing, and the trajectory of the particle was calculated as it passed through the grid matrix.

TABLE I

Comparison of Drag Forces on Spheres Calculated by Numerical Analysis,  $F_{Dn}$ , and Stokes Law,  $F_{DS}$

$D_p$ (um)	$F_{Dn}/F_{DS}$	Error %
2.0	1.035	3.5%
5.0	1.041	4.1%
10.0	1.015	1.5%

ponents and the pressure at each node point. Since numerical solution techniques have been used extensively and many cases reported in the literature, the techniques will not be described in detail here.

The particular solution technique that has been used in the work described here is the one described by Suhas Patankar,<sup>(7)</sup> and the reader is referred to his textbook for details of the technique. This technique is one that solves for the velocity vector components and the pressure at the node points rather than the stream function and vorticity. However, once the velocity vectors and pressure are known, the stream function and vorticity can be calculated if desired. The stream function is often calculated so that the stream lines (lines of constant stream function) can be shown to give a clearer understanding of the nature of the flow field.

Most of the work utilizing finite difference solutions to the Navier-Stokes equations has been in two dimensions, but three-dimensional solutions can be obtained.<sup>(5)</sup> Three-dimensional solutions, however, are much more costly in computer time than two-dimensional solutions. Although

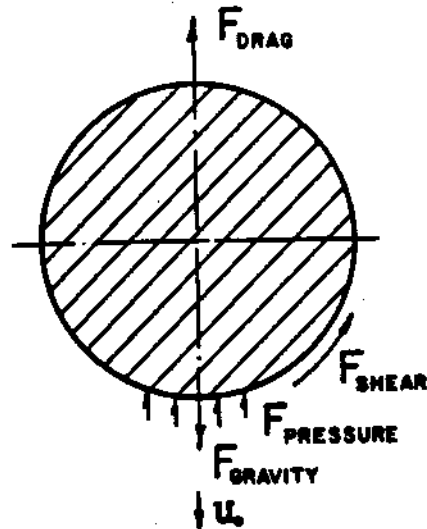


FIGURE 2. Numerical solution of drag acting on a sphere contributed by pressure and shear ( $D_p = 10$  um;  $U_o = 10$  cm/s).



FIGURE 3. Typical grid pattern for numerical solution.

## EQUIVALENT AERODYNAMIC DIAMETER OF PARTICLES

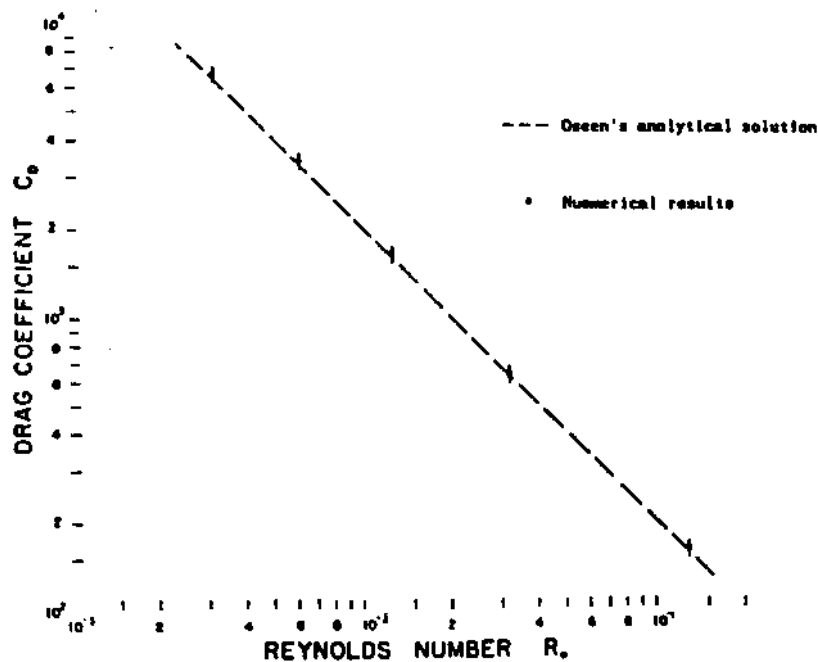


FIGURE 4. Drag coefficient of disks,  $C_D$ , Vs Reynolds number, comparison of Oseen's analytical solution with numerical results.

To study the flow around a particle and thus determine its drag and aerodynamic diameter, it is now necessary that the grid spacing be much smaller than the particle. The number of grid lines required to define the particle contour will depend upon the degree to which the features of the particle are to be described.

### Solution Technique as Applied to Particles

Since the object of the program is to determine the aerodynamic diameter of a particle and since the aerodynamic diameter is defined as the diameter of a unit density sphere which falls at the same speed as the particle in question, the problem reduces to one of determining the falling speed of a particle. As shown in Figure 2, this problem further reduces to one of determining at what speed the drag force is equal to the gravitational force on a particle, for these are the conditions which must exist when the particle is falling in equilibrium at its terminal settling speed.

The drag force on a particle will be the sum of both the pressure forces on the particle and the shear forces resulting from the fluid flowing past the surface of the particle. The numerical technique used here provides information on these two components of the drag force. For example, as shown in Figure 2, for a 10 micrometer diameter particle falling with a velocity of 10 cm/sec, the drag force due to the pressure difference is half the drag force due to the shear. This, incidentally, is the same ratio that will be found from analysis of the Stokes Drag Law.

Information on the drag force, presented in Figure 2, was found by application of the Navier-Stokes numerical analysis technique on a grid pattern such as that shown in Figure 3. Since the particle is a symmetrical sphere, the shape need only be defined as a semicircle as shown in the figure. The

coordinates are two-dimensional (radial and axial) cylindrical coordinates with no flow in the angular direction. Note that to define the particle with sufficient detail, the number of grid lines near the particle must be increased and the spacing between the grid lines decreased. The detail to which the contour of the particle can be defined is a function of the number of grid lines that are used.

In the technique described by Patankar,<sup>(6)</sup> the specification of the domain occupied by the particle is rather easy in that the viscosity is simply set to a very large number in this domain. The Navier-Stokes equations are then solved over the entire grid pattern (even through the particle). Since the viscosity is defined as being very large in the area of the particle, the flow does not move in this area and one has essentially defined an obstacle to the flow.

This same general technique will be used when three-dimensional analysis of the particles is performed. Due to the fact that the particles will no longer be symmetrical, no symmetry axis can be used, and the flow around the entire particle will be involved in the solution. However, the particle will still be defined by placing very high values of viscosity at all node points lying within the particle boundaries.

The grid shown in Figure 3 is in cylindrical coordinates so as to take advantage of the symmetry of a spherical particle. The same coordinate system is used when determining the drag force on a disk. However, in some cases it may be preferable to use rectangular coordinates, as in the case for an infinite cylinder in cross flow. Figure 3 could also represent the grid system for the cylinder in cross flow, but now the semicircle would represent one-half of a cylinder, and the coordinate system would be in x-y coordinates with no flow in the z direction. When the program is expanded into three dimensions, it may be advantageous to use rectangular rather than cylindrical coordinates for ease in defining the shape of the particle.

TABLE III

Comparison of Drag Forces, Shape Factors and Drag Coefficients for Disks Calculated by Numerical Analysis and by Oseen's Solution<sup>(10)</sup>

Re	$F_{Dn}/F_{Do}$	$K_n'$	$K_o'$	$C_{Dn}$	$C_{Do}$
$3.26 \times 10^{-3}$	1.058	0.898	0.849	$6.11 \times 10^3$	$6.25 \times 10^3$
$6.52 \times 10^{-3}$	1.05	0.891	0.849	$3.28 \times 10^3$	$3.125 \times 10^3$
$1.30 \times 10^{-2}$	1.045	0.887	0.849	$1.63 \times 10^3$	$1.563 \times 10^3$
$3.26 \times 10^{-2}$	1.02	0.865	0.849	$6.37 \times 10^2$	$6.25 \times 10^2$
$1.30 \times 10^{-1}$	1.015	0.861	0.849	$1.58 \times 10^2$	$1.56 \times 10^2$

$K_n'$  = Shape Factor obtained from numerical study.

$K_o'$  = Shape factor obtained by taking the limit case of the shape factor from Oseen's formula.

$C_{Dn}$  = Drag coefficient of disks obtained from numerical results.

$C_{Do}$  = Drag coefficient of disks obtained from Oseen's solution.

Results

The two-dimensional analysis has been applied to single spherical particles, cylinders in cross flow, disk shape particles, and spherical particles connected in chains. In all cases the shapes were selected because there was a prior determination of the drag force on the particle, either by analytical or experimental methods, and reported by other investigators, since it was the object of this portion of the project to gain confidence in a numerical technique.

For the single spherical particle, the drag force from the numerical solution was compared to the drag force predicted by Stokes law.<sup>(7)</sup> The results of this analysis are shown in Table I for particle diameters of 2, 5, and 10  $\mu$ m. In general, it was found that the calculation of the drag force on a particle agreed within four percent of that determined by Stokes law. This was believed to be quite good since the number of node points defining the particle was only approximately 40 in all cases. Thus, the sphere is actually approximated by 11 stacked cylinders, creating steps along the surface of the particle. As the number of grid points

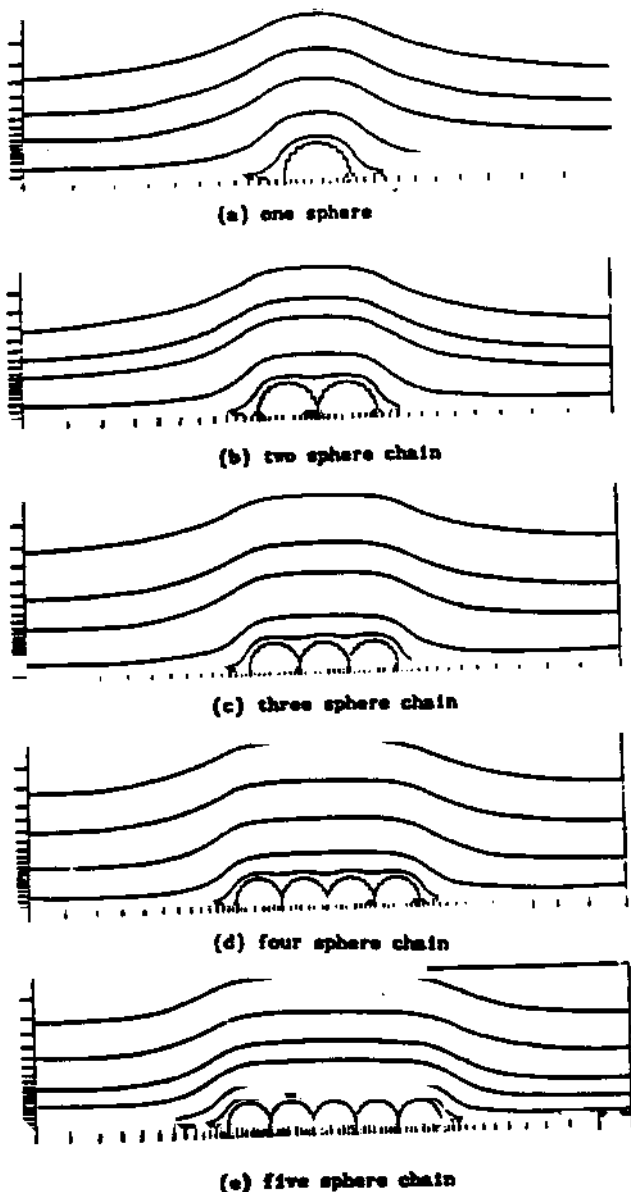


FIGURE 5. Flow field streamlines past a straight chain of spheres consisting of 1 to 5 spheres.

TABLE IV  
Comparison of Dynamic Shape Factor for Straight Chain Aggregates of Uniform Spheres Calculated by Numerical Analysis and Determined Experimentally by Stober<sup>(12)</sup>

No. of Sphere	Numerical Analysis Results				Experimental Results (Stober)
	$D_p = 0.4 \mu$ m	$D_p = 1 \mu$ m	$D_p = 4 \mu$ m	$D_p = 10 \mu$ m	
2	1.148	1.179	1.1225	1.1238	1.12
3	1.213	1.267	1.320	1.340	1.27
4	1.221	1.296	1.353	1.378	1.32
5	1.336	1.411	1.482	1.513	1.45

## EQUIVALENT AERODYNAMIC DIAMETER OF PARTICLES

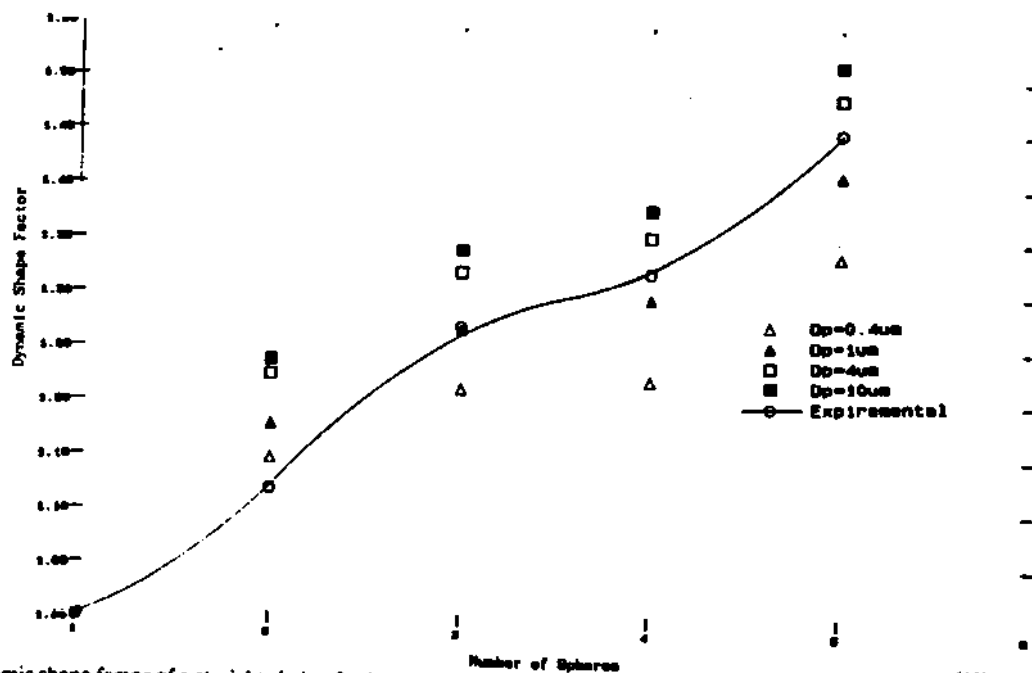


FIGURE 6. Dynamic shape factor of a straight chain of spheres, comparison of numerical results with experimental results,<sup>(12)</sup>  $D_p$  = Diameter of primary sphere.

(cylinders) increases, the size of the steps will decrease and more closely approximate the sphere.

For the case of cylinder in cross flow, which utilized rectangular coordinates, only one case was analyzed (10  $\mu$ m diameter) and compared to the analytical solution as defined by Tomokita and Aoi<sup>(8)</sup> and reported by White.<sup>(9)</sup> The result of this comparison is shown in Table II. There is good agreement between the two techniques. The difference is only approximately 2.5 percent. Again, the cylinder was defined by about 40 node points.

The next configuration studied was the disk in cross flow which again utilized cylindrical coordinates. The results of this test were compared to that of Oseen's solution<sup>(10)</sup> as reported by Fuchs.<sup>(11)</sup> Oseen studied the flow around ellipsoids, and in one limiting case, the ellipsoid can be made to resemble a disk. In the case of the disk the analysis was run for several values of the Reynolds Number. As shown in Table III, the error in the drag forces increased with decreasing Reynolds Number from approximately 1.5 percent at a Reynolds Number of 0.13 to about 6 percent at a Reynolds Number of 0.00326. The drag coefficients and the shape factor defined as the ratio of the drag force on an irregularly shaped particle to that on a sphere of the same frontal projected area are also presented in this table. The comparison of the drag coefficients for the two techniques for the disk are shown in Figure 4 and shows that the agreement is within the error bars on the numerical solution. These errors are estimates due to the inaccuracy in the numerical flow fields.

The final test of the numerical analysis technique was to study spherical straight chain agglomerates. Figure 5 shows the flow field around the chains containing from one to five spheres. In this case the dynamic shape factor of the straight chains was calculated and compared to those values reported from experiments performed by Stober<sup>(12)</sup> using a centrifuge to determine the shape factor. The numerical

technique was performed on primary spheres of sizes 0.4, 1, 4, and 10  $\mu$ m diameter and compared with the experimental results which used latex spheres of several particle sizes on the order of 1  $\mu$ m diameter. The results of the comparison are shown in Table IV and Figure 6. The agreement is seen to be quite good considering the uncertainties in the orientation of the particles in the centrifuge. It is interesting to note in Figure 6 that both experimental and numerical generated dynamic shape factor versus number of particle curves have "S" shapes. The reason for the "S" shape of the curves is not clear, but it is felt to be significant that both the experimental and numerical results give the same curve shape.

The numerical technique gives more detail on the forces of the particles than can be obtained experimentally. For example, in Figure 7, the percent of the total drag contributed by each sphere is presented as a function of the number of spheres in the chain. It is of interest to note that the drag force contributions by the leading and trailing spheres are nearly the same and approximately equal to twice the drag force on the intermediate spheres.

### Optimum Grid Pattern

As has been indicated earlier in this paper, a particle can be better defined by increasing the number of grid lines used to define the particle contour. However, as the number of grid lines increase, the number of node points over which the Navier-Stokes equations must be solved rapidly increases and soon becomes large enough to adversely affect the time and cost required to obtain a solution. Figure 8 shows the results of a study made in determining the drag on a sphere as a function of the node points used in the problem. This shows that as the number of node points increases, the percent error between the numerical solution and that obtained from Stokes Law rapidly decreases up to a value of ap-

# THE RESPIRABLE DUST CENTER

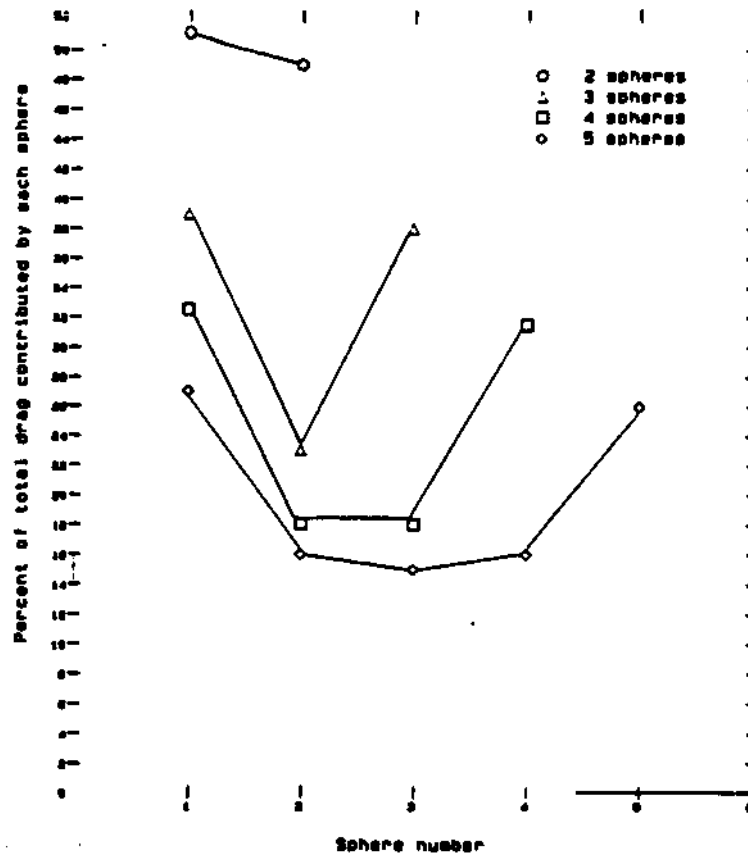


FIGURE 7. Drag distribution on a straight chain of spheres.

proximately 800 node points. As the number of node points is increased beyond 800, the increase in accuracy is only slight. Also shown on the chart is the computer central processing time, and this curve, although not as dramatic as the error curve, does increase at a more rapid rate for the larger number of node points. For this reason, we have used approximately 800 node points per problem definition.

In some cases it will be necessary to use more than 800 node points to define the outline of an irregularly shaped particle. To avoid the large cost associated with the large number of node points, it was decided to solve the problem in steps, with each step increasing the fraction of the area of interest covered by the particle. An example of this step process is shown in Figure 9. At the top of Figure 9 is the in-

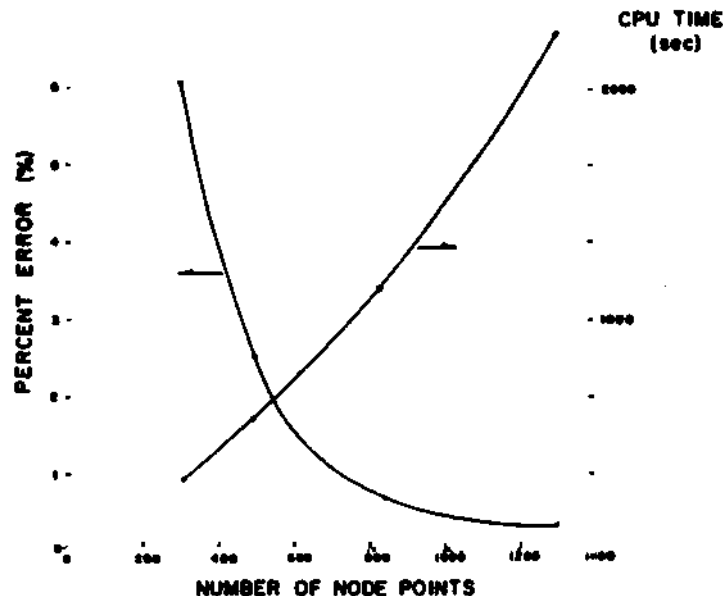


FIGURE 8. The effect of grid resolution on the accuracy of numerical solutions of spheres and on the computer time.

initial step where the particle is defined by only a few grid lines, with most of the space reserved for the flow around the particle. The reason for having such a large space around the particle is so that the boundary conditions can be assumed to be unaffected by the presence of the particle. The resulting solution of this problem will define a velocity profile at all grid points within the solution domain, as shown by the dashed lines in the upper figure. If the area within the dashed lines is now enlarged, there can be more grid lines used to define the outline of the particle and the boundary conditions are now those resulting from the first step.

This process can be continued in a stepwise fashion until sufficient definition of the particle contour has been obtained. In this manner, the flow around a very complex particle can be obtained and the number of node points kept on the order of 800, which is found to be optimum in obtaining an accurate answer at reasonable cost.

**Conclusion**

The two-dimensional numerical solution to the Navier-Stokes equations provides drag forces for particles that are in good agreement with those determined by other methods. For example, these drag forces on spheres agreed well with that given by the Stokes law. Similarly, cylinder drag agreed well with the analytical solution by Lamb, and the disk drag agreed with those determined by the Oseens solution. All solutions agreed within about five percent, and only about 40 node points were used to define the particle contour.

The technique, as applied to straight chains of spherical particles, also showed good agreement with experimental values of the dynamic shape factor determined by experimental centrifuge analysis. Although the numerical technique predicted dynamic shape factors somewhat larger than those determined experimentally, the dynamic shape factor as a function of the number of particles in the chain correlated well.

The two-dimensional analysis of particles, as reported in this paper, indicates that the contour of the particle can be satisfactorily defined with approximately 40 node points. It should, therefore, be possible to determine the drag force of irregularly shaped particles using three-dimensional numerical methods. For three-dimensional studies the computer time will be much more than for two dimensions, but information on the particle drag for these particles can be obtained in detail that is not obtainable by any other means. It is believed that any particle shape can be digitized, defined by a three-dimensional grid and analyzed to determine its aerodynamic diameter.

**Acknowledgment**

This research has been supported by the U.S. Department of Interior's Mineral Institutes program administered by the Bureau of Mines through the Generic Mineral Technology Center for Respirable Dust under allotment grant no. G1135142.

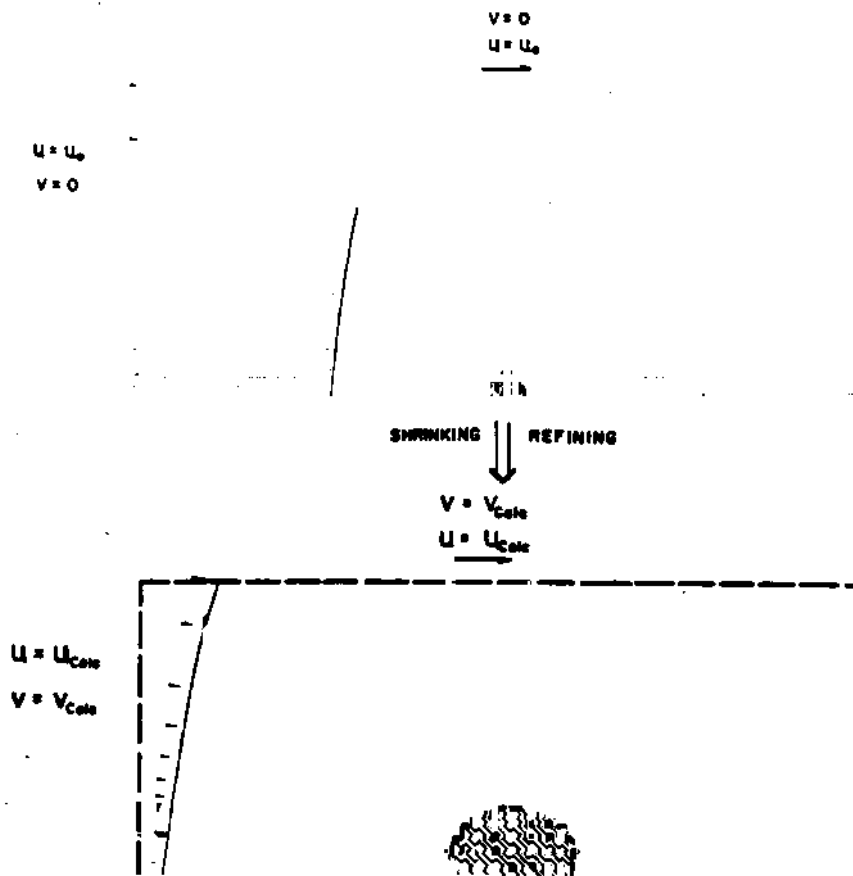


FIGURE 9. Grid lines used when shrinking calculation domain around a particle to increase resolution of the flow field.

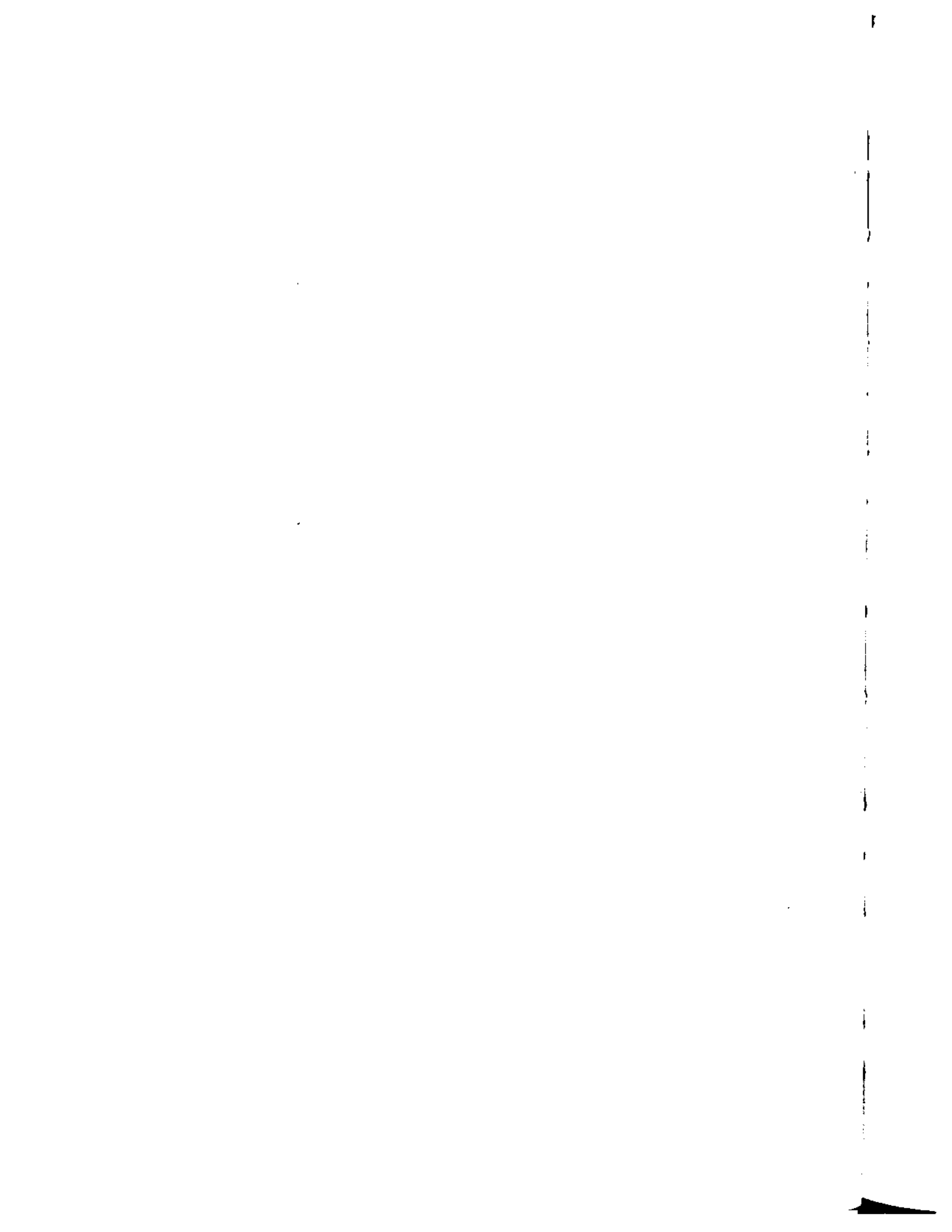
References

1. Hinds, W.C.: *Aerosol Technology*, pp. 104-126. John Wiley and Sons, New York (1982).
2. Marple, V.A.: A Fundamental Study of Inertial Impactors. Ph.D. Thesis, Mechanical Engineering Department, University of Minnesota, Minneapolis, MN (1970).
3. Agarwal, J.K.: Aerosol Sampling and Transport. Ph.D. Thesis. Mechanical Engineering Department, University of Minnesota, (1975).
4. Marple, V.A. and C.M. Chien: Virtual Impactors: A Theoretical Study. *Env. Sci. Tech.* 14:976-985 (1980).
5. Marple, V.A. and D.J. Rader: Recent Developments in the Application of Finite Difference Solutions to the Study of Flow Fields and Particle Trajectories. *Proceedings from Third Symposium on Advances in Particle Sampling and Measurement*, Daytona Beach, Florida, October 18-21 (1981).
6. Patankar, S.V.: *Numerical Heat Transfer and Fluid Flow*. McGraw-Hill-Hemisphere Publication, New York (1979).
7. Hinds, W.C.: *Aerosol Technology*, pp. 40-42. John Wiley and Sons, New York (1982).
8. Tomokita, S. and T. Aoi: The Steady Flow of Viscous Fluid Past a Sphere and Circular Cylinder at Small Reynolds number. *Q. J. Mech. Appl. Math.*, Vol. III, pp. 140-161 (1950).
9. White, F.M.: *Viscous Fluid Flow*. McGraw-Hill Book Company, New York (1974).
10. Oseen, C.: *Neuere Methoden und Ergebnisse in der Hydrodynamik*. Leipzig (1927).
11. Fuchs, N.: *Mechanics of Aerosols*, Chap. II, pp. 21-70, Pergamon Press, Oxford (1964).
12. Stober, W.: A Note on the Aerodynamic Diameter and the Mobility of Non-Spherical Aerosol Particles. *J. Aerosol Sci.*, pp. 453-456 (1971).

**III**

**Characterization of  
Dust Particles**





# Wetting Characteristics of Particles and Their Significance in Dust Abatement

S. Chander, B. R. Mohal and F. F. Aplan

Mineral Processing Section, The  
Pennsylvania State University

Dust abatement by water sprays involves the subprocesses of 1) collision between dust particles and water droplets, 2) adhesion of particles to droplets, and 3) engulfment of particles by the droplets. A review of the fundamental aspects of these subprocesses shows that collisions between particles and droplets are determined by aerodynamics and the size and surface charge of the particles and of the droplets. However, the adhesion and engulfment subprocesses depend upon the wetting characteristics of the particles. Although wetting agents (also known as surfactants) have been used as dust suppressants in several investigations, conflicting results are available regarding their effectiveness. In this paper, we show that these results can be explained if the effects of coal rank on surfactant adsorption and wetting characteristics are taken into account.

The influence of several nonionic surfactants containing polyethoxy adducts on the wetting behavior of coal is presented. The wetting was determined by a modified Walker Test method, and contact angle measurements. The results show that the wettability of coal depends upon coal rank, structure of the hydrocarbon chain of the surfactant, and the number of ethoxy groups in the molecule.

## Introduction

Due to the inherent nature of the mining process, a large number of particles are generated, a portion of which becomes airborne to create dust. Dust can be aesthetically and environmentally unacceptable and it can also be explosive. Fine particles in the respirable size range ( $< 5 \mu\text{m}$ ) are considered to cause lung diseases, namely, silicosis, pneumoconiosis, etc.<sup>(1)</sup> Several approaches to reduce dust in mine environments are practiced throughout the mining industry. These include decrease in generation of dust through improvements in mine machinery, ventilation (in which lower dust levels are achieved by dilution of contaminated air with clean air), and dust removal methods. Water sprays are most commonly used to remove dust particles. Recently, scrubbers are reported to have been installed on mining machines to remove dust,<sup>(2,3)</sup> which also make use of water sprays to reduce dust.

Wetting agents, also known as surfactants, are often used to increase the effectiveness of water sprays in capturing dust particles, particularly in the respirable dust range. This use of surfactants is not new. As early as 1924, a sulfonated hydrocarbon was found to be a very effective dust suppressant in both laboratory tests and underground trials.<sup>(4)</sup> Foams have been suggested as alternate to water sprays,<sup>(5)</sup> but their use also depends upon use of surfactants to create foams and improve adhesion.

The use of wetting agents to suppress dust in various coal mining and preparation stages has been increasing even though no consensus exists regarding their overall effectiveness. The following conclusions by various investigators illustrate this observation:

*"... surfactants act through several mechanisms - increase wettability of particles, ease atomization of water and increase dust adhesion."<sup>(6)</sup>*

*"... use of wetting agents reduced the dust loading of return air by 30% compared with the use of water alone."<sup>(7)</sup>*

*"... wetting agents ineffective when mining the high volatile coal of the Pittsburgh seam."<sup>(8)</sup>*

*"... a noticeable reduction in visible airborne dust in face areas resulted from adding a wetting agent to the water spray."<sup>(9)</sup>*

*"... one possible solution that has been in use in some coal mines for a number of years and is now receiving renewed interest is the use of chemical surfactants."<sup>(10)</sup>*

*"... laboratory tests indicate that 10 to 15 percent more respirable dust can be collected with wetting agents than with water alone."<sup>(11)</sup>*

"... we don't know why some agents work and some don't, some coals are wettable and some aren't."<sup>(12)</sup>

"... no significant correlations among the four wetting tests were observed."<sup>(13)</sup>

### Capture of Dust Particles by Water Sprays

The main objectives of water sprays used for in-mine dust removal are 1) to prevent particles from becoming airborne, and 2) to collect the airborne particles. The capture of dust particles by water droplets can be visualized in terms of a series of subprocesses which are:

1. Approach of dust particles to the droplet surface.
2. Adhesion of the dust particles with the droplet.
3. Engulfment of the particle within the droplet.

For effective dust control, all these sub-processes must be rapid, with the slowest sub-process determining the rate. The rate of capture of dust particles by water droplets can be written as:

$$\text{rate} = \text{collision frequency} \times \text{collision efficiency} \quad (1)$$

The collision frequency depends upon the following:

- Particle size and droplet size
- Aerodynamics of the system
- Number density of the particles and droplets

In case of water sprays, the droplet size is primarily determined by the nozzle characteristics and pressure drop across the nozzle. Typical droplet diameter varies from 150-360  $\mu\text{m}$ ,<sup>(14)</sup> with an average value of 250  $\mu\text{m}$ . The smaller the droplet size, the greater is the number density for the same amount of water sprayed. The particle size at the dust generation source would be from submicron sizes to ROM size coal. However, all the fragments produced in mining do not become airborne.<sup>(15)</sup> The characteristics of in-mine dust depends upon the nature of the mining method, coal seam, production rate, air velocities, etc.

The aerodynamics of the system are influenced by the particle and droplet sizes and their relative velocities. Three types of collision mechanisms can be envisaged, they are:

1. Inertial impaction
2. Flowline interception
3. Brownian diffusion.

Inertial impaction is the most common mode of collision for particles greater than 3 to 5  $\mu\text{m}$ , whereas Brownian diffusion is the predominant mode of collision for particles less than approximately 0.3  $\mu\text{m}$ . Flowline interception can be sig-

nificant when the dust particle must flow through a series of collectors as in filtration.

The collision efficiency, (i.e., the effectiveness of a collision to result in particle capture), depends upon the wetting characteristics of the particle. Also known by the names, attachment coefficient, sticking factor, etc., this parameter is often forgotten. Since capture of particles must involve both adhesion and engulfment processes, the wetting behavior of particles is an important consideration.

Three kinds of wetting phenomena are involved in capture and engulfment of particles: adhesional wetting, spreading wetting and immersional wetting. Adhesional wetting refers to the process of formation of a three phase contact between the dust particle, water droplet and air. Spreading wetting refers to the movement of the liquid/air interface along the surface of the particle such that the solid/liquid interfacial area increases and the solid/air interfacial area decreases. Immersional wetting refers to the process of transfer of the particle from air into water. The free energy changes for the three wetting processes can be represented by the following relations:

$$\begin{aligned} \text{Adhesion: } \Delta G_a &= \gamma_{SL} - \gamma_{SA} - \gamma_{LA} \\ &= -\gamma_{LA}(1 + \cos \Theta) \end{aligned} \quad (2)$$

$$\begin{aligned} \text{Spreading: } \Delta G_s &= \gamma_{SL} - \gamma_{SA} + \gamma_{LA} \\ &= \gamma_{LA}(1 - \cos \Theta) \end{aligned} \quad (3)$$

$$\begin{aligned} \text{Immersion: } \Delta G_i &= \gamma_{SL} - \gamma_{SA} \\ &= -\gamma_{LA} \cos \Theta \end{aligned} \quad (4)$$

where  $\gamma_{SL}$ ,  $\gamma_{SA}$  and  $\gamma_{LA}$  are the surface free energies of the solid/liquid, solid/air and liquid/air interfaces, and  $\Theta$  is the contact angle. The interfacial free energies and the contact angle, and hence the conditions for wetting can be altered through adsorption of surfactants. The free energies for the three wetting processes, plotted as a function of contact angle in Figure 1, are quite different from each other. Capture of particles by adhesional wetting is most likely to occur because  $\Delta G$  for this process is the smallest (or most negative). When particles are captured by this mode of wetting, they will remain at the surface of the droplet. For particles to be engulfed by the droplet, the liquid must spread on the particle surface before immersion can occur. Since  $G_s$  is positive for all values of  $\Theta$  except when  $\Theta = 0$ , a necessary condition for engulfment of particles is that  $\Theta = 0$ . Thus, for wetting agents to be effective, lowering of both  $\gamma_{LV}$  and  $\Theta$  are desired. Although the first condition, namely, lowering of  $\gamma_{LV}$ , is generally recognized, the second condition, namely, lowering of contact angle, is frequently overlooked. Figure 2 shows that the contact angle of coal is highly dependant upon rank parameters such as fixed carbon.<sup>(16)</sup> Therefore, dusts from mining of different coal types can be expected to behave very differently when exposed to water sprays. Wetting agents are of critical importance in wetting highly hydrophobic materials such as the higher rank coals. The remainder of this paper describes the effect of several different surfactants on the wetting behavior of coals of various ranks.

## WETTING CHARACTERISTICS OF PARTICLES

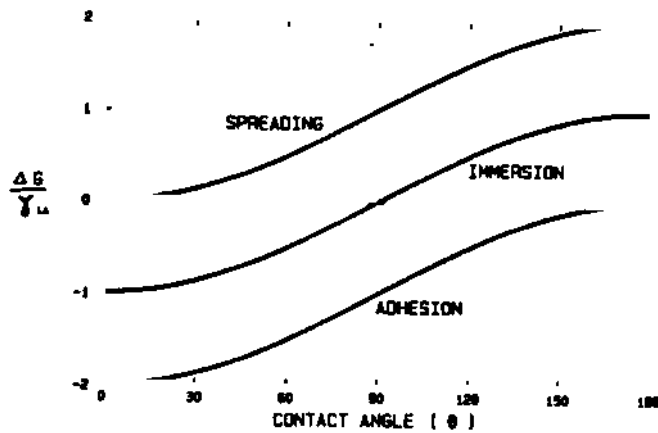


FIGURE 1. The free energies of spreading, immersional and adhesional wetting phenomena as a function of contact angle.

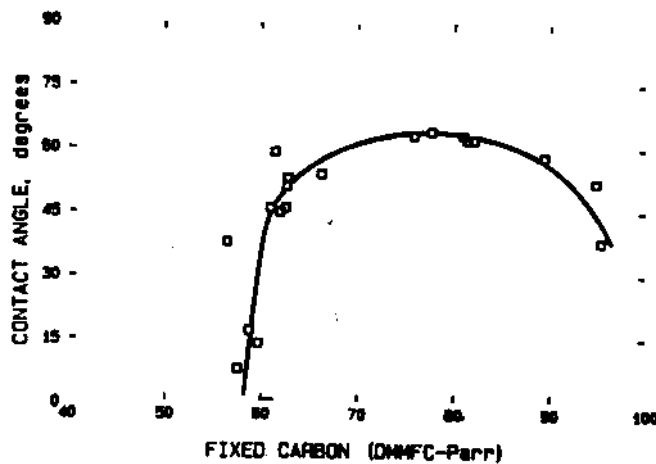


FIGURE 2. Captive bubble contact angles as a function of fixed carbon content for various coals.

### Loading of Water Droplets by Dust Particles

The effectiveness of water sprays can be greatly enhanced if particles are imbibed (engulfed) by water droplets rather than attached to the surface of the droplets. The following calculation, in which typical in-mine conditions are used, illustrate this fact.

The total mass of respirable dust generated in a typical coal mine is about 3.5 gram/pound of coal mined<sup>(15)</sup> which is equivalent to about 8.3 kilogram per minute of respirable dust generated. Since the total dust generated, and not the respirable fraction alone, will be seen by water sprays, on an average of about 25 kilogram per minute dust will be exposed to 15 gallon per minute water spray. For an average droplet diameter of 250  $\mu\text{m}$ , the surface area available for capture of dust is 22.7  $\text{m}^2/\text{sec}$ . The surface area occupied by a layer of dust particles in the same time period is 33.3  $\text{m}^2$  which implies that a particle loading factor of 150 percent is needed. For the same conditions, if particles could be imbibed into the droplet, the loading factor would be only about 25 per-

cent or less. Therefore, the capacity of water droplets to capture dust can be significantly increased if particles, on capture, were imbibed into a droplet rather than just adhering to the droplet surface. Kobrick<sup>(17)</sup> has reported that the cutters run dry even when 25 gallon per minute water is used in water sprays,<sup>(17)</sup> probably due to complete coating of water droplets by dust particles.

Particles which are not easily wetted by water alone can be wetted by the addition of wetting agents to water. The effect of additives on wetting behavior depends on the nature of particles themselves (i.e., their wetting characteristics) and on the nature of the surfactant used. These aspects are discussed in a later section.

### Experimental methods and materials

#### Wetting Rate - Modified Walker Technique

In this method, a 40 mg sample of 250 X 150  $\mu\text{m}$  coal was dropped on the surface of a surfactant solution and the amount of coal wetted by the liquid was measured by placing the pan of a Cahn electrobalance beneath the liquid surface. The initial wetting rates were determined from measurements of the amount of coal wetted as a function of time. The rate of wetting was found to be independent of the amount of the coal sample for the range 20-100 mg. The data reported for the wetting rates are an average of at least four replicate measurements in which the coefficient of variation was about 0.08. Additional details of the measurement technique are given elsewhere.<sup>(18)</sup>

#### Coal and Reagents

The coal sample used in this investigation was a HVA-bituminous coal from the Upper Freeport seam obtained from the Penn State Data bank (PSOC 1361P). The coal sample was crushed and screened to obtain a 250-150  $\mu\text{m}$  fraction which was then used for the wetting tests. The ethoxylated nonylphenol (Triton N-series) and octyl phenols (Triton X-series) were obtained from Rohm and Haas. The ethoxylated dodecylphenol (T-Det DD9) was obtained from Thomas Hayward Chemicals. Aerosol OT and Tween 80 were obtained from Fisher Scientific.

### Results and Discussion

The initial wetting rates for the HVA-bituminous coal are given as a function of the surfactant concentration in Figure 3. The hydrophilic group in this series of surfactants was kept constant (about 9-10 moles of ethylene oxide) and the hydrophobic group was varied from an 8 carbon to a 12 carbon chain. In the range investigated, the wetting rate increases linearly with the logarithm of concentration. The minimum concentration at which wetting occurs is referred to as the critical wetting concentration,  $C_{cr}$  and it is obtained by extrapolating the wetting rate versus logarithm of concentration. The slope of the curves increases with a decrease in length of the hydrophobic group. The differences in the effect of surfactants on wetting rates are attributed to differen-

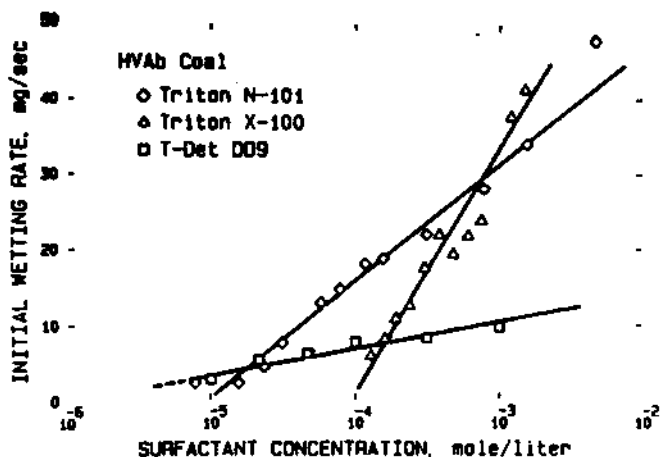


FIGURE 3. Initial wetting rates for a HVA bituminous coal for several surfactants with varying hydrophobic groups.

ces in the adsorption behavior of surfactants on the surface of coal.

The initial wetting rates for the coal versus surfactant concentration for different hydrophilic chain lengths are given in Figure 4. The hydrophobic portion of the surfactant was nonyl phenol in these cases and the hydrophilic chain length was varied by changing the number of ethoxy groups. The chain lengths of the hydrophilic group and other properties are included in Table I. The results in Figure 4 show that the concentration dependence of wetting rates, measured in terms of the slope of the wetting rate versus log concentration, first increases and then decreases with an increase in the number of ethoxy groups.

The hydrophilic-lipophilic-balance (HLB) is a number describing the relative attractions of a surfactant molecule for water and oil.<sup>(19)</sup> The HLB number for most nonionic surfactants increases with increase in the percentage weight

of the hydrophilic portion of the molecule. A higher HLB number also indicates a higher water solubility. The initial wetting rates of coal for a 0.1 wt% surfactant concentration are plotted versus the HLB value in Figure 5, for ethoxylated octyl and nonyl phenols. The wetting rates are maximum at an HLB value of 13.5 for both the ethoxylated octyl and nonyl phenols. At lower HLB values, the adsorbed surfactant molecule has low water solubility and hence a low wetting rate. At higher HLB values, the surfactant molecule has a much higher water solubility and its adsorption on the coal surface is reduced. Similar observations were made by Variali<sup>(20)</sup> on the effect of HLB on rheology of coal-water slurries.

The initial wetting rates versus surfactant concentration for three different surfactants are given in Figure 6. The Triton N-101 is an ethoxylated nonyl phenol, Tween 80 is an ethoxylated sorbitan mono oleate with an ethylene oxide chain length of 20, and Aerosol-OT is a dioctyl sulfosuccinate. For this coal, Triton N-101 appears to be the most effective wetting reagent.

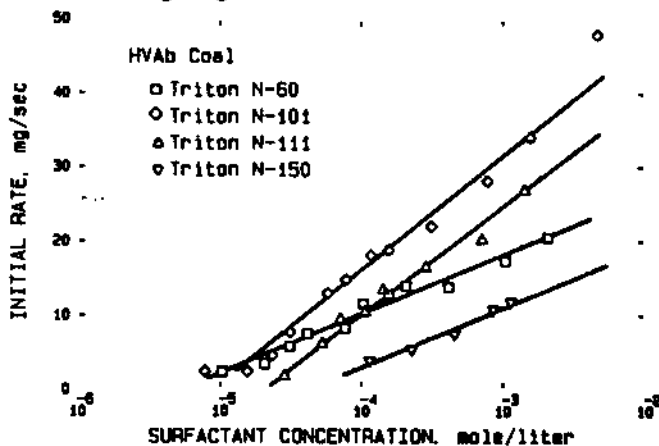


FIGURE 4. Initial wetting rates for a HVA bituminous coal for various ethoxylated nonyl phenols.

TABLE I

Hydrophile-Lipophile Balance of Surfactants Used in this Investigation.

Surfactant	Hydrophobic group	No. of ethoxy groups (-C <sub>2</sub> H <sub>5</sub> O-)	HLB.
Triton N-60	Nonylphenol	6	10.9
Triton N-1-	Nonylphenol	9-10	13.4
Triton N-111	Nonylphenol	11	13.8
Triton N-150	Nonylphenol	15	15.0
Triton X-100	Octylphenol	9-10	13.5
T-Det DD9	Dodecylphenol	9	12.0
Tween 80	Sorbitan monooleat	20	15.0
Aerosol OT	Dioctyl	(anionic)	

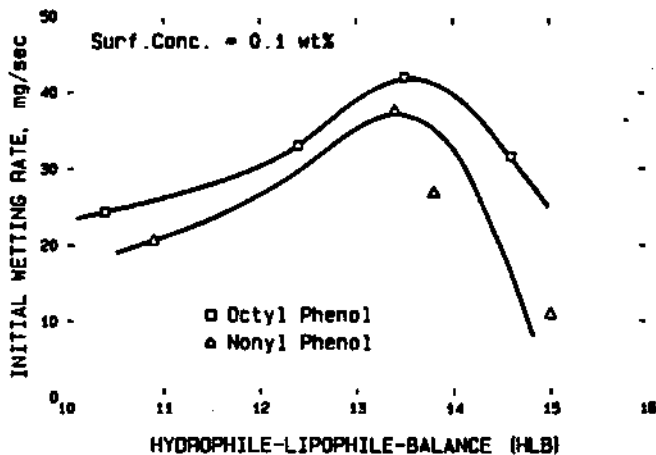


FIGURE 5. Initial wetting rates for a HVA bituminous coal as a function of the HLB number for a 0.1 wt% surfactant concentrations.

## WETTING CHARACTERISTICS OF PARTICLES

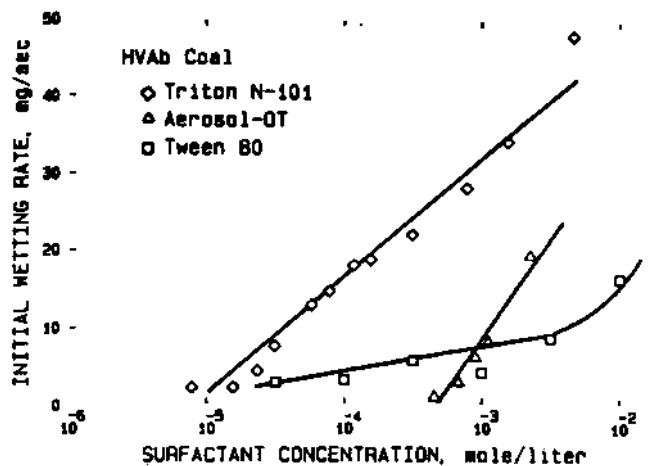


FIGURE 6. Initial wetting rates for a HVA bituminous coal as a function of surfactant concentration for Triton N-101, Aerosol-OT and Tween 80.

Results which have been reported elsewhere<sup>(18,21)</sup> show that the initial wetting rates in the presence of surfactants are a function of the coal type. When Triton N-101 is used as the surfactant, wetting rates decrease in the order: HVA-bituminous anthracite sub-bituminous, which is expected on the basis of the effect of coal rank on wettability of coal.

### Conclusions

A review of the subprocesses involved in capture of dust particles by water droplets shows that wetting agents can significantly enhance the effectiveness of water sprays. Adhisional wetting controls the capture of dust particles, whereas spreading and immersional wetting control their imbibition (engulfment).

Wetting of coal particles is shown to depend upon the coal rank, surfactant type and concentration. At low concentrations, a larger hydrophobic group gives a higher wetting rate (cf. Figure 3) whereas at high concentrations, the surfactant with a smaller hydrophilic group gives a higher wetting rate. The effect of hydrophilic group is more complex and can be discussed in terms of HLB. As the HLB number increases from a low value, the wetting rate first increases and then decreases, the maximum rates occur for an HLB number of 13.5. The largest wetting rates for a HVA bituminous coal were observed for Triton N-101, a nonionic surfactant.

### Acknowledgments

The authors acknowledge the support from the Mineral Institutes Program under Grant No. G1135142 from the Bureau of Mines, U.S. Department of the Interior, as part of the Generic Mineral Technology Center for Respirable Dust, The Pennsylvania State University.

### References

1. Naeye, R.G., J.K. Mahon and W.S. Dellinger: Rank of Coal and Coal Workers Pneumoconiosis. *Am. Rev. Resp. Dis.* 103:350-355 (1971).

2. Jayaraman, N.I.: Dust Control for a Borer-Type Continuous Mines using a Venturi Scrubber on a Transfer Car. *U.S.B.M. Rep. of Investigations 8408*, pp. 1-12 (1979).
3. Anon.: Peabody Opens Underground Mine in Kentucky. *Mining Engineering* 38:872 (1986).
4. Hartman I. and H.P. Greenwald: Use of Wetting Agents for Allaying Coal Dust in Mines. *U.S.B.M. Information Circular 7131*, pp. 1-11 (1940).
5. Volkwein, J.C., A.B. Cecilia and E.D. Thimons: Use of Foam for Dust Control in Mineral Processing. *U.S.B.M. Report of Investigations 8808*, pp. 1-11 (1983).
6. Walker, P.L., Jr., E.E. Peterson and C.C. Wright: Surface Active Agent Phenomena in Dust Abatement. *Ind. Eng. Chem.* 44:2389-2392 (1952).
7. Anderson, F.G., R.L. Evans and R.G. Peluso: A study of Dust Control Methods for Continuous Mining of Coal. *U.S.B.M. Information Circular 8205*, pp. 1-14 (1963).
8. Levo, N. Jr.: Dust Control in Coal Mines. *Trans. 53rd Nat. Safety Cong., Coal Min. Sesseions*, pp. 11-13 (1965).
9. Godard, R.R.: Dust Abatement Activities within United States Steel Coal Operations. *Coal Age* 72: 112 (1967).
10. Papic, M.M. and A.D. McIntyre: Surface Active Agents Evaluated in Canadian Study. *Coal Age* 78: 85-87 (1973).
11. Courtney, W.G. and L. Cheng: Control of Respirable Dust by Improved Water Sprays. *U.S.B.M. Information Circular 8753*, pp. 92-108 (1976).
12. Zeller, W.H., quoted by R. Harold: Surfactants vs. Dust - Do They Work? *Coal Age* 84:102-105 (1979).
13. Zeller, W.H.: Laboratory Tests for Selecting Wetting Agents for Coal Dust Control. *U.S.B.M. Report of Investigations 8815*, pp. 1-21 (1983).
14. Pigford, R.L. and C. Pyle: Performance Characteristics of Spray-Type Adsorption Equipment. *Ind. Eng. Chemistry* 43:1649-1662 (1951).
15. Cheng, L. and P.P. Zukovick: Respirable Dust Adhering to Run-of-Face Bituminous Coal. *U.S.B.M. Report of Investigations 7765*, pp. 1-9 (1973).
16. Gutierrez-Rodriguez, J.A., R.J. Purcell Jr. and F.F. Aplan: Estimating the Hydrophobicity of Coal. *Colloids and Surfaces* 12:1-25 (1984).
17. Kobrick, T.: Water as a Control Method - State of the Art Sprays and Wetting Agents. *U.S.B.M. Information Circular 8458*, pp. 122-133 (1970).

18. Chander, S., B.R. Mohal and F.F. Aplan: Wetting Behavior of Coal in the Presence of Some Nonionic Surfactants. *Colloids and Surfaces* (1986) (in press).
19. Anon.: *Kirk-Othmer Encyclopedia of Chemical Technology*, 3rd Ed., Vol. 8, pp. 910. John Wiley and Sons, New York (1980).
20. Varialli, G.: Coal-Water Slurry – Influence of Surfactants HLB on the Properties of Mineral Mixtures. Paper presented at 191st A.C.S. National Meeting, New York, April 13-18, 1986.
21. Mohal, B.R. and S. Chander: A New Technique to Determine Wettability of Powders – Imbibition Time Measurements. *Colloids and Surfaces* (1986) (in press).

# Wetting Behavior of Coal in the Presence of Some Nonionic Surfactants

S. Chander, B. R. Mohal and F. F. Aplan

Mineral Processing Section

Department of Mineral Engineering, The

Pennsylvania State University

## ABSTRACT

The wetting behavior of coal has been determined in the presence of nonyl and octyl series of nonionic surfactants containing polyethoxy groups of different sizes. The wetting behavior was determined by a modified Walker technique and contact angle measurements. The results show that the wetting rate of coal varies with coal rank, structure of the hydrocarbon chain and number of ethoxy groups in the hydrophilic group of the surfactant. A close relationship has been observed between the wetting rates and the short-time advancing contact angles.

## INTRODUCTION

Nonionic surfactants are used in many applications to improve wettability of solids. They can be used as dispersing agents [1] or dust suppressants [2-5] and to control the flotation, flocculation, filtration and flowability of particulates. This study was undertaken to study the effect of a series of nonionic surfactants on the wetting behavior of coal. Two series of surfactants, namely, ethoxylated nonyl and octyl phenols were used. The nonyl phenol series contains a linear hydrocarbon chain containing nine carbon atoms ( $(\text{CH}_3(\text{CH}_2)_8-\text{C}_6\text{H}_4-(\text{OC}_2\text{H}_4)_n$ , where  $n$  is the number of ethoxy groups). The octyl phenol series contains a branched hydrocarbon chain containing eight carbon atoms ( $(\text{CH}_3)_3\text{CCH}_2\text{C}(\text{CH}_3)_2-\text{C}_6\text{H}_4-(\text{OC}_2\text{H}_4)_n$ ).

### *Initial wetting rates — modified Walker technique*

Walker et al. [6] developed a sink test to determine the wettability of coal particles. In this technique, coal particles are dropped individually onto the surface of surfactant solutions of different concentrations, and the most dilute concentration in which coal would sink "instantaneously" is determined. This technique is a variation of a procedure initially developed by Draves and Clarkson [7] to determine the effect of surfactants on wettability of cotton fibers. In this procedure commonly known as the Draves test, the concentration of a surfactant required to give a 'sink time' of 25 s is determined.

Other investigators have used slight variations of the Walker method to study the wetting of fine particles [8-12], by measuring the time for wetting a given amount of powder. There are differences in the manner in which the time of wetting is measured, however. Some investigators measure the time for the



last trace of coal to disappear [8,11] whereas others determine the time for the vast majority of particles to sink [10]. Some investigators report a wetting rate [11] which is a value calculated on the basis of the time for the 'last traces of particles to sink'. The differences in choice of criterion for wetting can result in different values for wetting rates as illustrated in Fig. 1 which is based upon our measurements of the amount of powder wetted as a function of time. The procedure for wetting rate measurements is described in the next section. The technique in which time for disappearance of the 'last traces of particles' is determined gives the smallest value for the wetting rate, while the technique in which the time for wetting of the 'vast majority' of particles is determined will give intermediate rates. The terms 'last traces of particles' and 'vast majority of particles' are usually not defined explicitly and can lead to large differences in wetting rates measured by different investigators. Since our measurements show that the wetting rates for an assembly of powder decreases with time, we have used the initial wetting rates to compare the wetting behavior of coal in solutions of different surfactants.

#### EXPERIMENTAL METHODS AND MATERIALS

##### *Wetting rate — modified Walker technique*

To avoid some of the inherent difficulties associated with the measurement of time for wetting of powders, as discussed in the previous section, we have

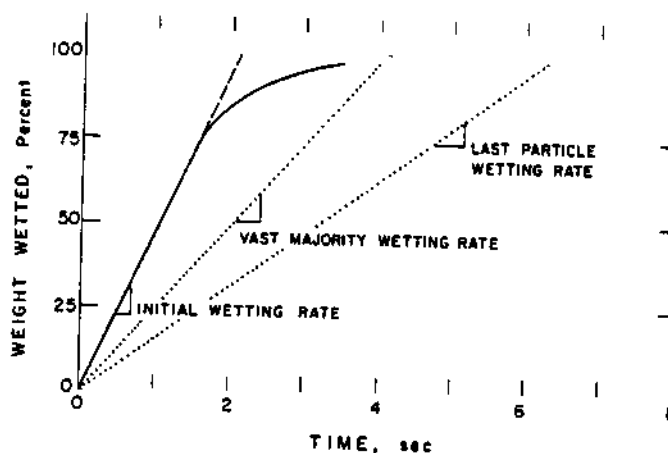


Fig. 1. The amount of a HVA-bituminous coal wetted by a  $4 \times 10^{-4} M$  Triton X-100 solution versus time in a typical wetting rate measurement.

modified the Walker method. In this method, shown schematically in Fig. 2, a 40 mg sample of  $250 \times 150 \mu m$  coal was dropped on the surface of a surfactant solution and the amount of coal imbibed into the liquid was measured by placing the pan of a Cahn electrobalance beneath the liquid surface. The initial wetting rates were determined from measurements of the amount of coal wetted as a function of time, as illustrated in Fig. 1. The rate of wetting was found to be independent of the amount of the coal sample in the range 20–100 mg. The data reported for the wetting rates is an average of at least four replicate measurements in which the coefficient of variation was about 0.08.

## WETTING BEHAVIOR OF COAL

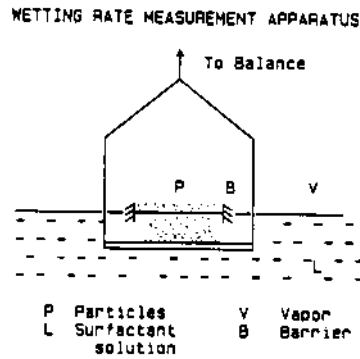


Fig. 2. A schematic diagram for the wetting rate measurement apparatus.

### *Contact angles*

The sessile drop contact angles were measured on carefully selected samples, avoiding those with cracks, locked particles of pyrite, mineral inclusions, etc. The coal was polished following the procedure of Gutierrez et al. [13]. Briefly, the procedure consisted of a rough polish on a series of emery papers followed by wet polishing on rotating laps (250 rpm) using, successively, 0.3 and 0.05  $\mu\text{m}$  levigated Linde Alumina. The samples were washed thoroughly with water to remove any adhering alumina particles and stored under distilled water. The contact angles were usually measured within ten minutes of sample preparation. Surgeon's gloves were used for the entire polishing sequence and all specimen handling was done with gloves or glass forceps to avoid contamination. The apparatus used for measuring the contact angle was the Ramé-Hart Model A-100 Contact Angle Goniometer.

### *Advancing contact angles*

The advancing contact angle measurements were made by observing the advance of the three-phase perimeter on a polished surface of coal. A drop of the surfactant solution (diameter  $\sim 2$  mm) was dropped from a height of 1 cm from a Gilmont microsyringe onto the polished specimen. The height of 1 cm was chosen to obtain a free falling drop. The progression of the drop was recorded using a Spin Physics Model SP2000 High Speed Motion Analysis System. The contact angle was measured during the period when the movement of the three-phase contact attained a constant velocity. This was taken to be the advancing contact angle.

### *Coal and reagents*

The three coal samples used in this investigation were: a HVA-bituminous coal from the Upper Freeport seam obtained from the Penn State Data Bank (PSOC 1361p), a sub-bituminous-A coal from Wyoming also obtained from the Penn State Data Bank (PSOC 512), and an anthracite coal obtained from Reading, PA. Proximate and ultimate analysis of the coal samples are given in Table 1. The coal samples were crushed and screened to obtain a  $250 \times 150 \mu\text{m}$  fraction which was then used for the wetting tests.

# THE RESPIRABLE DUST CENTER

TABLE 1

Proximate and ultimate analysis of coal samples

	HVA-bit.	Sub-bit.	Anthracite
Moisture	3.2%	10.24%	1.5%
Proximate analysis (dry basis %)			
Ash	8.47	6.64	8.2
VM	38.16	40.00	5.3
FC	53.37	53.36	86.4
Ultimate analysis (DAF basis %)			
C	81.94	75.42	94.3
H	5.70	5.15	2.3
N	1.54	0.84	0.9
S	2.12	0.35	0.6
O	8.7	18.22	1.9
Cl	—	0.22	—

The ethoxylated nonyl phenols (Triton N series) and octyl phenols (Triton X series) were obtained from Rohm and Haas and some of their properties are given in Table 2.

## RESULTS AND DISCUSSION

### *Wetting rates*

The initial wetting rates for a HVA-bituminous coal as determined by the modified Walker technique are given as a function of surfactant concentration in Fig. 3. The surfactants used in this series of tests were ethoxylated nonyl phenols with varying number of oxyethylene groups, the properties of which are given in Table 2. In the range investigated, the wetting rate increases linearly with the logarithm of concentration. The minimum concentration at which wetting occurs, obtained by extrapolating the wetting rate versus logarithm of concentration plots, is referred to as the critical wetting concentration,  $C_{cr}$ . In practical application in controlling wettability,  $C_{cr}$  would determine the minimum amount of surfactant needed to wet a given powder. Concentrations greater than  $C_{cr}$  will give higher rates of wetting. The  $C_{cr}$  values for various surfactants in the nonyl phenol series are shown by vertical arrows in Fig. 3 and are tabulated in Table 2.

The initial wetting rates, normalized with respect to the critical wetting concentration, are given in Fig. 4 for the nonyl phenol series and in Fig. 5 for the octyl phenol series of surfactants. The error bars for replicate measurements are given in Fig. 5, but are omitted from other figures for purpose of clarity. The results in Figs 4 and 5 show that the concentration dependence of wetting rates, measured in terms of the slope of the wetting rate versus log concentration, first increases and then decreases with an increase in the number of ethoxy groups. The slopes are given in the last column of Table 2. With the exception of Triton X-102, the  $C_{cr}$  increases with increase in the number of ethoxy groups. The ratio,  $C_{cr}/C_{CMC}$ , depends upon the number of ethoxy groups in the hydrophilic group of the surfactant and the nature of the hydrophobic group. This

# WETTING BEHAVIOR OF COAL

TABLE 2

Surfactant properties and parameters of coal wettability

Surfactant	No. of ethoxy groups	HLB	$C_{CMC}^a$ (M)	$C_{Cr}^b$ (M)	$C_{Cr}/C_{CMC}$	Slope <sup>c</sup>
<b>Nonyl Phenols</b>						
N-60	6	10.9	$2.7 \times 10^{-5}$	$5.4 \times 10^{-6}$	0.20	7.9
N-101	9-10	13.4	$3.3 \times 10^{-5}$	$8.2 \times 10^{-6}$	0.25	14.5
N-111	11	13.8	$6.0 \times 10^{-5}$	$1.8 \times 10^{-5}$	0.30	13.7
N-150	15	15.0	$9.3 \times 10^{-5}$	$4.5 \times 10^{-5}$	0.48	8.2
<b>Octyl Phenols</b>						
X-45	5	10.4	$(1.17 \times 10^{-4})$	$4.3 \times 10^{-5}$	0.37	14
X-114	7-8	12.4	$(2.1 \times 10^{-4})$	$5.7 \times 10^{-5}$	0.27	21.7
X-100	9-10	13.5	$2.2 \times 10^{-4}$	$1.3 \times 10^{-4}$	0.59	34.0
X-102	12-13	14.6	-	$9.0 \times 10^{-5}$	-	25.4

<sup>a</sup>The  $C_{CMC}$  value given in parentheses are from the literature [14], other values were obtained in this investigation.

<sup>b</sup>Critical wetting rate concentration, see text.

<sup>c</sup>Slope of the log surfactant concentration-initial wetting rate plot, see text.

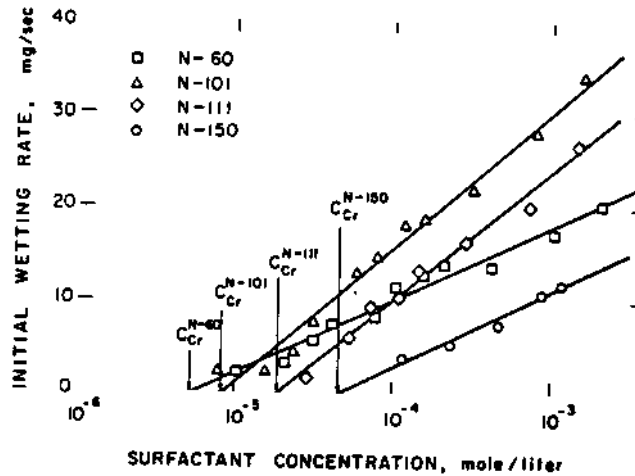


Fig. 3. The initial wetting rates for HVA-bituminous coal for various ethoxylated nonyl phenols.

is considered to reflect the importance of the adsorption phenomena at various interfaces in the three-phase system. These results are discussed later in the section on contact angles. The maximum in the slope occurs at about 9-10 ethoxy groups per molecule, or an HLB value of 13.5, for both the nonyl and the octyl phenol series of surfactants.

The initial wetting rates for three different coals, namely, an anthracite, a HVA-bituminous and a sub-bituminous, are given as a function of surfactant concentration in Fig. 6 for Triton N-101 and in Fig. 7 for Triton X-100. The effectiveness of the surfactant in wetting coal clearly depends upon both (a)

the coal rank and (b) the type of surfactant. For example, the rate of wetting for Triton N-101 follows the order:

HVA-bituminous > anthracite > sub-bituminous

whereas for Triton X-100, the order is:

anthracite  $\geq$  HVA-bituminous > sub-bituminous

These differences in the effect of surfactants on wetting rates are attributed to differences in the adsorption behavior of surfactants on the surface of coal and are discussed in the following section.

*Contact angles — sessile drop*

The sessile drop contact angles for HVA-bituminous and anthracite coals are given in Fig. 8 for Triton N-101 and in Fig. 9 for Triton X-100. As the concentration of the surfactant is gradually increased, the contact angle first increases and then decreases. The critical wetting concentration ( $C_{cr}$ ) as

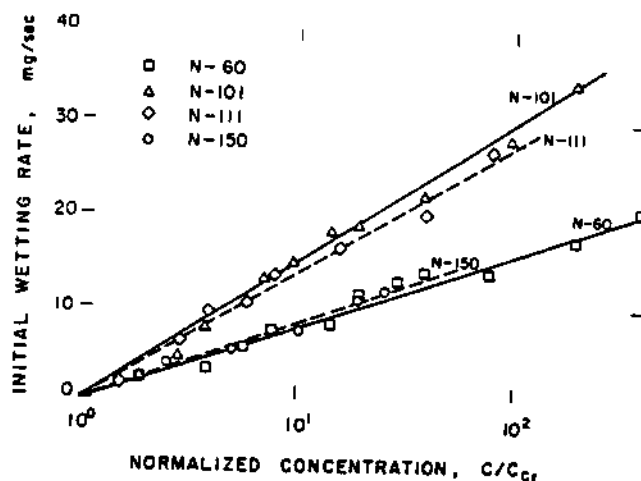


Fig. 4. The initial wetting rates for a HVA-bituminous coal as a function of normalized concentration for various ethoxylated nonyl phenols.

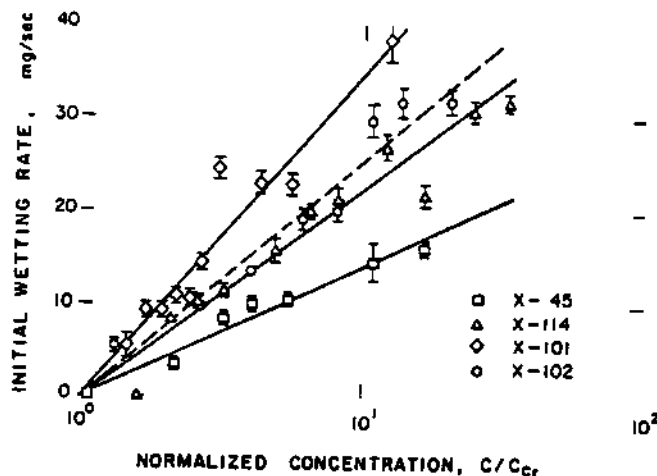


Fig. 5. The initial wetting rates for HVA-bituminous coal as a function of normalized concentrations for various ethoxylated octyl phenols.

## WETTING BEHAVIOR OF COAL

determined by wetting rate tests (Table 2) for these surfactants are shown by vertical arrows in both the figures.

The increase in contact angles at low concentration can be used to explain the zero wetting rate at concentrations below  $C_{cr}$ . At these concentrations the surfactant adsorbs on the hydrophilic sites at the coal surface through the polar head groups thus making coal more hydrophobic and non-wettable. Since coal consists of a distribution of hydrophilic sites on a hydrophobic surface [13], it is likely that at low surfactant concentrations, adsorption occurs simultaneously through hydrophobic interactions between the hydrocarbon chain and

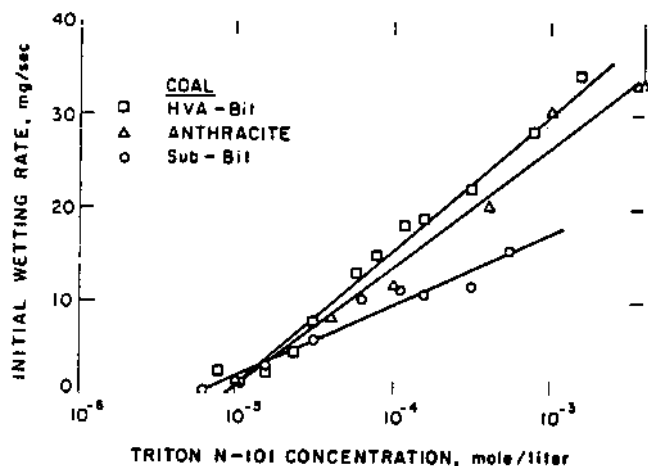


Fig. 6. The initial wetting rates for various coals as a function of Triton N-101 concentration.

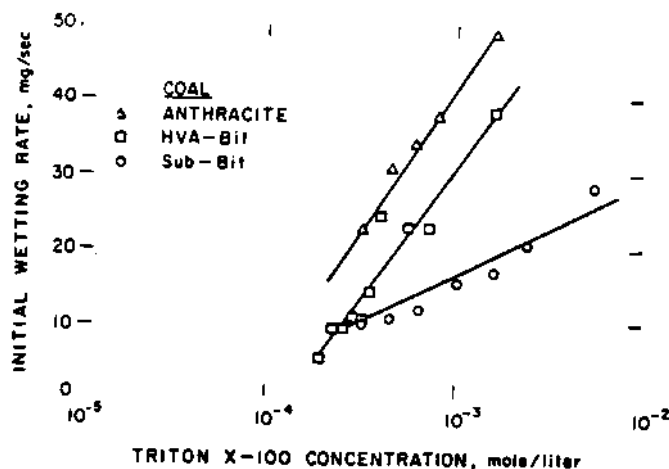


Fig. 7. The initial wetting rates for various coals as a function of Triton X-100 concentration.

the hydrophobic coal and through polar interactions between the ethoxylated group in the absorbed molecule and the hydrophilic sites at the surface of coal. At high surfactant concentrations, the surfactant molecules adsorb through hydrophobic chain interactions with a resultant decrease in contact angle and an increase in the rate of wetting. A direct correspondence between the wetting rates and the contact angles is not observed, however. For example, for Triton N-101 wetting occurs as soon as the concentration is such that the contact angle begins to decrease from its maximum value which is  $75^\circ$  for the HVA-

## THE RESPIRABLE DUST CENTER

bituminous coal and  $70^\circ$  for the anthracite. For Triton X-100, the contact angle must be reduced to  $\sim 55^\circ$  for the HVA-bituminous coal and to  $\sim 50^\circ$  for the anthracite coal before wetting is observed. Furthermore, on the basis of a thermodynamic analysis, involving the concept of immersional wetting ( $W_I = \gamma_{SL} - \gamma_{SV} = -\gamma_{LV}\cos\theta$ ), a large effect on wetting rate is not expected when contact angle changes from  $\sim 75^\circ$  to  $\sim 50^\circ$ .

### Contact angles — advancing

In an attempt to explain these observations, advancing contact angles were measured and the results are presented in Fig. 10. From the concept of immersional wetting the free energies involved in transfer of particles from air into

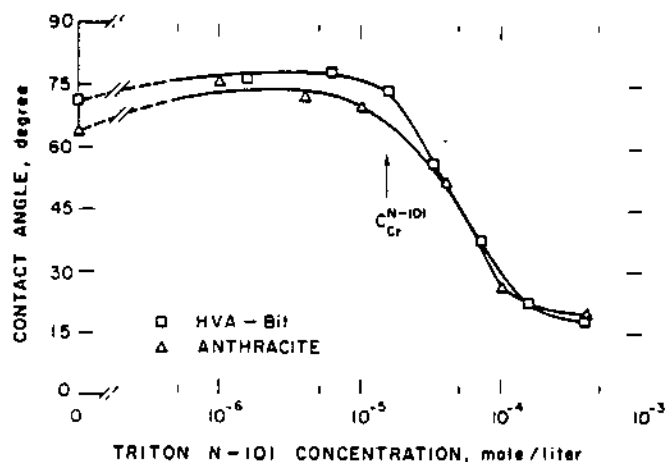


Fig. 8. The sessile drop contact angles for a HVA-bituminous coal and an anthracite coal as a function of Triton N-101 concentration.

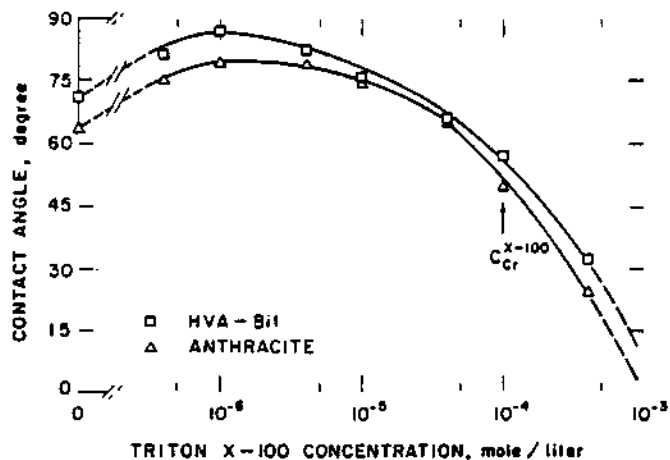


Fig. 9. The sessile drop contact angles for a HVA-bituminous coal and an anthracite coal as a function of Triton X-100 concentration.

## WETTING BEHAVIOR OF COAL

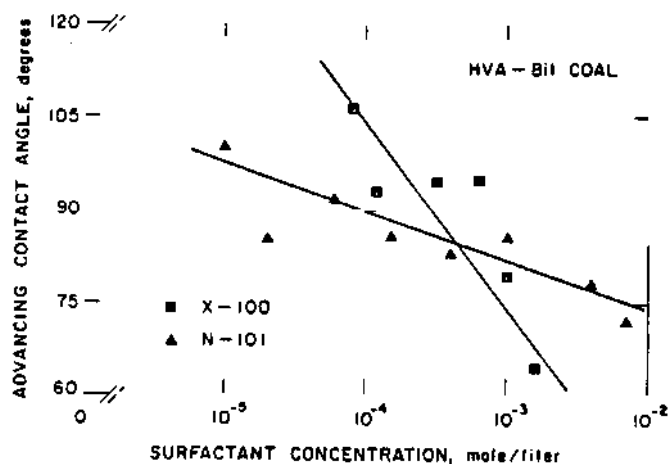


Fig. 10. The advancing contact angles for a HVA-bituminous coal as a function of concentration for Triton N-101 and Triton X-100.

an aqueous solution, wetting is expected when the contact angle is less than  $90^\circ$ . The results in Fig. 10 show that the effect of surfactant concentration on the advancing contact angle is very different for the two surfactants. In fact, the higher slope of the contact angle versus concentration plot for Triton X-100 than for Triton N-101 is in agreement with the slopes of the wetting rate versus concentration plots for these two surfactants. The minimum concentrations needed to decrease the advancing contact angles below  $90^\circ$  is higher for Triton X-100 ( $\sim 3 \times 10^{-4} M$ ) than for Triton N-101 ( $\sim 10^{-4} M$ ). The  $C_{cr}$  values for the above surfactants are  $1.3 \times 10^{-4} M$  and  $\sim 1 \times 10^{-5} M$ , respectively. These relate reasonably well but more importantly the slopes of the curves for the two surfactants (cf. Figs 4 and 5) for the wetting tests can be related to the slope of the curves in Fig. 10. Thus the concentration dependence of wetting rates can be explained in terms of the effect of surfactant concentration on advancing angles.

### SUMMARY

On the basis of the results reported in the previous section, it may be concluded that the wetting of coal particles depends upon the nature of interactions between coal surface and the surfactant. At low concentrations, the surfactant adsorbs through the polar ethoxy head group making coal non-wettable. Most likely, the hydrocarbon chains lie parallel to the surface resulting in an increased free energy of adsorption due to hydrophobic interactions between the hydrocarbon chain of the surfactant and the hydrophobic surface of coal. With increasing concentration, the contact angle decreases and the rate of wetting of coal increases. At higher concentrations, the orientation of adsorbed molecules is likely to be such that the polar ethoxy groups are oriented towards the solution.

The wetting behavior of coals by surfactant solutions varies with the coal rank because the nature of coal-surfactant interactions depends upon both the properties of the surfactant and type of hydrophilic and hydrophobic sites on the coal surface. Thus, the effectiveness of a given surfactant as a wetting agent for coal may be expected to vary with coal rank. For a HVA-bituminous coal, Triton-N-101 was found to be a superior wetting agent whereas for an anthracite coal, Triton X-100 was superior.



The results of wetting rate measurements correlate very well with the advancing contact angles. A comparison of the effect of surfactant concentration on wetting rate shows that the slope of the wetting rate versus logarithm of concentration plot for Triton X-100 is greater than the slope for Triton N-101 (cf. Figs 4 and 5). The slope of the advancing contact angle versus logarithm of concentration plots for Triton X-100 is also significantly greater than the slope for Triton N-101. Wetting is observed for conditions when the advancing contact angle decreases below about 100°. Thermodynamically, wetting is expected when the contact angle would be less than 90°. The slight difference is probably due to: (1) the differences in geometry of the system (the contact angles are measured on a polished surface whereas the wetting rate measurements are made with particles dropped onto an air/solution interface); (2) the effect of particle-particle interactions at the interface on wetting rate measurements. (More recently, through direct observation of a particle at interfaces, we have observed that the time of wetting of a particle is influenced by the presence of another particle at the interface.)

#### ACKNOWLEDGEMENTS

The authors acknowledge the support from the Mineral Institutes Program under Grant No. G1135142 from the Bureau of Mines, U.S. Department of the Interior, as part of the Generic Mineral Technology Center for Respirable Dust, The Pennsylvania State University. The support from the National Science Foundation, under equipment Grant No. CPE-8406276 is also acknowledged.

#### REFERENCES

- 1 G.D. Parfitt, *Dispersion of Powders in Liquids*, 3rd edn, Applied Science Publishers, Barking, 1982.
- 2 Anon., *Rock Prod.*, 65 (August 1962) 92-96.
- 3 R. Harold, *Coal Age*, 84 (June 1979) 102-105.
- 4 T. Kobrick, U.S. Bur. Mines Inf. Circ., 8458 (1969) 123-131.
- 5 P. Green, *Coal Age*, 87 (August 1982) 72-75.
- 6 P.L. Walker, E.E. Peterson and C.C. Wright, *Ind. Eng. Chem.*, 44 (1952) 2389-2392.
- 7 C.Z. Draves and R.C. Clarkson, *Am. Dyestuff Reporter*, 20 (March 1931) 109-116.
- 8 N. Feldstein, U.S. Bureau of Mines OFR 127-81, 1981, 47 pp., NTIS PB 82-104654.
- 9 M.M. Papic and A.D. McIntyre, *Coal Age*, 78 (June 1973) 85-87.
- 10 J.A. Kost, G.A. Shirey and C.T. Ford, U.S. Bureau of Mines OFR 30-82, 1980, 188 pp., NTIS PB 82-183344.
- 11 J.O. Glanville and J.P. Wightman, *Fuel*, 58 (1979) 819-822.
- 12 S. Garshve, S. Contreras and J. Goldfarb, *Colloid Polym. Sci.*, 256 (1978) 241-250.
- 13 J.A. Gutierrez-Rodriguez, R.J. Purcell Jr. and F.F. Aplan, *Colloids Surfaces*, 12 (1984) 1-25.
- 14 E.H. Crook, D.B. Fordyce and G.F. Trebbi, *J. Phys. Chem.*, 67 (1963) 1987-1994.

# A New Technique to Determine Wettability of Powders-Imbibition Time Measurements

**B. R. Mohal and S. Chander**

Mineral Processing Section  
Department of Mineral Engineering, The  
Pennsylvania State University

## ABSTRACT

A new technique to determine wettability of powders is presented in this paper. In this technique the times for immersion of individual particles from air into liquids, defined as imbibition times, are measured. Through the measurements of imbibition times for a large number of particles, it is possible to determine homogeneity/heterogeneity of a powder sample with regard to its wetting behavior. Quartz particles give a very narrow distribution of imbibition times showing a homogeneous wetting surface whereas coal particles give a broad distribution indicative of the heterogeneous nature of its surface. The imbibition time measurement technique is considered to have certain advantages over other methods to determine wettability of powders in surfactant solutions. In this study we have also compared the imbibition times with the wetting rate measurements obtained by a modified Walker test.

## INTRODUCTION

Several methods are available for determining wetting characteristics of solids. Each of the methods has been used in the past to obtain very valuable information for comparing wetting behavior of various solids in a given liquid or for comparing the wetting behavior of several liquids for a given solid. Each method measures a somewhat different aspect of wetting and therefore quantitative correlations between techniques have been difficult. A general approach is to use a method in which close similarity between the technique and the application (where results of wetting measurements are to be used) can be maintained. The objective of this investigation was to develop a method which could be used to determine the wetting characteristics of single particles in surfactant solutions. Wetting of individual particles is of importance in capture of dust particles by sprays of surfactant solutions.

## METHODS FOR DETERMINING WETTING — A BRIEF REVIEW

The various methods available for measuring wetting characteristics of solids include: contact angle, immersion/sink time, bubble pick-up, induction time, capillary rise, and displacement method measurements. Some of the methods are briefly reviewed in the paragraphs that follow.

\*Dedicated to the memory of Professor G.D. Parfitt.

\*\*To whom all correspondence may be addressed.

The contact angle method is perhaps the most widely used. Although there are some difficulties associated with the measurement, and interpretation of contact angles, it is one of the most common methods of assessing wettability. When done properly, contact angle measurements are simple and they provide very valuable information. The main difficulty of the technique, particularly in investigating the wetting behavior of coal, is that the sample must be carefully selected and polished, for measurements to be reliable [1]. Pellets made from pressing powders have been used by some investigators to estimate contact angles [2,3].

An immersion/sink time procedure was initially developed by Draves and Clarkson [4] to determine the effect of surfactants on wettability of cotton fibers. In this procedure, commonly known as Draves test, concentrations of the surfactant required to give a 'sink time' of 25 s is measured. The 'sink time' is measured as the time taken by a skein of cotton to sink after it has been immersed in the surfactant solution. Walker et al. [5] modified this test to determine the wetting ability of various surfactants for coal dusts. In this technique coal particles are dropped individually onto the surface of surfactant solutions of different concentrations. The most dilute concentration in which coal would sink instantaneously was determined. (The term 'instantaneously' was not defined by these authors. Results of the present study show that the wetting process could involve times of the order of milliseconds.) Other investigators modified the Walker technique in various ways. Some investigators report the time for wetting a given amount of powder [3,6,7] whereas others report wetting rate [8]. Also, there are differences in the manner in which the time of wetting is measured. Some investigators measured the time for the last trace of coal to disappear [3,8] whereas others have determined the times for the vast majority of particles to sink [7]. Our studies show that there is a gradual decrease in the wetting rate with time.

Bartell and Osterhof [9] used a method based upon measurement of the pressure with which one liquid will displace another from a packed bed of particles. Another similar method is the capillary rise method developed by Crowl and Wooldridge [10]. In this method a certain amount of powder is placed in a cylindrical glass tube one end of which has a filter paper or porous disc. The filter paper-end of the tube is placed in contact with the surface of the surfactant solution and the height to which the liquid rises is measured as a function of time. Neither of these methods is very suitable for determining wetting of powders in surfactant solutions due to surfactant depletion (through adsorption at the solid) effects at the liquid/gas interface.

Some investigators have used indirect methods, such as bubble pick-up [11], induction times [12], calorimetry [13,14], etc., to assess wetting characteristics of powders.

In this paper we have used a modified Walker technique to determine the rate of wetting of an assemblage of coal particles. In addition, we have developed a new technique of imbibition time measurements to determine wetting characteristics of individual particles in surfactant solutions. These techniques are discussed in the paragraphs that follow.

### THE WETTING RATE — MODIFIED WALKER TECHNIQUE

The difficulties associated with measurement of wetting rate of powders were discussed in the previous section. Therefore, we have introduced yet another modification to the Walker method of assessing wettability in surfactant solutions. The amount of coal imbibed into the liquid, and hence wetted, was mea-

## WETTING CHARACTERISTICS OF PARTICLES

sured by placing the pan of a Cahn electrobalance beneath the liquid surface. The wetting rates were determined from measurements of the amount of coal wetted as a function of time. Preliminary experiments showed that the wetting rate decreased gradually with time; a similar observation was made by Zeller [15]. This is perhaps the reason why some investigators have used somewhat arbitrary definitions of times at which wetting is considered to have occurred. Because of the dependence of wetting rate on time, we have used initial wetting rates to compare the wetting behavior of coals in different surfactant solutions.

### IMBIBITION TIME

For a highly heterogeneous substance like coal, the use of an averaged parameter to represent wetting characteristics is not very satisfactory and could in fact be misleading as shown later in this paper. Accordingly, a new technique to determine coal wettability was developed. In this technique, the imbibition time ( $\tau$ ), defined as the time between the instant the particle first impacts at the liquid-gas interface and the instant when the particle detaches from the interface, is measured. Totally hydrophilic particles pass directly into the liquid phase, the only impeding force to their passage being the fluid drag force experienced by the particle as it enters a dense phase. Totally hydrophobic particles make contact with the liquid, lose their kinetic energy and remain at the interface and are not imbibed. Particles with intermediate wetting behavior may remain at the interface until the movement of the three-phase contact completely engulfs the particle and the particle sinks.

The downward velocity of a particle as it passes through a gas/liquid interface is schematically shown in Fig. 1 for three kinds of particles. One may consider that the particle impacts the liquid surface with a velocity equal to its terminal settling velocity in air,  $(v_t)_{air}$ . Type I particles are the particles which are completely wetted by the liquid. The time at which such a particle is completely imbibed into the liquid is shown by a vertical arrow corresponding to an imbibition time of  $\tau$ . The particle in this case can enter the liquid at a velocity greater than the terminal settling velocity of the particle in the liquid,  $(v_t)_{liquid}$ . The quantity  $\tau$  is expected to depend on the kinetic energy of the particle at the time of impact at the gas/liquid interface. Type II particles are the completely hydrophobic particles which are not wetted by the liquid. These particles lose their kinetic energy after impact and remain at the interface. Type III particles are the particles with intermediate wettability which are

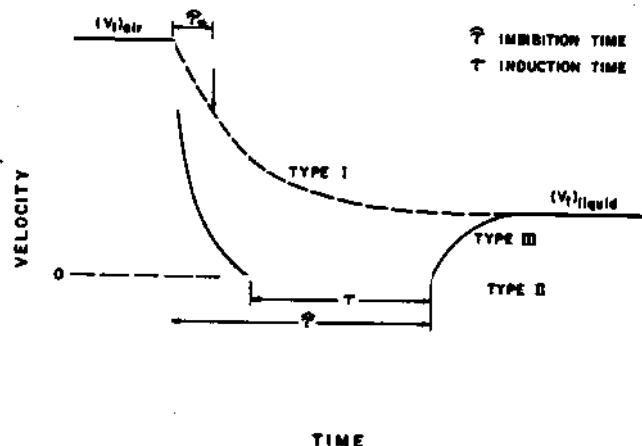


Fig. 1. Velocity of a particle passing through a gas-liquid interface versus time.

imbibed through gradual movement of the three-phase perimeter. The movement of the perimeter depends upon factors such as the adsorption of surfactants at various interfaces and the magnitude of interfacial tensions.

Although an induction time,  $\tau$ , can be defined to represent the time for which the particle remains at the interface after impact occurs and before imbibition starts, as defined by some investigators [12], experimental determination of this parameter is difficult. Since a hydrophilic particle of diameter  $200 \mu\text{m}$  is imbibed in about 0.5 ms, the difference between  $\tau$  and  $\tau$  is expected to be of the order 1 ms or less. The experimental values of  $\tau$  in coals/surfactant systems are in the range of 0.02–200 s. Therefore, imbibition times may be taken as a reasonable measure of induction times.

#### EXPERIMENTAL METHODS AND MATERIALS

The wetting rates were determined by measuring the amount of coal wetted as a function of time. The weight of coal wetted was measured by placing the pan of a recording electrobalance, Model Cahn 2000, beneath the surface of the liquid. The required amount of coal sample, typically 50 mg, was placed at the interface with a vibro-feeder. The feeder was held over the surface of the solution at a constant height of 1 cm. The initial wetting rate was determined from the plot of the weight of coal immersed versus time. An average of at least four experiments was taken as the initial wetting rate. The coefficient of variation in these experiments was less than 0.08.

A Spin Physics Model SP2000 High Speed Motion Analysis System was used to photograph the sequence of events during imbibition of particles into various solutions. The system is capable of recording images up to 12000 frames/s. Therefore, motion taking place at intervals of 0.083 ms can easily be distinguished. Imbibition times, as defined in the previous section, were determined from the recorded tape of events. The liquid was placed in a 1 cm wide spectrophotometer cell. Individual coal particles were dropped onto the liquid surface from a height of about 23 cm through a disposable pipet. The pipet ensured that the particles fall onto the specified viewing area, and also ensured by its length that all particles has the same kinetic energy before impinging on the liquid. The imbibition time was measured from the instant the particle appeared at the interface to the instant it detached from the liquid interface. To obtain the distribution of imbibition times approximately 75–100 particles were observed.

A hand-sorted sample of +2 in quartz was crushed and the +28 mesh fraction was acid leached and washed with distilled water until there was no change in pH of the wash water. The +28 mesh quartz was then wet ground in a porcelain ball mill. The material was dried at room temperature and stored in a dessicator until use.

The three coal samples used in this investigation were: a HVA-bituminous coal from the Upper Freeport seam obtained from the Penn State Data Bank (PSOC 1361p), a sub-bituminous A coal from Wyoming also obtained from the Penn State Data Bank (PSOC 512), and an anthracite sample obtained from Reading, PA. The proximate and ultimate analysis of these sample are given in Table 1. The coal samples were crushed and screened to obtain a  $250 \times 150 \mu\text{m}$  fraction which were used for wetting tests. The coal samples were stored in a dessicator at all times. Methanol and NaCl used were obtained as Bakers Analyzed Reagents. The surfactant Triton N-101 (a polyethoxylated nonyl-

# WETTING CHARACTERISTICS OF PARTICLES

phenol with an HLB of 13.4) was obtained from Rohm & Haas. Distilled water from a tin-lined still of specific resistivity greater than 2 Mohm was used in all the experiments conducted at 25°C.

## RESULTS AND DISCUSSION

### Wetting Rates

The initial wetting rates for coal as determined by the modified Walker technique are given as a function of surfactant concentration in Fig. 2. For Triton

TABLE 1

Proximate and ultimate analysis of coal samples

	HVA-bit-uminous	Sub-bit-uminous	Anthracite
H <sub>2</sub> O	3.2%	10.24%	1.5%
Proximate analysis (Dry basis%)			
Ash	8.47	6.64	8.2
VM	38.16	40.00	5.3
FC	53.37	53.36	86.4
Ultimate analysis (DAF basis%)			
C	81.94	75.42	94.3
H	5.70	5.15	2.3
N	1.54	0.84	0.9
O	2.12	0.35	0.6
Cl	—	18.22	1.9
		0.02	—

N-101, the largest wetting rates are observed for HVA-bituminous coal followed by anthracite and sub-bituminous coals. The results show that below approximately  $10^{-5}$  M surfactant concentration the wetting rate is zero. The surface tension of Triton N-101 at this limiting concentration was observed to be  $40 \text{ dyn cm}^{-1}$ . The close similarity of this surface tension and the critical surface tension of wetting of coals reported by Parekh and Aplan [16] is coincidental, however. We expect that the limiting surfactant concentration for zero wetting rate or the corresponding limiting surface tension will be dependent upon the surfactant type due to adsorption at the coal/surfactant solution interface. The significance of adsorption at the coal/solution interface was

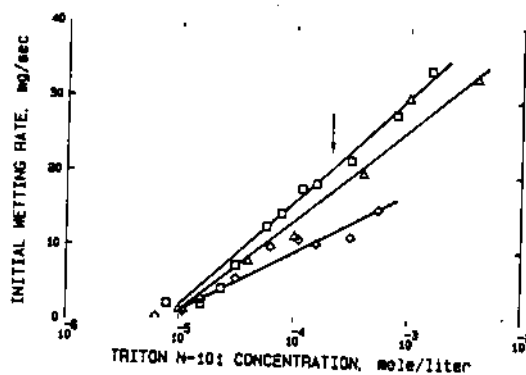


Fig. 2. Initial wetting rate for a HVA-bituminous ( $\square$ ), an anthracite ( $\Delta$ ), and a sub-bituminous ( $\diamond$ ) coal in aqueous solutions of Triton N-101. The vertical arrow represents the concentration at which imbibition time measurements were made.

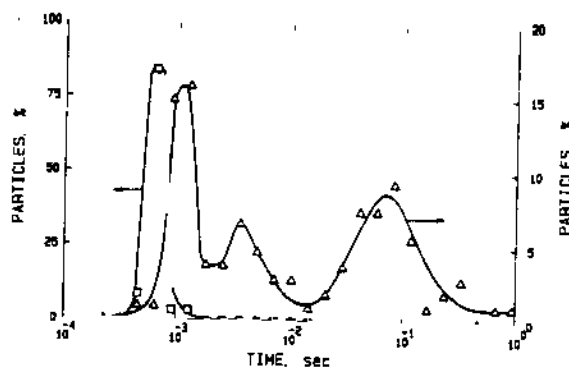


Fig. 3. Imbibition times for a wet ground quartz in aqueous  $2 \times 10^{-3} M$  NaCl ( $\square$ ) and a HVA-bituminous coal in a 60 vol. % methanol-water mixture ( $\Delta$ ).

discussed by Glanville and Wightman [17]. Our studies also show that the adsorption at the coal/water interface is a strong function of coal rank and surfactant type [18]. Due to the scatter in the data in Fig. 2, no definite conclusions can be drawn regarding the effect of micelle formation at concentration exceeding the CMC,  $3.5 \times 10^{-5} M$ .

#### *Imbibition times*

The imbibition times for a HVA-bituminous coal in a 60% methanol-water mixture are given in Fig. 3. The methanol-water mixture was used because the wetting rate measurements, presented in Fig. 1, show that coal particles require a surface tension of the liquid to be (approximately) less than  $35 \text{ dyn cm}^{-1}$  before they can be wetted. Similar observations were made by other investigators working with different coals [6,8]. For comparison with a hydrophilic material, times for imbibition of quartz in  $2 \times 10^{-3} M$  NaCl are also given in Fig. 3. Quartz being a relatively homogeneous hydrophilic solid gives a very sharp peak on the frequency plot in Fig. 3. The total distance moved by a particle for it to be completely imbibed, after initial contact with the liquid surface, is equal to its diameter which is about  $200 \mu\text{m}$  for the particles investigated. The time required for the particle to move this distance in air at its terminal settling velocity is about  $0.00016 \text{ s}$  and, similarly, the time required for the particle to move the same distance in water at its terminal settling velocity is about  $0.0082 \text{ s}$ . The mode of the imbibition time distribution plot for quartz in Fig. 4 is  $0.0005 \text{ s}$  which lies in between the two limits defined above. These results may be interpreted to mean that the quartz particle experiences an increased drag force immediately after impacting the liquid surface. The mode of the distribution time for quartz is less than  $\sqrt{0.0082 \times 0.00016}$  which is interpreted to mean that the particle enters the liquid phase at a velocity greater than the terminal settling velocity of the particle in the liquid. Direct measurements of the velocities of a quartz particle after having been imbibed into the liquid confirm this to be true.

The imbibition behavior of coal particles is quite different, however. Within the same coal sample, a large variation in imbibition times is observed. This was the reason for plotting the imbibition time data in Fig. 3 with times on a logarithmic scale. In this figure time intervals on  $\sqrt{2}$  scale were used with the geometric mean of the interval as the imbibition time of the interval. The wide distribution in imbibition times is considered to reflect the heterogeneous nature of the coal surface. Several investigators have suggested that coal surfaces con-

## WETTING CHARACTERISTICS OF PARTICLES

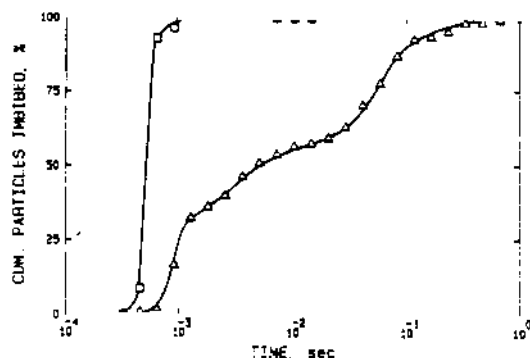


Fig. 4. Cumulative imbibition times for a wet ground quartz in aqueous  $2 \times 10^{-3} M$  NaCl ( $\square$ ) and a HVA-bituminous coal in a 60 vol. % methanol-water mixture ( $\triangle$ )

sist of a variety of hydrophilic and hydrophobic sites, but no techniques are available to quantitatively determine their relative proportions. We propose that the imbibition time distribution curves provide a means to assess the heterogeneities in wetting properties of coal. The trimodal distribution shown in Fig. 3 suggests that this coal can be considered to consist of three kinds of particles — a fast sinking fraction (least hydrophobic), a slow sinking fraction (most hydrophobic), and an intermediate fraction. The fast sinking fraction is most hydrophilic and its imbibition times in 60% methanol-water mixture are comparable to the imbibition times for quartz in  $2 \times 10^{-3} M$  NaCl. That is, the driving force to wet the fast sinking fraction of coal in 60% methanol-water mixture is comparable to the driving force to wet quartz in  $2 \times 10^{-3} M$  NaCl. The slow sinking fraction represents a very hydrophobic set of particles. Highly hydrophobic particles of certain coal macerals with a water contact angle of about  $120^\circ$  have been measured by Aplan and associates in recent studies at The Pennsylvania State University [19]. The particles with intermediate set of imbibition times could either represent locked particles or particles of intermediate wettability. Additional studies are being conducted to further characterize the three coal fractions.

The imbibition time data for quartz and coal are also plotted as cumulative percent of particles imbibed as a function of time on the logarithmic scale, Fig. 4. The relative proportions of fast-sinking, slow-sinking and intermediate fractions can be easily determined from such plots. The slope of the curves in Fig. 4 can be taken as a measure of the degree of homogeneity in the system. A large slope implies that the system is homogeneous as was observed for quartz and a small slope is an indication of a heterogeneous system as observed for coal. Both physical and chemical heterogeneities are expected to affect the imbibition time. Since crushed quartz with irregular shaped particles gave imbibition times in a narrow range, we believe that chemical heterogeneities predominantly contribute to the large variation in imbibition times for coal.

The cumulative imbibition time plots for wetting of three different coals in  $4 \times 10^{-4} M$  Triton N-101 are given in Fig. 5. This concentration is marked by a vertical arrow in Fig. 2 from which wetting rates can be obtained. A direct correlation between imbibition times and wetting rates is observed. The imbibition times for the sub-bituminous coal are several orders of magnitude greater than the HVA-bituminous coal indicating a very high sensitivity of these measurements.

A unimodal cumulative imbibition time curve can be conveniently described by two parameters:  $t_{50}$  and  $\sigma$ . The time parameter,  $t_{50}$ , is defined such that 50%



of the particles are imbibed in a time less than  $t_{50}$  (the remaining 50% imbibing at times greater than  $t_{50}$ ). The homogeneity index,  $\sigma$ , which is equal to the slope of the cumulative imbibition time curve at  $t_{50}$ , is a measure of the homogeneity of the sample; a large slope is indicative of a homogeneous sample whereas a small slope can be considered to represent a heterogeneous sample. As stated before, both chemical and physical heterogeneities may contribute to the homogeneity index. For polymodal distributions, a set of  $t_{50}$  and  $\sigma$  values are needed to describe the wetting behavior of the coal. The data in Figs 4 and 5 were used to calculate the  $t_{50}$  and  $\sigma$  values for various coals in different solutions and the calculated values are listed in Table 2. The results clearly show that coals consist of a mixture of particles which differ in their wetting behavior. The large value of  $\sigma$  for quartz suggests that the sample is fairly homogeneous in its wetting behavior even though the crushed particles were irregular

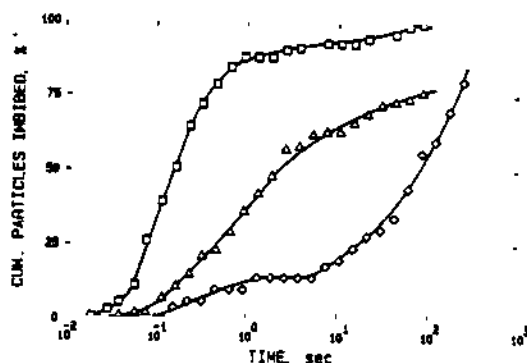


Fig. 5. Cumulative imbibition times for a HVA-Bituminous ( $\square$ ), an anthracite ( $\Delta$ ), and a sub-bituminous ( $\diamond$ ) coal in a  $4 \times 10^{-4} M$  solution of Triton N-101.

TABLE 2

The time parameter,  $t_{50}$ , and the homogeneity index,  $\sigma$ , for various coals in different solutions

System	$t_{50}$ (s)	$\sigma$	Type of distribution
Quartz/water	0.0005	6.42	Unimodal
HVA-bit./60% methanol	0.0009	5.5	Trimodal
	0.0021	1.71	
	0.0600	1.35	
HVA-bit./N-101	0.116	1.02	Bimodal
	35.7	1.67	
Anthracite/N-101	0.71	0.635	Bimodal
Sub-bit./N-101	0.33	0.81	Bimodal
	98.5	0.67	

in shape. A fraction of the HVA-bituminous coal is readily wetted by 60% methanol-water solution ( $t_{50} = 0.0009$  s,  $\sigma = 5.5$ ) whereas the remainder two fractions have longer  $t_{50}$  and smaller  $\sigma$  values. The change in  $t_{50}$  and  $\sigma$  in surfactant solutions is due to specific coal-surfactant interactions.

SUMMARY

A new technique to determine wettability of powders is presented in this paper. In this technique the times for imbibition of particles from air into liq-

## WETTING CHARACTERISTICS OF PARTICLES

uids are measured. The imbibition times for hydrophilic particles are of the order of half a millisecond whereas they are several orders of magnitude higher (ranging from 0.02 to 200 s or more) for hydrophobic coal particles. The imbibition times depend upon surfactant concentration and coal type which is not surprising because wetting is a three-phase phenomena. The most convenient way to represent the data is to plot cumulative percent particles imbibed as a function of time plotted on a logarithmic scale. The wetting behavior for a solid-surfactant system can be represented by two parameters. One is a time parameter,  $t_{50}$ , which is defined such that 50% of the particles are imbibed in a time less than  $t_{50}$ , and the second is a homogeneity index,  $\sigma$ , which is equal to the slope of the cumulative imbibition time curve at  $t_{50}$ . The wetting characteristics of a mixture of particles can be described by a set of such parameters, one set to represent each component in the mixture.

### ACKNOWLEDGEMENTS

The authors acknowledge the support from the Mineral Institutes Program under Grant No. G1135142 from the Bureau of Mines, U.S. Department of the Interior, as part of the Generic Mineral Technology Center for Respirable Dust, The Pennsylvania State University. The support from the National Science Foundation, under equipment Grant No. CPE-8406276, is also acknowledged.

### REFERENCES

- 1 J.A. Gutierrez-Rodriguez, R.J. Purcell Jr, and F.F. Aplan, *Colloids Surfaces*, 12 (1984) 1-25.
- 2 N.W.F. Kossen and P.M. Heertjes, *Chem. Eng. Sci.*, 20 (1965) 593-599.
- 3 N. Feldstein, BuMines OFR 127-81 (1981) 47 pp., NTIS PB 82-104654.
- 4 C.Z. Draves and R.G. Clarkson, *Am. Dyest. Rep.*, 20 (March 1931) 109-116.
- 5 P.L. Walker, E.E. Peterson and C.C. Wright, *Ind. Eng. Chem.*, 44 (10) (October 1952) 2389-2392.
- 6 M.M. Papic and A.D. McIntyre, *Coal Age*, 78 (June 1973) 85-87.
- 7 J.A. Kost, G.A. Shirey and C.T. Ford, BuMines OFR 30-82 (1980) 188 pp., NTIS PB 82-183344.
- 8 F.J.O. Glanville and J.P. Wightman, *Fuel*, 58 (1979) 819-822.
- 9 F.E. Bartell and H.J. Osterhof, *Ind. Eng. Chem.*, 19(11) (1927) 1277-1280.
- 10 V.T. Crowl and W.D.S. Wooldridge, *SCI Monograph*, Vol. 25, Society of Chemical Industry, London, 1967, pp. 200-212.
- 11 J.A. Finch and G.W. Smith, *Can. Metall. Q.*, 14(1) (1975) 47-51.
- 12 V.A. Glembotsky, *Izv. Akad. Nauk SSSR Otd. Tekh. Nauk*, (1953) 1524-1531 (in Russian).
- 13 A.C. Zettlemoyer, *J. Colloid Sci.*, 28 d(1968) 343.
- 14 R.W. Healy and D.W. Fuerstenau, *J. Colloid Sci.*, 20 (1965) 376.
- 15 W.H. Zeller, BuMines RI 8815 (1983) 21 pp.
- 16 B.K. Parekh and F.F. Aplan, *Rec. Dev. Sep. Sci.*, 4 (1978) 107.
- 17 J.O. Glanville and J.P. Wightman, *Fuel*, 59 (1980) 557-562.
- 18 B.R. Mohai, S. Chander and F.F. Aplan, unpublished work.
- 19 B.J. Arnold and F.F. Aplan, unpublished work.

# Estimation of Particle Size Distributions Using Pipet-Withdrawal Centrifuges

T. H. Dumm and R. Hogg

Mineral Processing Section  
Department of Mineral Engineering, The  
Pennsylvania State University

## Abstract

The mathematical treatments used in the evaluation of particle size distribution from pipet-withdrawal centrifuge data are reviewed. An error in the published procedure for multiple-sample withdrawal systems is pointed out and a corrected formulation is presented. An alternative treatment, based on a piece-wise linearization of the size distribution is described. Computer simulations of the analytical and data evaluation procedures indicate that the errors in the original formulation are not generally serious and that the corrected and alternative procedures lead to very similar estimates. Except for some cases involving very narrow size distributions, the alternative approach appears to give slightly closer estimates of the size distribution. Comparisons based on actual experimental data are also described.

## 1 Introduction

Sedimentation methods are widely used for the determination of particle size distributions. The procedures are relatively simple to use and the results are essentially absolute, requiring no external calibration. Gravity sedimentation is typically applicable to particles in the size range of about 1 to 50  $\mu\text{m}$  and generally involves measurement of the relative concentration of particles as a function of depth and time in a dilute suspension. Particle size is calculated using Stokes' law:

$$v = \frac{h}{t} = \frac{\Delta\rho g x^2}{18\mu} \quad (1)$$

Gravity sedimentation is limited, in the fine sizes, by the increasing importance of random, Brownian motion and by the excessively long settling times involved [1, 2]. The limiting size can be extended almost indefinitely through the use of centrifuges, but this introduces two additional complications in the analysis of data. In the first place, the force acting on the particles is no longer constant, but varies with distance from the center of rota-

tion of the centrifuge, i.e. with distance settled. Secondly, the settling is no longer unidimensional since particles move radially away from the center of rotation. This leads to dilution of the suspension at a fixed position, even for particles with identical settling velocities.

For centrifugal sedimentation, Eq. (1) must be replaced by:

$$v = \frac{dr}{dt} = \frac{\Delta\rho r\omega^2 x^2}{18\mu} \quad (2)$$

The relative concentration at position,  $r$ , and time,  $t$ , is given by:

$$Q(t) = \frac{c(r,t)}{c_0} = \int_0^{x_m} \frac{f(x)dx}{y(x)} \quad (3)$$

$f(x)dx$  is the mass fraction of particles in the size interval  $x$  to  $x + dx$ . Kamack [3] presented an approximate procedure for solving the integral equation.

Pipet withdrawal systems offer a simple, practical means for determining particle concentrations in settling suspensions and form the basis for the well-established Andreasen pipet used in gravity sedimentation. Allen and Svarovsky [4] have developed a disk centrifuge with pipet withdrawal which can be used for size analysis down to about 0.01  $\mu\text{m}$ . Since the withdrawal of suspension also leads to motion of the particles remaining in the centrifuge, the analysis is complicated still further when this technique is applied. The Kamack treatment can be applied up to the time of the first sample withdrawal and a complete size analysis can be obtained by repeating the procedure with a series of separate samples. Obviously, however, this is an inefficient and time-consuming process. Allen and Svarovsky [1, 4] have modified the Kamack procedure to allow for multiple sample withdrawals. Unfortunately, their treatment contains an error in the estimation of the dilution factors  $y(x)$ .

The purpose of this paper is to present a corrected version of the Allen/Svarovsky treatment as well as an alternative procedure for solving Eq. (3) for multiple withdrawal systems. Computer simulations are used to compare the results obtained using the different approaches. Some examples of their application to the analysis of fine powders are also given.

\* T. F. Dumm, Ph. D. Candidate in Mineral Processing, R. Hogg, Professor of Mineral Processing, The Pennsylvania State University, Department of Mineral Engineering, University Park, PA 16802 (USA).

2 Theory

2.1 Calculation of Particle Size

Integration of Eq. (2) from the surface of the suspension to the sampling location leads to

$$x^2 = \frac{\ln R/S_0}{kt} \quad (5)$$

where  $R$  and  $S_0$  are the distances from the center of rotation to the sampling position and the suspension surface respectively,  $k$  is a constant given by

$$k = \frac{\Delta\rho\omega^2}{18\mu} \quad (6)$$

For a single withdrawal at time,  $t$ , Eq. (5) defines the size of the largest particle in the sample.

In the case of multiple sample withdrawals, a particle of size,  $x_i$ , will fall an additional distance,  $\Delta z_{ij}$ , due to sample withdrawal at time,  $t_j$ . *Allen and Svarovsky* showed that this can be taken into account using a modified form of Eq. (5), i.e.,

$$x_i^2 = \frac{1}{kt_i} \ln(R/S_0) \prod_{j=1}^{i-1} \left[ \left( 1 + \frac{\Delta z_{ij}}{z_{ij}} \right)^{-1} \right] \quad (7)$$

with

$$z_{ij} = \begin{cases} S_0 \exp(x_i^2 t_j k) & j = 1 \\ S_0 \exp(x_i^2 t_j k) \prod_{l=1}^{j-1} \left( 1 + \frac{\Delta z_{il}}{z_{il}} \right) & 1 < j < i \end{cases} \quad (8)$$

$S_0$  denotes the initial location of the suspension surface. For a disk centrifuge of thickness,  $H$

$$\Delta z_{ij} (2z_{ij} + \Delta z_{ij}) = \frac{V}{\pi H} \quad (9)$$

where  $V$  is the volume of suspension extracted at each withdrawal. Eqs. (7), (8) and (9) can be solved iteratively to give the set of maximum particle sizes corresponding to the different sampling times.

2.2 Particle Size Distribution

To evaluate the distribution of particle sizes from measurements of the relative concentration,  $Q(t)$ , it is necessary to solve the integral equation, Eq. (3), *Kamack* [3] used an inverted form of the equation:

$$F(x) = \int_0^{Q(x)} y dQ \quad (10)$$

and described an approximate numerical scheme for evaluating the integral. In the absence of intermediate sample withdrawals, the dilution factor  $y(x)$  can be calculated from

$$y(x) = [R/S(x)]^2 \quad (11)$$

where  $S(x)$  is the initial radial location of a particle of size,  $x$ ,

which is in the sampling zone at time,  $t$ . It follows from Eqs. (5) and (11) that

$$y(x) = e^{2kx^2t} \quad (12)$$

For the largest particle (size  $x_m$ ) in the sampling zone,  $S$  is equal to  $S_0$ , the location of the surface of the suspension, and

$$y(x_m) = (R/S_0)^2 = e^{2kx_m^2t} \quad (13)$$

so that

$$y(x) = (R/S_0)^{2(x/x_m)^2} \quad (14)$$

Either Eq. (12) or Eq. (14) can be used in the solution of Eq. (10). *Kamack's* analysis leads to the following expression for the mass fraction finer than size  $x_i$ :

$$F(x_i) = 1/2 (y_{ii} - y_{i-1,i}) Q_i + \sum_{j=1}^{i-1} \left[ \frac{y_{ij} + y_{i-1,i}}{y_{j+1,i} + y_{ij}} - \frac{y_{ij} + y_{i-1,i}}{y_{ij} + y_{j-1,i}} \right] F(x_j) \quad (15)$$

in which

$$y_{ij} = (R/S_0)^{2(x_i/x_j)^2} \quad (16)$$

and the  $x_i$  and  $x_j$  are obtained from the appropriate substitutions into Eq. (5).  $i = 1$  refers to the sample extracted after the longest time.

For the case of multiple sample withdrawals, *Allen and Svarovsky* [4] replaced  $S_0$  in Eq. (16) by  $S_i$ , the location of the suspension surface immediately prior to the  $i$ -th extraction.  $S_i$  can be calculated from

$$S_i = \left[ \frac{(i-1)V}{\pi H} + S_0^2 \right]^{1/2} \quad (17)$$

Unfortunately, this substitution is incorrect since the displacement of a particle due to sample withdrawal depends on its location at the time of withdrawal. The use of  $S_i$  in Eq. (16) implies that all particles are displaced equally, regardless of their actual position.

A correct procedure for evaluating the dilution factors,  $y_{ij}$ , is to use a form of Eq. (12), i.e.

$$y_{ij} = e^{2kx_i^2t_j} \quad (18)$$

with  $x_i$  values calculated from Eq. (7). The *Allen/Svarovsky* approach implies the use of Eq. (5) which is not valid for multiple withdrawal systems.

2.3 An Alternative Procedure for Evaluating the Particle Size Distribution

Eq. (15) was obtained through the use of the trapezoid rule for numerical integration of Eq. (10). An alternative approach is to integrate Eq. (3) directly by making simplifying assumptions about the form of the cumulative size distribution,  $F(x)$ .

If it is assumed that  $F(x)$  is approximately linear between successive measurement sizes  $x_j$ ,

$$F(x) = a_j x + b_j \quad x_{j-1} \leq x \leq x_j \quad (19)$$

where  $a_j$  and  $b_j$  are constants. From the definition of the density function

$$f(x) = \frac{dF(x)}{dx} = a_j \quad x_{j-1} \leq x \leq x_j \quad (20)$$

From Eqs. (3) and (18),

$$Q_i = \int_0^{x_i} e^{-2kx^2 t_i} f(x) dx \quad (21)$$

after substitution from Eq. (20),

$$Q_i \cong a_1 \int_0^{x_1} e^{-2kx^2 t_i} dx + a_2 \int_{x_1}^{x_2} e^{-2kx^2 t_i} dx + \dots + a_j \int_{x_{j-1}}^{x_j} e^{-2kx^2 t_i} dx \quad (22)$$

or

$$Q_i \cong \sum_{j=1}^i a_j \left[ \int_0^{x_j} e^{-2kx^2 t_i} dx - \int_0^{x_{j-1}} e^{-2kx^2 t_i} dx \right] \quad (23)$$

with  $x_0$  equal to zero by definition.

The integrals in Eq. (23) can be expressed in terms of the Gaussian error function leading to

$$Q_i \cong 1/2 \left( \frac{\pi}{2kt_i} \right)^{1/2} \sum_{j=1}^i a_j (E_{ij} - E_{i,j-1}) \quad (24)$$

with

$$E_{ij} = \text{erf} [x_j (2kt_i)^{1/2}] \quad (25)$$

From Eq. (19),

$$a_j \cong \frac{F(x_j) - F(x_{j-1})}{x_j - x_{j-1}} \quad (26)$$

If Eq. (26) is applied to the final term ( $j = i$ ) in the summation in Eq. (24), the latter can be rearranged to give

$$F(x_i) \cong F(x_{i-1}) + \left( \frac{x_i - x_{i-1}}{E_{ii} - E_{i,i-1}} \right) \left[ \left( \frac{\pi}{2kt_i} \right)^{1/2} \frac{Q_i}{2} - \sum_{j=1}^{i-1} a_j (E_{ij} - E_{i,j-1}) \right] \quad (27)$$

Given experimental values of  $Q(t)$ , the values of  $x_i$  corresponding to each  $Q_i$  and  $t_i$  can be calculated using Eqs. (7), (8) and (9). Eq. (27) can then be used to obtain successive values of  $F(x_i)$ , starting from the smallest size,  $x_1$ .

### 3 Simulation Studies

The procedures described above for evaluating particle size distributions using pipet withdrawal centrifuges have been evaluated and compared by means of a simulation procedure.

For a known size distribution,  $F(x)$ , values of  $Q_i$  can be calculated by integration of Eq. (21), leading to a set of simulated experimental data. These, in turn, can be used to regenerate the size distribution. Comparison of the input and regenerated size distributions provides a direct measure of the error, etc. introduced by the interpretation procedures.

A similar procedure can be applied to real data where the true size distribution is not known. In this case, the calculated distributions can be used to regenerate the  $Q_i$  values by numerical integration of Eq. (21). Comparison of the regenerated  $Q_i$  values with the actual experimental data provides a check on the internal consistency of the calculations used to determine the size distribution.

Simulations were carried out using a variety of input size distributions based on the Schuhmann, Rosin-Rammler, and log-normal forms. For numerical integration of Eq. (21) to regenerate the  $Q_i$  values a one-dimensional, quasi-cubic hermite interpolation was performed on the calculated  $F_i$  values. The spline coefficients calculated from this procedure were used to determine the derivative of  $F(x)$  with respect to  $x$  using a cubic-spline, first-derivative evaluator. For each withdrawal time  $t_i$ , the derivatives of  $F(x_i)$  were substituted into Eq. (21). New spline coefficients were determined for each integrand expression at each time  $t_i$  and integration was carried out using a cubic spline quadrature.

Calculated size distributions were obtained using:

- the original *Allen/Svarovsky* modification of the *Kamack* analysis using Eqs. (15), (16) and (17) - designated (A/S)
  - the corrected *Allen/Svarovsky* method using Eqs. (15) and (18) - designated (A/S)<sub>corr</sub>
  - the alternative method based on Eq. (27) - designated ALT.
- Particles sizes were calculated using Eqs. (7), (8) and (9) in all cases.

The simulations were performed so as to correspond to sedimentation at 750 rpm in a disk centrifuge of diameter 16 cm and depth 1.02 cm containing 150 ml of a dilute suspension. The sample volume was 10 ml and the value of the constant,  $k$ , was about  $1.6 \times 10^3 \text{ cm}^{-2} \text{ sec}^{-1}$  in all cases. The calculated sizes correspond to sampling times of 2, 4, 8, 16, 32, 64 and 128 minutes.

A typical result, for a Rosin-Rammler size distribution with  $k_r = 2 \mu\text{m}$  and exponent  $m = 0.8$ , is shown in Table 1. It is clear that all three approaches provide estimates of the size distribution which agree closely with the "true" values. The error in the original *Allen/Svarovsky* treatment does not lead to serious errors in the results and the *Kamack* and alternative procedures for solving the integral equation lead to very similar estimates. The comparison can be simplified by computing the sums of squares of differences between the actual and estimated values of  $F(x)$  and the simulated and regenerated values of  $Q_i$ . These are given as  $SS_F$  and  $SS_Q$  respectively in Table 1. On this basis, it appears that the alternative approach (Eq. 27) is in slightly closer agreement with the true values than those based on the *Kamack* treatment, for this particular case. It should be emphasized, however, that the differences are small in all cases and would probably be within experimental error in a real measurement.

Similar simulations have been carried out using a broad range of the distribution parameters corresponding from very narrow to very broad distributions. The results are summarized in Tables 2, 3 and 4 using the  $SS_F$  and  $SS_Q$  criteria. For the majority of the cases studied, the alternative approach, Eq. (27), appears to provide the closest estimates of the actual distribution and to be the most self-consistent in regenerating the "experimental"  $Q$  values. Exceptions are found for the very narrow Schuhmann

# PARTICLE SIZE DISTRIBUTIONS

Table 1: Comparison of estimated size distributions from simulated pipet centrifuge data for a Rosin-Rammler size distribution with  $k_r = 2 \mu\text{m}$ ,  $m = 0.8$ .

Particle Size $x_i$ ( $\mu\text{m}$ )	True	Percent Finer $F(x_i)$			Relative Concentration $Q_i$			
		(A/S)	Estimated ( $A/S$ ) <sub>corr</sub>	ALT	Simulated (A/S)	Regenerated ( $A/S$ ) <sub>corr</sub>	ALT	
1.67	57.8	59.3	58.8	58.0	47.5	48.3	48.3	47.7
1.12	46.6	46.9	47.4	46.7	38.4	38.6	39.0	38.5
0.73	36.1	36.1	36.6	36.2	30.1	30.2	30.6	30.2
0.47	27.1	27.0	27.4	27.1	23.1	23.1	23.5	23.1
0.30	19.8	19.8	20.1	19.8	17.2	17.4	17.6	17.3
0.19	14.2	14.4	14.5	14.2	12.6	13.0	13.1	12.7
0.12	9.9	10.6	10.8	10.0	9.0	9.7	9.9	9.1
	$SS_F = 2.98$	3.05	0.08		$SS_Q = 1.37$	2.75	0.07	

Table 2: Comparison of size distribution estimation procedures for simulated Schumann size distributions:

$$F(x) = \left(\frac{x}{k}\right)^a$$

with  $k = 2 \mu\text{m}$ .

$a$	Deviations in Size Distribution Estimate, $SS_F$			Deviations in Regenerated Relative Concentration, $SS_Q$		
	(A/S)	(A/S) <sub>corr</sub>	ALT	(A/S)	(A/S) <sub>corr</sub>	ALT
5	0.47	0.24	4.16	0.05	0.04	1.17
4	1.46	0.85	3.73	0.19	0.18	1.06
3	3.69	2.24	2.47	0.58	0.60	0.81
2	7.18	4.66	0.77	1.34	1.63	0.32
1	8.27	6.25	0.00	2.05	3.47	0.00
0.9	8.00	6.29	0.01	2.20	3.84	0.01
0.8	7.75	6.52	0.03	2.52	4.65	0.03
0.7	7.59	7.07	0.01	3.08	5.86	0.11
0.5	12.33	11.40	0.51	7.85	11.98	0.57
0.3	20.92	29.20	2.54	23.26	33.90	3.04
0.1	70.20	344.28	12.10	70.04	353.07	14.68

Table 3: Comparison of size distribution estimation procedures for simulated Rosin-Rammler distributions:

$$F(x) = 1 - \exp\left[-\left(\frac{x}{k_r}\right)^m\right]$$

with  $k_r = 2 \mu\text{m}$ .

$m$	Deviations in Size Distribution Estimate, $SS_F$			Deviations in Regenerated Relative Concentration, $SS_Q$		
	(A/S)	(A/S) <sub>corr</sub>	ALT	(A/S)	(A/S) <sub>corr</sub>	ALT
5	0.46	0.26	2.35	0.06	0.05	0.62
4	1.33	0.80	1.66	0.20	0.18	0.51
3	2.92	1.84	0.71	0.49	0.52	0.29
2	4.46	3.05	0.06	0.92	1.21	0.04
1	3.38	2.88	0.06	0.99	1.90	0.03
0.9	3.14	2.88	0.05	1.12	2.24	0.03
0.8	2.98	3.05	0.08	1.37	2.75	0.07
0.7	3.14	3.65	0.14	1.93	3.72	0.13
0.5	5.26	7.32	0.48	5.29	8.76	0.54
0.3	13.54	19.13	1.92	15.55	22.05	2.34
0.1	35.62	48.54	6.43	37.29	50.95	7.73

and Rosin-Rammler distributions (large  $a$  or  $m$ ). For such cases, it appears that the *Kamack* integration procedure provides the better estimates and shows better internal consistency. For some

Table 4: Comparison of size distribution estimation procedures for simulated log-normal distributions:

$$F(x) = 1/2 \left[ 1 + \text{erf} \left( \frac{\ln x - \ln x_{50}}{\sqrt{2} \ln \sigma} \right) \right]$$

with  $x_{50} = 2 \mu\text{m}$ .

$\sigma$	Deviations in Size Distribution Estimate, $SS_F$			Deviations in Regenerated Relative Concentration, $SS_Q$		
	(A/S)	(A/S) <sub>corr</sub>	ALT	(A/S)	(A/S) <sub>corr</sub>	ALT
1.2	45.82	27.69	12.95	7.81	8.95	1.88
1.4	29.99	21.31	3.50	6.32	7.95	0.71
1.6	21.70	15.90	1.96	4.85	6.90	0.39
1.8	17.11	12.73	1.57	4.03	5.89	0.34
2.0	12.11	9.46	0.86	3.08	4.86	0.24
3.0	5.23	4.72	0.36	1.50	3.04	0.19
4.0	3.42	3.43	0.23	1.06	2.52	0.13
6.0	2.66	3.21	0.14	1.31	3.04	0.09
8.0	2.87	3.87	0.15	2.12	4.26	0.14
10.0	3.41	4.81	0.22	2.97	5.51	0.22
20.0	9.72	14.41	1.16	11.29	19.87	1.38

reason, this does not seem to apply to the very narrow log normal distributions (small  $\sigma$ ).

It should be noted that it is quite common for either of these procedures to yield  $F(x_i)$  estimates greater than 100 percent for the coarsest sizes (where the true  $F(x)$  values are very close to 100 percent). This is a consequence of the linear approximations made in both integration procedures. This occurrence, however, does not affect the smaller  $F(x)$  values and any apparent values greater than 100 percent can be taken to be 100 percent.

## 4 Experimental Studies

### 4.1 Methods and Materials

Samples of nominally  $\sim 10 \mu\text{m}$  coal (density  $1.38 \text{ g/cm}^3$ ), quartz (density  $2.65 \text{ g/cm}^3$ ) and kaolin clay (density  $2.65 \text{ g/cm}^3$ ) have been analyzed using a LADAL pipet centrifuge [3, 4]. Measurements were carried out using the manufacturer's recommended procedure. Since it was generally necessary to use dispersants, wetting agents etc., in order to obtain complete dispersion of the powders in water, it was found that membrane filtration of the samples taken from the centrifuge provided more reliable concentration data than the more commonly used

## THE RESPIRABLE DUST CENTER

evaporation procedure. Nuclepore filters, 25 mm diameter, 0.4  $\mu\text{m}$  pore size were used. The low tare weight of the filters (about 4 mg) led to greater sensitivity in the measurements allowing very low solids concentrations to be used in the centrifuge (about 0.1 weight percent), effectively eliminating hindered settling problems. Corrections for residual dispersant were un-

necessary since the solids could be thoroughly washed prior to drying and weighing. Because the filter substrates are hydrophobic, they do not absorb ambient moisture and require no desiccation before weighing. Following filtration, the filtrate was checked for clarity and, if necessary refiltered through the particle bed which had built up on the membrane.

Table 5: Experimental size distributions from the LADAL pipet centrifuge.

Solid	Sampling Time, $t_1$ (min.)	Particle Size, $x_1$ ( $\mu\text{m}$ )	Relative Concentration, $Q_i$ (Percent)			Weight Percent Finer	
			Measured	Regenerated		$(A/S)_{\text{corr}}$	ALT
			Internal radius: 8.0 cm				
			sampling radius: 7.0 cm				
			depth of bowl: 1.02 cm				
			sample volume: 11.44 $\text{cm}^3$ (13.91 $\text{cm}^3$ for coal)				
			speed: 885 rpm				
			initial suspension volume: 150 $\text{cm}^3$				
			liquid viscosity: 0.89 centipoise				
Coal ( $\rho = 1.38$ $\text{g/cm}^3$ )	2	4.63	57.3	58.8	57.0	85.6	83.0
	4	3.07	34.2	35.1	34.5	47.8	46.9
	8	1.98	20.9	21.4	21.2	28.6	28.2
	16	1.25	11.0	11.1	11.1	14.0	14.0
	32	0.77	5.5	5.6	5.6	6.4	6.4
	64	0.47	3.4	3.5	3.5	3.8	3.8
	128	0.27	2.0	2.1	2.0	2.2	2.2
			$SS_Q =$	3.35	0.21		
Clay ( $\rho = 2.65$ $\text{g/cm}^3$ )	2	2.22	57.1	58.1	57.5	67.9	67.4
	4	1.48	48.3	49.2	48.5	59.7	58.8
	8	0.96	37.7	38.3	37.7	45.9	45.2
	16	0.61	28.1	28.5	28.2	32.7	32.5
	32	0.38	22.2	22.6	22.3	27.0	26.5
	64	0.23	12.2	12.5	12.2	14.0	13.7
	128	0.14	7.5	7.9	7.5	8.6	8.2
			$SS_Q =$	2.74	0.22		
Quartz ( $\rho = 2.65$ $\text{g/cm}^3$ )	1	3.14	31.7	32.6	31.5	48.4	46.8
	2	2.09	18.2	18.7	18.2	26.6	25.8
	4	1.35	10.3	10.6	10.3	14.8	14.4
	8	0.86	4.9	5.0	4.9	6.8	6.6
	16	0.54	1.9	1.9	1.8	2.4	2.3
	32	0.33	0.84	0.89	0.81	1.0	0.94
			$SS_Q =$	1.16	0.05		

Table 6: Pipet centrifuge data of Allen [1] for zinc oxide particle (density 5.60  $\text{g/cm}^3$ ) conditions as in Table 5 except sample volume = 10.0  $\text{cm}^3$ , centrifuge speed = 750 rpm, and liquid viscosity = 0.01 poise.

Solid	Sampling Time, $t_1$ (min.)	Particle Size, $x_1$ ( $\mu\text{m}$ )	Relative Concentration, $Q_i$ (Percent)			Weight Percent Finer	
			Measured	Regenerated		$(A/S)_{\text{corr}}$	ALT
Zinc Oxide ( $\rho = 5.6$ $\text{g/cm}^3$ )	2	1.66	93.1	93.9	93.8	100.0	100.0
	4	1.11	87.2	88.3	88.0	100.0	100.0
	8	0.73	77.0	78.3	77.8	100.0	100.0
	16	0.47	50.2	51.3	50.1	69.8	68.2
	32	0.30	23.0	23.4	22.8	31.9	31.1
	64	0.19	6.2	6.1	5.9	8.1	7.9
128	0.12	1.2	1.1	0.96	1.4	1.3	
			$SS_Q =$	4.93	1.97		

# PARTICLE SIZE DISTRIBUTIONS

## 4.2 Results and Discussion

The results of the pipet centrifuge analyses are shown in Table 5 and Figure 1. The alternative calculation procedures (Eqs. 15 and 27) are compared in Table 5. As was the case for the simulations described above, it appears that the two approaches lead to very similar results but that Eq. (27) is slightly more self-consistent on the basis of the relative concentrations regenerated from the calculated size distributions. For completeness the same analyses have been applied to data for zinc oxide powder published by Allen [1]. The results, shown in Table 6, are in good agreement with those in Table 5.

The reproducibility of the pipet sedimentation technique has been evaluated by replicate measurements on the coal sample. The results are given in Table 7 and show excellent reproducibility, with standard deviations typically of the order of one or two percent.

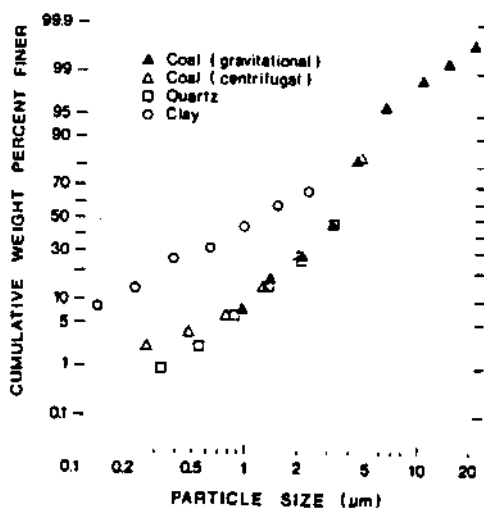


Fig. 1: Particle size distributions for coal, clay and quartz measured by pipet centrifuge. Gravity sedimentation (Andreasen pipet) data for coal are included for comparison.

Table 7: Reproducibility of LADAL pipet centrifuge analyses.

Size, $\mu\text{m}$	Cumulative Weight Percent Finer				Standard Deviation
	1	2	3	Avg.	
4.63	84.6	82.3	81.4	82.8	1.7
3.05	49.0	46.7	43.8	46.5	2.6
1.94	27.4	27.7	28.2	27.8	0.4
1.21	13.5	13.4	14.3	13.7	0.5
0.73	6.2	4.7	7.9	6.3	1.6
0.43	3.5	4.0	—	3.8	0.4

The particle size distributions are compared directly in Figure 1. The data for coal have been extended into the coarser size range using gravity sedimentation in an Andreasen pipet. The excellent agreement between the two methods in the overlap region (1 to 5  $\mu\text{m}$ ) provides further confirmation of the reliability of the pipet centrifuge technique for fine particle size analysis. Chung and Hogg [2] have shown similar agreement for kaolin clay.

## 5 Conclusions

The pipet-withdrawal centrifuge technique, as described by Allen and Svarovsky [1, 4] is a highly reproducible, reliable, absolute method for fine particle size analysis in the 0.1 to 10  $\mu\text{m}$  range. When correctly applied, the computation procedure originally suggested by Kamack [3] and modified by Allen and Svarovsky [4] provides very good estimates of particle size distribution from pipet centrifuge data. An alternative procedure, described in this paper, gives very similar agreement in simulation studies and appears to be slightly superior for broad size distributions. The corrected Allen/Svarovsky treatment may be superior for some kinds of very narrow distributions. A mathematical procedure for regenerating the measured relative concentrations from the calculated size distribution can provide a useful check on the self-consistency of the results and computations.

## 6 Acknowledgements

The work described in this paper was supported, in part, under The Mineral Institutes program by Grant No. G1135142 from the Bureau of Mines, U.S. Department of the Interior, as part of the Generic Mineral Technology Center for Respirable Dust.

## 7 Symbols and Abbreviations

<i>ALT</i>	procedure, based on Eq. (27), for estimating size distributions from pipet centrifuge data
<i>A/S</i>	Allen/Svarovsky procedure (Eqs. 15 and 16) for estimating size distributions from pipet centrifuge data
$(A/S)_{\text{corr}}$	corrected Allen/Svarovsky procedure (Eqs. 15 and 18)
$a_j$	constant in Eq. (19); approximate value for the particle size density, function in the $j$ -th size interval [ $L^{-1}$ ]
$b_j$	constant in Eq. (19) [—]
$c$	solids concentration [ $ML^{-3}$ ]
$c_0$	initial solids concentration [ $ML^{-3}$ ]
$E_{ij}$	the quantity: $\text{erf} [x_j (2kt_i)^{1/2}]$ [—]
$f(x)$	particle size density function [ $L^{-1}$ ]
$F(x)$	particle size distribution function [—]
$g$	acceleration due to gravity [ $LT^{-2}$ ]
$h$	sedimentation depth [ $L$ ]
$H$	thickness of disk centrifuge bowl [ $L$ ]
$k$	sedimentation constant defined by Eq. (6) [ $L^{-2}T^{-1}$ ]
$Q$	relative solids concentration ( $c/c_0$ ) [—]
$Q_i$	relative concentration in the $i$ -th sample [—]
$r$	radial distance in a centrifuge [ $L$ ]
$R$	radial distance from the center of rotation of the sampling location in a pipet centrifuge [ $L$ ]
$S$	radial distance from the initial position of a particle to the center of rotation [ $L$ ]
$S_0$	initial distance of suspension surface to center of rotation [ $L$ ]
$S_i$	distance from the centrifuge axis to the suspension surface at each extraction time [ $L$ ]
$SS_F$	sum of squares of differences between actual and calculated cumulative weight percent finer than size [—]



$SS_0$	sum of squares of differences between actual and regenerated relative solids concentration [-]
$t$	time [T]
$t_i$	time of withdrawal of $i$ -th sample [T]
$v$	Stokes' settling velocity of a particle [ $LT^{-1}$ ]
$V$	volume of sample extracted at each withdrawal [ $L^3$ ]
$x$	particle size [L]
$x_i$	maximum particle size in each withdrawal sample [L]
$x_m$	maximum measured particle size in powder [L]
$y$	dilution factor of largest particle in a withdrawn sample [-]
$y_{ij}$	dilution factor for particle smaller than largest particle in a withdrawn sample [-]
$z_{ij}$	position of particle $x_i$ from center of rotation at time $j$ [L]
$\Delta z_{ij}$	distance particle $i$ moves with fluid upon extraction at time $j$ [L]

$\mu$	fluid viscosity [ $ML^{-1}T^{-1}$ ]
$\Delta\rho$	density difference between particles and suspension fluid [ $ML^{-3}$ ]
$\omega$	angular velocity of centrifuge [ $T^{-1}$ ]

## 8 References

- [1] *T. Allen: Particle Size Measurement*. 3rd Ed., Chapman and Hall, New York 1981.
- [2] *H. S. Chung, R. Hogg: The Effect of Brownian Motion on Particle Size Analysis by Sedimentation*. Powder Technol. 41 (1985) 211-216.
- [3] *H. J. Kamack: Particle Size Determination by Centrifugal Pipet Sedimentation*. Anal. Chem. 23 (1951) 844-850.
- [4] *T. Allen, L. Svarovsky: A New High Speed Disc Centrifuge with Pipette Withdrawal*. Prepr. 1st Eur. Symp. Particle Size Measurement, Nürnberg, Dechema Monogr., Numbers 1589-1615 (1975) 279-292.

# Standard Respirable Dusts

T. F. Dumm and R. Hogg

Mineral Processing Section  
Department of Mineral Engineering, The  
Pennsylvania State University

There is a considerable need for standardized respirable dusts with consistent, reproducible characteristics which simulate those of actual mine dust. The availability of such materials should be a significant factor in promoting coordinated research into dust characterization and mine monitoring, dust control, and the biomedical aspects of dust toxicology. The use of an opposed-jet, fluid-energy grinding system in closed circuit with a cross-flow, centrifugal air classifier for preparing bulk quantities of respirable-size dust has been investigated, and appropriate, standardized procedures have been established. By stage-crushing, screening, and fine-grinding with a Donaldson Acucut classifier/mini-grinder system, it is possible to produce bulk quantities of respirable dust at relatively high rates. Using minor modifications to the system, broader or narrower size distributions can be prepared within the respirable range. The system has been shown to reach steady-state with respect to product size distribution very rapidly. However, preferential grinding/classification effects appear to lead to a slow build-up of mineral matter in the circulating load with a corresponding slow change in product composition with time. In those applications where the dust composition is required to match that of the feed coal, it may be necessary to allow considerable time for a true steady-state to be established.

Standard respirable dust samples have been prepared from coals representing the western (high volatile A bituminous), central (medium volatile bituminous) and eastern (anthracite) mining areas of Pennsylvania. Quartz and kaolin clay samples, representing important mineral constituents of coal dust have also been prepared. Extensive characterization studies have been performed on the samples to evaluate chemical and mineralogical composition and the distributions of particle size and specific gravity. Detailed information on the original coals is available from the Penn State Coal Data Base. The standard coal dust samples appear to simulate actual mine dust very well with respect to particle size and shape, but generally have somewhat lower ash content. Samples of these standard dusts have been made available to research groups concerned with respirable dust in mines.

## Introduction

Recently, there has been a large coordinated effort in research into finding the causes of Coal Workers' Pneumoconiosis and seeking remedies for it. There is a considerable need for standardized respirable dusts with consistent, reproducible characteristics which simulate those of actual coal mine dusts and can be made available for coordinated research on dust characterization and mine monitoring, dust control, and the biomedical aspects of dust toxicology.

The aim of the work described in this paper was to develop standardized procedures for producing bulk quantities of respirable dust at relatively high rates and to prepare and characterize a variety of such dusts, representing different coal seams and associated minerals.

## Preparation of Standard Dusts

### *Grinding System*

The process adopted in this study to produce the standard dust samples uses the Donaldson Acucut Classifier (Donaldson Co., Majac Division, St. Paul, Minnesota), shown in Figure 1, with an auxiliary jet mill grinding attachment. The classifier is a cross-flow device in which large volumes of air are brought through a centrifugal field containing air-entrained particles. Particles are separated on the basis of their aerodynamic diameter into a coarse fraction and a fine fraction with the separation size, or cut size, being determined by the force of the centrifugal field and the quantity of air flowing through the field.

The powder to be ground is fed into the system through a feeder/splitter apparatus as shown in Figure 2. The split stream of air and particles enters a grinder through two hoses connected to opposite ends of the mill. Powder at both ends of the mill then mixes with two opposing high-pressure air streams inside the mill and is comminuted as the particles collide with each other and with the mill surfaces. A pressure drop created by the aspirating action of the high pressure jets inside the mill provides the energy for air/particle flow from the feeder/splitter. All particles then leave the mill

and enter the Acucut Classifier at which point particles finer than the desired top size, are separated from the coarser material. The fine powder is collected using an air cyclone to remove the particles from the classifier overflow airstream. The coarse particles are ejected from the classifier and flow into the feeder/splitter assembly, mix with newly introduced powder and return to the jet mill.

The principal advantages of the Donaldson system for preparing standard dusts are that:

1. The process is a continuous, closed-circuit operation combining grinding and classification and is capable of producing dust at reasonably high rates. Fresh coal feed rates up to 3 g/min can be used so that a 500 g sample can be prepared in less than three hours.
2. The maximum particle size in the product can readily be controlled, in the range 1 to 30  $\mu\text{m}$ , through the classifier setting.
3. Since grinding is largely by particle impact, contamination of the product can be minimized.
4. Since the product is separated on the basis of an aerodynamic particle diameter, it should be possible to simulate airborne dust in mines.

The major disadvantage of the system is that selective grinding and/or classification can lead to concentration of specific organic or inorganic components.

**Materials**

Standard dusts were prepared from several coals, representing the western, central and eastern mining areas of Pennsylvania, and also from quartz and kaolin clay which are

important mineral constituents of coal mine dust. The coals are listed in Table I. The coal designated MP3 was used largely for preliminary test work etc., and was selected on the basis of immediate availability in the laboratory. The PSOC coals were obtained from the Penn State Coal Data Base and were originally collected as channel samples. Detailed information on these coals is given in Appendix A. The kaolin clay was obtained from the Georgia Kaolin Co., Dry Branch, Georgia, and the quartz was obtained from the Ashboro Quarry, Staley, North Carolina.

**Procedures**

Because of the coarse size of the as-received coal (approximately 50% > 4 mesh) the grinding to respirable size had to be performed in stages. For the initial crushing of all four coals, a Model 4-E Quakertown Mill (coffee grinder) was used. The grind setting was adjusted so as to produce the finest product possible which was typically 80 percent passing 70 mesh and all of the approximately 2500 g of each of the coal samples were ground. This material was then screened in 100-200 g increments using a Tylab Sieve Shaker to remove particles larger than 75  $\mu\text{m}$  (half the recommended top size for the fine grinding). This screened under-size product was ready for fine grinding. The quartz needed no initial crushing, but was prepared for fine grinding by placing about 150 grams into a ceramic Abbe ball mill and grinding for 1 hour and screened to remove the + 75  $\mu\text{m}$  particles. The kaolin clay required no crushing or fine grinding because the as-received material was already mostly of respirable size.

The grinding to produce respirable-size coal or quartz dust was carried out using the Donaldson grinding/classification system described previously. Operation was essentially according, to the manufactures instructions,<sup>(1)</sup> except

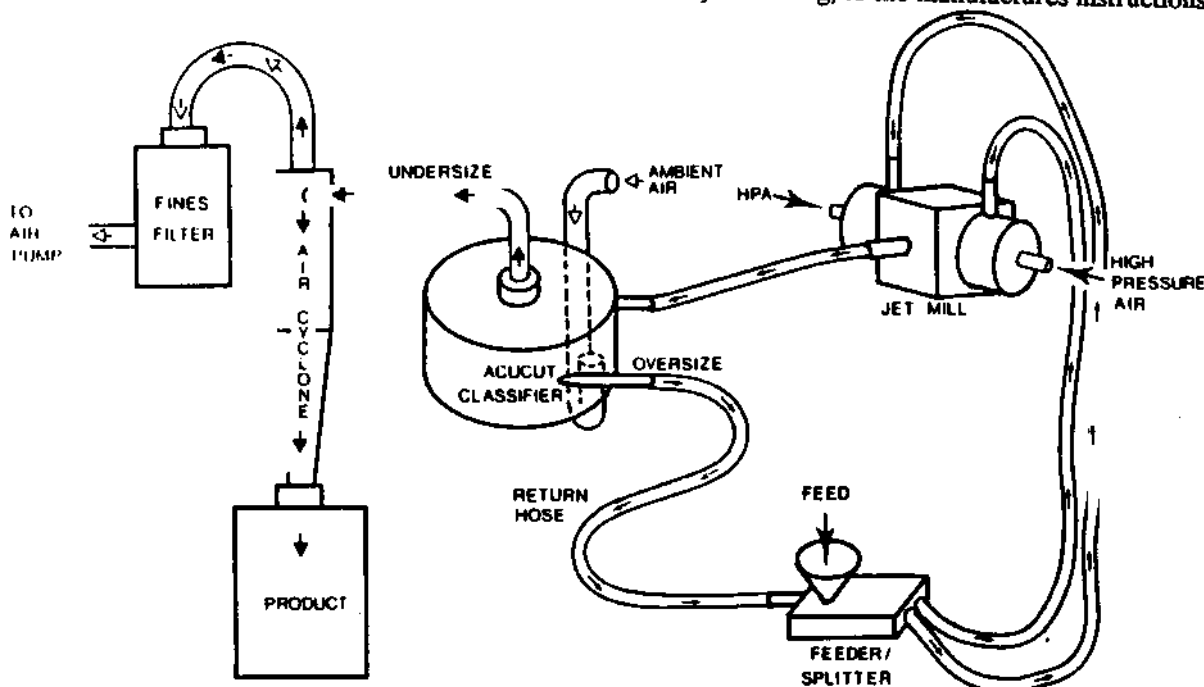


FIGURE 1. Diagram of Donaldson Acucut Classifier with auxiliary jet mill grinding attachment.

# STANDARD RESPIRABLE DUSTS

TABLE I

## Coals Used in These Investigations

Coal Designation	Seam	Seam Location, County	ASTM Rank
MP3 PSOC 1192 PSOC 1361P PSOC 867	U. Freeport L. Kittanning U. Freeport Primrose	Armstrong Clearfield Lawrence Schuylkill	High Vol. A Bit. Medium Vol. A Bit. High Vol. A Bit. Anthracite

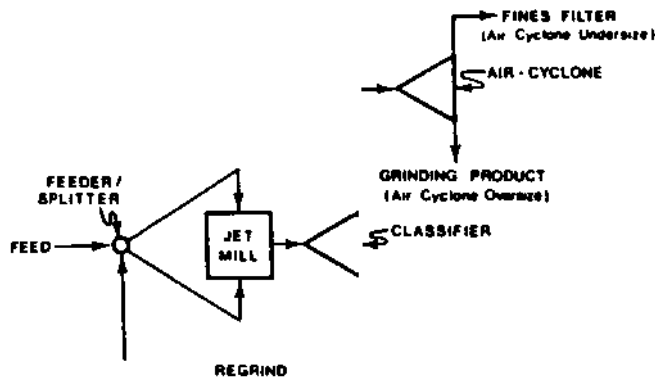


FIGURE 2. Schematic diagram of grinder/classifier system.

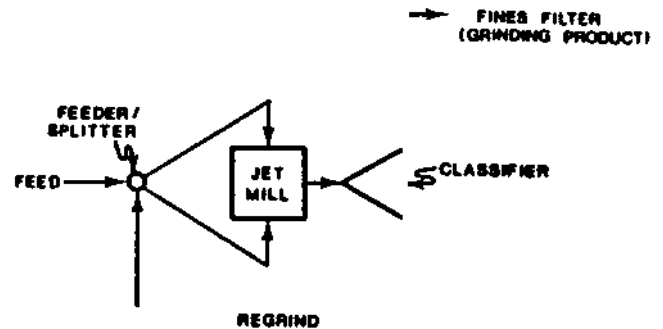


FIGURE 3. Schematic diagram of modified grinder/classifier system used for preparation of dusts with broad size distributions (MP3-3, PSOC 1192M).

that the high pressure air was at about 40 psig rather than 100 psig as recommended, since the higher pressures were not available, at sufficient volume, in our laboratories. The principal effect of the reduced pressure is to lower the system capacity. It is not believed to have significant effects on the overall product size distributions.<sup>(2)</sup>

The grinding/classification system, actually involves two-stage classification shown in Figure 2. The second stage, the air cyclone, is intended for gas-solid separation, but some size classification is probably inevitable. In order to investigate the influence of the air cyclone on product characteristics, three different circuit configurations were used for grinding of the MP3 coal. This was done by collecting the Acucut classifier undersize stream at the air cyclone inlet, oversize and undersize, (see Figure 2). Collecting the air cyclone oversize and undersize were straightforward. The oversize material falls into a collection jar as the grinding product and was designated MP3-2. The air cyclone undersize material leaves the air cyclone through the vortex finder and enters into a cylindrical, low pressure, high surface area filter where the fine particles become trapped. The fines filter was removed from the machine after grinding, and a snug-fitting collection container was placed around the open end of the filter. High-pressure air was blown through the clean side of the filter forcing the fine coal particles to fall into the collection container. It was not possible to remove all of the particles from the filter by this technique; usually about 70 weight percent were collected and these were assumed to be representative of the total amount. The particles not collected from the filter remained trapped within the depth of the filter's fibers. The coal sample collected by this

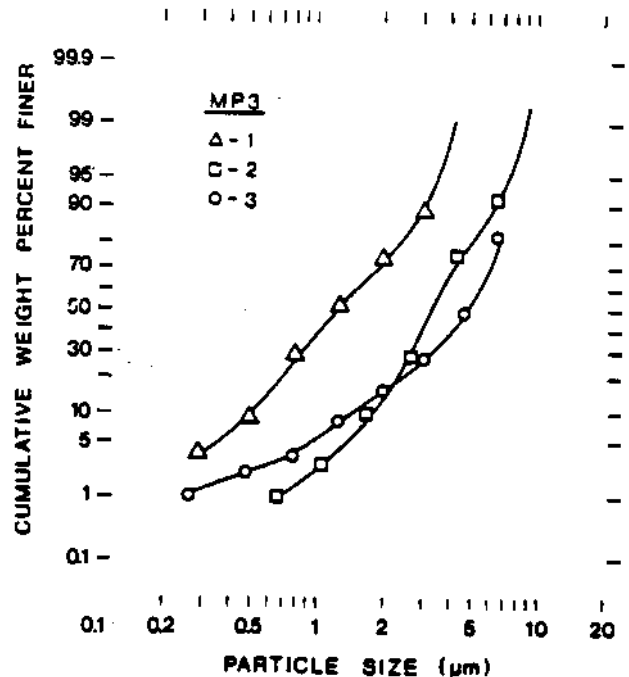


FIGURE 4. Size distributions of respirable dusts as determined by centrifugal sedimentation. MP3-1: air cyclone undersize; MP3-2: air cyclone oversize; MP3-3: air cyclone bypass.

procedure was labeled MP3-1. The modified classifier/grinder was then operated at the same conditions to achieve a cut size of 5 μm using MP3. When grinding was finished, the filter was removed and the coal sample was col-

lected in the same way as MP3-1. This sample of coal was designated MP3-3. It was assumed that this product has the same properties as the air cyclone inlet, which requires that the classifier performance does not change when the air cyclone is not in place. Figure 3 shows the modified system.

### Characterization of Standard Dusts

The standard respirable dusts have been characterized in terms of overall particle size distribution, size-specific gravity distribution, ash content and chemical and mineralogical composition.

#### Procedures

Particle size distributions were determined by centrifugal sedimentation using a Ladal pipet centrifuge<sup>(3)</sup> and by light scattering using a Leeds and Northrup Microtrac Small Particle Analyzer. Dumm<sup>(4)</sup> has investigated the correspondence between these two techniques and demonstrated that the results are quite consistent and can be inter-converted using a simple conversion factor.

Specific gravity distributions were evaluated by sink-float analyses in heavy liquids, using centrifuges. The procedure has been described in detail by Dumm.<sup>(4)</sup>

Ash analyses were performed by conventional high-temperature methods<sup>(4)</sup> and also by means of a Branson/IPC Low Temperature Asher.

Chemical (elemental) and mineralogical analyses were carried out by the Mineral Constitution Laboratory at Penn State. Elemental analyses were by plasma arc emission spectrometry and the mineralogical composition was determined by pressed KBr pellet infrared spectroscopy and powder X-ray diffraction techniques.

#### Results

##### Evaluation of the Grinding/Classification System

The effects of the air cyclone on the final product size distribution are shown in Figures 4 and 5. The normal circuit product, the cyclone oversize, (MP3-2) has the coarsest, narrowest size distribution, with very little submicron material. Apparently, the cyclone does indeed classify the dust, preferentially removing fine particles. As expected, the cyclone undersize contains the finest material (MP3-1), while the cyclone by-pass (MP3-3), which is intended to represent the feed to the cyclone, has the broadest distribution, being a combination of the other two products. It is apparent that these different circuit configurations can be used to prepare different size distributions, in the respirable range, from the same starting material. The cyclone by-pass arrangement has been used to prepare a modified dust from PSOC 1192 coal. This modified dust has been designated PSOC 1192 M.

##### Reproducibility of the Dust Preparation

For the standard respirable dusts to be useful in dust research, it is vital that the procedure used in their preparation be highly reproducible. An example of the reproducibility is given in Table II, in which the size distribution of a dust prepared in November 1984, is compared with that of a

second sample prepared in June 1986 from the same coal. It is clear from the results that the differences are quite small, essentially within experimental error, and that the procedure is indeed reproducible.

##### Particle Size Distribution

The particle size distributions of the standard dusts are shown in Figures 6 and 7. The three standard coal samples have similar distributions to one another and to sample MP3-1 (see Figure 4) sample PSOC 1192M has a somewhat broader size distribution, containing more submicron material, and is generally similar to MP3-1. The size distributions for the two mineral samples are shown in Figure 7. The distribution for quartz is quite similar to those for the coals.

The kaolin clay has a much broader size distribution and contains considerably more very fine particles than the other materials. This particular dust was not processed in any way

TABLE II

Reproducibility of Standard Dust Preparation with Respect to Particle Size Distribution (PSOC 1192)

Upper Limit of Size Interval (um)	Weight Percent in Sample 1 (Nov. 84)	Weight Percent in Sample 2 (June 86)
42.21	0.0	0.0
29.85	0.0	0.0
21.10	0.0	0.0
14.92	0.6	0.0
10.55	4.6	3.7
7.46	24.9	20.9
5.27	30.1	30.5
3.73	18.7	22.0
2.63	10.4	11.4
1.69	5.3	5.8
1.01	3.2	3.4
0.66	1.1	1.2
0.43	0.4	0.5
0.34	0.2	0.2
0.24	0.0	0.0
0.17	0.0	0.0
Mass Median Size:	4.26 um	3.99 um

and was used simply as-received. It should be emphasized that the mineral dusts were not intended to be directly representative of the mineral constituents in actual mine dusts.

A comparison of one of the synthetic dusts (MP3) with a sample of actual mine dust is shown in Figure 8. There appear to be no noticeable differences in particle size and shape between the two, indicating that the synthetic dusts may indeed be appropriate for research into coal mine dust and Coal Workers' Pneumoconiosis.

Particle size-specific gravity distributions for the PSOC 1192M, PSOC 1361P and PSOC 867 dusts are shown in Figures 9-11. The three distributions are distinctly bimodal, consisting of relatively clean coal (specific gravity < 1.7) and a very high ash fraction (specific gravity > 2). In other

STANDARD RESPIRABLE DUSTS

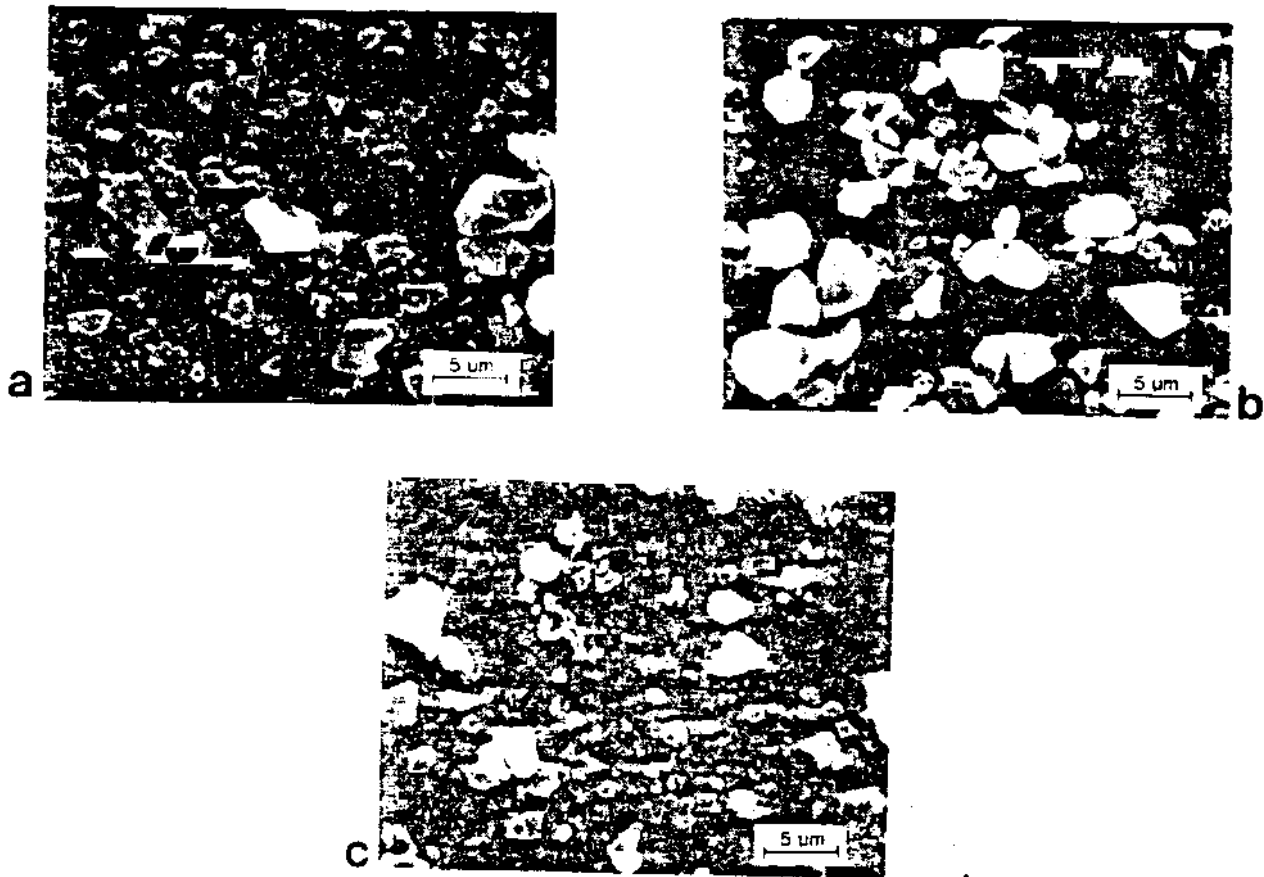


FIGURE 5. Scanning electron micrographs of a) air cyclone undersize (MP3-1) particles, b) air cyclone oversize (MP3-2) particles and c) air cyclone bypass (MP3-3) particles.

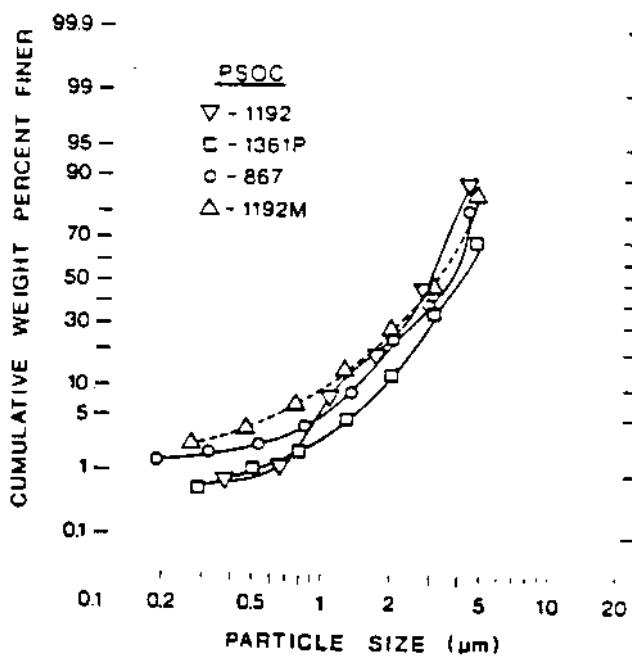


FIGURE 6. Size distributions of standard respirable dusts as determined by centrifugal sedimentation.

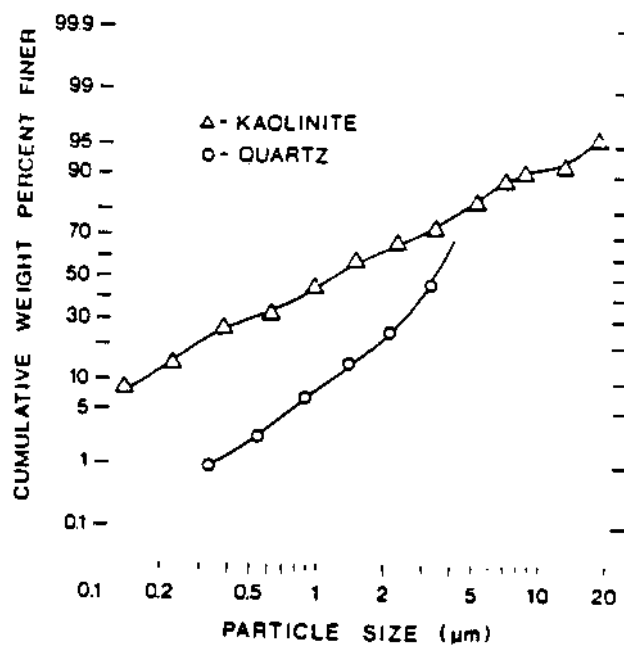


FIGURE 7. Size distributions of kaolinite and quartz standard respirable dusts as determined by centrifugal sedimentation.

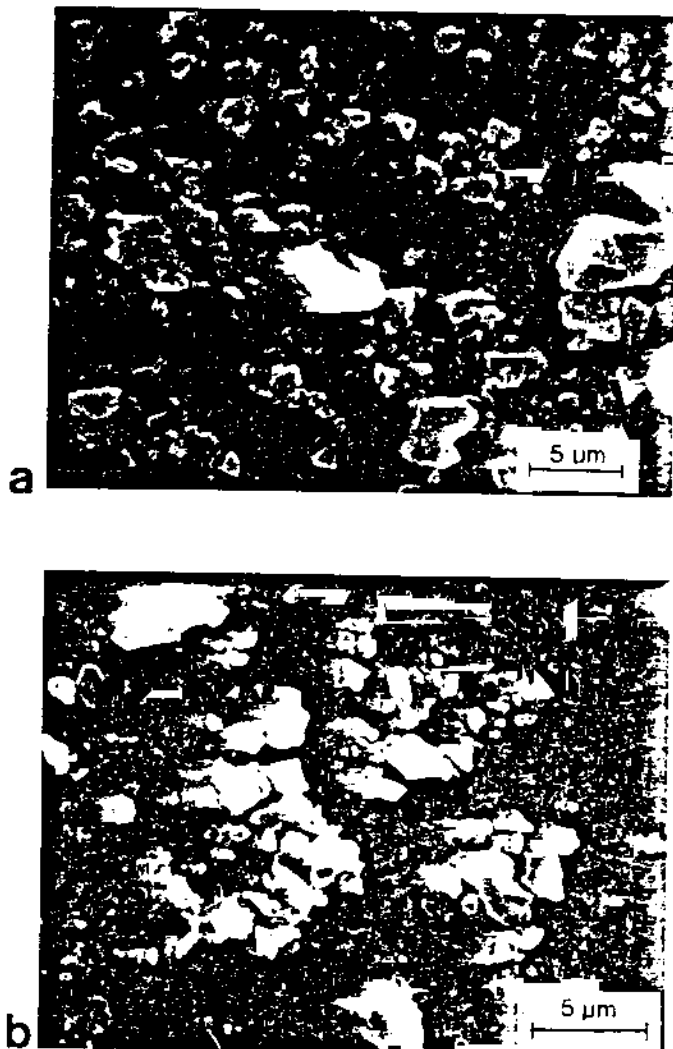


FIGURE 8. Scanning electron micrographs of a) standard respirable dust from Upper Freeport seam and b) actual coal mine dust from Brookville seam.

words, the dusts show a high degree of liberation between the organic material and mineral matter, as would generally be expected at such fine sizes. It can also be seen from the figures that the mineral matter tends to be slightly finer than the organic material.

#### Ash Content

The results of ash analyses on the standard respirable coal dusts and the corresponding feed coals are shown in Table III. It is clear that there is considerable discrepancy between the feed and the dust in each case. For the bituminous coals, the ash content of the dust is significantly lower than that of the original coal. It appears that the mineral matter does not break as rapidly as the organic coal constituents. This results in a larger than average amount of mineral particles remaining in the circulating load of the classifier/grinder system and a lower than average amount reporting to the respirable product container. For the anthracite, the opposite phenomenon is seen. The higher ash content of this respirable product compared to the feed is probably due to a large amount of very small clay particles that are already

TABLE III

#### Ash Contents of Feed Coals and Corresponding Respirable Dusts

Coal	Percent Ash	
	Feed	Respirable Dust
MP3-2	7.99	6.74
PSOC 1192	10.93	7.20
PSOC 867	12.65	21.2
PSOC 1361P	7.77	6.27

less than respirable size within the feed. These particles would pass immediately to the respirable product container along with a lower than average amount of comminuted organic particles. Given sufficient time, of course, the system should eventually reach a steady-state with the composition of the product identical to that of the feed. However, further experimentation has shown that the approach to such a steady-state is very slow. It is possible that this is a consequence of the reduced air pressure used in the grinding system.

#### Composition

Chemical and mineralogical analyses have been performed on each of the standard dusts.<sup>(5)</sup> The results are given in Appendix B.

#### Summary

By stage-crushing, screening, and fine grinding with the Donaldson Acucut classifier/grinder, it is possible to produce bulk quantities of respirable dust in relatively short periods of time. With certain modifications to the classifier/grinder, it is possible to produce different size distributions of a feed material without changing the top size of the products. The technique has been shown to be very reproducible as far as size distribution is concerned.

Although it appears that the product size distribution from the classifier/grinder reaches steady-state quickly, the composition does not. Differences in ash content between the feed coal and respirable coal dust product from the Donaldson Acucut classifier have been observed. These differences are attributed to differing breakage rates between the mineral and organic constituents of the coal. In addition, since the Acucut classifier is density dependent the varying densities between coal constituents will also contribute to differences in ash between the feed and product. If it is important that the composition of the standard respirable dust match the coal seam, or feed composition, considerably more time may be required to produce a standard respirable dust.

Standard dusts have been prepared from three different Pennsylvania coals and two minerals, quartz and kaolin, commonly associated with coal. Samples of these dusts can be made available for research. Their characteristics are listed in Appendix B.

# STANDARD RESPIRABLE DUSTS

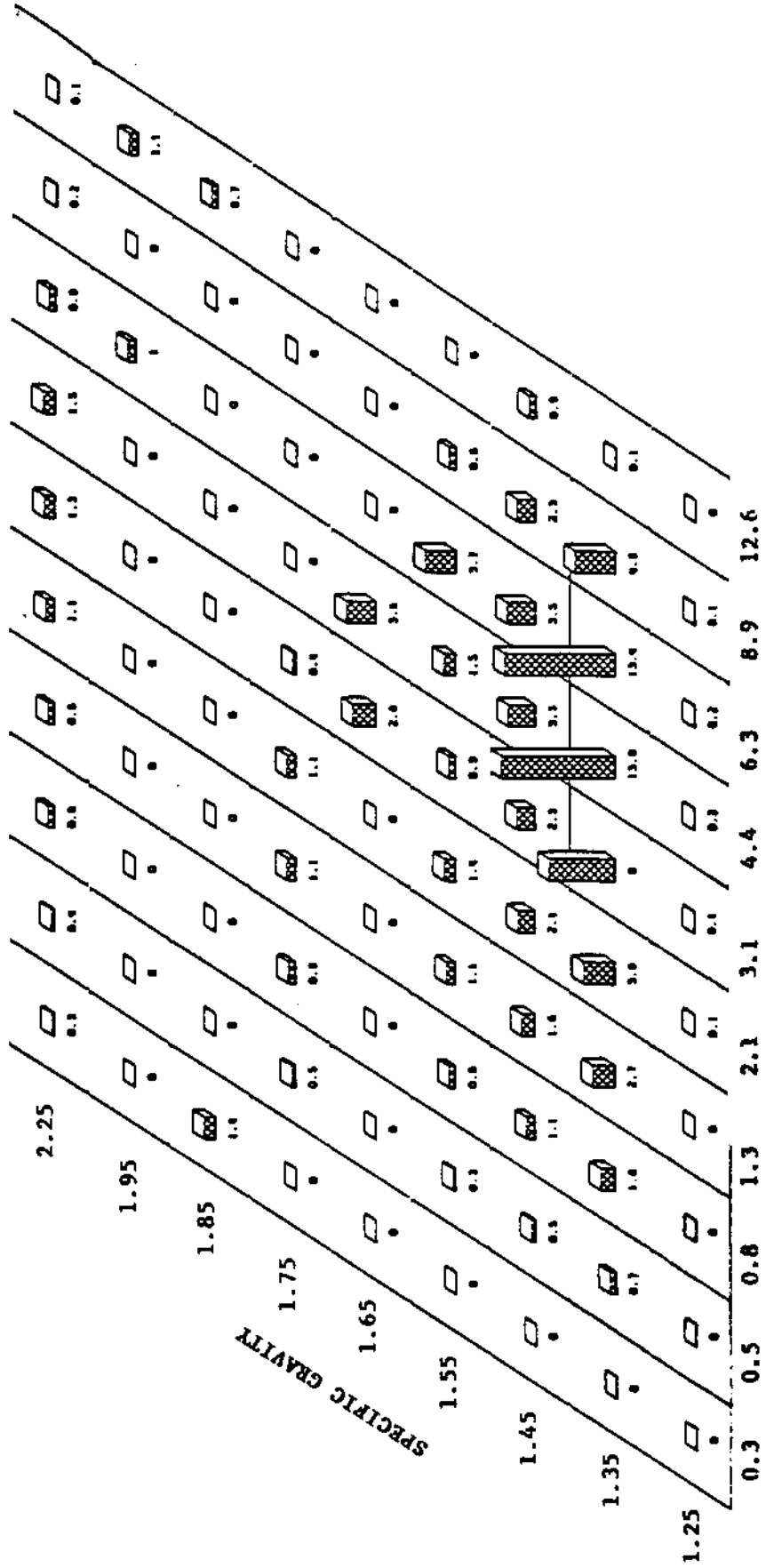
## Acknowledgments

The work described in this paper was supported by the Mineral Institutes program by Grant No. G1135142 from the Bureau of Mines, U.S. Department of Interior, as part of the Generic Mineral Technology Center for Respirable Dust.

## References

1. *Instruction Manual*, Donaldson Acucut Classifier. St. Paul, Minnesota (1978).
2. Personal Communication, Donaldson Corp., November (1983).
3. Allen, T.: *Particle Size Measurement*, 3rd Edition. Chapman and Hall (1981).
4. Dumm, T.F.: *An Evaluation of Techniques for Characterizing Respirable Coal Dust*. M.S. Thesis, The Pennsylvania State University (1986).
5. *ASTM Annual Book of Standards*, Designation D3174 (1982).





PARTICLE SIZE (µm)

FIGURE 9. Size-specific gravity distribution of standard respirable dust PSOC 1192M.

STANDARD RESPIRABLE DUSTS

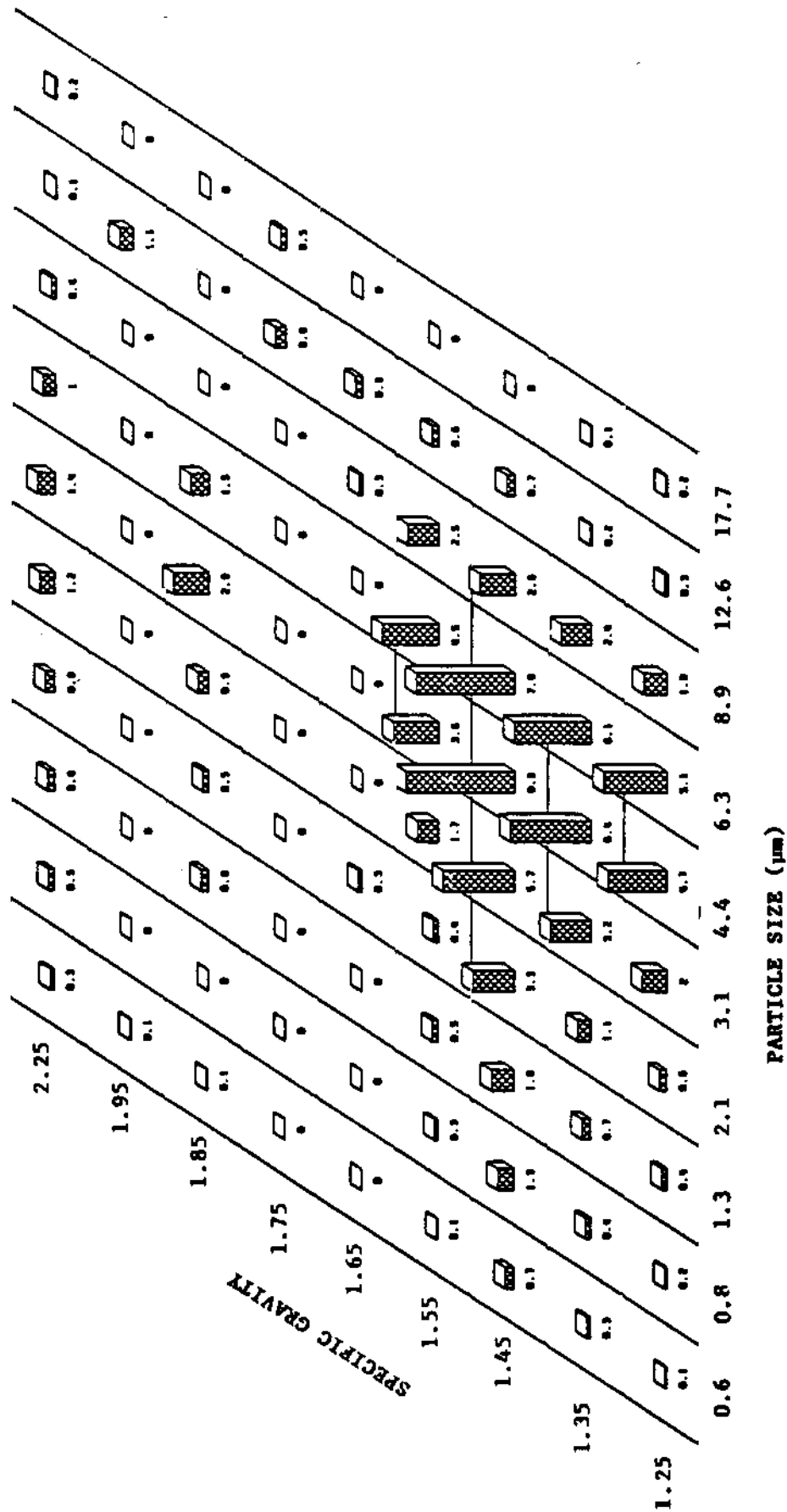


FIGURE 10. Size-specific gravity distribution of standard respirable dust PSOC 1361P.

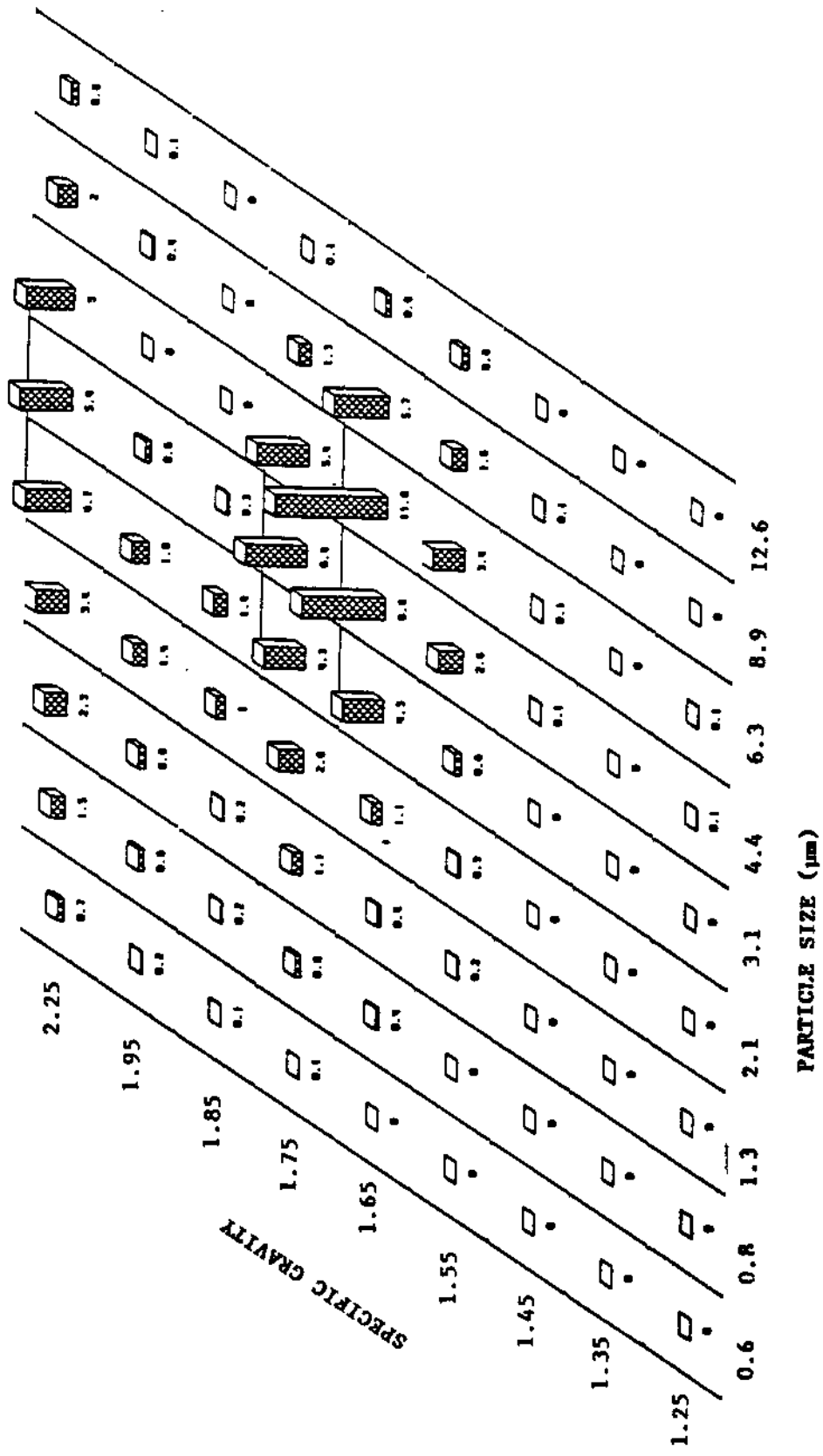


FIGURE 11. Size-specific gravity distribution of standard respirable dust PSOC 867.

# STANDARD RESPIRABLE DUSTS

## APPENDIX A

### Characteristics of Coals Used to Prepare Standard Dusts

Coal Identification: MP3

Coal Seam: Upper Freeport

Location: Plumcreek Township  
Armstrong County, PA  
Mine: Margaret No. 11

Collection: Hand-mined channel sample from freshly prepared face. Sealed in plastic-lined burlap bags. Returned to the laboratory at University Park.

Collection Date: September 27, 1979.

THE RESPIRABLE DUST CENTER

\*\* PENN STATE COAL DATA BASE \*\*

\*\*\*\*\*  
\*  
\* SAMPLE HISTORY \*  
\*  
\*\*\*\*\*

PENV STATE NUMBER PSOC-1192  
COLLECTED BY PENNSYLVANIA STATE UNIVERSITY  
COLLECTION DATE 10/16/79  
COLLECTOR'S NUMBER 1192  
REPORTED RANK  
SAMPLE TYPE CHANNEL WHOLE SEAM  
OTHER SAMPLE INFORMATION  
SAMPLE RESERVE 150  
SEAM NAME LOWER KITTANNING  
ALTERNATE SEAM NAME B SEAM  
TOTAL SEAM THICKNESS 1 FT. 10 IN.  
THICKNESS OF SEAM SAMPLED 1 FT. 10 IN.  
PORTION RECOVERED IN CORE  
DIAMETER OF CORE

SEAM NAME LOWER KITTANNING  
APPARENT RANK MEDIUM VOLATILE BITUMINOUS (MVB)  
\*\*\*\*\*  
\*  
\* GEOLOGIC INFORMATION \*  
\*  
\*\*\*\*\*

SYSTEM (AGE) PENNSYLVANIAN  
SERIES  
GROUP  
FORMATION ALLEGHENY  
OVERBURDEN LITHOLOGY SHALE  
FLOOR LITHOLOGY SHALE

# STANDARD RESPIRABLE DUSTS

\*\*\*\*\*  
\*  
\* CHEMICAL DATA 1 \*  
\*  
\*\*\*\*\*

<u>PROXIMATE ANALYSIS</u>	<u>AS REC'D</u>	<u>DRY</u>	<u>DAF</u>	<u>DMMF (PARR)</u>	<u>DMMF (PARR-G)</u>	<u>DMMF (DIR MM)</u>
% MOISTURE	0.67					
% ASH	11.40	11.48				
% VOLATILE MATTER	24.09	24.24	27.38	25.46	25.53	
% FIXED CARBON	63.85	64.28	72.62	74.54	74.47	

\*\*\*\*\*  
\*  
\* CHEMICAL DATA 2 \*  
\*  
\*\*\*\*\*

<u>ULTIMATE ANALYSIS</u>	<u>AS REC'D</u>	<u>DRY</u>	<u>DAF</u>	<u>DMMF (PARR)</u>
% ASH	11.40	11.48		(14.55 %MM)
% CARBON	76.08	76.59	86.52	89.64
% HYDROGEN	4.50*	4.53	5.12	5.30
% NITROGEN	1.42	1.43	1.62	1.67
% SULFUR	3.89	3.92	4.43	
% CHLORINE	0.08	0.09	0.10	0.10
% OXYGEN (DIFF)	1.95*	1.97	2.23	3.30
<u>SULFUR FORMS</u>				
	<u>% PYRITIC</u>	<u>% SULFATIC</u>	<u>% ORGANIC</u>	<u>% TOTAL</u>
DRY	3.14	0.02	0.76	3.92
DAF	3.55	0.02	0.86	4.43
OPTICAL				

<u>ELEMENTAL ANALYSIS</u>	<u>DRY</u>	<u>DMMF (MOD.P)</u>	<u>DMMF (DIR.)</u>
% CARBON	76.41	(14.49%MM) 89.36	( %MM)
% HYDROGEN	4.32	5.05	
% NITROGEN	1.43	1.67	
% ORGANIC SULFUR	0.76	0.89	
% OXYGEN (DIFF)	2.59	2.94	
% CHLORINE	0.09	0.10	
% MINERAL MATTER	14.49		
(INCLUDES S. R7 & PES2)			

THE RESPIRABLE DUST CENTER

\*\*\*\*\*  
 \*  
 \* CHEMICAL DATA 3 \*  
 \*  
 \*\*\*\*\*

% MOISTURE IN COAL = 0.40  
 % HIGH TEMPERATURE ASH = 11.70 AT 750 DEGREES C

TRACE ELEMENT ANALYSIS	PPM HTA	PPM TOTAL COAL	MAJOR ELEMENT ANALYSIS	OXIDE % OF HTA	ELEMENT % OF TOTAL DRY COAL
AG			SI02	34.20	1.87
B			AL2O3	23.10	1.43
BA	780	91	TIO2	0.90	0.06
BE	35	4	FE2O3	38.50	3.15
BI			MGO	0.45	0.03
CZ			CAO	1.12	0.09
CO			NA2O	0.21	0.02
CR	170	20	K2O	1.06	0.10
CU	95	11	P2O5	0.12	0.01
GA			SO3	1.20	0.06
GF					
LA					
LI					
MN					
MO			VOLATILES		PPM TOTAL COAL
NI	140	16	AS		
NB			BR		
PB			CD		
RB	50	6	CL		
SC			F		
SN			HG		
SR	370	43	SB		
TH			SE		
U					
V	250	29			
Y					
YB					
ZN	220	26			
ZR	220	26			

**STANDARD RESPIRABLE DUSTS**

\*\*\*\*\*  
 \*  
 \* PETROGRAPHIC DATA \*  
 \*  
 \*\*\*\*\*

**MACERAL COMPOSITION WHITE ANALYSIS ONLY**

	<u>DRY VOLUME %</u>	<u>DMMP VOLUME %</u>	<u>DRY WEIGHT %</u>
VITRINITE (CALC.)	80.5	87.1	74.4
INERTINITE (CALC.)	11.8	12.8	10.9
LIPTINITE (CALC.)	0.1	0.1	0.1
MINERAL MATTER (CALC.)	7.6		14.6
<b>VITRINOIDS</b>			
VITRINITE	79.4	85.9	73.4
PSEUDOVITRINITE	1.1	1.2	1.0
FUSINITE	2.5	2.7	2.3
SEMI-FUSINITE	7.0	7.6	6.5
MACRINITE	0.6	0.6	0.5
MICRINITE	1.8	1.9	1.6
SCLEROTINITE	0.0	0.0	0.0
SPORINITE			
CUTINITE			
EXINITE (ANAL.)	0.1	0.1	0.1
RESINITE	0.0	0.0	0.0
SUBERINITE			
EXUDATINITE			
FLUORINITE			
BITUMINITE			
ALGINITE	0.0	0.0	0.0
LIPTODETRINITE			
MINERAL MATTER(ANAL.)			
INERTINITE(ANAL.)			
LIPTINITE(ANAL.)			

<u>REFLECTANCE DATA (% IN OIL)</u>	<u>HIGH</u>	<u>LOW</u>	<u>RANGE</u>	<u>MEAN MAX</u>	<u>STAND.DEV.</u>
VITRINITE	1.49	1.20	0.29	1.32	0.05
PSEUDOVITRINITE					
VITRINOIDS					

<u>% VITRINOID REFLECTANCE</u>	<u>HALF-TYPE</u>	<u>VOLUME PERCENT</u>	<u>% VITRINOID REFLECTANCE</u>	<u>V-TYPE</u>	<u>VOLUME PERCENT</u>
1.20-1.24	VHT 1.225	7.00			
1.25-1.29	VHT 1.275	20.00			
1.30-1.34	VHT 1.325	41.00	1.20-1.29	V12	27.00
1.35-1.39	VHT 1.375	17.00			
1.40-1.44	VHT 1.425	4.00	1.30-1.39	V13	58.00
1.45-1.49	VHT 1.475	3.00	1.40-1.49	V14	7.00



THE RESPIRABLE DUST CENTER

\*\* PENN STATE COAL DATA BASE \*\*

\*\*\*\*\*  
\*  
\* SAMPLE HISTORY \*  
\*  
\*\*\*\*\*

PENN STATE NUMBER PSOC-1361P  
COLLECTED BY PENNSYLVANIA STATE UNIVERSITY  
COLLECTION DATE 2/24/82  
COLLECTOR'S NUMBER  
REPORTED RANK  
SAMPLE TYPE CHANNEL WHOLE SEAM  
OTHER SAMPLE INFORMATION PREMIUM SAMPLE  
SAMPLE RESERVE 80  
SEAM NAME UPPER FREEPORT  
ALTERNATE SEAM NAME E SEAM  
TOTAL SEAM THICKNESS 0 FT. 26 IN.  
THICKNESS OF SEAM SAMPLED 0 FT. 26 IN.  
PORTION RECOVERED IN CORE  
DIAMETER OF CORE

SEAM NAME UPPER FREEPORT  
APPARENT RANK HIGH VOLATILE A BITUMINOUS (HVAB)  
\*\*\*\*\*  
\* GEOLOGIC INFORMATION \*  
\*\*\*\*\*

SYSTEM (AGE) PENNSYLVANIAN  
SERIES  
GROUP ALLEGHENY  
FORMATION  
OVERBURDEN LITHOLOGY BLACK SHALE  
FLOOR LITHOLOGY CLAY

**STANDARD RESPIRABLE DUSTS**

\*\*\*\*\*  
\*  
\* CHEMICAL DATA 1 \*  
\*  
\*\*\*\*\*

<u>PROXIMATE ANALYSIS</u>	<u>AS REC'D</u>	<u>DRY</u>	<u>DAF</u>	<u>DMMF (PARR)</u>	<u>DMMF (PARR-G)</u>	<u>DMMF (DIR MM)</u>
% MOISTURE	1.90	---	---	---	---	---
% ASH	8.31	8.47	---	---	---	---
% VOLATILE MATTER	37.43	38.16	41.69	40.88	40.85	---
% FIXED CARBON	52.36	53.37	58.31	59.12	59.15	---

\*\*\*\*\*  
\*  
\* CHEMICAL DATA 2 \*  
\*  
\*\*\*\*\*

<u>ULTIMATE ANALYSIS</u>	<u>AS REC'D</u>	<u>DRY</u>	<u>DAF</u>	<u>DMMF (PARR)</u> (10.21 %MM)
% ASH	8.31	8.47	---	---
% CARBON	73.57	75.00	81.94	83.53
% HYDROGEN	5.12*	5.22	5.70	5.81
% NITROGEN	1.38	1.41	1.54	1.57
% SULFUR	1.90	1.94	2.12	---
% CHLORINE	---	---	---	---
% OXYGEN (DIFF)	7.81*	7.96	8.70	9.08

<u>SULFUR FORMS</u>	<u>% PYRITIC</u>	<u>% SULFATIC</u>	<u>% ORGANIC</u>	<u>% TOTAL</u>
DRY	1.17	0.05	0.72	1.94
DAF	1.28	0.05	0.79	2.12

<u>ELEMENTAL ANALYSIS</u>	<u>DRY</u>	<u>DMMF (MOD.P)</u> (10.12%MM)	<u>DMMF (DIR.)</u> (     %MM)
% CARBON	74.87	83.31	(     %MM)
% HYDROGEN	5.09	5.66	---
% NITROGEN	1.41	1.57	---
% ORGANIC SULFUR	0.72	0.80	---
% OXYGEN (DIFF)	7.79	8.66	---
% CHLORINE	---	---	---
% MINERAL MATTER (INCLUDES 2.19 % FES2)	10.12	---	---

THE RESPIRABLE DUST CENTER

.....  
 \*  
 \* CHEMICAL DATA 3 \*  
 \*  
 .....

% MOISTURE IN COAL = 1.90  
 % HIGH TEMPERATURE ASH = 9.27 AT 750 DEGREES C

TRACE ELEMENT ANALYSIS	PPM HTA	PPM TOTAL COAL	MAJOR ELEMENT ANALYSIS	OXIDE % OF HTA	ELEMENT % OF TOTAL DRY COAL
AG			SiO2	42.40	1.64
B			Al2O3	23.20	1.02
BA	1000	83	TiO2	1.02	0.05
BF	20	2	Fe2O3	26.40	1.53
BI			MgO	0.74	0.04
CK			CaO	1.15	0.07
CO			Na2O	0.38	0.02
CR	150	12	K2O	2.36	0.16
CU	190	16	P2O5	0.48	0.02
GA			S03	0.80	0.03
GF					
LA					
LI					
MN					
MO					
NI	150	12	VOLATILES		PPM TOTAL COAL
NB			AS		
PB			BR		
RB	90	7	CD		
SC			CL		
SN			F		
SR	1050	87	HG		
TH			SB		
U			SE		
V	160	13			
Y					
YB					
ZN	270	23			
ZR	230	19			

**STANDARD RESPIRABLE DUSTS**

\*\*\*\*\*  
\*  
\* PETROGRAPHIC DATA \*  
\*  
\*\*\*\*\*

**MACERAL COMPOSITION WHITE ANALYSIS ONLY**

	DRY VOLUME %	DMF VOLUME %	DRY WEIGHT %
VITRINITE (CALC.)	74.4	78.5	70.5
INERTINITE (CALC.)	15.1	15.9	14.3
LIPTINITE (CALC.)	5.3	5.6	5.0
MINERAL MATTER (CALC.)	5.2		10.2
<b>VITRINOIDS</b>			
VITRINITE	71.1	75.0	67.3
PSEUDOVITRINITE	3.3	3.5	3.1
FUSINITE	4.2	4.4	3.9
SEMI-FUSINITE	4.3	4.5	4.0
MACRINITE	0.9	0.9	0.9
MICRINITE	5.8	6.1	5.5
SCLEROTINITE	0.0	0.0	0.0
SPORINITE			
CUTINITE			
EXINITE (ANAL.)	4.7	5.0	4.5
RESINITE	0.6	0.6	0.5
SUBERINITE			
EXUDATINITE			
FLUORINITE			
BITUMINITE			
ALGINITE	0.0	0.0	0.0
LIPTOPETRINITE			
MINERAL MATTER (ANAL.)			
INERTINITE (ANAL.)			
LIPTINITE (ANAL.)			

REFLECTANCE DATA (% IN OIL)	HIGH	LOW	RANGE	MEAN MAX	STAND. DEV.
VITRINITE	0.93	0.73	0.20	0.83	0.04
PSEUDOVITRINITE					
VITRINOIDS					

% VITRINOID REFLECTANCE	HALF-TYPE	VOLUME PERCENT	% VITRINOID REFLECTANCE	V-TYPE	VOLUME PERCENT
0.70-0.74	VHT 0.725	2.00			
0.75-0.79	VHT 0.775	12.00	0.70-0.79	V7	14.00
0.80-0.84	VHT 0.825	55.00			
0.85-0.89	VHT 0.875	25.00	0.80-0.89	V8	80.00
0.90-0.94	VHT 0.925	6.00			
0.95-0.99	VHT 0.975		0.90-0.99	V9	5.00

THE RESPIRABLE DUST CENTER

\*\* PENN STATE COAL DATA BASE \*\*

\*\*\*\*\*  
 \*  
 \* SAMPLE HISTORY \*  
 \*  
 \*\*\*\*\*

PENN STATE NUMBER PSOC-867

COLLECTED BY PENNSYLVANIA STATE UNIVERSITY  
 COLLECTION DATE 8/29/76  
 COLLECTOR'S NUMBER 867

REPORTED RANK ANTHRACITE (AN)

SAMPLE TYPE CHANNEL WHOLE SEAM  
 OTHER SAMPLE INFORMATION  
 SAMPLE RESERVE 329

SEAM NAME PHIMROSE  
 ALTERNATE SEAM NAME

TOTAL SEAM THICKNESS 16 FT. 0 IN.  
 THICKNESS OF SEAM SAMPLED 16 FT. 0 IN.  
 PORTION RECOVERED IN CORE  
 DIAMETER OF CORE

SEAM NAME PHIMROSE  
 APPARENT RANK ANTHRACITE (AN)

\*\*\*\*\*  
 \*  
 \* GEOLOGIC INFORMATION \*  
 \*  
 \*\*\*\*\*

SYSTEM (AGE) PENNSYLVANIAN  
 SERIES  
 GROUP  
 FORMATION LLENWELLYN

OVERBURDEN LITHOLOGY SHALE  
 FLOOR LITHOLOGY SHALE

# STANDARD RESPIRABLE DUSTS

\*\*\*\*\*  
\*  
\* CHEMICAL DATA 1 \*  
\*  
\*\*\*\*\*

<u>PROXIMATE ANALYSIS</u>	<u>AS REC'D</u>	<u>DRY</u>	<u>DAF</u>	<u>DMHF (PARR)</u>	<u>DMHF (PARR-G)</u>	<u>DMHF (DIR MM)</u>
% MOISTURE	3.77					
% ASH	13.39	13.91				
% VOLATILE MATTER	3.57	3.71	4.31	2.82	1.88	
% FIXED CARBON	79.27	82.38	95.69	97.18	98.12	

\*\*\*\*\*  
\*  
\* CHEMICAL DATA 2 \*  
\*  
\*\*\*\*\*

<u>ULTIMATE ANALYSIS</u>	<u>AS REC'D</u>	<u>DRY</u>	<u>DAF</u>	<u>DMHF (PARR)</u>
				(15.31 %MM)
% ASH	13.39	13.91		
% CARBON	78.76	81.85	95.07	96.65
% HYDROGEN	1.02*	1.06	1.23	1.25
% NITROGEN	0.64	0.66	0.77	0.78
% SULFUR	0.50	0.52	0.60	
% CHLORINE	0.02	0.03	0.03	0.03
% OXYGEN (DIFF)	1.90*	1.97	2.30	1.30

<u>SULFUR FORMS</u>	<u>% PYRITIC</u>	<u>% SULFATIC</u>	<u>% ORGANIC</u>	<u>% TOTAL</u>
DRY	0.05	0.01	0.46	0.52
DAF	0.06	0.01	0.53	0.60
OPTICAL				

<u>ELEMENTAL ANALYSIS</u>	<u>DRY</u>	<u>DMHF (MOD. P)</u>	<u>DMHF (DIR.)</u>
		(15.75 %MM)	( %MM)
% CARBON	81.65	96.92	
% HYDROGEN	0.88	1.04	
% NITROGEN	0.66	0.78	
% ORGANIC SULFUR	0.46	0.55	
% OXYGEN (DIFF)	0.59	0.68	
% CHLORINE	0.03	0.03	
% MINERAL MATTER	15.75		
(INCLUDES 0.09 % FES2)			

THE RESPIRABLE DUST CENTER

\*\*\*\*\*  
 \*  
 \* CHEMICAL DATA 3 \*  
 \*  
 \*\*\*\*\*

% MOISTURE IN COAL = 1.23  
 % HIGH TEMPERATURE ASH = 13.67 AT 750 DEGREES C

TRACE ELEMENT ANALYSIS	PPM HTA	PPM TOTAL COAL	MAJOR ELEMENT ANALYSIS	OXIDE % OF HTA	ELEMENT % OF TOTAL DRY COAL
AG			SiO2	55.00	3.51
B			AL2O3	31.60	2.29
BA	1440	197	TiO2	1.93	0.16
BE	6	1	FE2O3	3.30	0.32
BI			MGO	0.86	0.07
CE			CAO	0.65	0.06
CO			NA2O	1.01	0.10
CR	260	36	K2O	3.38	0.38
CU	180	25	P2O5	0.26	0.02
GA			S03	0.60	0.03
GE					
LA					
LI					
MN					
MO					
NI	160	22	VOLATILES		PPM TOTAL COAL
NS			AS		
PB			BR		
RA	180	25	CD		
SC			CL		
SH			F		
SR	670	92	HG		
TH			SB		
U			SE		
V	220	30			
Y					
YB					
ZN	110	15			
ZR	340	46			

**STANDARD RESPIRABLE DUSTS**

\*\*\*\*\*  
 \*  
 \* PETROGRAPHIC DATA \*  
 \*  
 \*\*\*\*\*

**MACERAL COMPOSITION WHITE ANALYSIS ONLY**

	<u>DRY</u> <u>VOLUME %</u>	<u>DMMF</u> <u>VOLUME %</u>	<u>DRY</u> <u>WEIGHT %</u>		
VITRINITE (CALC.)	71.7	77.9	66.0		
INERTINITE (CALC.)	20.3	22.1	18.7		
LIPTINITE (CALC.)		0.0	0.0		
MINERAL MATTER (CALC.)	8.0		15.3		
<b>VITRINOIDS</b>					
VITRINITE	71.7	77.9	66.0		
PSEUDOVITRINITE	0.0	0.0	0.0		
FUSINITE	0.7	0.8	0.7		
SEMI-FUSINITE	19.5	21.2	17.9		
MACRINITE	0.1	0.1	0.1		
MICRINITE	0.0	0.0	0.0		
SCLEROTINITE	0.0	0.0	0.0		
SPORINITE	0.0	0.0	0.0		
CUTINITE	0.0	0.0	0.0		
EXINITE (ANAL.)					
RESINITE	0.0	0.0	0.0		
SUBERINITE					
EXUDATINITE					
FLUORINITE					
BITUMINITE					
ALGINITE	0.0	0.0	0.0		
LIPTODETRINITE					
MINERAL MATTER(ANAL.)					
INERTINITE(ANAL.)					
LIPTINITE(ANAL.)					
<b>REFLECTANCE DATA</b>					
(%, IN OIL)	<b>HIGH</b>	<b>LOW</b>	<b>RANGE</b>	<b>MEAN MAX</b>	<b>STAND.DEV.</b>
VITRINITE	5.80	4.86	0.94	5.77	0.38
PSEUDOVITRINITE					
VITRINOIDS					



**APPENDIX B**  
**Characteristics of Standard Respirable Dusts**

STANDARD RESPIRABLE DUSTS

TABLE 1  
Size Distribution of Standard Respirable Dusts as Determined by Ladal Pipet Centrifuge

X†	MP3-1		MP32		MP3-3		PSOC 1192		PSOC 1192M		PSOC 867		PSOC 1361P		Kaolinite		Quartz	
	F+	X	F	X	F	X	F	X	F	X	F	X	F	X	F	X	F	X
4.63	100.0	9.80	100.0	6.55	82.1	6.55	100.0	4.63	86.2	4.33	81.3	4.63	71.6	17.5+	95.7	3.14	46.8	
3.08	89.1	6.56	91.3	4.34	48.2	4.34	88.3	2.97	43.8	2.88	39.0	3.08	34.7	12.5+	91.9	2.09	25.8	
1.99	73.4	4.21	75.2	3.07	26.8	2.79	45.6	1.88	23.9	2.03	24.4	1.99	12.8	8.4+	90.8	1.35	14.4	
1.27	52.4	2.65	28.4	1.98	15.4	1.77	19.2	1.18	12.2	1.32	9.0	1.27	4.7	6.9+	88.5	0.86	6.6	
0.79	28.3	1.69	9.6	1.25	8.3	1.10	7.1	0.74	6.0	0.84	3.9	0.79	1.9	5.0+	82.7	0.54	2.3	
0.49	9.0	1.05	2.8	0.77	3.4	0.66	1.1	0.46	3.0	0.52	2.4	0.49	1.1	3.35+	73.1	0.33	0.94	
0.28	3.7	0.66	1.0	0.47	2.2	0.39	0.68	0.26	1.3	0.32	1.9	0.29	0.59	2.22	67.4			
				0.27	1.0					0.19	1.4			1.48	58.8			
														0.96	45.2			
														0.61	32.5			
														0.38	26.5			
														0.23	13.7			
														0.14	8.2			

† Size of particle in  $\mu\text{m}$ .  
\* Cumulative weight percent finer than size.  
+ Analysis extended with Andreasen Pipet.

TABLE 2  
Size Distribution of Standard Respirable Dusts as Determined by Microtrac Small Particle Analyser

Particle Size, um	Weight Percent Finer Than Size										Kaolinite	Quartz	
	MP3-1	MP3-2	MP3-3	PSOC 1192	PSOC 1192M	PSOC 1361P	PSOC 867	PSOC 1361P	PSOC 867	PSOC 1361P			
42.21	100.0	100.0	100.0	100.0	100.0	100.0	100.0	100.0	100.0	100.0	100.0	100.0	100.0
29.85	100.0	100.0	100.0	100.0	100.0	100.0	100.0	100.0	100.0	100.0	100.0	100.0	100.0
21.10	100.0	100.0	100.0	100.0	100.0	100.0	100.0	100.0	100.0	100.0	100.0	98.7	100.0
14.92	100.0	100.0	93.2	100.0	99.1	100.0	100.0	100.0	100.0	100.0	100.0	92.4	97.5
10.55	100.0	100.0	84.7	99.3	97.5	100.0	100.0	100.0	100.0	100.0	100.0	85.4	90.9
7.46	98.7	87.9	67.2	94.6	88.8	89.2	88.6	88.6	89.2	88.6	88.6	65.4	75.2
5.27	97.1	60.0	44.7	69.7	67.6	61.6	60.3	60.3	61.6	60.3	60.3	62.8	52.7
3.73	92.2	34.0	28.6	39.6	45.4	35.7	36.5	36.5	35.7	36.5	36.5	50.1	35.6
2.63	77.6	18.5	19.1	20.9	29.7	20.2	21.7	21.7	20.2	21.7	21.7	37.4	23.0
1.69	59.6	9.8	12.6	10.4	19.3	11.1	10.8	10.8	11.1	10.8	10.8	27.2	13.5
1.01	37.8	4.7	7.3	5.1	11.7	5.7	4.1	4.1	5.7	4.1	4.1	17.7	6.7
0.66	17.2	1.9	3.3	1.8	5.4	2.3	1.3	1.3	2.3	1.3	1.3	11.2	2.4
0.43	7.0	0.7	1.3	0.7	2.2	0.8	0.1	0.1	0.8	0.1	0.1	8.5	0.8
0.34	2.2	0.2	0.4	0.2	0.7	0.2	0.0	0.0	0.2	0.0	0.0	7.2	0.3
0.24	0.8	0.0	0.1	0.0	0.2	0.0	0.0	0.0	0.0	0.0	0.0	6.8	0.1
0.17	0.2	0.0	0.0	0.0	0.1	0.0	0.0	0.0	0.0	0.0	0.0	6.4	0.0

STANDARD RESPIRABLE DUSTS

TABLE 3  
 Mineralogical Composition of Standard Respirable Dusts  
 as Determined by the Mineral Constitution Laboratory of the Pennsylvania State University

Sample	PSOC 867	PSOC 1192M	PSOC 1361P	MP3-2
LTA	25.7%	9.58%	9.03%	10.1%
Quartz	14	4	8	12
Pyrite	n.d.	22	32	16
Kaolinite	35-45	30-40	30-40	25-35
Illite*	--	10-20	10-20	20-30
Illite plus mixed-layer clays*	20-30	--	--	--
Chlorite*	5-15	n.d.	n.d.	n.d.
Feldspars*	5-10	n.d.	n.d.	n.d.

n.d. = not detected.

\* = estimated value based on normative analysis.

TABLE 4  
Spectrochemical Analysis of Standard Respirable Dusts Expressed as Oxides  
Percent of High Temperature Ash

Oxide	Percent of High Temperature Ash						
	PSOC 867	PSOC 1192	PSOC 1192M	PSOC 1361P	MP3-2	Kaolinite	Quartz
SiO <sub>2</sub>	53.4	33.5	36.9	43.1	47.3	45.2	95
Al <sub>2</sub> O <sub>3</sub>	33.1	25.2	27.6	27.7	27.6	38.1	2.06
TiO <sub>2</sub>	1.46	1.02	1.27	1.12	1.35	1.36	< 0.1
Fe <sub>2</sub> O <sub>3</sub>	5.30	34.4	27.7	22.5	14.7	0.34	0.50
MgO	1.23	0.49	0.58	0.84	1.00	< 0.1	< 0.1
CaO	0.60	1.56	1.74	1.25	2.07	< 0.1	< 0.1
MnO	0.02	0.02	0.02	0.088	0.012	< 0.01	< 0.01
Na <sub>2</sub> O	0.93	0.17	0.21	0.27	0.26	0.05	0.10
K <sub>2</sub> O	2.84	1.24	1.38	1.77	2.60	0.12	0.39
P <sub>2</sub> O <sub>5</sub>	0.17	0.18	0.21	0.44	0.75	--	--
SO <sub>3</sub>	0.2	0.5	0.3	0.1	0.6	--	--
TOTAL	99.3%	98.3%	97.9%	99.1%	98.3%	85.2%*	98.0%

\* Loss of H<sub>2</sub>O on ignition (750°C) < 15.2%.

STANDARD RESPIRABLE DUSTS

TABLE 5  
Size-specific Gravity Distribution of FSO 1192M as a Percentage of the Total Coal

Size, um	% Total	Sink/Float													
		1.3	1.3 x 1.4	1.4 x 1.5	1.5 x 1.6	1.6 x 1.7	1.7 x 1.8	1.8 x 1.9	1.9 x 2.0	1.9 x 2.0	2.0				
42.21	0.0	0.0	0.0	0.0	0.0	0.0	0.0	0.0	0.0	0.0	0.0	0.0	0.0	0.0	0.0
29.85	0.0	0.0	0.0	0.0	0.0	0.0	0.0	0.0	0.0	0.0	0.0	0.0	0.0	0.0	0.0
21.10	2.1	0.0	0.1	0.4	0.0	0.0	0.0	0.0	0.0	0.0	0.0	0.5	1.0	0.1	0.0
14.92	0.8	0.0	0.0	0.5	0.0	0.0	0.0	0.0	0.0	0.0	0.0	0.2	0.1	0.0	0.0
10.55	8.3	0.1	4.9	2.3	0.9	0.0	0.0	0.0	0.0	0.0	0.0	0.0	0.0	0.2	0.0
7.42	22.7	0.2	13.4	3.5	2.7	0.0	0.0	0.0	0.0	0.0	0.0	0.0	1.0	0.9	0.0
6.27	23.9	0.2	13.8	3.3	1.5	3.6	0.0	0.0	0.0	0.0	0.0	0.0	0.0	1.5	0.0
3.73	15.8	0.1	8.0	2.3	0.9	2.8	0.4	0.0	0.0	0.0	0.0	0.0	0.0	1.3	0.0
2.63	9.6	0.1	3.8	2.1	1.4	0.0	1.1	0.0	0.0	0.0	0.0	0.0	0.0	1.1	0.0
1.69	7.3	0.0	2.7	1.6	1.1	0.0	1.1	0.0	0.0	0.0	0.0	0.0	0.0	0.8	0.0
1.01	5.4	0.0	1.8	1.1	0.8	0.0	0.9	0.0	0.0	0.0	0.0	0.0	0.0	0.8	0.0
0.66	2.5	0.0	0.7	0.5	0.3	0.0	0.5	0.0	0.0	0.0	0.0	0.6	0.0	0.4	0.0
0.43	1.1	0.0	0.0	0.0	0.0	0.0	0.0	0.0	0.0	0.0	0.0	0.9	0.0	0.2	0.0
0.34	0.4	0.0	0.0	0.0	0.0	0.0	0.0	0.0	0.0	0.0	0.0	0.4	0.0	0.0	0.0
0.24	0.1	0.0	0.0	0.0	0.0	0.0	0.0	0.0	0.0	0.0	0.0	0.1	0.0	0.0	0.0
0.17	0.0	0.0	0.0	0.0	0.0	0.0	0.0	0.0	0.0	0.0	0.0	0.1	0.0	0.0	0.0

TABLE 6  
Size-specific Gravity Distribution of PSOC 1361P as a Percentage of the Total Coal

Size, um	% Total	Sink/Float											
		1.3	1.3 x 1.4	1.4 x 1.5	1.5 x 1.6	1.6 x 1.7	1.7 x 1.8	1.8 x 1.9	1.9 x 2.0	2.0			
42.21	0.0	0.0	0.0	0.0	0.0	0.0	0.0	0.0	0.0	0.0	0.0	0.0	0.0
29.85	0.1	0.0	0.0	0.0	0.0	0.0	0.0	0.0	0.0	0.0	0.0	0.0	0.0
21.10	0.8	0.2	0.1	0.0	0.0	0.0	0.0	0.0	0.0	0.3	0.0	0.0	0.2
14.92	4.5	0.3	0.2	0.7	0.6	0.6	0.6	0.6	0.6	0.9	0.0	1.1	0.1
10.55	10.3	1.9	2.4	2.8	2.5	0.3	0.3	0.0	0.0	0.0	0.0	0.0	0.4
7.42	26.1	5.1	6.1	7.8	4.5	0.0	0.0	0.0	0.0	0.0	1.5	0.0	1.0
6.27	27.4	4.7	6.4	8.6	3.6	0.0	0.0	0.0	0.0	0.0	2.8	0.0	1.0
3.73	14.7	2.0	3.2	5.7	1.7	0.0	0.0	0.0	0.0	0.0	0.9	0.0	1.4
2.63	7.0	0.6	1.1	3.3	0.4	0.0	0.0	0.0	0.0	0.0	0.5	0.0	1.2
1.69	4.6	0.4	0.7	1.8	0.5	0.0	0.0	0.0	0.0	0.0	0.6	0.0	0.8
1.01	2.8	0.2	0.4	1.3	0.3	0.0	0.0	0.0	0.0	0.0	0.0	0.0	0.5
0.66	0.9	0.1	0.2	0.4	0.1	0.0	0.0	0.0	0.0	0.0	0.0	0.0	0.2
0.43	0.4	0.0	0.1	0.2	0.0	0.0	0.0	0.0	0.0	0.0	0.0	0.0	0.1
0.34	0.3	0.0	0.0	0.1	0.0	0.0	0.0	0.0	0.0	0.0	0.1	0.1	0.0
0.24	0.0	0.0	0.0	0.0	0.0	0.0	0.0	0.0	0.0	0.0	0.0	0.0	0.0
0.17	0.0	0.0	0.0	0.0	0.0	0.0	0.0	0.0	0.0	0.0	0.0	0.0	0.0

STANDARD RESPIRABLE DUSTS

TABLE 7  
Size-specific Gravity Distribution of P50C 867 as a Percentage of the Total Coal

Size, um	% Total	Sink/Float												
		1.3	1.3 x 1.4	1.4 x 1.5	1.5 x 1.6	1.6 x 1.7	1.7 x 1.8	1.8 x 1.9	1.9 x 2.0	2.0				
42.21	0.0	0.0	0.0	0.0	0.0	0.0	0.0	0.0	0.0	0.0	0.0	0.0	0.0	0.0
29.85	0.0	0.0	0.0	0.0	0.0	0.0	0.0	0.0	0.0	0.0	0.0	0.0	0.0	0.0
21.10	0.6	0.0	0.0	0.0	0.3	0.0	0.0	0.0	0.0	0.0	0.0	0.0	0.0	0.3
14.92	2.0	0.0	0.0	0.0	0.5	0.6	0.1	0.0	0.0	0.0	0.0	0.0	0.1	0.6
10.55	11.2	0.0	0.0	0.1	1.6	5.7	1.3	0.0	0.0	0.0	0.0	0.0	0.4	2.0
7.42	25.7	0.1	0.0	0.1	3.4	11.6	5.4	0.0	0.0	0.0	0.0	0.0	0.0	5.0
6.27	24.0	0.1	0.0	0.1	2.6	8.6	6.4	0.3	0.3	0.6	0.6	0.6	0.6	5.4
3.73	17.3	0.0	0.0	0.0	0.8	4.3	4.3	1.4	1.4	1.8	1.8	1.8	1.8	4.7
2.63	9.9	0.0	0.0	0.0	0.3	1.1	2.6	1.0	1.0	1.4	1.4	1.4	1.4	3.4
1.69	5.0	0.0	0.0	0.0	0.2	0.4	1.1	0.2	0.2	0.8	0.8	0.8	0.8	2.3
1.01	3.3	0.0	0.0	0.0	0.0	0.0	0.6	0.2	0.2	0.6	0.6	0.6	0.6	1.5
0.66	0.9	0.1	0.0	0.0	0.0	0.0	0.1	0.0	0.0	0.1	0.1	0.1	0.1	0.5
0.43	0.1	0.0	0.0	0.0	0.0	0.0	0.0	0.0	0.0	0.0	0.0	0.0	0.0	0.1
0.34	0.0	0.0	0.0	0.0	0.0	0.0	0.0	0.0	0.0	0.0	0.0	0.0	0.0	0.0
0.24	0.0	0.0	0.0	0.0	0.0	0.0	0.0	0.0	0.0	0.0	0.0	0.0	0.0	0.0
0.17	0.0	0.0	0.0	0.0	0.0	0.0	0.0	0.0	0.0	0.0	0.0	0.0	0.0	0.0



# A Procedure for Extensive Characterization of Coal Mine Dust Collected Using a Modified Personal Sampler

T. F. Dumm and R. Hogg

Mineral Processing Section  
Department of Mineral Engineering, The  
Pennsylvania State University

It is generally agreed that dust characteristics play a role in the development of Coal Workers' Pneumoconiosis (CWP). Unfortunately, there is a serious lack of information on what the characteristics of mine dust actually are and how they vary among different mining regions, coal seams, etc. This paucity of data can generally be attributed to the serious problems encountered in collecting sufficiently large quantities of dust for conventional analytical procedures.

Personal samplers are widely used in coal mines for regulatory and enforcement purposes. Generally, these provide information only on the total (respirable) dust loading in the mine atmosphere and on the mineral matter (primarily quartz) content of the respirable dust. A procedure has been developed by which samples collected with a slightly modified personal sampler can be analyzed for particle size distribution, total mineral matter content and elemental composition, in addition to the standard mass and quartz measurements. These analyses could readily be performed on a routine basis. Shape analysis by Scanning Electron Microscope (SEM) could easily be included if appropriate shape criteria are established. Extension of the procedure to include the determination of complete size/specific gravity (composition) distributions is quite straightforward provided sufficiently large samples (at least 10 mg) can be collected. Typical sample sizes for a personal sampler carried by a miner for one shift range from about 0.5 to 2 mg.

The basic procedure was developed and evaluated using synthetic mine dust prepared in the laboratory. Field tests in three working mines in Pennsylvania and West Virginia

have confirmed the applicability of the approach to the real world. Particle size distribution measurements on mine dust collected in the modified personal sampler were found to agree closely with the results of simultaneous *in situ* measurements obtained using cascade impactors.

## Introduction

The characteristics of the coal dust generated in the mining process play an important role in determining whether or not the inhaled dust will produce Coal Workers' Pneumoconiosis (CWP) over the working life span of a miner. It is commonly agreed that the quantity of respirable dust inhaled and the quartz content of that dust are two important characteristics which contribute to the development of CWP. It is also known that some coal mines have little incidence of the disease regardless of the dust levels and quartz content. This would indicate that other characteristics may also influence the pathogenesis of CWP.

Currently, the respirable dust concentration and in some cases, the quartz content of that dust are monitored for regulatory purposes. However, with a slight modification to the existing sampling apparatus, respirable coal dust can be collected in such a way as to provide considerably more information about the dust.

Laboratory tests using standard respirable dusts made at the Pennsylvania State University, have shown that it is possible to analyze very small quantities of respirable dust for mass loading, size distribution, low temperature ash, kaolinite and quartz content and in some cases, to perform

a specific gravity fractionation.

Having tested the characterization scheme in the laboratory, respirable dust samples were collected in three underground bituminous and mines in Pennsylvania and West Virginia. The dusts were returned to the laboratory and analyzed according to the suggested characterization scheme.

### Coal Dust Collection

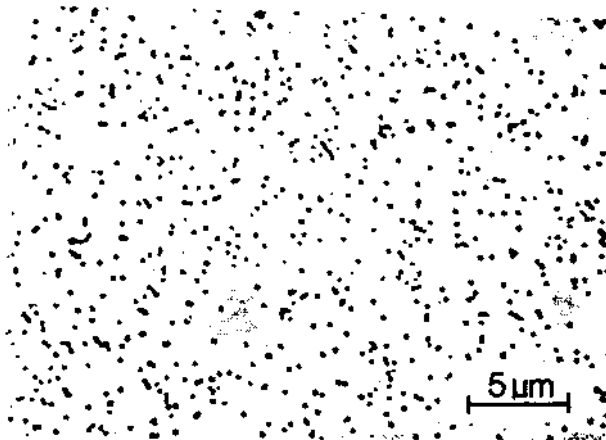
#### Collection System

The atmosphere in an operating coal mine section, especially close to the continuous miner, may contain particles as large as 30 to 40  $\mu\text{m}$ . In order to collect only the respirable particles, those less than 5  $\mu\text{m}$ , it is necessary to use a classifier when sampling. The 10 mm diameter nylon cyclone is commonly used in the U.S. to separate dust particles from mine atmospheres. When operated at its appropriate flowrate, the respirable fraction approximates the criterion for respirable dust defined by the American Conference of Governmental Industrial Hygienists (ACGIH).<sup>(1)</sup> The 10 mm diameter nylon cyclone is an integral part of the personal dust sampler units which measure the respirable dust concentration at the miner's work area (see Figure 1). In this arrangement, the dusty air is drawn into the inlet of the cyclone

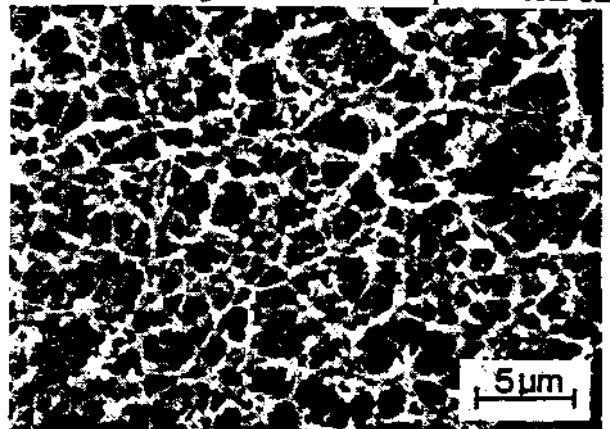
by a suitable 2 liter/minute constant flow pump. The oversize particles are deposited into a collection cap while the under-size, respirable particles are collected on a pre-weighed filter. After the mine air has been sampled for a set amount of time, the filter is weighed and, knowing the flow rate through the filter, the average concentration of dust that the miner was exposed to can be determined.<sup>(2)</sup>

In order to further analyze the respirable dust collected by the personal sampler, it is necessary to use a filter from which as much of the respirable dust as possible can be removed without bias with respect to particle size. The obvious filter for this purpose is a Nuclepore polycarbonate membrane filter which has a very flat surface. A 47 mm 0.2  $\mu\text{m}$  pore size Nuclepore membrane filter offers a pressure drop across it low enough that the necessary flow rate of 2 liters/minute can be maintained through the filter for several hours without exhausting the power supply of the pump. Figure 2 shows the filter surfaces of a Nuclepore membrane filter, a Gelman DM450 filter which is commonly used for mineralogical analysis of coal, and a Mine Safety Appliances Co. (MSA) filter which is used for routine sampling of coal mine atmospheres.

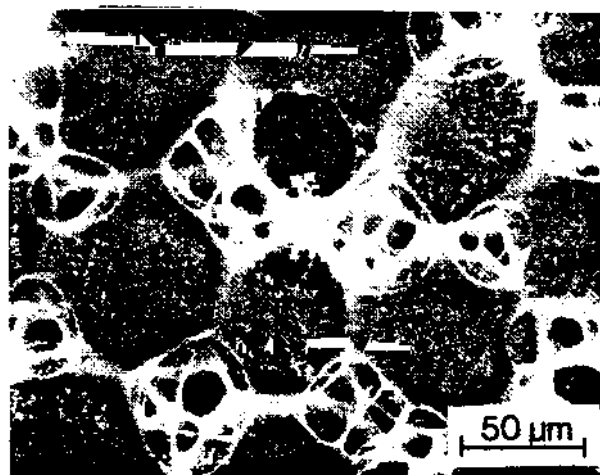
An experiment was performed in order to verify that the Nuclepore filters would have the same collecting capabilities as the MSA filters under typical loading conditions. Table I lists the mass loadings of a standard respirable coal dust



a



b



c

FIGURE 2. Scanning electron micrographs of a) 0.4  $\mu\text{m}$  pore size Nuclepore polycarbonate filter surface, b) 0.45  $\mu\text{m}$  pore size Gelman DM450 PVC acrylic copolymer filter surface and c) MSA personal sampler filter surface.

THE RESPIRABLE DUST CENTER

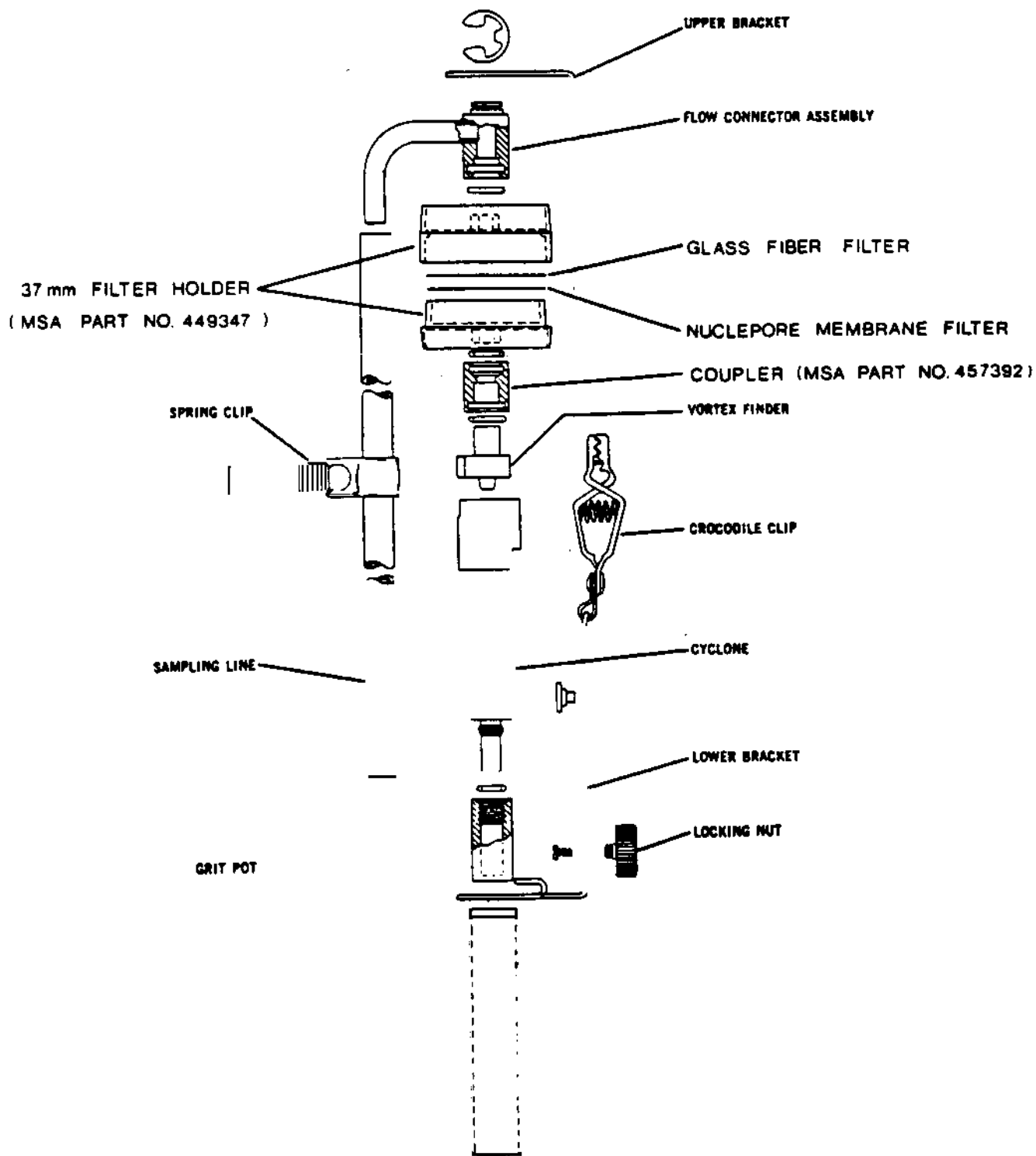


FIGURE 1. Schematic diagram of a MSA personal dust sampler showing the modifications necessary for the use of Nuclepore membrane filters.

which was dispersed in a chamber and sampled for eight hours by eight personal samplers. Four of the personal samplers contained the usual MSA filters while the other four contained 47 mm diameter 0.2 um pore size Nuclepore polycarbonate filters. As can be seen from the table, all of the filters gave about the same mass loadings.

The coal dust collection system thus consists of a 37 mm diameter Millipore filter cassette into which is loaded a 37 mm-diameter glass fiber back-up filter which provides support for the 47 mm 0.2 um pore size diameter Nuclepore membrane filter. The loaded cassette is wrapped with a cellulose band and placed into an MSA Gravimetric Dust Sampling Unit which is powered by an MSA Fixt-Flo pump.

*Mine Sampling*

Coal dust samples were collected at three underground coal mines in central Pennsylvania, northern West Virginia and western Pennsylvania, and are designated as mines A, B and C respectively. A personal sampler was placed in the return airway of mine A approximately 50 feet from the working face. The sampler was moved, but kept in the return airway as the continuous miner moved. Air was sampled for four hours. Mine B was sampled in a similar manner as mine A. This air was sampled for approximately three hours. Finally, for mine C, two personal samplers were used in addition to two total dust collection devices, which did not separate the respirable dust from the coarser particles. These devices were 47 mm diameter Nuclepore Open-Face Filter Holders which held 47 mm 0.2 um Nuclepore filters. These assemblies were connected to Fixt-Flo pumps which generated an airflow of 2 liters/minute. All samplers in mine C were placed on the return side of the continuous miner approximately 10 feet from the working face. Air was sampled for about three hours.

**Characterization of Respirable Dust**

*Mass Loading*

When all samples were returned to the laboratory, the respirable and coarse fractions were removed from the personal samplers. The respirable fraction was removed simply by taking the Nuclepore filter from the cassette. The coarse particles were washed from the cyclone into a beaker and filtered onto a 25 mm, 0.4 um Nuclepore filter. Both the coarse and respirable fractions were weighed to determine their mass. Generally the 10 mm cyclone deposited the coarse material into the bottom collection cap, however, for coal dust sampled at mine B, there was a significant deposit of coal on the cyclone walls. This material was initially kept separate from the coarse material but was combined with the coarse after weighing. Table II lists the mass loadings of coal collected at the three mines. In the normal routine analysis, only the respirable fraction of coal is used for analysis and not the cyclone underflow particles.

*Size Analysis*

The size distribution of the respirable coal dust particles dispersed in water is determined using the Microtrac Small Particle Analyzer (SPA). The Microtrac SPA, manufactured

by Leeds & Northrup, Inc., Largo, Florida, uses a combination of forward scattering and 90° scattering of light waves of varying wavelengths to size particles in the range of 0.12 to 42.2 um. The instrument is designed to directly relate the detector signal to the 2nd, 3rd and 4th powers of the particle diameter, to measure quantities such as total surface area, total volume, volume mean diameter, etc.

The Microtrac SPA uses a helium-neon laser to generate light of wavelength 633 nm to produce forward scattering from particles in the range 0.34 to 42.2 um. the diffraction pattern is analyzed according to Fraunhofer diffraction theory. In order to extend the size range of the Microtrac SPA, the instrument incorporates a tungsten lamp/filter assembly to produce three different wavelengths at two orthogonal polarizations. The scattering produced by these light sources is detected at 90° from the incident beam. This arrangement is used for analyzing particles between 0.12 to 0.34 um. Light scattering in this domain is described by the Mie theory.

Particles dispersed in water pass through the laser beam via a circulation system which pumps the suspension through tubing into a sample cell and back to the pump for recirculation. The Microtrac SPA was retrofitted with a small volume (~ 50 ml) sample recirculator which consists of a peristaltic pump connected in series with a small beaker and Tygon

TABLE I

Comparison of MSA and 0.2 um Pore Size Nuclepore Filters Collecting Dispersed Standard Respirable Dust in an Elpram Dust Chamber for 8 hours.

Filter No.	Type	Wt. Coal Collected, mg
1	MSA	2.837
2	MSA	2.854
3	MSA	2.873
4	MSA	2.858
		Avg. = 2.856 +/- 0.015 mg
		Avg. Conc. = 2.975 mg/m <sup>3</sup>
5	Nuclepore	2.936
6	Nuclepore	2.851
7	Nuclepore	2.737
8	Nuclepore	3.086
		Avg. = 2.903 +/- 0.147 mg
		Avg. Conc. = 3.024 mg/m <sup>3</sup>

tubing. This modification allows amounts of dust as small as about 0.5 mg to be accurately analyzed.

The "size" of a particle measured by the Microtrac is based on its projected area in random orientation in the turbulent suspension passing through the laser beam. The aerodynamic size, on the other hand, is based on the drag experienced by the particle as it moves through air. In a separate investigation, it was shown<sup>(3)</sup> that the size distribution of a dispersed dust as measured by the Microtrac SPA can be correlated with the aerodynamic size distribution as

TABLE II  
Weight of Coal Dust Collected in Mines.

Mine	Sample	Loadings, mg			% Resp.
		Respirable	Coarse	Total	
A	Personal	0.899	8.3	9.2	9.8
B	Personal	1.112	7.653	8.765	12.7
C	Personal #1	0.587	5.026	5.613	10.5
	Personal #2	1.094	9.762	10.856	10.1
	Total #1	—	—	9.364	—
	Total #2	—	—	18.872	—

measured by a cascade impactor by using a conversion factor of about 1.10.

Size analysis of the respirable dust sample collected on the Nuclepore filter first involves removing all of the dust from the filter. This is done simply by placing the filter into a beaker with a small amount of water containing wetting and dispersing agents. Ultrasonic energy is applied to help remove adhering particles and to completely disperse the system. The sample is then transferred to the small volume recirculator of the Microtrac SPA. Analysis time is typically about three minutes.

Knowing the weights of the coarse and respirable fractions of the dust, and their size distributions, it is possible to determine the size distribution of the dust that entered the personal sampler. From the mass balance

$$p(x) = q(x)Q = t(x)T/P$$

where:

$q(x)$ ,  $t(x)$ , and  $p(x)$  are the incremental weight fractions of the respirable, coarse and total size fractions, respectively

$Q$ ,  $T$ , and  $P$  are their respective weights.

From this relationship, the total size distribution was calculated using the data from the respirable and coarse fractions of the personal samplers.

The respirable and calculated total aerodynamic size distributions from mines A, B and C are shown in Figures 3, 4 and 5 respectively. In addition to the size distributions of dusts collected in the personal samplers, the size distributions of dusts sampled by Anderson Model 298 cascade impactors which were placed near the personal samplers are shown for comparison. Although the size distribution of the total dust as calculated from the respirable and coarse fractions sampled from mine A agree very well with the cascade impactor analysis, the cascade impactor size distributions are significantly coarser from mines B and C compared to

the calculated total. This is believed to be the result of agglomeration of the coal particles in the mine air. Evidence of this also exists in the fact that there was a significant amount of respirable particles (those less than about 5  $\mu$ m in diameter) in the coarse fraction of the dust.

#### Ash Analysis

When size analysis has been completed, it is possible to remove nearly all of the respirable dust particles from the Microtrac SPA.

This suspension is then deposited onto 25 mm, 0.4  $\mu$ m pore size Nuclepore polycarbonate filter membranes, dried and weighed. The weight of the deposited dust is recorded and the filters are placed into 10 ml beakers. The beakers are then placed in the chamber of the low temperature ashers and ashed for approximately three hours. The low temperature ash (LTA) remaining in the beakers is redispersed by adding water and redeposited onto similar Nuclepore membrane filters. The LTA content is determined by weighing the filters and dividing by the original weight of coal. The results of the low temperature ash analysis are presented in Table III.

The ash analysis of the Personal Sample #1 from the mine C is out of line with the other personal sample which gives a total ash content of about 17 percent and which agrees well with the ash content of the total samples from that mine. Although no errors were detected during the analysis of Personal Sample #1, there is always the chance one could have occurred. It is also possible that the sample could have been altered or contaminated during sample collection or transport from the mine to the laboratory. Incomplete low temperature ashing could have contributed to the higher LTA of the respirable fraction, but this does not explain the lower LTA value obtained for the coarse fraction. On the basis of just a few samples, one cannot rule out the possibility that the Personal Sample #1 data are correct and that there is a large sample variability. Judging from the values listed in Table II, it can be seen that there is a large difference in the amounts of coal collected by the mine C instruments, all of which were operating for the same amount of time in the same area. Whether or not this same variability applies to the ash content remains to be seen.

# CHARACTERIZATION OF COAL MINE DUST

## Mineralogical Analysis

Mineralogical analyses were performed using infrared spectrophotometry. The samples were first analyzed on the Nuclepore polycarbonate filters which were used to obtain their LTA weights. After infrared analysis on the Nuclepore filters, the ash was transferred to Gelman DM450 filters and the analysis was repeated. The infrared analysis follows the P7 procedure used by the Mine Safety and Health Administration (MSHA) in the routine analysis of quartz.<sup>(4)</sup>

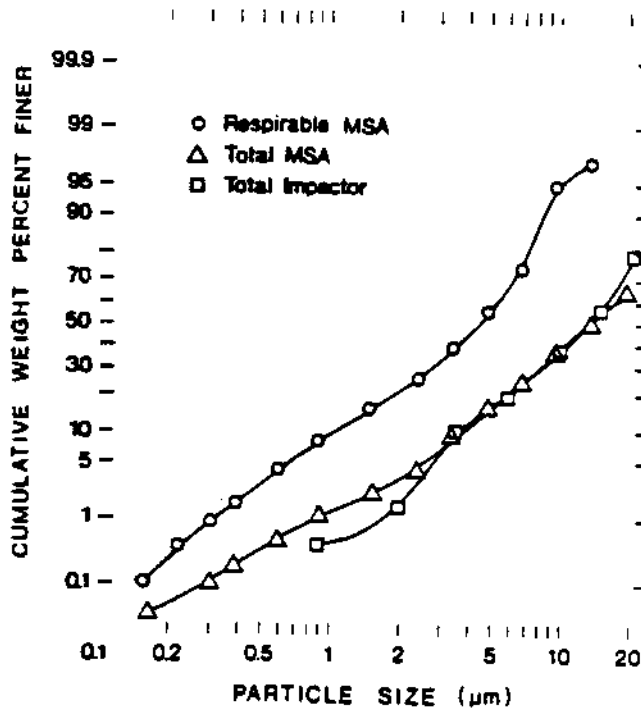


FIGURE 3. Aerodynamic size distributions of dust collected at mine A with a modified MSA personal sampler (converted from Microtrac SPA data). Cascade impactor size distribution is included for comparison.

TABLE III

LTA Content of Actual Coal Mine Dusts, Percent.

Mine	Sample	Respirable	Coarse	Total
B	Personal	42.1	21.6	24.9
C	Personal #1	61.3	6.1	11.9
	Personal #2	21.6	15.9	16.5
	Total #1	—	—	17.1
	Total #2	—	—	18.6

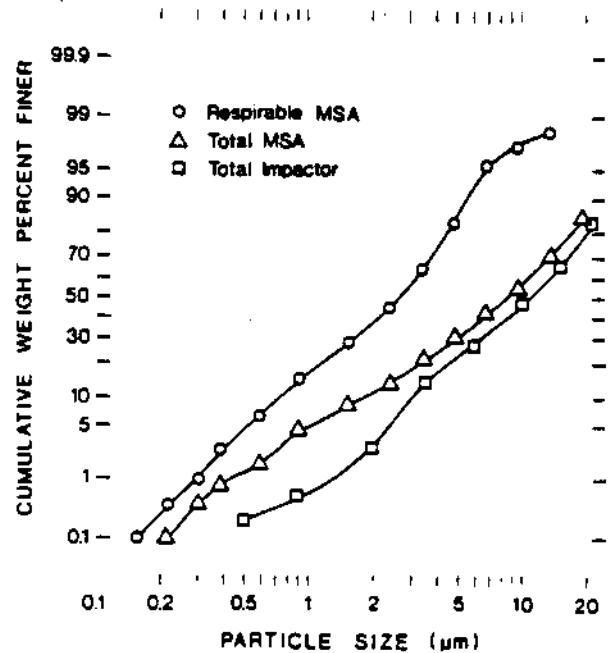


FIGURE 4. Aerodynamic size distributions of dust collected at mine B with a modified MSA personal sampler (converted from Microtrac SPA data). Cascade impactor size distribution is included for comparison.

The mineralogical assays for kaolinite and quartz, which are expressed as percentages of the whole dust, are listed in Table IV. The total quartz and kaolinite contents of the personal samplers were determined by adding their respective amounts from the respirable and coarse fractions and dividing by the total amount of coal. As can be seen from the table, the combined quartz content of the personal samplers agrees well with the total samples of the analyses for the mine C dusts.

If substantial quantities of minerals other than quartz and kaolinite exist within the respirable dust, x-ray diffraction could be used to determine their relative quantities. Although rigorous quantitative analysis of mineral powders requires the addition of an internal standard to the dust, sufficient accuracy can be achieved by using an external standard as described by Freedman.<sup>(5)</sup>

## Elemental Analysis

Lee and Mutmansky<sup>(6)</sup> have successfully applied Particle Induced X-ray Emission (PIXE) techniques to elemental analyses of respirable dust on cascade impactor substrates. Because this technique is non-destructive and only small quantities (10 ug) are necessary for adequate analysis, the elemental analysis of the coal dust could readily be incorporated into the characterization scheme. Elemental analysis could be performed on the low temperature ash after the mineralogical analysis since the latter technique is also non-destructive to the sample. Elemental analyses were not performed on the mine dust samples collected in this study.

TABLE IV

Kaolinite and Quartz Content of Actual Coal Mine Dusts by Infrared Spectroscopy

Mine	Sample	Kaolinite			Quartz		
		Respirable	Coarse	Total	Respirable	Coarse	Total
B		9	5	6	3	2	2
C	Personal #1	0	1	1	5	11	
	Personal #2	3	5	4	3	2	2
	Total #1	—	—	6	—	—	3
	Total #2	—	—	5	—	—	—

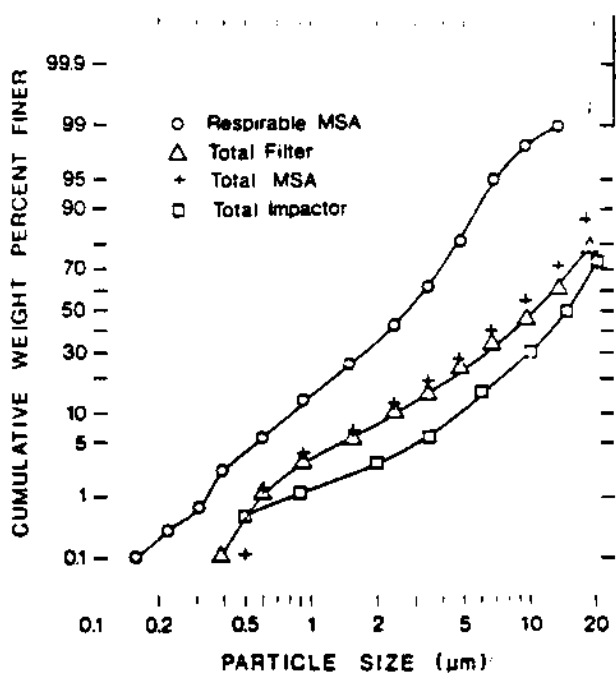


FIGURE 5. Aerodynamic size distributions of dust collected at mine C with a modified MSA personal sampler and an open-face filter (converted from Microtrac SPA data). Cascade impactor size distribution is included for comparison.

**Specific Gravity Fractionation**

If larger amounts (~10 mg) of respirable dust are collected, it is possible to perform a specific gravity fractionation on the coal dust. Although such quantities were not collected in the underground mine sampling, laboratory tests have demonstrated the feasibility of the technique.<sup>(3)</sup> The results of the gravity fractionation procedure can provide useful information on the relative distributions of the organic and mineral constituents in the dust.

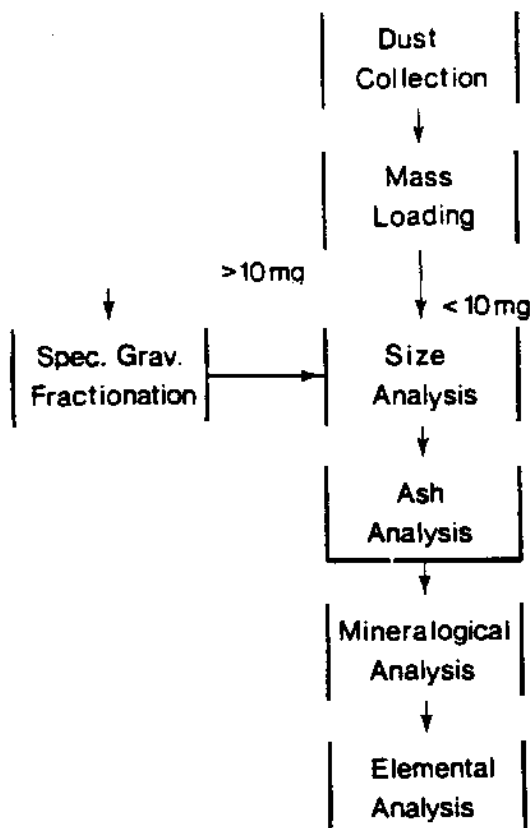


FIGURE 6. Recommended characterization scheme for respirable dust samples.

**Conclusions**

A systematic characterization scheme is suggested; Figure 6 is a diagram of the recommended procedure.

If more than 10 mg of respirable dust is collected, it would be possible to do at least one and perhaps two specific gravity fractionations. Otherwise, size analysis is performed using the modified Microtrac SPA after which the sample is collected and low temperature ashed. The ash can be weighed directly on a Nuclepore polycarbonate filter and transferred

to a Gelman DM450 filter, or just transferred to the Gelman DM450 filter directly from the low temperature asher if LTA weight is not necessary. Once deposited on an appropriate filter, the mineralogy of the LTA can be determined by x-ray diffraction and/or infrared spectroscopy. Since these techniques are non-destructive, elemental analysis of the LTA can then be performed.

The minimum amount of respirable coal dust necessary for these analyses, excluding the specific gravity fractionation is about 0.5 mg. This amount is about the limiting quantity for both the size analysis procedure using the Microtrac SPA, and the mineralogical procedure. The length of time required to perform the entire procedure, excluding the specific gravity fractionation, is approximately four hours per sample with three hours of this time being used for low-temperature ashing. It is possible, however, to process many samples simultaneously and thus reduce overall analysis time per sample. By including the specific gravity fractionation procedure, the analysis time would significantly increase depending on the number of fractionations desired. This procedure is not recommended as part of a routine analysis.

### Acknowledgments

The work described in this paper was supported by the Mineral Institutes program by Grant No. G1135142 from the Bureau of Mines, U.S. Department of Interior, as part of the Generic Mineral Technology Center for Respirable Dust.

### References

1. Measurement and Control of Respirable Dust in Mines, National Academy of Sciences, U.S. Bureau of Mines OFR 118-80 (1980).
2. Instruction Manual for MSA Gravimetric Dust Sampling Kit, Mine Safety Appliances Corp.
3. Dumm, T.F.: *An Evaluation of Techniques for Characterizing Respirable Coal Dust*. M.S. Thesis, The Pennsylvania State University, August (1986).
4. Infrared Determination of Quartz in Respirable Coal Mine Dust, Method No. P7, Mine Safety and Health Administration, 2nd Revision (1984).
5. Freedman, R.W.: Procedures for the Analysis of Respirable Dust as Related to Coal Workers' Pneumoconiosis. *Analytical Methods for Coal and Coal Products* 2:315-334 (1978).
6. Lee, C. and J.M. Mutmansky: Statistical Analysis of the Elemental Characteristics of Airborne Coal Mine Dust. *Proceedings Respirable Dust in the Mineral Industries Conference*, pp. 111-123. Univ. Park, PA (1986).



# Electron Spin Resonance Detection of Reactive Free Radicals in Fresh Coal Dust and Quartz Dust and Its Implications to Pneumoconiosis and Silicosis

N. S. Dalal, M. M. Suryan, B. Jafari and X. Shi  
Chemistry Department, West  
Virginia University

It is well known that prevalence and severity of coal worker's pneumoconiosis (CWP) differ markedly in different regions and mines despite comparable exposures. These variations in the pathogenicity of different coal mine dusts can only partially be explained by the mineral composition of the coal mine dust and the rank of coal. Laboratory studies also do not correlate with the human experience. One major difference between human exposure and laboratory studies is that the coal miner breathes dust from freshly broken coal, while the animals or cells are exposed to stale dust. In an effort to find biochemical clues for resolving this apparent paradox, we have carried experiments to detect differences in chemical reactivities of fresh versus stale coal dust from several U.S. coal mines. Electron spin resonance (ESR) was used as a technique for the direct detection of the concentration and reactivity of free radicals. ESR measurements of freshly ground coal dusts of different ranks and composition showed significant differences in the amount and reactivities of the organic free radicals produced. The half-lives and reactivity patterns of these newly formed species of free radicals seem to correlate with the expected toxicity and pathogenicity of the dust, thereby, providing new clues to the biochemical mechanisms and pathogenesis of CWP. Similar detection of free radicals in freshly crushed quartz suggest that free radicals might play a significant role in the pathogenicity of quartz in causing fibrosis and eventually silicosis.

## Introduction

The pathogenesis of coal workers' pneumoconiosis (CWP) has been an important topic of concern for decades, but the mechanism of CWP is still not understood. It is well known, for example, that the prevalence and severity of CWP differ markedly in different regions and mines despite comparable exposure<sup>(1,2)</sup> but these observations can only partially be explained by differences in mineral composition and rank of coal<sup>(3-5)</sup> Specifically, while epidemiological studies of coal miners indicate<sup>(1,2)</sup> that the effectiveness of coal in producing CWP correlates roughly with the rank (i.e. %

carbon content) of coal, such correlation has not been established via biological studies.<sup>(4-6)</sup>

In an effort to find additional clues to the biochemical mechanism of CWP, we have examined the possible role in CWP of organic radicals formed in coal dust during the cutting of coal. This study<sup>(7,8)</sup> was prompted by the following observations. Free radicals such as O<sub>2</sub><sup>-</sup> or its byproducts have been implicated in the pathogenicity of lung injury produced by activated macrophage or following radiation therapy. The relevance of free radicals in CWP was also suggested by our recent electron spin resonance (ESR) studies wherein a positive correlation was found between the severity of CWP and the concentration of organic free radicals in dry lung tissue of autopsied miners.<sup>(8)</sup> Moreover, three recent papers indicate that mechanical crushing of some coals leads to the formation of organic free radicals<sup>(9-11)</sup> In fact, Artmov and Reznik surmised that these radicals might be related to the pathogenicity of CWP<sup>(9)</sup> However, the authors did not establish any correlation between any property (say, concentration or reactivity) of the radicals and the dust pathogenicity. It was also not shown that dust from freshly crushed coals, termed as "fresh dust" here from now on, was more pathogenic than the same dust kept in air for several days, called "stale dust" here. At about the same time (1982), Retcofsky reported ESR detection of organic free radicals in a dry lung tissue sample of an autopsied coal miner.<sup>(12)</sup> He concluded that the free radicals detected in the lung tissue reflect essentially the presence of dust particles embedded in the tissue and exhibit no characteristic relevant to CWP. However, as mentioned earlier, our own ESR studies of tissue from lungs of autopsied workers who had worked in a variety of mines showed a positive correlation between the severity of CWP and the concentration of organic free radicals in the lung tissue. In order to study systematically the relationship of free radicals in fresh coal dust as well as in lung tissue with CWP, we have carried out the following experiments:

1. We have validated and extended the earlier report<sup>(7,9)</sup> by a detailed ESR spectroscopic analysis of free radicals produced by fracturing of two

# ELECTRON SPIN RESONANCE DETECTION

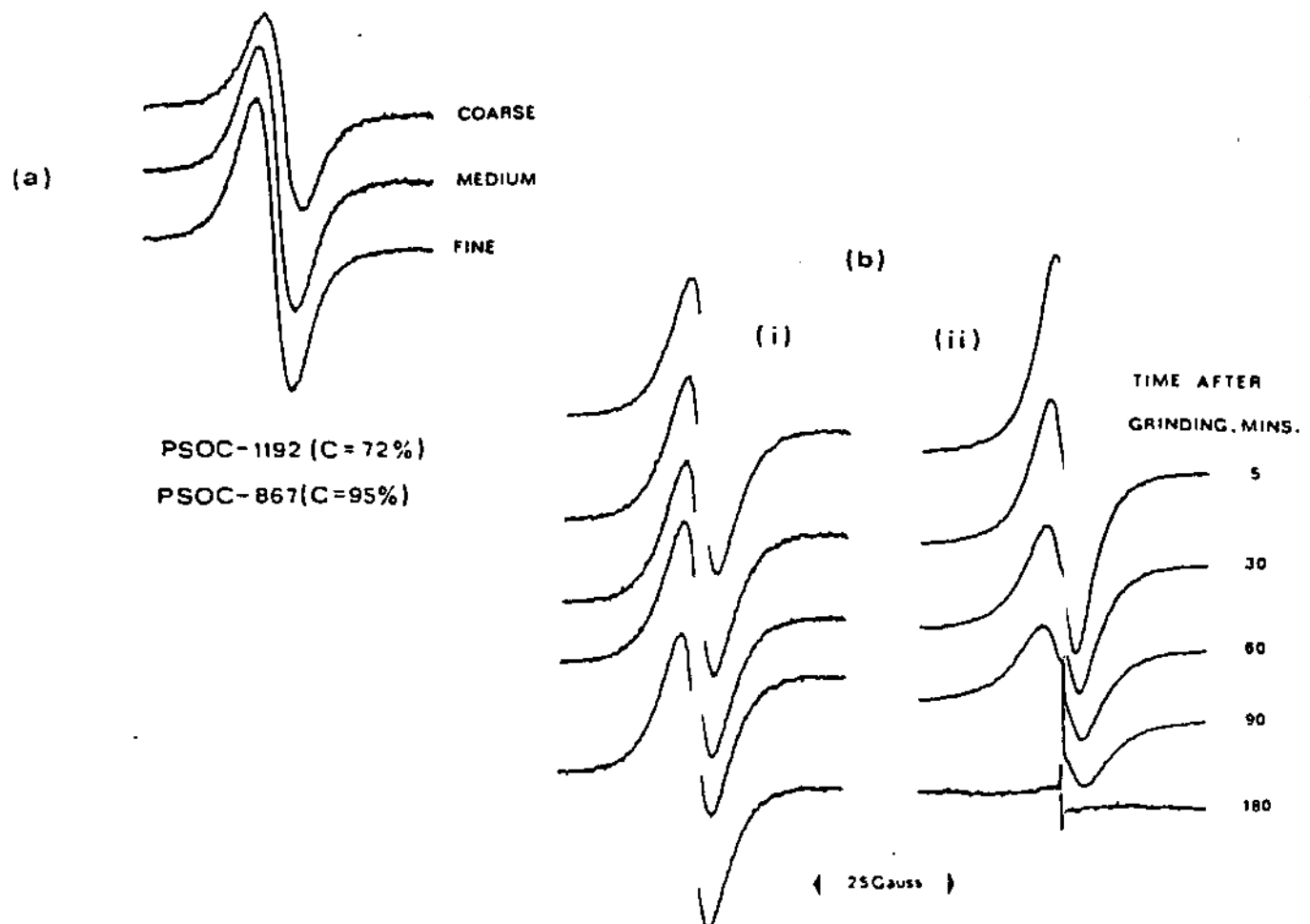


FIGURE 1. (a) Effect of grinding (under nitrogen) on the ESR signal intensity from a PSOC-1192 (bituminous coal); (b) Decay of (free radical) ESR signals after air exposure.

carefully selected U.S. coals under different environmental conditions.

2. We have initiated biochemical studies to determine the relative cytotoxicity of freshly fractured and stale coal dusts.
3. We have measured free radical concentrations in the lungs of autopsied coal miners with varying degrees of CWP. The results of this study are reported separately<sup>(8)</sup>
4. We have examined the production of free radicals in quartz particles ground under nitrogen and in air and measured the radical decay.

## Methodology

Electron spin resonance spectroscopy was used as a technique for the identification and reactivity studies of the free radicals.<sup>(12,13)</sup> The ESR measurements were made with an IBM (model ER200D) ESR spectrometer operative in the X-band (10 GHz) range, and equipped with an Aspect 2000 microcomputer for automatic data acquisition and processing. As usual, the area under the ESR signal was taken to be

proportional to the radical concentration. The two Pennsylvania coals studied here (PSOC-867, an anthracite, and PSOC 1192, a bituminous coal) and their composition data were obtained from the Pennsylvania State University coal data bank. For each ESR study, about 0.200 g of raw coal particles (a few millimeters in size) were outgassed for several hours to a vacuum of about  $10^{-5}$  mm Hg and then crushed in a glove box under dry nitrogen atmosphere so as to exclude oxygen reactions with the free radicals. The coal particles were crushed mechanically (using an agat mortar and pestle) to produce particles from respirable to larger size so as to mimic the situation during coal mining. The same methodology was employed for the quartz studies.

For ESR studies of free radicals in lung tissues of workers diagnosed as having CWP, 10-50 mg of lung tissues were obtained from the National Coal Workers Autopsy study, NIOSH, Morgantown, West Virginia. Samples were selected to represent a wide range of CWP severity. Cytotoxicity studies of fresh and stale coal dust were carried out at NIOSH using sheep red blood cell hemolysis developed by Vallyathan at NIOSH, as described elsewhere.<sup>(14)</sup>

Results and Discussion

Coal Studies

Figure 1 shows typical ESR spectra of the organic free radicals from the two Pennsylvania coals. The signals were assigned to organic free radicals from their similarity to ESR signals from organic radicals in parent coals.<sup>(12,13)</sup> As is well known, the absolute value of area under an ESR peak is proportional to the concentration of the species (radicals here). Thus Figure 1(a) shows the effect of the extent of crushing (as judged visually from the particle size) on the radical concentration for the bituminous coal sample (PSOC 1192, 72% carbon content). Here fine size was found to correspond roughly to the respirable size particles. We note that our grinding procedure is crude, but in this study our aim was to mimick the situation of coal production in a mine. It is seen that grinding produces free radicals. Perhaps an even more significant result was that the radical production was higher in the anthracite coal (PSOC 867 - 95% carbon content) for the same amount of grinding time, as may be seen from the ESR peaks in Figure 1(b). Moreover on exposure

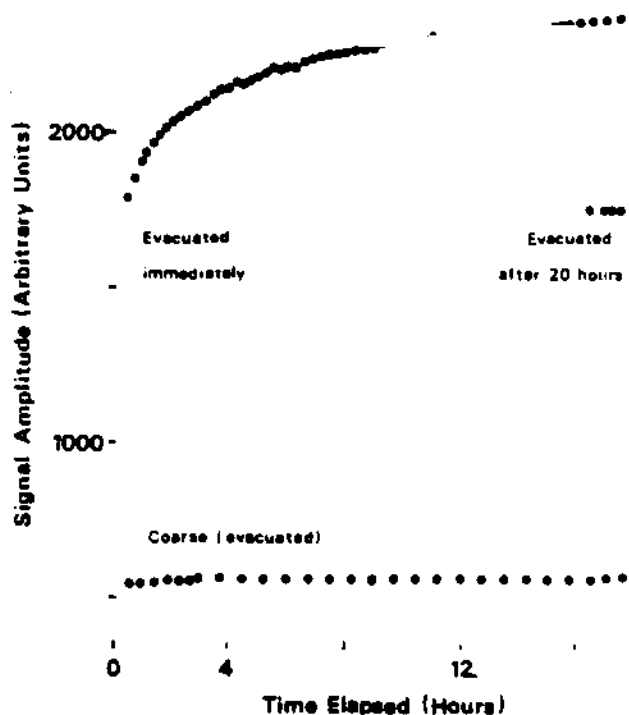


FIGURE 2. Time dependence of the decay of the free radical signals from a bituminous coal (PSOC-1192) crushed under nitrogen and exposed to air.

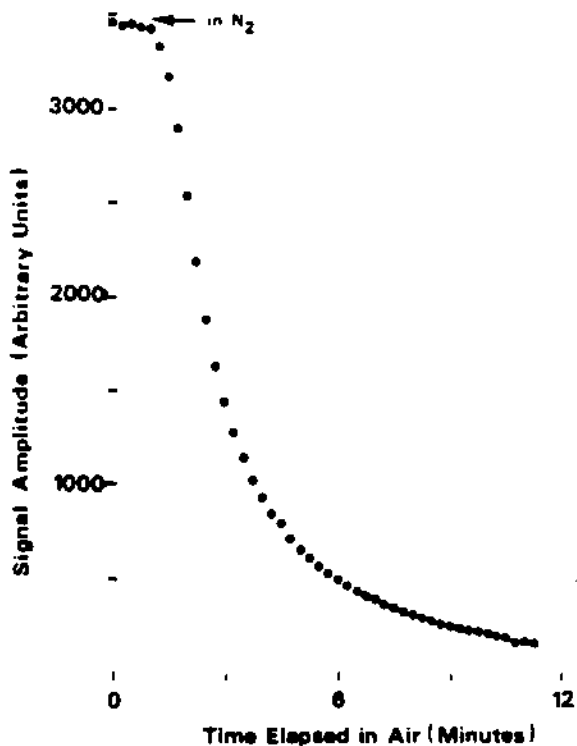


FIGURE 3. Decay pattern of the free radicals in an anthracite (PSOC 867) coal crushed under nitrogen and exposed to air.

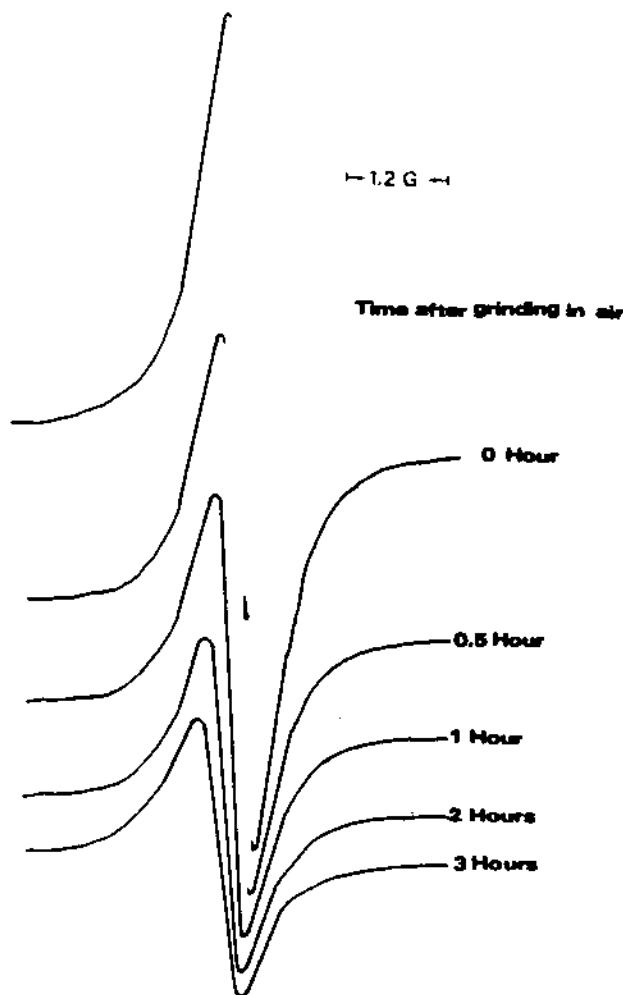


FIGURE 4. Decay pattern of free radicals from the same anthracite coal as in Figure 3 but crushed in air.

to  
(P  
in  
ly  
the  
1(  
for  
W  
ne  
to  
in  
the

FIG

the  
no  
co  
the  
th  
po  
mi  
ta  
ty  
fr  
th  
we  
ar  
th

le:  
of  
PS  
ov  
a  
ca  
ra  
ox

to air the free radicals produced in the anthracite coal (PSOC 867) decay at a much faster rate than those produced in the bituminous coal (PSOC 1192), as deduced qualitatively from the relative decreases with time (after grinding) in the ESR peaks of the two coals, as a function of time (Figure 1(b)). Figures 2 and 3 show these decreases quantitatively for the bituminous and the anthracite samples, respectively. While an accurate comparison of the radical decay rate needs more controlled grinding procedures (which we plan to complete in the future), the preliminary results presented in Figures 2 and 3 clearly show that the decay rate and hence the reactivity (with oxygen) of the free radicals produced in

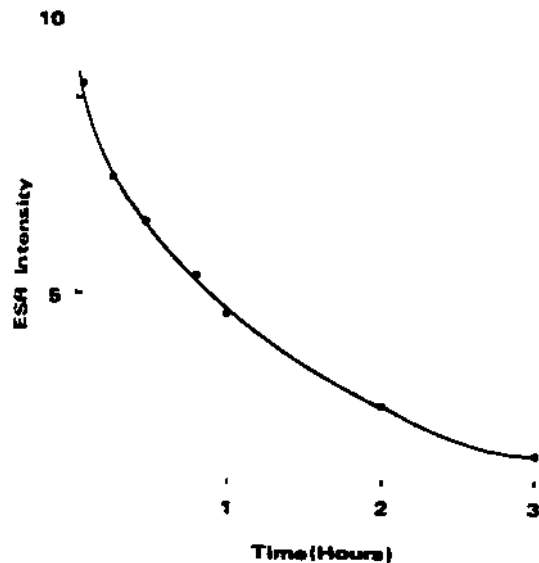


FIGURE 5. Time dependence of the decay of the free radicals in an air-crushed anthracite coal (PSOC-867).

the anthracite coal is about 300 percent higher than that in the bituminous sample. Another significant result to be noted from these figures is that under comparable grinding conditions, the yield of free radicals produced per gram from the anthracite coal is about an order of magnitude higher than from the bituminous coal. Thus for comparable exposures of fresh dust in an anthracite and bituminous coal mine, the anthracite miners would be exposed to dust containing significantly more quantity and also more reactive type of free radicals. If further experiments prove that these free radicals are involved in the mechanism of CWP, then the above results can be taken to provide a new clue to the well known but hitherto not understood observation that anthracite coal mine dust is significantly more pathogenic than bituminous dust.

We have also observed that crushing of coal in air also leads to the production of radicals which decay over a period of several hours. Figure 4 shows typical ESR signals of the PSOC 867 (anthracite) coal crushed in air and the changes over a period of three hours after crushing. Figure 5 shows a graphical representation of time dependence of the radical decay in air, after crushing in air. Again it is clear that the radicals produced decay smoothly by reaction with the oxygen in air.

### Free Radicals in Fresh Quartz Dust

It is known that fracturing of quartz under ultra-high vacuum ( $10^{-10}$  torr) results in the production of silicon-based free radicals.<sup>(15)</sup> These studies were conducted in relationship to the semiconductor-industrial applications. While it has been occasionally mentioned that free radicals on the surface of quartz particles might be relevant to the fibrogenicity of quartz, no systematic ESR measurements of such radicals have been reported, especially as related to the biological activity.<sup>(16)</sup> Our preliminary results are summarized below.

Figure 6 shows typical ESR spectra of quartz ( $\text{SiO}_2$ ) particles ground in air as a function of time after grinding. It is clearly seen that the radical concentration, as measured from the peak-to-peak height of an ESR spectrum, decreases with time as the quartz dust is left exposed to air. Figure 7 shows a plot of the time dependence of the radical concentration decrease. These results are somewhat similar to the radical decay pattern for the organic free radicals in fresh coal dust. Therefore, in this respect coal and quartz exhibit similar surface chemical reactivity.

### Implications to CWP and Silicosis

The above described ESR studies establish that the surfaces of fresh coal as well as quartz contain highly reactive free radical species, and hence the potential for cytotoxicity via chemical reaction (bond formation) with the cell membrane. Preliminary tests carried out using the sheep red-blood cell hemolysis<sup>(7)</sup> procedure indicate fresh coal dust, prepared by crushing of the anthracite (PSOC 867) coal exhibits significantly higher homolytic activity than the same dust left in air for several hours. Since exposure of fresh dust to air causes a decrease in the amount of the free radicals, as well as to a decrease in the cytotoxicity, it is possible that the free radicals do contribute to the coal dust's cytotoxicity. As for quartz, while hemolytic activity has not yet been studied, we have obtained an indirect evidence of the role of free radicals in the quartz's cytotoxicity: the free radical concentration decreases on heating freshly crushed quartz to about  $700^\circ\text{C}$  in a rough proportional manner to the decrease in the cytotoxicity of quartz as reported earlier.

Thus, while much further work remains to be done, the hypothesis that free radicals present in fresh quartz as well as coal dust contribute to their cytotoxicity seems to have some experimental basis.

### Acknowledgment

This research has been supported by the Department of the Interior's Mineral Institute program administered by the Bureau of Mines through the Generic Mineral Technology Center for Respirable Dust under grant number G1135142.

### References

1. Reisner, M.T.R. and K. Robock: Results in Epidemiological, Mineralogical and Cytotoxicological Studies of Pathogenicity of

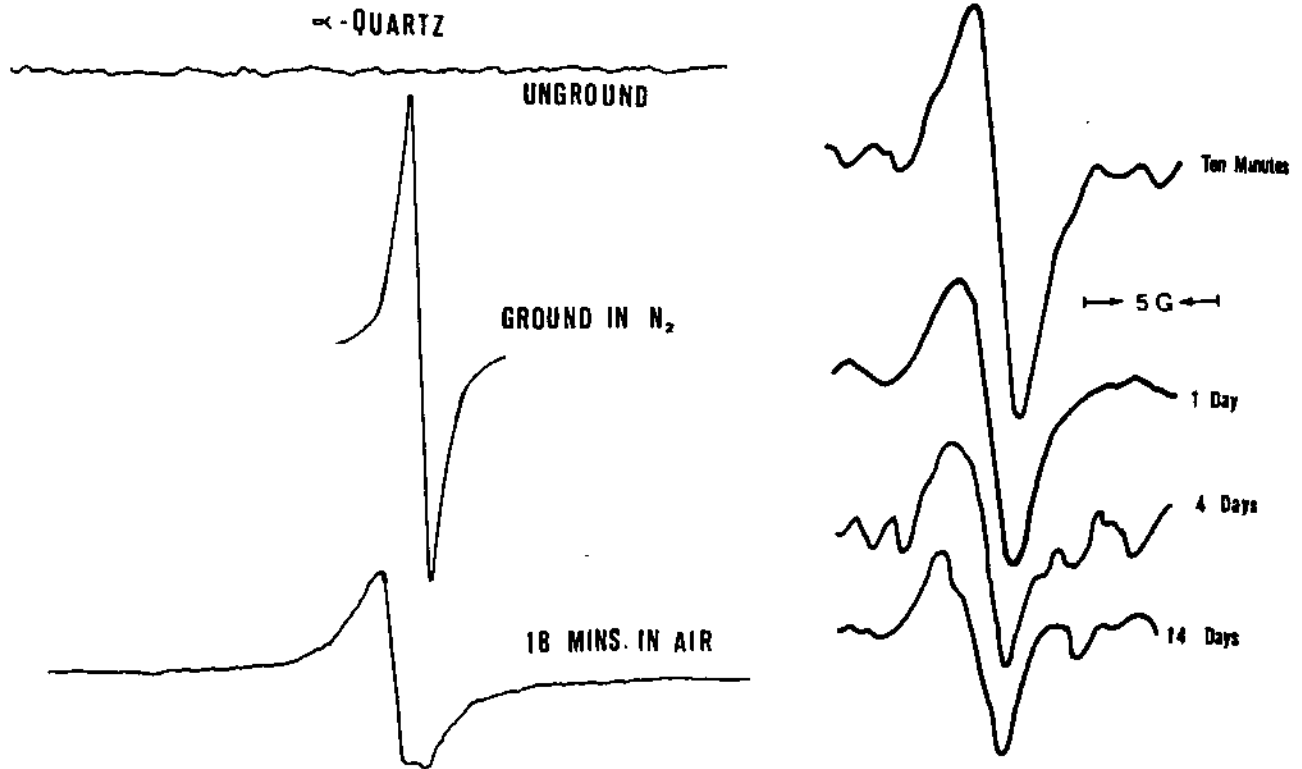


FIGURE 6. Typical ESR spectra of quartz particles crushed in air.

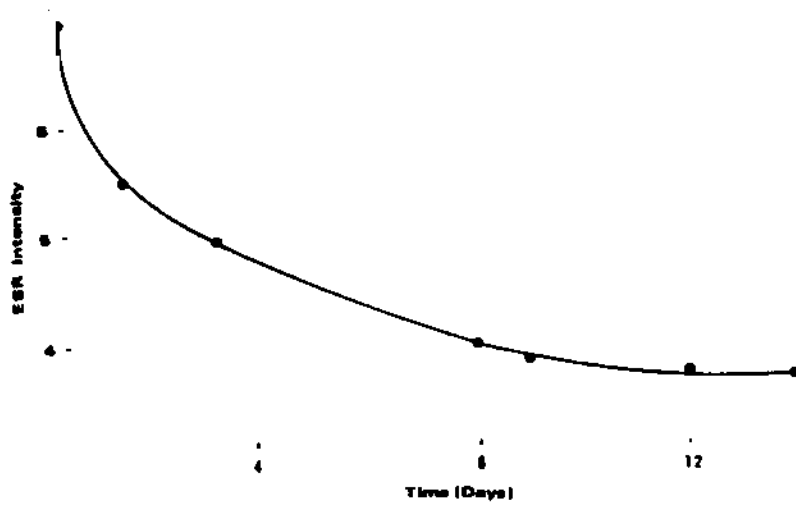


FIGURE 7. Time dependence of the decay of the free radicals in an air-crushed quartz sample.

- Coal-Mine Dusts. *Inhaled Particles* 4, p. 703 (1977).
2. Hurley, J.F. et al: *Simple Pneumoconiosis and Exposure to Respirable Dust: Relationships from Twenty-five Years' Research at Ten British Coal Mines*. Institute of Occupational Medicine Report, No. TM/79/13 (1979).
  3. Christian, R.T., J.B. Nelson, T.E. Cady et al: Coal Workers' Pneumoconiosis: *In Vitro* Study of the Chemical Composition and Particle Size as Causes of the Toxic Effects of Coal. *Environ. Res.* 20:358-365 (1979).
  4. Christian, R.T. and J. Nelson: Coal: Response of Cultured Mammalian Cells Corresponds to the Incidence of Coal Workers' Pneumoconiosis. *Environ. Res.* 15:232-241 (1978).
  5. Hatch, G.E., D.E. Gardener and D.B. Menzel: Stimulation of Oxidant Production in Alveolar Macrophages by Pollutant and Latex Particles. *Environ. Res.* 23:121-136 (1980).
  6. Heppleston, A.G.: Changes in the Lungs of Rabbits and Ponies Inhaling Coal Dust Underground. *J. Path. Bact.* 67:349-359 (1958).
  7. Dalal, N.S., M.M. Suryan, B. Jafari et al: Detection of Organic Free Radicals in Fresh Coal Dust and Its Implications to Pneumoconiosis. Presented at the Sixth International Symposium on Inhaled Particles, Cambridge, England (1985).
  8. Jafari, B., N.S. Dalal, V. Vallyathan and F.H.Y. Green: Detection of Organic Free Radicals in Coal-Dust Exposed Lung Tissue and Correlations with Their Histopathological Parameters. *Respirable Dust in the Mineral Industries: Health Effects, Characterization, and Control*, pp. XXXXX. Cincinnati, OH (1987).
  9. Artemov, A.V. and L.A. Reznik: Questions on the Methodology of Biological Investigations of the Fibrogenicity of Coal Dust. *Gib. Tr. Zabol.* 2:51-55 (1980).
  10. Lebedev, V.V., T.M. Khrenkova and M.L. Goldenko: The Formation of Paramagnetic Centers During Crushing of Coal. *Sol. Fuels Chem.* 12:117-119 (1978), and references to earlier Russian literature cited therein.
  11. Duliba, E.P. and R.B. Clarkson: A Magnetic Resonance Study of Native and Modified Illinois Coal. *Proc. Nato Summer School on Magnetic Resonance of Fossil Fuels*, a preprint (1984).
  12. Retcofsky, H.L.: Magnetic Resonance Studies of Coal. *Coal Science* 1:43-82 (1982).
  13. Petrakis, L. and D.W. Grandy: Free Radicals in Coals and Synthetic Fuels. Chap. III and IV. Elsevier, Amsterdam, (1983).
  14. See, for example, Wallace, W.E., V. Vallyathan, M.J. Keane, V. Robinson: *J. Toxic. Env. Health* 16:415-424 (1985).
  15. Hochstrasser, G. and J.F. Antonini: Surface States of Pristine Silica Surfaces. *J. Surface Sci.* 32:644-664 (1972).
  16. Gabar, S. and Z. Anca: Effect of Silica on Lipid Peroxidation in the Red Cells. *Int. Arch Arbeitsmed.* 32:327-332 (1974).

# Detection of Organic Free Radicals in Coal-dust Exposed Lung Tissue and Correlations with Their Histopathological Parameters

B. Jafari<sup>1</sup>, N. S. Dalal<sup>1</sup>, V. Vallyathan<sup>2</sup>  
and F. Y. H. Green<sup>2</sup>

<sup>1</sup>Chemistry Department, West Virginia University

<sup>2</sup>National Institute of Occupational Safety and Health,  
Morgantown, West Virginia

Using electron spin resonance (ESR) spectroscopy we have carried out a systematic study of the measurement of concentrations of organic free radicals in freeze-dried lung tissue. Sixty-six tissue samples were obtained from the National Coal Workers' Autopsy Study (NCWAS). The samples were characterized in terms of the concentration per gram of the free radicals, and examined in relationship to the histopathological parameters such as age, numbers of years in the mining atmosphere, the degree of disease, and smoking history. Preliminary results indicate a positive correlation between the free radicals in the lung tissue and the severity of pneumoconiosis.

## Introduction

This paper summarizes our electron spin resonance (ESR) measurements of the concentration of organic free radicals in the freeze-dried lung tissue of autopsied coal miners. This work was undertaken because it is well known that most coals contain carbon-centered organic free radicals,<sup>(1,2)</sup> and recent studies from our laboratories indicated that reactive free radicals might play a role in the biochemical mechanism of coal workers' pneumoconiosis (CWP).<sup>(3)</sup> Thus we obtained 144 lung-tissue samples from the National Institute for Occupational Safety and Health (NIOSH) in Morgantown. The samples came from the data bank of the National Coal Workers' Autopsy Study (NCWAS). This selection was unique because fairly detailed histopathological information was available for each sample.

Other recent studies in this field are those of Ohta *et al.*<sup>(4)</sup> who conducted ESR measurements on black dust deposited in autopsied human lungs, but no coal miner was included therein. Earlier Retcofsky<sup>(2)</sup> had examined one lung-tissue sample via ESR spectroscopy and had concluded that the free radicals in the lung tissue reflected simply the fusain (narrow component) ESR signals. The present study was thus undertaken to complement the earlier work<sup>(2-4)</sup> and the results indicate a positive correlation with the disease severity fairly strongly.

## Methodology

ESR measurements were made with an X-band, IBM-Bruker ER 200D, ESR spectrometer in conjunction with an Aspect 2000 microcomputer. The lung tissue samples were all used as thin slices, as received from NIOSH, and inserted into the microwave absorption cell (cavity) of the ESR Spectrometer using quartz sample tubes. Detailed ESR measurements were made at room temperature on all 144 samples, in a blind study. Of these 66 samples were used for statistical analysis since detailed histopathological data were available only for these samples from NIOSH. The average age was 55 +/- 8 years at time of death, with an average underground mining history of 31 +/- 13 years. Among these 94 percent were smokers and 6 percent non-smokers.

## Results

Figure 1 shows typical ESR spectra from two lung-tissue samples, Figure 1(a) is for a sample with only a preliminary coal dust exposure whereas 1(b) is that for a heavily-exposed tissue. These spectra were obtained over a wide range of magnetic field in order to measure both the free radicals and any paramagnetic transition-metal ions, such as Fe<sup>3+</sup>, as marked in the figure. The free radical spectra occur only in a narrow magnetic field range around 3400 G at X-band, as indicated by arrowheads in the figure. Since the focus of the present study was only the free radicals and not metal ions, detailed measurements were made only on the free radical features.

As is well known the concentration of the free radicals is proportional to the area under the free radical ESR signal.<sup>(1,2)</sup> The free radical concentration was thus measured per gram of the tissue sample used. Table I gives the details of the free radical concentration along with the histopathological data on the specimen studied. Here no disease refers to coal workers who had been classified to have no CWP. Macular refers to cases of simple pneumoconiosis whereas progressive massive fibrosis (PMF) refers to the

TABLE I  
Concentrations of Free Radicals in Coal Miners' Lungs With and Without Disease

Number of Cases	Age	Mining Tenure	Smoking History	Type of Disease	Free Radical Conc./GM
22	63 +/- 7	29 +/- 15	40 +/- 26	No disease	0.42 +/- 0.72
15	74 +/- 8	26 +/- 14	33 +/- 20	Macular disease	0.85 +/- 0.58
10	70 +/- 8	33 +/- 16	30 +/- 26	Progressive massive fibrosis	1.27 +/- 1.04
4	71 +/- 6	41 +/- 5	non-smokers	Progressive massive fibrosis	4.50 +/- 2.90
11	65 +/- 10	24 +/- 16	28 +/- 13	Cancer of the lung	3.76 +/- 2.23

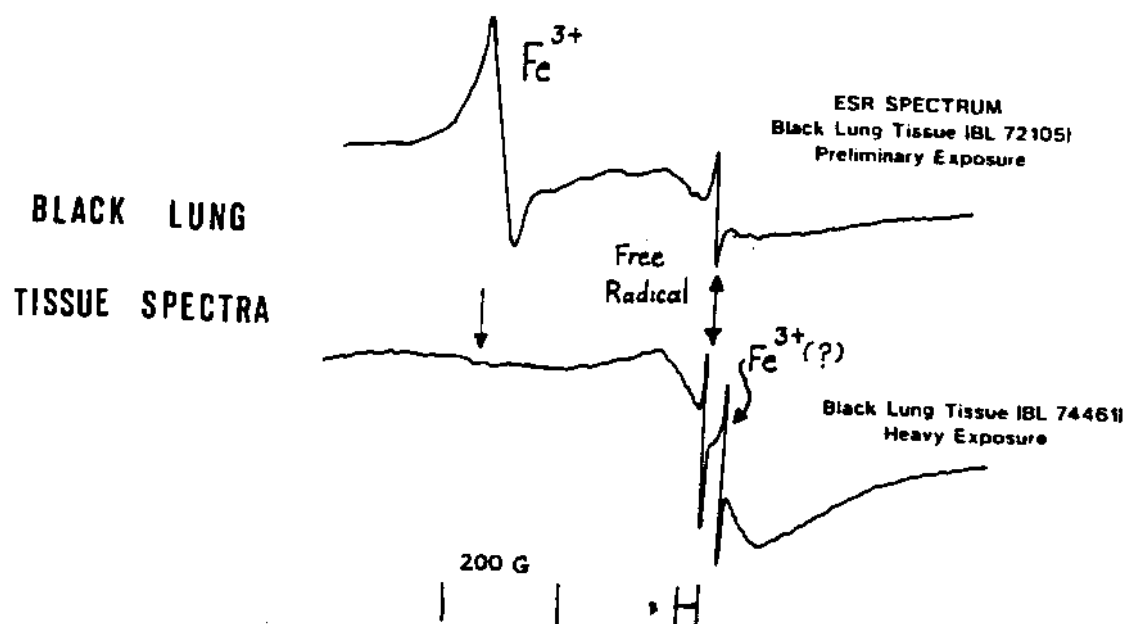


FIGURE 1. Typical ESR spectra of freeze-dried lung tissue (a) with preliminary exposure (b) with heavy exposure.

most advanced stage of the disease. It is seen that the free-radical concentration is the highest in samples with PMF and the lowest in those with "no disease." A graphical representation of the findings is given in Figure 2. Here the horizontal scale used is from zero to 14 as devised by NIOSH; zero corresponding to no disease and 14 to the highest PMF. It is again seen that the free radical concentration in the lung tissue increases sharply with the severity of CWP.

The results of Table I and Figure 2 also show that, for roughly the same degree of CWP, the free radical concentration is higher in the cases of non-smokers than smokers. This was surprising at first because cigarette smoke itself is known to contain organic free radicals.<sup>(5)</sup> Hence if there were no reaction between the free radicals in the coal dust and those in cigarette smoke, then one might expect that the total free radical concentration to be higher in the smokers, contrary to our findings. Thus while at present the nature of interac-

tions between the various types of free radicals in the lung tissue is not clear, it is apparent that these radicals are not inert.

## Conclusions

Preliminary conclusions from this study is that the amount of stable, carbon-centered free radicals in autopsied lung-tissue increases with the severity of CWP. We are in the process of comparing ESR signals from coal dust obtained from the same mines, to examine whether or not the free radicals in the lung tissue are the same as those found in the specific coal mine dust. It is hoped that the results would provide further clues to reactivity of the free radicals in the coal mine dust with lung tissue and cigarette smoke and thereby the pathogenicity of CWP.



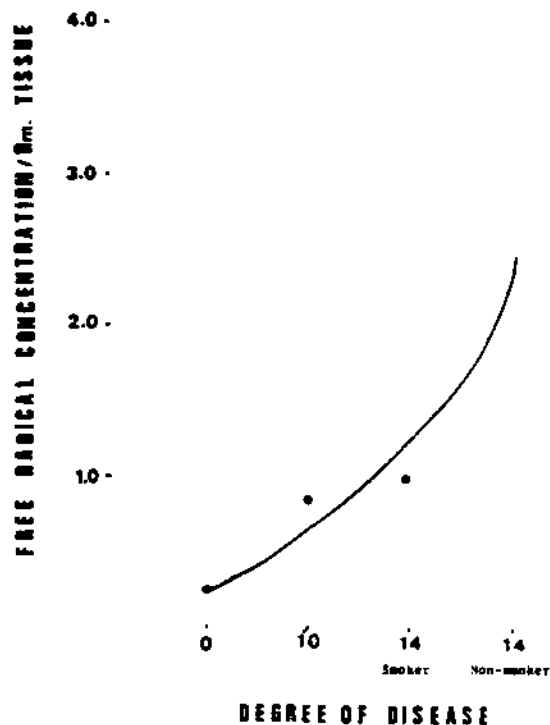


FIGURE 2. Correlation between the degree of CWP and the measured organic free radical concentration.

## Acknowledgment

This research has been supported by the Department of the Interior's Mineral Institute program administered by the Bureau of Mines through the Generic Mineral Technology Center for Respirable Dust under grant number G1135142.

## References

1. Petrakis, L. and D.W. Grandy: *Free Radicals in Coal and Fossil Fuels*. Elsevier (1983).
2. Retkofsky, H.L.: Magnetic Resonance Studies of Coal. *Coal Science* 1:43-82 (1982).
3. Dalal, N., M.M. Suryan, B. Jafari et al: *Detection of Reactive Free Radicals in Fresh Coal Mine Dust and Its Implications to Pneumoconiosis*. Paper presented at the Sixth International Symposium on Inhaled Particles. Cambridge, England (1985).
4. Ohta, Y., H. Shiraishi and Y. Tabata: An Electron Spin Resonance Study of Free Radicals in Black Dust Deposited in Human Lungs. *Arch. Environ. Health* 40:279-282 (1985).
5. Pryor, W.A., B.J. Hales, P. Premovic and D. Church: The Radicals in Cigarette Tars: Their Nature and Suggested Physiological Implications. *Science* 220:425-427 (1983).

# **Cascade Impactor Sampling & Data Analysis**

**edited by J. P. Lodge, Jr., Ph.D. and T. L. Chan, Ph.D.**

**ISBN #-932627-24-2**

**Copyright 1986**

**American Industrial Hygiene Association, 475 Wolf Ledges Parkway, Akron, OH 44311-1087**

# Theory and Design Guidelines - Chapter 4

V. A. Marple and K. L. Rubow

Particle Dispersion Laboratory  
Mechanical Engineering Department, University  
of Minnesota

## 4.1 Introduction

In previous chapters impactors have been described as useful instruments for classifying particles by their aerodynamic diameters and for measuring particle size distributions. These impactors can be used most reliably if the user has some understanding as to how the impactor classifies particles and what parameters are important in this classification process. This understanding can best be obtained by a theoretical inspection of inertial principles.

This chapter reviews the most recent theoretical impactor work and the latest theoretical efficiency curves. Procedures are then given for using these efficiency curves in the design and evaluation of cascade impactors. Finally, several examples are given comparing theoretical and experimental efficiency curves, pointing out when the theory can be used with great confidence and when the theory should be used only as a guideline.

Due to the rather simple principle of operation of an inertial impactor (i.e., the impingement of a jet of particle-laden air on a flat plate) the impactor readily lends itself to theoretical analysis. Three notable works in the early 1950's were those of Davies and Aylward (1951), Davies *et al.* (1951), and Ranz and Wong (1952).

Davies and Aylward (1951) used a method of conformal mapping to obtain an analytical solution to Euler's equation for the flow of a frictionless fluid through a rectangular impactor. Numerical calculations were then carried out whereby the equations of motion of the particles were solved in a stepwise manner, leading to a determination of the efficiency curves. Since this theory assumed potential flow, the effect of Reynolds numbers on the characteristics of the impactor could not be determined.

Ranz and Wong (1952) used an approximate flow field to calculate the efficiency of both round and rectangular nozzle impactors. In the vicinity of the stagnation point, the flow field was assumed to be that of frictionless stagnation flow. Here, the resulting equation of motion for the particles was found to be in a form similar to equations for free vibration with viscous damping. Therefore, the known solutions of the vibration equations were applied directly to the problem and the efficiency curves calculated. This solution technique, however, could not take into account the various geometric variations such as the jet-to-plate distance in the determination of the efficiency curves.

The work of Ranz and Wong (1952) was later modified by Mercer and Chow (1968) and Mercer and Stafford (1969) so that the rather simple flow fields of Ranz and Wong (1952) could be used to account for various jet-to-plate distances. The same techniques, however, were used to determine the impactor collection efficiency curves.

With the advent of high-speed computers and the development of numerical analysis techniques in the late 1960's it was possible to perform a detailed study of the flow fields and particle trajectories within impactors (Marple, 1970; Marple *et al.*, 1974a and 1974b; Marple and Liu, 1974; Marple and Liu, 1975). This not only resulted in obtaining theoretical efficiency curves as a function of the geometric parameters such as jet-to-plate distance and throat length, and fluid

mechanic parameters such as nozzle Reynolds number, but also a good insight into how an impactor must be designed and used. This theory was further updated in the early 1980's (Rader and Marple, 1985) to include second order effects such as ultra-Stokesian drag on the particles and particle interception at the impaction plate.

#### 4.2 Theoretical Collection Efficiency Curves

In the first comprehensive theoretical work utilizing high speed computers, the impactor efficiency curves were determined by numerical analysis techniques (Marple, 1970). This work, as well as that of Rader and Marple (1985), is for single-jet impactors. For the case of multiple-jet impactor stages, the jet-to-jet interaction may affect the cutoff characteristics.

The technique included the finite difference solution of the Navier-Stokes equations to determine the flow field (Marple, *et al.* 1974 a, b) and the subsequent calculation of particle trajectories in the flow field by numerically integrating the particles' equations of motion (Marple and Liu, 1974). This method was applied to the two-dimensional geometries of round (circular jet with diameter  $W$ ) and rectangular (rectangular slit of length  $L$  much greater than the nozzle width  $W$ ) impactors. The study determined the collection efficiency curves for both nozzle configurations as the dimensionless parameters of jet Reynolds number,  $Re$ , jet-to-plate distance,  $S/W$ , and nozzle throat length,  $T/W$ , were varied. Results of that parameteric study are presented in Figure 1 where the values of  $Re$ ,  $S/W$  and  $T/W$  are parameters. The symbols  $W$ ,  $S$  and  $T$  indicate the jet width or diameter, jet-to-plate distance, and nozzle throat length, respectively, as indicated in Figure 2.

In Figure 2 the particle size on the abscissa is expressed in dimensionless form as the square root of the Stokes number,  $\sqrt{St}$ , defined as:

$$\sqrt{St} = \sqrt{\frac{\rho_p V_o C D_p^2}{9\mu W}} \quad (1)$$

where  $\rho_p$  is the particle density,  $V_o$  is the average air velocity in the nozzle throat,  $C$  is the slip correction,  $D_p$  is the particle diameter,  $\mu$  is the fluid viscosity, and  $W$  is the nozzle diameter (round) or nozzle width (rectangular).

The Reynolds number,  $Re$ , is expressed as:

$$Re = \frac{\rho W V_o}{\mu} \quad (\text{round})$$

and

$$Re = \frac{2\rho W V_o}{\mu} \quad (\text{rectangular}) \quad (2)$$

where  $\rho$  is the air density.

The Reynolds number can also be expressed in terms of the air mass flow rate,  $\dot{m}$ , passing through the impactor as follows

$$Re = \frac{\dot{m} W}{\mu} \quad (\text{round})$$

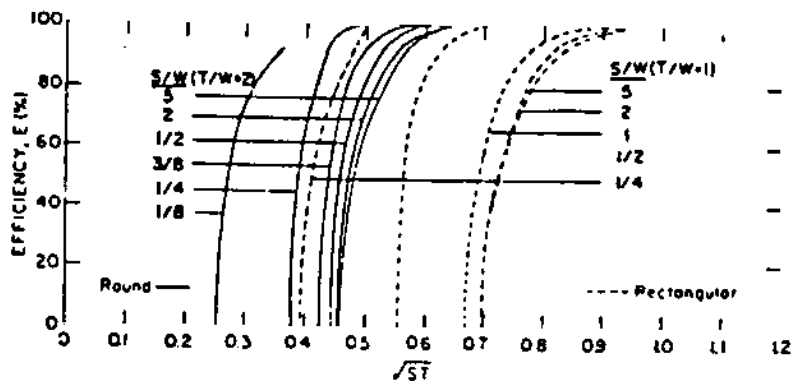
and

$$Re = \frac{2\dot{m} W}{\mu} \quad (\text{rectangular}) \quad (3)$$

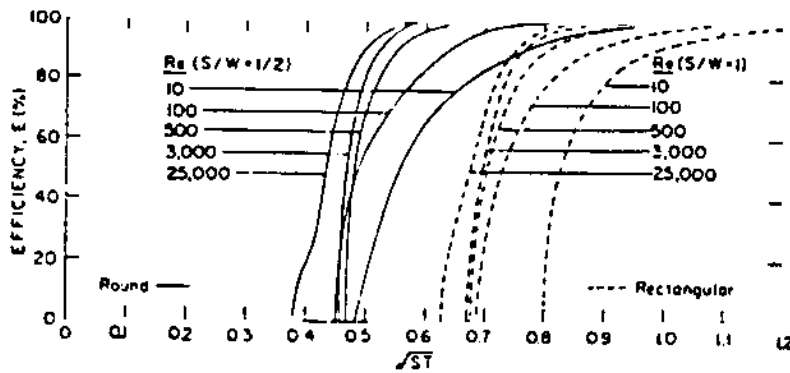
This form of the Reynolds number is advantageous since  $\dot{m}$  is a constant for all stages of the impactor.

It can be seen from the calculated efficiency curves in Figure 2 that the cutoff characteristics are good for efficiencies less than about 0.80. Above this value the cutoff characteristics are not

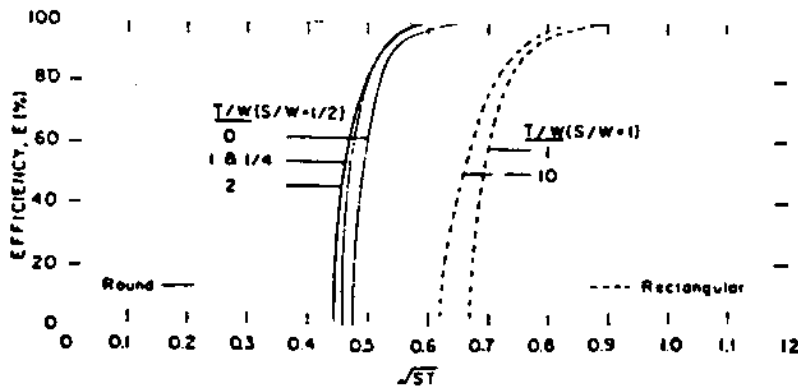
# THE RESPIRABLE DUST CENTER



(a) EFFECT OF JET TO PLATE DISTANCE ( $Re=3,000$ )



(b) EFFECT OF JET REYNOLDS NUMBER ( $T/W=1$ )



(c) EFFECT OF THROAT LENGTH ( $Re=3,000$ )

Figure 1. Original impactor efficiency curves for rectangular and round impactors showing the effect of jet-to-plate distance  $S$ , jet Reynolds number  $Re$ , and throat length  $T$  (from Marple, 1970).

as sharp due to the air and particles moving at lower velocities in the fluid boundary layer near the nozzle wall than in the central portion of the jet. Since the particle velocities are lower in this region, the particles must be larger to be collected, causing the nonsharp collection characteristics in the upper portion of the curves. A more detailed discussion of this phenomenon has been presented elsewhere (Marple and Liu, 1975).

Comparisons of the theoretical efficiency curves in Figure 2 to experimentally determined efficiency curves have indicated good agreement in most cases, if the nozzle configuration is similar to that shown in Figure 1. Differences between experimental and theoretical efficiency curves have primarily been in the shape of the efficiency curves. For example, in the portion of

## THEORY AND DESIGN GUIDELINES

the curve represented by efficiencies less than about 0.10, the experimental curves have tended to flare to the left (small values of  $\sqrt{St}$ ) while theoretical curves (Figure 2) tend to show sharp cutoff characteristics in this region. Thus, the actual experimental curve is "S" shaped while the theory predicted only the upper portion of the "S" curve. In addition the experimental efficiency curves have, in general, been steeper (sharper cutoff characteristics) than the theoretical curves shown in Figure 2.

In an attempt to define theoretical curves that are even in better agreement with experimental curves than the theory described above (steeper "S" shaped curves), the theoretical technique was revised in three areas and the efficiency curves recalculated (Rader and Marple, 1985). The first area of improvement was to make the grid finer over the area for which the Navier-Stokes equations were solved. This allowed for the flow field to be described more accurately. This grid refinement was made possible by the higher-speed and larger-capacity computers available now compared with those used in the earlier study. The second area of improvement was employment of a more accurate particle drag coefficient in the particle equation of motion. Finally, the third area was inclusion of the effect of the interception distance of the particle as it approached the impaction plate. This differs from the previous theoretical technique where the particles were assumed to be represented as point masses. The effect of these three revisions in the theoretical technique is described in detail by Rader and Marple (1985) and will not be described here. However, for most of the efficiency curves the effects were small.

The efficiency curves calculated by the revised theoretical technique are shown in Figure 3. These curves are too new to have had many comparisons with experimental curves; however, the agreement should be better. Comparison of the curves in Figures 2 and 3 will generally show that the efficiency curves in Figure 3 are steeper and have the characteristic S-shape found in experiments. Therefore, this most recent theory appears to be an improvement.

In the remainder of this chapter both sets of efficiency curves will be used. The original set (Figure 2) is presented since they have been in use for many years and many impactor designs, comparisons between theory and experiments, and impactor developments have been based upon these curves. The more recent curves, shown in Figure 3, are presented since they include more of the second order effects and should be the most accurate theoretical curves presently available. It is recommended that any future work be based upon the theoretical curves in Figure 3.

Although the revised theoretical curves in Figure 3 are to replace the original curves in Figure 2 that have been used for about 15 years, the basic guidelines have not changed, since

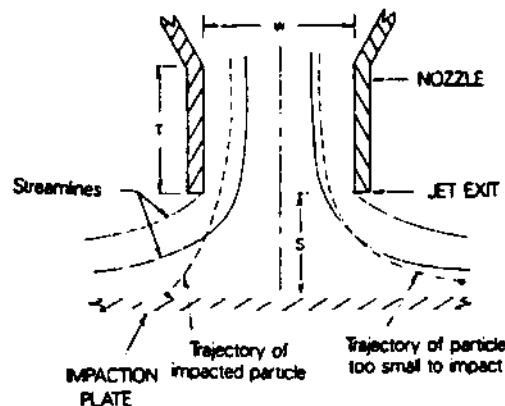


Figure 2. Schematic diagram of a typical impaction stage showing streamlines and particle trajectories.

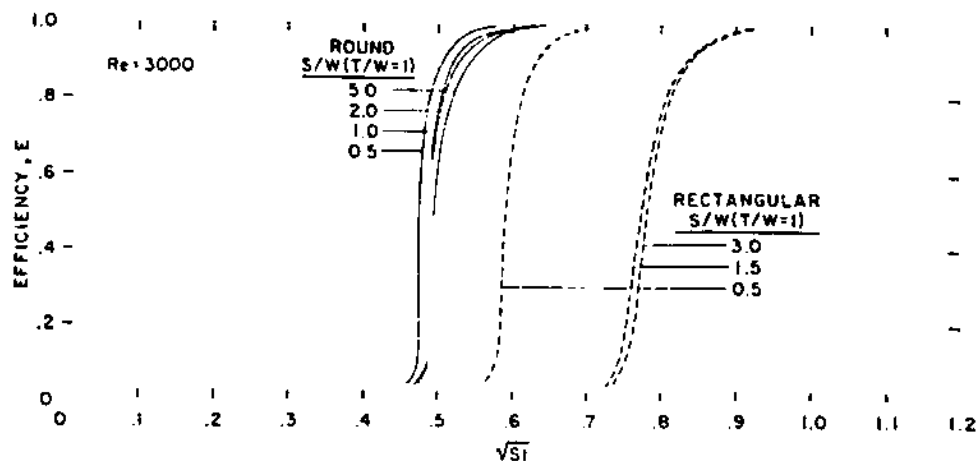
## THE RESPIRABLE DUST CENTER

the differences in the two sets of curves are slight in most cases. For example, both sets of curves indicate that  $S/W$  values should be greater than 1.0 for round impactors and 1.5 for rectangular impactors to avoid small changes in  $S/W$  radically changing  $\sqrt{St_{50}}$ , the Stokes number corresponding to 50% collection efficiency, and that the Reynolds number should be between about 500 and 3000 for both round and rectangular impactors to achieve efficiency curves with sharp cuts.

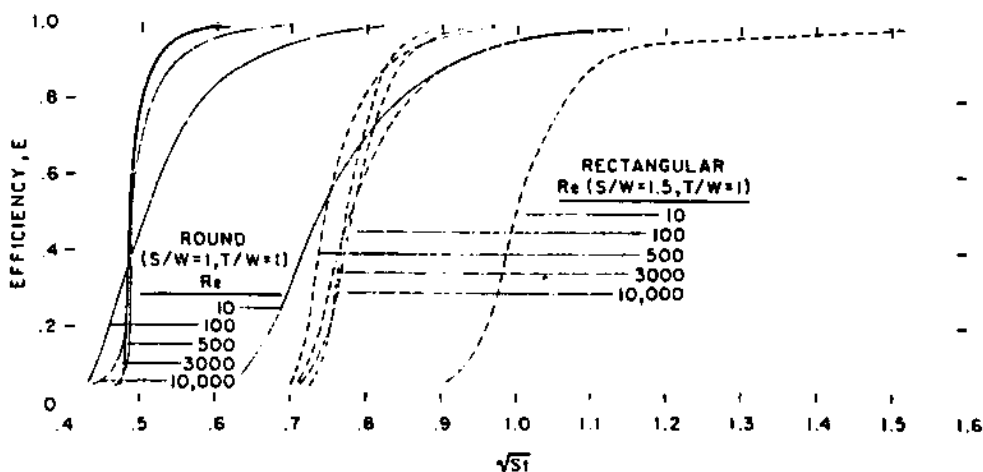
### 4.3 Slip Correction Considerations

In solving the Stokes number equation (equation 1) for the value of the particle diameter, a difficulty arises since the slip correction  $C$  is also a function of the particle diameter:

$$C = 1 + 1.257 \frac{2\lambda}{D_p} + 0.40 \frac{2\lambda}{D_p} \exp\left(-1.10 \frac{D_p}{2\lambda}\right) \quad (4)$$



(a) EFFECT OF JET TO PLATE DISTANCE ( $Re = 3000$ )



(b) EFFECT OF JET REYNOLDS NUMBER

Figure 3. Revised impactor efficiency curves for rectangular and round impactors showing effects of jet-to-plate distance  $S$ , and jet Reynolds number  $Re$  (from Rader and Marple, 1985).

where  $\lambda$  is the mean free path of the air molecules (Davies, 1945). Therefore, the solution of equation 1 for particle diameter normally is a value for  $\sqrt{C}D_p$  from which  $D_p$  must subsequently be solved. The value for the mean free path of the air molecules is taken as  $0.66 \times 10^{-5}$  cm at normal temperature of 20°C and pressure of 1 atm (101.3 kPa).

Although the mean free path is a function of both pressure and temperature, in most cases only the variation in the pressure as the aerosol passes through a cascade impactor must be considered.

The temperature is usually relatively constant and not far removed from the absolute normal temperature. Therefore, since the mean free path is inversely proportional to the pressure, it is possible to express the mean free path at a normal temperature of 20°C as:

$$\lambda = 0.66 \times 10^{-5}/P \quad (5)$$

where  $\lambda$  and  $P$  are in units of centimeters and atmospheres, respectively. The slip correction can now be expressed as:

$$C = 1 + \frac{1.659 \times 10^{-5}}{D_p P} + \frac{5.28 \times 10^{-6}}{D_p P} \exp(-83,300 D_p P) \quad (6)$$

One method for obtaining  $D_p$  when the value of  $\sqrt{C}D_p$  is known is by iteration. With this technique a value for  $D_p$  is selected,  $C$  calculated from equation 4 and then the value of  $\sqrt{C}D_p$  compared to the known value from equation 1. Next a new value of  $D_p$  is selected and the process repeated. This continues until the value of  $D_p$  has been found.

A more straightforward method of obtaining  $D_p$  from equation 6 is to express  $\sqrt{C}D_p P$  as a function of  $D_p P$  (Marple, 1986). This is possible since  $C$  is a function of  $D_p P$  (equation 6). By plotting the relationship of  $\sqrt{C}D_p P$  versus  $D_p P$  as shown in Figure 4, it is quite easy to obtain  $D_p$  when  $\sqrt{C}D_p$  is known. This is done by multiplying the known value of  $\sqrt{C}D_p$  by the pressure  $P$  in atmospheres. From Figure 4 the corresponding value  $D_p P$  can be found on the abscissa. Division of this value of  $D_p P$  by  $P$  gives the value of  $D_p$ .

The value of  $C$  versus  $D_p P$  from equation 6 is also shown in Figure 4. This indicates that for values of  $D_p P$  greater than 10  $\mu\text{m}$ -atmospheres the value of  $C$  is unity and this solution technique need not be used.

One final use of Figure 4 is the determination of the aerodynamic diameter  $D_w$  (diameter of a unit density sphere with same settling velocity) when the diameter of a particle  $D_p$  of non-unit density is known. The governing relationship is:

$$\sqrt{\rho_p} \sqrt{C_{D_w}} D_w = \sqrt{\rho_p} \sqrt{C_{D_p}} D_p \quad (7)$$

when  $\rho_p = 1 \text{ g/cm}^3$ . If  $D_p$  and  $\rho_p$  are large enough so that  $D_p$  and  $D_w$  are in the regime where  $C_{D_w}$  and  $C_{D_p}$  are unity then:

$$D_w = \sqrt{\rho_p/\rho_p} D_p \quad (8)$$

However, if the  $C$ 's are greater than unity, then Figure 4 can be used by multiplying both sides of equation 7 by the pressure  $P$ :

$$\sqrt{\rho_p} \sqrt{C_{D_w}} D_w P = \sqrt{\rho_p} \sqrt{C_{D_p}} D_p P \quad (9)$$

As illustrated in the insert in Figure 4, the procedure for finding  $D_w$  is to first multiply  $D_p$  by  $P$  and find  $\sqrt{C_{D_p}} D_p P$ . Multiply this value by  $\sqrt{\rho_p}$ , the result of which is equal to  $\sqrt{C_{D_w}} D_w P$ , since  $\rho_p = 1$ . The value of  $D_w P$  can now be found from Figure 4 and the division by  $P$  gives  $D_w$ . If the value of  $D_w$  is known,  $D_p$  can be found by simply reversing the above procedure.

#### 4.4 Importance of the Flow Field

Since impactors collect particles by making use of the particles' inertial properties to move the particles through the air streamlines onto the impaction plate, the fluid flow field within an impactor is very important. For example, Marple and Liu (1974) showed that impactors with sharp collection efficiency curves can be obtained if the velocity profiles at the nozzle exit are uniform across the nozzle. The theoretical analysis, resulting in the efficiency curves in Figures 2 and 3, indicate that the two parameters of primary importance in controlling the flow field are the impactor configuration and the Reynolds number of the fluid at the nozzle.

Basically there is not much that can be done with the configuration to achieve uniform flow at the nozzle exit with the exception of controlling the jet-to-plate distance. We have already shown that the  $S/W$  value should be greater than 1.0 and 1.5 for round and rectangular



# THE RESPIRABLE DUST CENTER

impactors, respectively, to avoid sizable changes in particle cutoff size as a result of small changes in jet-to-plate distance.

The Reynolds number of the fluid at the nozzle throat, however, is very important in achieving a uniform velocity at the nozzle exit. If the Reynolds number is too low, a large viscous boundary layer exists at the nozzle wall and the velocity profile becomes parabolic. Smaller particles are collected from the center of the nozzle where the fluid velocity is higher than near the wall where the velocity is low. This leads to a particle collection efficiency curve that has poor sharpness-of-cut characteristics as shown in Figure 3 for low Reynolds numbers.

Marple and Willeke (1976) investigated controlling the Reynolds number by controlling the number of nozzles used per stage of the impactor. This resulted in the development of a set of design curves for both round and rectangular impactors shown in Figures 5 and 6.

Figure 5 is actually three sets of curves for Reynolds numbers of 500, 3000 and 10000. In each set, the ordinate is the total flow rate through the impactor stage and the abscissa the number of nozzles in that stage. In this analysis there is a one-to-one relationship between the value of the  $\sqrt{C}D_p$  and the nozzle diameter  $W$ . Therefore,  $\sqrt{C}D_p$  and  $W$  are used as parameters for the curves in each set.

The curves in Figure 5 are to be used only as a guideline in analyzing or designing impactors. For example, if an impactor is to be designed with a Reynolds number of 3000 and a total flow rate of 10 L/min, the number of nozzles to achieve a cutoff size of  $\sqrt{C}D_{50} = 1 \mu\text{m}$  will be 5. The nozzle diameter for this stage would be about 0.113 cm. If the Reynolds number was to be lowered to 500, the same cutoff size would be achieved with about 30 nozzles of 0.0894 cm diameter. If the Reynolds number was to be raised to 10000, then the impactor would take less than one nozzle and, thus, could not be a solution to the problem.

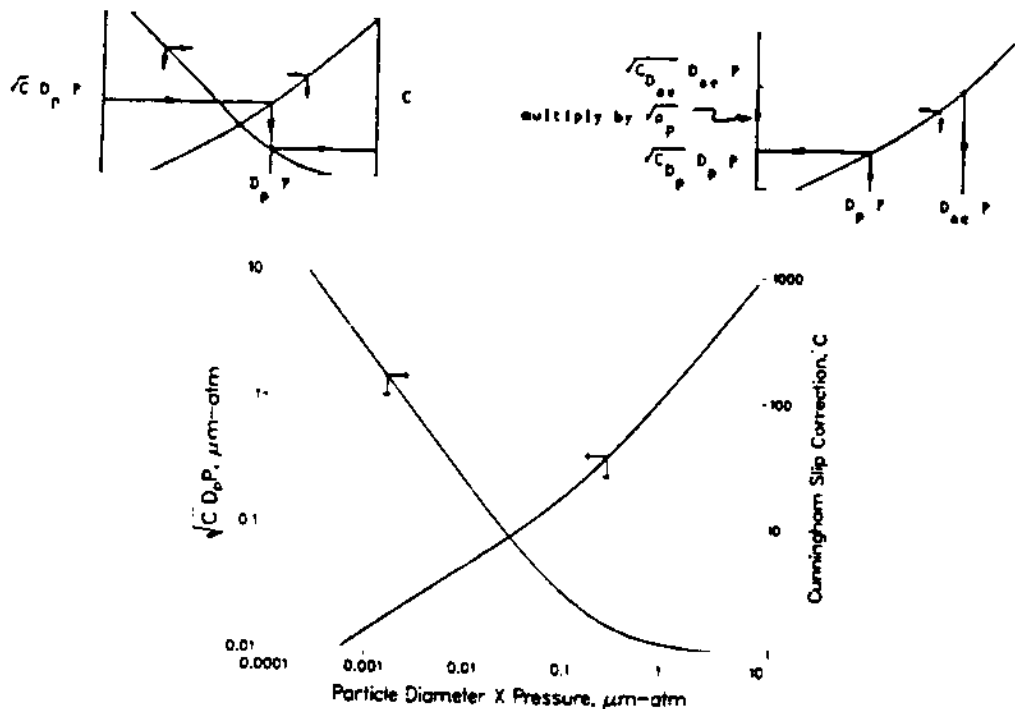


Figure 4.  $\sqrt{C}D_p P$  vs.  $D_p P$  and  $C$  vs.  $D_p P$ . (A detailed plot is included in the instruction manual for the circular slide rule.)

# THEORY AND DESIGN GUIDELINES

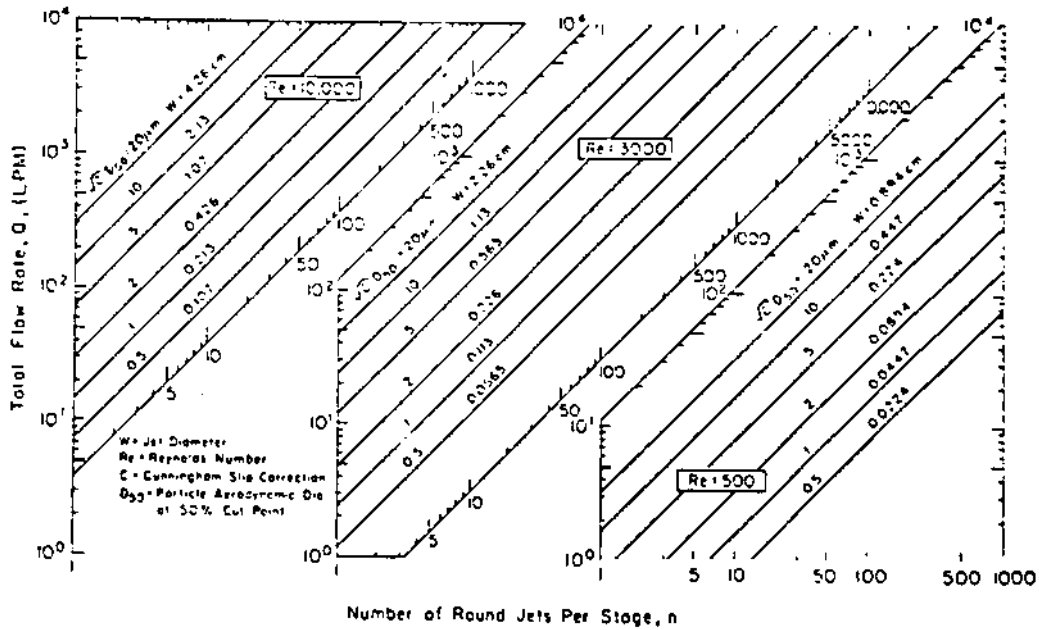


Figure 5. Design chart for round impactors ( $D_{50}$  = aerodynamic diameter at 50% cut point), from Marple and Willeke (1976).

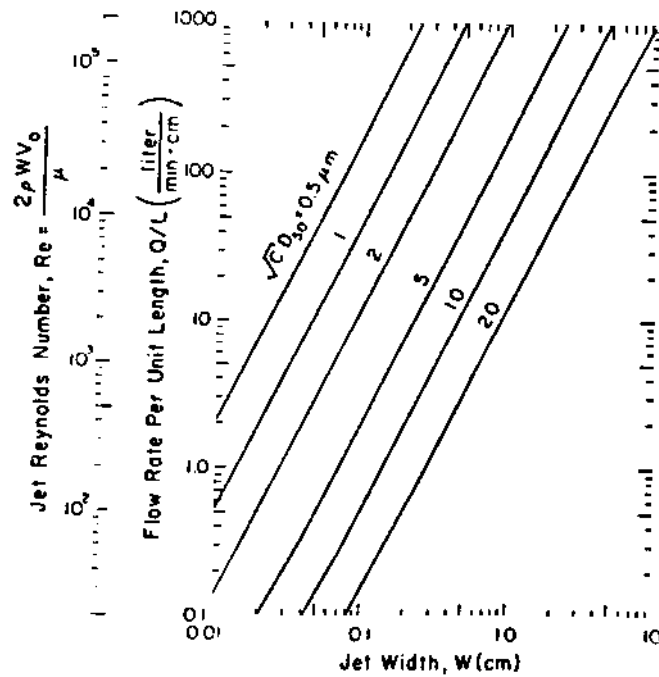


Figure 6. Design chart for rectangular impactors ( $D_{50}$  = aerodynamic diameter at 50% cut point), from Marple and Willeke (1976).

Although using multiple round nozzles in a stage of an impactor to control the Reynolds number is effective for round nozzles, it is not the case for rectangular impactors. If the nozzle of the rectangular impactor is divided into smaller nozzles the width of the nozzle remains constant and only the length and number of nozzles changes. This does not serve to change the Reynolds number or the cutoff size of the impactor. Therefore, the design curves for the rectangular impactors shown in Figure 6 indicate a one-to-one relationship between the Reynolds number and the flow rate per unit length. If a specific Reynolds number is desired, the flow rate per unit length is dictated as well as the nozzle width  $W$  for a specific cutoff  $\sqrt{CD_p}$ . For example, if the Reynolds number is to be kept at 3000 and the cutoff size is to be  $1 \mu\text{m}$ , then Figure 6 shows that a nozzle width of about 0.06 cm is needed and the flow rate will be about 16 L/min/cm. If the flow rate was to be 10 L/min then the length of the nozzle would be 0.625 cm. This stage could be designed with a one 0.625 cm by 0.06 cm wide nozzle or the length could be divided into any number of segments desired; the total length would have to be held at 0.625 cm.

It must be noted that the curves of Figures 5 and 6 were developed at the time when only efficiency curves of Figure 2 were in existence. Thus, these curves pertain only to Figure 2. However, in development of Figures 5 and 6 only the value of  $\sqrt{CD_{50}}$  as a function of the Reynolds number at 500, 3000 and 10000 were used. Since these values are very similar for the efficiency curves in Figures 2 and 3 the design curves of Figures 5 and 6 are still valid. As explained above, the curves in Figures 5 and 6 are to be used only as guidelines in designing or analyzing impactors.

#### 4.5 Summary of Theoretical Considerations

Before starting a design one must first have at hand the necessary curves, equations and design criteria. Although some of this information has been presented in previous sections of this chapter it will be summarized here also.

1. The collection efficiency curves in Figure 3 are the most recent theoretical results.
2. The minimum value of  $S/W$  should be:

$$S/W = 1 \quad (\text{round impactor})$$

and

$$S/W = 1.5 \quad (\text{rectangular impactor}) \quad (10)$$

so that small changes in  $S/W$  do not alter the value of  $D_{50}$ . The theory does not predict an upper value of  $S/W$  but designs close to the values in equation 10 are preferred. For small nozzle diameters,  $S/W$  values may have to be as large as 5 or 10. In such cases, an experimental study should be performed to ascertain the sensitivity of the particle cut size to the nozzle-to-plate distance.

3. The Reynolds number should be between 500 and 3000 to achieve as sharp a collection efficiency curve as possible.

4. The value of the Reynolds number in the nozzle can be controlled by the number of nozzles per stage for round impactors and by the flow rate per unit length for rectangular impactors. Figures 5 and 6 should be used in estimating the number of nozzles that will be needed (round) or the flow rate per unit length (rectangular) required.

5. The Stokes number equation can be used to predict the cut size (size of particles collected at 50% efficiency) if the  $St_{50}$  (Stokes number at 50% collection efficiency) is used in equation 1. Thus,

$$\sqrt{CD_{50}} = \sqrt{\frac{St_{50} 9 \mu W}{\rho_p V_o}} \quad (11)$$

is a governing equation for determining the cut size when the Stokes number is known.  $D_{50}$  is found from  $\sqrt{CD_{50}}$  by use of Figure 4. Based on conditions 2 and 3 above,  $\sqrt{St_{50}}$  is 0.49 and 0.77 for round and rectangular nozzles, respectively.

## THEORY AND DESIGN GUIDELINES

It is often more convenient to express equation 11 in terms of the flow rate per nozzle  $q$  rather than the velocity  $V_o$ . Using the relationships

$$V_o = \frac{q}{\pi W^2/4} \quad (\text{Round})$$

$$V_o = \frac{q}{LW} \quad (\text{Rectangular}) \quad (12)$$

equation 11 becomes:

$$\sqrt{C} D_{50} = \sqrt{\frac{9St_{50}\pi\mu W^3}{4q\rho_p}} \quad (\text{Round})$$

$$\sqrt{C} D_{50} = \sqrt{\frac{9St_{50}\mu\left(\frac{L}{W}\right)W^3}{q\rho_p}} \quad (\text{Rectangular}) \quad (13)$$

6. It is necessary to know the pressure in the impaction region so that the slip correction  $C$  can be calculated and the volumetric flow rate  $q$  or the velocity  $V_o$  can be adjusted. Both of these parameters influence the calculation of the cut size,  $D_{50}$ , in equations 11 and 13.

The dependency of  $C$  on pressure has already been discussed. The only question that remains is what pressure to use; the pressure upstream or downstream of a nozzle. Both pressures have been used at various times by various researchers. In actuality, the local static pressure at the particle should be used as the particle passes through the nozzle. However, since this is not known, and since the static pressure in the stagnation region at the impaction plate is probably close to the static pressure at the nozzle inlet, the authors have generally used the static pressure upstream of the nozzle in the calculation of  $C$ . Thus the static pressure at the impaction region is being approximated by the upstream static pressure.

The same reasoning does not hold true in the calculation of  $q$  or  $V_o$ , since  $V_o$  is the velocity of the air in the nozzle throat. Therefore,  $q$  and  $V_o$  must be calculated at conditions in the throat. The calculation of  $q$  or  $V_o$  is not difficult if it is realized that the mass flowrate of air is constant for all stages. Therefore,  $q$  is inversely proportional to pressure.

$$q_2 = q_1 \left( \frac{P_1}{P_2} \right) \quad (14)$$

where subscripts 1 and 2 refer to conditions at the impactor inlet and the impaction plate in question, respectively. The velocity is calculated from the relationship

$$V_o = q/A, \quad (15)$$

where  $A$ , is the throat area.

The only difficult step is the determination of the pressure appropriate for these calculations. Normally, it is assumed that the dynamic pressure of the jet at any stage is lost to turbulence. Therefore,

$$\Delta P = \frac{1}{2} \rho V_o^2 \quad (16)$$

where  $\Delta P$  is the pressure drop across a stage. The values for  $\rho$  and  $V_o$  should be calculated at the downstream pressure. The ideal gas equation can be assumed for the calculation of  $\rho$ . Therefore, an iterative procedure must be used in the solution of equation 16. It is realized that this is a simplistic approach to dealing with the influence of pressure, in that such phenomena as pressure recovery in the impaction zone are ignored, but experience has shown that it is a satisfactory procedure for most impactor calculations.

#### 4.6 Design Procedure

Marple and Willeke (1976) presented a step-by-step design procedure for designing a cascade impactor. That procedure is described below for a cascade impactor of either round or rectangular design. The details have been modified so that the design procedure corresponds with the curves, equations, etc. presented in this chapter. The procedure starts with the design of the first stage (i.e., stage with largest particle cutoff size).

1. Choose a desired cutoff diameter,  $D_p$ , for first stage. Although the Stokes number equation (equation 11 or 13) is applicable to particles of any density, it is generally easier to design an impactor if the cutoff size is expressed as the equivalent aerodynamic diameter  $D_{ae}$ . The relationship between  $D_p$  and  $D_{ae}$  has been presented in equations 7 through 9. In addition, the procedure using Figure 4 to solve for  $D_{ae}$  when the slip correction is important has already been described.

2a. (Round) Use Figure 5 and determine the number and size of nozzles required for the desired operating Reynolds number and the aerodynamic cutoff size  $\sqrt{C}D_{50}$ . The curves for Reynolds number 3000 should be satisfactory for this step.

2b. (Rectangular) Use Figure 6 and choose a desired Reynolds number ( $Re = 3000$  should be satisfactory) and determine the flow rate per unit length, and the nozzle width for the desired aerodynamic cutoff size  $\sqrt{C}D_{50}$ . From the values of  $Q/L$  and  $Q$ , the nozzle length  $L$  must be calculated and compared to the nozzle width  $W$  to be assured that the nozzle is actually a rectangular slit. If  $L$  and  $W$  are approximately equal, the nozzle would act as a round nozzle. It is felt that  $L$  should be on the order of about  $10W$  for the nozzle to be rectangular.

3. Select a convenient nozzle diameter (or nozzle width) which is close to the value found in step 2. For a round impactor this would be a standard reamer size, and for a rectangular impactor it may be a standard slitting saw width.

4. For this value of nozzle diameter (or nozzle width), check the Reynolds number using equation 2. If the Reynolds number is far removed from the value assumed in step 2, repeat the process in step 2.

5. At this point it is important to calculate the pressure in the impaction region of the impactor so that corrections can be made in the value of flow rate  $Q$ . It is usually assumed, for stages collecting particles of 1  $\mu\text{m}$  diameter or greater, that the pressure drop across the nozzle is negligible, and that the flow rate and pressure can be assumed to be that of the impactor entrance. However, as the air passes through the stages of a cascade impactor, the pressure drop can become appreciable at the lower stages.

The pressure for any stage,  $P_n$ , can be calculated using equation 16 to give

$$P_n = P_{n-1} - \frac{1}{2} \rho V_n^2 \quad (17)$$

6. Determine the value of  $\sqrt{S}t_{50}$  from Figure 3 and calculate the cutoff size  $\sqrt{C}D_p$  using equation 13.

7. Determine the particle cutoff size  $D_p$  from  $\sqrt{C}D_p$  by the procedure outlined in Figure 4.

8. Repeat the steps, starting at step 1, for the next stage of impactor and continue until the entire impactor has been designed.

Remember that for all stages the value of  $S/W$  should be kept at

$$\begin{aligned} S/W &\geq 1.0 \text{ (Round)} \\ S/W &\geq 1.5 \text{ (Rectangular)} \end{aligned} \quad (18)$$

Also for the impactors to have sharp cuts the Reynolds number should be

$$500 < Re < 3000 \quad (19)$$

for both round and rectangular impactors.

## 4.7 Case Studies

The authors of this chapter have used the above theory to design many impactor stages that have subsequently been calibrated. In this section, a few examples are presented, as well as how the theoretical and experimental efficiency curves agreed.

## 4.7.1 Single Stage, Single Round Nozzle Impactor

The object of this design was to design two single stage impactors with single round nozzles to provide cuts at either 2.5  $\mu\text{m}$  or 10  $\mu\text{m}$  aerodynamic diameters. These impactors are used in the MST Indoor Air Sampler (MSP Corp., Maple Plain, MN 55359). This design is of particular interest in that the boundary conditions in the impactor are exactly matched to theory, since the theory considers only single nozzles. The only design constraint was that the flow rate had to be 4 L/min.

With this information, and using the design procedures outlined, the impactor described in Table 1 and shown in Figure 7 was designed. As can be seen in Table 1, the values of  $S/W$  and  $Re$  are within the guidelines for good impactor operation. It was expected, then, that the theoretical and experimental collection efficiency curves should be in good agreement, and this was found to be true as shown in Figure 8. The theoretical curves are taken from Figure 3. The experimental data points were generated with monodispersed aerosols of oleic acid droplets tagged with a uranine dye tracer. The quantities of dye collected on the impaction plate and afterfilter were determined using a fluorometer and the subsequent collection efficiency calculated. Since the sharpness of cut was so steep for these stages ( $\sigma_g = 1.02$  and 1.09 for the 2.5 and 10  $\mu\text{m}$  impactor, respectively), special care had to be taken to measure the quantity of doublet and triplet particles generated by the vibrating orifice aerosol generator and back out their higher collection efficiency from the calculations of collection efficiency.

Figure 8 shows the comparison between the theoretical and experimental collection efficiency curves. The agreement is excellent for the 2.5  $\mu\text{m}$  impactor, but shows a 6% discrepancy for

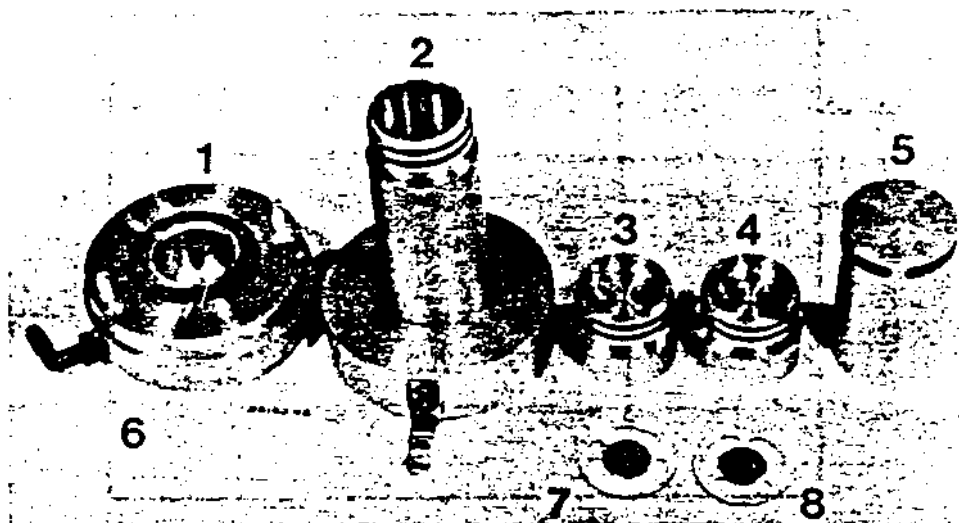


Figure 7. The MST Indoor Air Sampler Showing: (1) Base and Filter holder, (2) Cover for afterfilter and support for impactor stages, (3 & 4) Impaction stages with same cut size to decrease probability of overloading, (5) Cover, (6) Afterfilter, and (7 & 8) Impaction plates.

the 10  $\mu\text{m}$  impactor. This discrepancy is thought to be due to gravitation effects and is discussed in greater detail in Section 4.7.2. It should be noted that in the design procedure, the first estimate of the nozzle diameter was 0.248 cm which provided for an experimental cutoff size of 2.60  $\mu\text{m}$ . Since this cut size was 4% larger than desired, the nozzle diameter was changed to 0.244 cm, which provided the cutoff size of 2.52  $\mu\text{m}$ . A similar iteration was experienced

# THE RESPIRABLE DUST CENTER

**TABLE 1. Design parameters and cutoff diameters of the impactors in the MST indoor air sampler**

Nominal Cutoff Diameters, $\mu\text{m}$	2.5	10
Nozzle Diameter, cm	0.244	0.620
S/W	2.0	0.86
Re	2140	900
Cutoff Diameter, $\mu\text{m}$		
Theoretical	2.52	10.4
Experimental	2.52	9.8

**TABLE 2. Design parameters and cutoff diameters of Marple Personal Cascade Impactor (from Rubow *et al.*, 1986)**

Stage	1	2	3	4	5	6	7	8
Nozzle Shape	slot	slot	slot	slot	slot	slot	round	round
Number of Nozzles	6	6	6	6	6	6	12	12
Nozzle-width, cm	0.264	0.145	0.0813	0.0432	0.0254	0.0173	—	—
-diameter, cm	—	—	—	—	—	—	0.0457	0.0318
Slot Length, cm	0.953	0.953	0.953	0.953	0.953	0.480	—	—
S/W	1.2	2.2	1.3	2.4	2.0	2.9	1.7	2.4
Re	76	76	76	76	76	230	490	710
Cutoff Diameter, $\mu\text{m}$ :								
Theoretical	35.8	19.6	11.0	5.8	3.38	1.59	0.94	0.52
Experimental	21.3	14.8	9.8	6.0	3.5	1.55	0.93	0.52

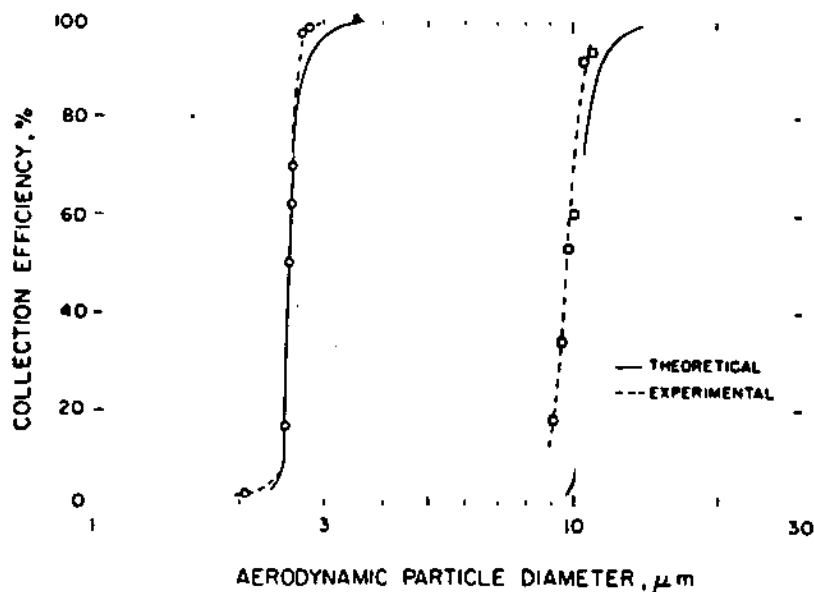


Figure 8. Comparison of the theoretically and experimentally determined collection efficiency curves for the impaction stages ( $D_{50}$ 's of 2.5 or 10  $\mu\text{m}$ ) used in the MST Indoor Air Sampler.

The design of an entire cascade impactor is a lengthy process and will not be described in detail here. However, several points of interest concerning the design procedures and the agreement between the experimental and theoretical efficiency curves will be discussed.

First note that the agreement between theoretical and experimental efficiency cutoff diameters is quite good for diameters of 10  $\mu\text{m}$  and less. For larger cutoff sizes, the theory predicts a larger cutoff size than found experimentally, which has been the case for nearly all impactors the authors have designed. It is felt that these differences may be due to gravitational effects for these larger particles, and this is currently being investigated.

Another area of interest, and where special care must be taken, is in designing impactors with small cutoff sizes as in Stage 8. Here the pressure drop is sufficient to increase the volumetric flow rate, and the particles are small enough so that the slip correction must be considered. In Stage 8, the pressure was measured to be 100.0 kPa compared to 101.3 kPa at the inlet. Therefore, the volumetric flow rate is 1.013 times larger or 2.03 L/min instead of 2 L/min as for the upper stages. Although the correction for volumetric flow rate was not large for this particular impactor, for impactors with cutoff sizes less than 0.5  $\mu\text{m}$  it can become much more significant. The slip correction can be much larger than the volumetric flow correction. In the particular impactor considered here, for a cutoff size of 0.5  $\mu\text{m}$  and a pressure of 0.997 atmospheres, the slip correction from Figure 4 is found to be 1.33. If the slip correction had been assumed to be unity, the theory would have predicted a cutoff size of 0.60  $\mu\text{m}$ .

#### 4.7.3 *Impactors With Respirable Cutoff Characteristics*

Most of the information presented in this chapter has been on how to design an impactor with sharp cutoff characteristics. However, at times it may be desirable to design an impactor stage with classification characteristics that match a specific curve. This was a case in designing an impactor stage with a penetration curve that approximated the American Conference of Governmental Industrial Hygienists (ACGIH) respirable curve (Marple, 1978, Marple and McCormack, 1983, and Marple and Rubow, 1983). An impactor of this design is shown in Figure 10.

If a single nozzle impactor is designed to approximate the respirable curve, the 50% value can be designed to be correct, but the cutoff characteristics will be too sharp. The approximation can be improved by using a stage with multiple nozzles of two different sizes so the respirable curve is approximated in two steps. Even better approximation can be obtained by using multiple nozzle stages with nozzles of even more sizes. We have found that three nozzle sizes are usually satisfactory.

The procedure for such a design is rather simple. As shown in Figure 11, the respirable curve is divided into three equal segments of collection efficiency (i.e., 0 to 33 $\frac{1}{3}$ %, 33 $\frac{1}{3}$ % to 66 $\frac{2}{3}$ % and 66 $\frac{2}{3}$ % to 100%). Nozzle diameters must now be sized so that the 50% cut points correspond to the particle sizes at the midpoints of the three segments (i.e. particle sizes corresponding to 17%, 50% and 83%). The flow rate through each size of nozzle must be  $\frac{1}{3}$  of the total flow rate. The first nozzle diameter to be designed must be that of the largest cut size, and this can be accomplished with a single nozzle. Since the pressure drop is the same across all nozzles, the velocity through all nozzles will be approximately the same. Thus, the velocity through the with the 10  $\mu\text{m}$  cut impactor. The process of designing an impactor stage is, therefore, one of iteration. The theory is used to obtain the best estimate of the correct nozzle diameter. In many cases, the resulting true cutoff size, as determined by experimentation, is close enough to the desired cutoff size to be satisfactory. However, if closer agreement is desired, a second iteration is necessary. It must be noted, however, that to do this iteration, the experimental determination of the collection efficiency curve must be painstakingly performed or the experimentally determined cutoff size will be in greater error than the theoretically determined size.

#### 4.7.2 *Cascade Impactor With Multiple, Rectangular and Round Nozzles*

The object of this project was to design a personal cascade impactor with a flow rate of 2 L/min. This impactor is the Marple Personal Cascade Impactor (Andersen Samplers, Inc., Atlanta, GA 30336). A more complete description, together with the calibration data, is given by Rubow *et al.* 1986). Rectangular nozzles were used for the upper six stages and round nozzles



for the two lower stages. The parameters describing the impactor are given in Table 2, along with the theoretical and experimental 50% cutoff diameters (Figure 3 was used for the theoretical design). The experimental efficiency curves are shown in Figure 9. The theoretical curves are not shown because parameters were such as to require interpolation of the curves in Figure 3. Only the theoretical 50% cutoff diameters were determined (Table 2).

nozzle designed for the largest cut size must be calculated and this velocity used in the calculation for the nozzle diameters of the smaller two cut sizes. By knowing the cut size and the velocity, the nozzle diameters for these two cut sizes can now be calculated. The final step is to determine the number of nozzles of each size which is needed for the lower two cut sizes, and this can be determined by using the known nozzle diameters and velocities for these cut sizes and by providing enough nozzles to obtain 1/3 of the total flow. The impactor stage is now designed.

This procedure can be used to design impactors with a variety of flow rates, number of nozzle sizes, and respirable curves. We have used the technique for approximating the ACGIH and the British MRC respirable curves, as shown in Figure 12. Note in these figures that the experimentally determined efficiency curves are very nearly that predicted by the theory, and they both approximate the respirable curves quite well.

Impactors with a variety of flow rates have been designed using this procedure, as indicated in Table 3. The impactors with 2 L/min flow rates have been used for personal samplers where a personal sampling pump has been used as the air mover, and the impactor with 30 L/min flow rates have been used as a respirable sampler standard in an aerosol test chamber in our laboratory.

#### 4.8 Impactor Calculator

As has been described in previous sections of this chapter, the important considerations in designing an impactor are control of the Reynolds number, the Stokes number and the jet-to-plate distance. Therefore, in the design of an impactor, there are repetitious calculations of the Reynolds number and the Stokes number, or manipulation of these equations, which must be made to find flow rates or nozzle diameters to give a specific cutoff size. To facilitate the solution of these equations a circular slide rule is included in an envelope of this book. Side 1 of the slide rule is used for solving the Stokes number equation, and Side 2 is used for solving the Reynolds number equation. The instruction booklet with the slide rule gives details on its use as well as some examples. Furthermore, in the instruction manual, Figure 4 is reproduced, and instructions are given on how to solve for the value of  $D_p$  when the value of  $\sqrt{CD_p}$  is known.

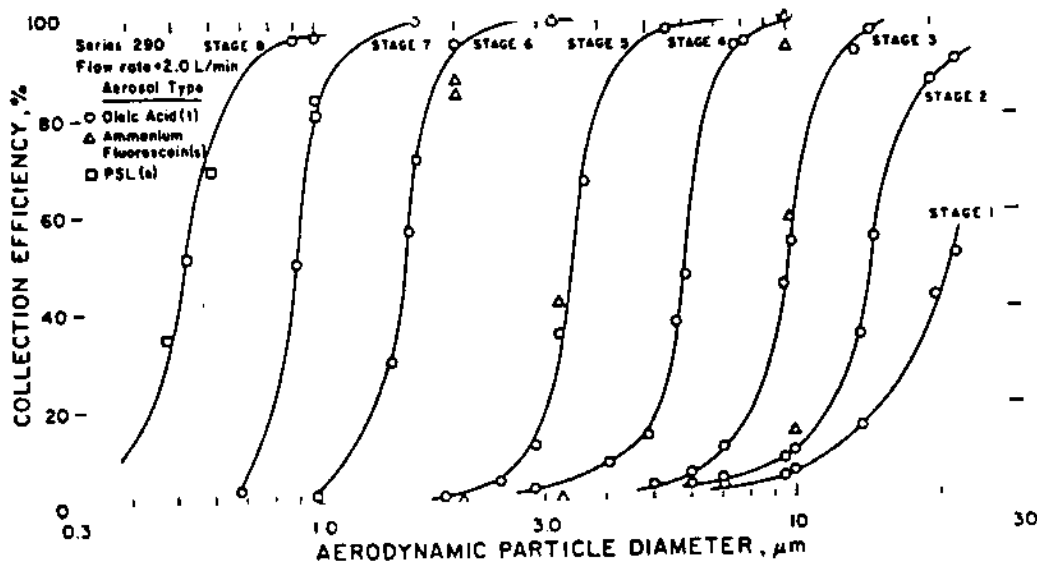


Figure 9. Experimentally determined collection curves for the Marple Personal Cascade Impactor (from Rubow *et al.* 1986).



1

2

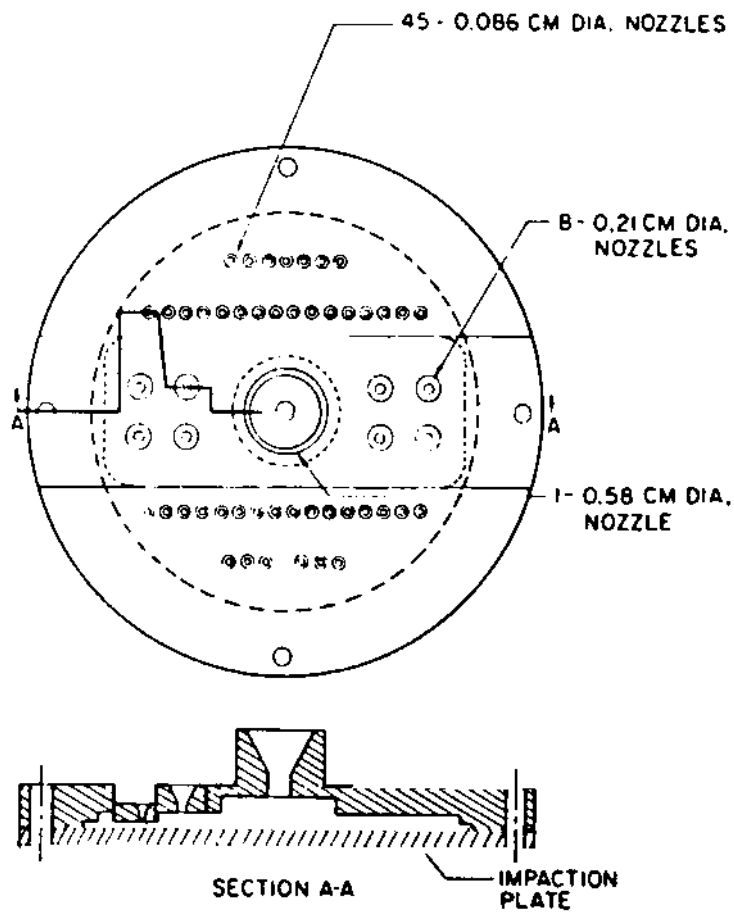


Figure 10. Three-nozzle size impactor designed for a flow rate of 28.3 L/min (from Marple, 1978).

**THE RESPIRABLE DUST CENTER**

**TABLE 3. Impactor designs with penetration characteristics that simulate respirable penetration curves (from Marple & Rubow, 1983)**

Impactor	Total Flowrate (liter/min)	Respirable Curve	No. of Nozzle Sizes	Nozzle Cut Diam. ( $\mu\text{m}$ )	Nozzle Diam. (cm)	No. of Nozzles
A	2	ACGIH	2	5.0	0.25	1
				2.5	0.063	16
B	2	ACGIH	3	5.8	0.24	1
				3.5	0.087	8
				2.2	0.033	53
C	2	BMRC	2	6.1	0.28	1
				3.5	0.093	9
D	2	BMRC	3	6.4	0.26	1
				5.0	0.15	3
				2.9	0.048	28
E	28	ACGIH	2	5.0	0.60	1
				2.5	0.16	14
F	28	ACGIH	3	5.8	0.58	1
				3.5	0.21	8
				2.2	0.086	45
G	40	ACGIH	3	5.8	0.65	1
				3.5	0.24	8
				2.2	0.097	45

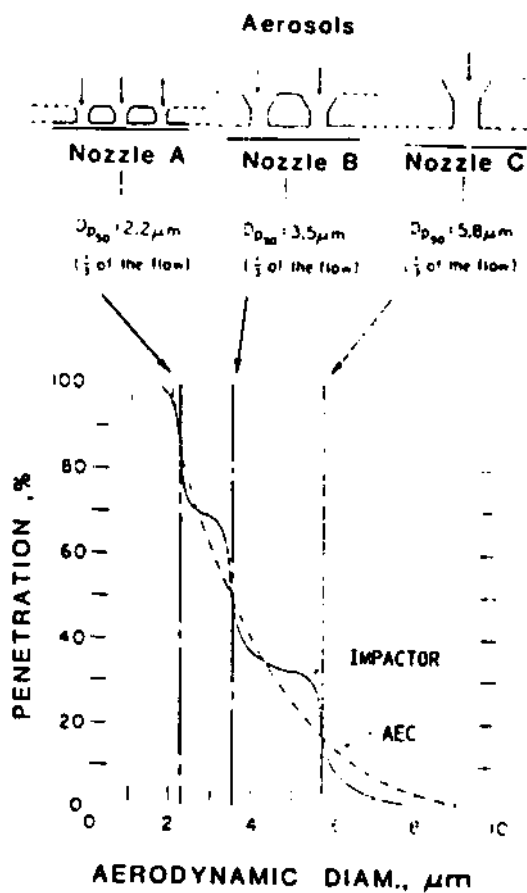


Figure 11. Approximation of the penetration curve for the single-stage impactor with three nozzle sizes to the AEC-ACGIH criteria for respirable mass sampling (from Marple and Rubow, 1983).

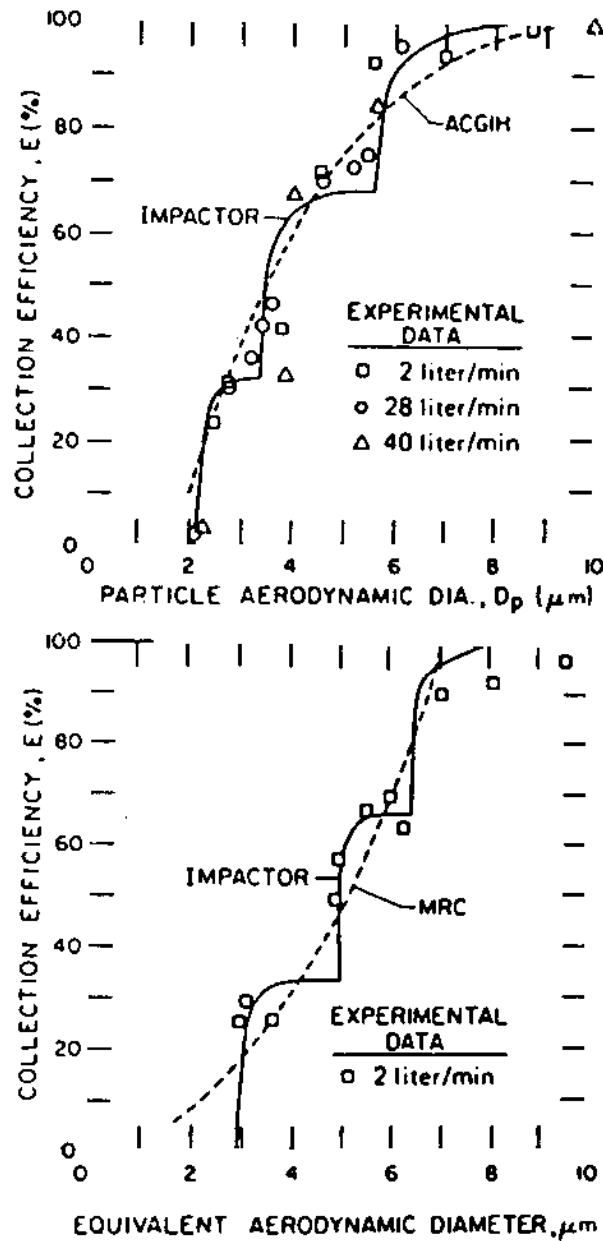


Figure 12. Comparison of the experimentally and theoretically-determined collection efficiency curves for three single-stage impactors with the ACGIH and BMRC respirable curves (from Marple and Rubow, 1983).

## THEORY AND DESIGN GUIDELINES

### References

- Davies C. N. (1945) Definitive equation for the fluid resistance of spheres. *Proc. Phys. Soc.* 57:259-270.
- Davies C. N. and Aylward M. (1951) The trajectories of heavy, solid particles in a two-dimensional jet of ideal fluid impinging normally on a plate. *Proc. Roy. Soc. London B64*:889-911.
- Davies C. N., Aylward M. and Leacey D. (1951) Impingement of dust from air jets. *AMA Arch. Ind. Hyg. Occup. Med.* 4:354-397.
- Marple V. A. (1970) *A Fundamental Study of Inertial Impactors*. Ph.D. Thesis, University of Minnesota, Minneapolis, MN.
- Marple V. A. (1978) Simulation of respirable penetration characteristics by inertial impaction. *J. Aerosol Sci.* 9:125-134.
- Marple V. A. (1986) A procedure for the calculation of particle size when the slip correction must be considered. *Aerosol Sci. & Technol.* (in press).
- Marple V. A. and Liu B. Y. H. (1974) Characteristics of laminar jet impactors. *Envir. Sci. & Technol.* 8:648-654.
- Marple V. A. and Liu B. Y. H. (1975) On fluid flow and aerosol impaction in inertial impactors. *J. Coll. & Interface Sci.* 53:31-34.
- Marple V. A., Liu B. Y. H. and Whitby K. T. (1974a) Fluid mechanics of the laminar flow aerosol impactor. *J. Aerosol Sci.* 5:1-16.
- Marple V. A., Liu B. Y. H. and Whitby K. T. (1974b) On the flow fields of inertial impactors. *J. Fluids Eng.* 96:394-400.
- Marple V. A. and McCormack J. E. (1983) Personal sampling impactors with respirable aerosol penetration characteristics. *Am. Ind. Hyg. Assoc. J.* 44:916-922.
- Marple V. A. and Rubow K. L. (1983) Impactors for respirable dust sampling. In *Aerosols in the Mining and Industrial Work Environments* (edited by V. A. Marple and B. Y. H. Liu), V. 3, pp. 847-860.
- Marple V. A. and Willeke K. (1976) Impactor design. *Atmos. Envir.* 10:891-896.
- Mercer T. T. and Chow H. Y. (1968) Impaction from rectangular jets. *J. Coll. Interface Sci.* 27:75-83.
- Mercer T. T. and Stafford R. G. (1969) Impaction from round jets. *Ann. Occup. Hyg.* 12:41-48.
- Rader D. J. and Marple V. A. (1985) Effect of ultra-Stokesian drag and particle interception on impaction characteristics. *Aerosol Sci. & Technol.* 4:141-156.
- Ranz W. E. and Wong J. B. (1952) Impaction of dust and smoke particles. *Ind. Eng. Chem.* 44:1371-1381.
- Rubow K. L., Marple V. A., Olin J. and McCawley M. A. (1986) A personal cascade impactor: Design, evaluation and calibration. *Am. Ind. Hyg. Assoc. J.* (in press).

### ACKNOWLEDGEMENTS

This research has been supported by the Department of the Interior's Mineral Institute program administered by the Bureau of Mines through the Generic Mineral Technology Center for Respirable Dust under grant number G1135142.

# Low-Pressure and Micro-Orifice Impactors - Chapter 5

Susanne V. Hering

Department of Chemical Engineering,  
University of California, Los Angeles  
Virgil A. Marple

Particle Dispersion Laboratory  
Mechanical Engineering Department, University  
of Minnesota

## 5.1 Introduction

Traditional impactors do not offer much size resolution for submicrometer particles; typically their finest size cut is around  $0.4 \mu\text{m}$ . Yet for many aerosol applications it is useful to be able to size segregate aerosols in the size range below  $0.4 \mu\text{m}$ . Diesel emissions, welding fumes, cigarette smokes and photochemically generated smog aerosols typically exhibit mass median diameters between  $0.1$  and  $0.6 \mu\text{m}$ . When sampling these aerosols with a traditional impactor, fifty percent or more of the aerosol mass can penetrate the final impactor stage. Although the material can still be collected on a backup filter, the filter gives no size resolution. As a result, the investigator has no size information on a substantial portion of the sample. One needs a sampler that size-segregates the majority of the aerosol mass. A lower size cut of  $0.1 \mu\text{m}$  or less is required for most combustion smokes and smog aerosols.

To obtain smaller cutpoints two types of impactors have been developed, namely low-pressure impactors and micro-orifice impactors. Both instruments can provide cutpoints as small as  $0.05 \mu\text{m}$ . Low-pressure impactors were introduced more than twenty years ago (Stern *et al.*, 1962), and a variety of these samplers are in use today. Micro-orifice impactors have been developed at the University of Minnesota within the last five years (Marple *et al.*, 1981). To date theirs are the only examples of these instruments in use.

## 5.2 Operating Principles

The low-pressure and micro-orifice impactors use two different approaches to achieve their very small particle-size cuts. Low pressure impactors resemble ordinary impactors, but are operated at reduced pressures of  $5\text{-}40 \text{ kPa}$  ( $0.05 - 0.4 \text{ atm}$ ). They take advantage of the decreased aerodynamic drag on particles that occurs when the mean free path in the air is as large or larger than the particle diameter. Micro-orifice impactors operate at near atmospheric pressure, but employ very small orifices,  $40 \mu\text{m}$  to  $200 \mu\text{m}$  in diameter. The streamlines of the air impinging upon the impaction plate have correspondingly smaller radii of curvature; the air is accelerated more quickly, making it more difficult for the particles to follow.

The basic operating principles for both types of impactors are evident from the particle Stokes number, defined as:

$$St = \frac{\rho_p D_p^2 V C}{9\mu W} \quad (1)$$

where  $\rho_p$  = particle density,  $D_p$  = particle diameter,  $V$  = jet velocity,  $C$  = Cunningham slip factor,  $\mu$  = air viscosity, and  $W$  = jet diameter. The Stokes number is a dimensionless parameter that characterizes particle deposition in an impactor. It does not account for the undesired effects of wall losses or particle bounce, but accurately predicts whether a particle will impact on the collection surface. Physically, the Stokes number is proportional to the ratio of the particle

## LOW-PRESSURE AND MICRO-ORIFICE IMPACTORS

stopping distance to the jet diameter. Alternatively, it may be viewed as the ratio of particle relaxation time to the transit time of the airflow across the impaction plate. (The relaxation time is the time for a particle initially at rest to achieve  $1/e$  of the velocity of the airstream, where  $e$  is the base of natural logarithms.)

Impactor stages with similar geometry, but varying jet diameters or flow rates, will have collection efficiencies that tend to fall on a common curve when plotted as a function of  $St$ . The critical Stokes number,  $St_{50}$ , corresponds to a collection efficiency of fifty percent. Its value is between 0.22 and 0.25 for most round jet impactors. Even impactors of quite different design have very similar values for  $St_{50}$ .

Small particles can be collected in an impactor only when  $\rho_p D_p^2 = (9\mu St_{50})(W/CV)$  is small. There is not much latitude for variation in many of these parameters. The value of  $St_{50}$  is nearly constant, as is the air viscosity  $\mu$ , which is independent of pressure and only slightly dependent on temperature. The jet velocity  $V$  is limited to sonic velocity for a converging nozzle, and in practice is usually kept below 100 m/s where the flow is approximately incompressible. For an impactor stage with a 0.5 mm diameter round jet operated at 100 m/s, the cutoff diameter would be about 0.35  $\mu\text{m}$ . To collect smaller particles, either the slip factor  $C$  must be larger, or the jet diameter  $W$  must be smaller. Low-pressure impactors operate at large  $C$ , and micro-orifice impactors at small  $W$ .

The slip factor,  $C$ , is a dimensionless number which appears in the expression for the aerodynamic drag on a particle:

$$F_{\text{drag}} = 3\pi\mu D_p (V_p - V)/C \quad (2)$$

where  $V_p$  is the particle velocity and  $V$  is the airstream velocity. It is a function of the ratio between the particle diameter ( $D_p$ ) and the mean free path ( $\lambda$ ) of the surrounding gas (Davies, 1945):

$$C = 1 + 1.257 \frac{2\lambda}{D_p} + 0.40 \frac{2\lambda}{D_p} \exp\left(-1.10 \frac{D_p}{2\lambda}\right) \quad (3)$$

The slip factor accounts for the reduction in the drag on a particle in the transition between the continuum and free molecular regimes. In the continuum regime the particle diameter is large by comparison with the air mean free path; the drag force is proportional to the particle diameter, and the slip factor has a value of one. In the free molecular regime the particle diameter is much smaller than the air mean free path, and the drag force is proportional to the square of the particle diameter. The slip factor is large, and is inversely proportional to particle diameter.

Values for the slip factor in air at 101 kPa (atmospheric pressure) and at 6.6 kPa (0.066 atm) are shown in Figure 1. At 101 kPa (1 atm) and 20°C the mean free path in air is 0.066  $\mu\text{m}$ , and the value of the slip factor is less than 3 for particles larger than 0.1  $\mu\text{m}$ . At 6.6 kPa (and 20°C)

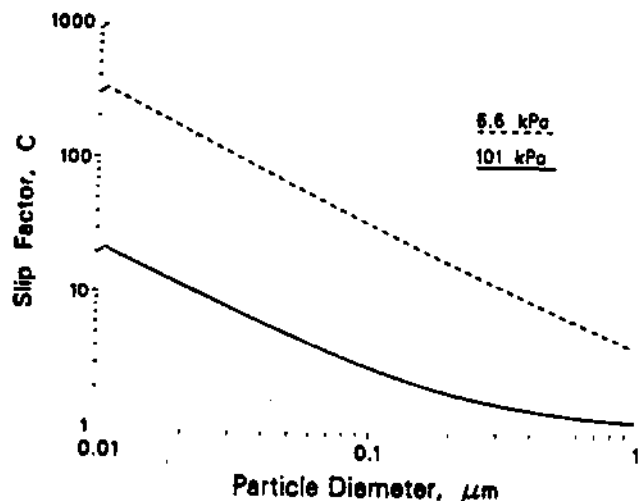


Figure 1. The Cunningham slip factor is shown as a function of particle diameter for pressures of 101 kPa (1 atm) and 6.6 kPa (0.066 atm) at 20°C. Since the air mean free path equals 1  $\mu\text{m}$  for the 6.6 kPa conditions, this curve also gives the slip factor as a function of the dimensionless ratio of particle diameter to mean free path.



the mean free path is  $1 \mu\text{m}$ , and the slip factor for a  $0.1 \mu\text{m}$  particle is 34. The corresponding value of  $V/W$  (jet velocity/jet diameter) can be  $\frac{3}{4}$  as large, and still yield the same collection efficiency for  $0.1 \mu\text{m}$  particles by impaction. In our earlier example of an atmospheric-pressure impactor with  $100 \text{ m/s}$  flow through a  $0.5 \text{ mm}$  diameter round jet, we showed that a  $0.35 \mu\text{m}$  particle would be collected with roughly 50% efficiency. If the same impaction stage were operated at  $6.6 \text{ kPa}$ , again with a flow of  $100 \text{ m/s}$ , the corresponding 50% cutoff diameter would be (approximately)  $0.05 \mu\text{m}$ . At the lower pressure the aerodynamic drag on the particles is reduced, thus enabling their collection.

Micro-orifice impactors operate at near atmospheric pressure using  $0.04 \text{ mm}$  to  $0.06 \text{ mm}$  ( $40 \mu\text{m}$ – $60 \mu\text{m}$ ) jets to obtain the lower size cuts. With a jet velocity of  $100 \text{ m/s}$ , the cutpoint for the  $0.04 \text{ mm}$  jet is about  $0.1 \mu\text{m}$ . The instruments are inherently multijet impactors since many jets must be used to obtain a reasonable flow rate. For example, the lower stages of the University of Minnesota micro-orifice impactors use 2000 jets each to give  $30 \text{ L/min}$  flow.

### 5.3 Development and Applications of Low-Pressure and Micro-Orifice Impactors

The development of low-pressure impactors predates that of the micro-orifice impactors. The behavior of impactors at low pressures was first investigated by Stern *et al.* (1962). They showed that the Stokes number properly accounted for the collection efficiency of impactors when the ratio of air mean free path to particle diameter is large. McFarland and Zeller (1963) applied these principles to an impactor used for stratospheric aerosol sampling, and then later McFarland *et al.* (1973) built a ground-based low-pressure impactor by adding three low-pressure stages to the commercially available Andersen 2000 multijet impactor (Andersen Instruments, Inc., Atlanta, GA 30336). This sampler operated at  $28 \text{ L/min}$ , with pressures of  $2.9$  to  $3.3 \text{ kPa}$  on the low-pressure stages. The corresponding pumping requirements were large, and the instrument is no longer in use. Parker and Buchholz (1968) built an  $8 \text{ L/min}$  multijet sampler, also similar in appearance to the Andersen sampler, which operated at  $4$  to  $6 \text{ kPa}$  with a lower cutoff diameter of  $0.05 \mu\text{m}$ . Although laboratory calibration work showed that the particle cutoff diameters were close to the calculated values, its use appears to have been very limited. Recently Fernandez de la Mora *et al.* (1984) used a single stage, low-pressure impactor to demonstrate inertial effects for heavy molecules suspended in a light carrier gas.

Several different low-pressure impactors currently are available commercially: an Andersen low-pressure impactor (Andersen, Atlanta GA), the Berner Impactor (Hauke-Aeras, Gmunden, Austria), the Hering LPI (ATEC, Calabasas, CA), the PIXE impactor (PIXE International, Tallahassee FL), QCM impactors (California Measurements, Sierra Madre, CA and QCM Inc., Laguna Beach, CA), and the University of Washington Source Test Impactor of Pilat *et al.*, 1978, (Pollution Control Systems, Renton, WA). The Andersen low-pressure impactor is the newest of these, and applications of this instrument have not yet appeared in the literature. The PIXE impactor is similar in design to the Hering LPI (Bauman *et al.*, 1981).

The QCM impactors use piezoelectric quartz crystals as collection substrates for real time determinations of mass size distributions. The final stages of the impactor operate at pressures of  $74$ – $89 \text{ kPa}$  ( $0.74$ – $0.89 \text{ atm}$ ). Calibration curves are given by Fairchild and Wheat (1984). The QCM has been used for both ground-based and stratospheric sampling of atmospheric aerosols (Hering, 1986).

The Berner impactor has been used for a variety of atmospheric measurements, including ambient size distributions for sulfate, nitrate and carbon and other elements in Vienna, Austria (Puxbaum and Wopenka, 1984), for sulfate, nitrate and ammonium ion and acid in Southern California (John *et al.*, 1985), for ion analyses by secondary ion mass spectrometry (Klaus, 1983, 1984), and for mass distributions of urban aerosols (Berner *et al.*, 1979, 1983, and Hitzengerger and Husar, 1984), and traffic-derived aerosols (Berner and Lürzer, 1980, Berner *et al.*, 1984). The Berner impactor has also been used in laboratory studies of particle agglomeration in intense acoustic fields (Cheng *et al.*, 1983) and in studies of the aerodynamics of irregularly shaped particles (Kasper and Shaw, 1983).

The Hering LPI has been used primarily for ambient sulfur size distributions, including measurements in Columbus, OH (McMurry and Wilson, 1983), in St. Louis, MO (Vossler and Macias, 1986), in Los Angeles, CA (Hering and Friedlander, 1982), and in the southwestern US

desert (Hering *et al.*, 1981, Macias *et al.*, 1981). Sulfur distributions in power plant plumes are reported by Richards *et al.*, (1985), and those from smog chamber studies are given by McMurry and Friedlander, (1979). The Hering LPI has also been used for ambient distributions of elements (Quimette and Flagan, 1982), polycyclic aromatic hydrocarbons (Miguel, 1982) and soot (Miguel and Friedlander, 1978). Taylor and Flagan (1981) have measured elemental distributions in laboratory studies of combustion-generated aerosols. Calibration data are presented by Hering *et al.* (1979).

The micro-orifice impactor has been developed more recently (Kuhlmeiy *et al.*, 1981 and Marple *et al.*, 1981). Calibration data for one of the prototype instruments are given by Rubow and Marple (1984). It has been used for elemental size distribution analyses (Macias *et al.*, 1981, Dzubay *et al.*, 1984), and for carbon, sulfate and nitrate distributions in the southwestern U.S. (Hasan and Dzubay, 1985, Hering and McMurry, 1985, McMurry and Marple, 1986). Recently the micro-orifice impactor has been used to distinguish between coal and diesel particles in laboratory studies (Rubow *et al.*, 1986) and in mining operations (Cantrell *et al.*, 1986).

Examples of size distributions measured with the Berner, Hering and micro-orifice impactors are given in Figure 2. All of the data shown are for ambient sulfate aerosols from Los Angeles, CA. The micro-orifice and Hering LPI data were collected simultaneously, but the Berner impactor data are from a different year. All three instruments have lower size cuts below  $0.1 \mu\text{m}$ , and are able to resolve the details of the submicrometer sulfate distribution. Both the micro-orifice and Hering LPI show similar results for the ambient sulfate aerosols, both in the distributions and in the total sulfate loadings. The similarity of the data for the Berner impactor is in part coincidental, as it is known that the distribution of ambient sulfates in Los Angeles can vary.

### 5.4 Low-Pressure Impactors

#### 5.4.1 Design

As with traditional impactors, the optimal design for low-pressure impactors depends, in part, on their intended use. We describe below two different types of low pressure impactors; the Berner impactor used for both gravimetric and chemical analyses, and the Hering LPI, designed for direct elemental analyses.

**Berner Impactor:** The Berner low-pressure impactor was designed to provide sufficient sample for gravimetric determinations of aerosol mass distributions, and for chemical analyses requiring sample extraction. There are several models, with flow rates from 2 L/min to 150 L/min. The most commonly used is the model 30/.06/2 which is a multijet impactor with a flow rate of 30 L/min, as measured at the inlet temperature and pressure. The design and operating parameters are given in Table 1. Except for the first stage, the impactor has between 7 and 130 equal-diameter jets per stage. The jets are arranged in a circle, as shown in Figure 3. The collection plate has a large hole in the center for the air to pass to the subsequent stage. This flow arrangement gives a symmetrical flow pattern, and thus equal deposits under each jet. The flow rate through the impactor is controlled by a critical orifice downstream of the final collection stage.

In Table 1 the stagnation pressure in the impactor stage below each jet is listed in terms of the ambient pressure at the impactor inlet,  $P_a$ . The pressures and jet velocities are those given by Berner *et al.* (1979). Note that only the last three stages operate at reduced pressures; particles greater than  $0.5 \mu\text{m}$  are collected at atmospheric or near-atmospheric pressure.

The calculated particle-diameter cutpoints for the Berner impactor are 0.06, 0.125, 0.25, 0.5, 1.0, 2.0, 4.0, 8.0, 16.0  $\mu\text{m}$ . The jet Reynolds numbers fall in the range between 1000 and 4000, which according the impactor theory (Chapter 4) should give sharp particle size cutoffs. Recently John *et al.* (1986) calibrated the impactor with sticky particles. Their experimental cutpoints were sharp, and agreed with the calculated values.

## THE RESPIRABLE DUST CENTER

**Hering LPI:** In contrast to the Berner impactor, the Hering low-pressure impactor (LPI) has just one circular jet per stage, as shown in Figure 4. It was designed to make use of direct analysis techniques, which are generally more sensitive than those that require sample extraction, but which require the aerosol to be concentrated in a small deposit area. For example, aerosol deposited within a 20 mm<sup>2</sup> area can be analyzed for sulfur at the nanogram level by the method of flash volatilization with flame-photometric detection of the evolved gases. Elemental analysis by proton-induced X-ray emissions is also suitable for spot analyses, and is sensitive at the 10 nanogram level for many elements. The sample flow rate is 1 L/min at ambient temperature and pressure, which is sufficient with nanogram sensitivities to produce easily measurable samples for sulfur in 0.5–5 hours of sampling. The lower mass flow rate reduces

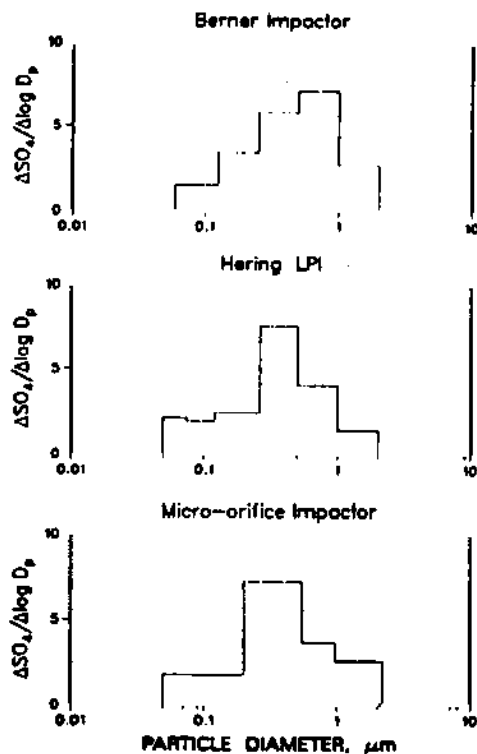


Figure 2. Ambient sulfate size distributions in Los Angeles measured using a) the Berner low-pressure impactor on 8/9-10/83, b) the Hering low-pressure impactor on 8/8/84 (1832-1944 PDT), and c) the University of Minnesota micro-orifice impactor (MOUDI) on 8/8/84 (1657-2015 PDT). The data from the Hering LPI and the MOUDI were collected side by side.

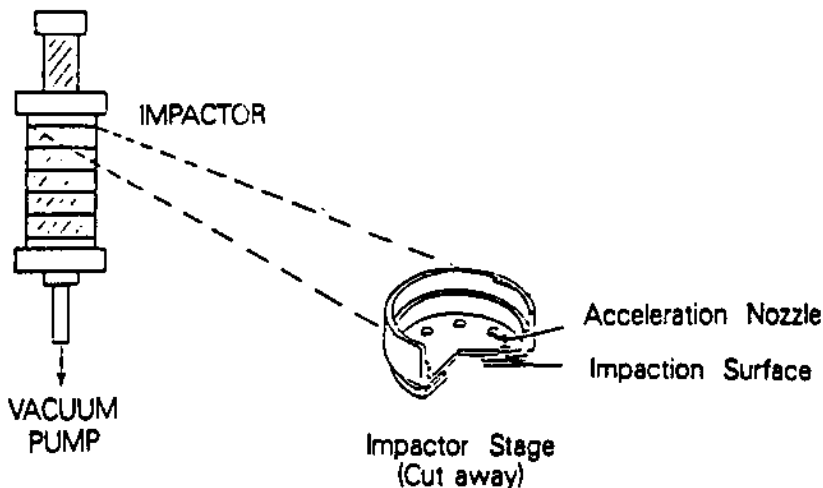
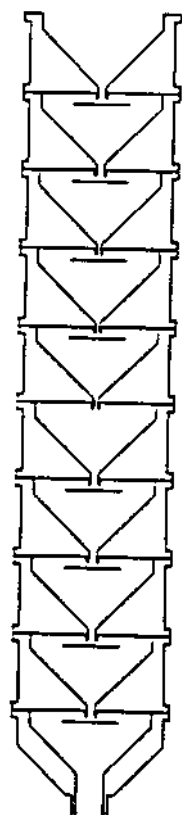


Figure 3. The Berner low-pressure cascade impactor, with details of one stage showing the orifice and collection plates. (Adapted from John *et al.* 1986).

# LOW-PRESSURE AND MICRO-ORIFICE IMPACTORS

**TABLE 1. Design and operating parameters for the Berner Low-pressure Impactor, Flow rate = 30 L/min.**

Stage #	No. of Jets	Jet Diameter (mm)	$P/P_0$	Jet Velocity (m/s)	$Re$	$D_{50}$ ( $\mu\text{m}$ )
9	1	16.60	1.000	2.31	2549	16.0
8	7	5.50	1.000	3.01	1099	8.0
7	13	2.80	1.000	6.25	1162	4.0
6	26	1.40	0.995	12.50	1162	2.0
5	50	0.75	0.991	26.00	1128	1.0
4	30	0.60	0.954	64.00	2351	0.50
3	22	0.50	0.814	153.00	3847	0.25
2	30	0.40	0.515	227.00	3526	0.125
1	130	0.25	0.324	227.00	1302	0.06



PRESSURE	CUTPOINT
100 kPa	4 $\mu\text{m}$
100 kPa	2 $\mu\text{m}$
99 kPa	1 $\mu\text{m}$
95 kPa	0.5 $\mu\text{m}$
Critical orifice	
19 kPa	0.26 $\mu\text{m}$
15 kPa	0.12 $\mu\text{m}$
7 kPa	0.075 $\mu\text{m}$
3 kPa	0.05 $\mu\text{m}$

Figure 4. Schematic drawing of the Hering low-pressure cascade impactor showing the operating pressures and calibrated cutoff diameters at an inlet pressure of 99 kPa.

the pumping requirements, making the Hering LPI a portable instrument suitable for both ground based and aircraft sampling.

Design and operating parameters of the impactor are listed in Table 2. It is an eight stage impactor with aerodynamic cutoff diameters (corresponding to particles collected with an efficiency of 50%) of 0.05, 0.075, 0.12, 0.26, 0.5, 1.0, 2.0 and 4.0  $\mu\text{m}$ . Particles larger than 0.5  $\mu\text{m}$  are sampled at ambient pressure using the first four stages of the Battelle impactor (Mitchell and Pilcher, 1959). Four additional stages, operating at pressures below 0.2  $P_0$ , size-segregate the smaller particles. A critical orifice separates the atmospheric and low-pressure stages, and determines the sample flow rate. A 47 mm fiber filter may be operated after the final stage without affecting the impactor performance. Calibration curves obtained with solid particles on greased surfaces are shown in Figure 5. These data were obtained for operation at 99 kPa and room temperature. Impactor cutoffs for operation at high temperatures and low pressures are given by Biswas and Flagan (1984).

TABLE 2. Design and operating parameters for the Hering Low-pressure Impactor, Flow rate = 1.0 L/min.

Stage #	No. of Jets	Jet Diameter (mm)	S/W	P/P <sub>0</sub>	Average Jet Velocity (m/s)	Jet Core Velocity (m/s)	Re	D <sub>50</sub> ( $\mu\text{m}$ )
1	1	2.49	0.5	1.000	3	0	566	4.0
2	1	1.40	0.5	1.000	11	0	1007	2.0
3	1	0.99	0.5	0.990	22	41	1425	1.0
4	1	0.65	0.5	0.952	53	81	2170	0.5
orifice	1	0.36	—	0.206	—	313	3918	—
5	1	1.10	0.5	0.185	93	134	1282	0.26
6	1	0.99	0.5	0.146	143	196	1425	0.12
7	1	0.99	0.5	0.070	271	313	1425	0.075
8	1	1.40	0.5	0.032	290	313	1007	0.05

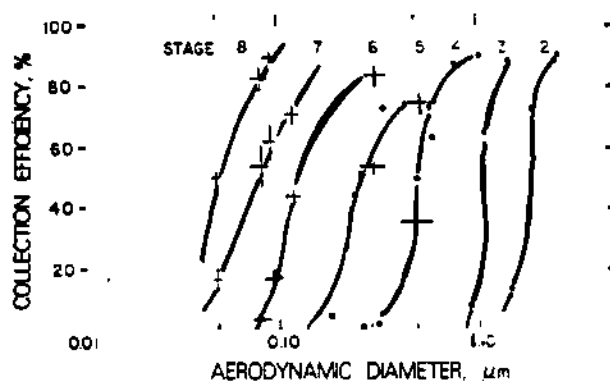


Figure 5. Experimental collection efficiencies for the Hering LPI collected on Vaseline<sup>®</sup> coated substrates at an inlet pressure of 99 kPa. Calibration aerosols are uranine (+) and polystyrene latex (o).

From Table 2 we note that the jet diameters for the low-pressure stages do not become smaller with each stage. In fact the eighth, or smallest cutoff stage, has the larger jet diameter. The mechanism used to obtain smaller cutoff diameters is the successive reduction of the stagnation

pressure on each stage. The lower pressures have the combined effect of increasing the jet velocity (since the mass flow rate per jet is constant) and increasing the effect of particle slip. This successive reduction in stagnation pressure on the last four stages arises from the high jet velocities, corresponding to compressible flow conditions. In all of these stages the air mean free path in the collection region above the impaction plate is greater than the diameter of the particle collected with 50% efficiency. The corresponding values for the slip factor at the cutoff diameter,  $C(D_{50})$ , vary from 5 to 60.

The two jet velocity values listed in Table 2 correspond to the average velocity in the jet, calculated assuming adiabatic flow, and the velocity in the core of the jet, calculated assuming isentropic (adiabatic and inviscid) flow, as discussed below. The velocity generally used in the calculation of Stokes numbers is the average velocity in the jet. The isentropic core velocity is also instructive; here it shows that the final two stages of the Hering LPI have sonic velocity jets. Further reduction of the pressure downstream of the final stage below the value needed to make the flow sonic does not affect the stage performance. Thus the pressure below that stage is listed simply as less than  $0.032 P_0$ . This point may be argued from theoretical grounds, but has also been verified experimentally.

In the calibration of Hering *et al.* (1979), wall losses were assessed by comparing the sum of material collected on the impactor stages and after filter with the amount collected on a parallel filter. Since solid particles were used for the calibration, the data only give a lower limit for overall wall losses, but should well represent diffusional losses. As shown in Figure 6, no significant losses are found for particles larger than  $0.05 \mu\text{m}$ . Washing of the impactor after several calibration runs showed no significant losses within the critical orifice, although some losses do occur downstream of the orifice, at the entrance of the fifth stage.

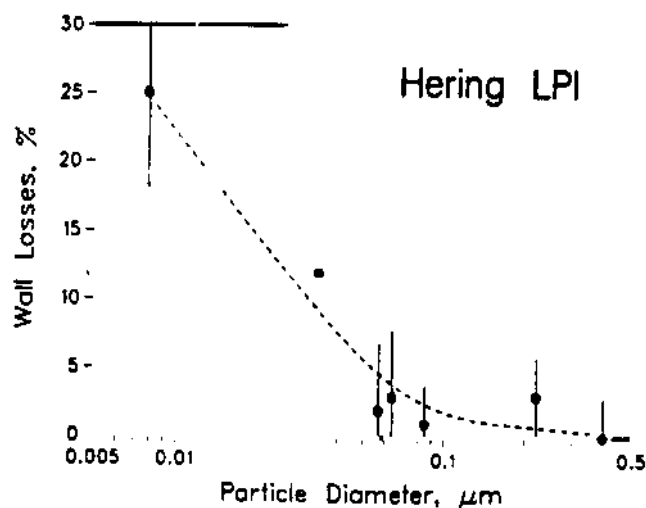


Figure 6. Solid-particle wall losses in the Hering LPI as a function of the physical particle diameter. Losses are attributed to diffusion.

#### 5.4.2 Operation of Low-Pressure Impactors

The operation of low-pressure impactors is quite similar to that of traditional impactors; substrates must be carefully prepared and properly mounted; flow rates should be checked. Two points require special attention. First, since the instrument operates at reduced pressure, care must be taken to insure that there are no leaks in the system. Second, the jet velocities can be quite high, and care should be taken to insure there are no losses from particles rebounding from the collection stages.

Leaks not only cause contamination of the sample, but will affect the pressure drops in the instrument, thereby changing the size cuts. One simple method to check for leaks is to use a vacuum gage attached to one of the lower impaction stages. The impactor inlet can be sealed and the impactor evacuated with the sampling pump. After evacuation the valve to the pump is closed and the vacuum gage is watched for any rise in pressure. Generally low-pressure im-

factories use o-rings which provide excellent vacuum seals. Leaks can arise in the connections to the pump, or to the vacuum gage itself. It is considered good practice to leak-check the impactor for each day it is used.

Although the flow rate should be checked with each use, this is not a sufficient check that the impactor is leak-tight. For the Hering LPI, which has its rate-controlling orifice ahead of the low-pressure stages, the flow rate can be unaffected by leaks downstream of the orifice. The design pressure below the orifice is  $0.206 P_0$ . Yet the flow rate in the instrument will be correct unless the pressure below the orifice is above  $0.5 P_0$ . Only a fairly large leak would perturb the flow rate.

The second point of concern is that of particle bounce, or rebound of the particles from the collection substrate. Solid particles will bounce in these impactors because of the high jet velocities used for impaction. Although it is often assumed that small particles are not susceptible to particle bounce, both laboratory and field studies show that solid particles are not efficiently collected when using uncoated stages. In Figure 7, the collection efficiency for  $0.22 \mu\text{m}$  polystyrene latex spheres is shown for greased and ungreased surfaces. These measurements are for a  $0.15 \mu\text{m}$ -cutpoint impactor stage, operated at 10 kPa with a jet velocity of 86 m/s. Particle penetration is detected using an optical particle counter downstream of the impactor stage (Hering, 1986). The uncoated surface gives a collection efficiency of 28%, compared with 95-98% for a well-greased surface. When a relatively light grease coating was tested, solid-particle collection efficiencies decreased with loading on the collection surface.

For the Hering LPI it is recommended that an adhesive coating always be used on the collection substrates. For the Berner impactor, samples have been collected without using grease coatings on the stages; however, it is important to verify that particle bounce is not a problem for the particular aerosol being sampled (Berner *et al.*, 1980).

#### 5.4.3 Limitations

Problems may arise in the sampling of volatile materials with a low pressure impactor for two reasons: (1) the collected aerosol is exposed to low pressure during sampling, which can cause volatilization, and (2) the high-velocity flow in the critical orifice and final impactor stages is

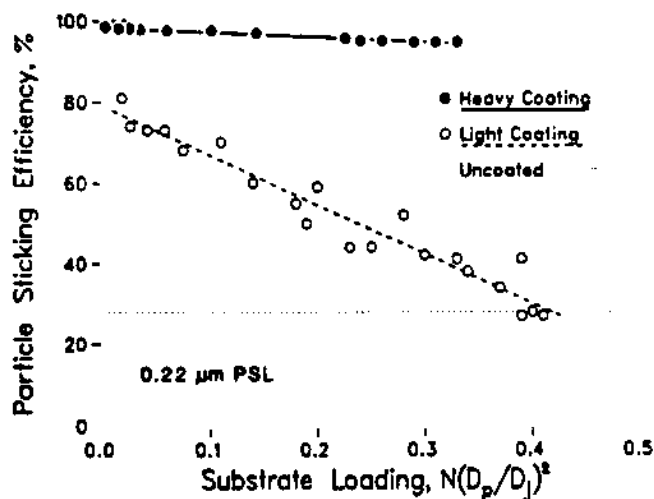


Figure 7. Collection efficiencies for  $0.22 \mu\text{m}$  polystyrene latex particles on bare glass and Vaseline<sup>®</sup> coated substrates. The ordinate gives the ratio of the cross-sectional area of the deposited aerosol to the cross-sectional area of the jet. For the lightly-coated substrate the collection efficiency decreases as the collection surface becomes coated with particles.

accompanied by large temperature drops in the jets, which could potentially cause condensation from the gas phase. The magnitude of these effects is just now being studied.

We first examine losses during sampling of volatile species deposited on the impactor collection surface. Recently John *et al.* (1986) investigated evaporative losses of ammonium nitrate collected in the Berner impactor. Tests were conducted with a 0.16  $\mu\text{m}$  mass median diameter polydisperse aerosol, which predominantly collects on the low pressure impactor stages. Their experiments consisted of first collecting the nitrate aerosol in the impactor, removing a small portion of the sample for analysis, and then sampling dry, clean air through the impactor placed in an environmental chamber at 35°C. Losses in the impactor for exposures of 6 to 24 hours were 3–7%. The same test conducted for Teflon<sup>®</sup> membrane filters showed 80–95% losses. The losses for this volatile species are actually much greater from filter sampling than from the low pressure impactor.

John's explanation of the lower losses from the impactor is that the exposed surface area of the aerosol collected on the filter is much greater than for the aerosol collected in the impactor. In the impactor the particles collect in a small pile, and only those on the outer layer are subject to evaporation. His hypothesis is supported by additional experiments showing that the volatilization losses for both the filter and the impactor are dependent on the areal loading. One concludes that with sufficient particle loadings, this problem can be minimized.

The second issue to be addressed is the potential for changing particle size during sampling with a low pressure impactor. At the reduced pressures, water associated with the aerosol may evaporate. While not affecting the chemical assays of the collected sample, the water loss can change the size of the particle before impaction. If a hygroscopic material such as ammonium sulfate loses its water, then the particle diameter can decrease dramatically. At the same time the particle density increases, and the decrease in aerodynamic diameter is not as great as the decrease in the physical (volume equivalent) diameter. For example, at deliquescence the physical diameter of ammonium sulfate changes by 50%, whereas its aerodynamic diameter changes by 15–30% (depending on particle size relative to the mean free path).

The effects of changes in relative humidity due to pressure and temperature drops in the impactor jets have been examined by Hochrainer and Zebel (1981), and more recently by Biswas *et al.* (1986). Both examined impactors with high jet velocities (greater than 200 m/s), which have temperature drops of greater than 30°C in the jet. There are two competing factors in these high velocity jets: the drop in pressure decreases the relative humidity while the drop in temperature increases it. Deliquescent salts can either gain or lose water, with corresponding changes in particle diameter.

In their experiments, Hochrainer and Zebel did not observe any substantial water condensation on the particles during sampling. They attributed the lack of particle growth to the brief residence time of the particles in the jet. On the other hand, Biswas *et al.* (1986) find there can be measurable changes in particle sizes for the Hering LPI. Their calculations and experiments with 0.05–0.2  $\mu\text{m}$  ammonium sulfate particles show decreases in particle diameter for the fifth and sixth LPI stages, and increases for the seventh stage. Biswas also applied his model to the Berner impactor, and predicted condensational growth for ammonium sulfate particles at high humidities on the final three Berner impactor stages. However this was not observed experimentally (John *et al.*, 1986). Although there is disagreement on this issue, the investigator should be aware that impactor sizing could be in error for deliquescent salts near their deliquescence point or at humidities above 90%.

### 5.5 Micro-Orifice Impactors

#### 5.5.1 Design

The micro-orifice sampler developed at the University of Minnesota is a multijet cascade impactor designed for a flow rate of 30 L/min (Kuhlmeier *et al.*, 1981, Marple *et al.*, 1981, Marple and Rubow, 1984a). The instrument is designed to provide adequate sample for gravimetric mass measurements, and for chemical assays from the sampling of atmospheric aerosols. The collection substrates are 37 mm in diameter, and can be of nearly any material. However usually a foil or filter substrate is used. Calibrated cutpoints below 1  $\mu\text{m}$  show a slight variation in the cutoff diameters with different types of substrate.



## THE RESPIRABLE DUST CENTER

There are several prototype versions of the instrument, and a commercial version is just becoming available. The specifications for one of the prototype designs are given in Table 3. In this design the final two stages are a micro-orifice design with 2000 nozzles in each stage. The nozzle diameters range from 46 to 124  $\mu\text{m}$ , and are formed by chemical etching. The upper four stages, which collect super-micrometer particles, resemble more traditional impactors, with ten jets per stage formed by drilling. The impactor has two 1  $\mu\text{m}$ -cutpoint stages to insure that large particles do not enter the micro-orifice stages.

**TABLE 3. Design and operating parameters for the  
Micro-orifice Impactor MOUDI, Flow rate = 30 L/min.**

Stages #	No. of Jets	Jet Diameter (mm)	S/W	P/P <sub>0</sub>	Average Jet Velocity (m/s)	Re	D <sub>50</sub> Al* ( $\mu\text{m}$ )	D <sub>50</sub> Filter ( $\mu\text{m}$ )
1	10	3.45	1	1.000	5	1226	4.90	4.90
2	10	2.18	1	0.998	13	1941	2.60	2.60
3	10	1.18	1	0.983	46	3586	1.00	0.97
4	10	1.18	1	0.968	47	3586	1.00	0.97
5	80	0.47	1.5	0.957	36	1000	0.60	0.53
6	2000	0.07	10	0.917	63	286	0.23	0.20
7	2000	0.06	10	0.814	122	378	0.103	0.092

\* Al: Aluminum substrate

A second feature of this impactor is the ability to provide uniform deposits. The arrangement of the nozzles on the orifice plate is such that when the collection substrate is rotated during collection, a uniform deposit results. The advantage of the uniform deposit is it allows direct analysis of the sample by X-ray fluorescence. It also permits the collection of a larger sample before the impaction substrate becomes overloaded or the jet to plate distance is affected by the aerosol deposit.

A schematic diagram of one of the stages is shown in Figure 8. Each impactor stage consists of the collection plate for the stage above and the nozzle plate for the stage below. The jet-to-plate distance is controlled by the thickness of the nozzle support ring. With this design, alternating stages can be rotated, providing uniform deposits on all of the collection substrates. The rotated version of the instrument is called the MOUDI, for *Micro-Orifice Uniform Deposit Impactor*.

The 127-m/s jet velocity used to obtain the 0.1  $\mu\text{m}$ -cutoff in the micro-orifice impactor is not much lower than the 143-m/s velocity used for the 0.12  $\mu\text{m}$ -cutoff stage in the Hering LPI. The pressure, however, is much closer to ambient. For the micro-orifice instrument the upstream stagnation pressure, which approximates the pressure at the collection plate, is 92% of the ambient pressure. For the low-pressure impactor, the pressure above the 0.12  $\mu\text{m}$ -stage is 19% of ambient. This can have important implications for sampling volatile aerosols.

The jet Reynolds numbers for the micro-orifice stages are lower than for the low pressure impactors, but for the 0.1 and 0.2  $\mu\text{m}$  cutpoints are sufficient to provide reasonably sharp cutpoints, as has been verified by the experiment. Typical calibration curves for the micro-orifice stages are shown in Figure 9. These data are for a prototype version similar to that described in Table 3.

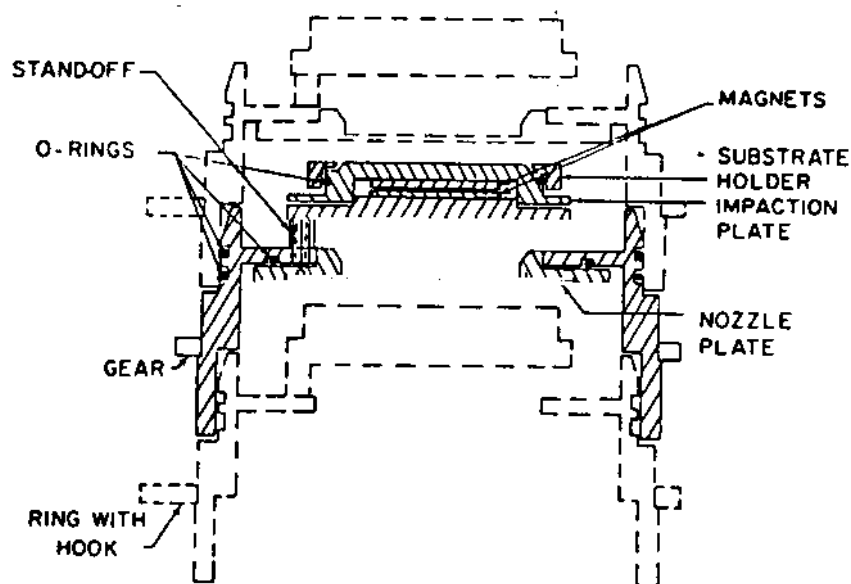


Figure 8. Schematic diagram of a typical stage of a uniform deposit impactor.

### 5.5.2 Operation of Micro-orifice Impactors

The micro-orifice impactor can be used with nearly any particle collection substrate as long as it is 37 mm in diameter. Substrates of foils and filters have both been used. For example, aluminum foil substrates are used when carbon analyses are to be made on the deposited particles, and Teflon® filter substrates are used for inorganic and elemental measurements. In addition, the substrates can be greased or ungreased. Ungreased substrates were used for the carbon and the inorganic and elemental measurements.

Another feature of the micro-orifice impactor is that the impaction plates and filter holder can easily be removed from the impactor. The purpose of this feature is to allow the substrates and backup filter to be loaded onto the impaction plates and filter holder in the laboratory, taken to the field for a test and then returned to the laboratory where the substrates and backup filter holder are removed. Sealed covers for the impaction plates and backup filter holder are provided so the deposits are not damaged during transport. Generally, two sets of impaction plates and backup filter holders are used with a single impactor so that the impactor can be collecting data with one set while the substrates are being changed in the second set.

When using a micro-orifice impactor, some care must be taken to keep the orifice plates clean. Since the nozzles are very small, they can become partially blocked during handling, or sometimes when sampling for extended periods of time. The plates may be cleaned using an ultrasonic bath. While operating the impactor, the pressure drop across the first stage is monitored to indicate the flow rate through the impactor. In addition, the pressure drop across the final stage is monitored to indicate if the nozzles are becoming dirty.

## 5.6 Aerodynamic Diameter and Data Interpretation

Two factors need to be considered in interpreting low pressure and micro-orifice impactor data. First, impactors size particles according to their aerodynamic behavior at the operating pressure of the impactor stage. For stages operating at reduced pressures, this is not quite the same as the aerodynamic diameter of the particle at atmospheric pressure. The atmospheric-pressure aerodynamic diameter may differ from the stage-pressure aerodynamic diameter by as much as  $\sqrt{\rho_p/\rho_o}$  (where  $\rho_p$  = particle density, and  $\rho_o = 1 \text{ g/cm}^3$ ), although usually the corrections are smaller.

## THE RESPIRABLE DUST CENTER

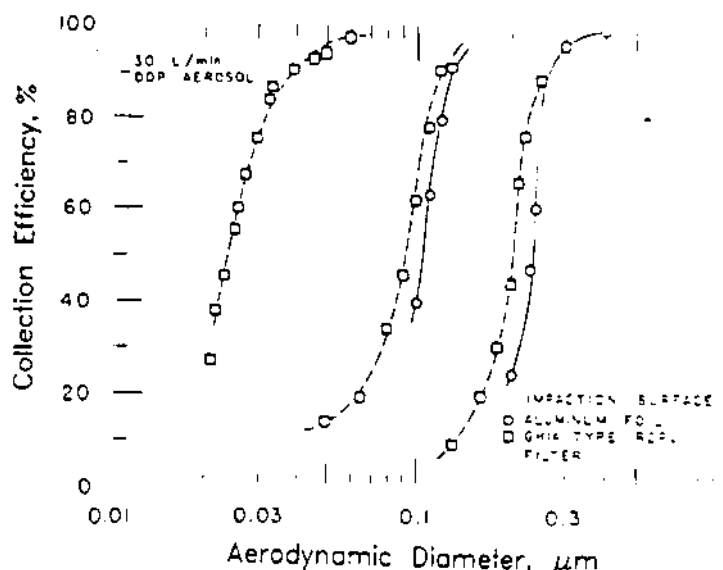


Figure 9. Experimental collection efficiency curves for the micro-orifice impactor stages with aluminum foil or Ghia<sup>®</sup> filter as impaction substrates.

Second, for particles below 0.2–0.4  $\mu\text{m}$ , the aerodynamic diameter is often not of as much interest as the Stokes diameter, which can be directly related to the diffusion coefficient. Stokes diameter is the value for particle diameter which appears in the Stokes number. For a smooth spherical particle, it is just the actual, physical diameter. For a nonspherical particle it is the diameter of a round particle that has the same density and settling velocity.

Traditional impactors cover the size range above 0.4  $\mu\text{m}$  where aerodynamic diameter is the quantity of interest. For these particles, aerodynamic diameter is the parameter that enters into the equations for transport and deposition. For smaller particles sampled in the lower stages of low-pressure and micro-orifice impactors, diffusion is often more important than inertial mechanisms. In these cases the Stokes diameter may be more useful. The particle diffusion coefficient  $\mathcal{D}$  is explicitly given in terms of the Stokes diameter by the Stokes-Einstein relation:

$$\mathcal{D} = \frac{kTC}{3\pi\mu D_p}$$

The relationship between aerodynamic and Stokes diameter depends on the particle density, as does the ratio between atmospheric-pressure aerodynamic diameter and stage-pressure aerodynamic diameter. Based on chemical analysis, the investigator can generally estimate the density of the aerosol sampled. Thus the Stokes diameter and the atmospheric-pressure aerodynamic diameter can be evaluated from the stage-pressure aerodynamic diameter (a known quantity) and the estimated particle density. For particles with densities 1  $\text{g}/\text{cm}^3$ , the low-pressure aerodynamic diameter is the same as the atmospheric-pressure aerodynamic diameter, and is also the same as the Stokes diameter.

**Stokes Diameter:** For particles with non-unit density, the Stokes diameter is calculated from the stage-pressure aerodynamic diameter using:

$$D_p = \left[ \frac{\rho_p C(D_{st}, \lambda_s)}{\rho_a C(D_p, \lambda_s)} \right]^{1/2} D_{st} \quad (4)$$

Here  $C(D_p, \lambda_s)$  and  $C(D_{st}, \lambda_s)$  are the slip factors for the Stokes and stage-pressure aerodynamic diameters respectively, evaluated for the mean free path at the stagnation pressure above the impactor jet ( $\lambda_s$ ).

The scaling with density is different between the continuum and free molecular regimes. At reduced pressures, when the mean free path is larger than the particle diameter ( $C \sim D_p^{-1}$ ), the aerodynamic diameter is related to the Stokes diameter according to:

$$D_{st} = \frac{\rho_p D_p}{\rho_a} \quad (\lambda \gg D_p)$$

For the continuum regime, when the mean free path is much smaller than the particle diameter, the aerodynamic diameter is given by the familiar expression:

$$D_w = \sqrt{\frac{\rho_p}{\rho_a}} D_p \quad (\lambda \ll D_p)$$

Because the slip factor itself depends on particle diameter, equation (4) reduces to the continuum and free molecular expressions for the appropriate limiting cases.

*Atmospheric-Pressure Aerodynamic Diameter:* In a low-pressure impactor, a particle may be collected on the basis of its aerodynamic behavior in the free molecular regime, when at atmospheric pressure its behavior is best described by the continuum expression. The particle size that is measured by a low-pressure impaction stage is dependent upon the stage pressure.

To calculate the atmospheric-pressure aerodynamic diameter, one must first evaluate the Stokes diameter using equation (4). Then the aerodynamic diameter at atmospheric pressure is given by:

$$D_w = \left[ \frac{\rho_p C(D_p, \lambda)}{\rho_a C(D_w, \lambda)} \right]^{1/2} D_p \quad (4a)$$

where  $C(D_p, \lambda)$  and  $C(D_w, \lambda)$  are the slip factors for the Stokes and atmospheric-pressure aerodynamic diameters respectively, evaluated for the mean free path at atmospheric pressure ( $\lambda = 0.066 \mu\text{m}$ ).

Values for the atmospheric pressure (101 kPa) aerodynamic cutoff diameters for the Hering LPI are given in Table 4. The largest differences between the atmospheric- and stage-pressure aerodynamic diameters are for particles in the transition regime. For very small particles the low-pressure impactor gives a good estimate of the atmospheric aerodynamic diameter because the particle is already near the free molecular regime at atmospheric pressures.

*Data Presentation:* Whether the investigator chooses to plot his data in terms of Stokes or aerodynamic diameter will depend on the application at hand. Sometimes, such as in the lung deposition of 0.1–0.5  $\mu\text{m}$  particles, both types of information are needed. To accommodate the need to know the aerodynamic diameter for large particles, and the Stokes diameter for small particles, Hering and Friedlander (1982) proposed plotting size distributions as a function of  $\sqrt{\rho_p/\rho_a} D_p$ . For particles greater than 0.5  $\mu\text{m}$ , this is essentially the same as the aerodynamic diameter. For smaller particles, which are collected on the low pressure impaction stages, one must assume a particle density, from which the Stokes diameter is obtained using equation (4). Also, the scaling of Stokes diameter with respect to density is consistent over the entire size range, which is not true for the aerodynamic diameter.

Values for the Hering LPI cutoff diameters, expressed as  $\sqrt{\rho_p/\rho_a} D_p$  are given in Table 4. For the atmospheric pressure stages ( $D_p > 0.5 \mu\text{m}$ ) this quantity has the same value as the aerodynamic diameter. Expressing the cutoff as  $\sqrt{\rho_p/\rho_a} D_p$  does not require knowledge of the particle density. For the low-pressure stages, one estimates the particle density on the basis of the particle chemistry. Generally the same value is used for each stage. The Stokes diameter can be readily obtained from the stated particle density, and yet the data for the entire size range are presented in a consistent manner.

### 5.7 Design Considerations for Low-Pressure and Micro-Orifice Impactors

As pointed out in Chapter 4, impactor stages should be designed with jet Reynolds numbers between 500 and 3000 to give sharp cuts. Inspection of the expression for the Stokes number shows that the only means of obtaining small cutoffs at large Reynolds number is to use large jet velocities.

The particle Stokes number is proportional to jet velocity divided by jet diameter:

$$St \sim CD_p^2 \frac{V}{W}$$

## THE RESPIRABLE DUST CENTER

For incompressible flow, the jet Reynolds number is directly proportional to the product of jet diameter and pressure:

$$Re \sim PWV$$

Combining these two proportionalities for a pressure of one atmosphere gives, for the jet velocity:

$$V^2 \sim \frac{Re \cdot St}{CD_p^2} \quad (\text{at atmospheric pressure})$$

When the particle diameter is smaller than the mean free path, the Cunningham slip factor is inversely proportional to the pressure and particle diameter. The expression for the proportionality between jet velocity, particle diameter,  $Re$  and  $St$  becomes:

$$V^2 \sim \frac{Re \cdot St}{D_p} \quad (\text{low pressure, } \lambda > 3D_p)$$

For a fixed particle cutoff diameter, larger jet Reynolds numbers can only be obtained at larger jet velocities. For large diameter cutoffs it is not difficult to maintain Reynolds numbers above 500 for moderate jet velocities. But at small cutoffs, below a few tenths of a micrometer, relatively large velocities are required even to get a Reynolds number of 200.

In Figure 10 jet velocities at  $Re = 200$  are shown as a function of cutoff diameter. Two cases are presented: (1) a micro-orifice impactor operating at atmospheric pressure, and (2) a low-pressure impactor operating at pressures such that the mean free path is more than 3 times the

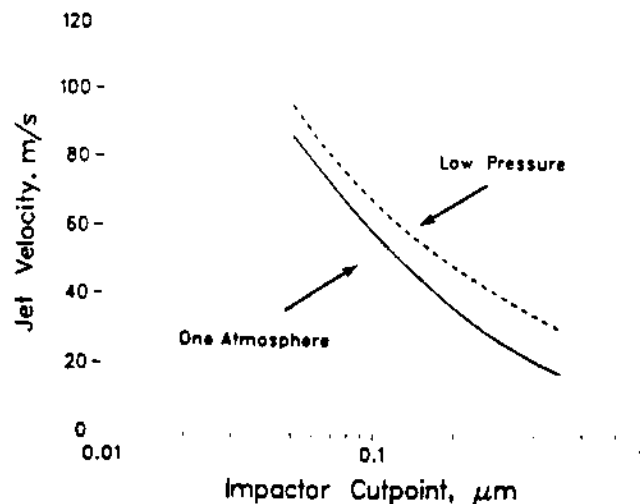


Figure 10. Jet Velocities needed to obtain the given cutpoints for round jet impactors operated at a jet Reynolds number of 200. The upper curve (---) corresponds to a low-pressure impactor at  $\lambda > 3D_p$ . The lower curve (—) corresponds to the micro-orifice impactor operated at 101 kPa (1 atm).

cutpoint diameter. Calculations are for round-jet impactors operating at velocities below 100 m/s (incompressible flow).

We find that the jet velocities required by the micro-orifice are not quite as large as those required by the low-pressure impactors. However, at cutoff diameters below 0.2  $\mu\text{m}$ , the micro-orifice jet velocities are less than 15% lower than those for a low pressure impactor operating at the same jet Reynolds number.

At higher Reynolds numbers, jet velocities larger than those shown in Figure 10 are required to obtain the small cutpoints. One of the recommended design criteria given in Chapter 4 is that the jet Reynolds numbers be greater than 500. However, for particle cutpoints of less than 0.1  $\mu\text{m}$ , to obtain  $Re \geq 500$  requires jet velocities greater than 90 m/s for micro-orifice impactors, and greater than 105 m/s for low-pressure impactors. Thus, it is difficult to obtain small cutoffs without using relatively high jet velocities. Two types of sampling problems can arise

## LOW-PRESSURE AND MICRO-ORIFICE IMPACTORS

for large jet velocities. There are potential problems of particle rebound from the collection surface. For velocities above 150 m/s, there are also substantial pressure drops across the jets that may create artifacts for volatile species. These factors must be considered in the design of small-cutpoint impactors.

### 5.8 Calibration of Low-Pressure and Micro-Orifice Impactors

The calibration of low-pressure impactors involves the generation of monodisperse aerosols as small as 0.03  $\mu\text{m}$ . This is generally achieved using an electrostatic classifier (TSI Model 3071, St. Paul, MN). First, a polydisperse aerosol is generated using an atomizer or condensation aerosol generator. The charge on the dried aerosol is neutralized by exposure to a  $^{85}\text{Kr}$  source. The neutralization process places an equilibrium bipolar charge distribution on the aerosol. Overall the aerosol is neutral, but individual particles can still carry a net charge. The percentage of particles carrying 0,  $\pm 1$ ,  $\pm 2$ , or higher charges depends on particle diameter, as described by the Boltzmann equilibrium charge distribution. Within the classifier, the aerosol

**TABLE 4.** Cutpoints for the Hering LPI expressed in terms of atmospheric-pressure aerodynamic diameter,  $D_w$ , atm; and  $\sqrt{\rho_p/\rho_w}D_p$  for varying particle densities.

Stage	Cutpoint, $D_w$	$\rho_p/\rho_w$	$D_w$ , atm	$\sqrt{\rho_p/\rho_w}D_p$
Stage 8	0.05 $\mu\text{m}$	0.5	0.056	0.070
		1.0	0.050	0.050
		1.5	0.048	0.041
		2.0	0.047	0.036
		4.0	0.045	0.025
		6.0	0.045	0.021
		10.0	0.044	0.016
Stage 7	0.075 $\mu\text{m}$	0.5	0.086	0.103
		1.0	0.075	0.075
		1.5	0.071	0.062
		2.0	0.069	0.054
		4.0	0.066	0.038
		6.0	0.065	0.031
		10.0	0.064	0.024
Stage 6	0.12 $\mu\text{m}$	0.5	0.139	0.160
		1.0	0.120	0.120
		1.5	0.112	0.100
		2.0	0.108	0.088
		4.0	0.101	0.063
		6.0	0.099	0.052
		10.0	0.097	0.040
Stage 5	0.26 $\mu\text{m}$	0.5	0.302	0.326
		1.0	0.260	0.260
		1.5	0.239	0.223
		2.0	0.227	0.198
		4.0	0.205	0.146
		6.0	0.197	0.121
		10.0	0.190	0.094
Stage 4	0.50 $\mu\text{m}$	0.5	0.498	0.522
		1.0	0.500	0.500
		1.5	0.502	0.483
		2.0	0.503	0.469
		4.0	0.506	0.426
		6.0	0.507	0.394
		10.0	0.507	0.349

flow is introduced in an annular ring around a column of particle-free sheath air. The positively charged aerosol is drawn toward a central collector rod by a cylindrically symmetric electric field. By varying the collector rod voltage, aerosol of a chosen electrical mobility is made to pass through a slit at the base of the rod. Singly charged particles will all have the same Stokes diameter, but some larger doubly and triply charged particles will also be found. The percentage of the larger particles can be minimized by tailoring the input polydisperse aerosol so that its number median diameter is smaller than the diameter of the singly charged aerosol exiting the classifier.

As with any other impactor, calibrations should be performed with both solid and liquid particles. Solid particles are subject to particle bounce, while liquid particles are more susceptible to wall losses. The calibration aerosols often consist of fluorescein, or fluorescein-tagged particles. The mass collected on each impactor stage and the mass lost to the walls can then readily be detected by a simple fluorescence measurement of the extracted deposit. Calibration curves for the Hering LPI obtained in this manner are shown in Figure 5. In the calibration of the micro-orifice impactor, Marple and Rubow (1984b) used an electrical aerosol detector, which measured the total charge on an aerosol, to measure changes in the aerosol concentrations upstream and downstream of each impaction stage. Typical curves are presented in Figure 9.

### 5.9 Calculations of Jet Velocities and Stokes Numbers for Compressible-Flow Impactors.

The flow through the jets of the final three stages of the Hering LPI and Berner impactors is compressible; that is the velocities are greater than one third the speed of sound. This is in part a consequence of the fact that larger velocities are needed at low pressure to maintain the same mass flow rate through the jets. It is also a consequence of the desire to maintain large jet Reynolds numbers. When the impactor jet velocities are greater than one third the speed of sound, or 100 m/s for normal-temperature operation, then there are appreciable pressure drops across the jet. Since the flow is approximately adiabatic, the air temperature drops as well. This is because the air no longer behaves like an incompressible fluid, but expands as it passes through the jet. It is perhaps easier to think of the flow as "expansible" rather than "compressible".

The velocity that appears in the Stokes number is the velocity at the exit of the jet. The average velocity can be calculated from the mass flow rate and jet cross-sectional area, provided the temperature and pressure at the jet exit are known. Mass conservation gives:

$$V = \frac{q_v P_o T}{A P T_o} \quad (5)$$

where  $A$  is the cross-sectional area of the jet, and  $q_v$  is the volumetric flow rate per jet measured at the impactor inlet temperature,  $T_o$ , and pressure,  $P_o$ .  $T$  and  $P$  refer to the temperature and pressure at the jet exit.

Energy conservation for adiabatic flow relates the air velocity to the change in specific enthalpy  $h$ , which for an ideal gas gives:

$$V^2 = -2\Delta h = \frac{2\gamma R}{\gamma - 1} (T - T_o) \quad (6)$$

where  $R$  is the ideal gas constant, and  $\gamma$  is the ratio of the heat capacities. Combining equations (5) and (6) gives:

$$V = \frac{q_v P_o}{A P} \left\{ 1 - V^2 \frac{(\gamma - 1)}{(2\gamma R T_o)} \right\} \quad (7)$$

This is the average velocity in the jet assuming adiabatic conditions. It holds for both viscous and inviscid flow.

One can also calculate the velocity in the core of the jet assuming inviscid, adiabatic flow. This is given by the isentropic relations:

$$V_{\text{core}} = \left\{ \frac{2\gamma RT_o}{\gamma - 1} \left[ 1 - \left( \frac{P_{\text{below}}}{P_{\text{above}}} \right)^{(\gamma-1)/\gamma} \right] \right\}^{1/2} \quad (\text{subsonic flow})$$

$$V_{\text{core}} = \left[ \frac{2\gamma RT_o}{\gamma + 1} \right]^{1/2} \quad (\text{sonic flow})$$

where  $P_{\text{above}}$  and  $P_{\text{below}}$  are the stagnation pressures above and below the jet. Again  $T_o$  is the temperature at the impactor inlet. This velocity corresponds to the flow in the core of the jet when viscous dissipation is negligible. The second equation gives the velocity for choked flow, that is, when the sonic velocity limit has been reached.

Whereas the jet velocity is calculated using the air density at the jet exit, the Cunningham slip factor is calculated using the air density at the jet inlet. This is because the deviation of particles from the airstream lines is most important immediately above the impaction plate. The static pressure in the region of the collection surface is approximately equal to the upstream stagnation pressure. Experimentally determined impactor cutoffs for high-velocity jets support calculations of the slip factor based on the upstream stagnation conditions.

### 5.10 Summary

Low-pressure and micro-orifice impactors both offer a means of collecting particles as small as 0.05  $\mu\text{m}$  by inertial impaction. This is important for the study of submicrometer aerosols, such as found in photochemical smogs or combustion-generated smokes. Several low-pressure impactors are available, and the micro-orifice impactors are increasingly in use. Both require some care in their operation. Jet velocities are generally higher than found in traditional impactors, and particle rebound from the collection surface can be a problem. Low-pressure impactors are susceptible to artifacts when sampling volatile species; however, the magnitude of these problems is just now being evaluated. To aid in the design of low-pressure and micro-orifice impactors, we have presented some considerations of the relationship between jet Reynolds number and the Stokes numbers for small particles. We have also presented methods for calculating jet velocities and Stokes numbers for impactors with high-velocity jets.

### References

- Bauman S., Houmère P. D. and Nelson J. W. (1981) Cascade impactor aerosol samples for PIXE and PESA analyses. *Nuclear Instruments & Methods* 181:499-502.
- Berner A., Lürzer C., Pohl F., Preining O. and Wagner P. (1979) The size distribution of the urban aerosol in Vienna. *Sci. Tot. Envir.* 13:245-261.
- Berner A. and Lürzer C. (1980) Mass distributions of traffic aerosols in Vienna. *J. Phys. Chem.* 84:2079-2083.
- Berner A., Reischl G. and Winkelmayr W. (1983) A Sahara dust episode in Vienna. *Sci. Tot. Envir.* 31:277-281.
- Berner A., Reischl G. and Puxbaum H. (1984) Size distributions of traffic-derived aerosols. *Sci. Tot. Envir.* 36: 299-303.
- Biswas P. and Flagan R. C. (1984) High-velocity inertial impactors. *Envir. Sci. Technol.* 18:611-616.
- Biswas P., Jones C. L. and Flagan R. C. (1986) Distortion of size distributions of dry aerosol sampling instruments. Submitted to *Aerosol. Sci. & Technol.*
- Buchholz H. (1970) An underpressure cascade impactor. *Staub Reinhalt. Luft* 30:17-20.
- Cantrell B., Rubow K. L. and Cocalis J. (1986) In-mine measurement of diesel and dust aerosol size distributions using a micro-orifice uniform deposit impactor. Presented at the American Industrial Hygiene Conference, May 19-23 in Dallas, TX.
- Cheng M. T., Lee P. S., Berner A. and Shaw D. T. (1983) Orthokinetic agglomeration in an intense acoustic field. *J. Coll. & Interface Sci.* 91:176-187.
- Davies C. N. (1945) Definitive equation for the fluid resistance for spheres. *Proc. Phys. Soc.* 57:259-270.
- Dzubay T. G., Stevens R. K. and Haugenson P. L. (1984) Composition and origins of aerosol at a forested mountain in Soviet Georgia. *Envir. Sci. & Technol.* 18:873-883.
- Fairchild C. I. and Wheat L. D. (1984) Calibration and evaluation of a real-time cascade impactor. *Am. Ind. Hyg. Assoc. J.* 45:205-211.
- Fernandez de la Mora J., Halpern B. L. and Wilson J. A. (1984) Inertial impaction of heavy molecules. *J. Fluid Mech.* 149:217-233.



## THE RESPIRABLE DUST CENTER

- Flagan R. C. (1982) Compressible flow inertial impactors. *J. Coll. & Interface Sci.* 87:291-299.
- Hasan H. and Dzubay T. G. (1986) Size distribution of species in fine particles in Denver using a micro-orifice impactor. *Aerosol Sci. & Technol.* (in press).
- Hering S. V., Flagan R. C. and Friedlander S. K. (1978) Design and evaluation of new low pressure impactor. 1. *Envir. Sci. & Technol.* 12:667-673.
- Hering S. V., Friedlander S. K., Collins J. J. and Richards L. W. (1979) Design and evaluation of new low pressure impactor. 2. *Envir. Sci. & Technol.* 13:184-188.
- Hering S. V., Bowen J. L., Wengert J. G. and Richards L. W. (1981) Characterization of the regional haze in the southwestern United States. *Atmos. Envir.* 15:1999-2009.
- Hering S. V. and Friedlander S. K. (1982) Origins of aerosol sulfur size distributions in the Los Angeles basin. *Atmos. Envir.* 16:2647-2656.
- Hering S. V. and McMurry P. H. (1985) Comparison of impactor methods for determining the 0.05-2.5  $\mu\text{m}$  size distributions of carbon and sulfur. Presented at the AAAR annual meeting, November 18-23 in Albuquerque, NM.
- Hering S. V. (1986) Calibration of the QCM impactor for stratospheric sampling. *Aerosol Sci. & Technol.* (In press)
- Hitzenberger R. and Husar R. B. (1984) A comparison of extinction and size distribution data measured at two urban sites in the U.S. and Europe. *Atmos. Envir.* 18:448-452.
- Hochrainer D. and Zebel G. (1981) The influence of the expansion humidity on the deposition of particles in impactor. *J. Aerosol Sci.* 12:49-53.
- John W., Wall S. M. and Ondo J. L. (1985) Dry acid deposition on materials and vegetation: concentrations in ambient air. AIHL report #CA/DOH/AIHL/SP-34.
- John W., Wall S. M., Ondo J. L. and Wang H. C. (1986) Dry deposition of acidic gases and particles. AIHL report #CA/DOH/AIHL/SP-40.
- Kasper G. and Shaw D. T. (1983) Comparative size distribution measurements on chain aggregates. *Aerosol Sci. & Technol.* 2:369-381.
- Klaus N. (1983) Urban aerosols, analyzed by secondary ion mass spectrometry. *Sci. Tot. Envir.* 31:263-275.
- Klaus N. (1984) The effect of the substrate material on SIMS analysis of aerosols. *Sci. Tot. Envir.* 35:1-12.
- Kuhlmeiy G. A., Liu B. Y. H. and Marple V. A. (1981) Micro-orifice impactor for submicron aerosol size classification. *Am. Ind. Hyg. Assoc. J.* 42:790-795.
- Macias E. S., Zwicker J. O., Ouimette J. R., Hering S. V., Friedlander S. K., Cahill T. A., Kuhlmeiy G. A. and Richards L. W. (1981) Regional haze case studies in the southwestern U.S. I. Aerosol chemical composition. *Atmos. Envir.* 15:1971-1986.
- Marple V. A., Liu B. Y. H. and Kuhlmeiy G. A. (1981) A uniform deposit impactor. *J. Aerosol Sci.* 11:333-337.
- Marple V. A. and Rubow K. L. (1984a) Development of a micro-orifice uniform deposit impactor. U.S. Department of Energy report #DOE/PC/61255.
- Marple V. A. and Rubow K. L. (1984b) Calibration of micro-orifice impactor. USEPA report #3D3376NAEX.
- McFarland A. R. and Zeller H. W. (1963) Study of a large volume impactor for high altitude aerosol collection. U.S. Atomic Energy Commission report #USAEC/TID-18624.
- McFarland A. R., Nye H. S. and Erickson C. H. (1973) Development of a low-pressure impactor. USEPA report #EPA-650/2-74-014.
- McMurry P. H. and Friedlander S. K. (1979) New particle formation in the presence of an aerosol. *Atmos. Envir.* 13:1635-1651.
- McMurry P. H. and Wilson W. E. (1983) Droplet phase (heterogeneous) and gas phase (homogeneous) contributions to secondary ambient aerosol formation as functions of relative humidity. *J. Geophys. Res.* 88:5101-5108.
- McMurry P. H. and Marple V. A. (1986) Measurements of submicron size resolved aerosol chemical composition with the micro-orifice uniform deposit impactor. Presented at the Air Pollution Control Association annual meeting, June 23-27 in Minneapolis, MN.
- Mitchell R. I. and Pilcher J. M. (1959) Improved cascade impactor for measuring aerosol particle sizes. *Ind. Eng. Chem.* 51:1039-1042.
- Miguel A. H. and Friedlander S. K. (1978) Distribution of benzo(a)pyrene and coronene with respect to particle size in Pasadena aerosols in the submicron range. *Atmos. Envir.* 12:2407-2413.
- Miguel A. H. (1982) On the determination of benzo(a)pyrene in atmospheric aerosols fractionated by a low-pressure impactor, by TLC separation and *in situ* spectrophotofluorometry at the picogram level. *Int. J. Envir. Anal. Chem.* 12:17-25.
- Ouimette J. R. and Flagan R. C. (1982) The extinction coefficient of multicomponent aerosols. *Atmos. Envir.* 16:2405-2419.
- Parker G. and Buchholz H. (1968) Size classification of submicron particles by a low-pressure cascade impactor. Oak Ridge National Laboratory report #ORNL-4226.
- Pilat M. J., Raemhild G. A., Powell E. B., Fioretti G. M. and Meyer D. F. (1978) Development of a cascade impactor system for sampling 0.02-20  $\mu\text{m}$  diameter particles. Electric Power Research Institute report #FP-844, Palo Alto, CA.
- Puxbaum H. and Wopenka B. (1984) Chemical composition of nucleation and accumulation mode particles collected in Vienna. *Atmos. Envir.* 18:573-580.
- Rubow K. L., Marple V. A., Kittelson D. B. and Fang C. (1986) Use of the micro-orifice uniform deposit impactor to determine the size distribution of coal/diesel aerosol mixture. Presented at the American Industrial Hygiene Conference, May 19-23 in Dallas, TX.
- Stern S. C., Zeller H. W. and Schekman A. I. (1962) Collection efficiency of jet impactors at reduced pressures. *Ind. & Engrg. Chem. Fund.* 1:273-277.

## LOW-PRESSURE AND MICRO-ORIFICE IMPACTORS

Taylor D. D. and Flagan R. C. (1981) Aerosols from a laboratory pulverized coal combustor. In *Atmospheric Aerosol Source/Air Quality Relationships* (edited by E. S. Macias and P. K. Hopke), ACS Symposium Series #167, pp. 157-172.

Vossler T. L. and Macias E. S. (1986) The contribution of fine particle sulfates to light scattering. Submitted to *Envir. Sci. & Technol.*

### ACKNOWLEDGEMENTS

This research has been supported by the Department of the Interior's Mineral Institute program administered by the Bureau of Mines through the Generic Mineral Technology Center for Respirable Dust under grant number G1135142.

# Micro-orifice Uniform Deposit Impactor

V. Marple<sup>1</sup>, K. Rubow<sup>1</sup>, G. Ananth<sup>1</sup> and H.J. Fissan<sup>2</sup>

<sup>1</sup>Particle Dispersion Laboratory  
Mechanical Engineering Department,  
University of Minnesota

<sup>2</sup>University of Duisburg, Duisburg,  
F.R.G.

## INTRODUCTION

Over the past several years a new type of cascade impactor that utilizes small nozzle diameters (micro-orifice nozzles) has been under development (Kuhlmey *et al.*, 1981; Marple *et al.*, 1981). The small nozzle dimensions allow for particles to be collected as small as  $0.024 \mu\text{m}$  aerodynamic diameter on the last stage of the impactor. To obtain a reasonable flow rate of  $30 \text{ l min}^{-1}$  through the impactor, a large number of nozzles (up to 2000) are required per stage.

Furthermore, by locating the nozzles of multi-nozzle stages in a prescribed manner (described in detail by Marple *et al.*, 1981) and rotating the impaction plates relative to the nozzle plates, uniform deposits can be achieved on the impaction plates. As described by Marple *et al.* (1981), the advantages of a uniform deposit impactor over the conventional impactor that collects particles only beneath stationary nozzles are: (1) maximum use of the impaction substrate surface, reducing both particle bounce (if substrates are greased) and tare weights of the substrates (if particle mass is measured gravimetrically); (2) deposited particles can be analyzed for elemental composition by X-ray fluorescence (Dzubay and Riekkel, 1978); and (3) the pressure in the impactor can be kept relatively high compared to low pressure impactors that depend on a large slip correction to achieve small particle collection (some types of particles may evaporate at low pressures). The work described in this paper investigates two additional advantages of a uniform deposit impactor. These are: (1) the possibility of collecting two separate deposits at one time on one stage for two types of analysis techniques, and (2) the possibility of utilizing piezoelectric quartz crystal impaction plates more effectively by eliminating the deposit location sensitivity nature of the crystals (Schulze-Fröhlich, 1981).

## MICRO-ORIFICE UNIFORM DEPOSIT IMPACTOR (MOUDI)

A photograph of an eight-stage MOUDI is shown in Fig. 1. Each stage body of the impactor supports the impaction plate for the stage above and the nozzle plate for the stage below as shown in Fig. 2. By rotating alternate stage bodies, while holding the other stage bodies stationary, the impaction plates (or nozzle plates) will be rotated relative to the nozzle plates (or impaction plates).

Rotation of the alternate stage bodies is achieved by gears on these bodies that mesh with gears on an electrically driven drive shaft of a rotating mechanism (Fig. 1). The alternate stage bodies are restrained from rotation by pins that rest on the drive shaft.

The MOUDI has been calibrated with both solid and liquid monodisperse particles utilizing a vibrating orifice monodisperse aerosol generator (Berglund and Liu, 1973) for particles greater than  $1.0 \mu\text{m}$  diameter and an electrostatic classifier (Liu and Pui, 1974) for

the submicron aerosols. Calibration curves for DOP aerosols for two stages of interest in this paper are presented in Fig. 3. These stages are labeled B and E with cut sizes of 0.60 and 0.23  $\mu\text{m}$  diameter, respectively.

#### PIEZOELECTRIC QUARTZ CRYSTAL TESTS

Several investigators have found that the sensitivity of a piezoelectric crystal to measure the mass of particles deposited upon it is a function of the location of the particles on the crystal (Schulze-Fröhlich, 1981; Sauerbrey, 1959; Sauerbrey, 1964; Schaper, 1982; Daley and Lundgren, 1975). This means that the mass indicated by the frequency shift of a crystal will be a function of not only the mass of particles but also the location and shape of the particle deposit. Realizing that this undesirable characteristic could be eliminated by depositing the particles uniformly on the crystal, the feasibility of incorporating piezoelectric quartz crystal impaction surfaces into the MOUDI was investigated.

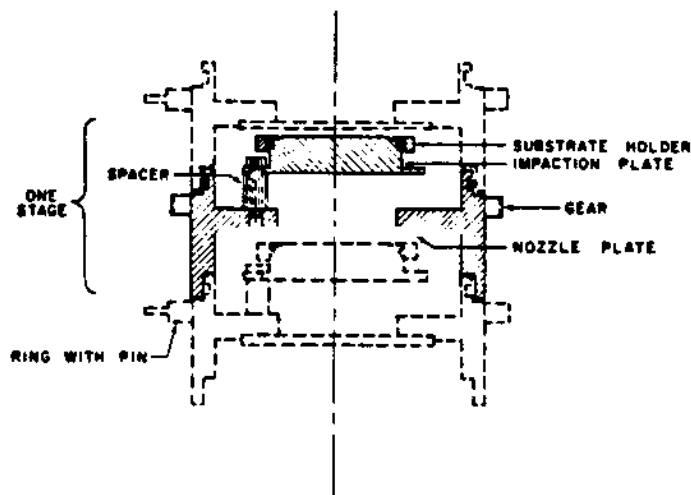


Fig 1 Micro-orifice uniform deposit impactor.

## THE RESPIRABLE DUST CENTER

Figure 4 shows an impaction plate that was constructed by TSI Inc. containing a piezoelectric quartz crystal mounted flush with the surface. Also shown in Fig. 4 is an annular foil impaction substrate that can be placed on the same impaction plate holding the crystal. Thus, particles can be collected on the foil and on the piezoelectric crystal simultaneously. By measuring the mass of particles collected on the foil (weigh foil before and after a test) the piezoelectric crystal can be calibrated.

Prior to piezoelectric crystal calibration, however, the effective area of the annular foil must be determined. A calculated ratio of areas indicates that 80.7% of the impaction surface was covered by the foil. This ratio was verified by mass measurements of particles collected on the annular foil and foils covering the entire surface. Two such tests of 0.5  $\mu\text{m}$  diameter particles deposited on stage E gave mass ratios of 79.1 and 80.0%. The close agreement



VERTICAL UNIFORM DEPOSIT IMPACTOR

Fig. 2. Schematic diagram of typical impactor stage.

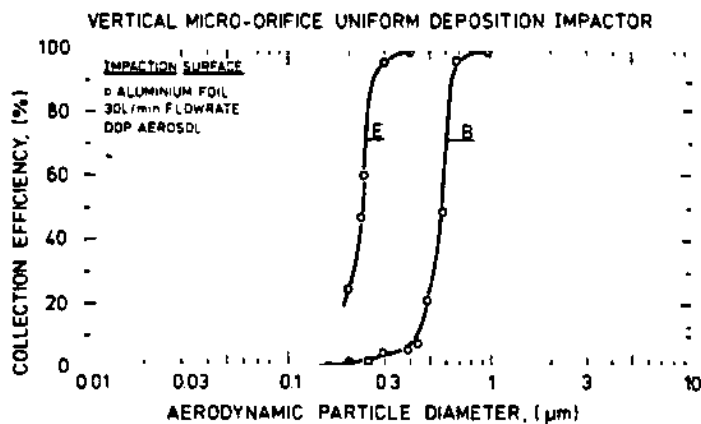


Fig. 3. Collection efficiency curves.

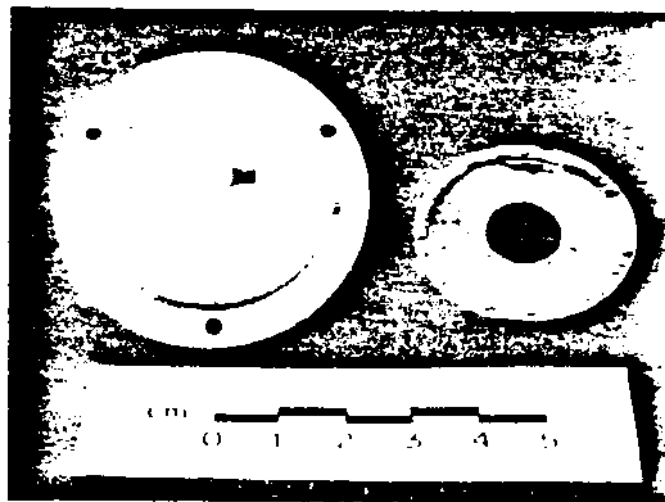


Fig. 4. Mounted piezoelectric quartz crystal and annual collection foil.

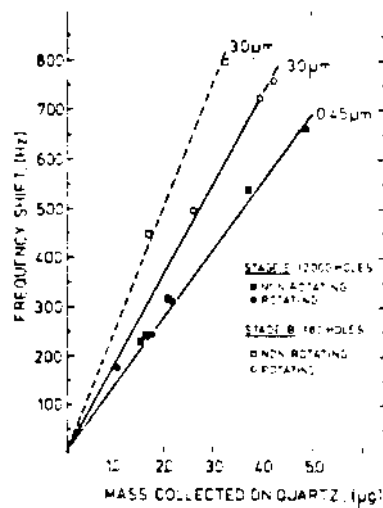


Fig. 5. Piezoelectric quartz crystal calibration curves

between the calculated and measured area ratios indicates that the deposit is indeed uniform, at least on this rather broad scale.

Using the above determined area of the foil and a crystal sensitive area of  $0.317 \text{ cm}^2$  (corresponding to a 0.25 inch diameter electrode area), the calibration curves shown in Fig. 5 were obtained. In the tests for stage B there were only about four nozzles depositing particles on the crystal since there are only 80 nozzles in the nozzle plate. Thus, different calibration curves were obtained for the nonrotating and the rotating cases. This was expected, since the rotating case provided a more uniform deposit than the four stationary nozzles of the nonrotating case. Tests with stage E containing 2000 nozzles showed no differences between the nonrotating and rotating cases. For E, approximately 100 nozzles impinge upon the crystal and this provides for a sufficiently uniform deposit in the nonrotating case to give the same calibration curve as the rotating case.

The differences between the calibration curves for the rotating stage B case and the stage E cases is due to the few nozzles near the center in stage B providing rings that are not completely uniform. Thus, these four cases show that, as the deposit becomes progressively more uniform, the calibration curve approaches the stage E calibration curves. The sensitivity of this crystal was, therefore, determined to be  $143 \text{ Hz } \mu\text{g}^{-1}$ .

CONCLUSIONS

The MOUDI has previously been demonstrated to have the advantages of maximum use of impaction surface area, adaptability to analysis techniques requiring a uniform deposit (such as X-ray fluorescence elemental analysis) and relatively low pressure drop through the nozzles. It has been demonstrated here that the MOUDI has the additional advantages of being able to collect particles simultaneously on two different substrates and to take maximum advantage of the piezoelectric quartz crystal mass sensing abilities. By using the crystal and an annular foil (gravimetric standard) as the two substrates, it is possible to calibrate the crystal directly on the particles it is to measure.

REFERENCES

- Berglund, R. N. and Liu, B. Y. H. (1973) *Environ. Sci. Technol.* 7, 147-153.  
Daley, P. S. and Lundgren, D. A. (1975) *Am. Ind. Hyg. Assoc. J.* 518-532.  
Dzubay, T. G. and Rickel, D. G. (1978) *Electron Microscopy and X-Ray Applications* (Edited by Russell, P. A. and Hutchings, A. E.), pp. 3-20. Ann Arbor Science, Ann Arbor, Michigan.  
Kuhlmey, G. A., Liu, B. Y. H. and Marple, V. A. (1981) *Am. Ind. Hyg. Assoc. J.* 42, 790-795.  
Liu, B. Y. H. and Pui, D. Y. H. (1974) *J. Colloid Interface Sci.* 47, 155-171.  
Marple, V. A., Liu, B. Y. H. and Kuhlmey, G. A. (1981) *J. Aerosol Sci.* 12, 333-337.  
Sauerbrey (1959) *Z. Phys.* 155, 106-222.  
Sauerbrey (1964) *Arch. elekt. Übertr.* 18, 617-624.  
Schaper, R. (1982) *Process- and Aerosol Measurement Technology*. Internal report No. 98, University of Duisburg, F.R.G.  
Schulze-Fröhlich, D. F. (1981) *Grundlagenuntersuchung an massesensitiven Schwingquarzen als Impaktionsflächen*. Lang, Frankfurt.

ACKNOWLEDGEMENTS

This research has been supported by the Department of the Interior's Mineral Institute program administered by the Bureau of Mines through the Generic Mineral Technology Center for Respirable Dust under grant number G1135142.

# A Hypothesis on the Possible Contribution of Coal Cleats to CWP

Thomas P. Meloy

Particle Analysis Center, West  
Virginia University

The presence of respirable quartz-bearing mineral particles has been well documented in many coal mines, and the Mine Safety and Health Administration regulations address the quartz content of mine dusts. Unfortunately, the correlation between the quantity of respirable quartz-bearing mineral particles and the pathogenicity of the dust is not strong. Work is currently underway by the National Institute for Occupational Safety and Health/U.S. Bureau of Mines and work is being included in the Respirable Dust Center Program by Dr. Seehra to determine the surface availability of quartz in mixed composition mine dusts. However, this paper propose a possible source of surface quartz or a special region in the coal that may contribute to the pathogenicity of selected particles in the respirable dust.

Assumed in this model is the hypothesis that either the cleat surface is coated with quartz or some cytotoxic substance that in the body is capable of destroying macrophage and thus inducing a fibrotic response,<sup>(1)</sup> that during the fragmentation a reasonable proportion of the respirable size coal particles contain some of the original cleat surface and that these particles have the same order of *in vivo* cytotoxicity as do the quartz particles. It may be that these cleat surfaced respirable size particles are only contributory to the overall pathogenicity of the coal dust, nevertheless, there are enough of these particles to be considered as a potential source of the cytotoxic dust particles.

This paper demonstrates that if the cleat surfaces are mineralized with quartz or have a pathogenic coating, then in many mines there will be enough respirable coal dust particles containing some cleat surface to cause a fibrotic reaction. To understand why some of the dust particles contain as part of their surface some of the cleat surface, consider what happens when a beer bottle is broken. While there are a large number of beer bottle fragments, many of the fragments, particularly the larger fragment sizes, will have as a fraction of their surface part of the original beer bottle surface. The model and mathematics of this problem have been worked out by Meloy.<sup>(2-4)</sup>

In the homogeneous IAC model,<sup>(2,5)</sup> a fragment or particle resulting from comminution is equally likely to occur anywhere in the material being broken. Therefore the prob-

ability of a particle of size  $x$  having part of the cleat surface in it,  $p(x)$ , is proportional to  $x$ . Thus:

$$p(x) = kx \quad (1)$$

where:

$k$  is a constant.

To quantify  $k$ , one must know the surface area of the cleats per cubic meter, which is the number of cleats per meter,  $n$ , times the surface area of the cleat, times 2 — the cleat has two surfaces. Thus a coal with 100 cleats per meter, has 200 square meters of cleat surface per cubic meter.

For a particle of size  $x$  to contain part of the cleat surface, it must be within a distance of plus or minus half the particles diameter,  $x/2$ , from a cleat surface.<sup>(2)</sup> The probability of a fragment of size  $x$  being in this region is the ratio of the volume of plus or minus half the fragment diameter times the cleat surface area,  $2nx$ , divided by the total volume of the block, one meter cubed. Thus:

$$p(x) = 2nx/1 \quad (2)$$

Hence:

$$k = 2nx.$$

Before proceeding further with the quantification, two concepts must be understood. First, when a fragment containing part of the cleat surface is formed, actually two fragments are formed, one on either side of the cleat surface. This is known as the two step process. Considering now the two step breakage problem: in the IAC model, when a fragment forms that contains the cleat surface, the fragmentation proceeds thru the cleat surface and completes the fragmentation on the other side of the cleat surface. However, since the cleat is a double surface, the fragment is further divided at the cleat surface into two smaller particles — the two step fragmentation process.

Secondly, during this two step fragment formation, larger particles secondarily break into smaller particles. These par-



ticles have their own size distribution as derived by Meloy and Clark.<sup>(4)</sup> For the sake of simplicity, it will be assumed that the two particles are half the size of the original particle — two hemispheres of thickness  $x$ . Therefore, since the original size particle is  $2x$ , and since it broke into 2 equally sized particles of thickness  $x$ , the probability of a respirable size particle containing some of the original cleat surface forming is, from equation 2:

$$p(x) = 8nx/1 \quad (3)$$

To obtain the probability of a particle of size  $x$  not containing part of the cleat surface, one takes the volume where a non cleat particle must form, and ratios it to the total volume, 1 minus equation 1. Thus the probability that a particle of size  $x$  will not contain cleat surface,  $p(x)nc$  becomes:

$$p(x) = (1-nx)/1 \quad (4)$$

To find the ratio of fragments of size  $x$  containing cleat surface to those not containing cleat surface, one ratios the respective probabilities, equations 3 and 4. One obtains:

$$\text{ratio} = 8nx/(1-nx) \quad (5)$$

where  $nx$  in the denominator is small compared to 1, and thus the ratio becomes  $8nx$ .

If one assumes that  $n$  is equal to 800 cleats per meter — Preston County bright layer coals and the particle size is 5 microns, then 3.2 percent of the respirable size coal particles have some of the original cleat surface on their surface. Because quartz has twice the density of coal, this is equivalent to saying that 3.2 mg/m<sup>3</sup> of quartz are present in a respirable dust that contains 50 milligrams of coal dust or 6.4 mg/m<sup>3</sup> of quartz are present in a respirable silica mine dust. For 10 cleats per meter this is equivalent to 0.4 and 0.8 mg/m<sup>3</sup> respectively.

## Discussion

As presented, the model contains two parts: the prediction that the cleat surface fragments will be cytotoxic and that there will be enough particles in the dust with some cleat surface to be a significant source of cytotoxicity. If one considers that the average coal fragment containing cleat surface is six sided, then in theory it would have only 1/6th the toxicity of a quartz particle. On the other hand, it only takes one corner or edge to make the particle toxic. This is and will probably remain an unresolved problem for quite some time.

Providing that there is no other major source of cytotoxic internal communicating surface in coal, this hypothesis predicts that for a given level proportional to the cleat surface in the coal. Naturally there may be other sources of pathogenic particles that mask the above predicted relationship.

The calculation of the percent of respirable size coal dust particles that are likely to be present, while a simplified calculation, is relatively conservative. Though the discussion has been limited to cleat surface, it applies equally well to any other internal coal surface that is both cytotoxic and is likely to appear on a respirable size dust particle. However, assuming cleat surface cytotoxicity, there are more than enough particles containing cleat surface, present in coal dusts to be a significant source of particles that are

pathogenic to anyone inhaling a sufficient quantity.

In the literature there is very little information on either the total amount of connected internal surface, its surface composition, or how much of this surface is likely to be present in the dust. This is one area that should be investigated.

## Conclusion

This theoretical paper presents the hypothesis that respirable size coal particles containing some of the cleat surface may be a significant source of the pathogenic particles in the dust. Specifically:

1. In coal seams that contain between 10 and 80 cleats per decimeter, the respirable coal dust contains the equivalent of .6 to 6 percent by weight of silica particles.
2. The pathogenicity of the coal is proportional to the cleat or communicating internal surface area of the coal.
3. A more definitive calculation as to the amount of respirable cleat surface dust particles present in dusts.
4. One should measure the cytotoxic behavior of coal particles containing a thin layer of silica.
5. Work needs to be done to determine the composition of cleat surfaces, its cytotoxic behavior, how much cleat surface is present in coals and how much other communicating internal surface is present in coals.

## Acknowledgment

This research has been supported by the Department of the Interior's Mineral Institute program administered by the Bureau of Mines through the Generic Mineral Technology Center for Respirable Dust under grant number G1135142.

## References

1. Meloy, T.P.: Liberation Theory — Eight Useful Theorems. *Int. J. Miner. Process.* 13:113-124 (1984).
2. Meloy, T.P., U. Preti and G. Ferrara: Volume and Mass Locking Profiles Derived — Theoretical and Practical Conclusions. *Int. J. Miner. Process.* (to be published). (1986)
3. Meloy, T.P. and N.N. Clark: Generalized Locking Profile of Angular Particles — Locked Particle Theory. *Part. Charact.*, pp. 63-67 (1986)
4. Meloy, T.P. and N.N. Clark: Locking Profile of Diamond Shaped Particles — of all Aspect Ratios. *Int. J. Miner. Process.* (to be published) (1987).
5. Meloy, T.P.: A Working Hypothesis on How Silica and Surfaces May Cause Silicosis and CWP. *Proceedings Respirable Dust in the Mineral Industries*, pp. 15-18. Univ. Park, Pa. (1987).

# A Working Hypothesis on How Silica and Silica Surface May Cause Silicosis and CWP

Thomas P. Meloy

Particle Analysis Center, West  
Virginia University

This paper presents an interim progress report on our recently begun research project on respirable dusts. We are reporting on a sophisticated, predictive, probably correct, testable hypothesis that postulates a mechanism by which some natively cytotoxic respirable size mineral particles, such as kaolin, are not harmful to the lungs, while other equally cytotoxic particles, such as quartz, are, even in small quantities, very harmful. In essence the hypothesis predicts that some mineral particles, not normally present in the earth's ambient dust, causes the lungs dust defense mechanisms to turn on the lung and harm it. However fruitful the hypothesis may be, it is a hypothesis and much work remains to be done before it can be accepted as a theory.

While I may make the presentation and be the PI, my co-PI, Dr. William Wallace of NIOSH, has and will continue to make at least as much contribution to the project as I. Our sophisticated hypothesis is deeply scientifically based and unfortunately, in spite of the multifaceted aspects of this project, there is virtually nothing in the literature to guide our work. This means we must go back to the classical physics to develop the models for calculating the powerful electrical effects near particle edges, and we must measure the fundamental biological constants associated with pulmonary macrophage. While there are daily discussions on Boltzman distributions, Einstein's Brownian Motion paper, the Nernst Equation, and sophisticated semi- *in vivo* biological time constant measurements, we are aware that this is not an easy problem and we are not likely to have irrefutable closed solutions to these problems by next Monday morning.

## Hypothesis

Let me now turn to our hypothesis. In order to occupy all the naturally occurring surface areas on the earth, man, during his long evolution from fish, had to evolve effective defenses against all the naturally occurring cytotoxic respirable mineral dusts. For example, clays, which are often the main component in naturally occurring respirable mineral dusts, are quite cytotoxic but do not harm the lung. However, for respirable mineral dusts that contain significant amounts of nonnaturally occurring but equally cytotoxic quartz and asbestos particles, the body has not had

to evolve an effective defense mechanism, and thus respirable mineral dusts containing these particles may harm the lung. Our hypothesis is, therefore, that a few nonambient minerals such as quartz, cause the body's dust defensive system to harm the body in a manner analogous to Lupus or MS, diseases of the immune system.

For respirable size mineral dusts that enter the alveoli of the lung, the body has evolved three main defense mechanisms: surfactant coating of the particles which acts as a protective sheath, ingestion and eventual removal of the particle from the lung by macrophage — phagocytosis, and when the afore mentioned mechanisms fail, walling off the affected area by scarring — fibrosis. In the case of the clays, the first two defense mechanisms work, while in the case of quartz, some types of coal particles and perhaps some other minerals, such as asbestos, the first two mechanisms fail and the body responds by initiating fibrosis, characteristic of silicosis, progressive massive fibrosis and asbestosis. It is believed that when a macrophage is killed, some type of chemical messenger is released, when present in sufficient quantities, initiates fibrosis.

To understand how the body responds to respirable mineral dust particles, consider the fate of two respirable size particles, 2 to 5  $\mu\text{m}$ , when they enter the lung's alveoli. Let one of the particles be kaolin, a typical clay, and the other a freshly broken, sharp edged, quartz particle. Immediately, both particles are wetted and then covered by a protective coating of the lung's surfactants, primarily lecithin. In time, the lung's free scavenger cells, pulmonary macrophages, ingest by a mechanism called phagocytosis both the clay and the quartz particles. After ingestion, both particles are exposed to the digestive, lytic enzymes of the macrophage. While the kaolin particle remains in the macrophage and is eventually removed from the lung, the quartz particle destroys the macrophage and remains in the lung.

Wallace *et al*<sup>(1)</sup> mimicked experimentally the events that take place in the lung by first coating respirable size kaolin and quartz particles with lecithin, digesting this coating with the lytic enzymes of the macrophage, and then testing the cytotoxicity of these treated kaolin and quartz particles. With one or two hours of enzyme exposure, most of the protective coating remains on the kaolin particle with some modifica-

tion of the outer adsorbed layer. On the other hand, the lytic enzymes rapidly removed most of the coating from the quartz particles thus retoxifying them, and these stripped particles were again cytotoxic. (Both kaolin and quartz particles uncoated are equally cytotoxic, but when both particles are coated with the pulmonary surfactant lecithin, both are noncytotoxic.) As a test the lecithin coating, enzyme digestion, cytotoxic testing test has wider application.

The writer believes that a modification of the above described dust test may now be used for quantitatively testing the cytotoxicity of quartz bearing respirable mineral dusts and thus presumably the pathogenicity of said dusts. Furthermore, in the relatively near future, this test may well be shown to apply to a variety of other minerals and solids that cause pulmonary fibrosis. This test, a research tool now, may well become the standard laboratory test of monitoring and predicting the quantitative pathogenicity of respirable mineral dusts. Currently, Dr. Wallace is measuring longer digestion time behavior of the dusts in the test systems to investigate the possible role of such interactions in the pathogenesis of pneumoconiosis and to determine if the phenomenon might provide a basis for more predictive cytotoxic testing. Additional test parameters are also being investigated.

Since the body evolved a simple effective protective mechanism that covers a large variety of naturally occurring respirable size mineral particles such as clays, oxides, carbonates, hydroxides, halides, silicates, borates, sulfides, sulfates and phosphates, why is this mechanism not effective against the silica minerals: quartz, cristobalite and tridymite? What is so unusual about these silica minerals. Quartz, which is characteristic of these silica minerals, has four unusual properties: it is relatively inert chemically, piezoelectric, in physiological saline it has a very high surface charge, and it has extraordinarily sharp edges and corners. Quartz's chemical inertness means that it does not bind surface coatings strongly and thus they are easily removed by the microphage's lytic enzymes. Combined with quartz's extremely sharp edges and corners, the high surface charge means that at the sharp edges and corners very powerful electrical effects are present; so powerful in fact, that when an edge with these electrical effects is brought close to a cell's membrane, it will rip that membrane apart. Finally, quartz being piezoelectric can generate large voltages when impacted.

Clays, in contrast to quartz, are quite active chemically, binding surface coatings tightly, and do not have sharp edges and corners. However, clays, because of their layered structure which consists of alternate layers of positive and negative charges, also have very powerful electrical effects on their edges, which, when uncoated with a surfactant, are as cytotoxic as quartz.

Coal particles, which normally would be considered benign, sometimes have a quartz surface and thus would behave as if they were a quartz particle. Meloy<sup>(2)</sup> has postulated that the cleats in coal, which act as conduits for underground water, have their surfaces coated with quartz, and he has shown that the amount of respirable size quartz-coated coal dust particles present in an unregulated coal mine is sufficient to cause the characteristic fibrosis.

However, these quartz-coated coal particles would have a quartz assay that would be very low compared to the number of quartz-coated particles present. Obviously, the number of quartz-coated coal particles present must be measured experimentally by a variety of approaches — something we are currently setting up to do.

One can speculate that the *in vitro* test described above may predict which type of mineral particles will be cytotoxic because the test itself mimics the action of the body defense so closely. Those particles that do not destroy macrophage will not test positive, will not be cytotoxic, and will not be fibrogenic. Those particles that do test positive, will probably also destroy macrophage, be cytotoxic, and initiate fibrosis. Therefore, there is the possibility that this proposed work will lead to a generalized mineral dust test.

### Sub Programs

In a hypothesis as sophisticated and promising as the one presented above, there are number of related but independent programs that must be done before the hypothesis can be considered a viable theory. We must show that the "in vitro" mimicking of the macrophage's phagocytosis is as postulated, and we must also explore the envelope of the pulmonary surfactants and lytic enzymes. In addition, we must show that the powerful electrical effects exist for both the uncoated quartz and clay particles; that these electrical effects are strong enough to disrupt cell membranes, that experimentally modified (rounded) quartz particles are not cytotoxic, that experimentally quartz particles really have these unusually sharp edges and corners, that a significant amount of quartz-surfaced particles exist to initiate pulmonary fibrosis, and that cleat surfaces are silica coated.

### Electrical Effects

Because there is no extant method for measuring the electrical affects near a sharp edge or corner, extending out 30 to 50 A, these effects must be calculated. Since the Chapman Gouy and similar models were developed for flat or gently curving surfaces and are not applicable near sharp edges and corners, an entirely new model to describe the electrical fields near these sharp features has been developed. Until actual SEM measurements are available characterizing the sharpness of quartz, we must calculate these electrical effects by making the fundamental calculation of the distribution of the ions and surface charges near the edges, using the Boltzman distribution and Nernst equation and then seeking to integrate the Poisson equation in a region near a tip or edge of known radius of curvature. In addition, since the respirable quartz particles are small and subject to Brownian motion that results in rather high peak velocities, we must calculate the effect of this motion on the electrical effects. Quartz being piezoelectric, will generate voltages when struck by molecules during its Brownian motion dance. Because these calculations go back to the basis of classical physics and involve noncontinuum fluid flow, they are not easy. While we are confident that we will get accurate answers, currently, we are trying to calculate the bounds on these electrical effects before getting the broader solutions.

In addition to the edge effects, we also must show that the molecules that comprise the surface membrane of cells can be disrupted by the electrical fields calculated above. This is done by showing that the neutral molecules with a charge separation in a unit membrane can be disorganized when closely approached by an electrical field of the strength and divergence calculated above. While there may be experimental methods of showing this to be true, the cost and time to do the experimental work is prohibitive.

Finally, in this program we must show that the uncoated layered clay particles have electrical effects also sufficiently powerful to disrupt cell membranes. Part of the work done above may be applicable to the clay edge problem. Once again, one is working with discontinuous charge distributions and non-Newtonian fluid flow. Experimental measurements do not appear to be feasible.

### Macrophage – Mimicking

When a respirable particle deposits in a pulmonary alveolus, its first contact will be with the pulmonary surfactant lining the wet alveolar surface. The possibility that the major component in the surfactant could adsorb onto a respirable particle has been investigated by Wallace *et al.*<sup>(3)</sup> Following the surface adsorption on both the clay and quartz particles, the cytotoxicity of both coated particles is neutralized.<sup>(4)</sup> We presume that such coated particles in the lung are phagocytized by pulmonary macrophage and subjected to an enzymatic digestion process within the cell. These processes are being modeled by "in vitro" enzymatic digestion of lecithin treated dusts.<sup>(1,5)</sup> Currently, the results of these reported studies are being used as the basis for extension of the studies to longer digestion times, full surfactant and full enzyme use, and testing using macrophage in culture. The tests are designed to determine the time course of enzymatic digestion of protective surfactants from various dust (mineral) surfaces to determine if there are mineral-specific difference which might be significant to the initiation of pulmonary disease process. These studies are performed in concert with NIOSH projects on "Effective Silica Indices for Respirable Mineral Dusts, Evaluating Prophylactic Coatings for Silica Dusts," and the NIOSH - USBM Interagency Agreement on "Correlation of Free Silica and Active Silica Content of Respirable Coal Mine Dust Fractions Associated with Coal and Overburden Mineralogy."

### Dust Test

Currently, we are doing our dust testing at NIOSH, but we are in the process of setting up the simple "in vitro" dust test in my laboratory at CCMER. Cytotoxicity of a variety of respirable size dust particles will be tested as a function of surfactant morphology, surface charge and surface coating. In addition, we plan to test raw respirable mineral dusts from coal and perhaps other mines as well as artificially generated dust samples. We anticipate having a full load of work for the dust test laboratory. We do not claim that our dust cytotoxic test is fully developed or even proven, but it is a powerful research tool, and, imperfect as it may be, it does mimic the *in vivo* defense of the body to respirable size mineral dust particles.

### SEM – Shape Characterization

Key to the proposed hypothesis of the cytotoxicity of quartz particles is the sharpness of the corners and edges of quartz particles. Since once again there is nothing quantitative in the literature on the sharpness of quartz's edges, these parameters must be measured with an SEM. Fortunately, we hope we may soon purchase a new SEM with sufficient brightness and resolving power to measure the radius of curvature of these edges. From other work we believe that the sharpness will be on the order of 8 Å. For an SEM to make this measurement it must not only have the brightness and resolving power, but it also must have two orthogonal angles of specimen tilt, a goniometer, so that the edge of the particle will be parallel to the beam. Current SEMs available to us do not have the needed resolving power, brightness, or extra angle of tilt. Probably a field emission SEM with a resolving power of 15 Å will be required.

Should the SEM available to us not be able to resolve the sharpness of the corners and angles, then we will probably work with the National Electron Microscope Laboratory located in Berkeley, California. We are in contact with the Scientific Director and applying for the necessary time and status to use their facilities if needed. One of the problems in working with quartz is that high kvs smashes quartz, therefore high magnification with low kvs is required. It will probably be sufficient to show that the radius of curvature at an edge is less than 15 Å. In any event, to calculate the electrical field effects at an edge or corner, it is necessary to postulate the sharpness of that corner.

### Cleat Surfaces – A Possible Source of Cytotoxic Particles

The presence of respirable quartz-bearing mineral particles has been well documented in many coal mines, and MSHA regulations address the quartz content of mine dusts. Work is currently underway by NIOSH-USBU, and work is being included in the Respirable Dust Center Program by Dr. Seehra to determine the surface availability of quartz in mixed composition mine dusts. Prof. Ting<sup>(6)</sup> and I are preparing a study to determine if some quartz bearing dust originates from quartz deposited on organic coal substrates, a study which would compliment the above effort and the Shape and Surface Characteristics project.

Meloy<sup>(2)</sup> has demonstrated that if the cleat surfaces are mineralized with quartz, then in many mines there will be enough quartz coated coal particles to cause a fibrotic reaction. From locked particle theory,<sup>(7-10)</sup> it is predicted that only one coal particle in two to five hundred will show a quartz coating. Proposed, by Profs. Ting and Meloy, is an additional approach to look directly at the cleat surface to see if they are mineralized with silica.

### Summary

What I have presented is an explanation of how quartz and clay particles are and are not cytotoxic depending on whether they are coated or not. This explanation depends solely on physical effects – electrical fields and mechanics

from the classical physics — not on traditional biological explanations. In the long view all biological and even all chemical reactions are governed by physics. As Prof Philip Morrison of MIT once said, "We are cousin to the clouds and brother to the stones" and the law of physics that effect them also effect us.

### Acknowledgment

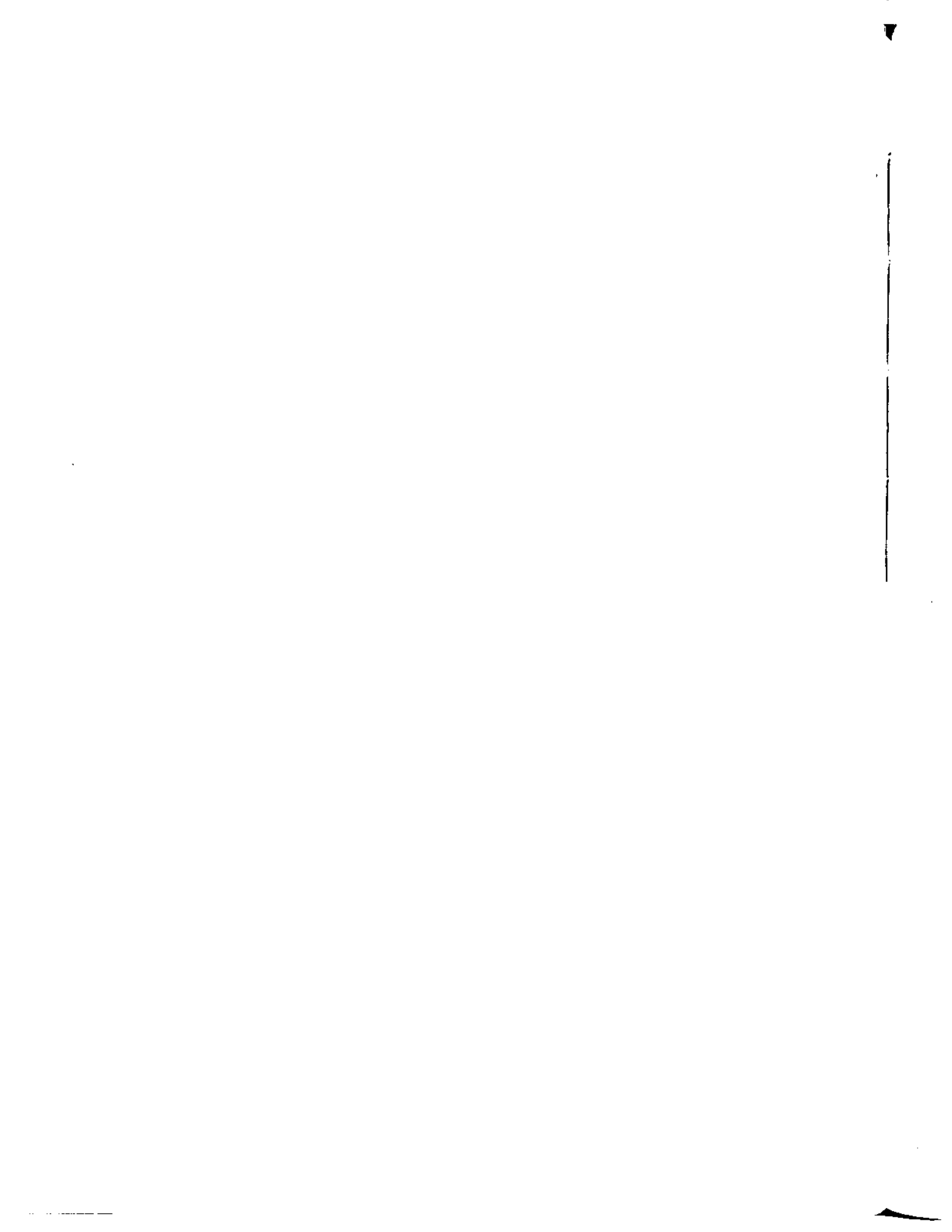
This research has been supported by the Department of the Interior's Mineral Institute program administered by the Bureau of Mines through the Generic Mineral Technology Center for Respirable Dust under grant number G1135142.

### References

1. Wallace, W.E. et al: *Proceedings Coal Mine Dust Conf.* Morgantown, WV (1984).
2. Meloy, T.P.: A Hypothesis on the Possible Contribution of Coal Cleats to CWP. *Proceedings Respirable Dust in the Mineral Industries Conference*, pp. 240-241. Univ. Park, PA (1986).
3. Wallace, W.E. et al: *J. Colloid Interface Science* 52: 535 (1975).
4. Wallace, W.E. et al: *J. Toxicol. Environ. Health* 16: 415 (1985).
5. Wallace, W.E. et al: *Proceedings Inhaled Particle Conference*. Cambridge, England (September 1985) (To be published).
6. Ting, F.T.C.: Origin and Spacing of Cleats in Coal. *Trans. AIME*, Vol. 99. J. Press., Vessel Tech. (1977).
7. Meloy, T.P.: Liberation Theory — Eight Useful Theorems. *Int. J. Miner. Proc.* 13:113-124 (1984).
8. Meloy, T.P., U. Preti and G. Ferrara: Volume and Mass Locking Profiles Derived — Theoretical and Practical Conclusions. *Int. J. Miner Proc.* (1986) (To be published).
9. Meloy, T.P. and N.N. Clark: Generalized Locking Profile of Angular Particles — Locked Particle Theory. *Part. Charact.*, pp. 63-67 (1986).
10. Meloy, T.P. and N.N. Clark: Locking Profile of Diamond Shaped Particles — of all Aspect Ratios. *Int. J. Miner Proc.* (1987) (To be published.).

**IV**

**Interaction of Dust  
and Lungs**



# Measurement of Superoxide Release From Single Pulmonary Alveolar Macrophages

K. A. DiGregorio, E. V. Cilento and R. C. Lantz

Departments of Chemical Engineering and Anatomy, West Virginia University

An electro-optical method was used to quantify superoxide (SO) release from single rat pulmonary alveolar macrophages (PAM) exposed *in vitro* to respirable quartz and kaolin dusts and *in vivo* to quartz. Release was determined by measuring the reduction of nitroblue tetrazolium (NBT) to a diformazan precipitate at 550 nm from video-recorded images of individual cells. *In vitro* exposure to 0.025 or 0.05 mg/ml kaolin for 40 minutes resulted in no significant differences in either the total diformazan produced (max) or the maximum rate of diformazan production (R). *In vitro* exposure to 0.025 mg/ml quartz decreased max 38 percent while no significant change was found using 0.05 mg/ml. However, R was decreased 31 percent and 24 percent for the low and high dose, respectively. In contrast, PAM obtained from animals exposed *in vivo* to quartz dust for two or four weeks in inhalation chambers exhibited increased production of diformazan. However, only PAM analyzed three days post-exposure showed significant increases, while PAM from animals sacrificed ten or 31 days post-exposure were not significantly different from control. The combined *in vitro* and *in vivo* quartz results might suggest that there is an initial acute response to exposure that decreases the ability of PAM to produce SO, followed by recruitment of production of PAM with increased SO producing capability. It appears that removal of animals from the source of exposure permits PAM to return to control levels of SO production by 31 days. Whether this would be true for chronic exposure remains to be elucidated.

## Introduction

Pulmonary alveolar macrophages (PAM) protect the lungs by phagocytizing foreign debris and bacteria.<sup>(1)</sup> This process involves ingestion as well as destruction of foreign matter. Phagocytosis usually is accompanied by a respiratory burst which increases cellular oxygen consumption leading to the release of highly reactive oxygen metabolites.<sup>(2)</sup> These agents have been implicated in the killing of bacteria by phagocytes, but they have also been shown to be toxic and

have been linked to cancer, emphysema, arthritis, diabetes, and other diseases.<sup>(3)</sup> Toxic effects may be a result of 1) an abnormally low production of metabolites, resulting in damage to lung tissue by the respired bacteria and/or dusts; or 2) an abnormally high production resulting in direct damage to lung tissue by metabolites themselves.

The initial oxygen metabolite released is thought to be superoxide anion (SO) produced from the reduction of oxygen by NADPH oxidase.<sup>(2)</sup> Superoxide can readily dismutate to form hydrogen peroxide and subsequently, other antimicrobial agents.<sup>(2,3)</sup> Exposure of PAM to respirable dusts may lead to hyper- or hypo-secretion of superoxide resulting in either too much or too little of these antimicrobial agents. This may then lead to pneumoconiosis, silicosis, or other respiratory disease.

In this study an electro-optical technique was used to quantitatively measure the release of superoxide from single cells which had been obtained from animals exposed *in vivo* in inhalation chambers or *in vitro* to respirable quartz, or *in vitro* to kaolin dusts. NBT reduction to a diformazan precipitate by SO was measured from single PAM during adherence. The initial (maximum) rate of productions and total mass of diformazan produced were measured and compared among the different dusts.

## Materials and Methods

PAM were obtained from male Long-Evans hooded rats (Charles River) weighing between 250 and 300 grams using the tracheal lavage method developed by Myrvik *et al.*<sup>(4)</sup> Briefly, the diaphragm was severed, the animal exsanguinated, and a 15 gauge needle inserted through an incision in the trachea. Lavage fluid (145 mM NaCl, 5 mM KCl, 1.9 mM NaH<sub>2</sub>PO<sub>4</sub>, 9.35 mM Na<sub>2</sub>HPO<sub>4</sub>, and 5 mM glucose) at pH 7.4 and 4°C was injected into the lung through the needle and slowly withdrawn to obtain cells. A total of 80 ml of lavage fluid was collected by repeating this process approximately 12 times. PAM collected were centrifuged at 500 g for five minutes at 4°C and resuspended in HEPES-buffered medium (140 mM NaCl, 5 mM KCl, 1.5 mM CaCl<sub>2</sub>, 10 mM Na-HEPES [N-2-hydroxyethyl] piperazine-N'-2-ethane



TABLE I

The Mean (+/- SE) Total Diformazan Produced (max) and Initial Rate of Diformazan Production (R) for PAM Exposed *in vitro* to Either Respirable Quartz or Kaolin Dust

	Total Diformazan Production (fmoles)		Diformazan Production Rate (10 <sup>-3</sup> fmoles/sec)	
	Quartz	Kaolin	Quartz	Kaolin
CON*	15.3 +/- 1.6	11.7 +/- 1.0	24.5 +/- 2.3	10.5 +/- 0.8
LOW	9.5 +/- 1.5**	10.2 +/- 1.5	16.8 +/- 1.7**	10.5 +/- 1.4
HIGH	13.0 +/- 1.6	8.1 +/- 0.9	18.6 +/- 2.1**	10.6 +/- 1.4

\* CON = control; LOW = 0.26 mg/ml; HIGH = 0.05 mg/ml.

\*\* p < 0.05.

n = 18 cells in each case.

sulfonic acid] and 5 mM glucose) at pH 7.4 and 4°C. Following a second wash, PAM were resuspended in approximately 6 ml of HEPES-buffered medium and placed in an ice-water bath.

Nitrobluc tetrazolium (NBT) was added to the HEPES-buffered medium to obtain soluble NBT solutions at a concentration of 2.0 mg/ml. NBT, in the presence of a strong reducing agent such as superoxide, is reduced to an insoluble diformazan product which absorbs light at 550 nm. Three ml of NBT solution at 37°C was placed in a tissue culture dish (Falcon 3001) and an aliquot of 400 µL of the cell suspension ( $2 - 5 \times 10^5$  cells), was added. A layer of paraffin oil (37°C) was placed on top of the aqueous layer to reduce evaporation.

The culture dish was placed on a temperature-controlled (37°C) heating element located on the stage of an Olympus (model IMT) inverted light microscope and trans-illuminated at 550 nm. A microscopic field of at least six PAM was televised using a low light-level Cohu (model 4410) silicon-vidicon television camera and videorecorded for 40 minutes using a 3/4-inch Sony (model V05600) videocassette recorder. PAM were stimulated to release superoxide by adherence to the bottom of the culture dish.

Temporal changes in light intensity over single PAM were determined by play back of videorecorded images through an IPM (model 204A) video photometric analyzer. The analyzer generates two windows which act as phototransistors sensitive to changes in average light intensity in the window area. Each window was placed over a single PAM and the output video voltage from each window was digitized (12 bit) using a Keithley DAS (model 520) every ten seconds for 40 minutes, and stored on an IBM PCXT. This procedure was repeated to obtain measurements from at least six PAM in each videorecorded image.

Background light intensity was determined in regions of the image containing no cells. Following correction for any background variation, changes in optical density (OD) for each cell were calculated using the Beer-Lambert Law. The

OD value was multiplied by the window area and the molar extinction coefficient ( $30,000 \text{ M}^{-1} \text{ cm}^{-1}$ ) to determine the mass of diformazan produced.

Temporal changes in mass of diformazan produced, M, exhibited a time delay followed by an exponential-like increase to an asymptotic maximum value (max). Therefore, the data were fit to the following first-order equation:

$$M = \max[1 - \exp(-(t - t_d)/T)]$$

where:

t = time

$t_d$  = delay time measured between stimulation and detection of diformazan production

T = time constant

The total diformazan produced, max, was determined from an average of the last six values of M (1 min) and  $t_d$  was estimated by observing the point at which diformazan production increased significantly above baseline. T was determined by fitting the data to the log linearized form of this equation. The maximum (initial) rate of diformazan production, R, was calculated from the derivative of the equation at time  $t_d$ ; that is, as  $\max/T$ .

The effects of *in vitro* exposure to respirable quartz and kaolin on superoxide release were tested using concentrations of 0.025 or 0.05 mg/ml added to NBT solutions just prior to addition of PAM. PAM were added to dishes containing either the high or low dust concentrations as well as a control dish containing no dust.

The effects of *in vivo* exposure of PAM to respirable quartz ( $20 \text{ mg/m}^3$ , 16 hr/day, 5 days/wk of MIN-U-SIL 10, 95% < 5 µm) was tested by housing six animals each for two or four weeks in the West Virginia University (WVU) inhalation facilities. Six control (no quartz) animals were also kept in the inhalation chambers for two or four weeks. Following exposure, animals were removed from the inhalation chambers and housed in WVU animal-care facilities for 3, 10, or

31 days post-exposure, at which time animals were removed for analysis of superoxide production. At each analysis period PAM were obtained from two exposed and two control animals. This approach permitted analysis of the effects of exposure and post-exposure time.

Experiments were analyzed using ANOVA at the 95 percent confidence level. When significant differences were found, the Newman-Keuls test was used to determine the significant differences among means.

**Results**

*In vitro* exposure of PAM to the low dose of quartz (0.025 mg/ml) decreased max 38 percent compared to control while exposure of PAM to the high dose (0.05 mg/ml) did not significantly change max. The maximum rate of diformazan production, R, decreased 31 percent for the low dose and 24 percent for the high dose when compared to control (Table I). *In vitro* exposure to either the low or high dose of kaolin did not significantly change either max or R.

*In vivo* exposure of all animals (including animals exposed for both two and four weeks and analyzed at 3, 10, and 31 days) to quartz dust increased max 36 percent and R 29 percent compared to control animals. No significant differences were obtained between animals exposed for two or four weeks, therefore, data for *in vivo* experiments in Table II represent a combined average. Max was increased 69 percent for quartz-exposed animals analyzed three days post-exposure compared to control animals analyzed three days post-exposure, but the 10- and 31-day groups were not significantly increased above their respective controls. The 3-day group was also significantly increased (61%) compared to 31 days post-exposure.

**Discussion**

Superoxide release may play an important role in silicosis and other respiratory diseases. *In vitro* assays on large numbers of cells in culture using hemolysis of red blood cells or release of enzymes from PAM following dust exposure have been used to analyze cytotoxicity. In such systems, kaolin has been found to have an activity comparable to quartz on a mass basis.<sup>(5)</sup> However, *in vivo* quartz is highly fibrogenic resulting in silicosis while kaolin is relatively inert biologically.<sup>(5)</sup> Therefore, these cellular assays do not correlate with the *in vivo* effects of quartz and kaolin. It has been hypothesized that the difference between assay results and *in vivo* data may be due to dust interaction with pulmonary surfactant in the lung.<sup>(5)</sup> In this study, *in vitro* exposure of PAM to quartz resulted in decreased production of diformazan while *in vitro* exposure to kaolin did not significantly effect PAM compared to control. These results correlate with *in vivo* effects of quartz being toxic and kaolin being inert and helps support the usefulness of this superoxide assay in evaluating the effects of respirable dusts on cell function.

The low dose of quartz resulted in less diformazan production compared to the high dose in the *in vitro* experiments. The reason for this difference is at present unknown and further studies are needed to elucidate this discrepancy.

Interestingly, *in vivo* exposure to quartz resulted in increased production of diformazan rather than the decreased production observed *in vitro*. This difference may be due to a change in cellular function from the *in vivo* to the *in vitro* environment. However, the *in vitro* results also may be due to an initial (acute) response to quartz, since PAM were analyzed for 40 minutes immediately after contacting dusts.

TABLE II

The Mean (+/- SE) Total Diformazan Produced (max) and Initial Rate of Diformazan Production (R) for PAM Exposed *in vivo* to Respirable Quartz Dust

	Total Diformazan Production (fmoles)	Diformazan Production Rate (10-3 fmoles/sec)
CON (72)*	7.6 +/- 0.5	16.1 +/- 1.3
3 Days (23)	12.4 +/- 2.5**	19.3 +/- 2.6
10 Days (24)	11.0 +/- 0.9	19.6 +/- 2.5
31 Days (24)	7.7 +/- 0.9	23.1 +/- 2.9

\* CON = control; 3, 10, 31 days post-exposure; n given in parentheses as number of cells.

\*\* p < 0.05.

In contrast, the *in vivo* responses were considered more long-term since animals were exposed for two or four weeks followed by a post-exposure period before analyses were made. Thus, it may be possible that quartz causes an initial injury to PAM resulting in decreased production of superoxide followed by recruitment or activation of PAM having increased production capabilities.

Further support is the significant increase in production of diformazan observed in PAM analyzed three days following *in vivo* exposure compared to the control levels generated by PAM analyzed ten and 31 days post-exposure. Thus, after removal from dust exposure, PAM continue increased superoxide production initially but gradually fall back to control values by ten to 31 days post-exposure.

Finally, the quartz-exposed PAM analyzed three days post-exposure exhibited a wider range than the control and 10- and 31-day post-exposure groups. Heterogeneity has been reported by this lab and others and may explain this variation.<sup>(6-8)</sup> However, the range exhibited here seems to indicate more than the usual biological variation. Specifically, perhaps due to quartz exposure two populations of PAM were present: 1) cells injured by initial or long-term dust contact, resulting in decreased superoxide production; and 2) recruited or activated PAM which exhibited increased superoxide production. In conclusion, studies to examine this further as well as the effects of *in vitro* and *in vivo* exposure to PAM to respirable coal dusts are currently in progress.

### Acknowledgments

The authors wish to acknowledge the support of this research by the Department of Interior's Mineral Institute program administered by the Bureau of Mines through the Generic Mineral Technology Center for Respirable Dust under grant number G1135142 and CDC-NIOSH grant number 1K01-Oh00019-01.

### References

1. Miles, P.R., V. Castranova and P. Lee: Reactive Forms of Oxygen and Chemiluminescence in Phagocytizing Rabbit Alveolar Macrophages. *Am. J. Physiol.* 235(3):C103-C108 (1978).
2. Babior, B.M.: The Respiratory Burst of Phagocytes. *J. Clin. Invest.* 73:599-601 (1984).
3. Klebanoff, S.J.: Oxygen Metabolism and the Toxic Properties of Phagocytes. *Ann. Int. Med.* 93:480-489 (1980).
4. Myrvik, Q.N., E.S. Leake and B. Fariss: Studies on Pulmonary Alveolar Macrophages from the Normal Rabbit: A Technique to Produce them in a High State of Purity. *J. Immunol.* 86:128-132 (1961).
5. Wallace, Jr., W.E., V. Vallyathan, M.J. Keane and V. Robinson: *In vitro* Biologic Toxicity of Native and Surface-modified Silica and Kaolin. *J. Toxicol. Environ. Health* 16:415-424 (1985).
6. DiGregorio, K.A., E.V. Cilento and R.C. Lantz: Superoxide Release from Single Pulmonary Alveolar Macrophages. *Fed. Proc.* 45(3):309 (1986).
7. Hollan, A., J.H. Dauber, M.S. Diamond and R.P. Daniele: Separation of Bronchoalveolar Cells from the Guinea Pig on Continuous Gradient of Percoll: Functional Properties of Fractionated Lung Macrophages. *J. Reticuloend. Soc.* 33:157-164 (1983).
8. Zwillig, B.S., L.B. Campolito and N.A. Reiches: Alveolar Macrophage Subpopulations Identified by Differential Centrifugation on a Discontinuous Albumin Density Gradient. *Am. Rev. Respir. Dis.* 125:448-452 (1982).

# The Effect of Lecithin Surfactant and Phospholipase Enzyme Treatment on Some Cytotoxic Properties of Respirable Quartz and Kaolin Dusts

W. E. Wallace<sup>1</sup>, M. J. Keane<sup>2</sup>, V. Vallyathan<sup>2</sup>, F. Saus<sup>2</sup>, V. Castranova<sup>2</sup>, D. Bates<sup>2</sup> and C. A. Hill<sup>3</sup>

<sup>1</sup>Division of Respiratory Disease Studies, National Institute for Occupational Safety and Health (NIOSH) and West Virginia University

<sup>2</sup>Division of Respiratory Disease Studies, National Institute for Occupational Safety and Health (NIOSH)

<sup>3</sup>West Virginia University

Two *in vitro* systems are being developed to model initial stages in the interaction of respired dusts with the acinar region of the lung. Incubation of quartz and kaolin with dipalmitoyl glycerophosphorylcholine, a major component of pulmonary surfactant, suppresses the prompt cytotoxicity of both dusts as measured by *in vitro* enzyme release from pulmonary macrophages or assay by erythrocyte hemolysis. Additional data is presented to quantitate the detoxification of quartz and kaolin by dipalmitoyl lecithin. Subsequent incubation of lecithin treated dusts with phospholipase enzymes results in partial to complete restoration of the assayed cytotoxic potentials, dependent on the lipase activity applied, the incubation time, and the mineral. Restored cytotoxic potential is due to removal of the prophylactic lecithin surface coating and/or due to residual lysolecithin which is produced by the partial enzymatic digestion of lecithin. Data is presented on the contribution of each mechanism to the restored toxicity. Again, this is dependent on the mineral used, the lipase activity applied, and digestion time. Additionally, a system is under development to challenge pulmonary macrophages in culture with native and surfactant treated dusts. A preliminary test of the dipalmitoyl lecithin - quartz - rabbit pulmonary macrophage system is presented to illustrate the method.

## Introduction

Respirable quartz dust exposure is known to cause fibrotic lung disease; respirable clay dust exposure is less likely to do so as indicated by epidemiologic data on occupational exposures and by animal model studies.<sup>(1-7)</sup> The hypothesis that damage to pulmonary macrophages in the acinar region of the lung by respired dusts is an early event in the disease process requires consideration because kaolin clay and quartz dusts are comparably cytotoxic to pulmonary macrophages *in vitro*.<sup>(8,9)</sup>

Simulating dust interaction in the lung, quartz and kaolin dusts have been assayed for their cytotoxicity both in their native state and after incubation with an emulsion of dipal-

mitoyl glycerophosphorylcholine (DPL), called dipalmitoyl lecithin.<sup>(8,9)</sup> Lecithins are a major component of pulmonary surfactants which stabilize the surface properties of the hypophase coating of pulmonary alveoli.<sup>(10)</sup> This surfactant adsorbs to kaolin and to quartz from emulsion in physiologic saline. Adsorption isotherms for these dusts have been measured.<sup>(11,12)</sup> The cytotoxicity of both dusts is suppressed by such DPL adsorption at 37°C<sup>(8,9,12)</sup> as assayed *in vitro* by macrophage release of cytosolic and lysosomal enzymes or erythrocyte hemolysis. Lecithins are also major components of cellular membranes. Interactions of quartz with the bilayer lipid membrane have been proposed as a mechanism of cell lysis; and effects of dust surface crystallinity and coatings on this lysis have been studied.<sup>(13-15)</sup> Our simulation of pulmonary surfactant interaction with respired dusts replaced a false positive toxicity assay for kaolin with a false negative assay for quartz.

Removal of serum protein from phagocytized silica has been observed.<sup>(16)</sup> As a research hypothesis, we presume that the prophylactic surfactant coating adsorbed on a respired particle following contact with pulmonary surfactant is subject to enzymatic digestion following phagocytosis by pulmonary macrophages. We have been exploring this hypothesis by *in vitro* studies using dipalmitoyl lecithin in physiologic saline for alveolar hypophase surfactant and phospholipase enzymes A2 and C for two lysosomal enzymatic digestion processes. We used pulmonary macrophage cytosolic or lysosomal enzyme release or erythrocyte hemolysis assays to monitor the cytotoxicity of the quartz and kaolin dusts treated in different experimental protocols.<sup>(8,9,12)</sup>

In this report we provide quantitative data showing suppression of hemolytic potential of quartz and kaolin dusts as a function of DPL dose. We provide more data on the effects of phospholipase enzymes A2 and C on treated dusts. We discuss the bases for enzymatic restoration of cytotoxicity of treated dusts by providing initial data on the time course of enzymatic digestion and retoxification.

Although this simulation provides for detailed analyses of some proposed steps in the interaction of a mineral particle with pulmonary surfactant and macrophages, the adequacy

of the selected parameters to model the complex *in vivo* situation must be questioned. We are developing a complementary method which may model that reality more closely, but which thereby poses more problems of interpretation. In this system, pulmonary macrophages are challenged *in vitro* with surfactant-treated or native dusts. The attempt is then made to maintain their viability in culture for a sufficient period of time to detect macrophage attrition due to the surfactant treated dusts at levels above those for negative controls, i.e., macrophages which have not been challenged with dust. We discuss the method using preliminary data for rabbit pulmonary macrophages challenged with DPL treated and untreated quartz.

## Materials and Methods

Alpha quartz used is at least 98.5 percent pure as determined by x-ray energy spectrometric analysis. It has a specific surface area of  $3.97 \text{ m}^2/\text{g}$  as determined by nitrogen adsorption. Kaolin used is at least 96 percent pure, contains no crystalline silica, and has a specific surface area of  $13.25 \text{ m}^2/\text{g}$ .

Erythrocytes were obtained for hemolysis assay from a sheep maintained on a fixed diet. Pulmonary macrophages were obtained by lavage of rats or rabbits, as indicated, using Hank's Balanced Salt Solution (HBSS). Cells were washed twice and resuspended in HBSS.

Commercially obtained L-alpha-dipalmitoyl glycerophosphorylcholine (DPL) (Calbiochem) was

ultrasonically dispersed in  $0.165 \text{ M}$  sodium chloride to produce emulsions of the desired DPL concentration. Dry quartz or kaolin dust at the ratio of mass of dust to mass and concentration of DPL desired were dispersed into DPL emulsion and the mixtures incubated for one hour at  $37^\circ\text{C}$  in a shaking water bath. Dusts were then centrifuged for ten minutes at  $990 \text{ g}$  and resuspended in calcium and magnesium free Dulbecco's phosphate-buffered saline (PBS).

Commercially supplied Phospholipase A2 was obtained from: porcine pancreas (Sigma) or from *Crotalus adamanteus* venom (Cooper Biomedical), as indicated. Phospholipase C from *Clostridium perfringens* was obtained from Sigma. Enzymes were dissolved in phosphate-buffered saline (PBS) containing  $2.0 \text{ mM}$  calcium chloride, to provide specific activities for designed digestion steps. Amounts of native or DPL-treated dusts were resuspended in PBS with  $2.0 \text{ mM}$   $\text{CaCl}_2$ , desired amounts of the enzyme solution added, and the samples incubated for specified times at  $37^\circ\text{C}$  in a shaking water bath. Following incubation, the dusts were resuspended in PBS containing  $2.0 \text{ mM}$  EDTA to stop the enzymatic digestion, and then resuspended in PBS alone. For conceptual purposes, we have expressed phospholipase activity in terms of "activity equivalents" which equal  $0.0817$  units of phospholipase. Using the equilibrium amounts of DPL adsorbed on kaolin from the adsorption isotherm study,<sup>(9)</sup> one activity equivalent would ideally remove that amount of DPL within one hour at  $37^\circ\text{C}$ .

Hemolytic potential of variously treated dusts was assayed by the erythrocyte hemolysis assay of Harrington *et*

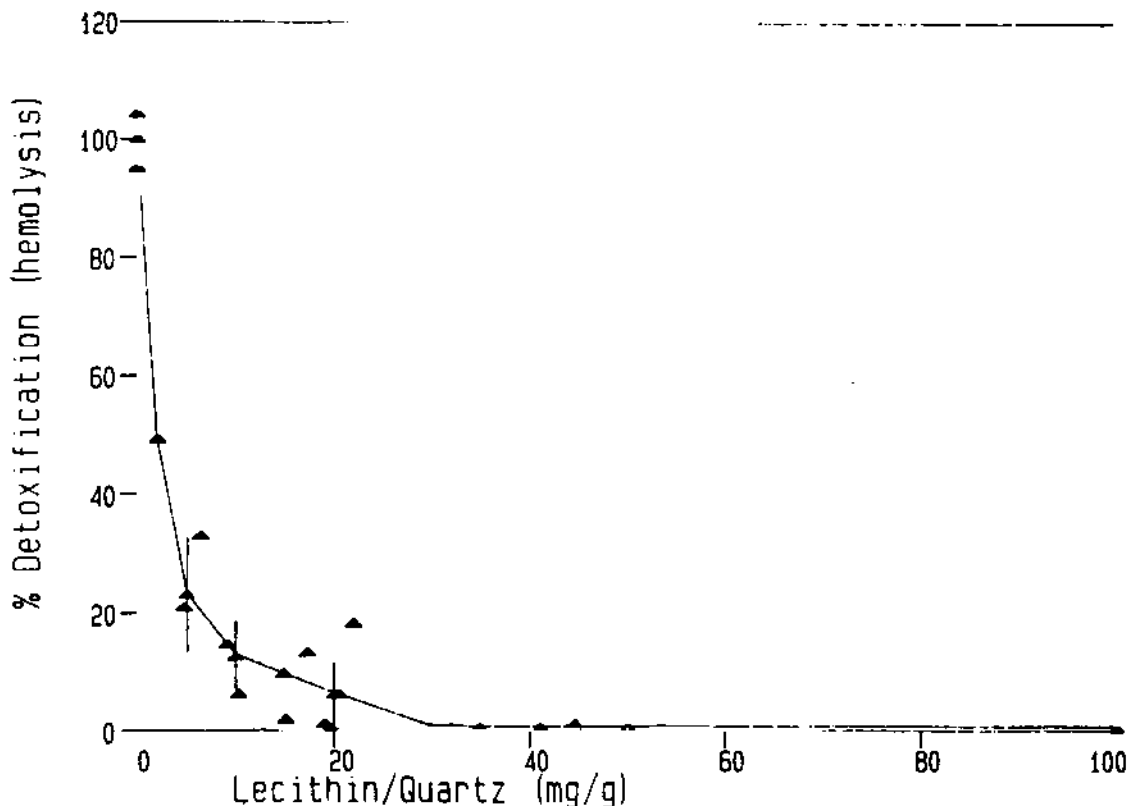


FIGURE 1. Hemolytic potential of quartz versus dipalmitoyl lecithin treatment. Erythrocyte hemolysis values are given as percentages of the value for untreated quartz. Open triangles connected by line segments show the diminution as a function of DPL added to the system. Line segments are connected between average values; and the bars show the ranges measured. The solid triangle scatter graph shows values from additional measurements where abscissa values are the amounts of lecithin actually adsorbed as measured by elution from the particles.

*al.*<sup>(17)</sup> Suspensions of erythrocytes (2% by volume) and 1.0 mg dust per ml were incubated in PBS at 37°C for one hour. After centrifugation at 500 g, the optical density of the supernatant was spectrophotometrically determined at 540 nm wavelength to measure the hemoglobin concentration.

The release of lactate dehydrogenase from pulmonary macrophages was determined by the method of Reeves and Fimignari,<sup>(18)</sup> beta-N-acetyl glucosaminidase by the method of Lockart and Kennedy,<sup>(19)</sup> and beta-glucuronidase by the method of Sellinger *et al.*<sup>(20)</sup>

DPL or lysolecithin (L-alpha-lecithin, beta palmitoyl) adsorbed to dusts was measured by freeze drying the dust, eluting phospholipids from the dust with methanol/chloroform (2/1 by volume), separating by thin layer chromatography, and phosphate quantitating by the method of Bartlett.<sup>(21)</sup>

Suppression of the hemolytic cytotoxicity of quartz and of kaolin by DPL was measured after incubation of each dust in DPL emulsion at concentrations calculated to provide coatings from 2 to 200 mg lecithin per gram dust, assuming total adsorption of the lecithin in emulsion. Some experiments were run with parallel samples which were then analyzed for amount of DPL adsorbed as measured by the phosphate assay.

Combined effect of DPL and lysolecithin (which is itself a lytic agent) adsorbed to quartz and to kaolin on their hemolytic potentials was similarly measured, except that the dusts were incubated with DPL emulsion containing an equal molar concentration of dissolved lysolecithin.

Time course experiments for the effect of PLA<sub>2</sub>, from porcine pancreas, on DPL-treated dust hemolytic potential was determined for dusts incubated at 7.5 mg dust per ml of DPL emulsion. The emulsion concentration was 10 mg DPL per ml saline. This is sufficient to provide saturation as determined by the adsorption isotherm measurements. Enzyme activity at levels from 10 to 300 activity equivalents was applied for periods of 2 to 216 hours. Following the incubation with enzymes and washing procedures, the hemolytic strengths of the dusts were measured and the amounts of residually adsorbed DPL and lysolecithin measured.

For tests in a simulated long-term system, pulmonary macrophages were obtained from rabbits and maintained in tissue culture for different periods of time. Cells were washed twice with HBSS and resuspended in Medium 199 containing 10% fetal calf serum and penicillin/streptomycin 100 ug/ml. Approximately  $4 \times 10^6$  cells were placed in individual culture wells, permitted to stabilize for 24 hours at 37°C, 5% CO<sub>2</sub>, and 90% relative humidity, and then challenged with native or DPL-treated quartz at levels of 400 ug dust per  $4 \times 10^6$  cells. Cells which were not challenged with dust were also maintained to determine the background rate of macrophage damage. Cytotoxicity was assayed by LDH and beta-N-acetyl glucosaminidase release.

## Results

Hemolytic potentials of DPL-treated quartz are shown with respect to untreated quartz in Figure 1. The highest abscissa value is around 50 mg lecithin per gram quartz, in concert with adsorption isotherm values.<sup>(12)</sup> The hemolytic strength of quartz is reduced by adsorbed lecithin, reaching

background levels between 20 and 30 mg/g adsorbed lecithin. Figure 2 similarly quantitates the hemolytic potential of kaolin. Maximum specific lecithin adsorption is about 130 mg/g; and values approach background between 80 and 100 mg/g. When comparing values between the quartz and kaolin dusts used, one should note the ratios of their specific surface areas, the kaolin having about three times the value of the quartz for surface area per gram.

Hemolytic potentials of quartz and kaolin treated with DPL and lysolecithin in combination were also measured. We have previously reported that the retoxification of dusts treated first with DPL and then with phospholipase enzymes can be due to a combination of functionally available particle surface activity and to adsorbed lysolecithin produced by the enzymatic digestion of lecithin.<sup>(8,12)</sup> Figure 3 shows the hemolytic potential for quartz treated with equimolar concentration of lecithin and lysolecithin together in physiologic saline. Figure 4 presents comparable data on the hemolytic potentials of lecithin and lysolecithin-treated kaolin. In both Figures 3 and 4, the maximum values of hemolytic potential reached are limited by the measurement conditions; that is, all the erythrocytes have been lysed. The hemolytic potentials above the untreated dust levels are presumed to be due to lysolecithin adsorbed to the dust or adsorbed to lecithin on the dust. In general the amount of lysolecithin eluted was less than the lecithin eluted, the lysolecithin being substantially more soluble in saline than the lecithin. Figure 5 presents the 37°C adsorption isotherm for lysolecithin on quartz and kaolin in physiologic saline; the corresponding lecithin isotherms have been presented elsewhere for these dusts.<sup>(12)</sup>

The hemolytic potential of DPL-treated quartz after phospholipase A<sub>2</sub> digestion *in vitro* is shown in Figure 6. Hemolysis is shown as a function of enzyme activity and digestion time. With the exception of one point at the highest enzyme activity, the potential rises with digestion time to approach untreated quartz levels between 44 and 72 hours. Parallel samples were eluted with organic solvent, the eluted material separated by thin layer chromatography, and measured by phosphate analysis. Figure 7 shows the amount of DPL remaining on the quartz following digestion. This is shown as a function of applied enzyme activity and time of enzymatic digestion. There is a rapid decrease in the amount of adsorbed DPL by the end of two hours, the shortest digestion time used. At 72 hours the levels detected are within the background for this method of separation and quantitation. Figure 8 shows similar measurements of the lysolecithin which was separated from DPL by the thin layer chromatography of eluted material. Much lower amounts of lysolecithin are seen, which decrease to background levels around 44 hours. The hemolysis and DPL retention data are overlaid on the maps of hemolytic potential of DPL and lysolecithin treated quartz in Figure 9. Values typically fall in the region indicating contributions to the cytotoxicity from both mechanisms, with the dust surface contribution increasing with digestion time.

The hemolytic potential of DPL-treated kaolin after digestion with phospholipase A<sub>2</sub> is shown in Figure 10. Unlike the quartz results, the kaolin potential generally is significantly greater than that of untreated kaolin. Somewhere between 20 and 44 hours these potentials drop to values

## LECITHIN SUPPRESSION OF KAOLIN HEMOLYTIC POTENTIAL

120

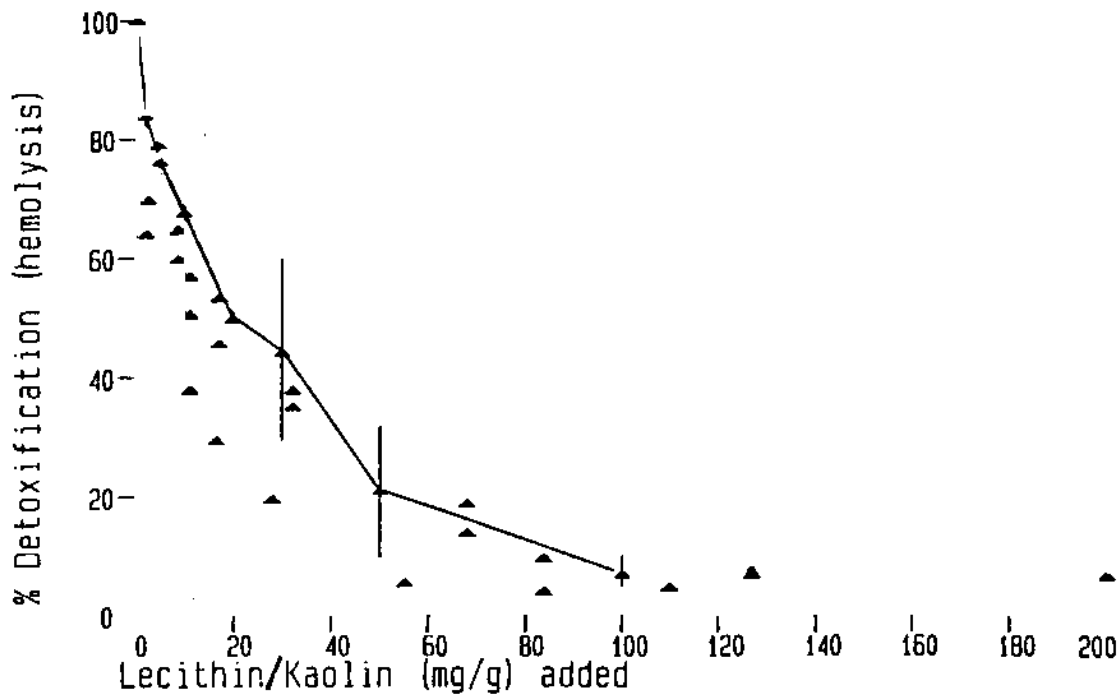


FIGURE 2. Hemolytic potential of kaolin versus dipalmitoyl lecithin treatment. Open triangles connected by line segments have as their abscissa values the amounts of lecithin added. The solid triangle scatter graph shows the potentials versus DPL eluted from the particles.

below that of native kaolin. At 72 hours, the potential is rising back toward the native dust levels. Figure 11 shows the amounts of DPL remaining on the kaolin as a function of enzyme activity and of time of digestion. This is measured by elution, chromatography, and phosphate analysis as for the quartz. Relatively high levels of DPL are retained on the kaolin to 44 hours as shown, in contrast to the quartz behavior. Figure 12 shows the corresponding lysolecithin retention data. Again, in contrast to quartz, high levels are retained in general out to the 44-hour data point. Figure 13 displays the hemolytic potential and retained DPL data for kaolin on the map of potential versus adsorbed DPL and lysolecithin for kaolin. Lower enzymatic activities and digestion times are seen to result in potentials which can be attributed to enzymatically produced lysolecithin. Longer digestion times result in potentials which might be attributed at least in part to surface effects. That the high hemolytic potentials above those of native kaolin can be attributed to adherent lysolecithin has been demonstrated by additional mixed enzyme studies to those previously reported,<sup>(12)</sup> comparing the effects of one hour digestions with 300 activity equivalents of phospholipase A<sub>2</sub>, from *Crotalus adamanteus* venom, and mixtures of it with equal activities of phospholipase C. The double enzyme treatment reduces the hemolytic potentials and adsorbed DPL levels from system saturation values for kaolin to values consistent with fractional exposed surface toxicity with little lysolecithin con-

tribution. The quartz potential after double lipase treatment is partially reduced from levels manifesting some combined effects of surface and lysolecithin to values consistent with activity due principally to exposed surface activity.

Development is underway in our lab on a system to challenge pulmonary macrophages *in vitro* with dusts treated with pulmonary surfactant, radiolabeled components of pulmonary surfactant, or proposed prophylactic agents. The attempt will then be to maintain the cells in culture long enough to measure any restoration of cytotoxic effects above those displayed by negative controls, that is, by cells not dosed with dusts. Figures 14 and 15 demonstrate, in part, the method and its major difficulty — maintaining viable control cells. The figures show the percentage of lactate dehydrogenase and beta-N-acetyl glucosaminidase which is released from the cells as a function of time since dust exposure. The top line is the release from cells challenged with untreated quartz. Cell damage or death is presumed to be indicated if both enzymes are released. The partial suppression of quartz hemolytic potential for the first 3 days is attributed to prophylactic effects of various biochemicals in the culture nutrient media. The bottom line shows the attrition of cells treated identically except that they have not been challenged with quartz. The data for cells challenged with DPL-treated quartz are initially at the levels for the negative controls. This may be due principally to the prophylactic effects of DPL on phagocytized dusts; we have observed that

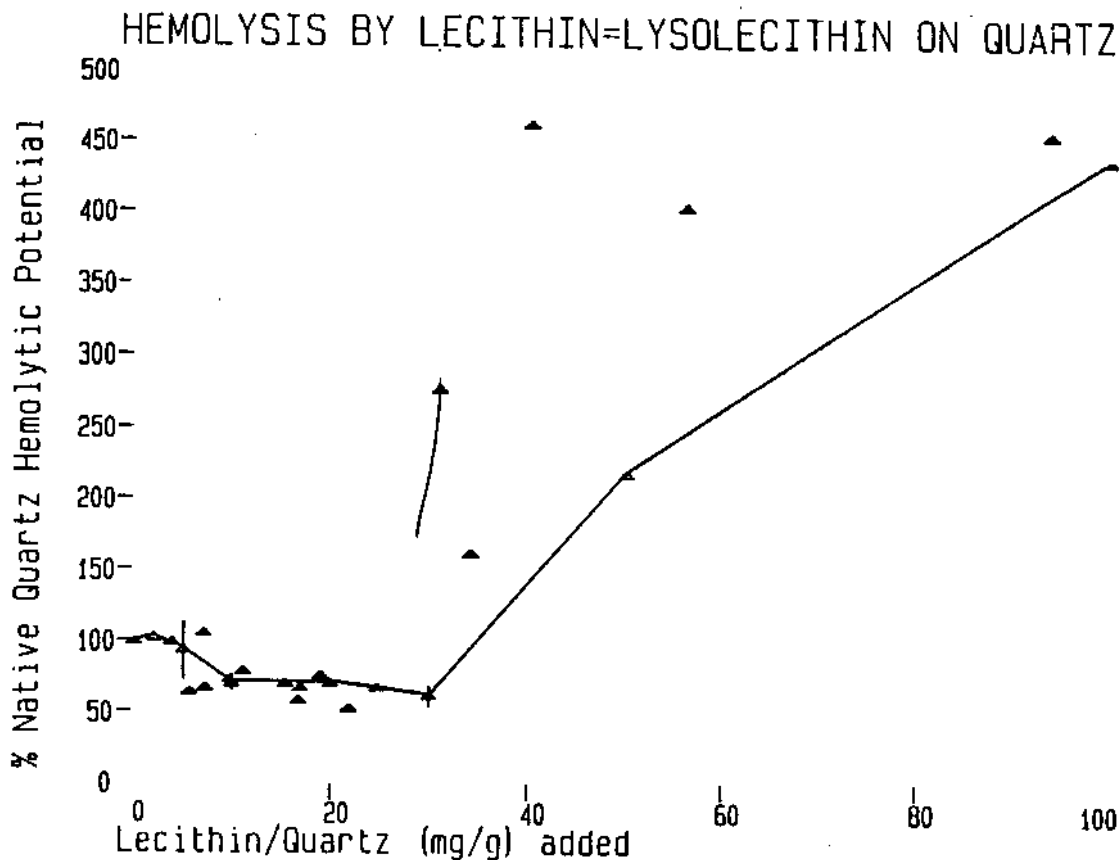


FIGURE 3. Hemolytic potential of quartz versus treatment by lysolecithin and dipalmitoyl lecithin added in equal molar amounts. Ordinate values are expressed as percentages of the value for untreated quartz. Open triangles with line segments have DPL added as their abscissa values. Solid triangle abscissa values are amounts of DPL eluted.

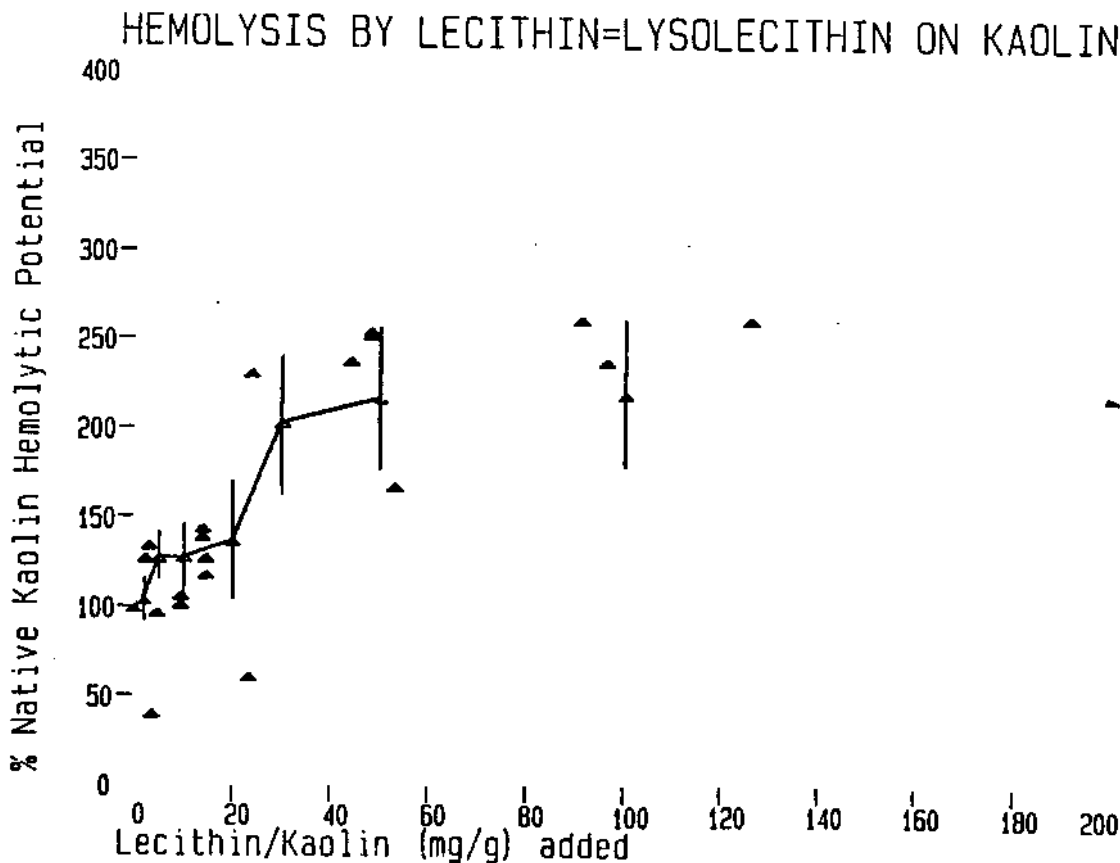


FIGURE 4. Hemolytic potential of kaolin treated with lysolecithin and dipalmitoyl Lecithin in equal molar amounts. Ordinate values are expressed as percentages of the value for untreated kaolin.



ADSORPTION OF LYSOLECITHIN ON KAOLIN AND ON SILICA

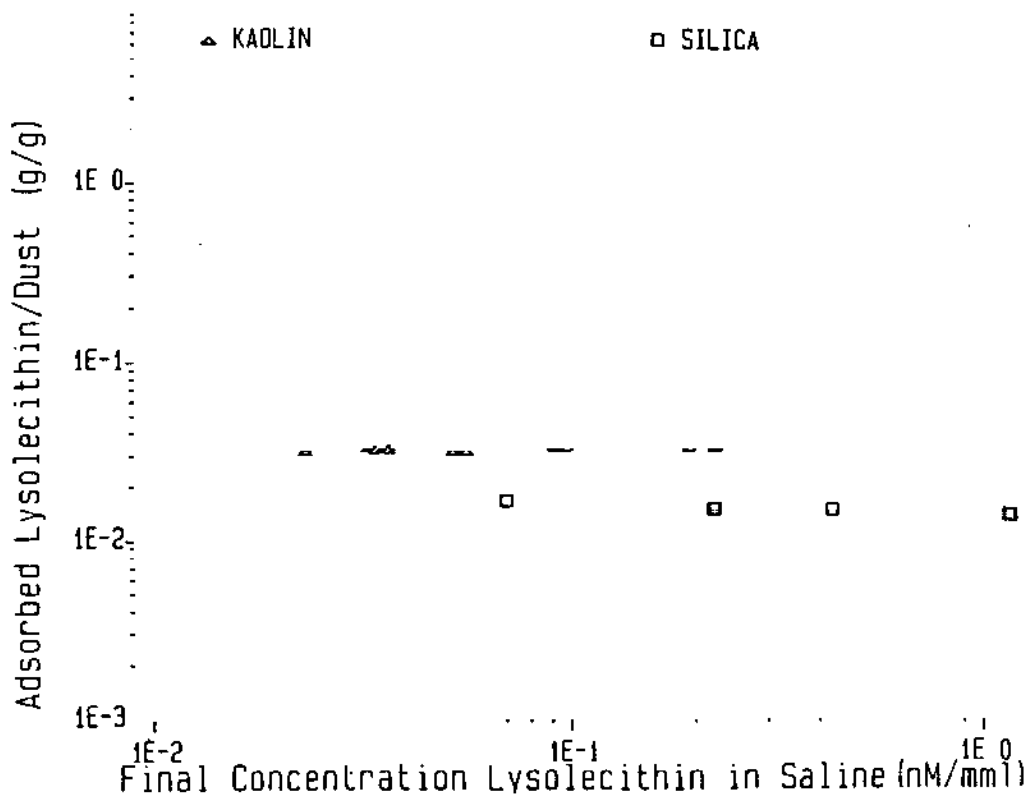


FIGURE 5. Adsorption isotherm for lysolecithin adsorption on kaolin and on quartz from saline at 37C. Ordinate values are mass specific adsorption as measured from initial and final concentration of lysolecithin in solution.

LACTATE DEHYDROGENASE RELEASE- QUARTZ + MACROPHAGE

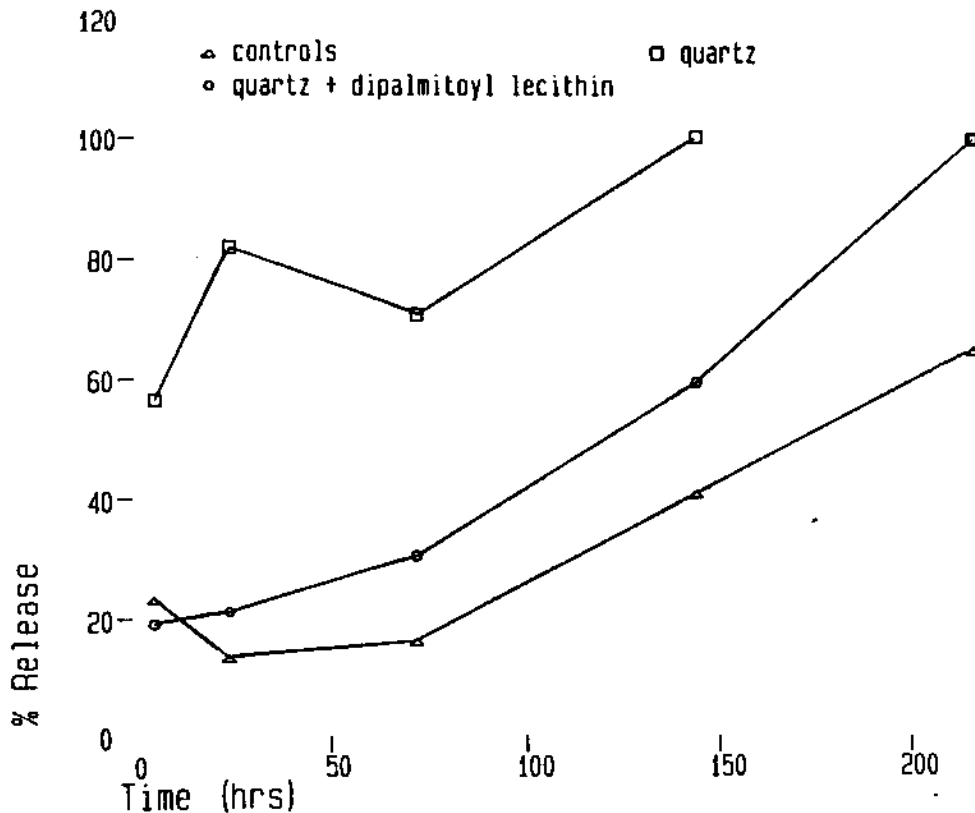


FIGURE 6. Erythrocyte hemolysis by dipalmitoyl lecithin and phospholipase A2 treated quartz versus time of incubation with the lipase. Data is shown for different levels of applied enzyme activity, expressed in terms of 'activity equivalents' defined in the text.

LECITHIN SURFACTANT/PHOSPHOLIPASE ENZYME TREATMENT

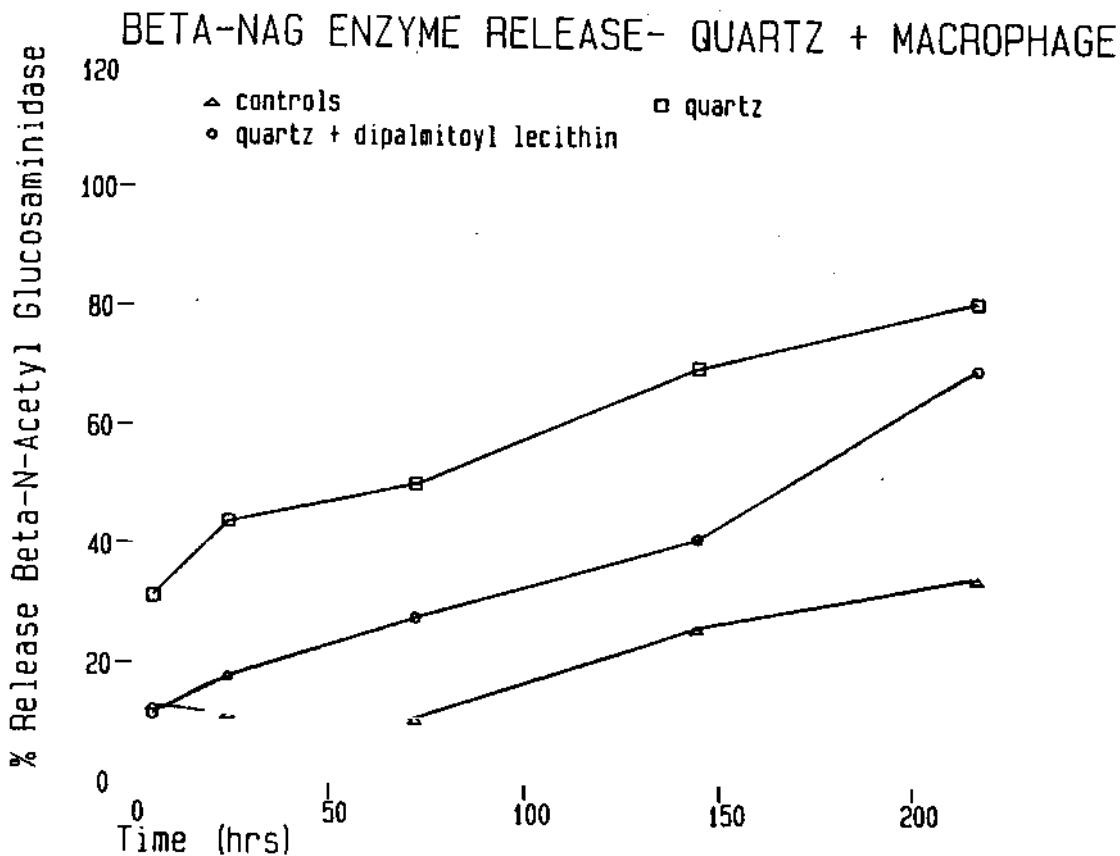


FIGURE 7. Dipalmitoyl lecithin retained on quartz following treatment with phospholipase A2 versus time of incubation with the lipase. Data is shown for different levels of applied enzyme activity expressed as "activity equivalents."

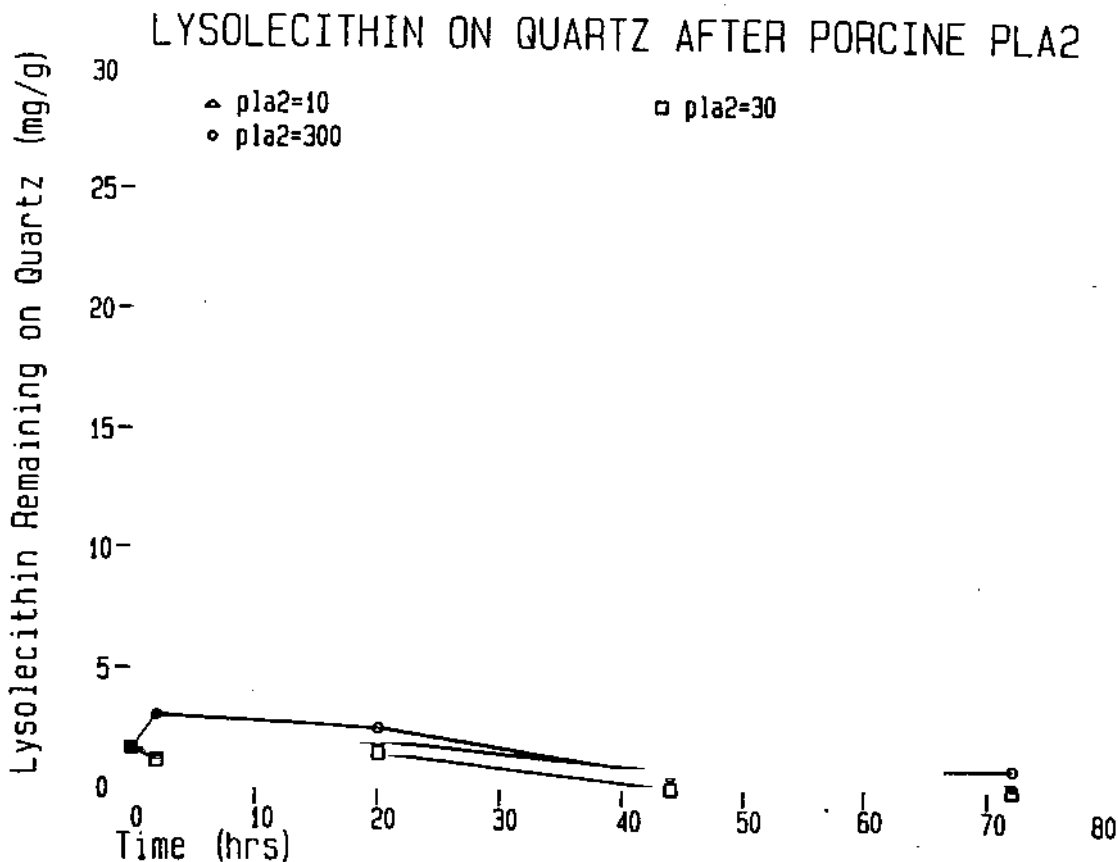


FIGURE 8. Lysolecithin retained on quartz following treatment with phospholipase A2 versus time of incubation with the lipase. Data is shown for different levels of applied enzyme activity expressed as "activity equivalents."

PLA2 DIGESTION VS TIME, ACTIVITY-LECITHIN ON QUARTZ

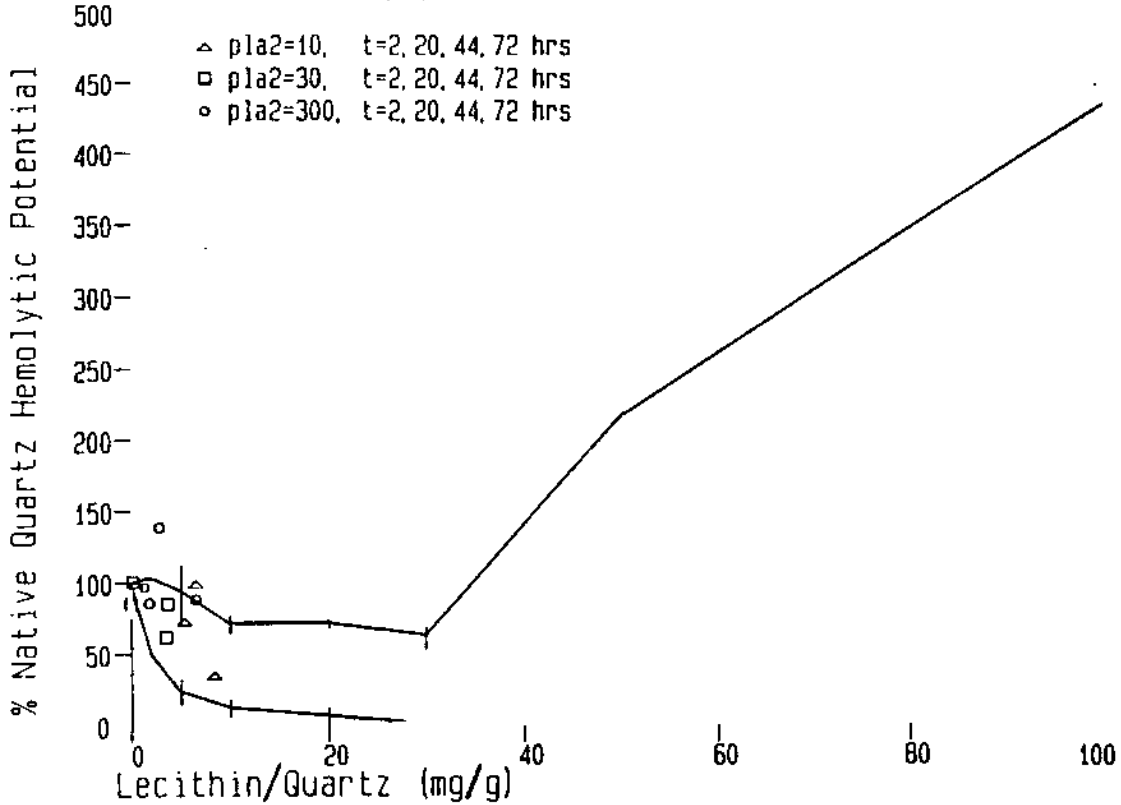


FIGURE 9. Erythrocyte hemolytic potential and retained dipalmitoyl lecithin for lecithin and phospholipase A2 treated quartz. Data from Figures 6 and 7 are presented on the map of quartz hemolytic potential versus lecithin and lysolecithin treatment from Figures 1 and 3.

HEMOLYSIS BY LECITHIN AND PLA2 TREATED KAOLIN

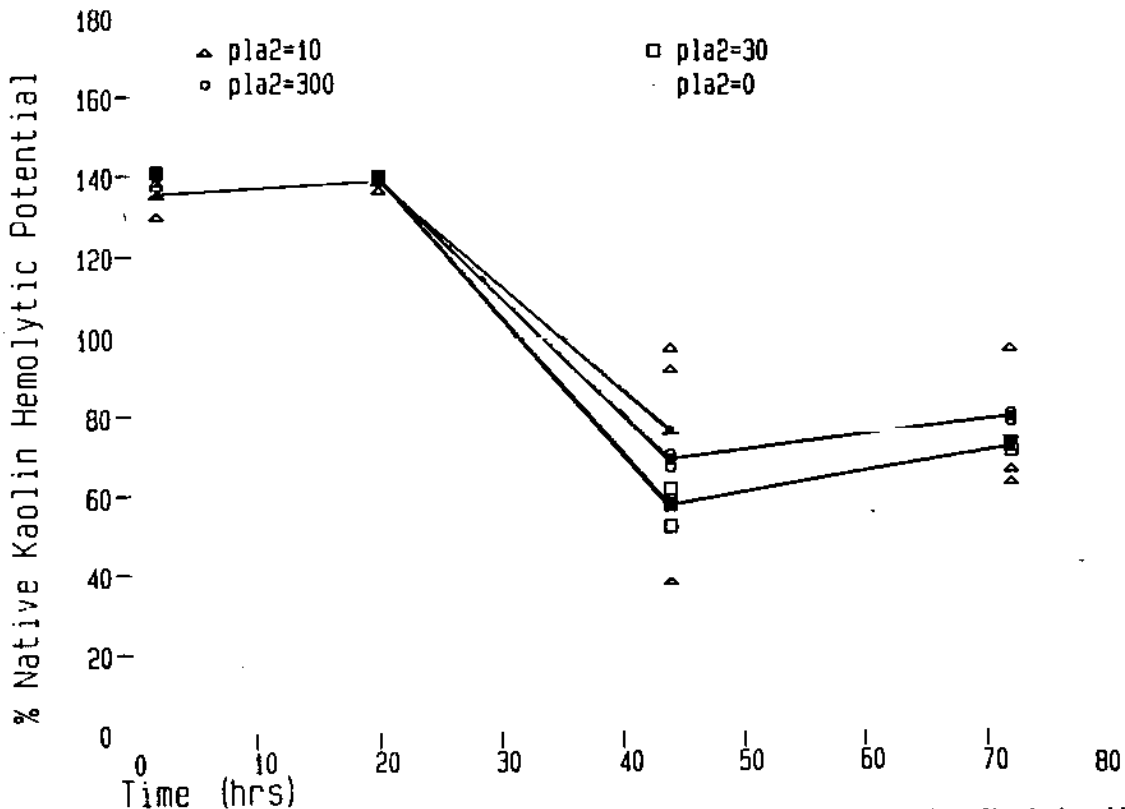


FIGURE 10. Erythrocyte hemolysis by dipalmitoyl lecithin and phospholipase A2 treated kaolin versus time of incubation with the lipase. Data is shown for different levels of applied enzyme activity, expressed in terms of "activity equivalents" defined in the text.

LECITHIN SURFACTANT/PHOSPHOLIPASE ENZYME TREATMENT

LECITHIN ON KAOLIN AFTER PORCINE PLA2 DIGESTION

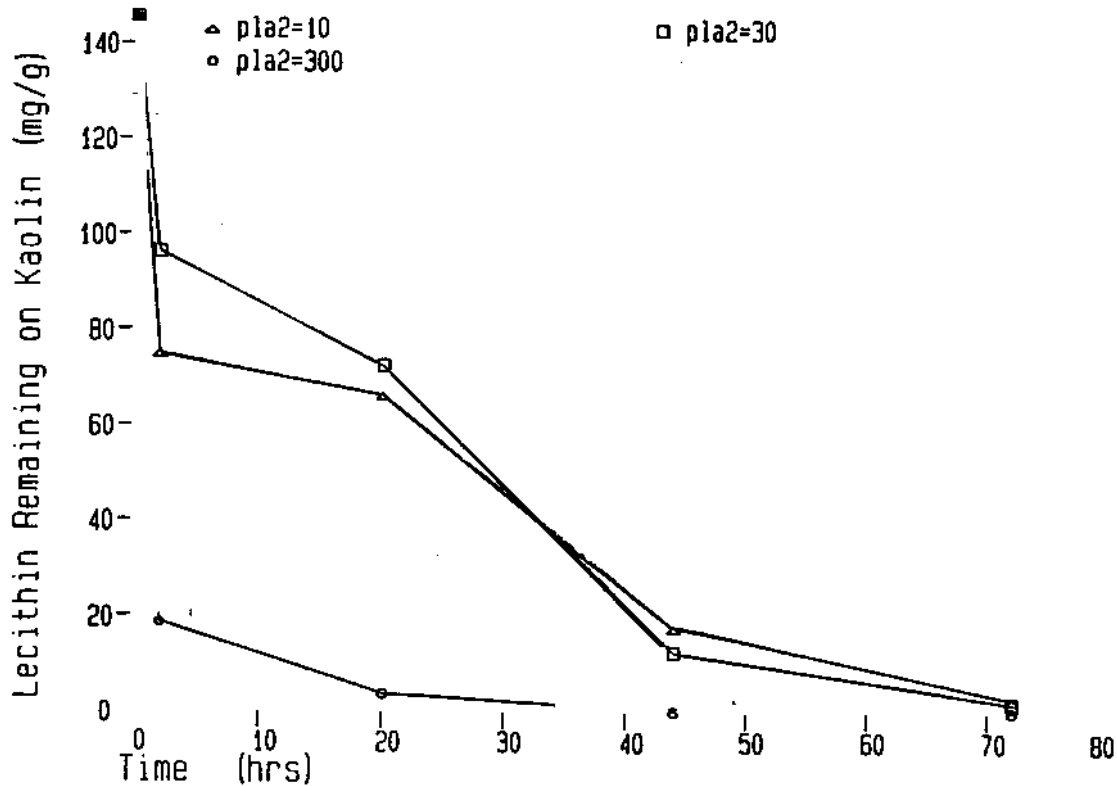


FIGURE 11. Dipalmitoyl lecithin retained on kaolin following treatment with phospholipase A2 versus time of incubation with the lipase. Data is shown for different levels of applied enzyme activity expressed as "activity equivalents."

LYSOLECITHIN ON KAOLIN AFTER PORCINE PLA2

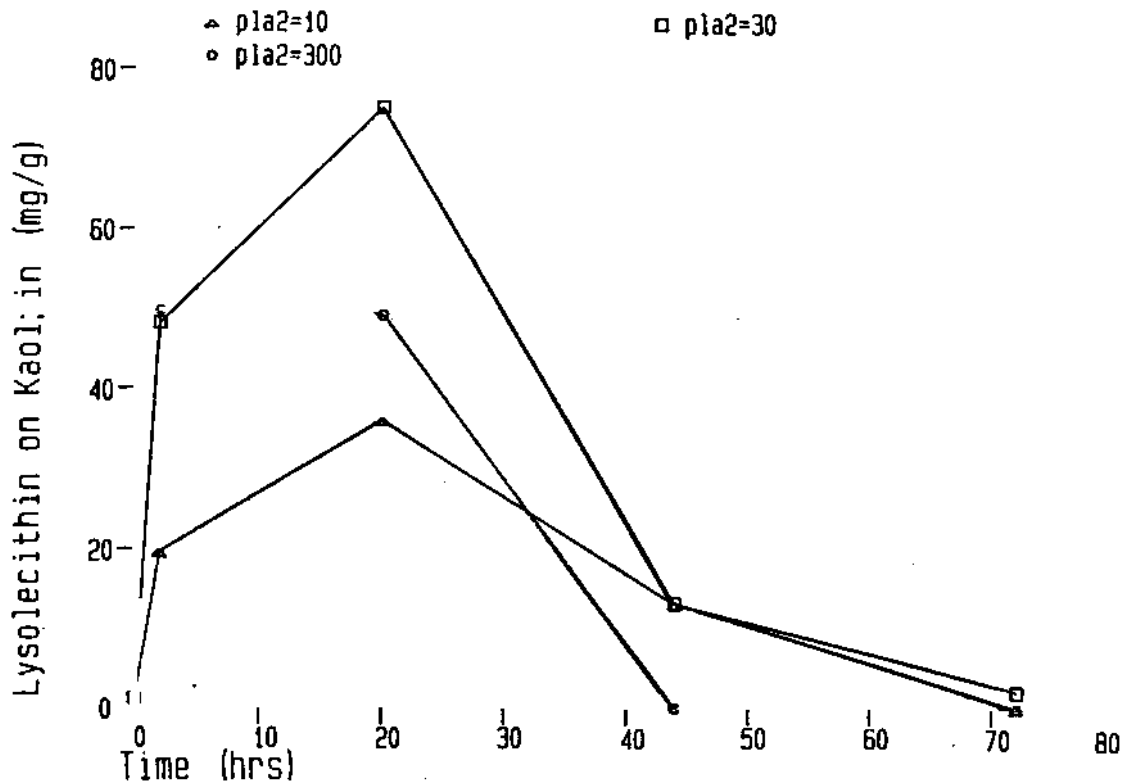


FIGURE 12. Lysolecithin retained on kaolin following treatment with phospholipase A2 versus time of incubation with the lipase. Data is shown for different levels of applied enzyme activity expressed as "activity equivalents."

the DPL treatment also slows uptake of quartz by the cells. The high attrition rates in this experiment do not permit unequivocal interpretation of the longer time values. We currently are testing modifications of the system to improve the viability of the controls.

**Discussion**

Adsorption of pulmonary surfactant by a respired particle may suppress prompt cytotoxic damage to alveolar macrophages and epithelial cells in the lung. Dipalmitoyl lecithin, a major component of pulmonary surfactant, suppresses the *in vitro* hemolytic potential of both quartz and kaolin, and also suppresses their potential to cause major damage to pulmonary macrophages *in vitro* as measured by cytosolic and lysosomal enzyme release. Comparison of estimated amounts of surfactant in a healthy lung and DPL adsorption data indicate *in vivo* pulmonary surfactant levels are adequate to provide a defense against the prompt lytic effects of silicate or aluminosilicate dusts at typical occupational exposure levels.<sup>(11)</sup> Instillation of quartz and kaolin in animal lungs does not produce prompt permanent damage;<sup>(22)</sup> acute but transient inflammatory cellular response *in vivo* which is observed for both dusts<sup>(22)</sup> indicate some non-mineral specific effect of respired dusts. The effect or lack of effect of surfactant on dust induced release of antigenic factors by pulmonary macrophages has not been investigated.

Phospholipase A2 enzymatic digestion *in vitro* of DPL-coated quartz or kaolin can remove all or most of the ad-

sorbed DPL over the period of a few days for the enzymatic activities used. There appear to be mineral specific differences in the rates of digestion and in the degree of adherence of lipase-produced lysolecithin to the DPL-dust complex at intermediate stages of digestion. Mineral specific rate differences might result from differing free energies of adsorption or from conformational differences in adsorbed DPL which provide different levels of steric hindrance to the lipase action. Phospholipase activity is affected by the physical state of its phospholipid substrate.<sup>(23)</sup>

Adsorption of lecithin to aluminosilicate dust surface may involve electrostatic and hydrogen bonding. Alumina surface is a better catalyst than silica for hydrolysis of lecithin in organic media,<sup>(24)</sup> indicating more effective interaction of alumina surface hydroxyls with the ester bonds to the glycerol moiety of lecithin. Lecithin is a zwitterion with the choline head group cationic and the phosphate group anionic. Silanol groups on the surface of quartz in aqueous media partially dissociate to produce negatively charged surface sites, with an isoelectric point around pH 1.5;<sup>(25)</sup> that is, part of the adsorption of DPL to quartz may be attributed to electrostatic interaction between the choline group at the tip of the DPL and the dissociated silanol groups on the quartz surface.<sup>(26)</sup> Kaolin has a structure of alternate layers of silica tetrahedra and alumina octahedra. Hydroxyl groups on the surface of alumina have an isoelectric point of about pH 9.4,<sup>(25)</sup> the surface of alumina bearing a net positive charge. Adsorption of DPL to kaolin should involve in part electrostatic interaction between the alumina octahedra positively charged surface sites and the negatively charged phosphate

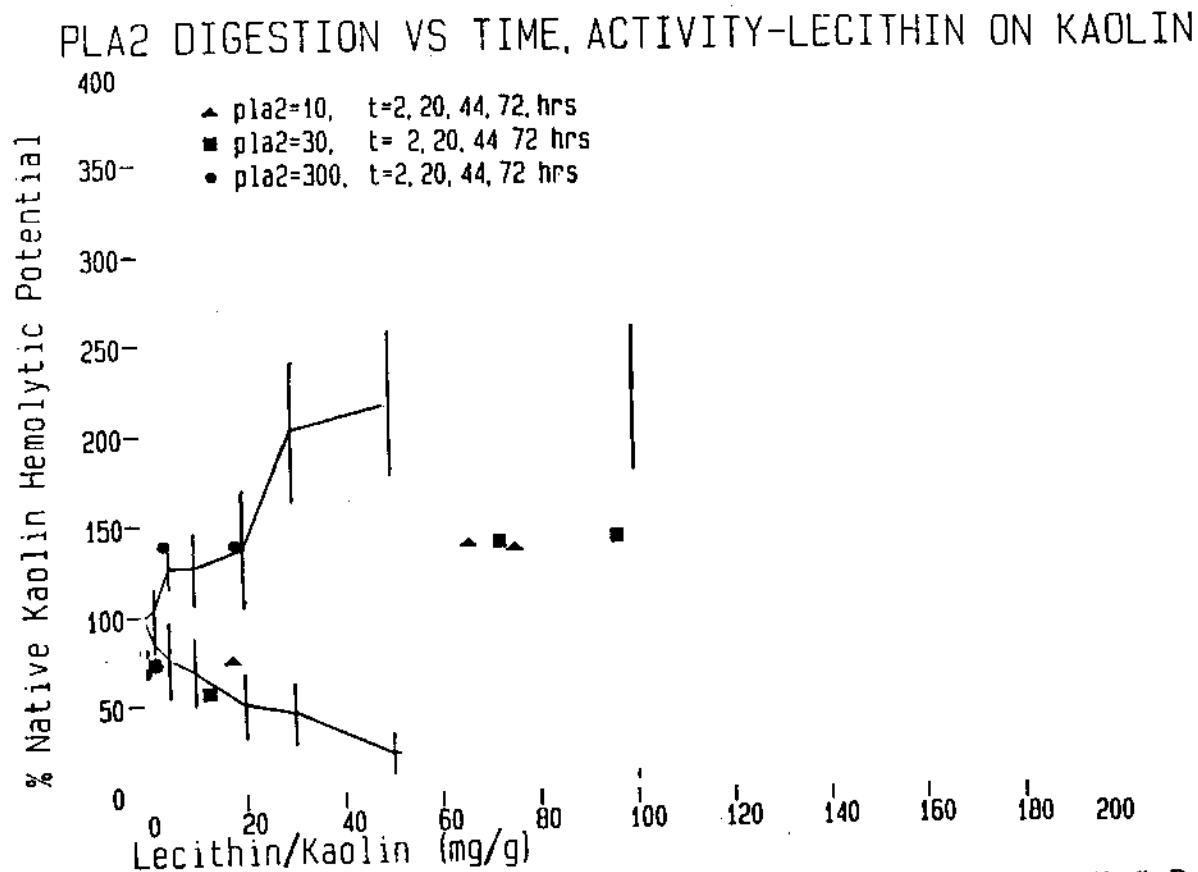


FIGURE 13. Erythrocyte hemolytic potential and retained dipalmitoyl lecithin for lecithin and phospholipase A2 treated kaolin. Data from Figures 10 and 11 are presented on the map of kaolin hemolytic potential versus lecithin and lysolecithin treatment from Figures 2 and 4.

LECITHIN SURFACTANT/PHOSPHOLIPASE ENZYME TREATMENT

LECITHIN ON QUARTZ AFTER PORCINE PLA2 DIGESTION

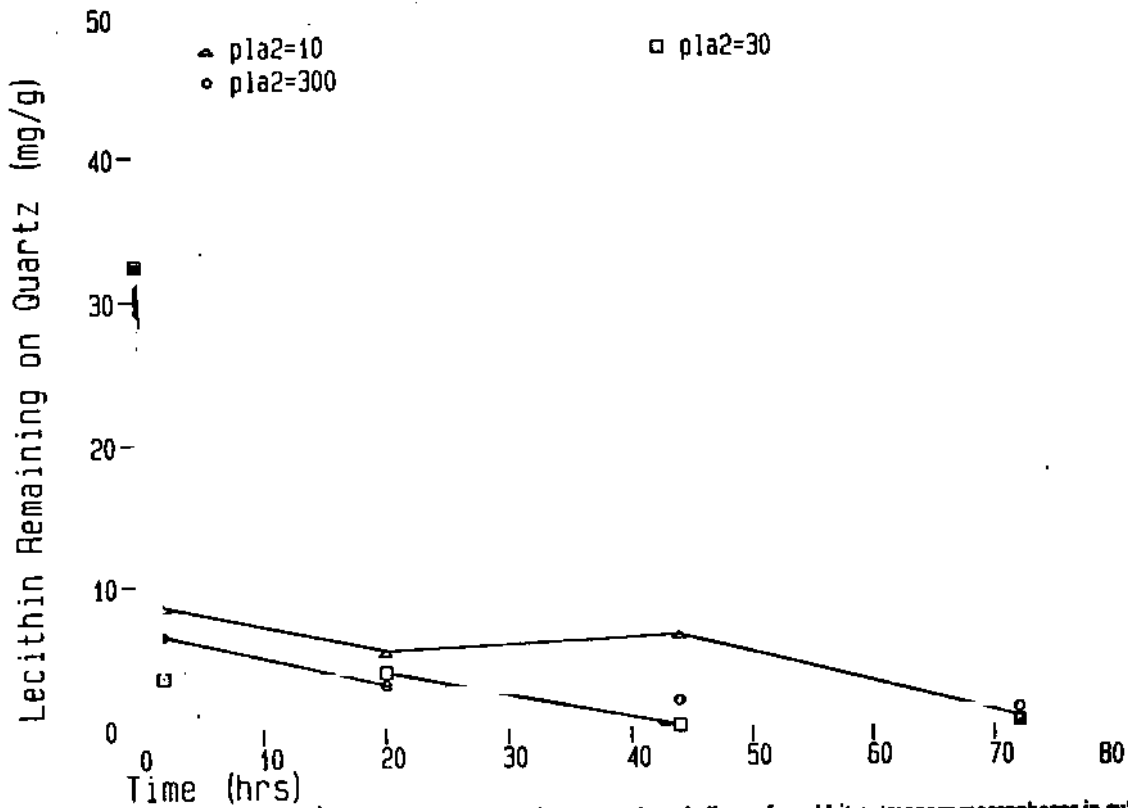


FIGURE 14. Release of lysosomal enzyme versus time following quartz dust challenge for rabbit pulmonary macrophages in culture. Data is shown for negative controls, i.e., macrophages not challenged with quartz; for positive controls, i.e., for challenge with untreated quartz; and for challenge with lecithin treated quartz.

HEMOLYSIS BY LECITHIN & PLA2 TREATED QUARTZ

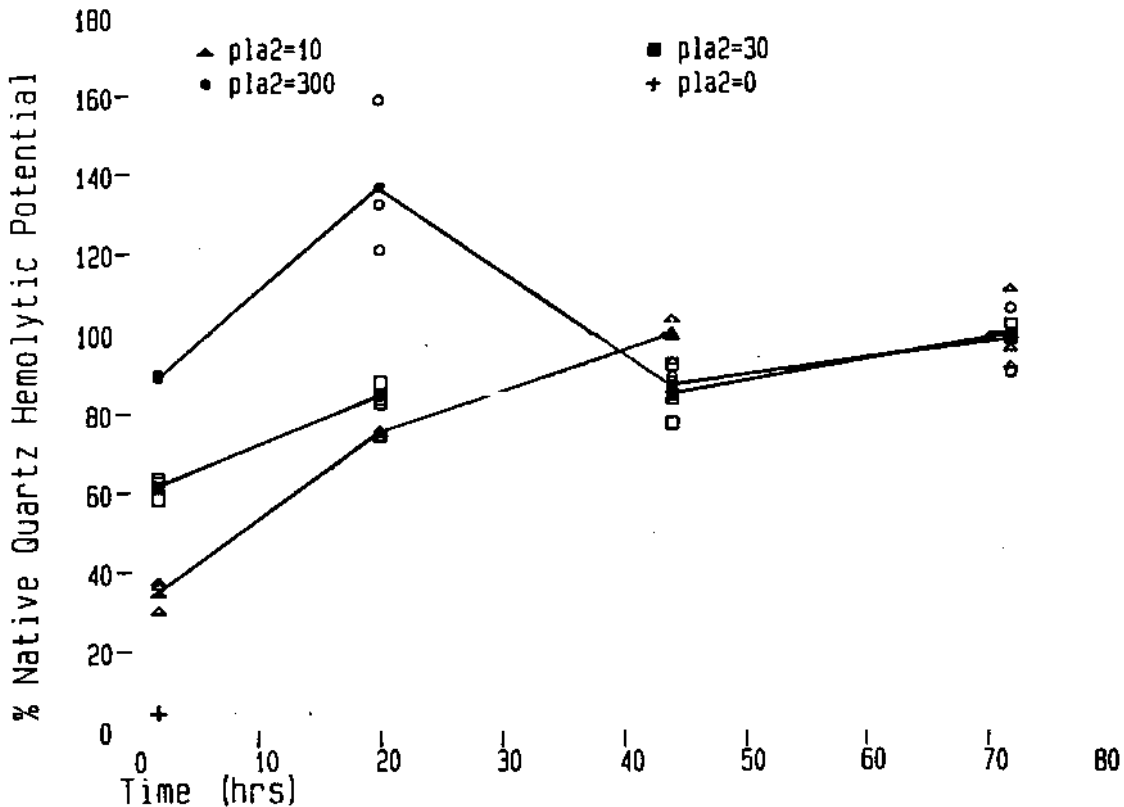


FIGURE 15. Release of cytosolic enzyme versus time following quartz dust challenge for rabbit pulmonary macrophages in culture. Data is shown for macrophages not challenged with quartz, challenged with untreated quartz, or challenged with lecithin treated quartz.

moiety of DPL. The phosphate-glycerol bond is hydrolyzed under the enzymatic action of Phospholipase C and the adjacent ester linkage of glycerol to a fatty acid acyl group is hydrolyzed by the action of Phospholipase A2. An adsorbed phospholipid conformation in which phosphate groups are directed toward alumina surface groups of aluminosilicate dust might hinder enzymatic hydrolysis of the target ester linkages.

Lysolecithin is adsorbed to a more limited extent than DPL by both quartz and kaolin in single compound adsorption isotherm measurements. Adsorption of lysolecithin at intermediate stages of the phospholipase A2 digestion of DPL on dusts may be due in part to lysolecithin association with adsorbed DPL. Lysolecithin on quartz and kaolin decreases as DPL is digested away. We have not determined the degree of mineral adsorption of hydrolysis produced by fatty acids or their contribution to cytotoxicity suppression. In the phagolysosome of a pulmonary macrophage, a number of enzymes would act upon a surfactant coated particle. Our limited experiments with phospholipase A2 and C in combination indicate that the mixed activity can significantly diminish the lysolecithin contribution to the hemolytic potential compared to the single enzyme treatment result. To provide a useful basis for analysis of physiologic effects, these *in vitro* digestion studies must be extended to use damaged surfactants, full lysosomal enzyme applied at acidic conditions representative of the phagolysosomal interior, and representative relative amounts of surfactant, enzyme activity, and dusts. We are currently measuring the DPL-digesting activity of full lysosomal enzyme, which we obtain by density gradient centrifugation methods<sup>(28)</sup> from rat liver homogenate.

Complementary to these *in vitro* digestion experiments, the long-term macrophage challenge system is an attempt to obtain time course information on the suppression of dust cytotoxic properties after challenge and phagocytosis of surfactant treated dusts. If macrophages can be maintained viable in culture long enough to unequivocally distinguish dust induced effects, then the possible correlation of induced effects with the fate of the initial coating of labeled surfactant will be tested. Comparing the time course for retoxification of kaolin with that of quartz should indicate whether or not these interactions are significant in distinguishing the pathogenicity of respirable quartz dust.

### Acknowledgment

This research has been supported by the Department of the Interior's Mineral Institute program administered by the Bureau of Mines through the Generic Mineral Technology Center for Respirable Dust under grant number G1135142.

### References

1. Morgan, W.K.C. and A. Seaton: *Occupational Lung Diseases*, Saunders, Philadelphia (1975).
2. Hamilton, A. and H.L. Hardy: *Industrial Toxicology*, 3rd ed., p. 448. Publishing Sciences Group, Acton, MA (1974).
3. Parker, W.R.: *Occupational Lung Disorders*, p. 338. Butterworths, London (1974).

4. Hunter, D.: *The Diseases of Occupations*, 5th ed., p. 992. English Universities Press, London (1975).
5. Sheers, G.: Prevalence of Pneumoconiosis in Cornish Kaolin Workers. *Br. J. Ind. Med.* 21:218 (1964).
6. Warraki, S. and Y. Herant: Pneumoconiosis in China-Clay Workers. *Br. J. Ind. Med.* 20:226 (1963).
7. Lynch, K. and F.A. Melver: Pneumoconiosis from Exposure to Kaolin Dust: Kaolinosis. *Am. J. Path.* 30:1117 (1954).
8. Wallace, W.E., M.J. Keane, V. Vallyathan et al: Pulmonary Surfactant Interaction with Respirable Dust. *Proceedings - Generic Mineral Technology Center for Respirable Dust, Coal Mine Dust Conference*, pp. 180-187. S. Peng, Ed. (1984). Report No. BP86 169380/AS. National Technical Information Service, Springfield, VA (1986).
9. Wallace, W.E., V. Vallyathan, M.J. Keane and V. Robinson: *In vitro* Biologic Toxicity of Native and Surface-modified Silica and Kaolin. *J. Toxicol. Environ. Health* 16:415 (1985).
10. Clements, J.A., J. Nellenboger and H.J. Trahan: Pulmonary Surfactant and Evolution of the Lungs. *Science* 169:603 (1970).
11. Wallace, W.E., Jr., L.C. Headley and K.C. Weber: Dipalmitoyl Lecithin Surfactant Adsorption by Kaolin Dust *in vitro*. *J. Colloid Interface Sci.* 51:535 (1975).
12. Wallace, W.E., M.J. Keane, V. Vallyathan et al: Suppression of Inhaled Particle Cytotoxicity by Pulmonary Surfactant and Re-Toxicification by Phospholipase--Distinguishing Properties of Quartz and Kaolin. *Proceedings - British Occupational Health Society, Inhaled Particles Conference, 1985*. (To be published).
13. Nolan, R.P., A.M. Langer, J.S. Harington et al: Quartz Hemolysis as Related to its Surface Functionalities. *Environ. Res.* 26:503 (1981).
14. Marks, J.: The Neutralization of Silica Toxicity *in vitro*. *Br. J. Ind. Med.* 14:81 (1957).
15. Stalder, K. and W. Stober: Haemolytic Activity of Suspensions of Different Silica Modifications and Inert Dusts. *Nature* 207:874 (1965).
16. Allison, A.C.: *Respiratory Defense Mechanisms, Part II*, pp. 1075-1102. J.D. Brain, D.F. Proctor and L.M. Reid. Eds. Marcel Dekker, Inc., New York (1977).
17. Harington, J., K. Miller and G. Macnab: Hemolysis by Asbestos. *Environ. Res.* 4:95-117 (1971).
18. Reeves, W.J. and G.M. Fimignari: An Improved Procedure for the Preparation of Crystalline Lactic Dehydrogenase from Hog Heart. *J. Biol. Chem.* 238:3853 (1963).
19. Lockard, V. and R. Kennedy: Alterations in Rabbit Alveolar Macrophages as a Result of Traumatic Shock. *Lab. Invest.* 35:501-506 (1976).
20. Sellinger, O.Z., H. Beaufay, P. Jacques et al: Intracellular Distribution and Properties of beta-N-Acetylglucosaminidase and beta-N-

- galactosidase in Rat Liver. *Biochem. J.* 74:450-456 (1960).
21. Bartlett, G.R.: Phosphorus Assay in Column Chromatography. *J. Biolog. Chem.* 234:466 (1959).
  22. Vallyathan, V., D. Schwegler, M. Reasor et al: Comparative *in vitro*. Cytotoxicity and Relative Pathogenicity of Mineral Dusts. *Proceedings — British Occupational Health Society, Inhaled Particles Conference, 1985* (to be published).
  23. Matsuzawa, Y., and K.Y. Hostetler: Properties of Phospholipase C Isolated from Rat Liver Lysosomes. *J. Biolog. Chem.* 255:646 (1980).
  24. Renkonen, O.: Breakdown of Lecithin on Aluminum Oxide Columns. *J. Lipid Res.* 3:181 (1962).
  25. Ginn, M.E.: Adsorption of Cationic Surfactants on Mineral Substrates. *Cationic Surfactants*, Chap. 10, p. 347. E. Jungerman, Ed. Marcel Dekker, Inc., New York (1977).
  26. Langer, A.M.: Crystal Faces and Cleavage Planes in Quartz as Templates in Biological Processes. *Q. Rev. Biophysics* 11:543 (1978).



# Effects of Coal Dust and Alveolar Macrophages on Growth of Lung Fibroblasts

G. E. Bartlett and A. B. Pederson

Department of Pathology, The Milton S. Hershey Medical Center, The Pennsylvania State University

As a part of our study of how coal mine dusts injure the lung we have studied the effects of dusts and dust-exposed pulmonary alveolar macrophages (PAMs) on the growth of lung fibroblasts (LF). Fibroblasts were cultured near confluence in low-serum medium, either alone or in the presence of dusts, dusts plus PAMs, dust leachates or supernatants of dust-exposed PAM cultures. We report here provisional conclusions, based on initial observations. Rat LF were relatively unresponsive to direct effects of dusts, showing weak stimulation in only a few cultures, and there was no evidence that dust-exposed rat PAMs had released any growth-regulatory products. In contrast, guinea pig cells were more responsive to the dusts. The pattern of responses was quite complex. Three of the dusts stimulated LF directly (with no mediation by PAMs). Two dusts were essentially inert when added directly to fibroblast cultures, either with or without PAMs, but their leachates were active: 867 leachate was inhibitory and RF leachate was stimulatory. Dust 1361, either directly in the cultures or as an aqueous leachate, was stimulatory, and it activated cocultured PAMs to stimulate LF growth; however, supernatant products of 1361-stimulated PAMs were inhibitory. Direct exposure to 1192 stimulated LF, but its leachate was inert; cocultured PAMs exposed to 1192 had weak stimulatory effects, but supernatants of 1192-exposed PAMs were mildly inhibitory. MP3-3 had effects similar to 1192, except that the cocultured, dust-exposed PAMs had no effect on growth. We conclude 1) that guinea pig lung cells are more responsive to dusts than are rat lung cells, 2) that dusts can influence growth of LF by four kinds of interaction (by direct dust-cell interaction, by release of soluble dust components into the culture medium, by activating PAMs to exert direct cell-cell interactions, and by activating PAMs to release growth regulatory products into the culture medium), 3) that each kind of interaction may be neutral, inhibitory or stimulatory, depending on the dust tested, 4) that four of the dusts tested were neutral, inhibitory or stimulatory, depending on the assay (the fifth dust was either neutral or stimulatory), and 5) that the effects of soluble mediators (leachates or products of activated PAMs) frequently did not correspond with the

direct dust-cell or PAM-fibroblast effects. These results suggest that the nature of the dust-lung interaction at the level of cells and molecules is exceedingly complex. These observations need to be confirmed and extended to determine what characteristics of the dusts determine the nature of the cellular responses, and to determine which patterns of responses are detrimental and which are beneficial in the overall health of the dust-exposed lung.

## Introduction

Chronic occupational exposure to the dusts in coal mines commonly results in coal worker's pneumoconiosis (CWP), the progressive accumulation of coal mine dusts in the substance of the lung. The effects on pulmonary function may range from minimal to debilitating. One common feature of the degenerative changes that occur in CWP is the production of increased amounts of fibrous connective tissue ("scar"). This process of fibrosis converts the normally pliable, elastic lung tissue into a more or less rigid, nonelastic organ. Even when fibrosis is minimal, it exerts traction on surrounding delicate alveolar walls, contributing to the emphysema that is a part of the milder forms of CWP. If the dust-lung interaction could be characterized sufficiently to define the sequence of events that leads to fibrosis, it might be possible to prevent the development of fibrosis in CWP by modulating the lung's response to dust. Likewise, prevention of CWP would be facilitated if the characteristics of dusts that trigger the fibrotic process could be identified, leading to the recognition of which dusts are most likely to cause serious disease. Our long range objective is to learn how to prevent CWP. To that end we are studying the interaction of coal dusts and lung cells in cell culture in order to determine how that interaction results in fibrosis and to determine whether dusts with different physical and chemical characteristics interact with lung cells in qualitatively or quantitatively different ways.

A key component of the fibrotic process is the proliferation of the fiber-producing cells of the lung, called lung fibroblasts (LF). In the normal, healthy lung the LF are a part of the supporting framework of the lung and are

generally quiescent. They undergo division only rarely, so they synthesize DNA at a low rate. When the lung is responding to injury, the LF are mobilized to produce the new fibers necessary to patch up the area of injury. Part of that mobilization response is an increase in the rate of cell division in order to increase the numbers of LF available to carry out the repair. The response of most tissues to injury is orchestrated, in large part, by a class of mobile, protective cells called macrophages; in the lung they are called pulmonary alveolar macrophages (PAMs). Studies of pneumoconiosis and pulmonary fibrosis due to other agents have suggested that when macrophages ingest the inhaled particulates they are "activated," resulting in increased synthesis and secretion of several different compounds that regulate various aspects of the inflammatory, repair and immune processes.<sup>(1-9)</sup> In particular, it has been shown that PAMs exposed to asbestos release more fibroblast growth factor than do control PAMs.<sup>(10)</sup> Similar studies have been performed with other agents,<sup>(11-14)</sup> but not with well-characterized coal dusts. Likewise, many such studies have used macrophages from parts of the body other than the lung (i.e., from the peritoneal cavity)<sup>(9,15-17)</sup> and have used fibroblasts either from other sites, such as skin<sup>(9,15-18)</sup> or from established, heterologous cell lines in culture.<sup>(11)</sup> The overall purpose of this study is to test the hypothesis that exposure of PAMs to coal dusts causes the PAMs to secrete factors that stimulate growth of LF; related hypotheses and corollaries are tested in the course of the study. To our knowledge, this is the only investigation that uses coal dusts, PAMs and LF.

## Materials & Methods

### Animals

Female Hartley random-bred guinea pigs were purchased from Hazelton Research, Denver, Pennsylvania. Female Fisher 344 inbred rats were purchased from Charles River Laboratories, Kingston, New York.

### Macrophages

PAMs were obtained by bronchial lavage of adult female rats or guinea pigs under nembutal anesthesia. Five ml of phosphate buffered saline (pH 7.4) with 0.1 percent ethylenediamine tetraacetic acid was instilled through the trachea, flushed five times and collected in a sterile plastic centrifuge tube on ice. Each animal was lavaged three times. Cells from different rats were pooled, but cells from different guinea pigs were not pooled. The cell suspensions were centrifuged at 400 g for 15 min, and resuspended at  $2 \times 10^5$  cells/ml in Dulbecco's Minimal Essential Medium (DMEM) containing fetal calf serum (FCS), 1 percent for cocultures or 0.5 percent for supernatant production.

### Supernatants and Leachates

Products of stimulated guinea pig PAMs were prepared as described by Lemaire.<sup>(10)</sup> Briefly, PAMs were added to the 24 mm diameter wells of 12-well cluster plates at the rate of 0.5 ml ( $10^6$  cells)/well, and incubated at 37°C for one hour to allow the cells to adhere. One hour later, 0.5 ml of dust suspension was added to each well containing  $10^6$  newly

plated PAMs, so that the final nutrient volume was 1.0 ml and the final FCS concentration was 0.5 percent. The cells were incubated at 37°C 5 percent CO<sub>2</sub> for 24 hours. At the end of the incubation period, the nutrient medium was aspirated from each well, and the supernatants of replicate wells (same additive, same concentration, cells from different donor animals) were pooled. Supernatant pools were centrifuged at 1600 g for 15 min, distributed in 1 ml aliquots in plastic tubes and frozen at -70°C. Leachates were prepared in parallel with the supernatants, incubating the dust in 1 ml of DMEM (0.5 percent FCS) without PAMs for 24 hours.

### Lung Fibroblasts (LF)

Young adult guinea pigs (approximately 2 months old) were killed by an overdose of nembutal, and the lungs were removed aseptically. Small fragments of lung tissue ( $< 1 \text{ mm}^3$ ) were placed in dry 35 mm plastic tissue culture dishes; after several minutes to permit firm attachment to the dish, the explants were covered with 2 ml DMEM (20 percent FCS). Fibroblasts were permitted to grow out of the explants, and when they covered a majority of the surface of the primary culture dish, they were harvested and passed to larger culture vessels for expansion of the population. Cells were harvested by 10 min incubation in 0.05 percent trypsin, washed in DMEM with 20 percent FCS and counted in a hemacytometer. In some experiments, rat lung fibroblasts were prepared from 60-80 gm weanling rats and used in the same fashion.

### Coal Dust Samples

Five different coal dusts have been tested thus far. For each of the first four dusts, the coal sample was collected in the mine, transported to the Mineral Engineering laboratory at Pennsylvania State University, crushed, screened and milled to produce dust with a size distribution predominantly in the respirable range ( $< 5 \mu\text{m}$  diameter). Those specimens include: MP3-3 (Upper Freeport, Bituminous); PSOC-867 (Primrose, Anthracite); PSOC-1192 (Lower Kittanning, Bituminous); and PSOC-1361P (Upper Freeport, Bituminous). The first was kindly provided by Professor R. Hogg, Pennsylvania State University, and the latter three were provided by the Generic Technology Center for Respirable Dust. The fifth dust is the respirable fraction of a coal mine dust sample collected in the Arkwright Mine by Joe Parenty (Pittsburgh, Bituminous), and distributed by the Generic Technology Center.

Dust aliquots were preweighed and autoclaved dry. Under aseptic conditions they were suspended at 1 gm/100 ml in DMEM containing 0.4 percent Tween 80, centrifuged (1600 g, 15 min), washed in medium without FCS or Tween, then resuspended at  $10^{-3}$  gm/ml in DMEM and stored frozen in 1 ml aliquots.

### Growth of LF

Monolayers of LF were harvested just as they reached confluence. The cells were washed in DMEM and resuspended at  $2 \times 10^5$  cells/ml in DMEM with 20 percent FCS. The cell suspension was added to the wells of 96-well cluster plates, usually 20,000 cells per well. Radioactive

THE RESPIRABLE DUST CENTER

TABLE I

Growth of Rat LF\* Exposed to Dusts in Culture With or Without Cocultured PAMs (CPM/well x 10<sup>3</sup>)

Concentration of Dust (Log, gm/ml)	LF Only		LF + PAMs		Concentration of Dust (Log, gm/ml)	LF Only		LF + PAMs	
	Mean	+/- SEM**	Mean	+/- SEM***		Mean	+/- SEM**	Mean	+/- SEM***
<b>MP3-3</b>					-8	9.1 +/- 1.7	7.1 +/- 1.1		
0	2.2 +/- 0.1		2.6 +/- 0.3		-7	18.5 +/- 2.2+	12.5 +/- 1.0		
-10	1.9 +/- 0.2		2.3 +/- 0.1		-6	13.8 +/- 2.5	12.4 +/- 0.8		
-9	2.0 +/- 0.5		2.2 +/- 0.2		-5	13.0 +/- 1.8	12.1 +/- 0.8		
-8	1.9 +/- 0.2		2.6 +/- 0.3		-4	7.1 +/- 0.4-	7.0 +/- 0.2		
-7	1.9 +/- 0.3		2.9 +/- 0.3		<b>PSOC-1361</b>				
-6	1.9 +/- 0.2		1.9 +/- 0.1		0	9.4 +/- 0.8	8.8 +/- 1.9		
-5	1.7 +/- 0.3		2.2 +/- 0.5		-10	11.6 +/- 0.7	11.7 +/- 1.7		
-4	2.0 +/- 0.3		2.3 +/- 0.1		-9	10.4 +/- 0.3	9.6 +/- 1.0		
<b>PSOC-867</b>					-8	10.3 +/- 0.7	10.7 +/- 1.5		
0	20.2 +/- 3.4		19.3 +/- 3.6		-7	14.7 +/- 0.8++	11.9 +/- 1.2		
-10	25.1 +/- 3.6		22.6 +/- 1.7		-6	14.1 +/- 0.7++	12.9 +/- 2.3		
-9	21.5 +/- 2.2		21.1 +/- 3.1		-5	12.8 +/- 1.4	12.9 +/- 1.1		
-8	21.4 +/- 0.8		23.3 +/- 0.8		-4	7.2 +/- 0.2	7.9 +/- 0.4		
-7	36.8 +/- 3.6+		31.4 +/- 0.2		<b>CMD-RF</b>				
-6	34.5 +/- 2.4+		34.7 +/- 2.4		0	10.2 +/- 1.4	10.8 +/- 1.7		
-5	33.1 +/- 4.0		34.7 +/- 2.4		-10	8.5 +/- 1.4	9.7 +/- 1.0		
-4	22.3 +/- 0.8		22.1 +/- 1.6		-9	7.7 +/- 0.9	9.0 +/- 1.6		
<b>PSOC-1192</b>					-8	9.3 +/- 1.4	9.5 +/- 1.6		
0	9.8 +/- 0.8		9.3 +/- 1.9		-7	11.9 +/- 3.1	10.7 +/- 0.8		
-10	9.5 +/- 0.6		7.9 +/- 0.9		-6	11.6 +/- 1.7	11.3 +/- 1.2		
-9	7.2 +/- 0.8		8.1 +/- 0.9		-5	13.6 +/- 1.5	11.4 +/- 0.6		
					-4	9.0 +/- 1.4	8.9 +/- 0.5		

Notes:

\* 20,000 LF seeded/well in DMEM with 0.5 percent FCS; 5000 PAMs and/or dusts added after overnight incubation. 1 uCi/well 3H-TdR added 2 hour, cells harvested 48 hours after addition of dusts. PAMs only, 198 +/- 13 CPM/well. Triplicate wells for each condition.

\*\* + = stimulation, - = inhibition of growth compared to control wells (0 gm/ml dust), (t-Test): one symbol, p < 0.05; two symbols, p < 0.02.

\*\*\* Growth of LF in the presence of PAMs was not different from growth of LF alone.

tracer, tritiated thymidine (<sup>3</sup>H-TdR, 1 uCi/well) was added to the culture medium to assess proliferative activity by incorporation of 3H-TdR into DNA of growing cells. For harvest, each well was treated with 0.05 percent trypsin at 37 C for 10 minutes. Then the cells were aspirated with a multiple-well automated sample harvester, deposited on glass fiber filters, washed, dried, suspended in Betafluor (Beckman) and counted in a liquid scintillation counter. Other conditions (concentrations, times, etc.) are described with each experiment. Results were recorded as counts per minute (CPM)/well, and values for triplicate wells are reported in the tables as mean CPM/well +/- the standard error of the mean (SEM) in thousands (i.e., x 10<sup>-3</sup>). Differences between experimental and control values were tested for statistical significance using the Student's t-Test.

Results

Effects of Coal Dusts on Growth of Rat LF

This series of tests was performed to test the hypothesis that aqueous suspensions of coal dusts would have a direct

effect on growth of rat LF, without the intervention of PAMs. Based on preliminary experiments it was expected that the dusts would be relatively inert in this assay, except for some inhibition of proliferation at the highest concentration (100 ug/ml). Rat LF were incubated in DMEM with 0.5 percent for 48 hours, either alone or in the presence of dust suspensions (10<sup>-10</sup> to 10<sup>-4</sup> gm/ml). The cells were labelled continuously during the experiment with <sup>3</sup>H-TdR. The results of this assay for the five dust samples are shown in the left column of Table I. In the experiment testing MP3-3, growth of fibroblasts in all wells was unusually low, suggesting that, for unknown reasons, the cells in that experiment were not suitable for detecting growth effects of the dust. Among the tests of the other four dusts, only (1192) had a significantly inhibitory effect on the cells, and that was only at the highest dose tested (100 ug/ml). Three of the dusts (867, 1192 and 1361) showed significant stimulation of LF growth, but only at one or two doses. The respirable fraction of dust from the Arkwright Mine had no significant effect on cell growth. We conclude that three dusts have a weak direct stimulatory effect on growth of rat LF.

GROWTH OF FIBROBLASTS

TABLE II

Growth of Guinea Pig LF\* Exposed to Dusts in Culture With or Without Cocultured PAMs (CPM/well x 10<sup>3</sup>)

Concentration of Dust (Log, gm/ml)	LF Only		LF + PAMs		Concentration of Dust (Log, gm/ml)	LF Only		LF + PAMs	
	Mean +/- SEM**		Mean +/- SEM***			Mean +/- SEM**		Mean +/- SEM***	
<b>MP3-3</b>									
0	20.3 +/- 2.0		26.6 +/- 0.8+		-6	70.3 +/- 6.0++		64.9 +/- 1.7	
-10	25.1 +/- 2.0		26.0 +/- 2.5		-5	59.8 +/- 5.7		62.7 +/- 6.3	
-9	30.6 +/- 4.0		31.5 +/- 5.4		-4	26.6 +/- 1.9--		32.5 +/- 1.1	
-8	33.0 +/- 2.8+		29.0 +/- 1.1		<b>PSOC-1361</b>				
-7	37.7 +/- 4.4+		25.8 +/- 2.4		0	27.3 +/- 1.0		42.0 +/- 2.1+++	
-6	27.2 +/- 1.0+		26.0 +/- 1.2		-10	35.0 +/- 0.1+++		51.1 +/- 3.7++	
-5	30.8 +/- 0.4+++		36.2 +/- 2.5		-9	32.2 +/- 0.5+++		55.2 +/- 2.3++++	
-4	16.6 +/- 1.2		20.0 +/- 0.9		-8	51.5 +/- 6.1++		68.1 +/- 0.2	
<b>PSOC-867</b>									
0	65.3 +/- 11.3		74.3 +/- 3.9		-7	61.7 +/- 6.1++		65.8 +/- 2.4	
-10	78.3 +/- 6.8		75.5 +/- 3.7		-6	62.6 +/- 4.0++		66.0 +/- 5.7	
-9	65.2 +/- 14.3		68.5 +/- 12.3		-5	45.9 +/- 0.6++++		75.0 +/- 0.1++++	
-8	63.2 +/- 4.4		64.9 +/- 13.6		-4	22.5 +/- 2.8		28.6 +/- 2.1	
-7	72.7 +/- 9.9		76.4 +/- 4.6		<b>CMD-RF</b>				
-6	65.2 +/- 6.5		79.2 +/- 5.9		0	60.1 +/- 5.3		45.5 +/- 7.4	
-5	51.2 +/- 4.0		51.6 +/- 4.5		-10	60.0 +/- 4.5		51.6 +/- 1.7	
-4	32.1 +/- 0.8-		31.6 +/- 3.0		-9	60.5 +/- 4.1		44.1 +/- 6.1	
<b>PSOC-1192</b>									
0	45.7 +/- 2.1		58.7 +/- 7.5		-8	55.7 +/- 2.6		49.0 +/- 5.3	
-10	48.8 +/- 0.3		66.5 +/- 1.4++++		-7	66.2 +/- 2.1		57.6 +/- 7.3	
-9	52.5 +/- 5.9		50.2 +/- 6.7		-6	57.6 +/- 0.7		78.3 +/- 12.8	
-8	63.6 +/- 6.0+		54.4 +/- 7.1		-5	58.7 +/- 4.3		52.2 +/- 0.8	
-7	56.1 +/- 2.0+		71.8 +/- 3.2++		-4	35.4 +/- 2.0--		33.5 +/- 2.1	

Notes:

\* 20,000 LF seeded/well in DMEM with 0.5 percent FCS; 5000 PAMs and/or dusts added after overnight incubation. 1 uCi/well <sup>3</sup>H-TdR added 2 hour, cells harvested 48 hours after addition of dusts. Triplicate wells for each condition.

\*\* + = stimulation, - = inhibition of growth compared to control wells (0 gm/ml dust) (t-Test): one symbol, p < 0.05; two symbols, p < 0.02; three symbols, p < 0.01; four symbols, p < 0.001.

\*\*\* + = stimulation, - = inhibition of growth compared to the adjacent leachate control: one symbol, p < 0.05; two symbols, p < 0.02; three symbols, p < 0.01; four symbols, p < 0.001.

*Effects of Dust-Exposed PAMs on Growth of Cocultured Rat LF*

The next experiments were done to test the hypothesis that dust-exposed rat PAMs would affect growth of cocultured rat LF, compared to growth of the LF in the presence of the same concentration of dust without PAMs. As part of the each experiment described above, replicate wells were incubated with LF and dusts as described, plus 5000 PAMs per well that were added at the time of dust exposure. The results are in the right column of Table I; each value is to be compared to the adjacent value in the left column to determine if the presence of the PAMs had any significant effect on LF growth. Again the test with MP3-3 was uninterpretable. For the remaining four dusts, growth of LF in the presence of dust and PAMs was not significantly different from growth of LF in the presence of the dust alone. Thus, we conclude that under these conditions, the dusts

tested here did not stimulate any growth-regulatory activity of the PAMs.

*Effects of Coal Dusts on Growth of Guinea Pig LF*

Because rat LF & PAMs were relatively unresponsive to coal dusts, we next used guinea pig LF to test the hypothesis that coal dusts would have a direct effect on growth of guinea pig LF. These tests were performed under identical conditions to those described above, except that guinea pig LF were used. The results are in the left column of Table II. Three dusts (867, 1192 and RF) were inhibitory at the highest concentration tested (100 ug/ml). Two of those three dusts (867 and RF) had no effect on fibroblast growth at any of the lower concentrations. The other three dusts each stimulated fibroblast growth to a significant degree over a range of concentrations. The most consistent effect was by 1361, stimulating proliferation of LF from 100 pg/ml to 10 ug/ml; 1192 and MP3-3 were stimulatory from a low concentration of 10

ng/ml to a high concentration of 1 or 10 ug/ml respectively. We conclude 1) that dusts differ in their toxicity for guinea pig fibroblasts, 2) that dusts differ in their ability to stimulate guinea pig fibroblasts, 3) that the same dust may be either toxic or stimulatory at different concentrations, and 4) that guinea pigs and rats differ in their susceptibility to either toxic or stimulatory effects of coal dusts for LF.

#### *Effects of Dust-Exposed PAMs on Growth of Cocultured Guinea Pig LF*

The next experiments were done to test the hypothesis that dust-exposed guinea pig PAMs would affect growth of cocultured guinea pig LF, compared to growth of the LF in the presence of the same concentrations of dust without PAMs. As part of the each experiment described in the previous paragraph, replicate wells were incubated with LF and dusts as described, plus 5000 PAMs per well that were added at the time of dust exposure. The results are in the right column of Table II. Each value is to be compared to the adjacent value in the left column to determine if the presence of the PAMs had any significant effect on fibroblast growth. In two experiments, PAMs alone had a weak or moderate stimulatory effect on growth of LF in the absence of dusts. Three dusts (MP3-3, 867 and RF) did not cause the PAMs to exert any growth regulatory effect at any dust concentration. PAMs exposed to two different concentrations of 1192 stimulated fibroblast growth, and PAMs exposed to 1361 were stimulatory at three concentrations. We conclude that, in contrast to rat PAMs, guinea pig PAMs may be activated by two of the five dusts to stimulate growth of cocultured guinea pig LF.

#### *Effects of Dust Leachates on Growth of Guinea Pig LF*

Since LF are nonphagocytic, and since suspensions of dust particles can stimulate or inhibit LF growth without the mediation of phagocytic cells (Table II, left column), it is important to determine whether the effects of the dusts are mediated by direct contact with the cells or by some constituent of the dust that becomes dissolved in the aqueous medium. Therefore, this series of experiments tested the hypothesis that aqueous leachates of the dusts would either inhibit or stimulate growth of guinea pig LF. After overnight incubation of 20,000 guinea pig fibroblasts/well, the medium was removed and replaced with 100 ul/well DMEM containing 0.5 percent FCS. Then each well received 100 ul of dust leachate and 1 uCi <sup>3</sup>H-TDR, and cells were harvested 24 hours later. The results are in the left column of Table III. Leachates of 1192 had no effect and those from MP3-3 had a weak effect at only one concentration. Two dusts, 1361 and RF, produced leachates that stimulated LF growth in the middle to higher concentration range. In contrast, the leachates from 867 had significant inhibitory effects on fibroblast growth across the whole spectrum of concentrations tested. We conclude 1) that some dusts (MP3-3 and 1192) do not contain aqueous extractable components that alter growth of guinea pig LF, 2) that aqueous extracts of other dusts (1361 and RF) stimulate LF growth, and 3) that aqueous extracts of surprisingly small amounts of dust 867 are inhibitory for growth of guinea pig LF.

#### *Effects of Supernatants from Dust-Exposed PAM Cultures on Growth of Guinea Pig LF*

Table II showed that dust-exposed PAMs had growth stimulatory properties on cocultured LF. The following experiments were to test the hypothesis that growth-regulatory effects of dust-exposed PAMs are mediated by soluble products secreted by the PAMs into the culture medium. They were performed as part of each of the leachate experiments described in the previous paragraph, using replicate wells of cultured LF. Supernatant media were collected after 24 hour incubation in the presence of PAMs and various concentrations of the five dusts, and they were added to cultures of guinea pig LF and labelled for 24 hours. The results are shown in the right column of Table III. Such supernatants would be expected to contain both the products released by activated PAMs and any components of the dusts extracted by the aqueous medium. Therefore, each experimental value is to be compared with the adjacent leachate control to determine to what extent the products of dust-exposed PAMs altered growth, as distinct from effects of the leachate. Media from PAMs exposed to RF were essentially inert, having no significant effect at most concentrations when compared to the effects of the same concentration of leachate. Supernatants from 867-exposed PAMs were significantly stimulatory across the entire range of concentrations. In contrast, the other three dusts caused the PAMs to release into the medium soluble materials that inhibited fibroblast growth. We conclude 1) that one of the dusts (RF) did not activate PAMs to secrete growth-regulatory products, 2) that three dusts (MP3-3, 1192 and 1361) caused PAMs to release growth inhibitory products, 3) that one dust, 867, activated PAMs to secrete growth stimulatory products, and 4) that the growth regulatory effects of soluble products of dust-exposed PAMs do not correspond to the growth regulatory effects of cocultured, dust-exposed PAMs.

## Discussion

The experiments reported here have not yet been repeated for confirmation, so the conclusions drawn are, of necessity, provisional. The data are based on results of triplicate cultures; in some instances duplicate values were used if results from one well of a set were not obtainable for technical reasons, or if one well of a set deviated substantially from the mean of the other two ("outliers"). Differences between experimental and control wells were tested for statistical significance by the Student's t-Test. We hope to perform a more comprehensive statistical evaluation of these (or subsequent) data using the analysis of variance test with the Newman-Keuls and Dunnett tests. Because results of multiple-comparison assays were tested with a pair-wise statistic, statements about the significance of inhibitory or stimulatory effects reflected an assessment of the pattern of effects over a range of several dust doses; isolated values that were significant by the t-test were not regarded as biologically significant.

The major working hypothesis for this phase of our study was that coal dusts stimulate PAMs to secrete materials that

GROWTH OF FIBROBLASTS

TABLE III

Growth of Guinea Pig LF\* Exposed in Culture to Dust Leachates or to Supernatants of Dust-exposed PAMs (CPM/well X 10<sup>3</sup>)

Dust in Preculture (Log, gm/ml)	LF + Leachates Mean + SEM**	LF + Supernatants Mean + SEM***	Dust in Preculture (Log; gm/ml)	LF + Leachates Mean + SEM**	LF + Supernatants Mean + SEM***
<b>MP3-3</b>					
0	11.6 +/- 0.7	9.3 +/- 0.3-	-8	11.5 +/- 0.9	8.6 +/- 0.4-
-10	12.1 +/- 0.5	10.2 +/- 0.6	-7	13.3 +/- 1.1	9.4 +/- 0.8-
-9	11.9 +/- 0.7	8.3 +/- 0.5--	-6	19.2 +/- 1.5	15.1 +/- 2.1
-8	12.5 +/- 0.4	8.6 +/- 0.1---	-5	16.6 +/- 0.9	11.3 +/- 0.4--
-7	13.8 +/- 1.6	10.7 +/- 0.7	-4	11.7 +/- 0.8	10.2 +/- 0.9
-6	14.7 +/- 0.6+	7.6 +/- 0.3---	<b>PSOC-1361</b>		
-5	15.1 +/- 1.1	8.4 +/- 0.7--	0	52.9 +/- 1.3	38.2 +/- 0.7--
-4	13.0 +/- 1.8	9.9 +/- 0.7	-10	46.2 +/- 1.5-	36.6 +/- 1.0--
<b>PSOC-867</b>					
0	45.0 +/- 1.7	43.7 +/- 1.9	-9	43.5 +/- 4.0	33.2 +/- 3.3
-10	30.8 +/- 1.9--	38.9 +/- 1.5+	-8	45.5 +/- 3.2	34.5 +/- 0.8-
-9	27.1 +/- 2.0--	37.1 +/- 1.5++	-7	73.3 +/- 4.9++	72.3 +/- 1.5
-8	25.5 +/- 3.4--	37.8 +/- 2.2+	-6	73.1 +/- 4.6++	55.5 +/- 1.4--
-7	26.0 +/- 0.4--	33.0 +/- 0.1+++	-5	75.2 +/- 1.6+++	51.2 +/- 1.9--
-6	28.4 +/- 3.0--	37.9 +/- 6.6	-4	34.5 +/- 1.7--	26.6 +/- 0.4-
-5	28.4 +/- 4.6-	44.6 +/- 0.6+	<b>CMD-RF</b>		
-4	20.0 +/- 3.3--	44.6 +/- 3.1+++	0	81.0 +/- 0.9	81.7 +/- 7.7
<b>PSOC-1192</b>					
0	14.1 +/- 1.2	11.1 +/- 0.5	-10	85.3 +/- 10.1	86.5 +/- 11.3
-10	12.1 +/- 2.0	10.1 +/- 1.0	-9	85.3 +/- 2.2	87.9 +/- 11.1
-9	12.2 +/- 0.4	8.5 +/- 0.4--	-8	93.0 +/- 7.3	83.9 +/- 12.4
			-7	106.9 +/- 3.0+++	87.8 +/- 4.4-
			-6	99.9 +/- 4.7++	81.6 +/- 13.4
			-5	103.9 +/- 6.6+	88.3 +/- 6.9
			-4	96.1 +/- 1.5+++	89.5 +/- 8.9

Notes:

\* 20,000 fibroblasts seeded/well in DMEM with 0.5 percent FCS; leachates or supernatants added after overnight incubation. Labeled with 1 ug/well 3H-TdR 24 hours after addition of dusts. Triplicate wells for each condition.

\*\* + = stimulation, - = inhibition of growth compared to control wells (0 gm/ml dust) (t-Test): one symbol, p < 0.05; two symbols, p < 0.02; three symbols, p < 0.01; four symbols, p < 0.001.

\*\*\* + = stimulation, - = inhibition of growth compared to the adjacent leachate control (t-Test): one symbol, p < 0.05; two symbols, p < 0.02; three symbols, p < 0.01; four symbols, p < 0.001.

stimulate the growth of fibroblasts. The results of Table III confirm that, at least for the one anthracite sample we tested, the hypothesis is true. Supernatants of PAMs exposed to dust 867 caused up to a two-fold increase in the rate of proliferation of LF. However that conclusion is not generally applicable since in the same series of experiments, supernatants of PAMs exposed to three of the bituminous samples caused up to 40 percent inhibition of LF proliferation, and supernatants induced by the respirable fraction of mine dust were inactive as far as LF proliferation is concerned. It is tempting to view the stimulatory effects of 867-induced supernatants as detrimental and the inhibitory or inactive supernatants as biologically neutral, and that would conform to the conventional wisdom that the pension was added to each well containing 10<sup>6</sup> newly plated areas. However, under some circumstances, inhibition of the proliferation needed to maintain normal homeostasis would be detrimental. Therefore, much more on assay and that different dusts induce secretion

*A priori* one might predict that any PAM-mediated effects on LF would be at least qualitatively similar whether assessed with cell-free PAM culture supernatants or with PAMs growing in direct contact with the LF. However, our results showed that results of the two assays were not qualitatively similar. In two instances, dust-stimulation of PAM-LF cocultures had no effect on LF growth while the supernatants of PAMs stimulated by those dusts were inhibitory and stimulatory respectively. Further, two dusts that had stimulatory effects in PAM-LF cocultures induced production by PAMs of inhibitory supernatants. At this early stage of the study it is not evident how the cocultured PAMs affect LF growth other than by their secreted products. Presumably the dust-stimulated PAMs in LF-coculture secrete into the shared medium the same kinds and same amounts of products that they secrete into medium when they are cultured without LF. So, the proliferative rate that was observed must be the net result of the of rat LF

In addition to the PAM-mediated effects on LF growth mentioned above, these experiments revealed that dust or dust leachates can modulate growth of LF without the mediation of PAMs. Three dusts were mildly to moderately stimulatory when in direct contact with LF (in the absence of PAMs), and for one dust that stimulation could be repeated using a centrifuged leachate of the dust. In contrast, leachates of the other two dusts were inactive, suggesting that the stimulatory effects of those dusts was due to direct dust-LF contact, not to water-soluble dust components conveyed by the culture medium. Finally, two dusts that had no effect when in direct contact with the LF released soluble components into the leachate that had potent inhibitory effects in one case and moderate stimulatory effects in the other case. Again, it is not yet possible to conclude that one kind of dust-cell interaction of "bad" and that others are "good," but it is clear that coal dusts can have potent, and sometimes opposite, effects on LF proliferation, independent of PAMs.

It should be mentioned that the nature of the dust effects (stimulatory/inhibitory) and their pattern may reflect not only the character of the dust and the way it was assayed in these experiments, but may depend to some extent on other experimental conditions that were not varied in this study. For instance, the methods of collecting and culturing PAMs might alter their reactivity in small or large ways. Likewise, this system is only one of a variety of experimental conditions that can be used to assess the proliferative behavior of LF. As done here (20,000 cells/well and low serum concentration [0.5 percent]), the cells are relatively quiescent. In other systems, LF could be studied during a maximal growth phase (low cell density and high serum concentration), and at various times in their growth pattern. Experiments testing some of those variables are planned.

From a practical standpoint it is important to emphasize the major species difference in responses to coal dusts that we have observed. Both rats and guinea pigs have been used extensively to study lung diseases and to study the functions of macrophages. However, most cell culture studies of macrophage function in the rat have used macrophages from the peritoneal cavity. We have observed that that rat PAMs are not functionally equivalent to peritoneal macrophages or to PAMs of other species. Rat and guinea pig macrophages from the lung, from the peritoneum and from inflammatory exudates were stimulated with tetradecanoyl phorbol acetate. Each class of macrophages, except rat PAMs, promptly released a significant amount of superoxide anion radical. (19) The results presented here further indicate that rat PAMs and LF are not equivalent to guinea pig PAMs in terms of response to coal dusts. On that admittedly limited evidence we have decided to use the guinea pig for most of our studies in the near future. It will not be possible to determine which species' response pattern is most representative of human responses until similar experiments can be performed using human cells.

The major conclusion to be drawn from this work is that, even at this preliminary stage of investigation, there are clear differences in the ways in which different coal dusts affect PAMs and LF of the guinea pig. The response patterns are complex, and for reasons stated above it is not possible to

identify any particular pattern as "good" or "bad." However, the existence of these intersample differences means that it will soon be possible to design experiments to identify which chemical or physical characteristics of the dusts are responsible for the various kinds of responses, and how those responses are mediated at the cellular and molecular level.

## Acknowledgment

This research has been supported by the Department of the Interior's Mineral Institute program administered by the Bureau of Mines through the Generic Mineral Technology Center for Respirable Dust under grant number G1135142.

## References

1. Koretzky, G.A., J.A. Elias, S.L. Kay et al: Spontaneous Production of Interleukin-1 by Human Alveolar Macrophages. *Clin. Immunol. Immunopathol.* 29:443-450 (1983).
2. Hunninghake, G.W.: Release of Interleukin-1 by Alveolar Macrophages of Patients with Active Pulmonary Sarcoidosis. *Am. Rev. Respir. Dis.* 129:569-572 (1984).
3. Martin, T.R., L.C. Altman, R.K. Albert and W.R. Henderson: Leukotriene B4 Production by the Human Alveolar Macrophage: A Potential Mechanism for Amplifying Inflammation in the Lung. *Am. Rev. Respir. Dis.* 129:106-111 (1984).
4. Sherman, M.P. and R.I. Lehrer: Superoxide Generation by Neonatal and Adult Rabbit Alveolar Macrophages. *J. Leukocyte Biol.* 36:39-50 (1984).
5. Tate R.M., H.G. Morris, W.R. Schroeder and J.E. Repine: Oxygen Metabolites Stimulate Thromboxane Production and Vasoconstriction in Isolated Saline-perfused Rabbit Lungs. *J. Clin. Invest.* 74:608-613 (1984).
6. Vilim, V., J. Wilhelm, P. Brzak and J. Hurych: The Chemiluminescence of Rabbit Alveolar Macrophages Induced by Quartz Dust Particles. *Immunol. Lett.* 8:69-73 (1984).
7. Kouzan, S., A.R. Brody, P. Nettesheim and T. Eling: Production of Arachidonic Acid Metabolites by Macrophages Exposed in vitro to Asbestos, Carbonyl Iron Particles or Calcium Ionophore. *Am. Rev. Respir. Dis.* 131:624-632 (1984).
8. Nugent, K.M., J. Glazier, M.M. Monick and G.W. Hunninghake: Stimulated Human Alveolar Macrophages Secrete Interferon. *Am. Rev. Respir. Dis.* 131:714-718 (1985).
9. Kampschmidt, R.F., M.L. Worthington III and M.I. Mesecher: Release of Interleukin-1 (IL-1) and IL-1-like Factors from Rabbit Macrophages with Silica. *J. Leukocyte Biol.* 39:123-132 (1986).
10. Lemaire, I., H. Beaudoin, S. Masse and C. Grondin: *Am. J. Path.* 122:205-211 (1986).

## GROWTH OF FIBROBLASTS

11. Burrell, R. and M. Anderson: The Induction of Fibrogenesis by Silica-treated Alveolar Macrophages. *Environ. Res.* 6:389-394 (1973).
12. Nourse, L.D., P.N. Nourse, H. Botes and H.M. Schwartz: The Effects of Macrophages Isolated from the Lungs of Guinea Pigs Dusted with Silica on Collagen Biosynthesis by Guinea Pig Fibroblasts in Cell Culture. *Environ. Res.* 9:115-127 (1975).
13. Lugano, E.M., J.H. Dauber, J.A. Elias et al: The Regulation of Lung Fibroblast Proliferation by Alveolar Macrophages in Experimental Silicosis. *Am. Rev. Resp. Dis.* 129:767-771 (1984).
14. Kovacs, E.J. and J. Kelley: Secretion of Macrophage-derived Growth Factor During Acute Lung Injury Induced by Bleomycin. *J. Leukocyte Biol.* 37:1-14 (1985).
15. Harington, J.S., M. Ritchie, P.C. King and K. Miller: The *in-vitro* Effects of Silica-treated Hamster Macrophages on Collagen Production by Hamster Fibroblasts. *J. Path.* 109:21-37 (1971).
16. Aalto, M. and A.G. Heppleston: Fibrogenesis by Mineral Fibres: An *in-vitro* Study of the Roles of the Macrophage and Fibre Length. *Brit. J. Exp. Path.* 65:91-99 (1984).
17. Hart, P.H., L.W. Powell, W.G.E. Cooksley and J.W. Halliday: Mononuclear Cell Factors that Inhibit Fibroblast Collagen Synthesis. I. *In vitro* Conditions Determining Their Production and Expression.



# The Effects of Coal Mine Dust Particles on the Metabolism of Arachidonic Acid By Pulmonary Alveolar Macrophages

L. M. Demers, R. E. Edelson, M. P. Rose and D. T. Superdock

Department of Pathology, The Milton S. Hershey Medical Center, The Pennsylvania State University

The pulmonary alveolar macrophage is a major defensive cell which counteracts the invasive properties of bacteria and particles when these substances invade the pulmonary environment. Pulmonary exposure to coal dust particles is believed to activate these macrophages to release a host of chemical mediators which can neutralize or contribute to the harmful effects of these dust particles. Our efforts have been concerned with assessing a specific family of mediator substances produced by the alveolar macrophage from arachidonic acid when these cells are in contact with activating substances such as coal dust. Metabolites of arachidonic acid produce a vast array of effects which can impact significantly on pulmonary function both with normal pulmonary events and with pathologic processes of the lung. Our studies demonstrate that isolated alveolar macrophages obtained from rats or guinea pigs cultured *in vitro* release appreciable amounts of the cyclooxygenase products prostaglandin E<sub>2</sub> and thromboxane A<sub>2</sub> and release significant amounts of the lipoxygenase products, 5-HETE and LTB<sub>4</sub>. In the presence of  $1 \times 10^{-4}$  -  $1 \times 10^{-7}$  g/ml of a coal dust suspension, alveolar macrophages from the rats and guinea pigs alters their pattern of arachidonic acid metabolite release. In the rat, exposure of alveolar macrophages *in vitro* to the higher concentrations of coal dust causes a significant reduction in PGE<sub>2</sub>, TXB<sub>2</sub> and LTB<sub>4</sub> in a 4 hour time course study. In contrast, macrophages from the guinea pig in response to coal dust had little change in TXB<sub>2</sub> release, only a slight inhibition in PGE<sub>2</sub> production and an initial stimulation in LTB<sub>4</sub> release over the 4 hour time course. Cells from guinea pigs released considerably more TXB<sub>2</sub> than the rat under these conditions while rat cells formed considerably more LTB<sub>4</sub> than guinea pig alveolar macrophages. These findings support the following conclusions.

1. Alveolar macrophages from rats and guinea pigs form significant amount of the arachidonic acid metabolites PGE<sub>2</sub>, TXB<sub>2</sub>, LTB<sub>4</sub>.
2. Exposure of the alveolar macrophage to coal dust induces an alteration in the pattern of arachidonic

acid metabolism which is different between rats and guinea pigs.

3. At high concentration of coal dust ( $1 \times 10^{-4}$  g/ml), there is a significant reduction in mediator release by rat alveolar macrophages. In contrast, guinea pig cells appear to augment their production of leukotriene LTB<sub>4</sub> in response to coal dust exposure.
4. Electron microscopy of the coal dust exposed macrophages reveals intense phagocytosis and internalization of coal dust particles by these cells in culture.

In conclusion, the reactivity of the alveolar macrophage to coal mine dust exposure involves alterations in macrophage arachidonic acid mediator release which varies between different species.

## Introduction

Coal workers' pneumoconiosis (CWP) is associated with a build up of black deposits in the lung from chronic exposure to coal dust.<sup>(1)</sup> CWP presents with few clinical symptoms itself but if left unattended leads to a progressive, complicated respiratory disease process with extensive pulmonary fibrosis, severe respiratory compromise and eventually death. Both CWP and its associated pulmonary fibrosis are believed to be a result of chronic exposure to a particular type of coal dust. Exposure levels to dust is also considered to be an important contributor to the onset of CWP.

The alveolar macrophage is a major defensive white blood cell which resides within the pulmonary space to counteract the invasive properties of microorganisms and foreign particles when they present to the lungs.<sup>(2)</sup> Their principal function is to maintain a sterile environment in the lower respiratory tract. Bacteria,<sup>(3)</sup> fungi and viruses<sup>(4)</sup> as well as non-infectious foreign particles<sup>(5)</sup> are normally neutralized by the alveolar macrophage through phagocytosis preventing entry into the systemic circulation.

## METABOLISM OF ARACHIDONIC ACID

With activation, the alveolar macrophage exhibits an increase in metabolic activity including increased oxygen consumption, rapid glucose utilization, increased superoxide production<sup>(6)</sup> and the release of several important chemical mediators which affect the functional role of the alveolar macrophage as well as other cells and tissues in the pulmonary environment.<sup>(7,8)</sup>

Several metabolites of arachidonic acid are formed by the alveolar macrophage when activated and released as mediators of the inflammatory response.

Arachidonic acid is a 20 carbon fatty acid stored in most cells as phospholipid and released when the cells become activated. In the alveolar macrophage, at least two distinct metabolic pathways for arachidonic acid exist<sup>(9)</sup> (Figure 1). A cyclooxygenase enzyme system catalyzes the formation of prostaglandins and thromboxane from released arachidonic acid. Leukotrienes and hydroxy fatty acids are formed by a second major pathway catalyzed by a lipoxygenase enzyme. These metabolites produced a variety of effects in the lungs and can impact significantly on both normal and abnormal pulmonary function.<sup>(10,11)</sup> Chronic release of these metabolites in the lungs are associated with damage to the lung and if left unchallenged can evoke many of the pathologic changes associated with miners lung disease.

The interaction of the pulmonary alveolar macrophage with non-infectious particles such as asbestos has been shown to evoke a stimulation in arachidonic acid derived mediator release.<sup>(8)</sup> Although little information is available regarding coal dust effects on alveolar macrophage

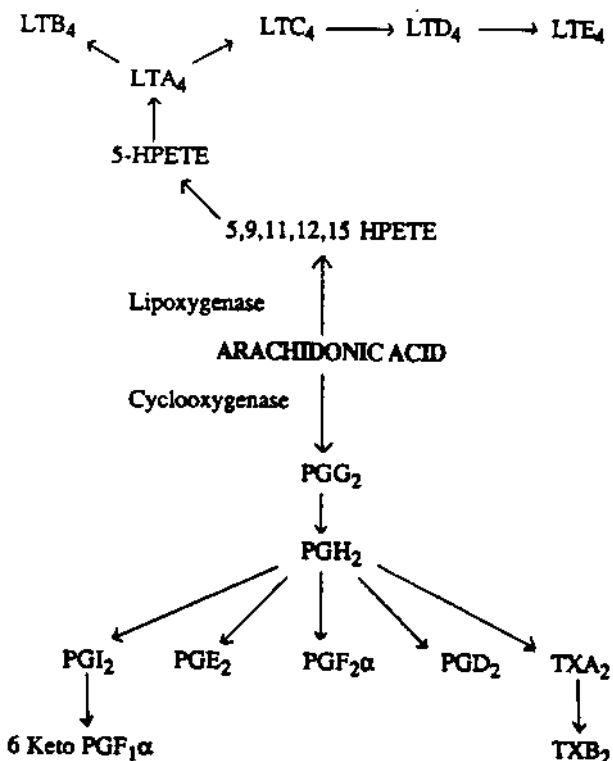


FIGURE 1. Metabolic pathways of arachidonic acid.

arachidonic acid metabolism, there is evidence to show intense phagocytosis of coal dust particles by these cells.<sup>(12)</sup>

Our present study was designed to investigate the interaction of coal dust particles with the alveolar macrophage *in vitro*, specifically assessing the metabolism of arachidonic acid to products of the cyclooxygenase and lipoxygenase pathway following exposure of these cells to coal dust particles in suspension.

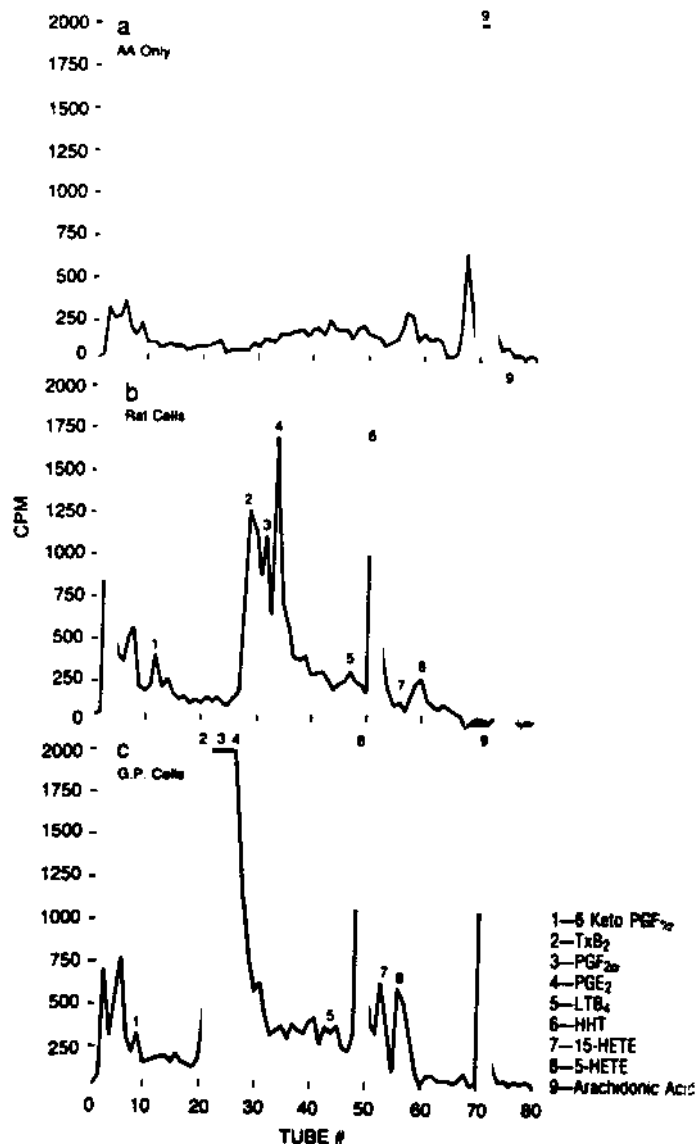


FIGURE 2. Products of arachidonic acid metabolism by rat and guinea pig alveolar macrophages after 4 hour incubation with <sup>14</sup>C-arachidonic acid. Cells were prepared as described in Materials and methods. a) Arachidonic acid only, b) Rat alveolar macrophages, c) Guinea pig alveolar macrophages.

### Materials and Methods

#### Cell Culture of Alveolar Macrophages

Rat and guinea pig lung macrophages were obtained by pulmonary lavage with Ca<sup>2+</sup> and Mg<sup>2+</sup>-free phosphate buffered saline containing 0.1 percent (w/v) ethylene-

diaminetetraacetic acid. The lungs were lavaged 3x each with an 8 ml volume of lavage fluid. The resulting cell suspension was centrifuged at 600 xg for 10 minutes and the cell pellet washed with Medium 199. The cells were resuspended in 2 mls Medium 199 and enumerated by counting in a hemocytometer. Viability was assessed by trypan blue exclusion. The cells were diluted to  $0.5 \times 10^6$ /ml and 2 ml of the suspension were placed in wells of multi-well plates. The cells were incubated for 1 hour at 37°C in a humidified CO<sub>2</sub> controlled atmosphere (5 percent CO<sub>2</sub> in air). The medium was then removed and the adherent cells were washed 3x with M-199. The medium was replaced and the cells were incubated for varying times in the presence of coal dust preparations, or known effectors of arachidonic acid metabolism. In certain experiments <sup>14</sup>C-arachidonic acid (New England Nuclear, 400,000 cpm/well) was added.

*Analysis of Metabolites of Arachidonic Acid*

*Analysis of <sup>14</sup>C-Labelled Metabolites by High performance liquid chromatography*

At the end of each incubation, medium was collected and acidified by the addition of .01 M citric acid (25 ul/ml). Radiolabelled metabolites were extracted by shaking for 10 minutes with an equal volume of cyclohexane:ethylacetate (1:1 v/v) in silanised glass extraction tubes. Phase separation was achieved by centrifugation at 600 xg for 10 minutes. The organic layer was transferred to a second silanised tube and the solvent was evaporated under nitrogen. The residue was redissolved in 50 ul of HPLC Solvent A (acetonitrile: water 26:74 v/v, pH 3.0 with phosphoric acid). Arachidonic acid metabolites were separated on a Waters C18 radial compression cartridge using 2 solvent systems. Solvent system 1 consisted of HPLC Solvent A pumped isocratically for 26 minutes at 3 mls/min. This was followed by solvent system 2 which consisted of a linear gradient over 60 minutes for 100 percent Solvent A to 22 percent Solvent A and 78 percent Solvent B (acetonitrile:water 95:5 v/v, pH 3.0 with phosphoric acid) flow rate was maintained at 3 mls/min. Eluting solvent was collected into 1 ml fractions and 7 mls scintillation fluid (ACS, Amersham) was added. Radioactivity was determined by counting in a Searle Delta 300 liquid scintillation system. Retention times of arachidonic acid metabolites were compared with those of authentic standards.

*Quantitative Determination of Arachidonic Acid Metabolites*

Prostaglandin E<sub>2</sub>, prostaglandin F<sub>2</sub> and thromboxane B<sub>2</sub> were determined by radioimmunoassay as previously described from this laboratory.<sup>(13)</sup> Culture medium from the alveolar macrophage cultures were analyzed by RIA following a cyclohexane:ethyl acetate extraction step.

Leukotriene B<sub>4</sub> was determined by radioimmunoassay using reagents purchased from Seragen Inc. (Waltham, Mass.)

*Coal Dust Samples*

Samples of coal dust prepared to respirable quality by the Department of Mineral Engineering, Pennsylvania State University, were obtained and suspended in Medium 199 by the addition of 1 percent tween followed by sonication.

*Chemicals*

All chemicals used in these studies including the calcium ionophore A23187 and nordihydroguaiaretic acid (NDGA) were obtained from the sigma Chemical Company.

**Results**

*Metabolism of <sup>14</sup>C-Arachidonic Acid by Alveolar Macrophages*

Alveolar macrophages isolated from the lungs of both guinea pigs and rats metabolized in culture under basal conditions <sup>14</sup>C-arachidonic acid to a variety of compounds of both the lipoxygenase and cyclooxygenase pathways. The major cyclooxygenase products released into the medium were identified as thromboxane B<sub>2</sub> (TXB<sub>2</sub>), PGF<sub>2</sub> PGE<sub>2</sub>, and hydroxyheptadecatrienoic acid (HHT). Lipoxygenase products identified included LTB<sub>4</sub>, 15-hydroxyeicosatetraenoic acid (15-HETE) and 5-hydroxyeicosatetraenoic acid (5-HETE). Figure 2 reflects the pattern of products produced from AA when alveolar macrophages from rats and guinea pigs were incubated with <sup>14</sup>C-arachidonic acid for four hours.

As shown in Figure 3, exposure of these cells to a known lipoxygenase stimulant such as the calcium ionophore (10 ug/ml) augmented the release of HETE products and LTB<sub>4</sub>

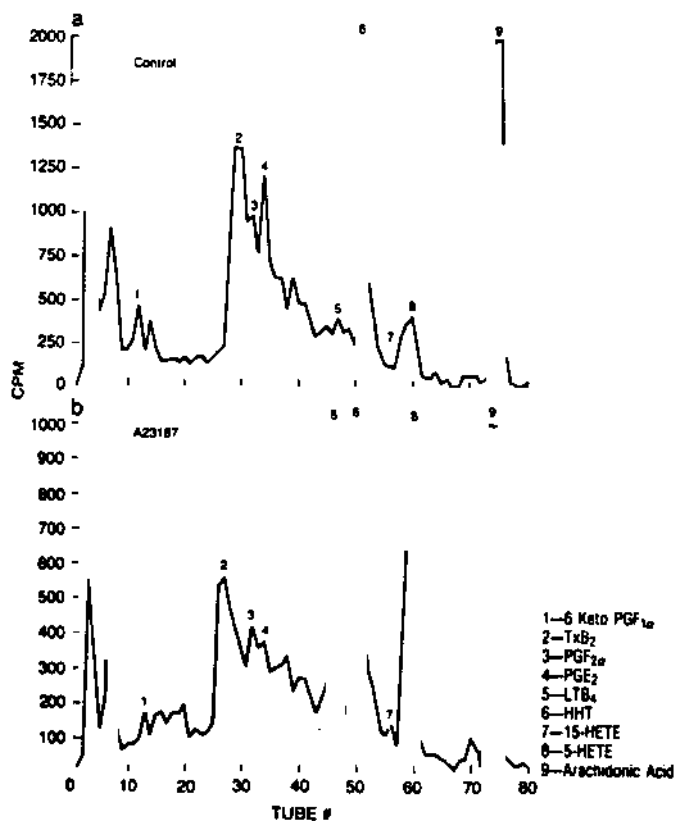


FIGURE 3. Stimulation of lipoxygenase pathways by calcium ionophore. a) Baseline conversion of arachidonic acid by rat macrophages. b) Stimulation of lipoxygenase products LTB<sub>4</sub> and HETE by calcium ionophore (10 ug/ml). Cells were prepared as previously described and incubated for 4 hours with arachidonic acid in the presence or absence of calcium ionophore.

## METABOLISM OF ARACHIDONIC ACID

into the medium. Although not shown, the addition of the lipoxygenase inhibitor NDGA ( $10^{-5}$ M) was effective in reducing the formation of HETE products to 20 percent of the control response. Addition of various preparations of

coal dust in suspension to the culture medium was shown to inhibit the conversion of  $^{14}$ C-arachidonic acid to cyclooxygenase products by rat alveolar macrophages (Figure 4).

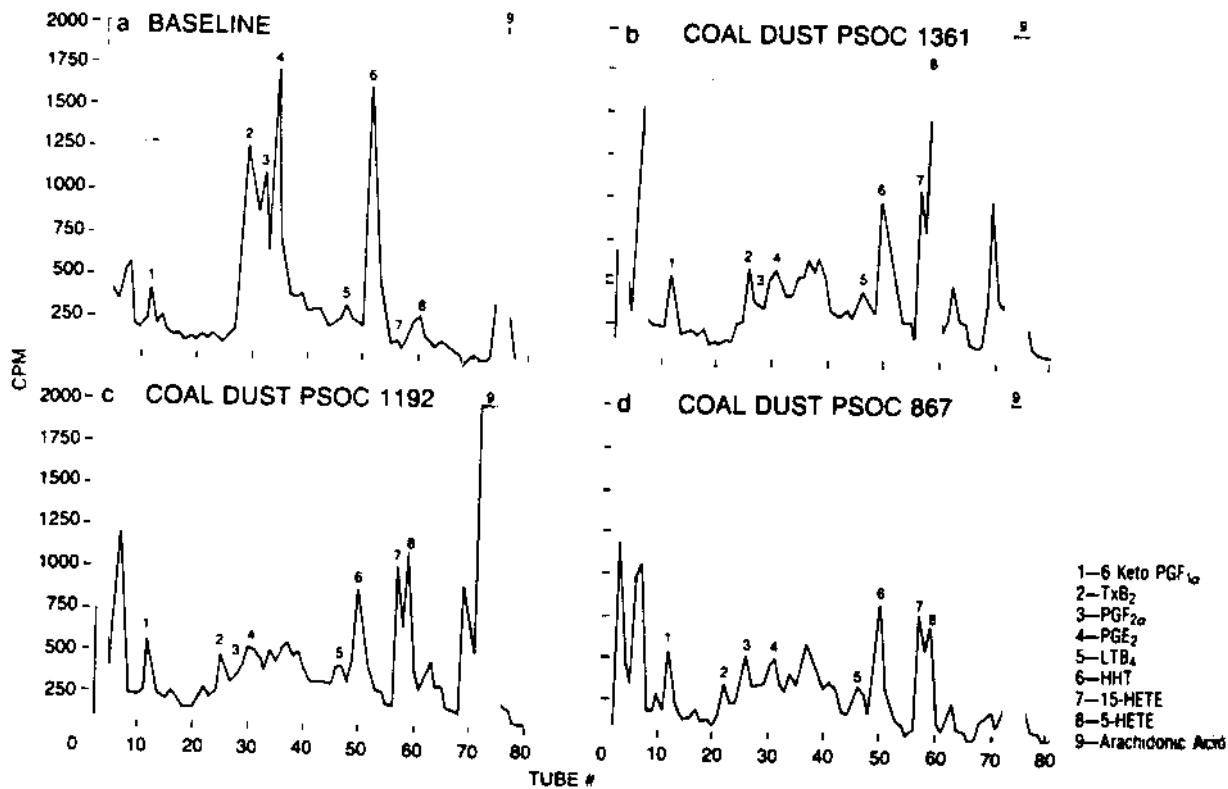


FIGURE 4. Effect of various coal dust preparation on metabolism of  $^{14}$ C-arachidonic acid. a) No addition, b) Coal dust PSOC 1361, c) Coal dust PSOC 1192, d) Coal dust PSOC 867.

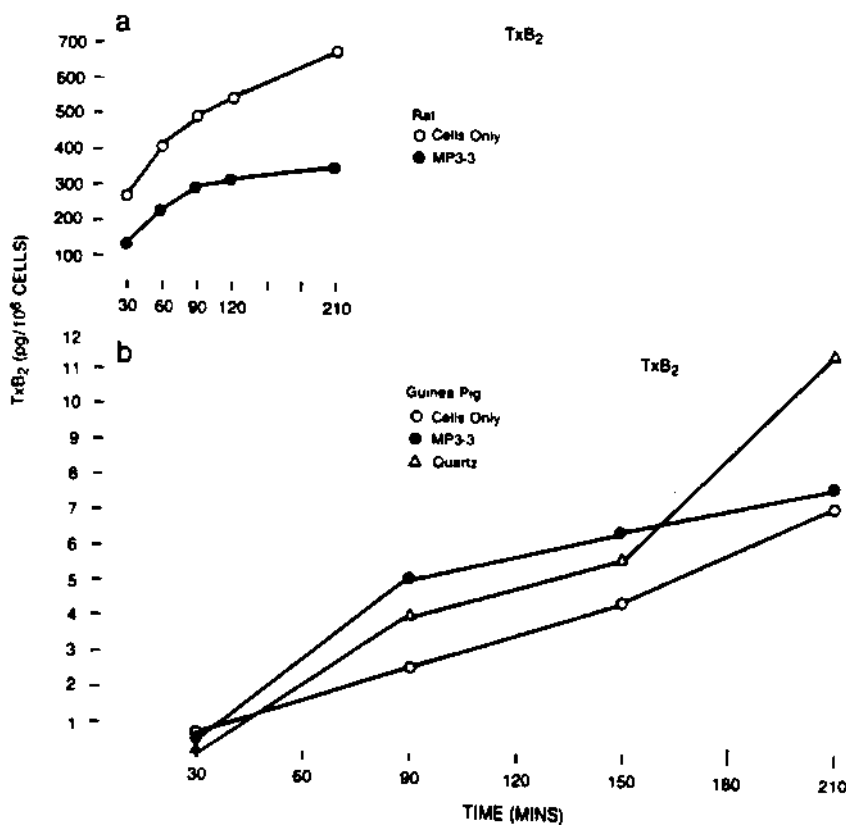


FIGURE 5. Time course of release of thromboxane as measured by TxB<sub>2</sub> radioimmunoassay by rat (a) and guinea pig (b) alveolar macrophages in the presence and absence of coal dust MP3-3 (100 ug/ml).

Quantitation of Arachidonic Acid Metabolites

In time course experiments, it was observed that the presence of coal dust (MP3-3, 100 ug/ml) appeared to inhibit the release of thromboxane from incubated rat alveolar macrophages. Interestingly, the alveolar macrophages from the guinea pig were only slightly affected by the coal dust preparations (Figure 5). It was also noted that guinea pig alveolar macrophages released in quantity substantially more thromboxane (approximately 10-fold) than did the rat alveolar macrophages.

The release of PGE<sub>2</sub> into the medium when assessed quantitatively was not markedly affected by the presence of MP3-3 (100 ug/ml) during early periods of exposure but did appear to be compromised by 3 1/2 hours (Figure 6). It was also observed that guinea pig cells released more PGE<sub>2</sub> than did the rat cells.

Changes in lipoxygenase product formation were affected differently by the coal dust exposure. As shown in Figure 7, although the release of LTB<sub>4</sub> from the rat alveolar macrophage appeared to be suppressed by the presence of coal dust (MP3, 100 ug/ml), the release of this lipoxygenase product by guinea pig alveolar macrophages appeared to be stimulated at earlier time points reaching a plateau as shown in Figure 7.

The effects of different concentrations of coal dust on the arachidonic acid metabolites is shown in Figure 8. Products of the cyclooxygenase pathway were suppressed by high concentrations of coal dust MP3-3 whereas LTB<sub>4</sub> release was suppressed more at the lower concentrations.

In Figure 9 are depicted the effects of different coal dust matter on PGE<sub>2</sub> and TXB<sub>2</sub> production by these cells. As noted previously, coal dust such as the MP3-3 produced a modest suppression of both these products. The effects of limestone, however, was more pronounced in suppressing TXB<sub>2</sub> release when compared to PGE<sub>2</sub> release by these cells.

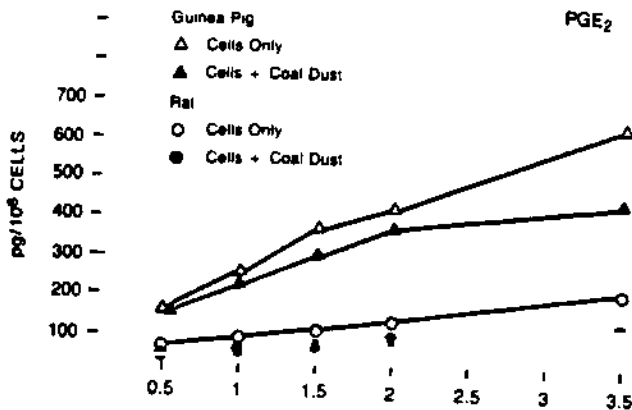


FIGURE 6. Time course of release of PGE<sub>2</sub> by rat and guinea pig alveolar macrophages in the presence and absence of coal dust MP3-3 (100 ug/ml).

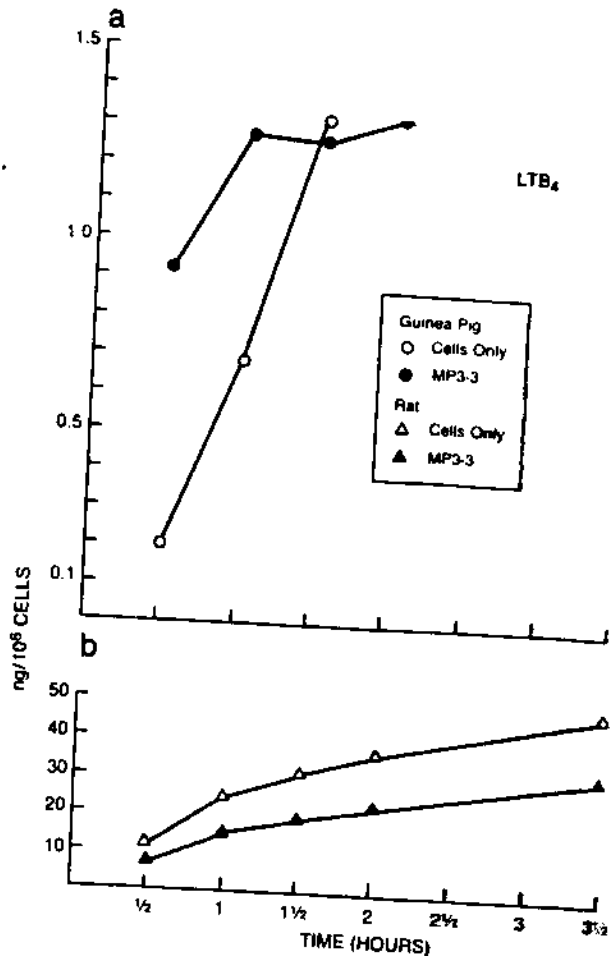


FIGURE 7. Time course of release of LTB<sub>4</sub> by rat and guinea pig alveolar macrophages in the presence and absence of coal dust MP3-3 (100 ug/ml).

Electron Microscopy

Electron micrographs were prepared of the cells exposed to coal dust. Figure 10 is a representative figure revealing the internalization of the coal dust particles by the alveolar macrophage in culture.

Discussion

The aims of the experiments described were to determine whether alveolar macrophages could react *in vitro* with coal dust particles and whether this interaction has any effect on arachidonic acid metabolism.

We observed that alveolar macrophages from both rats and guinea pigs are able to metabolize arachidonic acid to a variety of lipoxygenase and cyclooxygenase products and that the pathways can be altered by known modulators of arachidonic acid metabolism. It was also evident that alveolar macrophages from rats and guinea pigs have differing capacities to produce arachidonic acid metabolites.

It was postulated that the interaction of coal mine dust particles with alveolar macrophage may lead to activation of the cells and release of immunologic mediators such as arachidonic acid metabolites, in a fashion similar to that of

## METABOLISM OF ARACHIDONIC ACID

asbestos particles. These mediators could in turn, through activation of the immune system, lead to pathogenic events.

In rat alveolar macrophage cultures we were unable to demonstrate a significant stimulation of arachidonic acid metabolism after exposure to coal dust. Any alterations observed tended to be of an inhibitory nature. The alveolar macrophages of guinea pigs did not appear to be as sensitive to the effects of coal dust preparations at the levels tested.

Although fibrous particles such as asbestos may stimulate arachidonic acid metabolism as do other non-infectious particles such as carbonyl iron particles,<sup>(8)</sup> not all phagocytosed particles may be as effective. It has been observed that phagocytosis of latex particles has no effect on prostaglandin synthesis in pulmonary macrophages.<sup>(7)</sup> The interaction of small particles with macrophages depends on many factors. Phagocytosis may be enhanced by opsonizing factors and in the absence of antibody-antigen reactions, physical properties such as surface charge may play a role.

The absence of a stimulatory effect of coal dust particles on rat alveolar macrophages could be due to coal dust particles, which are not fibrous, behaving more like latex particles than asbestos particles. If this is true then the observed pathology of CWP could be partially accounted for by a failure of the pulmonary immune response thus leading to ineffective clearance of dust particles and a build up of molecules. Unknown physical or chemical properties of

various coal dusts could lead to toxic effects on cells which have ingested the particles,<sup>(12)</sup> causing cell death and release of inflammatory cellular components.

However, our results also suggest that there are basic differences in arachidonic acid metabolism between species, and that there could be variations in the response of different species to coal dust particles. There is evidence to suggest that in coal miners there may be inter-individual susceptibility to altered lung function<sup>(14)</sup> and that different ranks of coal are associated with a different prevalence of pneumoconiosis.<sup>(15)</sup>

The pathogenic events which could lead to CWP and PMF and altered pulmonary function may depend on the ability of the individual to respond to the damaging effects of particles which in turn may depend on duration of exposure level and type of particle involved. Given the different particulate mix of coal dust in any one mine, it may well be that a combination of factors may synergize the pathologic response. Studies are continuing to explore further the differing effects of different coal dust preparations on the macrophage processing of arachidonic acid.

### Acknowledgment

This research has been supported by the Department of the Interior's Mineral Institute program administered by the

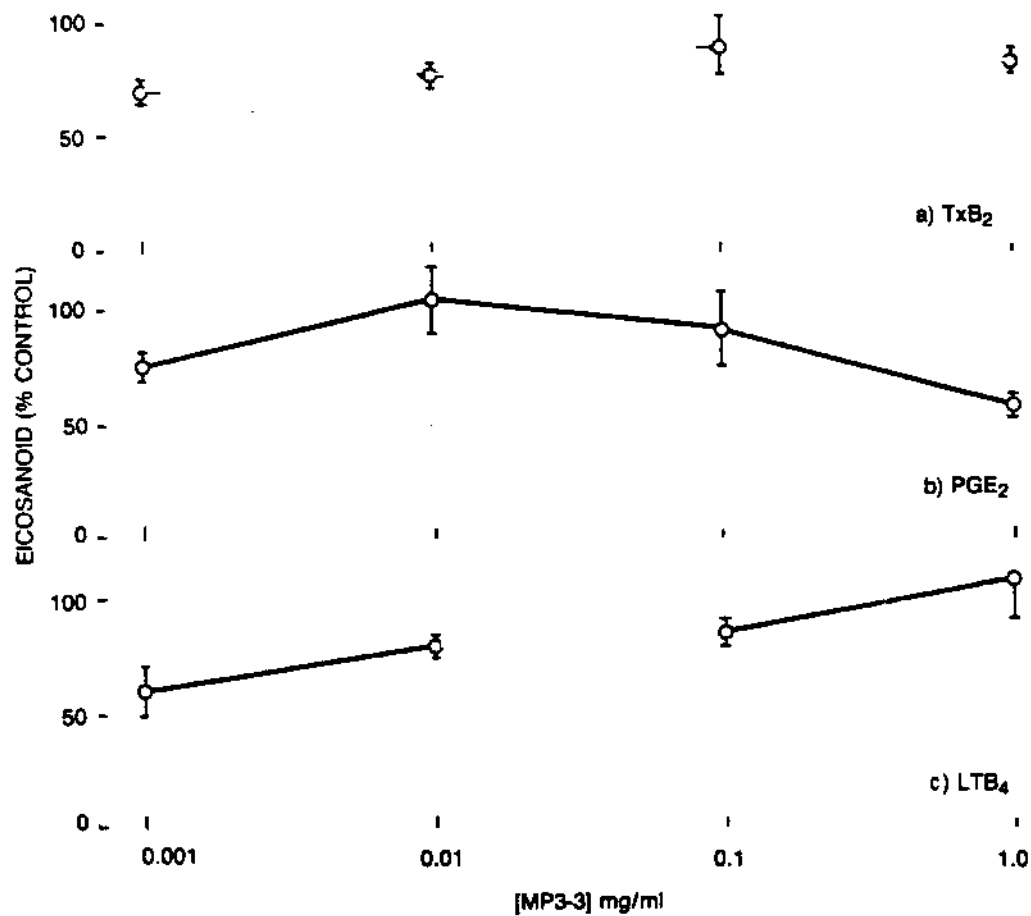


FIGURE 8. Release of arachidonic acid metabolites by rat alveolar macrophages in the presence of different concentration of coal dust MP3-3 after 1 hour incubation.

Bureau of Mines through the Generic Mineral Technology Center for Respirable Dust under grant number G1135142.

References

1. Morgan, W.K.C.: *Occupational Lung Diseases*, pp. 149-215. W.B. Saunders Co. (1975).
2. Hunninghake, G.W., J.E. Gadek, O. Kawanami et al: Inflammatory and Immune Processes in the Human Lung in Health and Disease: Evaluation by Bronchoalveolar Lavage. *Am. J. Pathol.* 97(1): 149-205 (1979).
3. Harris, J.O., E.W. Swenson and J.E. Johnson, III: Human Alveolar Macrophages: Comparison of Phagocytic Ability, Glucose Utilization and Ultrastructure in Smokers and Nonsmokers. *J. Clin. Invest.* 49:2086-2096 (1970).
4. Drew, W.L., L. Mintz, R. Hoo and T.N. Finley: Growth of Herpes Simplex and Cytomegalovirus in Cultured Human Alveolar Macrophages. *Am. Rev. Resp. Dis.* 119:287-291 (1979).
5. Yeager, H., Jr., S.M. Zimmet and S.L. Schwartz: Pinocytosis of Human Alveolar Macrophages. Comparison of Smokers and Non-smokers. *J. Clin. Invest.* 54:247-251 (1974).
6. Hoidal, J.R.: Alveolar Macrophages from Young, Asymptomatic Cigarette Smokers and Non-smokers Use Equal Amounts of O<sub>2</sub> and Glucose but Smokers make more Superoxide Anion. *Am. Rev. Resp. Dis.* 119:222A (1979).
7. Hsueh, W.: Prostaglandin Biosynthesis in Pulmonary Macrophages. *Am. J. Pathol.* 97:137-148 (1979).
8. Kouzan, S., A.R. Brody, P. Nettesheim and T. Eling: Production of Arachidonic Acid Metabolites by Macrophages Exposed *in vitro* to Asbestos Carbonyl Iron Particles or Calcium Ionophore. *Am. Rev. Resp. Dis.* 131:624-632 (1985).
9. Needleman, P., J. Turk, B.A. Jakschik et al: Arachidonic Acid Metabolism. *Ann. Rev. Biochem.* 55:69-102 (1986).
10. Fantone, J.C., S.L. Kunkel and P.A. Ward: Chemotactic Mediators in Neutrophil-dependent Lung Injury. *Ann. Rev. Physiol.* 44:283-293 (1982).
11. Hyman, A.L., E.W. Spannake and P.J. Kadowitz: Prostaglandins and the Lung. *Am. Rev. Respir. Dis.* 117:111-136 (1978).
12. Tilkes, F. and E.G. Beck: Macrophage Functions After Exposure to Nonfibrous Mineral Dusts. *Environ. Health Persp.* 51:167-171 (1983).
13. Demers, L.M.: Prostaglandins, Thromboxane and Leukotrienes. *Laboratory Medicine*. G. Race, Ed. Harper & Row, New York (1983).
14. Hurley, J.F. and C.A. Soutar: Can Exposure to Coal Mine Dust Cause a Severe Impairment of Lung Function? *Brit. J. Ind. Med.* 43:150-157 (1986).
15. Morgan, W.K.C.: Prevalence of Coal Workers' Pneumoconiosis. *Am. Rev. Respir. Dis.* 98:306-310 (1968).

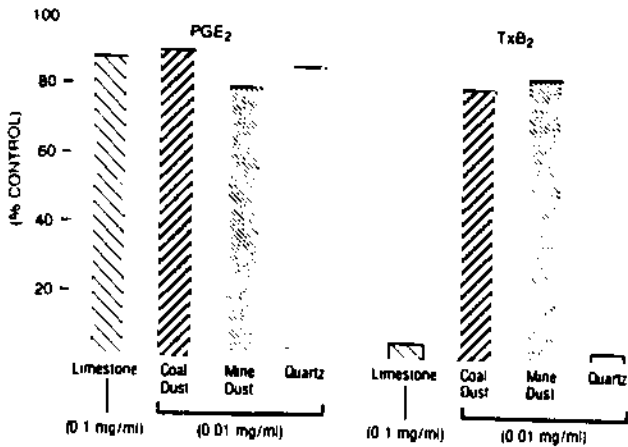


FIGURE 9. Effect of different coal dust particles on PGE<sub>2</sub> and TXB<sub>2</sub> production by rat alveolar macrophage.

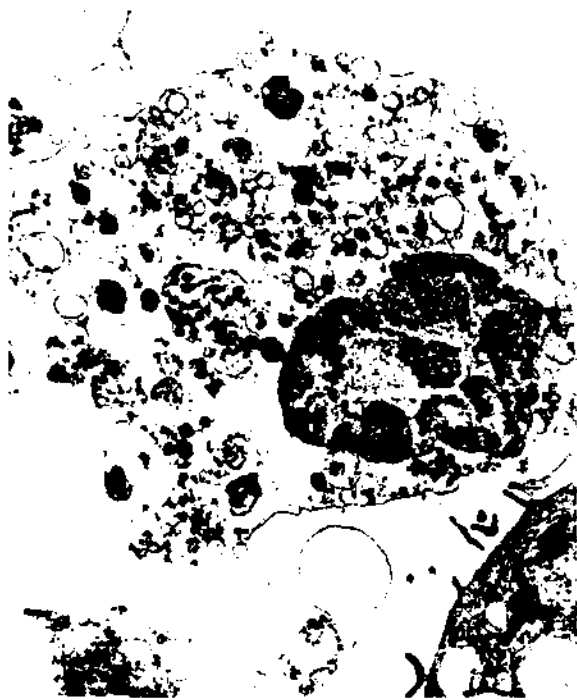


FIGURE 10. Transmission electron micrograph of alveolar macrophage following exposure to coal dust under in vitro conditions.

# Development of Alterations in the Lung Induced by Inhaled Silica: a Morphometric Study

R. Clark Lantz<sup>1</sup>, Charles Stanley<sup>2</sup> and David E. Hinton<sup>1</sup>

<sup>1</sup>Department of Anatomy, West Virginia University

<sup>2</sup>Department of Mechanical Engineering, West Virginia University

Morphometric examination of lung alterations following exposure to toxic and pathogenic substances is invaluable in detecting subtle changes which might otherwise be overlooked. Results, from evaluation of initial structural alterations, support and guide subsequent non-morphological techniques and, when coupled appropriately, can lead to a better understanding of the pathogenesis of a disease. Morphometry is a technique which can be used to determine, quantitatively, the site, extent, development, and progression of a disease state. Determination of the extent of tissue and cellular involvement in the response to inhalation of silica has been performed in order to gain a better understanding of the development of fibrosis following inhalation of this toxicant. In addition, since silica has been postulated as one of the important pathogenic minerals in coal mine dust, it is important to understand the lung tissue response to silica prior to evaluating the effects of inhaled coal mine dusts. Male Syrian golden hamsters were placed in Hazelton 1000 inhalation chambers and were exposed to either filtered air (controls,  $n = 24$ ) or filtered air plus  $30 \text{ mg/m}^3$  silica (Min-U-Sil 10, 95% of particles  $< 5 \text{ } \mu\text{m}$ ,  $n = 24$ ) for 16 hours per day, five days per week, for two weeks. Animals were returned to the animal quarters prior to subsequent tissue processing at 1, 4, and 12 weeks following exposure. This schedule was designed to allow time for the development of fibrosis. Lungs were fixed by intratracheal perfusion of 1/2 strength Karnovsky's fixative at a pressure of  $20 \text{ cm H}_2\text{O}$  and tissues were taken for embedment and analysis at the light level. Determination of site, extent, and development of alterations was performed using a multitiered approach. Changes in large structures (airways, blood vessels) was determined prior to evaluation of changes at the septal tissue level. Data will be presented outlining the progression of changes. Results indicate the usefulness of morphometric analysis of lungs following inhalation of toxic substances in quantitatively defining the structural alterations.

## Introduction

Silica is a known fibrogenic agent when inhaled alone and has also been postulated as an important causative agent in coal workers' pneumoconiosis. Although efforts have been made to elucidate the mechanism of pathogenesis of silicosis, the events which lead to the deposition of collagen and fibrosis in the lung following silica exposure are not completely understood. Several investigators have attempted to describe the tissue and cellular responses following silica exposure either following intratracheal instillation or inhalation.<sup>(1-4)</sup> However, these studies have used relatively high doses and have only been concerned with qualitative evaluation of the morphological alterations. The purpose of this report is to describe, in quantitative terms using morphometric techniques, the structural alterations in the lung following inhalation of silica. Use of these techniques permits objective evaluation of structural alteration, permits statistical testing of differences between control and exposed animals, allows structural data to be correlated with other biochemical and physiological data, and can be a sensitive method for detection of subtle differences in structural alteration.

## Materials and Methods

### *Animals*

Male Syrian golden hamsters (90-110 g body weight obtained from Engle Laboratories, Farmersburg, IN) were used throughout the study. When not in the inhalation chambers, animals were housed in the WVU Basic Science animal quarters, given food and water ad lib and maintained on a 12 hour on - 12 hour off light/dark cycle.

### *Inhalation Exposure*

Hamsters were exposed to silica in the West Virginia University inhalation facility. The facility consists of two



Hazelton HIC-1000 chambers. Both chambers received air (10 l/min) which had been filtered, cooled, dehumidified, and reheated and humidified to 70°F, 45 percent relative humidity. Animals were selected at random and placed in either the control chamber, which received only the filtered air, or the exposure chamber, which received silica in addition to filtered air. Silica (Min-U-Sil 10, 95% of particles < 5  $\mu$ m) was aerosolized using a TSI 9310 fluidized bed aerosol generator and animals were exposed to 30 mg/m<sup>3</sup> of silica 16 hours per day, five days per week for two weeks. At one week (N = 7), four weeks (N = 7) and 12 weeks (N = 8) following the end of exposure animals were processed for morphological and morphometric examination. Control animals (N = 10) were also taken at each time point.

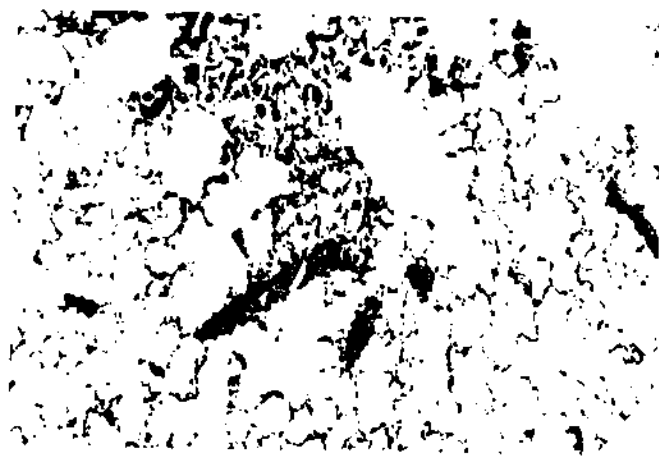


FIGURE 1. Light micrograph of hamster distal lung. Note cellular accumulation in alveoli. Silica treated animal 12 weeks postexposure. H & E stained paraffin section. X80.

#### General Morphologic Methods

All animals were anesthetized by a single i.p. injection (0.6 ml/100 g body weight) of 1.0 percent aqueous Brevital sodium (Lilly). After exposure of the trachea, a catheter was inserted between the second and third tracheal cartilaginous rings. The catheter was connected to a three way valve allowing maintenance of a patent airway. At this time the anterior abdominal wall was opened and the diaphragm was punctured permitting collapse of the lung against atmospheric pressure and flow of fixative (1/2 strength Karnovsky's fluid containing 0.01 percent picric acid in 0.1M phosphate buffer, pH 7.4) into the lungs was initiated. This fixative was selected since it has been shown to be satisfactory for light and electron microscopy. Lungs were inflated against a constant pressure of 20 cm H<sub>2</sub>O for one hour at which time the trachea was ligated and lungs, heart and other components of the mediastinum were removed, immersed in fixative and stored at 4°C overnight. Total lung volume (via fluid displacement) and weights of right (apical, middle, caudal and infracardiac lobes) and left (left lobe) lungs of each animal were recorded.

After fixation, each lobe was dissected free and sliced along the axis of the major intrapulmonary airway from the

hilus to the periphery.<sup>(5)</sup> Slices were taken from each lobe for routine light microscopy (LM) (paraffin embedment and staining of 5  $\mu$ m sections, taken at 1 mm intervals, with hematoxylin and eosin. Slices from right caudal and left lung lobes of each animal were used for high resolution light microscopy (HRLM). These were gently minced into 1 mm<sup>3</sup> pieces, rinsed in phosphate buffer as above, postfixed in OsO<sub>4</sub> for one hour, dehydrated in graded ethanol solutions, passed through propylene oxide and embedded in Epon-Araldite. Semithin sections (1  $\mu$ m) of Epon-Araldite embedded material were cut with glass knives and stained with toluidine blue for HRLM. Randomization was assured at the lung lobe level<sup>(6)</sup> since approximately 100 pieces from individual lobes were mixed in vials of fixative prior to removal of ten pieces for HRLM.

#### Morphometric Procedures

Standard point counting techniques as described for the lung<sup>(7)</sup> were used. Point counting of all light microscopic material was performed directly from glass slides using a drawing tube attachment which superimposed an image of the square lattice over the image of the tissue section. Analysis of H & E — stained, paraffin embedded sections, from each lobe of each lung was performed using a grid overlay of 100 points with an interpoint distance (as determined by stage micrometer) of 0.2 mm. The number of points overlying structures of interest was used to estimate volume densities ( $V_v$ ) for large blood vessels and airways as well as distal lung (respiratory bronchiole, alveolar ducts, sacs and alveoli) in 10 fields/animal. The second level of analysis was HRLM material. Slides were viewed at 625X and a grid overlay of 100 total points with interpoint distance of 20  $\mu$ m was used. Points over air space and alveolar septal tissue were used to estimate  $V_v$  of each. Surface density of alveolar epithelium was estimated by counting intercepts of test lines with the epithelial surface.

Arithmetic mean barrier thickness of alveolar septa was calculated by dividing the volume density of septal compartment by the epithelial surface densities. Alveolar mean linear intercept length was calculated from the volume density of distal lung airspace and surface density of alveolar epithelial cells.

#### Statistics

Statistical differences between experimental groups were determined by using analysis of variance<sup>(8)</sup> with  $P < 0.05$  being considered as significant.

#### Results

Qualitative evaluation of light micrographs from animals exposed to silica show responses typical of toxic dust exposures. Examination of tissue demonstrated cellular accumulations in the alveolar spaces (Figures 1 and 2) and apparent thickening of the alveolar septa (Figure 2). These changes were present in animals at 1, 4, and 12 weeks following the termination of the two week exposure to silica.

# ALTERATIONS IN THE LUNG INDUCED BY INHALED SILICA

**TABLE I**  
Effect of Silica Exposure on Hamster Lung

Parameter	Time After Silica Exposure			
	Control	1 week	4 weeks	12 weeks
Total lung volume (cm <sup>3</sup> )	4.99 +/- 0.19	4.36 +/- 0.17	4.79 +/- 0.16	5.84 +/- 0.30 <sup>a</sup>
Large airways (cm <sup>3</sup> )	0.46 +/- 0.05	0.30 +/- 0.02	0.49 +/- 0.07	0.39 +/- 0.05
Large blood vessels (cm <sup>3</sup> )	0.39 +/- 0.03	0.36 +/- 0.03	0.49 +/- 0.03	0.44 +/- 0.05
Distal lung (cm <sup>3</sup> )	4.14 +/- 0.18	3.70 +/- 0.16	3.81 +/- 0.20	5.01 +/- 0.25 <sup>a</sup>
Distal lung airspace (cm <sup>3</sup> )	3.60 +/- 0.13	3.14 +/- 0.15	3.25 +/- 0.19	4.15 +/- 0.20 <sup>a</sup>
Alveolar septa (cm <sup>3</sup> )	0.54 +/- 0.07	0.55 +/- 0.04	0.56 +/- 0.03	0.86 +/- 0.09 <sup>a</sup>
Alveolar mean linear intercept (um)	55.5 +/- 2.6	55.1 +/- 2.5	57.3 +/- 2.3	50.6 +/- 2.9
Septal thickness (um)	1.99 +/- 0.15	2.45 +/- 0.15 <sup>b</sup>	2.47 +/- 0.07 <sup>b</sup>	2.55 +/- 0.19 <sup>b</sup>

Values are mean +/- SEM

<sup>a</sup>Significantly different from all other groups (p < 0.05).

<sup>b</sup>Significantly different from control (p < 0.05).

Light microscopic morphometric data are presented in Table I. Values for volumes are presented as absolute values so that any change in various tissue compartment volumes could be detected. Although control animals were examined at all three time points following the end of exposure, no significant differences were seen between any of the controls and therefore all control animal values were placed in a single group.

Twelve weeks following silica exposure significant increase in total lung volume was seen versus all other groups. When the total lung volume was divided into its constitutive parts it was determined that the increase in lung volume was caused by increases in both the distal lung airspace and alveolar septal volumes (Table I).

In order to determine if the changes in volume of distal lung compartments represents septal thickening and/or emphysema, alveolar mean linear intercept (the average distance between alveolar septal walls) and the septal thickness were calculated. No significant differences were seen in alveolar mean linear intercept. Alveolar septa were thicker in the 12 week group but significant increases in this parameter over controls were also seen in the one and four week postexposure groups.

## Discussion

Qualitative descriptions of the response of the lung to inhaled silica have been previously reported by numerous investigators.<sup>(1,4)</sup> Although descriptive accounts of the progression of the tissue responses is useful, quantitative determinations of the site and extent of alteration cannot be obtained by these methods. Morphometric examination of lung alterations following exposure to toxic and pathogenic

substances is invaluable in detecting subtle changes which might otherwise be overlooked. Results, from evaluation of initial structural alterations, support and guide subsequent nonmorphological techniques and, when coupled appropriately, can lead to a better understanding of the pathogenesis of a disease. Morphometry is a technique which can be used to determine, quantitatively, the site, extent, development and progression of a disease state. Determination of the extent of tissue and cellular involvement in the response to inhalation of silica has been performed in order to gain a better understanding of the development of fibrosis following inhalation of this toxicant.

Data presented in this light microscopic study support and extend the findings of qualitative evaluation of pulmonary tissue following silica exposure. Wehner *et al*<sup>(4)</sup> reported that inhalation of silica lead to increases in lung volume as early as four months postexposure. They did not however, present data as to the exact cause and site of the increase in lung volume. Our study has also found a similar increase in lung volume in silica exposed animals at 12 weeks postexposure but by using morphometric techniques it was determined that the increase is due to changes in both the distal lung airspace and septal volumes.

Alteration in these volumes may be expected if, as is well documented, silica exposure leads to fibrosis and also to emphysema. However, this conclusion is not substantiated by our data. If emphysema were present in the silica exposed animals, alveolar mean linear intercept values should increase. No significant differences were seen in this parameter at 12 weeks postexposure. In addition, if increases in septal lung volume is due only to increases in the septal thickness, then increases should only be present in the 12 week group and not in all groups of exposed animals. Since

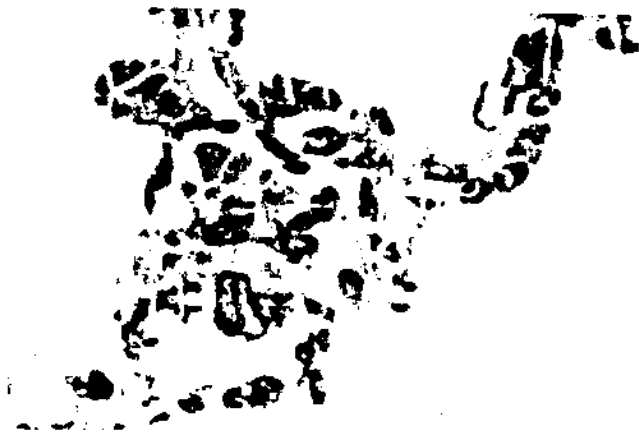


FIGURE 2. High resolution light micrograph of hamster distal lung. Cellular accumulation in alveoli and apparent thickening of alveolar septa are present. Silica treated animal 12 weeks postexposure. Toluidine blue stained epon embedded tissue. X600.

tissue volume and air space have increased without an increase in alveolar size one interpretation of the data is that the number of alveoli has increased in the silica exposed group 12 weeks after the end of the exposure. Similar increases in alveolar number in response to toxic inhalants has been reported previously by Hyde *et al.*<sup>(9)</sup>

Increases in septal thickness at all time points following the termination of exposure may be an indication of either interstitial edema, interstitial cellular accumulation and/or fibrosis. The exact nature of the septal response and the cells involved in the response are currently under investigation by performing morphometric examination of the electron microscopic levels. Data obtained at that level of investigation should enhance the understanding of the cellular and tissue responses following silica inhalation.

### Acknowledgment

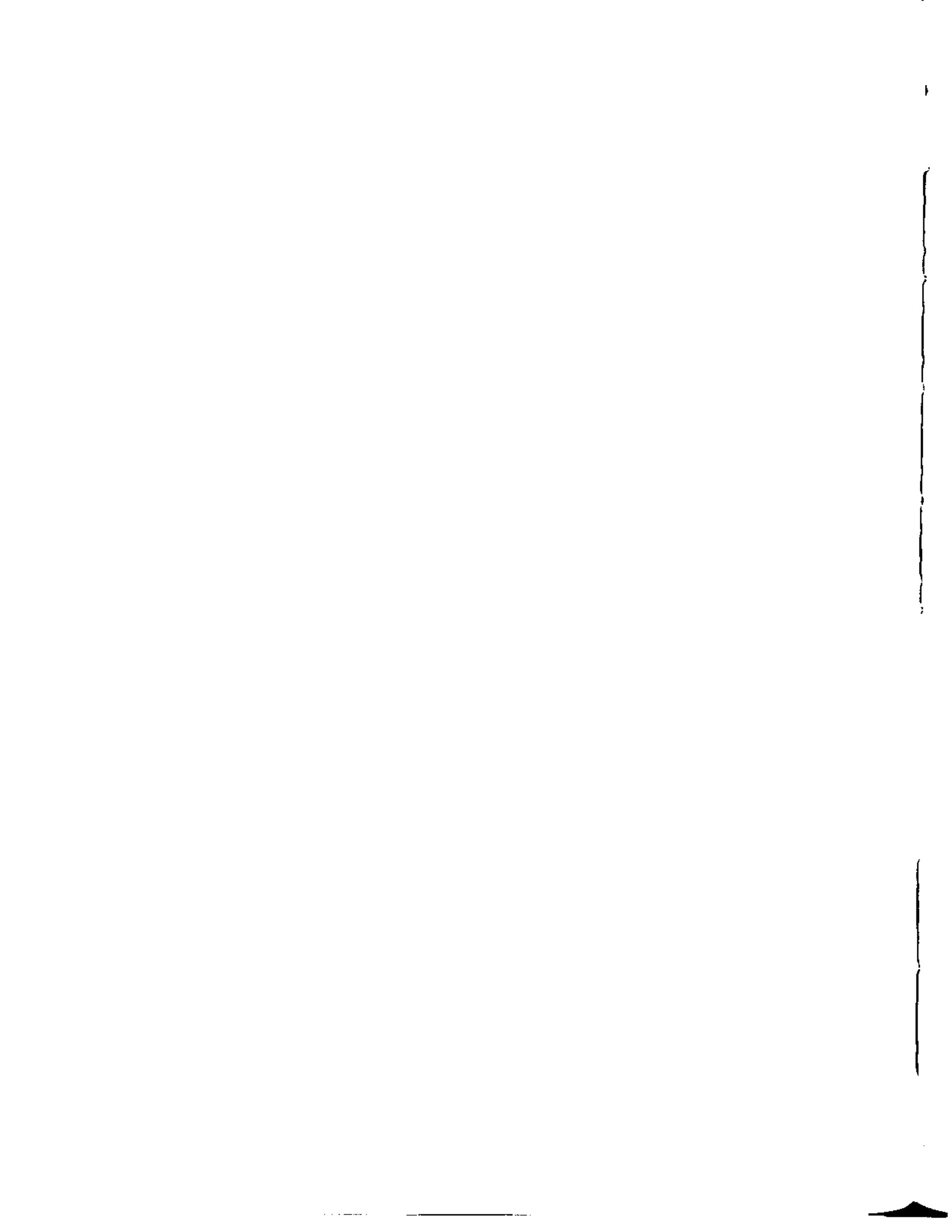
This research has been supported by the Department of the Interior's Mineral Institute program administered by the Bureau of Mines through the Generic Mineral Technology Center for Respirable Dust under grant number G1135142.

### References

1. Martin, J.C., H. Daniel and L. Le Bouffant: Short- and Long-term Experimental Study of the Toxicity of Coal-mine Dust and Some of Its Constituents. *Inhaled Particles IV*, pp. 361-372. British Occupational Hygiene Society, London (1977).
2. Dauber, J.H., M.D. Rossman, G.G. Pietra et al: Experimental Silicosis: Morphologic and Biochemical Abnormalities Produced by Intratracheal Instillation of Quartz into Guinea Pig Lungs. *Am. J. Pathol.* 101:595-612 (1980).
3. Martin, T.R., E.Y. Chi, D.S. Covert et al: Comparative Effects of Inhaled Volcanic Ash and Quartz in Rats. *Am. Rev. Resp. Dis.* 128:144-152 (1983).
4. Wehner, A.P., G.E. Dagle and M.L. Clark: Lung Changes in Rats Inhaling Volcanic Ash for One Year. *Am. Rev. Resp. Dis.* 128:926-932 (1983).
5. Dungworth, D.L., L.W. Schwartz and W. Tyler: Morphological Methods of Evaluation of Pulmonary Toxicity in Animals. *Ann. Rev. Pharmacol. Toxicol.* 16:381-400 (1976).
6. Rohr, H., M. Oberholzer, G. Bartsch and M. Keller: Morphometry in Experimental Pathology: Methods, Baseline Data and Applications. *Int. Rev. Exp. Pathol.* 15:233-325 (1976).
7. Weibel, E.R.: *Stereological Methods: Practical Methods for Biological Morphometry*. Academic Press, New York, NY (1979).
8. Winer, B.J.: *Statistical Principles in Experimental Design*. McGraw-Hill, New York, NY (1971).
9. Hyde, D.M., M.Y. Stovall, A.Y. Kyhos and D.A. Samuelson: Estimation of Alveolar and Alveolar Duct Number and Size in Nitrogen Dioxide-Induced Emphysema. *Acta. Stereol.* 2:159-162 (1983).

V

**Relationship of Mine Environment,  
Geology and Seam Characteristics  
To Dust Generation  
and Mobility**



# A Strategy for Coal Mine Respirable Dust Sampling Using Multi-stage Impactors for Characterization Purposes

C. Lee and J. M. Mutmanský  
Department of Mineral Engineering, The  
Pennsylvania State University

## Introduction

Recognition of Coal Workers' Pneumoconiosis (CWP) as a major occupational disease has affected various aspects of the coal mining industry in the United States as well as in almost all major coal producing countries. Regulations related to the control of coal mine dust forced mine operators to modify their mining and ventilation practices. As the coal production record of the last 15 years shows, this had both direct and indirect impacts on the productivity and production costs.

To identify the causes of CWP, many research efforts have been made throughout the world. Most of these studies were epidemiological in nature, attempting to pinpoint exposure and seam variables that affected the incidence of the disease. Other studies have been oriented toward the elemental and mineralogical composition of the coal dust in the mine atmosphere and in the miners' lungs. These studies indicate that there may exist some relationships between the characteristics of the coal mine dust and the prevalence of the disease. Some of the variables that are thought to affect the occurrence of CWP are the mass of the dust in the working place, the rank of the coal, the existence of certain trace elements, the free silica content of the coal, and the existence of other minerals in the respirable dust. A more complete description of these previous research studies has appeared elsewhere (Mutmanský and Lee, 1984).

The behavior of particles in the human lung is known to be governed by their aerodynamic diameter, which is defined as the diameter of a hypothetical spherical particle with unit density that exhibits the same settling velocity as the given particle. Because of this fact, the aerodynamic size distribution of coal mine dust

is one of the parameters to be determined along with the other physical, elemental, and mineralogical characteristics. The objective of this paper is to establish a strategy for providing coal mine respirable dust samples for characterization purposes using instruments that classify according to the aerodynamic diameter. In addition, several findings concerning characterization methods will be presented.

## Choice of Samplers

Most of the gravimetric dust collection devices that can be utilized in a mine environment can be classified as either single- or multi-stage samplers. Personal dust samplers that collect compliance dust samples and single-stage impactor samplers that simulate the characteristic curve of the human lung belong in the former category. Because these samplers normally collect dust on filters, the dust must be separated from the collection filter and dispersed in a gaseous or liquid suspension medium to obtain size distributions. During these preparation procedures, important information about the agglomeration and deagglomeration is likely to be lost. Furthermore, the sizing in the different size analyzers may not be based on the aerodynamic diameter. To avoid problems of this type, it was decided to utilize multi-stage cascade impactors for respirable coal mine dust collection in our research.

In choosing a multi-stage impactor for use in an underground coal mine, a number of different requirements must be met. First, the impactor must be powered by a permissible pump. This more or less limits the samplers to those that can utilize the standard 2 l/min permissible pumps now available on the market. Second, the sampler must be relatively compact, rugged enough for

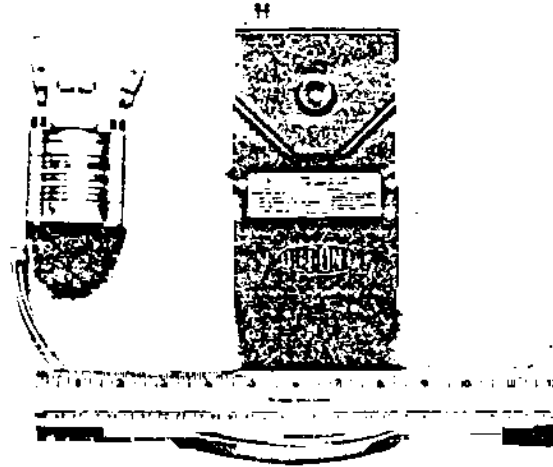


Figure 1. Sierra Model 298 cascade impactor connected to a DuPont Model P2500A pump.

underground use, and able to be transported underground without special handling. There are only a few multi-stage impactors that can meet these requirements. We chose the Sierra Model 298 Marple personal cascade impactor now marketed by Anderson Samplers, Inc. (Rubow et al., 1985). This multi-stage sampler was designed to be used on a personal basis and hence is rather compact. As shown in Figure 1, the sampler has been combined with a DuPont Model P2500A pump to form a manageable package for use underground.

The Sierra Model 298 consists of eight stages and a backup filter. It is shown in its disassembled form in Figure 2. The dust-laden air enters the instrument at the top and passes through a series of progressively smaller jets. At each stage, there is a collection substrate of mylar or stainless steel on which particles are impacted according to their aerodynamic diameters. The cut points range from 0.5 to 21  $\mu\text{m}$  for this impactor. A 34-mm PVC backup filter with a five-micron pore size is used to gather the dust that is not impacted on the mylar substrates. A grease or other collection medium is normally used on the substrates to provide a more efficient collection process. It should be noted that we used mylar substrates in all of our research. More information will be given on that subject later in this paper.

To provide accurate estimates of the mass of dust on each of the substrates, a microbalance capable of determining the masses of the substrates plus dust to a precision of 1  $\mu\text{g}$  was used. To insure that moisture did not affect the mass determinations, the substrates were

greased and placed in a desiccation chamber overnight before being weighed. The substrates loaded with dust were likewise placed in a desiccation chamber overnight before the final mass determinations were performed. The PVC filters were handled in an identical manner except that no collection grease was applied. To overcome the effects of any static charges that might build up on the surface of the mylar substrates, a small polonium 210 radiation source was located in the weighing chamber. The substrates were passed over the source before weighing to remove the static charges.

#### Equipment Testing

To test the selected equipment and to determine the optimal sampling parameters for use in the underground environment, a test chamber and auxiliary equipment were set up in our respirable dust lab. Details on each of these components of the test equipment are provided below.

**Aerosol Test Chamber.** The aerosol chamber used in the tests of the impactors was manufactured by Elpram Systems, Inc. and is shown in figure 3. The design of the chamber has been described in detail elsewhere (Marple and Rubow, 1983) but the general characteristics of the chamber bear repeating here. The chamber is approximately 3 m (10 feet) high and has a hexagonal horizontal cross section of about 1.1  $\text{m}^2$  (12  $\text{ft}^2$ ). The intake air containing the aerosol (coal dust, in this case) is introduced at the top of the chamber, passes through a honeycomb flow-straightener, and flows toward the bottom of the chamber. The chamber

## COAL MINE RESPIRABLE DUST SAMPLING

is designed to have a uniform distribution of the aerosol across the entire cross section. However, to insure that the instruments subjected to the aerosol within the chamber have a uniform exposure, all instruments are placed upon a turntable that is kept rotating during any given test.

A variety of features help to make the chamber more easily used and maintained. The support frame has several areas for placement of auxiliary equipment. Three removable Plexiglas windows are positioned around the chamber so that the chamber activity can be viewed during the test and so that access can be readily achieved. A set of glove ports is located below each window so that entry can be made into the chamber during a test without disturbing the stability of the chamber environment.

**Auxiliary Equipment.** The auxiliary equipment necessary to operate the aerosol test chamber includes a dust generator, a dessicator for drying intake air, a mixing apparatus for combining clean and dust-laden air, and a radioactive source to remove static charges from the dust particles introduced into the chamber. The dust generator used in our lab is a TSI Model 3400 that utilizes a fluidized bed of brass beads of 100  $\mu\text{m}$  diameter in a 5.1 cm diameter chamber to introduce the dust into the intake air stream. The dust is introduced into the fluidized bed by a No. 3 ball chain (2.3 mm diameter balls on 3.1 mm centers) that passes through the dust holding chamber and the fluidized bed. More technical information on this aerosol generator can be found in the paper by Marple, Liu, and Rubow (1978).

Other auxiliary equipment for the aerosol chamber includes a TSI Model 3074 air supply system which contains equipment for regulating the pressure and a dessication chamber for removing moisture from the air supply. A mixing valve, which is simply a calibrated variable-orifice two-way valve, and two flow meters were supplied with the chamber. These devices insure that the intake air stream is provided with the correct mixture of clean and dust-laden air. Finally, a TSI Model 3012 aerosol neutralizer was placed at the outlet of the dust generator. This device is a pass-through chamber containing a krypton 85 radiation source to remove the surface charges that may be present on the dust particles discharged from the fluidized bed dust generator.

### Sampling Experiments

To insure that the equipment was operating properly and to provide realistic sampling procedures and times, a series of experiments was run in the aerosol test chamber prior to any field experiments. The collection efficiency of different greases was first tested to insure that the impactors were operating satisfactorily with a coal dust aerosol. Sampling time experiments were then conducted to gather raw data upon which proper sampling times could be determined. This data set was then analyzed to determine the optimal sampling times for use in underground coal mines.

**Impactor Collection Efficiency.** The use of an aerosol impactor in dust collection work normally requires that the substrates be coated with a relatively sticky liquid or solid substance to aid in the collection of

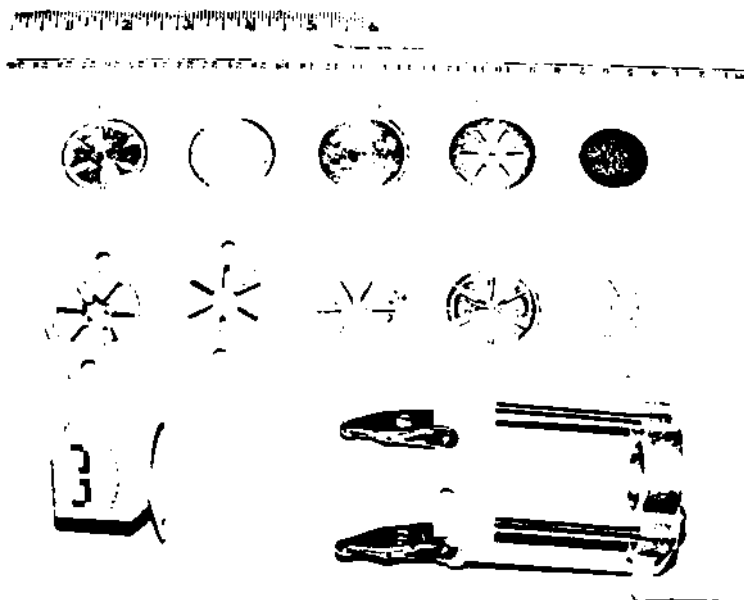


Figure 2. Components of the Sierra Model 298 cascade impactor.



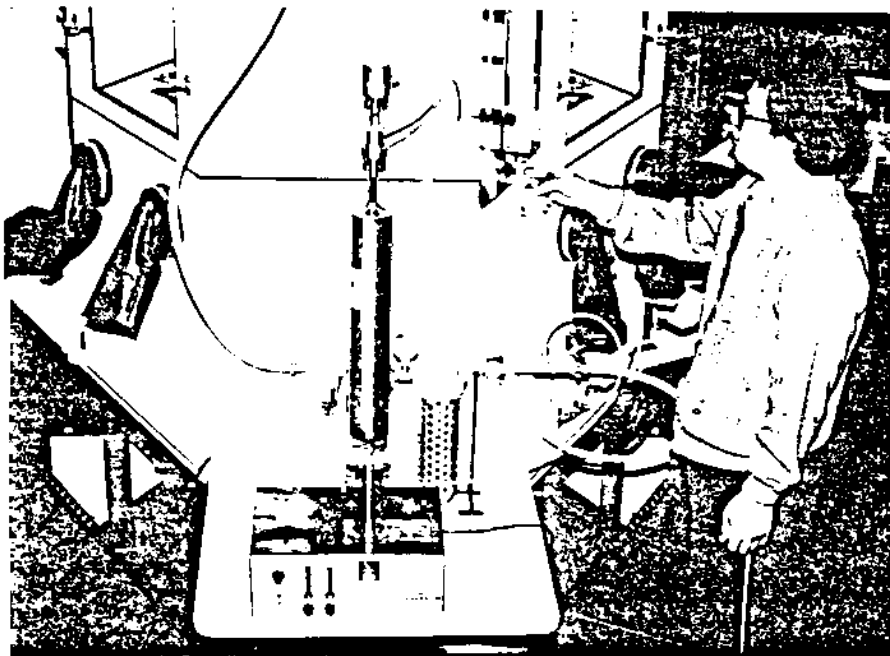


Figure 3. Elpram Systems Inc. aerosol test chamber and auxiliary equipment.

the aerosol particles while helping to prevent particle bounce. This improves the collection efficiency of the impactors and reduces the number of particles that are misclassified. Many aerosol researchers use vacuum greases for collection purposes because the physical characteristics of these greases are quite favorable. In our research, we were interested in using a pure organic grease because of the desire to determine the elemental composition of the dust without interference from the substrate coating.

Only two organic coatings, paraffin and petroleum jelly, were known to have been used in the past on impactor substrates. These two organic substances were tested against a vacuum grease, Apiezon L, commonly used on impactor substrates. To apply these greases to the substrates, spraying techniques using an artist's air brush were attempted. Based upon the advice of other aerosol researchers, the spraying was performed using toluene to thin the coating for spraying. The greases used were typically sprayed on the substrates as a liquid consisting of about 20% by weight of the grease dissolved in toluene. The substrates were then sprayed under a hood using an air brush operated at about 200 kPa (30 psi) and, when the toluene had evaporated, were weighed using the techniques described earlier.

In the collection efficiency studies, six of the Sierra Model 298 impactors were prepared for use in

the aerosol chamber. Petroleum jelly, Apiezon L, and paraffin were used as the impaction coatings, two of the impactors loaded with each coating. The impactors were then simultaneously subjected to an atmosphere containing approximately  $2.0 \text{ mg/m}^3$  of respirable coal dust in the aerosol test chamber for a period of several hours. The resulting mass distribution of the dust on the substrates for each of the coatings is provided in Table 1 and shown in graphical form in Figure 4. It can be seen that the petroleum jelly is a more efficient coating for the substrates than either paraffin or Apiezon L. It appears that the reason for this is that the petroleum jelly is more efficient in retaining particles on the proper substrate. The higher cumulative percentages of particles in the finer size range evident on the curves for Apiezon L and paraffin are apparently due to particle bounce (when the particle bounces off the substrate) and blow-off (when the particle sticks but is blown off later). The phenomena have been discussed in the paper by Esmen and Lee (1980). As a result of the tests, it was concluded that petroleum jelly is the best of the three impactor coatings for use with coal dust. Thus petroleum jelly has been used in all of our underground work because of its efficiency as a collector and its pure organic composition.

Sampling Time Experiments. To determine the optimal sampling time for use of the samplers under varying aerosol concentrations, it was

## COAL MINE RESPIRABLE DUST SAMPLING

decided to use the impactors in the aerosol test chamber until the distribution determined during the sampling period was identical to some known or standard distribution. To accomplish this, it was assumed that the log-normal distribution with two parameters was the best distribution to use to describe the dust size distribution. The measured distribution determined during a test in the aerosol chamber was then assumed to be equal to the known distribution when the two parameters of the measured distribution (the geometric mean and the geometric standard deviation) are equal to the parameters of the known or standard distribution.

To carry out this series of tests, a standard coal dust consisting primarily of particles in the respirable size range was prepared in the lab. This coal dust was then dispersed in the chamber while a number of impactors were in operation. The mass distribution of the impactors were then measured and the average assumed to be the known distribution. The results of this testing are given in Table 2. This standard dust was then used to produce aerosol concentrations of about  $1 \text{ mg/m}^3$ ,  $2 \text{ mg/m}^3$ , and  $4 \text{ mg/m}^3$  and each of these concentrations was run for periods of 90, 180, and 270 minutes. Each of these tests was run by first bringing the chamber up to the desired dust concentration as determined by the readings from an instantaneous dust monitor, GCA Model PDM-1 Mini-RAM, connected to an output printer for convenient data

recording. Typically, it takes the chamber two to four hours to stabilize at a given mass concentration and the concentration is controlled by varying the fluidized bed feed chain velocity and the volume of dilution air added to the input air stream. As a result of the stabilization time required, no attempt was made to achieve a precise value of the desired mass concentration. Instead, an approximation of the desired concentration and stability of the chamber environment was sought before each test proceeded.

A suite of six impactors was used for each combination of concentration and sampling time and the resulting distributions were averaged. The geometric mean and the geometric standard deviation were then determined for each combination using linear regression on log-normal probability paper. The results of these determinations are shown in Table 3. The geometric mean of this measured distribution was then compared with the geometric mean of the standard distribution ( $3.3 \text{ }\mu\text{m}$ ) using the well-known t-test. Similarly, the geometric standard deviation of the measured distribution was compared with the geometric standard deviation of the standard distribution ( $2.5 \text{ }\mu\text{m}$ ) using the F-test. The statistical test results are shown in Table 4.

The statistical tests run at or near  $1 \text{ mg/m}^3$  (Group 1 tests) indicate that 180 minutes was the shortest

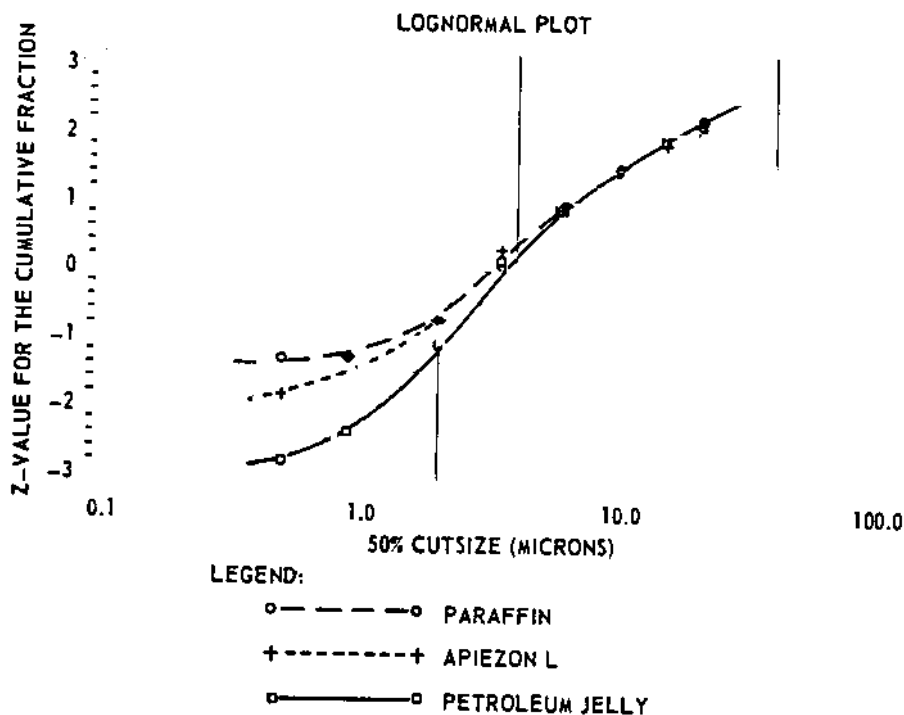


Figure 4. Lognormal plot of the mass distribution of coal dust using three different impactor substrate coatings.

# THE RESPIRABLE DUST CENTER

Table 1. Mass distribution of coal dust particles on the Sierra Model 298 impactor using three different collection coatings.

50% cut size	Petroleum Jelly		Apiezon L		Paraffin	
	z	Z	z	Z	z	Z
21 $\mu\text{m}$	2.13	98.34	2.20	98.60	2.20	98.60
15	1.94	97.36	1.84	96.74	1.87	96.92
10	1.44	92.56	1.47	92.90	1.48	93.12
6	0.92	82.05	0.93	82.29	0.91	81.90
3.5	0.07	52.78	0.28	61.10	0.13	54.98
2	- 1.13	12.97	- 0.78	21.67	- 0.75	22.65
0.9	- 2.40	0.83	- 1.35	8.80	- 1.31	9.53
0.5	- 2.81	0.24	- 1.86	3.16	- 1.34	8.98

z standard normal variable of the cumulative Z

Z cumulative percent of mass below the cut size

time for which it could be stated that the measured distribution was equal to the known distribution. In addition, it can be seen from the data that the significance level increases as the sampling time goes to 270 minutes. The two distributions derived from the 180-minute and the 270-minute samplings were not significantly different from each other but one of the impactors used in the 180-minute sampling was somewhat underloaded with dust in the upper and lower stages. This indicates that the sampling time should probably be greater than 180 minutes. As a result of these tests, it was concluded that the optimal sampling time was about four hours if the dust concentration is approximately  $1 \text{ mg/m}^3$ .

In the Group 2 tests run in dust concentrations of about  $2 \text{ mg/m}^3$ , it was found that sampling the dust for a period of 180 minutes or more with the impactor yielded accurate distributions. However, the substrates on the impactors used for 270 minutes in a concentration of  $2 \text{ mg/m}^3$  were somewhat overloaded, leading to the conclusion that about three hours or 180 minutes was the optimal sampling time. The optimal sampling time dropped significantly when dust concentrations of about  $4 \text{ mg/m}^3$  were used (Group 3). The measured distributions differed significantly from the standard distribution at this concentration because of overloading of the substrates. Thus, it was concluded that the optimal sampling time should be shorter than 90 minutes. It was estimated that the optimal sampling time would be about 45 minutes for dust concentrations of  $4 \text{ mg/m}^3$ . This was later verified in underground coal mine sampling. Dust concentrations of about  $4 \text{ mg/m}^3$  in locations behind the line brattice near an operating continuous miner yielded properly loaded substrates when

operated for one cut, typically 30 to 60 minutes. Our conclusion is therefore that the proper sampling time is approximately 45 minutes.

#### Mine Sampling Locations

The primary objective of this research study is to collect coal mine airborne dust at various locations in continuous miner development openings for characterization purposes and to identify sources in the mine that contribute to the various characteristics. Eventually it is hoped that the study will contribute to the engineering control measures in operating mines. Therefore, to choose locations for sampling that would provide as much information as possible, the following criteria were applied.

- \* Characteristics of dust originating from continuous miners and roof bolters were to be studied separately when possible in order to determine the quantitative and qualitative contribution of each equipment type to the dust.
- \* The sources and characteristics of the dust generated from secondary sources such as re-entrainment were to be determined.
- \* The distance of influence of each dust source in terms of its downstream dust concentration was to be determined.
- \* The effects of various face ventilation methods were to be analyzed.

## COAL MINE RESPIRABLE DUST SAMPLING

Table 2. Size distribution of the standard dust sample.

Impactor Stage	50% Cut Size ( $\mu\text{m}$ )	Cumulative % Smaller
1	21.0	99.1
2	15.0	96.5
3	10.0	87.7
4	6.0	65.7
5	3.5	40.4
6	2.0	23.8
7	0.9	8.8
8	0.5	6.0

Geometric mean = 3.3  $\mu\text{m}$

Geometric standard deviation = 2.5  $\mu\text{m}$

Table 3. Experimental data.

Test Group	Sampling Time (minutes)	Dust Concentration ( $\text{mg}/\text{m}^3$ )	Geometric Mean ( $\mu\text{m}$ )	Geometric Standard Deviation ( $\mu\text{m}$ )
1	90	1.0	2.1	2.2
	180	0.9	3.0	2.0
	270	0.6	3.2	2.7
2	90	2.0	4.5	2.4
	180	2.5	3.1	2.6
	270	1.8	2.9	2.7
3	90	5.0	4.0	2.4
	180	3.5	4.9	2.0
	270	4.6	4.3	2.5

\* The properties of the coal and rock were to be correlated with the dust properties through the taking of channel samples.

To limit the analysis, only continuous miner development sections were considered as candidates for sampling. Applying these criteria to such a section with a double-split ventilation setup and line brattice for face ventilation, the scheme shown in Figure 5 was devised. It should be noted that this scheme is basically a fixed-point sampling plan with sampler #1 located in the intake airstream outby the section dust sources. Samplers 2, 3, 4, and 5 are associated with the continuous miner while samplers 6, 7, 8, and 9 are associated with the roof bolter.

While the sampling plan shown is a fixed-point method, most of the samplers are not stationary. When the continuous miner and the roof bolter move, all samplers except those in the intake airway are repositioned to maintain their same position in the air stream with respect to these two pieces of equipment. The samplers 2, 3, 4, and 5 are moved when the continuous miner moves and samplers 6, 7, 8, and 9 move with the roof bolter.

The basic logic of this sampling scheme is also applied to systems using single-split ventilation and to face ventilation with auxiliary fans and vent tubing. However, the scheme must be varied somewhat for each case. In a single-split system, the continuous miner and roof bolter will be required to work in the same split of air. Under these conditions, it is more difficult to separate the effect of the miner and bolter on the dust. Thus it is more important to carefully locate the samplers so that the differences in dust collected on the intake and return side of the equipment can be used to determine the effect of the equipment. In systems using vent tubing, it is difficult or impossible to sample within the tubing and thus a return air stream sample must be taken at the face close to the end of the tubing. This location should be carefully checked to insure it is within the dust cloud of the pertinent equipment.

### Field Application

The sampling strategy outlined above has been applied to a number of mines in Pennsylvania and West Virginia. During this field work,

# THE RESPIRABLE DUST CENTER

Table 4. Statistical test results.

Hypothesis	Test Value	Conclusion
$\sigma_g^2(1,90) = \sigma_g^2(\text{known})$ $\mu_g(1,90) = \mu_g(\text{known})$	F = 0.77 t = 0.99	Variances Equal Level of Significance < 35%
$\sigma_g^2(1,180) = \sigma_g^2(\text{known})$ $\mu_g(1,180) = \mu_g(\text{known})$	F = 0.64 t = 0.22	Variances Equal Level of Significance > 80%
$\sigma_g^2(1,270) = \sigma_g^2(\text{known})$ $\mu_g(1,270) = \mu_g(\text{known})$	F = 1.17 t = 0.06	Variances Equal Level of Significance > 90%
$\sigma_g^2(1,90) = \sigma_g^2(1,180)$ $\mu_g(1,90) = \mu_g(1,180)$	F = 1.21 t = 0.90	Variances Equal Level of Significance < 40%
$\sigma_g^2(1,180) = \sigma_g^2(1,270)$ $\mu_g(1,180) = \mu_g(1,270)$	F = 0.55 t = 0.14	Variances Equal Level of Significance > 85%
<hr/>		
$\sigma_g^2(2,90) = \sigma_g^2(\text{known})$ $\mu_g(2,90) = \mu_g(\text{known})$	F = 0.92 t = 0.65	Variances Equal Level of Significance < 55%
$\sigma_g^2(2,180) = \sigma_g^2(\text{known})$ $\mu_g(2,180) = \mu_g(\text{known})$	F = 1.08 t = 0.13	Variances Equal Level of Significance > 90%
$\sigma_g^2(2,270) = \sigma_g^2(\text{known})$ $\mu_g(2,270) = \mu_g(\text{known})$	F = 0.77 t = 0.28	Variances Equal Level of Significance > 75%
$\sigma_g^2(2,90) = \sigma_g^2(2,180)$ $\mu_g(2,90) = \mu_g(2,180)$	F = 0.36 t = 0.76	Variances Equal Level of Significance < 50%
$\sigma_g^2(2,180) = \sigma_g^2(2,270)$ $\mu_g(2,180) = \mu_g(2,270)$	F = 1.40 t = 0.14	Variances Equal Level of Significance > 85%
<hr/>		
$\sigma_g^2(3,90) = \sigma_g^2(\text{known})$ $\mu_g(3,90) = \mu_g(\text{known})$	F = 0.92 t = 0.40	Variances Equal Level of Significance > 75%
$\sigma_g^2(3,180) = \sigma_g^2(\text{known})$ $\mu_g(3,180) = \mu_g(\text{known})$	F = 0.64 t = 0.91	Variances Equal Level of Significance < 40%
$\sigma_g^2(3,270) = \sigma_g^2(\text{known})$ $\mu_g(3,270) = \mu_g(\text{known})$	F = 1.00 t = 0.54	Variances Equal Level of Significance < 60%

Note:  $\sigma_g^2(\text{known})$  is the geometric standard deviation of the known or standard distribution.

$\mu_g^2(\text{known})$  is the geometric mean of the known or standard distribution.

$\sigma_g^2(1,90)$  is the geometric standard deviation of the sample from test group 1 that had a sampling time of 90 minutes.

$\mu_g(1,90)$  is the geometric mean of the samples from test group 1 that had a sampling time of 90 minutes.

## COAL MINE RESPIRABLE DUST SAMPLING

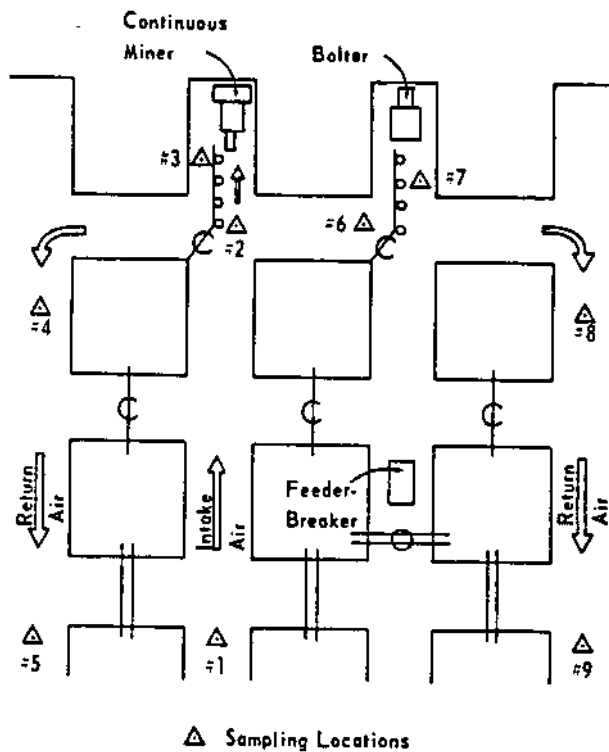


Figure 5. Sampling locations for a continuous miner development section using line brattice and a double-split ventilation plan.

the experiences with different operating sections indicated that a slightly different operating procedure was necessary for each mine. In this section, several observations based upon our field work are outlined. Potential users of this technique should also review the paper by Burkhart, McCawley, and Wheeler (1983) for other sampling observations.

Samplers used in the section were run for periods from 30 to 60 minutes in the return air location closest to the continuous miner to an entire shift for the sampler located in the intake air stream. Typically, it is generally easy to predict a sampling time to correctly load the impactors from the dust conditions in the section. However, the use of an instantaneous dust concentration measuring instrument will reduce the quesswork and insure a proper impactor loading.

Generally, the location for taking channel samples and the sampler locations themselves had to be planned so they were out of the way of the equipment. The impactors and pumps were connected together by velcro strips and hung as a unit, normally from the roof bolt bearing plates. The sampling package was normally placed about 1.3 m (4 feet) from either rib and about 0.3 m (1 foot) below the roof of the opening. Channel sampling was typically

performed in the crosscut closest to the face where no equipment traffic was expected. These locations presented no unexpected problems.

When setting up instruments in the section, the rock dusting practices should be studied for its effects on the sampling plan. When rock dusting is periodically performed, it is generally necessary to turn off the sampler during the dusting operation. This may be necessary after every cut. The use of a trickle duster associated with auxiliary fans presents a different problem. These dusters must be turned off to get valid samples for characterization purposes.

When ventilation systems using auxiliary fans and vent tubing were visited, it was necessary to place the nearest return side sampler associated with the miner or bolter outside the tubing and still get a valid sample for characterization purposes. The experience we had with this ventilation system indicated that placing the samplers below the tubing about 1.5 m (5 feet) from the end was a successful procedure. This location always appeared to be within the dust cloud generated by the machinery without interfering with its operation.

One final comment concerning the practical aspects of field application relates to the face. These samplers had an uncomfortably high probability of

## THE RESPIRABLE DUST CENTER

being hit by water sprayed by the miner. As a result, the inlet cowl of the impactors were redesigned with a hood that more adequately protected the inlet port. This hood was designed to wrap around the inlet port without increasing the resistance to air flow within the instrument.

### Characterization Procedures

The primary purpose in providing impactor samples is to characterize the dust in terms of its physical, chemical, and mineralogical composition. The impactors also provide a direct method of obtaining the size distribution of the airborne particles. However, the maximum amount of sample from a single stage is around 1 mg. This amount is normally collected on the upper stages of the impactor while the lower stages often collect less than 0.5 mg when properly loaded. In addition to this, the impactors placed in the intake airway are often underloaded. Thus, any analytical methods used on these samples must be capable of working with extremely small samples and must also be non-destructive in order to preserve the samples for other purposes.

The techniques for analyzing the physical characteristics of the dust are perhaps the best developed of the procedures. The use of a scanning electron microscope and image analysis techniques can be used to characterize the shape of the particles. While these techniques are well established and accepted, the elemental and mineralogical analysis procedures will require more careful scrutiny before they are used.

When researching methods for performing elemental analyses on our impactor samples, the most common of the conventional procedures using X-ray fluorescence were found to be lacking because of the requirement for a significantly greater dust mass than what was being collected. However, one reference in the literature (Ahlberg, Leslie and Winchester; 1983) outlined the use of proton-induced X-ray emission (PIXE) spectroscopy for aerosol samples. In PIXE analysis, a beam of protons is passed through the dust particles on the substrate and interacts with the electrons of the elements present (Johansson and Johansson, 1976). The X-rays emitted as a result of these interactions are analyzed to determine the elements that originated the various wave lengths. By counting the number of X-rays that are emitted in any given range of wave lengths, the amount of each element in the dust can be estimated with an error that can be determined

statistically for each element. The PIXE method quantifies the mass of all elements simultaneously but has one limitation. The commercially available PIXE analysis services are set up to determine only those elements that possess an atomic number greater than or equal to sodium. The cost of determining this set of elements is typically \$25 to \$50 per sample, depending upon the number of samples run at any given time.

The impactor substrates are not an ideal matchup with a typical PIXE instrument because the proton beam of the instrument will not encompass the entire dust mass on the substrate. As a result, it would take six separate periods of irradiation to analyze the entire dust mass. As a result of the cost of such a practice, PIXE analyses were performed on the six dust submasses on several substrates in order to judge the statistical effectiveness of analyzing only some of the six submasses. As a result, we concluded that subjecting two submasses of dust from each substrate and three substrates from each impactor would be sufficient for our purposes. This strategy will be reevaluated when the analyses from our summer field work of 1985 have been completed.

The final characterization area of interest to us deals with the mineralogical makeup of the dust. This is an area where the state of the art requires very labor-intensive and prolonged procedures to identify the minerals in an aerosol sample of the type found on an impactor substrate. Lee (1978) has outlined a procedure using both energy-dispersive microscopy on a scanning electron microscope and selected area electron diffraction on a high-voltage electron microscope. While this may be a feasible procedure, it is not cost effective where many samples are to be analyzed. As a result, other researchers at Penn State and West Virginia University associated with the Generic Technology Center on Respirable Dust are carrying out research efforts to provide more efficient and useful mineralogical characterization procedures. In general, these characterization procedures have not as yet been fully tested and analyzed. However, a great deal of progress has been made in the characterization area.

### Conclusions

Multi-stage cascade impactors have advantages over other single-stage samplers because they provide aerosol size data as well as samples classified according to the aerodynamic diameter. A major objective of the research described here has been to design a sampling

## COAL MINE RESPIRABLE DUST SAMPLING

strategy to gather sized dust samples for characterization purposes. This strategy has been designed and successfully applied to underground continuous miner development sections. Characterization of these samples is now in progress and the researchers involved are looking forward to the analysis of the results.

### Acknowledgements

The authors gratefully acknowledge that the Generic Mineral Technology Center for Respirable Dust supported this project. The Center is funded by the U.S. Bureau of Mines through the Pennsylvania Mining and Mineral Resources Research Institute at The Pennsylvania State University. The authors appreciate the support of these organizations. Grant Number G1135142

### Disclaimer

The opinions and conclusions expressed in this paper are those of the authors alone and do not represent the opinions of the Generic Mineral Technology Center for Respirable Dust, the Pennsylvania Mining and Mineral Resources Research Institute, or the U.S. Bureau of Mines. Citation of manufacturers' names in the paper were made for general information purposes and do not imply endorsement of the products by the authors.

### References

- Ahlberg, M.S., Leslie, A.C.D., and Winchester, J.W., 1978, "Environmental and Occupational Health Analysis Using Proton-Induced X-Ray Emission," Chap. 4 in Electron Microscopy and X-Ray Applications to Environmental and Occupational Health Analysis, Russell, P.A., and Hutchings, A.E., Eds., Ann Arbor Science Publishers, Ann Arbor, Mich., pp. 41-46.
- Burkhart, J.E., McCawley, M.A., and Wheeler, R.W., 1983, "Particle Size Distributions in Underground Coal Mines," A paper presented at AIHA Conference, Philadelphia, PA.
- Esmen, N.A., and Lee, T.C., 1980, "Distortion of Cascade Impactor Measured Size Distributions due to Bounce and Blow-off," American Industrial Hygiene Association Journal, Vol. 41, No. 6, June, pp. 410-419.
- Johansson, S.A.E., and Johansson, T.B., 1976, "Analytical Application of Particle Induced X-Ray Emission," Nuclear Instruments and Methods, Vol. 137, North-Holland Publishing Co., Amsterdam, pp. 473-516.
- Lee, R.J., 1978, "Electron Optical Identification of Particulates," Chap. 16 in Electron Microscopy and Occupational Health Analysis, Russell, P.A., and Hutchings, A.E., Eds., Ann Arbor Science Publishers, Ann Arbor, Mich., pp. 175-188.
- Marple, V.A., Liu, B.Y.H., and Rubow, K.L., 1978, "A Dust Generator for Laboratory Use," American Industrial Hygiene Association Journal, Vol. 39, No. 1, Jan., pp. 26-32.
- Marple, V.A., and Rubow, K.L., 1983, "An Aerosol Chamber for Instrument Evaluation and Calibration," American Industrial Hygiene Association Journal, Vol. 44, No. 5, May, pp. 361-367.
- Mitmansky, J.M., and Lee, C., 1984, "An Analysis of Coal and Geologic Variables Related to Coal Workers' Pneumoconiosis," Proceedings of the Coal Mine Dust Conference, West Virginia University, Morgantown, West Virginia, pp. 235-249.
- Rubow, K.L., et al., 1985, "A Personal Cascade Impactor: Design, Evaluation and Calibration," Publication No. 469, Particle Technology Lab, University of Minnesota, Minneapolis, April.



# Statistical Analysis of the Elemental Characteristics of Airborne Coal Mine Dust

C. Lee and J. M. Mutmansky

Department of Mineral Engineering, The Pennsylvania State University

This paper outlines some of the work associated with a research study into the relationship between the characteristics of coal mine dust and the incidence of coal workers' pneumoconiosis (CWP). The project involves study of the chemical, mineralogical, and morphological characteristics of the dust. Early stages of the study have dealt primarily with the size analysis and elemental composition of airborne dust in continuous miner sections. This paper outlines the procedures and findings of the elemental analysis portion of the study.

Most of the previous elemental analyses of coal were made available in the quest for information on the combustibility of coal dust or on causal agents and prevalence of CWP. However, no extensive studies have been performed to date, primarily due to the limitations of the analytical methods. A review of the analytical methods for elemental characterization of coal and coal dust particles is presented. The comparisons are made based on the sample mass required, the sample preparation required, the destructivity of the test, and the capability of providing an easy multi-element analysis. The reasons for selecting the proton-induced x-ray emission spectroscopy (PIXE) method are outlined.

The PIXE method was applied to both the airborne coal mine dust and channel samples collected from seven continuous miner sections in six different mines. Channel samples of the coal, roof and floor were collected and analyzed. Airborne dust sampling was performed using multi-stage cascade impactors and permissible 2.0 l/min pumps. Sampler locations were fixed in the sections with respect to the continuous miner and roof bolter or with respect to the intake and return airways. Sampling times varied from 45 minutes to 6 hours, depending on the dust concentration.

The statistical analysis of the resulting elemental data is presented. Of particular importance are the analyses of the variation of elemental composition with size and the variation in elemental composition over the working section. One interesting finding is outlined showing the multivariate statistical analysis of the trace elements and its implications in the identification of the dust sources. The paper concludes with an analysis of the ramifications of the elemental data to related medical studies.

## Introduction

The significance of coal mine dust in the development of coal workers' pneumoconiosis has long been recognized. As a result, various medical and environmental studies have been carried out in order to identify the variables of coal mine dust that are related to CWP. These studies have revealed that a wide variation in the incidence of CWP exists from coalfield to coalfield, opening the door to a number of hypotheses. Most of these hypotheses deal with geologic variables such as coal rank, organic structure of the coal and the mineral and elemental characteristics of the coal and the surrounding geologic sediments.

Although many epidemiological studies indicate that a significant positive correlation exists between the incidence of CWP and the rank of coal mined, many researchers feel that the rank is not the causal variable. Criticism of the "rank cause" hypothesis is largely centered around the possible synergistic effects of other variables and the questionable representativeness of the samples of coal workers studied. This question and the effects of free silica have drawn considerable attention from many researchers.<sup>(1)</sup>

Additional studies of the characterization of coal, coal mine airborne dust, and dust from deceased miners' lungs have showed the possible association of the elemental composition of coal to the development of CWP. Concentration of some elements have been found to vary significantly in different coalfields.<sup>(2,3)</sup> Additionally, other studies have also related the significant differences in elemental compositions with the incidence and progression of CWP.<sup>(4-7)</sup> This led to a study by the authors on the elemental composition and rank of coal in three Pennsylvania coalfields. The results showed that elemental composition varied significantly with rank and that a successful discriminant analysis was possible using the elemental compositions as a basis for the discrimination.<sup>(8)</sup>

The primary objective of this paper is to carry the study of elemental characteristics one step further by the systematic study of airborne coal mine dusts in continuous miner sections. The overall study involves determining the elemental, mineralogical, and physical characteristics of the dust but only the elemental compositions of the dust will be analyzed here. The work involves analysis of the elemental

composition of the dust as a function of its size, its location in the mining section and its association with the materials being mined. The ultimate purpose for this work is to identify dust characteristics that are worthy of further study by medical personnel.

### Sample Collection

In assessing the sample collection possibilities, one major concern was the necessity for determining the properties of dust as a function of the size. The second major concern was the ability to classify the particles by aerodynamic diameter with a minimum of handling or alteration. In addition, the ability to utilize permissible pumps and a reasonably small sampler size was very desirable. As a result, Sierra Model 298 eight-stage cascade impactors were used, powered by Dupont Model P2500A pumps. The pumps and samplers were first tested in an aerosol chamber for proper sampling times as a function of dust concentration and in a simulated mine tunnel to determine whether isokinetic inlets were necessary (they were not).

A standardized sampling scheme was established and applied to all the mining sections sampled. In the sections employing a double-split ventilation scheme, mine sampling locations were selected to study the effects of different dust sources and the locational variability. One sampler was placed in the intake airway, outby the effects of section activity. Two samplers were assigned to the primary dust sources, the continuous miner and the roof bolter. One of these samplers was placed in the air of the immediate intake of the machine and the other was placed in the immediate return air. Two additional samplers were used in each return airway of the two machines, one at two blocks outby the pertinent machine. In a single-split ventilation plan, it was not possible to differentiate between the returns of the bolter and the miner. As a result, only two samples were placed in the return airway, one at two blocks and one at four blocks outby the closest machine.

During the sampling operation, all samplers were fixed relative to the face equipment. As a result, the samplers were moved each time an equipment face change occurred. In addition to airborne dust samples, channel samples were taken as close as possible to the continuous miner location. These were used to correlate the coal and airborne dust properties. More complete details on the sampling scheme can be found elsewhere.<sup>(9)</sup>

### The Elemental Analysis Method

Among the variety of elemental analysis methods, only a few are applicable to the elemental characterization of coal mine dust. An optical method, emission spectroscopy, has been used for the analysis of heavy metals in coal dust found in miners' lung tissue.<sup>(10,11)</sup> Spark source mass spectroscopy and the neutron activation method have been applied to respirable coal mine dust samples gathered from a mine atmosphere.<sup>(12,13)</sup> Finally, the atomic absorption method has been used with application both to coal mine dust and to coal dust in lung tissue.<sup>(11,13,14)</sup>

In selecting an elemental analysis method for airborne coal mine dust collected by cascade impactors, the most

restrictive requirement was the ability to perform the analysis at a relatively low cost on very small samples. Typically, the weight of the dust sample from a properly loaded stage of an impactor is usually in the range of 0.05 to 1.0 mg while the backup filter possesses a sample of about 0.01 mg. Furthermore, except on the backup filter, a sample on each stage is divided into six or twelve submasses. Therefore, the analytical method must be capable of performing multi-element analysis on an extremely small weight of sample. Another crucial requirement in the project was that the dust samples were needed intact for later mineralogical and morphological analysis. Thus, methods requiring ashing or chemical treatments of the samples were excluded.

Our literature research indicated that a non-destructive analytical method that can perform rapid multi-element analysis of extremely small samples at nanogram sensitivity had been applied to atmospheric samples collected by cascade impactors.<sup>(15,16)</sup> This method, proton-induced x-ray emission (PIXE) spectroscopy, uses a proton beam for excitation of the atoms of a sample prepared as a thin layer (usually a thickness of less than 5 mg/cm<sup>2</sup>). Matrix absorption of characteristic x-rays is known to be negligible in this range of thickness. In our case, the thickness of samples on the substrates of the cascade impactors has consistently been smaller than this value and thus thin-sample PIXE analysis is applicable. One advantage of the PIXE method is that the variables related to the characteristic x-ray yield are known or can be experimentally determined.<sup>(17)</sup> Therefore, it is an absolute method that does not require standard samples. The PIXE method can also be applied to thick samples if they are in standard pellet form so that compensation for the absorbed x-rays can be made.<sup>(18)</sup> Therefore, the PIXE method was applicable to channel samples if the sample was crushed, blended, ground to 200 mesh, and pressed into pellets. As a result, both channel and aerosol samples were analyzed by the PIXE method in this project. The samples were prepared by project personnel and sent to a commercial lab for analysis.

### Application to Impactor Sample

In the PIXE method, the analytical instrument was capable of generating a proton beam of up to 5/8-inch diameter. As a result, the beam is capable of irradiating only one dust submass at a time. In analyzing substrates from a multi-stage impactor, the large number of substrates and submasses involved can result in very large analysis costs. As a result, the investigators decided to limit the number of substrates to which the elemental analysis procedure was applied. In choosing selected substrates, it was decided to utilize substrates that are normally loaded to an appropriate level and to span both the respirable and nonrespirable size ranges. This led us to choose the third-stage (10 to 15  $\mu$ m), fifth-stage (3.5 to 6  $\mu$ m), and seventh-stage (0.9 to 2  $\mu$ m) substrates for analysis. Before deciding the number of submasses to be analyzed per substrate, a statistical analysis of the submass variation was conducted.

The entire dust mass on any given substrate can be analyzed using six irradiations of the proton beam. As a measure of the variation in any given irradiation on a substrate, the coefficient of variation (CV) in the weight per-

**THE RESPIRABLE DUST CENTER**

centage of the elements on a given substrate was determined. The airborne dust collected in the immediate return of the continuous miner in a development section was used for this purpose. When considering the major elements (Mg, Al, Si, P, S, K, Ca, Ti and Fe), the CVs were relatively small on the third and fifth stages of the impactor with most CVs being less than 20 percent. On the seventh stage, the CVs were higher relative to the upper stages with most values being less than 50 percent. Submass-to-submass variation of the trace elements was much higher with numerous CVs above 100 percent. However, most of the trace elements with CVs greater than 100 percent had extremely low concentrations, usually less than 1 ppm by weight. This clearly leads to higher variations because some elements will be recorded as non-

existent if their concentrations fall below the detection limit. As in the major elements, the submass-to-submass variation increased in the lower stages.

In addition to the relatively small variance in the data, one also obtains a strong feeling for the stability in values of the non-organic portion of the dust by studying the ratios of the major element weight percentages to that of silicon. Using this procedure, the analysis from each dust submass on a given substrate shows a remarkable resemblance as a result of the fact that the effects of the organic elements are removed. As a result of these results, it was decided by the investigators that two submasses from each substrate would be appropriate for analysis by the PIXE method.

**TABLE I**  
**Effects of Size on the Major Element Composition**

Elements <sup>(1)</sup>	Comparison <sup>(2)</sup>	Stage/Mean <sup>(3)</sup>
Sampling Location: CI (intake of continuous miner)		
SI	5,3 > 3,7	5/ 55.676, 3/ 41.517, 7/ 9.513
S	3,5 > 7	3/ 16.850, 5/ 13.288, 7/ 6.102
Ca	3,5 > 5,7	3/ 83.128, 5/ 46.313, 7/ 5.333
Ti	3,5 > 7	3/ 2.274, 5/ 1.567, 7/ 0.202
Fe	3 > 5,7	3/ 36.981, 5/ 14.616, 7/ 2.533
MONOVA Test		
Wilks' Lambda = 0.036	F(128,366) = 1.68	Pr > F = 0.0001
Pillai's Trace = 2.526	F(128,448) = 1.61	Pr > F = 0.0002
Sampling Location: CR (immediate return of continuous miner)		
Al	3 > 5 > 7	3/ 52.123, 5/ 30.384, 7/ 10.208
Si	3 > 5 > 7	3/ 92.256, 5/ 47.916, 7/ 14.394
P	7 > 5,3	7/ 2.090, 5/ 1.116, 3/ 1.000
S	3 > 5,7	3/ 16.538, 5/ 9.247, 7/ 6.545
K	3 > 5,7	3/ 8.939, 5/ 5.608, 7/ 3.593
Ca	3,5 > 5,7	3/ 31.507, 5/ 19.325, 7/ 6.108
Ti	3 > 5 > 7	3/ 4.391, 5/ 2.299, 7/ 0.496
Fe	3,5 > 7	3/ 19.223, 5/ 14.696, 7/ 3.040
Wilks' Lambda = 0.183	F ( 18, 92) = 6.84	Pr > F = 0.0001
Pillai's Trace = 0.987	F ( 18, 94) = 5.09	Pr > F = 0.0001
Sampling Location: RI (intake of the roof bolter)		
Al	5,3 > 7	5/ 66.296, 3/ 58.844, 7/ 17.022
Si	5,3 > 7	5/120.350, 3/116.320, 7/ 22.400
S	3 > 5 > 7	3/ 21.693, 5/ 12.183, 7/ 5.302
Ca	3,5 > 5,7	3/ 31.078, 5/ 21.509, 7/ 4.815
Wilks' Lambda = 0.106	F ( 18, 26) = 2.99	Pr > F = 0.0055
Pillai's Trace = 1.267	F ( 18, 28) = 2.69	Pr > F = 0.0093
Sampling Location: RR (immediate return of the roof bolter)		
Mg	3,5 > 5,7	3/ 2.947, 5/ 1.517, 7/ 0.574
Al	3 > 5 > 7	3/ 61.936, 5/ 41.807, 7/ 15.187
Si	3 > 5 > 7	3/113.760, 5/ 72.140, 3/ 22.070
S	3 > 5,7	3/ 19.137, 5/ 8.242, 7/ 6.397
K	3 > 5,7	3/ 14.989, 5/ 9.953, 7/ 3.323
Ca	3 > 5,7	3/ 43.562, 5/ 20.357, 7/ 5.590
Ti	3,5 > 7	3/ 4.041, 5/ 2.802, 7/ 0.799
Fe	3,5 > 7	3/ 36.894, 5/ 24.860, 7/ 6.639
Wilks' Lambda = 0.101	F ( 18, 50) = 5.95	Pr > F = 0.0001
Pillai's Trace = 1.269	F ( 18, 52) = 5.02	Pr > F = 0.0001

# STATISTICAL ANALYSIS

## TABLE I (Continued)

Elements <sup>(1)</sup>	Comparison <sup>(2)</sup>	Stage/Mean <sup>(3)</sup>
Sampling Location: 2X (two crosscuts outby the face operations)		
Mg	3,5 > 5,7	3/ 1.673, 5/ 1.199, 7/ 0.294
Al	3,5 > 7	3/ 47.591, 5/ 36.000, 7/ 9.310
Si	3,5 > 7	3/ 80.187, 5/ 58.695, 7/ 13.814
S	3 > 5,7	3/ 30.219, 5/ 18.714, 7/ 7.595
K	3,5 > 7	3/ 10.292, 5/ 8.322, 7/ 1.945
Ca	3 > 5,7	3/ 42.408, 5/ 14.579, 7/ 5.182
Ti	3,5 > 7	3/ 5.626, 5/ 4.099, 7/ 0.600
Wilks' Lambda = 0.089	F ( 18, 38) = 4.96	Pr > F = 0.0001
Pillai's Trace = 1.370	F ( 18, 40) = 4.83	Pr > F = 0.0001
Sampling Location: 4X (four crosscuts outby the face operations)		
Al	5,3 > 7	5/ 35.579, 3/ 31.965, 7/ 8.143
Si	5,3 > 7	5/ 57.216, 3/ 54.495, 7/ 11.305
S	3,5 > 7	3/ 19.045, 5/ 17.081, 7/ 6.877
K	5,3 > 7	5/ 7.710, 3/ 7.249, 7/ 1.546
Ca	3 > 5,7	3/ 37.649, 5/ 17.557, 7/ 4.436
Ti	3,5 > 7	3/ 3.234, 5/ 2.983, 7/ 0.410
Fe	3,5 > 5,7	3/ 52.753, 5/ 26.702, 7/ 2.749
Wilks' Lambda = 0.010	F ( 18, 26) = 12.57	Pr > F = 0.0001
Pillai's Trace = 1.329	F ( 18, 28) = 3.08	Pr > F = 0.0037

**Notes:**

- (1) Only the elements showing significant size effects at an alpha risk of 5 percent by ANOVA are listed.
- (2) Comparisons are based upon the multiple F-test, REGW. Stages connected by a comma indicate no significant difference between them.
- (3) The unit for the mean values is 102 x percent by weight.

### Results of Field Studies

Data for the elemental composition studies reported here were collected in seven different continuous miner sections located in six bituminous coal mines in Pennsylvania. Five of the seven sections sampled in this portion of the study were using single-split ventilation schemes. As a result, return airway samples associated with the miner and bolter operations are not differentiated. The elemental data used in the paper are relative values expressed as weight percentages. Because of the volume of data (over 7000 values of elemental weight percentages), the data is not presented here. However, the complete data set will be available through the Generic Technology Center for Respirable Dust at The Pennsylvania State University. The study results reported here are confined to the topics of relating the elemental compositions to the size of the dust, the location of the samplers in the mine layout, and the materials being cut.

#### Size Dependency of Elemental Compositions

The size dependency of the elemental composition characteristics of airborne coal mine dust was tested using standard univariate and multivariate statistical methods. At each sampling location, a multiple F-test known as the Ryan-Einot-Gabriel-Welsch (REGW) test was performed along with the analysis of variance (ANOVA) procedure to com-

pare the concentrations of the individual elements in the three size fractions that were analyzed. Then, taking into account the correlation structure among the elements, the multivariate analysis of variance (MANOVA) procedure was applied to test the significance of the differences in the overall elemental compositions of the dust samples in the three size fractions. In all of these statistical tests, the trace elements were analyzed separately from the major elements.

Tables I and II contain the elements that showed a significant size dependency at an alpha value (level of significance) of 5 percent and the results of the equality tests by the multiple F-test at each of the sampling locations. Also included are results of the MANOVA for significance of the differences in the centroids of the 9 major element and the 21 trace elements for the three different size fractions.

As shown in Table I, airborne coal mine dust samples from all the sampling locations show significant size effects in the overall composition of the major elements; however, samples from the immediate return of the bolter operation have a relatively weak size dependency compared to the other sampling locations. Significant size dependency is observed in the two elements most common in the clay minerals, Al and Si, at all locations except at the intake of the miner. In the samples from the immediate returns of the miner and bolter operations, these two elements show their highest concentrations on the third stage, while no sig-

**THE RESPIRABLE DUST CENTER**

**TABLE II**  
**Effects of Size on the Trace Element Compositions**

Elements <sup>(1)</sup>	Comparison <sup>(2)</sup>	Stage/Mean <sup>(3)</sup>
Sampling Location: CI		
Mn	3,5 > 7	3/ 0.319, 3/ 0.152, 7/ 0.029
Ni	3 > 5,7	3/ 0.132, 5/ 0.024, 7/ 0.007
Br	3 > 5,7	3/ 0.105, 5/ 0.035, 3/ 0.006
Sr	3 > 5,7	3/ 0.447, 3/ 0.123, 7/ 0.017
Zr	3 > 5,7	3/ 0.194, 5/ 0.033, 7/ 0.013
MANOVA Test		
Wilks' Lambda = 0.060	F ( 32, 24) = 2.31	Pr > F = 0.0185
Pillai's Trace = 1.307	F ( 32, 26) = 1.31	Pr > F = 0.1336
Sampling Location: CR		
Cl	3 > 5,7	3/ 2.433, 3/ 1.298, 7/ 0.795
V	3 > 5 > 7	3/ 0.137, 5/ 0.079, 7/ 0.002
Cr	3,5 > 7	3/ 0.081, 5/ 0.059, 3/ 0.008
Ni	3,5 > 7	3/ 0.037, 3/ 0.036, 7/ 0.008
Br	3,5 > 7	3/ 0.074, 5/ 0.038, 7/ 0.022
Rb	3,5 > 7	3/ 0.101, 5/ 0.068, 7/ 0.024
Sr	3 > 5 > 7	3/ 0.248, 5/ 0.130, 7/ 0.021
Zr	3 > 5 > 7	3/ 0.120, 5/ 0.066, 7/ 0.023
Mo	3 > 5,7	3/ 0.044, 5/ 0.007, 7/ 0.003
Pb	3,5 > 7	3/ 0.078, 5/ 0.049, 7/ 0.011
Wilks' Lambda = 0.215F ( 32, 78) = 2.81Pr > F = 0.0001		
Pillai's Trace = 1.045	F ( 32, 80) = 2.74	Pr > F = 0.0001
Sampling Location: RI		
None of the elements shows significant variation among the three different size fractions.		
Sampling Location: RR		
V	3 > 5,7	3/ 0.148, 5/ 0.068, 7/ 0.005
Mn	3,5 > 7	3/ 0.394, 5/ 0.281, 3/ 0.084
Ge	7 > 3,5	7/ 0.002, 3/ 0.000, 5/ 0.000
Br	3,5 > 5,7	3/ 0.049, 5/ 0.035, 7/ 0.021
Rb	3,5 > 5,7	3/ 0.201, 5/ 0.120, 7/ 0.027
Sr	3 > 5 > 7	3/ 0.213, 5/ 0.125, 7/ 0.036
Zr	5,3 > 7	3/ 0.121, 5/ 0.109, 7/ 0.024
Pb	3 > 5,7	3/ 0.176, 5/ 0.099, 7/ 0.038
Wilks' Lambda = 0.135		
Pillai's Trace = 1.242	F ( 32, 36) = 1.94	Pr > F = 0.0279
	F ( 32, 38) = 1.95	Pr > F = 0.0250
Sampling Location: 2x		
Cl	3 > 5 > 7	3/ 2.892, 5/ 1.685, 7/ 0.547
Cu	3,5 > 5,7	3/ 0.678, 5/ 0.442, 3/ 0.067
Sr	3 > 5,7	3/ 0.700, 5/ 0.196, 7/ 0.019
Wilks' Lambda = 0.037		
Pillai's Trace = 1.586	F ( 32, 24) = 3.17	Pr > F = 0.0023
	F ( 32, 26) = 3.11	Pr > F = 0.0020
Sampling Location: 4x		
Cl	5,3 > 3,7	5/ 2.304, 3/ 1.766, 7/ 0.650
V	5,3 > 3,7	5/ 0.075, 3/ 0.038, 7/ 0.003
Cr	5,3 > 7	5/ 0.093, 3/ 0.060, 7/ 0.013
Mn	3,5 > 5,7	3/ 0.449, 5/ 0.229, 7/ 0.022
Ni	3,5 > 5,7	3/ 0.109, 5/ 0.056, 7/ 0.011
Zn	3 > 5,7	3/ 6.852, 5/ 1.373, 7/ 0.622
Sr	3 > 5,7	3/ 0.360, 5/ 0.157, 7/ 0.016
Pb	3,5 > 7	3/ 0.286, 5/ 0.238, 7/ 0.012
Wilks' Lambda = 0.002		
Pillai's Trace = 1.780	F ( 32, 12) = 8.21	Pr > F = 0.0002
	F ( 32, 14) = 3.53	Pr > F = 0.0075

Notes: See the Notes for Table I.

## STATISTICAL ANALYSIS

nificant difference is observed between the third and fifth stages at the other sampling locations. Major elements showing a significant size dependency at all the locations are Si, S, and Ca.

A noticeable difference between the immediate return samples of the miner and bolter operations is that Mg, a major element in rock dust, shows a size dependency only in the return of the roof bolter. A size dependency of Mg is also found at two crosscuts outby the face operation but disappears at four crosscuts outby. An increase in the number of major elements showing size dependency can be seen in the returns of the miner and bolter operations compared to that in their intakes. Concentrations of many of the major elements do not show significant differences between the third and fifth stages, but those on the seventh stage are smaller.

The element P, which shows significant size effects in the samples from the immediate return of the miner is the only element that shows its highest concentration on the seventh stage.

In Table II, where trace element statistical results are shown, the MANOVA test results indicate no significant difference in the overall trace element compositions in the intake airways of the miner and bolter operations. However, the trace element compositions showed significant size dependency in the immediate return of the miner with a less significant size dependency detected in the immediate return of the bolter. Parallel to that for the major elements, the immediate return of the miner shows the most significant size dependencies in the trace element compositions as well as the largest number of elements showing size dependency.

**TABLE III**

**ANOVA Tests for Locational Variability of the Total Weight Fractions of the Major and Trace elements and Organic Component**

Variables	Comparison <sup>(1)</sup>	Location/Mean <sup>(2)</sup>
<b>On the Third Stage (10-15 <math>\mu</math>m)</b>		
Major Elements	no difference	
Trace Elements	IN > the other locations	IN/ 35.261 2X/ 13.183 4X/ 11.180 CI/ 8.830 RR/ 4.795 RI/ 4.673 CR/ 4.337
Organic Fraction	no difference	
<b>On the Fifth Stage (3.5-6 <math>\mu</math>m)</b>		
Major Elements	IN, RI > RI, RR 2X, CI, 4X, CR	IN/510.370 RI/304.400 RR/182.710 2X/180.500 CI/172.370 4X/167.110 CR/131.120
Trace Elements	IN > the other locations	IN/ 30.905 2X/ 6.686 RI/ 6.288 4X/ 5.362 CI/ 5.107 RR/ 3.486 CR/ 2.888
Organic Fraction	CR, 4X, CI, RR, 2X, RI RI, IN	CR/ 98.660 4X/ 98.275 CI/ 98.225 RR/ 98.138 2X/ 98.128 RI/ 96.893 IN/ 94.587
<b>On the Seventh Stage (0.9-2 <math>\mu</math>m)</b>		
Major Elements	RR, RI, CR, 2x CR, 2X, 4X, IN, CI	RR/ 62.349 RI/ 62.075 CR/ 47.205 2x/ 45.551 4X/ 37.579 IN/ 33.538 CI/ 33.270
Trace Elements	No difference	
Organic Fraction	CI, IN, 4X, 2X, CR 2X, CR, RI, RR	CI/ 99.649 IN/ 99.645 4X/ 99.610 2X/ 99.527 CR/ 99.511 RI/ 99.365 RR/ 99.360

Notes:

(1) Comparisons are made based upon the multiple F-test, REGW. Locations connected by a comma indicate no significant difference between them.

(2) The unit is 102 x percent by weight except in the organic component; percent by weight for the organic component.

**THE RESPIRABLE DUST CENTER**

In general, the samples associated with the bolter indicate the weakest size effects among the trace elements. V, Br, Rb, Sr and Zr indicate significant size dependency in the immediate returns of the miner and bolter while the concentrations of Cl, Cr, Ni and Mo vary with size only in the immediate return of the miner operation. In the size dependencies shown for the trace elements, all had lower concentrations in the finer size ranges.

It should be mentioned that all the elements below Na in the periodic table are not analyzed by the PIXE method. Most of the undetected material will be the organic components of the coal which are predominantly composed of C, H and O. Therefore, the weight fraction of the airborne

coal mine dust sample other than that of the major and minor elements detected has been designated as the organic fraction in this paper. As shown in Table III, the organic fraction shows its highest concentrations in the size range of 0.9 to 2 um at all the sampling locations. This indicates that this size range is made up of more organic material than the other coarser size ranges.

One additional comment concerning the elemental composition and its relationship to the size is the general trend observed. The concentrations of most of the elements detected by the PIXE method were higher in the coarser size ranges. This led the investigators to question whether the PIXE method was providing weight percentages of the ele-

**TABLE IV**  
**MANOVA Tests for Locational Variation of the Major Element Composition**

Elements <sup>(1)</sup>	Comparison <sup>(2)</sup>	Location/Mean <sup>(3)</sup>
On the Third Stage (10-15 um)		
P	IN > the other locations	IN/ 36.921 CI/ 2.200 RR/ 2.110 RI/ 1.666 4X/ 1.650 2X/ 1.563 CR/ 1.000
S	IN > the other locations	IN/140.880 2X/ 30.220 RI/ 21.690 RR/ 19.140 4X/ 19.050 CI/ 16.850 CR/ 16.54
K	RI, RR, 2X, CR > RR, 2X, CR, 4X > 2X, CR, 4X, CI, IN	RI/ 17.182 RR/ 14.989 2X/ 10.292 CR/ 8.938 4X/ 7.248 CI/ 4.673 IN/ 0.894
MANOVA Test		
Wilks' Lambda = 0.122	F (54, 300) = 2.84	Prob > F = 0.0001
Pillai's Trace = 1.632	F (54, 378) = 2.62	Prob > F = 0.0001
On the Fifth Stage (3,5-6 um)		
Mg	RI, CI, RR, 2X, 4X, CR, CI, RR, 2X 2X, 4X, CR, IN	RI/ 3.694 CI/ 2.693 RR/ 1.517 2X/ 1.199 4X/ 0.939 CR/ 0.532 IN/ 0.000
Si	IN, RI, RR, RI, RR, 2X, 4X, CI, CR	IN/130.290 RI/120.350 RR/ 72.140 2X/ 58.700 4X/ 57.220 CI/ 55.680 CR/ 47.920
P	IN > the other locations	IN/ 22.672 CI/ 2.815 4X/ 1.346 RI/ 1.340 2X/ 1.124 CR/ 1.116 RR/ 8.240
S	IN > the other locations	IN/129.400 2X/ 18.710 4X/ 17.080 CI/ 13.290 RI/ 12.180 CR/ 9.250 RR/ 1.029
K	RI, RR > RR, 2X, 4X, CI, IN, CR	RI/ 18.939 RR/ 9.953 2X/ 8.322 4X/ 7.710 CI/ 7.000 IN/ 6.239 CR/ 5.608
Ca	IN, CI, CI, RI, RR, CR, 4X, 2X	IN/ 78.123 CI/ 46.313 RI/ 21.509 RR/ 20.357 CR/ 19.325 4X/ 17.557 2X/ 14.579
Fe	IN, RI, 2X, 4X RR, RI, 2X, 4X, RR, CR, CI	IN/ 78.334 RI/ 54.023 2X/ 37.764 4X/ 26.702 RR/ 24.860 CR/ 14.696 CI/ 14.616
Wilks' Lambda = 0.048	F (54, 300) = 4.52	Prob > F = 0.0001
Pillai's Trace = 1.878	F (54, 378) = 3.19	Prob > F = 0.0001

STATISTICAL ANALYSIS

TABLE IV (Continued)

Elements(1)	Comparison(2)	Location/Mean(3)
On the Seventh Stage (0.9-2 um)		
Al	RI, RR, CR > RR, CR, 2X, 4X CR, 2X, 4X, CI, IN	RI/ 17.022 RR/ 15.187 CR/ 10.208 2X/ 9.310 4X/ 8.143 CI/ 5.896 IN/ 3.751
Si	RI, RR > RR, CR 2X, 4X, CI, IN IN/ 7.768	RI/ 22.399 RR/ 22.072 CR/ 14.394 2X/ 13.814 4X/ 11.305 CI/ 9.513
Fe	RR, 2X, RI, IN > 2X, RI, IN, CR, 4X, CI	RR/ 6.639 2X/ 5.138 RI/ 4.133 IN/ 3.436 CR/ 3.040 4X/ 2.749 CI/ 2.533
MANOVA Test		
Wilks' Lambda = 0.234	F (54, 300) = 1.83	Prob > F = 0.0009
Pillai's Trace = 1.131	F (54, 378) = 1.63	Prob > F = 0.0053

Notes:

- (1) This column contains the elements showing significant locational variability at an alpha risk of 5 percent by ANOVA
- (2) Comparisons are made based upon the multiple F-test, REGW. All the locations connected by commas indicate no significant difference between them.
- (3) The unit for the means is 102 x percent by weight.

ments that were dependent upon the total weight on each substrate or whether the weights were biasing the results. To answer this question, correlations between the weight percentages of the elements and the sample weights was tested in the course of this study. Considering the result that none of the elements showed a significant positive correlation, it does not seem that the size dependency of elemental compositions observed in this study is due to the lack of sensitivity of the PIXE method or bias related to the sample weight.

Variation With Section Location

In assessing the variation in elemental composition with the section location, a similar suite of statistical procedures was used but stepwise discriminant analysis was used in addition to identify those elements that provide a significant contribution to the locational variability. The tests were performed separately on the dust samples from the three different size fractions.

As shown in Table IV, the major element compositions in all three size ranges show significant differences among the seven different sampling locations. In the size range of 10 to 15 um, concentrations of P, S and K vary significantly over the various locations according to the MANOVA tests as well as the stepwise discriminant analysis which is summarized in Table V. These three elements show the highest concentrations in the intake air while the immediate return of the miner operation appears to contain the lowest levels even though the differences among the locations other than the intake airways are not statistically significant.

In the size range from 3.5 to 6 um, Si and K show significant locational variation and have their highest concentrations near the roof bolter operation. In addition, Ca shows a significant locational variation in this size range with

the most enriched values occurring in the intake air. Because Ca occurs in abundance in rock dust, this occurrence may be due to rock dust being reentrained in the intake air stream. In the finest size range from 0.9 to 2 um, Al and Si show much higher concentrations near the miner and bolter and are significantly enriched near the bolter. This is hypothesized to be a result of the minerals present in the roof rock. As shown in Table IV, locational variation of the total weight percentages of the 9 major elements are not statistically significant in the 10 to 15 um range; however, the differences become significant in the finer size ranges. In general, the pattern that exists is that the higher weight percentage of the major elements are associated with the bolter operation in the minus 6 um range of dust size.

Table VI indicates significant locational variation of the overall compositions of the trace elements in all three size ranges. In the size range of 10 to 15 um, V, Zn and Sr are the trace elements showing significant locational variation. V and Zn are highly enriched near the face operations and in the intake airway, respectively, while Sr shows less concentration near the face. In the size range of 3.5 to 6 um, Cl, As and Rb indicate significant locational variation. Rb shows higher concentrations near the roof bolter operation, while Cl and As have lower concentrations near the face operations. In the finest size range of 0.9 to 2 um, the element As has higher concentrations in the return airway, while Br and Mo are enriched near the face operations and roof bolter, respectively. In terms of the total weight percentages of the trace elements, the intake airway shows the highest values in the size range above 3.5 um, while locational variation is not significant in the size range of 0.9 to 2 um. As shown in Table VII, in the size range below 6 um, sampling locations near the miner operation contain significantly higher organic



## THE RESPIRABLE DUST CENTER

fractions compared to the bolter operation. However, the differences are not significant in the size range of 10 to 15  $\mu$ m.

### *Effects of Geologic Materials Mined on the Elemental Composition*

Effects of the materials being cut on the elemental characteristics of airborne coal mine dust can be studied by measuring the similarity in characteristics between them. The similarity can be quantified through the coefficient of proportional similarity which is the cosine of the angle between the two vectors of the overall elemental compositions in the n-space of the n compositions being considered. For example, the elemental composition of the dust samples in

each size fraction from the impactor in the immediate return of the miner can be compared with that of the channel samples taken at the working face. If numerous types of geologic material (bottom rock, coal, rock parting, bony coal, roof rock) are separately sampled, then the elemental characteristics of each geologic material may be tested for similarity with the airborne dust. Only a summary of the findings are discussed in this section. A detailed description of the study and analyses of the results will be available in another paper being prepared by the authors.

As a general conclusion, it can be said that the major element compositions of the dust samples from the immediate return of the miner operation are very closely associated with the coal seam, regardless of the size range of airborne dust

**TABLE V**

**Stepwise Discriminant Analysis for Locational Variability of the Major and Trace Elements**

Step	Selected <sup>(1)</sup> Elements	F Statistic	Prob > F	Wilk's Lambda	Prob > Wilk's Lambda
<b>For the Major Elements</b>					
<b>On the Third Stage (10-15 <math>\mu</math>m)</b>					
1	P	5.363	0.0001	0.672	0.0001
2	K	4.845	0.0004	0.464	0.0000
3	Si	3.958	0.0020	0.339	0.0000
4	S	3.551	0.0043	0.253	0.0000
5	Ca	3.186	0.0086	0.193	0.0000
<b>On the Fifth Stage (3.5 - 6 <math>\mu</math>m)</b>					
1	K	3.679	0.0033	0.475	0.0000
2	Si	5.628	0.0001	0.311	0.0000
3	Al	15.359	0.0001	0.126	0.0000
4	Ti	3.445	0.0053	0.105	0.0000
5	Ca	2.747	0.0197	0.083	0.0000
<b>On the Seventh Stage (0.9 - 2 <math>\mu</math>m)</b>					
1	Si	6.691	0.0001	0.622	0.0000
2	Mg	2.320	0.0432	0.512	0.0000
3	Al	2.195	0.0548	0.425	0.0000
<b>For the Trace Elements</b>					
<b>On the Third Stage (10-15 <math>\mu</math>m)</b>					
1	Sr	2.834	0.0163	0.594	0.0004
2	V	3.508	0.0046	0.447	0.0000
3	Zn	2.656	0.0232	0.357	0.0000
4	As	1.933	0.0894	0.300	0.0000
5	Mn	1.893	0.0965	0.253	0.0000
6	Ni	3.615	0.0040	0.186	0.0000
<b>On the Fifth Stage (3.5 - 6 <math>\mu</math>m)</b>					
1	Cl	3.617	0.0037	0.753	0.0037
2	As	2.922	0.0138	0.593	0.0004
3	Rb	2.802	0.0175	0.469	0.0000
<b>On the Seventh Stage (0.9 - 2 <math>\mu</math>m)</b>					
1	As	3.811	0.0025	0.743	0.0025
2	Mo	2.811	0.0171	0.590	0.0004
3	Mn	2.384	0.0385	0.482	0.0001
4	Br	2.746	0.0196	0.382	0.0000
5	Cr	2.478	0.0326	0.308	0.0000
6	Cu	1.927	0.0906	0.259	0.0000

Note: The selected elements denote the final selection of elements excluding all the removed elements at an alpha risk of 15 percent.

## STATISTICAL ANALYSIS

samples and presence of noncoal bands in the coal seam. This relationship has been observed in the samples from all seven sections studied in this paper. However, the relationship based upon the trace elements is not consistent. In some sections, the trace element compositions of the dust particles in all three size ranges show high similarities with the coal bands in the seam. In other cases, their close association is

observed only in the fine size range of 0.9 to 2  $\mu$ m, while the noncoal bands show much higher similarities in the other size ranges. The opposite relationship is also observed in other occasions; noncoal bands show much higher similarities with dust samples in the fine size range and, in the coarser size ranges, coal bands indicate higher similarities. These dis-

**TABLE VI**  
**MANOVA Tests for Locational Variation of the Trace Element Composition**

Elements <sup>(1)</sup>	Comparison <sup>(2)</sup>	Location/Mean <sup>(3)</sup>
<b>On the Third Stage (10-15 <math>\mu</math>m)</b>		
Cl	IN > the other locations	IN/ 15.602 2X/ 2.892 CR/ 2.433 CI/ 2.162 4X/ 1.766 RR/ 1.656 RI/ 1.399
V	2X, RR, RI, CR, CI > RR, RI, CR, CI, 4X, IN	2X/ 0.434 RR/ 0.148 RI/ 0.141 CR/ 0.137 CI/ 0.042 4X/ 0.048 IN/ 0.000
Cu	no difference	2Z/ 0.678 CI/ 0.533 RI/ 0.297 IN/ 0.295 4X/ 0.292 RR/ 0.240 CR/ 0.140
Zn	IN > the other locations	IN/ 17.120 4X/ 6.852 CI/ 3.942 2X/ 3.801 RI/ 1.533 RR/ 1.271 CR/ 0.669
Sr	2X, CI, 4X, CR, RR CI, 4X, CR, RR, RI, IN	2X/ 0.700 CI/ 0.447 4X/ 0.360 CR/ 0.248 RR/ 0.213 RI/ 0.154 IN/ 0.014
<b>MANOVA Test</b>		
Wilks' Lambda = 0.089	F (96, 295) = 1.64	Prob > F = 0.0009
Pillai's Trace = 1.899	F (96, 336) = 1.62	Prob > F = 0.0010
<b>On the Fifth Stage (3.5 - 6 <math>\mu</math>m)</b>		
Cl	IN > the other locations	IN/ 12.402 RI/ 2.458 4X/ 2.304 2X/ 1.685 CI/ 1.666 RR/ 1.528 CR/ 1.298
Mn	IN, RI, RR > RI, RR, 2X, 4X, CI, CR	IN/ 0.793 RI/ 0.565 RR/ 0.281 2X/ 0.247 4X/ 0.229 CI/ 0.152 CR/ 0.114
Cu	IN, 2X, CI, RI, 4X > 2X, CI, RI, 4X, CR, RR	IN/ 0.788 2X/ 0.442 CI/ 0.357 RI/ 0.321 4X/ 0.246 CR/ 0.143 RR/ 0.108
As	2X > the other locations	2X/ 0.040 CI/ 0.010 RR/ 0.006 4X/ 0.006 RI/ 0.005 CR/ 0.004 IN/ 0.000
Rb	RI, 2X, RR, 4X > 2X, RR, 4X, CR, CI, IN	RI/ 0.328 2X/ 0.187 RR/ 0.120 4X/ 0.109 CR/ 0.068 CI/ 0.035 IN/ 0.007
Zr	IN, 2X > 2X, RI, 4X, RR, CR, CI	IN/ 0.497 2X/ 0.209 RI/ 0.183 4X/ 0.141 RR/ 0.121 CR/ 0.066 CI/ 0.033
<b>MANOVA Tests on the Fifth Stage</b>		
Wilks' Lambda = 0.037	F (96, 295) = 2.42	Prob > F = 0.0001
Pillai's Trace = 2.400	F (96, 336) = 2.33	Prob > F = 0.0001

crepancies may be due to the differences in the modes of occurrences of the trace elements as minerals or impurities in the organic coal or in the rock materials. However, without any information concerning these characteristics, further explanation cannot be made on the causes of the differences in the trace element compositions of the airborne coal mine dust and the materials being cut

**Summary and Conclusions**

The size dependency of the major and trace elements in airborne coal mine dust was shown to be significant at almost all locations in underground coal mine sections utilizing continuous miners. In general, the size effects were more significant near the miner operation and the immediate return of the face operation indicated higher size dependency than the immediate intake.

The elemental compositions of airborne coal mine dust varied significantly among the various sampling locations. However, the elements showing significant locational variation were different in the different size ranges analyzed. Most of the elements with significant locational variability were found to be enriched near the bolter operation. The organic fraction of airborne coal mine dust was higher in the fine size range of 0.9 to 2  $\mu$ m and near the miner operation.

Concentrations of almost all elements detected by the PIXE method were relatively higher in the coarser size ran-

ges. Statistical tests indicated that this result was not due to bias in the analytical procedure. It is thought that this result is a function of the size of the salts and minerals that are the source of the trace elements.

The major element composition of airborne coal mine dust generated from the face was shown to be very similar to that of the coal seam. However, characterization of the mineral components and study of the occurrence mode of the trace elements are necessary to explain the discrepancies in the relationship of the trace element composition between the airborne coal mine dust and materials being cut a different sections.

As a final point of discussion, it should be mentioned that this study of elemental compositions is a part of a larger and more encompassing study that will consider the mineralogical and morphological characteristics as well. However, this study has proven that airborne coal mine dust is certainly not a homogeneous material. The composition is clearly shown to vary with size, the location in the mine workings, and with the characteristics of the source materials. This has very clear implications in further studies, particularly with regard to the types of coal used in medical studies related to CWP development.

TABLE VI (Continued)

Elements <sup>(1)</sup>	Comparison <sup>(2)</sup>	Location/Mean <sup>(3)</sup>
On the Seventh Stage (0.9 - 2 $\mu$ m)		
MN	no difference	RR/ 0.084 RI/ 0.049 IN/ 0.047 CR/ 0.045 CI/ 0.029 2X/ 0.028 4X/ 0.022
Zn	2X, IN, CI, RR, 4X, CR > CI, RR 4X, CR, RI	2X/ 0.944 IN/ 0.922 CI/ 0.826 RR/ 0.722 4X/ 0.622 CR/ 0.602 RI/ 0.505
As	2X, 4X > 4X, IN, RR, CI, RI, CR	2X/ 0.025 4X/ 0.011 IN/ 0.009 RR/ 0.007 CI/ 0.004 RI/ 0.003 CR/ 0.002
Br	CR, IN, RR, 2X, CI, RI > IN, RR, 2X, CI, RI, 4X	CR/ 0.022 IN/ 0.021 RR/ 0.021 2X/ 0.018 CI/ 0.017 RI/ 0.005 4X/ 0.005
Mo	In, 2X, RR, CI, RI > 2X, RR, CI, RI, CR, 4X	IN/ 0.033 2X/ 0.024 RR/ 0.015 CI/ 0.013 RI/ 0.003 CR/ 0.003 4X/ 0.000

MANOVA Test

Wilks' Lambda = 0.096

Pillai's Trace = 1.798

F(96,295) = 1.58 Prob > F = 0.0021

F(96,336) = 1.50 Prob > F = 0.0049

Notes:

(1) This column contains the elements showing significant locational variability at an alpha risk of 5 percent by ANOVA.

(2) Comparisons are made based upon the multiple F-test, REGW. All the locations connected by comma indicate no significant difference between them.

(3) The mean is in unit of 102 x % by weight.

# STATISTICAL ANALYSIS

## TABLE VII

**Variation in the Total Weight Fractions of the Major and Trace Elements and the Organic Components of Coal Mine Dust**

Sampling Locations	Weight Percentages <sup>(2)</sup>									
	Major Elements			Trace Elements			Organic Components			
	Stage <sup>(1)</sup>	3	5	7	3	5	7	3	5	7
IN <sup>(3)</sup>		485.31/	510.37/	33.54	35.26/	30.91/	1.98	94.79/	94.59/	99.65
CI		213.14/	172.37/	33.27	8.83/	5.11/	1.93	97.78/	98.23/	99.65
CR		227.16/	131.03/	47.21	4.34/	2.89/	1.65	97.69/	98.66/	99.51
RI		286.51/	304.40/	62.08	4.67/	6.29/	1.40	97.09/	96.89/	99.37
RR		299.38/	182.71/	62.35	4.80/	3.49/	1.60	98.21/	98.14/	99.36
2X		387.19/	180.50/	45.55	13.18/	6.69/	1.78	96.00/	98.13/	99.53
4X		209.93/	167.11/	37.58	11.18/	5.36/	1.46	97.79/	98.28/	99.61

Notes:

(1) The columns headed by 3, 5 and 7 indicate the weight percentages on the third, fifth and seventh stages in the cascade impactors.

(2) The unit for the major and trace elements is 102 x percent by weight, percent by weight for the organic components.

(3) See Table I for identification of sampling location codes.

### Acknowledgment

This research has been supported by the Department of the Interior's Mineral Institute program administered by the Bureau of Mines through the Generic Mineral Technology Center for Respirable Dust under grant number G1135142.

### References

- Hamilton, R.J.: *Industrial Health and Safety*. A synthesis report on research supported by the Commission of the European Community during the period 1977-82, Luxembourg (1985).
- O'Gorman, J.V.: *Studies on Mineral Matter and Trace Elements in North American Coals*. Unpublished Ph.D. Thesis, The Pennsylvania State University, University Park, PA (1971).
- Glick, D.C.: *Variability in the Inorganic Content of United States' Coals*, A Multivariate Statistical Study. Unpublished M.S. Thesis, The Pennsylvania State University, University Park, PA (1984).
- Carlberg, J.R., J.V. Crable, L.P. Limhaco et al: *Total Dust, Coal, Free Silica, and Trace Metal Concentrations in Bituminous Coal Miners' Lungs*. *Am. Ind. Hyg. Assoc. J.* 32:432-440 (1971).
- Sweet, D.V., W.E. Crouse, J.V. Crable et al: *The Relationship of Total Dust, Free Silica, and Trace Metal Concentrations to the Occupational Respiratory Disease of Bituminous Coal Miners*. *Am. Ind. Hyg. Assoc. J.* 5:479-485 (1974).
- Sorenson, J.J., T.E. Kober and H.G. Petering: *The Connection of Cd, Cu, Fe, Ni, Pb and Zn in Bituminous Coals from Mines with Differing Incidences of Coalworkers' Pneumoconiosis*. *Am. Ind. Hyg. Assoc. J.* 35:93-98 (1974).
- Wesson, T.C. and F.E. Armstrong: *Elemental Composition of Coal Mine Dust*. U.S. Bureau of Mines RI 7992 (1975).
- Mutmansky, J.M. and C. Lee: *An Analysis of Coal and Geological Variables Related to Coal Workers' Pneumoconiosis*. *Proceedings of the Coal Mine Dust Conference*. West Virginia University, Morgantown, WV (1984).
- Lee, C. and J.M. Mutmansky: *A Strategy for Coal Mine Respirable Dust Sampling Using Multi-Stage Impactors for Characterization Purposes*. *Proceedings of the Symposium on Engineering Health and Safety in Coal Mining*. A.W. Khair, Ed. Society of Mining Engineers of AIME, Littleton, CO (1986).
- Crable, J.V., R.G. Keenan, R.E. Kinser et al: *Metal and Mineral Concentrations in Lungs of Bituminous Coal Miners*. *Am. Ind. Hyg. Assoc. J.* 29:106-110 (1968).
- Keenan, R.G., J.V. Crable, A.W. Smallwood and J.R. Carlberg: *Chemical Composition of the Coal Miners' Lung*. *Am. Ind. Hyg. Assoc. J.* 32:392-397 (1971).
- Sharkey, A.G. Jr., T. Kessler and R.A. Friedel: *Trace Elements in Coal Dusts by Spark-Source*

- Mass Spectrometry. *Trace Elements in Fuel*, Advances in Chemistry Series No. 141, Ch. 4. S.P. Babu Ed. American Chemistry Society, Chicago, IL (1975).
3. **Freedman, R.W.:** Procedures for Analysis of Respirable Dust as Related to Coal Workers' Pneumoconiosis. *Analytical Methods for Coal and Coal Products*, Vol. II, Ch. 28. K. Clarence, Jr., Ed. Academic Press Inc., NY (1978).
4. **Corn, M., F. Stein, Y. Hammad et al:** Physical and Chemical Properties of Respirable Coal Dust from Two United States Mines. *Am. Ind. Hyg. Assoc. J.* 33:295-285 (1973).
5. **Ahlbert, M.S., A.C.D. Leslie and J.W. Winchester:** Environmental and Occupational Health Analysis Using Proton-Induced X-Ray Emission. Electron Microscopy and X-ray *Applications to Environmental and Occupational Health Analysis*, Ch. 4. P.S. Russel and A.E. Hutchings, Eds. Ann Arbor Science, Ann Arbor, MI (1978).
16. **Hudson, G.M., H.C. Kaufman, J.W. Nelson and M.A. Bonacci:** Advances in the Use of PIXE and PESA for Air Pollution Sampling. *Nuclear Instruments and Methods* 168:259-263. North-Holland Publishing Co., Amsterdam (1980).
17. **Johansson, S.A.E. and T.B. Johansson:** Analytical Application of Particle Induced X-ray Emission. *Nuclear Instrument and Methods* 137:473-516. North Holland Publishing Co., Amsterdam (1976).
18. **Chen, J.R., H. Kneis, B. Martin et al:** Trace Elemental Analysis of Bituminous Coals Using the Heidelberg Proton Microprobe. *Nuclear Instruments and Methods* 181:151-157. North-Holland Publishing Co., Amsterdam (1981).

# Variation in Mineral and Elemental Composition of Respirable Coal Mine Dusts by Worker Location and Coal Seam

R. A. Andre<sup>1</sup>, T. Simonyi<sup>2</sup> and R. L. Grayson<sup>2</sup>

<sup>1</sup>West Virginia Geological Survey

<sup>2</sup>Department of Mining Engineering, West Virginia University

The purpose of this paper is to disclose analytical, statistical, and observational results relating to mineralogy and trace elements in respirable dust samples collected from two different mines in West Virginia. Samples were taken from longwall panels, and the panels operated in different coal seams, one located in the northern part of the state and the other in the southern region. Mining conditions and equipment arrangements on the panels will be described along with dust control techniques used. Results from sample analyses are summarized with emphasis on relationships between mineralogy, trace elements, and mineral particle size to worker locations. Correlations are made between micro x-ray diffraction and energy dispersive x-ray analyses for sample mineralogy.

## Introduction

Through the work of many researchers worldwide, the health of coal miners in modern societies is now protected from harmful exposure to respirable coal mine dust. A vast amount of research culminated in the exposure-response model of Jacobsen, *et al.*,<sup>(1)</sup> which has been used to establish the 2 mg/m<sup>3</sup> exposure limit in the United States. According to the model, exposure to respirable dust for 35 years at this level or less would prevent the occurrence of a clinically significant case of coal workers' pneumoconiosis (CWP) in a miner. The exposure limit, of course, must be adjusted whenever greater than five percent free silica exists in the respirable dust.

The Jacobsen model was built around a mean mass concentration exposure, which generally showed the highest correlation with both incidence and progression of CWP. As Morgan, *et al.* noted, however, the quantity of respirable dust inhaled is not the only significant factor.<sup>(2)</sup> They noted that although mass of respirable dust correlates highest with the incidence of CWP, it is not a causal factor. Admittedly, the insidious processes causing the disease occur at the lung cell-dust particle level.

A look at past and present research is helpful in determining the properties of respirable coal mine dust warranting characterization. Studying the cytotoxicity of respirable

coal dusts, Reisner and Robock correlated cell damage positively with mineral content.<sup>(3)</sup> Earlier, Leiteritz, Bauer, and Bruckman concluded that the incidence of CWP is related to both quartz and fine dust concentration.<sup>(4)</sup> The mineral composition of respirable coal mine dust requires closer scrutiny, however, since Walton, Hadden, and Jacobsen suggested that mineral matter may be a protective factor<sup>(5)</sup>, whereas Davis, Ottery, and LeRoux found that the severity of CWP increased in miners with the occurrence of quartz and clay mineral enrichment.<sup>(6)</sup> A review of research throughout Europe indicates significant activity in mineralogical characterization of respirable coal dusts.<sup>(7)</sup> An interesting finding in France revealed that not a single case of CWP has occurred in a mine located in the Provence coalfield where a high level of calcite was detected in the dust.

A study of chest x-rays taken of coal miners participating in the National Coal Study illustrated that the incidence of category 1 CWP and progression of the disease to more complicated forms is higher in certain parts of the United States.<sup>(8)</sup> An analysis by the authors of 87 West Virginia cases of "dust disease of the lung," as reported in the 1984 Health and Safety Analysis Center (HSAC) data base, revealed that 75 cases were initiated from mines operating in the southern part of the state, seven originated from mid-state locations, and five were filed in the northern part of the state. Research is continuing on correlating reported lung diseases and coal seams in which the victims work.

Because of known toxicity of quartz, its characterization is important, but Morgan, as well as Davis, Ottery, and LeRoux, concluded that quartz is not the only cause of progression from CWP to progressive massive fibrosis.<sup>(6,9)</sup> Mutmanský emphasized that attention should also be placed on the potential relationship between trace elements in respirable dust and CWP.<sup>(10)</sup> Stein and Corn suggested that more research is needed into the physical and chemical properties of coal mine dusts and the dependence of these properties on mine of origin and particle size.<sup>(11)</sup> With regard to these properties, it is important that characterization of respirable dusts taken from coal mines be coordinated with research designed to characterize respirable

dusts in the lungs of miners. It is also important that analytical results be correlated with mining conditions and methods, worker locations, and coal seams.

In summary, more research is needed in coordinating respirable mass concentration with other physical and chemical properties of respirable dusts. Through such research an explanation of the processes causing incidence of CWP may be achieved. It is evident that mineral composition, trace element existence, and mineral particle size distributions are all aspects warranting closer scrutiny. It is important to note, however, as did Sharkey, Kessler, and Friedel, that there exists a great degree of deviation in the composition of respirable dust from parent material mined.<sup>(12)</sup> This applies both to mineral and trace element constituents. Therefore, the mechanics of dust generation and transport and the utilization of dust control methods must be described concurrently to explore the reasons for such variability in composition.

### Description of Longwall Panels

The longwall panel operating in the Pittsburgh seam, located in Northern West Virginia, had a 167.6 m (550 ft) long face and was equipped with a double-ended ranging drum shearer. The shearer took a 762 mm (30 in) cut and loaded coal onto a 732 mm (28.8 in) wide armored face conveyor. A crusher was mounted on the stage loader to reduce the size of rock, which frequently fell from exposed roof. An average mining height of 1.98 m (78 in) was maintained, with an average of 0.20 m (8 in) of floor mined. Normal practice was to cut from the tailgate to the headgate with the leading drum raised and the tail drum lowered, cutting bottom. After reaching the headgate, the shearer was reversed and both drums lowered for a clean-up pass. The last 12.2 m (40 ft) of the face on the tailgate end was cut on the clean-up pass. The shearer traveled at a speed ranging from 0.054 m/s (10.7 fpm) to 0.093 m/s (18.3 fpm) while cutting, depending on physical conditions. Varying roof conditions were observed, with as much as 0.91 m (3 ft) of drawslate falling from the roof over a distance of forty shields. Generally, however, local areas of bad roof were observed, usually limited to a ten- to twenty-shield span. Production during sampling ranged from 1397 t (1540 st) to 2286 t (2520 st) per shift with an average cutting time of 157 minutes.

For dust control purposes, the shearer in the first panel was equipped with two banks of four water sprays each and two large, "flood" sprays on the headgate end and one bank of three sprays and one "flood" spray on the tailgate end. Additionally, sixteen sprays were located behind the cutting bits on each drum. The spray system was operated at 0.586 MPa (85 psi), delivering 307 liters of water per minute (81 gpm) to knock down dust. The two large, "flood" sprays and the gob-side bank of four sprays on an extension arm at the headgate end of the shearer were directed against the air flow causing roll back of dust over the shearer operators.

Fresh air was provided to the face via the track heading and a parallel intake entry. The air was split at the headgate with 2.36 m<sup>3</sup>/s (5000 cfm) routed down the belt entry and the remaining 8.97 m<sup>3</sup>/s (19,000 cfm) to 12.74 m<sup>3</sup>/s (27,000 cfm) directed toward the face. Between 5.75 m<sup>3</sup>/s (12,180 cfm)

and 8.03 m<sup>3</sup>/s (17,010 cfm) actually reached the tailgate location. No ventilating check curtain was used between the first shield and the solid rib to prevent air from leaking into the gob, but the minimum air velocity of 1.524 m/s (300 fpm) required on the face by the ventilation plan was maintained. A ventilating check curtain was used between the stage loader and the pillar being mined to prevent dust-laden air from flowing over the shearer operator during cut-out into the headgate entry. The direction of air flow on the face was opposite that of coal flow on the conveyor (non-homotropol).

The other panel, located in the Beckley seam in Southern West Virginia, had a 127.1 m (417 ft) long face and was equipped with a high-speed plow. The plow sliced off a 101.6 mm (4 in) cut of coal each pass. The average mining height was 1.17 m (46 in) with no roof or floor being mined. Some roof rock would fall onto the conveyor at times, but workers generally were able to control the size of such rocks. Unlike the first panel, workers were stationed on the panel and remained there for the entire shift. Production during the sampling period ranged from 816 t (900 st) to 2380 t (2624 st) per shift, as the plow averaged 1.81 m/s (356 fpm) in traveling up and down the face.

Solenoid-activated water sprays were mounted along the armored face conveyor, one per pan section. The water system was operated at 200 psi, delivering 6.8 lpm per water spray. Fresh air was provided at both the headgate and tailgate entries, but only headgate air was directed down the face. A minimum volume of 4.58 m<sup>3</sup>/s (9,700 cfm) of air was observed on the panel. No ventilating check curtains were used on the panel unless methane became a problem. Airflow was non-homotropol on this face relative to coal travel.

### Methodology

#### Dust Sampling Procedures

Respirable dust samples which met the criteria required of coal operators for compliance sampling were obtained for characterization.<sup>(13)</sup> Gravimetric samples were collected from fixed positions on the longwall faces using MSA personal sampling units equipped with Dorr-Oliver 10-mm cyclones and DuPont P2500 constant flow pumps calibrated to operate at 2 lpm. Sampling units were hung from shields and on the shearer in panel 1 at a height which approximated the level of the nose and mouth of employees. Personal sampling of shieldmen on panel 1 was also done. In order to obtain a good approximation of the average respirable mass concentrations for the different locations over time, ninety nearly full shift samples were collected from panel 1 and seventy samples from panel 2.

Locations sampled on panel 1 included: 1) intake air, 2) headgate, 3) 1/2 face, 4) 3/4 face, 5) tailgate, 6) lead shearer, 7) mid-shearer, 8) tail shearer, and 9) shieldman. Locations sampled on panel 2 were: 1) head intake, 2) headgate, 3) 1/4 face, 4) 1/2 face, 5) 3/4 face, 6) tailgate, and 7) tail intake.

Pre-weighed MSA PVC filters, 37-mm in diameter with a 0.5 µm mean pore size, were used for sampling. These filters were checked routinely by the Mine Safety and Health Administration (MSHA) for accuracy of weighings, but addi-

## VARIATION IN RESPIRABLE DUST COAL MINE DUSTS

tional checks were made to ensure that deviations remained less than 0.1 mg. A Sartorius, Type 2462S00Z0, semi-automatic, electronic analytical balance with digital readout was used for weighing samples to the nearest 0.01 mg, both before and after sampling.

During sampling on a shift, supplemental notes were taken regarding cutting time, downtime, the amount and location of bad roof areas, tram speed of the cutting machine, the type of cutting, and the cross-sectional area and air velocity at sampling locations. Ventilation arrangements, dust control procedures used, work habits of employees, the amount of mineral partings and floor mined, and shift productivity were logged.

Following determination of mass concentrations, twenty-seven samples from the first panel and twenty-one samples from the second panel were designated for mineral and elemental composition analysis and mineral particle sizing using available scanning electron microscopes (SEM's). The samples were selected from shifts which had varying conditions.

### Scanning Electron Microscope Analysis

Respirable dust was ultrasonically bathed from a field sample in a beaker of alcohol. A portion of the dust-alcohol suspension was immediately transferred to a polished carbon stud and allowed to evaporate such that dust particles appeared to be uniformly dispersed on the background. The sample mount was then coated with a conductive layer of gold to prevent surface charging.

Two Cambridge Stereoscan SEM's (Model 150 and Model 180) were available for identification of elements and minerals and particle size analysis. Kevex 7000 analytical spectrometers were interfaced with the SEM's in order to identify elements on the basis of their energy levels (energy dispersive x-ray analysis).

The mineralogy of a particle was determined by comparing the EDX spectrum obtained for major and minor elements (Si, Al, K, S, Ca, Fe) with the known standard elemental spectra of minerals. The electron beam accelerating voltage used for mineral identification was typically 20 KV. Time of exposure to electron bombardment varied, but generally 20 to 74 seconds were needed to accurately determine the proportionality of elements and positively identify the mineralogy of an individual particle.

A scanning screen was used to randomly locate a field on the sample mount. Each particle within the field was "spotted" and bombarded for identification. Following identification, particle size (Feret's diameter) was determined by superimposing a graticule and scale onto the focused image on the screen. A total of 100 inorganic particles were analyzed for each mounted sample.

### Micro X-ray Diffraction Analysis

Very small quantities of dust are collected in respirable sampling, generally ranging from 0.1 to 3.2 mg on longwall panels for a full shift. Standard X-ray diffraction techniques, which can be used to determine the mineral composition of materials semi-quantitatively based upon the crystalline structure of its components, require samples containing at least 100 mg of dust. X-ray diffraction analysis can be done on respirable dust samples, however, by mounting the dust,

along with a minimum amount of Apiezon-L substrate, onto a thin glass spline mounted in wax on a copper stud. The sample to be x-rayed is placed into a large Phillips Debye-Scherrer powder camera, which is then mounted on an X-ray generator. The aligned, rotating sample is bombarded with copper radiation for 4 to 18 hours to obtain a good film pattern. The exposure time depends on the amount of sample.

A properly exposed film contains a number of sharply defined lines forming a concentric pattern in the forward direction. According to Bragg's Law, the positions of these lines are dependent on the interplanar d-spacings of the crystalline materials in the sample. From a list of d-spacings for common minerals in coal dust, the mineralogy of the sample can be determined. The intensity of a diffraction line on the film is directly proportional to the amount of material that produced it. A microphotodensitometer is used to measure intensities from the film pattern, and the resulting diffraction trace contains a peak for each line on the film (Figure 1). The height of a peak is directly proportional to the darkness of the corresponding line.

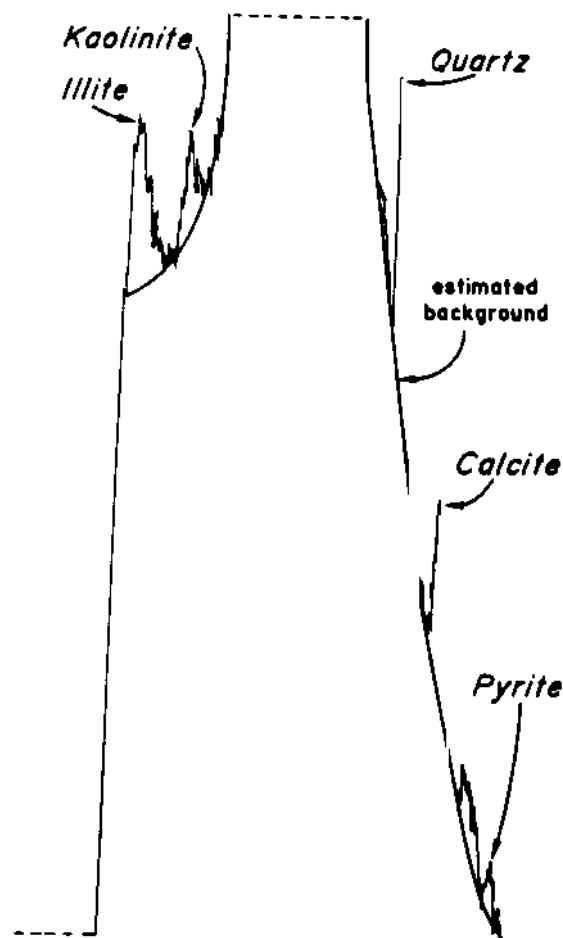


FIGURE 1. X-ray diffraction trace generated by a microphotodensitometer.

tions of roof in order to describe the variability in the various respirable dust characteristics being analyzed.



TABLE I

Percent Composition of Respirable Mineral Dust by Panel Based on Particle Count Using SEM/EDS

Panel	Mineral				
	Calcite	Illite	Quartz	Kaolinite	Pyrite
1 Pittsburgh Seam (N = 2682)	20.7	55.8	8.7	2.0	6.0
2 Beckley Seam (N = 400)	47.3	29.3	8.5	8.0	0.5

The mineralogy of a respirable dust sample can be estimated semi-quantitatively from a trace following the procedure of Renton.<sup>(14)</sup> In this procedure, the height of each peak is measured and the estimated background, which occurs primarily because of the grease and the organic matrix of coal dust, is subtracted out. The raw intensities are then multiplied by weighting factors determined by Renton. The weighting factors compensate for differences in crystallinity of minerals. The weighting factor used for illite, for example, is large since illite is poorly crystalline relative to other minerals in West Virginia coals and does not diffract X-rays efficiently. Mineral percentages are then determined using the sum of weighted intensities as the denominator. The overall accuracy of determinations is approximately +/- 15 percent, which includes uncertainty associated with background estimation and the weighting procedure. The weighting factor reflects not only the crystallinity of a mineral, which can vary substantially as it does for illite, but also the diffraction method used.

## Discussion of Results

### Mineralogy

Based upon availability of in-house technology, the mineralogy of respirable dust samples was determined using an energy dispersive X-ray analysis system interfaced with a scanning electron microscope. This procedure facilitated simultaneous mineral particle size analysis. The mineral composition of each sample was determined by identifying the mineralogy of each of 100 particles. Realizing the variability inherent in this procedure, corroboration was sought using the micro X-ray diffraction technique, which is also semi-quantitative but involves a larger amount of material. Twenty-seven respirable dust samples were analyzed using SEM/EDS for the first panel and four (out of twenty-one) have been completed for the second panel. To date, seven samples have been characterized by both SEM/EDS and XRD.

TABLE II

Percent Composition of Respirable Mineral Dust by Location Within Panel 1 Based on Particle Count Using SEM/EDS

Location	Mineral				
	Calcite	Illite	Quartz	Kaolinite	Pyrite
Intake	54.3	13.0	14.3	0.3	0.7
Headgate	50.7	25.0	7.0	2.0	2.3
1/2 Face	10.7	70.7	7.3	0.7	4.3
3/4 Face	8.2	71.5	10.2	1.8	6.2
Tailgate	6.5	77.2	7.8	1.8	3.8
Shearer	10.5	58.0	6.8	1.5	15.8
Shieldman	25.0	52.0	6.0	6.7	4.7

Table I shows the average mineralogy of respirable mineral dust by panel based on SEM/EDS analysis of 2682 particles for panel 1 and 400 particles, thus far, for panel 2. The mineral composition is quite different for the two panels. Quartz content is nearly identical at 8.5 percent, but pyrite and kaolinite contents differ, with more kaolinite found in the Beckley seam and more pyrite detected in the Pittsburgh seam. Illite was the dominant mineral found in the Pittsburgh seam, followed by calcite. In the Beckley seam, the roles are reversed.

Table II depicts the mineral composition of respirable mineral dust by location in panel 1. Values for each location are derived from analysis of approximately 300 particles. Definite trends are seen for the variation of calcite and illite by location. A fitted, multiple linear regression model for the variation of illite content by location yielded the equation:

$$I = -8.45 + 37.61X - 3.99X^2$$

where:

I is percent illite at face location X and X is the proportionally-coded face location (1, . . ., 5).

The model reveals that illite content increases along the longwall face but at a decreasing rate. The model explains 78 percent of the variability in illite content and is statistically significant ( $F = 17.95$ ).

A fitted, multiple linear regression model for the variation of calcite content by location yielded the equation:

$$C = 82.84 - 36.43X + 4.20X^2$$

where:

C is percent calcite at face location X.

## VARIATION IN RESPIRABLE DUST COAL MINE DUSTS

This model reveals that calcite content decreases along the face but at a decreasing rate. The model explains 80 percent of the variability in calcite content and is also statistically significant ( $F = 19.49$ ).

**TABLE III**

**Percent Composition of Respirable Mineral Dust by Location Within Panel 2 Based on Particle Count Using SEM/EDS**

Location	Mineral				
	Calcite	Illite	Quartz	Kaolinite	Pyrite
Head Intake	63.0	20.0	8.0	5.0	0
1/4 Face	40.0	33.0	10.0	10.0	1.0
1/2 Face	25.0	46.0	10.0	10.0	1.0
Tail Intake	61.0	18.0	6.0	7.0	0

No general relationship was found for quartz, kaolinite, or pyrite content variation by location on panel 1. Table II indicates that quartz and kaolinite content of respirable mineral dust was relatively constant on the face, but a significant increase in the amount of pyrite (15.8%) was detected at the shearer locations. This latter phenomenon can be attributed to the rollback of the dust cloud generated from the cutting action over the shearer operators. The inability to find a relationship for quartz, kaolinite, and pyrite is not surprising because of the high variability in SEM/EDS determinations for minerals that are present in small percentages. Hundreds of particles would have to be analyzed for each sample to determine accurate percentages for such quantities. The important point here is that quartz, kaolinite,

and pyrite do exist in small amounts, whereas illite and calcite exist in much larger amounts.

Table III provides mineralogical results to date for the second panel. However, only 100 particles for each location have been analyzed to date, with seventeen samples pending analysis. The second panel differed from the first one in the provision of fresh air up the tailgate entry, which impacted the mineralogy at that location. Because of this situation and generally smaller amounts of illite, calcite is the dominant mineral. The same general trends for calcite and illite content variation by location exist for this panel, but not enough data is presently available to develop regression models. Thus far, it can be said that illite content increases linearly with face location, except at the tailgate. Calcite content appears to decrease at a decreasing rate, except at the tailgate, but the rate of decrease is slower for panel 2 than it was for panel 1.

Comparison of Table III with Table II reveals that 1) kaolinite content is much higher in panel 2; 2) pyrite content is much lower in panel 2; 3) quartz content is not much different; 4) calcite content is higher in panel 2 at each location; and 5) illite content is considerably lower in most locations in panel 2.

Correlation of SEM/EDS and XRD mineralogical results is made by mineral type in Figures 2 through 5. Figure 2

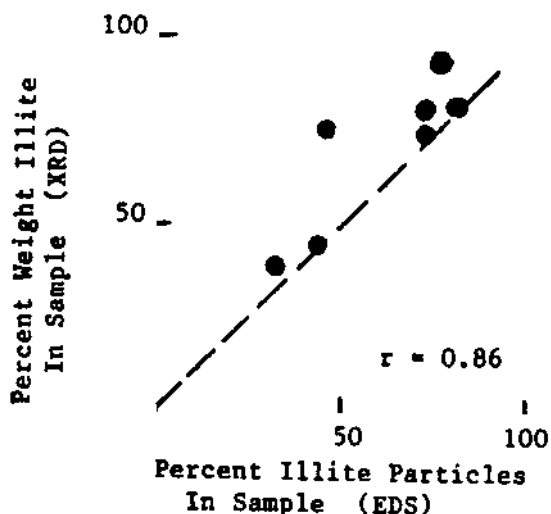


FIGURE 2. XRD versus EDS results for illite.

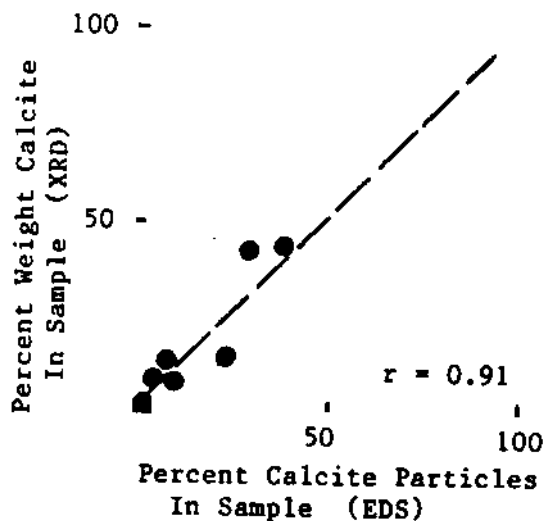


FIGURE 3. XRD versus EDS results for calcite.

reveals that a high correlation ( $r = 0.86$ ) exists between illite content determinations by the different methods, with either XRD slightly overestimating illite content or SEM/EDS slightly underestimating it. Figure 3 shows a higher correlation ( $r = 0.91$ ) between results for calcite content, with no trends apparent in method bias. Figure 4 shows either a possible overestimation of kaolinite content by XRD or an underestimation by SEM/EDS, but a good correlation ( $r = 0.79$ ) was obtained. Figure 5 indicates either possible overestimation of pyrite content by SEM/EDS or underestimation by XRD, but, again, good correlation ( $r = 0.79$ ) exists. Results for quartz content are not shown because of poor correlation ( $r = 0.12$ ), with no trends in bias apparent.

Correlation results are very good considering 1) weight percentages are compared with number percentages, and 2) sources for error in the two analytical methods. Since particles are in the respirable fraction of mine dust and mean particle sizes were similar in magnitude, number percentages are tantamount to weight percentages, thereby yielding good correlations. Estimation of the background and the use of unadjusted weighting factors in XRD analysis appear ade-

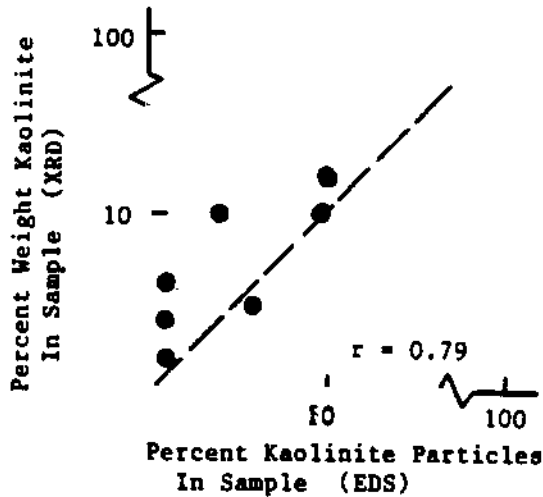


FIGURE 4. XRD versus EDS results for kaolinite.

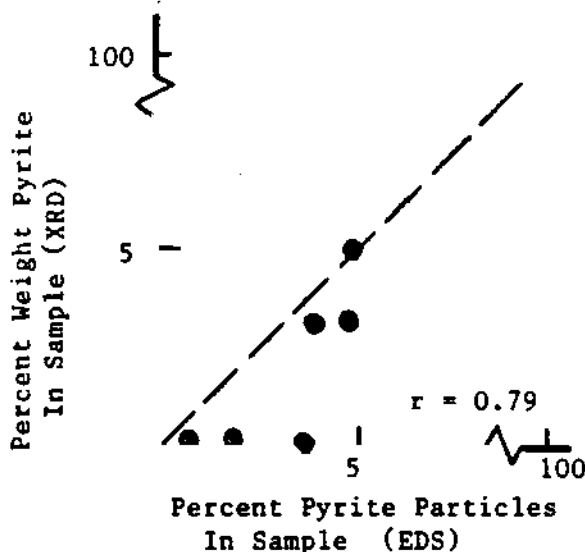


FIGURE 5. XRD versus EDS results for pyrite.

quate for gross determination of mineralogy, except in the case of quartz. Classification of clay minerals as either illite or kaolinite in the SEM/EDS analysis hinges on the ratio of aluminum to silicon and the presence of a potassium peak in a particle, and results indicate that good judgment has been exercised. Determinations of pyrite content by XRD depends on the crystalline structure of pyrite, which has been seen to vary considerably. Defects in the crystal structure of some pyrites may explain the non-existence of this mineral

in many of the XRD determinations while it was detected in the SEM/EDS analysis. Quartz content determinations present a real problem but may be related to the amount of contamination in a particle. Only 28 percent of the quartz particles analyzed in panel 1 were possibly uncontaminated by other elements. In contrast, over 68 percent of the quartz particles in panel 2 were potentially uncontaminated. However, the answer to the problem may lie in the use of a weighting factor that is too low since most of the data indicate that the XRD method underestimates quartz content relative to SEM/EDS.

Trace Elements

During SEM/EDS analysis of dust samples for mineralogy, elements which showed a peak energy level above the gold background but were not primary in determining the mineralogy of a particle were logged as trace elements for that particle. In this way, the number of occurrences could be tabulated. Table IV shows the results of this procedure. The elements listed in Table IV are those which were identified more than one time. The percent of occurrence for each element is determined based on the total number of particles analyzed per panel. The denominator for panel 1 is therefore 2682, while the denominator for panel 2 is presently only 400. Elements such as aluminum, potassium, iron, silicon, sulfur, and calcium, although they quite frequently showed up in trace amounts, are not included because they consistently occur as major or minor constituents of other minerals.

Table IV indicates that chlorine and magnesium occur more frequently in panel 1 than they do in panel 2. It also indicates that sodium and titanium occur more frequently but in a smaller ratio. Levels of chromium, which Mutmanský hypothesized may be associated with causes of CWP,<sup>(11)</sup> and levels of manganese are virtually the same.

Table V breaks down the percent occurrence of trace elements by location for panel 1. Chlorine occurrences appear to be particularly high in intake air and somewhat higher at the shearer positions. The data for magnesium indicates a trend of increasing occurrence from headgate to tailgate along the face, much like the trend for illite in the mineralogical analysis. No other relationships are evident, except for the possible reduction in the occurrence of sodium from headgate to tailgate along the face. No relationships can be concluded from the minimum amount of data for panel 2, which is shown in Table VI.

TABLE IV

Percent Trace Element Occurrence by Panel Based on Particle-by-Particle SEM/EDS Analysis

Panel	Element					
	Cl	Cr	Mg	Mn	Na	Ti
1	5.3	4.5	16.1	2.8	2.4	7.8
2	1.0	5.0	5.3	3.5	0.5	4.0

## VARIATION IN RESPIRABLE DUST COAL MINE DUSTS

### Mineral Particle Size

As mentioned previously, Feret's diameter was recorded for each mineral particle analyzed under SEM to determine

important to note that no difference in mineral particle size was detected by date, especially since physical conditions on the panel changed. It is also significant to note that the mean particle size obtained for the shieldman reflects the fact that he spends two-thirds of his time in intake air rather than on the face.

**TABLE V**

**Percent Trace Element Occurrence by Location Within Panel 1 Based on Particle-by-Particle SEM/EDS Analysis**

Location	Element					
	Cl	Cr	Mg	Mn	Na	Ti
Intake	15.7	5.3	18.0	2.3	6.3	3.3
Headgate	3.7	2.7	11.3	5.7	3.3	8.7
1/2 Face	0.3	4.7	15.0	2.0	2.0	8.7
3/4 Face	4.3	5.8	19.0	1.0	1.0	9.3
Tailgate	1.8	3.0	21.5	3.3	0.8	6.5
Shearer	6.2	4.5	15.7	2.7	2.2	9.2
Shieldman	5.0	6.7	13.3	3.7	1.3	8.7

**TABLE VI**

**Percent Trace Element Occurrence by Location Within Panel 2 Based on Particle-by-Particle SEM/EDS Analysis**

Location	Element					
	Cl	Cr	Mg	Mn	Ni	Ti
Head Intake	1.0	4.0	7.0	2.0	1.0	3.0
1/4 Face	1.0	4.0	5.0	3.0	0	4.0
1/2 Face	0	6.0	6.0	4.0	0	7.0
Tail Intake	2.0	6.0	3.0	5.0	1.0	2.0

size distributions for minerals and to detect differences in mineral particle size by location. Table VII reveals the results of mineral particle sizing by location on panel 1. A minimum of 300 particles were sized for each location. An analysis-of-variance (ANOVA) performed on diameter means by location (three means per location) indicated that the mean mineral particle size at the tailgate is significantly smaller than those for all other locations. Results, using Fisher's least significant difference test following a significant F-test, are presented in Table VII by grouping. It is

**TABLE VII**

**Variation of Mineral Particle Size (Feret's Diameter) by Location on Panel 1**

Location	Mean Feret's Diameter (um)	Least Significant Difference Test Group
Tailgate	1.17	A
1/2 Face	1.55	B
Shearer	1.56	B
3/4 Face	1.66	B
Headgat	1.67	B
Shieldman	1.75	B
Intake	1.82	B

**TABLE VIII**

**Variation of Mineral Particle Size (Feret's Diameter) by Mineral Type of Panel 1**

Location	Mineral			
	Quartz	Illite	Calcite	Pyrite
Intake	1.40	2.17	1.74	--
Headgate	1.28	1.53	1.70	1.72*
1/2 Face	1.39	1.54	1.74	1.34
3/4 Face	1.61	1.64	1.61	1.30
Tailgate	0.97	1.22	1.28	1.01
Shearer	1.56	1.55	1.69	1.23
Shieldman	1.18	1.64	1.77	1.50
Average	1.38	1.53	1.65	1.29

\*Only one sample of three had greater than 3 particles.

Table VIII lists the mean particle size of minerals by location on panel 1, as well as the overall mean particle size for each mineral. Performing an analysis-of-variance on this data revealed that the mean diameters of quartz (1.38  $\mu\text{m}$ ) and pyrite (1.29  $\mu\text{m}$ ) are significantly smaller than those of illite (1.53  $\mu\text{m}$ ) and calcite (1.65  $\mu\text{m}$ ). From this table, it is also seen that the trend for smaller particle size at the tailgate is demonstrated by all minerals.

At this time not enough data exists for an analysis of particle size by location on panel 2, but, thus far, the average mineral particle size (for 400 particles) is 1.36  $\mu\text{m}$ , which is smaller than the average for panel 1 (1.58  $\mu\text{m}$ ).

## Conclusions

Determination of variations in mineralogical and elemental composition of respirable coal mine dusts and in mineral particle size by worker locations on production panels and across different coal seams may eventually lead to discoveries regarding the causes of CWP. Causes are still unclear, and contradictions exist relative to the role of quartz and other minerals. Although major progress has been achieved in prevention of CWP, no definitive answers concerning causes have been revealed. Potentially, results from mineralogical, elemental and particle size analyses of lung sections taken from disease victims, when coupled with knowledge regarding work history, may lead to important correlations with data from analysis of in-mine samples.

This paper has presented two methods for determining gross mineralogy of respirable coal mine dust samples. Good correlation was obtained between particle-by-particle SEM/EDS and small-quantity micro-XRD results. Differences in mineralogy by coal seam and by worker location on a production panel can be detected using analysis-of-variance techniques, and relationships between the percentage of an existing mineral and worker location can be developed. Many of the differences and relationships can be explained by phenomena observed in mines. Some variations, for example, can be explained by physical conditions, panel configurations, equipment arrangements, or work practices.

Along with mineralogical results, information relative to the existence of trace elements in respirable dust and mineral particle size data can be obtained from SEM/EDS analyses. Differences in the occurrence of different trace elements in particles and in mineral particle sizes can be determined. For example, more magnesium and chlorine were found to exist in the Pittsburgh seam than in the Beckley seam, and mineral particles at the tailgate location on a longwall panel were found to be significantly smaller than particles at other locations. Also, quartz and pyrite particles were smaller than illite and calcite particles in the longwall panel operating in the Pittsburgh seam.

## Acknowledgment

This research has been supported by the Department of the Interior's Mineral Institute program administered by the Bureau of Mines through the Generic Mineral Technology Center for Respirable Dust under grant number G1135142

## References

1. Jacobsen, M. et al: The Relationship Between Pneumoconiosis and Dust Exposure in British Coal Mines. *Inhaled Particles III*, pp. 903-917. W.H. Walton, Ed. Unwin Bros., Old Woking, Surrey (1971).
2. Morgan, W.K.C. et al: The Prevalence of Coal Workers' Pneumoconiosis in U.S. Coal Miners. *Arch. Environ. Health* 27:221-226 (1973).
3. Reisner, M.T.R. and K. Robock: Results of Epidemiological, Mineralogical, and Cytotoxicological Studies on the Pathogenicity of Coal-Mine Dusts. *Inhaled Particles IV*, pp. 703-715. W.H. Walton, Ed. Unwin Bros., Old Woking, Surrey (1977).
4. Leiteritz, H., D. Bauer and E. Bruckman: Mineralogical Characteristics of Airborne Dust in Coal Mines of Western Germany and Their Relations to Pulmonary Changes in Coal Hewers. *Inhaled Particles III*, pp. 729-743. W.H. Walton, Ed. Unwin Bros., Old Woking Surrey (1971).
5. Walton, W.H., G.G. Hadden and M. Jacobsen: The Effect of Quartz and Other Non-coal Dusts in Coalworkers' Pneumoconiosis, Part I, Epidemiological Studies. *Inhaled Particles IV*, pp. 669-690. W.H. Walton, Ed. Unwin Bros., Old Woking, Surrey (1975).
6. Davis, J.M.G., J. Ottery and A. LeRoux: The Effect of Quartz and Other Non-coal Dusts in Coalworkers' Pneumoconiosis, Part II, Lung Autopsy Study. *Inhaled Particles IV*, pp. 691-702. W.H. Walton, Ed. Unwin Bros., Old Woking, Surrey (1975).
7. Industrial Health and Safety: *A Synthesis Report on Research Supported by the Commission During the Period 1977-82*. R.J. Hamilton, Ed. Commission of the European Communities, Luxembourg (1985).
8. Attfield, M. R. Reger and R. Glenn: The Incidence and Progression of Pneumoconiosis Over Nine Years in U.S. Coal Miners: II. Relationship with Dust Exposure and Other Potential Causative Factors. *Am. J. Ind. Med.* 6:417-425 (1984).
9. Morgan, W.K.C.: Coal Workers' Pneumoconiosis. *Am. Ind. Hyg. Assoc. J.* 32:29-34 (1971).
10. Mutmansky, J.M. and C. Lee: An Analysis of Coal and Geologic Variables Related to Coal Workers' Pneumoconiosis. *Proc. Coal Mine Dust Conference, Morgantown, 1984*, pp. 236-249. S.S. Peng, Ed. West Virginia University (1984).
11. Stein, F. and M. Corn: Shape Factors of Narrow Size Range Samples of Respirable Coal Mine Dust. *Powder Technology* 13:133-141 (1976).
12. Sharkey, A.G., T. Kessler and R.A. Friedel: Trace Elements in Coal Dust by Spark-source Mass Spectrometry. *Trace Elements in Fuel*, pp. 48-56. S.B. Babu, Ed. American Chemical Society, Washington (1975).

## VARIATION IN RESPIRABLE DUST COAL MINE DUSTS

13. 30 CFR Part 70 Subpart B.

14. Renton, J.J.: Use of Weighted X-ray Diffraction Data for Semi-Quantitative Estimation of Minerals

in Low-Temperature Ashes of Bituminous Coals and in Shale. Technical Report MERC/CR-79/5. U.S. Department of Energy (1979).

# Characterization of Respirable Dust on a Longwall Panel -- A Case Study

R. L. Grayson and S. S. Peng  
Department of Mining Engineering, West  
Virginia University

**Abstract.** Sampling of respirable dust and analyses of samples have been partially completed for a longwall panel. Physical and compositional properties which have been characterized include:

1. Respirable mass concentration,
2. Mineral composition,
3. Particle size distribution by mineral,
4. Particle shape distribution by mineral,
5. Particle angularity distribution by mineral, and
6. Respirable size distribution.

Analytical techniques used in the characterization of samples are described, and results are reported with emphasis placed on relationships between the various characteristics and worker locations. Details of existing mining conditions, equipment arrangements, dust control methods and operating system parameters are presented.

## INTRODUCTION

Through the work of many researchers worldwide, the health of coal miners in modern societies is now protected from dangerous exposure to respirable coal mine dust. A vast amount of research culminated in the exposure-response model of Jacobsen, et al. (1971) which has been used to establish the 2mg/m<sup>3</sup> exposure limit in the United States. According to the model, exposure to respirable dust for 35 years at this level or less would prevent the

occurrence of a clinically significant case of coal workers' pneumoconiosis (CWP). The exposure limit, of course, must be adjusted whenever greater than five percent free silica exists in the respirable dust.

The Jacobsen model was built around a mass concentration exposure, which showed the highest correlation with incidence and progression of CWP. As Morgan, et al. (1973) noted, however, the quantity of respirable dust inhaled is not the only significant factor. It is noted that although mass of respirable dust correlates highest with the incidence of CWP, it is not a causal factor. Indeed, the insidious processes causing the disease occur on the cell-particle scale, requiring microscopic investigation.

Stein and Corn (1976) suggested that more research is needed into the physical and chemical properties of the dust and the dependence of these properties on mine of origin and particle diameter. It is important that characterization of dust properties be guided by requirements of coordinated research in cytotoxicology, epidemiology, and immunology, be related to realistic mining conditions, and be designed to detect differences in properties due to mining methods, worker locations, and coal seams.

A look at past research is helpful in determining the properties warranting characterization. Studying the cytotoxicity of respirable coal dusts, Reisner and Robock (1977) correlated cell damage positively with mineral content. Leiteritz, Bauer, and Bruckman (1971) concluded that the incidence of CWP is related to both quartz concentration and fine dust

## RESPIRABLE DUST ON A LONGWALL PANEL

concentration. The mineral composition of respirable dust requires closer scrutiny since Walton, Hadden, and Jacobsen (1975) suggested that mineral matter may be a protective factor, whereas Davis, Ottery, and Le Roux (1975) saw that the severity of CWP increased in miners with the occurrence of quartz and clay mineral enrichment. Concerning particle size, Leiteritz, Bauer, and Bruckman (1971) and Corn, et al. (1973) showed that ash and quartz increased with decreasing median particle diameter. It is realized that quartz characterization is important, however, Morgan (1971), as well as Davis, Ottery, and Le Roux (1975), concluded that quartz is not the only cause of progression from CWP to progressive massive fibrosis (PMF). Emphasis must also be placed on the potential relationship between the size and shape of mineral particles and health effects (Shedd, Virta, and Wylie, 1982).

From the above comments, it is apparent that much more research is needed in coordinating mass concentration with other physical and chemical properties of respirable dust to explain processes causing incidence of CWP and its progression to more complicated forms. Particle size distributions, especially in the mineral-enriched smaller size fractions, mineral composition, trace element existence and particle shape and angularity are all aspects warranting closer scrutiny. It is important to note, however, as did Sharkey, Kessler, and Friedel (1975), that there exists a great degree of deviation in the composition of respirable dust from parent material mined. This applies both to mineral and trace element constituents. Thus, the mechanisms of dust generation and transport and the utilization of dust control methods must be described concurrently to explain the reasons for such great variability in composition.

The focus of this research has been to characterize the mineral composition of respirable dust and describe the size, shape, and angularity of mineral particles. Respirable dust samples and coal seam channel samples have been collected from three panels, and most of the samples have been analyzed for the first panel. The mining conditions and equipment arrangements on this panel, a longwall setup operating in the Pittsburgh seam, will be described along with dust control techniques used. Results from sample analyses will be summarized with emphasis on

relationships between specific dust characteristics and worker locations.

### DESCRIPTION OF THE LONGWALL PANEL

The 167.6 m (550 ft) longwall face was equipped with a double-ended ranging shearer, which cuts a 762 mm (30 in) web, loading onto a 732 mm (28.8 in) wide armored face conveyor. A crusher was used at the headgate, outby the stage loader, to reduce the size of rock which frequently fell from exposed roof. An average mining height of 1.98 m (78 in) was maintained, with an average of 0.20 m (8 in) of floor mined. Normal practice was to cut from the tailgate to the headgate with the leading drum raised and the tail drum lowered cutting bottom. After reaching the headgate, the shearer was reversed and both drums lowered for a clean-up pass. The last 12.2 m (40 ft) of face on the tailgate end was cut on the clean-up pass. The shearer traveled at 0.054 m/s (10.7 fpm) to 0.093 m/s (18.3 fpm) while cutting, depending on physical conditions. Varying conditions were observed, with as much as 0.91 m (3 ft) of drawslate falling over a distance of forty shields. Generally, however, relatively local areas of bad roof were encountered, usually limited to a ten to twenty shield span. Production during sampling ranged from 1397 t (1540 st) to 2286 t (2520 st) per shift.

The shearer was equipped with two banks of four water sprays each and two large, "flood" sprays on the headgate end and one bank of three sprays and one "flood" spray on the tailgate end. Additionally, sixteen sprays were located behind the cutting bits on each drum. A minimum of 45 sprays were required to be kept operating at all times. The spray system was operated at 0.586 MPa (85 psi) and water sprays were rated at 6.8 lpm (1.8 gpm). A minimum total flow of 189.3 lpm (50 gpm) was required at the shearer at a minimum pressure of 0.345 MPa (50 psi) according to the ventilation plan. It was noted that the two large, "flood" sprays and the gob-side bank of four sprays on the headgate end of the shearer were directed against the air flow causing rollback of dust over the shearer operators.

Intake air was provided to the longwall face via the track entry. The air was split at the headgate with 2.36 m<sup>3</sup>/s (5000 cfm) routed down the belt entry and the remaining 8.97 m<sup>3</sup>/s (19 000 cfm) to 12.74 m<sup>3</sup>/s (27 000 cfm) directed toward the face. Between 5.75 m<sup>3</sup>/s (12 180 cfm) and 8.03 m<sup>3</sup>/s (17 010



## THE RESPIRABLE DUST CENTER

cfm) reached the tailgate location. No check was used between the first shield and the solid rib, but the minimum air velocity of 1.524 m/s (300 fpm) required by the ventilation plan at the tenth shield was maintained at all times. It should be noted that the velocity is not optimal for dust control. A check was used between the stage loader and the pillar being mined to prevent dust-laden air from flowing over the lead shearer operator. The direction of air flow on the face was opposite that of coal flow on the conveyor. The cross-sectional area for air flow ranged from 3.25 m<sup>2</sup> (35 ft<sup>2</sup>) at the shearer to 7.43 m<sup>2</sup> (80 ft<sup>2</sup>) on the gates. An average area of 4.92 m<sup>2</sup> (53 ft<sup>2</sup>) was measured at other locations.

It was noted that shieldmen worked only 15.3% of their 480-minute shift on the face (on the average). Cutting time per shift ranged from 111.3 min to 218.9 min, averaging 157.1 min. Shieldmen worked on the face only during the clean-up pass, approximately 73.6 min per shift average. It was also seen that a number of men relieved the shearer operators at frequent intervals during the shift.

### METHODOLOGY

#### Dust Sampling Procedures

Respirable dust samples which approximate the size distribution defined by the American Conference of Governmental Industrial Hygienists (Hinds, 1982) and also meet the criteria required of coal operators for compliance sampling (30 CFR Part 70 Subpart B) were desired for characterization. Therefore, gravimetric samples were collected from fixed positions on the longwall face using MSA personal sampling units equipped with Dorr-Oliver 10-mm cyclones and DuPont P2500 constant flow pumps calibrated to operate at 2 lpm. Sampling units were hung from shields and on the shearer at a height which approximated the level of the nose and mouth of employees working on the panel. A unit was also located on one of the shieldmen. In order to obtain a good approximation of the average respirable mass concentrations for the different locations over time, ten nearly full shift samples were taken over a 35-day period.

Locations sampled on the panel included:

1. Intake air,
2. Number 1 shield (headgate),

3. Number 55 shield (mid-face),
4. Number 75 shield (3/4-face),
5. Number 112 shield (tailgate),
6. Lead shearer,
7. Mid-shearer,
8. Tail shearer, and
9. Shield mover.

Pre-weighed MSA PVC filters, 37-mm in diameter with 0.5  $\mu$ m mean pore size, were used for sampling. These filters are checked routinely by MSHA to ensure accuracy of weighings, but additional checks were made to ensure that deviations remained less than  $\pm 0.1$  mg. A Sartorius, Type 2462S0020, semi-automatic, electronic, analytical balance with digital readout was used for weighing samples to the nearest 0.01 mg, both before and after sampling.

MRE-equivalent, respirable mass concentrations were determined and normalized for full-shift (portal-to-portal) equivalence using the formula:

$$(1) \quad C_M = \frac{C_p (T_p) + C_I (T_I)}{T_p + T_I}$$

where:

$C_M$  is the full-shift, normalized, MRE-equivalent respirable mass concentration,

$C_p$  is the MRE-equivalent, respirable mass concentration measured on the panel,

$T_p$  is the actual time spent on the panel by the worker during mining,

$C_I$  is the MRE-equivalent, respirable mass concentration measured in the intake air, and

$T_I$  is the time after mining was stopped until the end of the shift.

During sampling for a shift, supplemental notes were taken regarding cutting time, downtime, the amount and location of bad roof areas, tram speed of the shearer, the type of cutting (one-way or two-way), and the cross-sectional area and air velocity at

# RESPIRABLE DUST ON A LONGWALL PANEL

sampling locations. Ventilation arrangements, dust control procedures used, work habits of employees, the amount of mineral partings and floor mined, and shift productivity were also noted.

## Distribution of Samples for Analysis

Following determination of mass concentrations, it was decided that three samples would be analyzed for mineral composition, mineral sizing, and mineral shape and angularity characteristics using available scanning electron microscopes (SEM's). Laboratory personnel required one set of samples for refining their analytical techniques of preparing and mounting samples and for practicing determinations or measurements of the desired characteristics. Three other samples for each location were designated for determination of alpha quartz percentages using infrared spectrometry. Total respirable dust size distributions were desired from the remaining three sets of samples.

## Scanning Electron Microscope Analysis

Cambridge Stereoscan 150 scanning electron microscopes were available for identification of minerals, particle sizing, and particle shape/angularity micro-analysis. Kevex 7000 analytical spectrometers are interfaced with the SEM's for describing X-rays in terms of their energy (energy dispersive X-ray analysis). Analyses were made for 100 particles from each sample.

Time of exposure for individual particles to X-ray bombardment varied, but generally 20 to 74 seconds were needed to positively identify the mineralogy based on proportional counts of elements displayed on a cathode ray tube (CRT). Figure 1 shows a typical X-ray spectrum (in energy levels) for illite. The normal energy level used for the electron beam was 20KV during mineral identification. Specimens were coated with gold to prevent surface charging.

The scanning screen was used to randomly locate particles in a field. A selected particle was then "spotted" and bombarded for identification. Following identification, the size of the particle was determined from the focused image on the screen to the nearest 0.5  $\mu\text{m}$  using a superimposed scale. The shape of the particle was ranked according to the following system:

- 1 - equiaxial
- 2 - oblate

- 3 - tabular
- 4 - irregular
- 5 - prolate
- 6 - acicular

Photographs were taken of some of the particles to show the different rankings (see Figure 2). The key result in shape

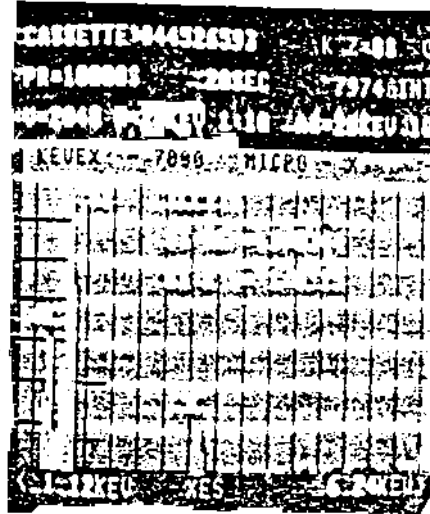


Figure 1. Energy Dispersive X-ray Spectrum for Illite.

characterization with respect to health effects is believed to be the percentage of prolate and acicular particles present in a sample. These particles approach the fibrous structure of other minerals where fibrosity was correlated with sarcoma production (Shedd, Virta, and Wylie, 1982). This percentage should be adequately determined by use of the shape ranking system.

A ranking system (after Powers, 1953) was also used to characterize the angularity of particles. The rankings are:

- 1 - very round
- 2 - round
- 3 - sub-round
- 4 - sub-angular
- 5 - angular
- 6 - very angular

The key result is the percentage of particles which were ranked as angular or very angular. Photographs of one hundred particles for one sample in each

set will be taken so that fractal dimensions of particle profiles can be manually determined (Mandelbrot, 1977; Kaye, 1984) and correlations made with particle ranks.

#### Infrared Spectrometry Analysis

Alpha quartz percentages for individual samples were determined by infrared spectrometry using the USBM developed chemical method number P7 (USBM, 1982). In this method, the MSA filters containing respirable dust are low-temperature ashed to destroy organic materials. After the remaining mineral matter is redeposited on another membrane filter, the sample is scanned by infrared spectrometry to determine the presence of quartz. The weight of the quartz in the sample is determined from using measured quartz peak absorbance units and the calibration curve (linear) for a quartz standard. Minus 5  $\mu\text{m}$  Min-U-Sil was used as the standard since its performance has been tested and found reliable (Kacsmar and Tomb, 1984).

#### Total Respirable Dust Sizing

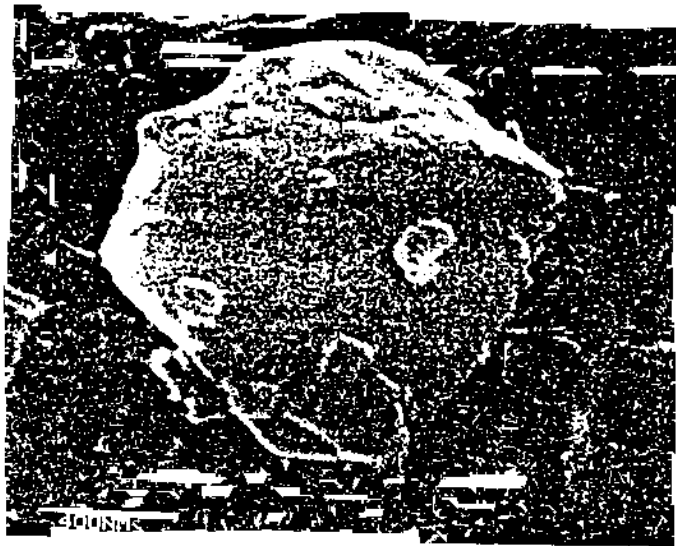
The sizing of total respirable dust was originally planned to be accomplished using 6-stage, personal cascade impactors. Following several determinations, however, it was decided that the short sampling time involved (12 to 15 min before substrate overloading occurred) led to nonrepresentative samples of average full-shift coal dust exposure for workers. The longwall panel was frequently not producing coal and also intermittently mining roof rock (due to bad roof areas). Accurate determinations of actual cutting time, shield moving time, rock crushing time, and the effect of cutting rock at different locations during the sampling period would be necessary in order to estimate representative exposures.

In lieu of using impactors, a TSI, Inc., Aerodynamic Particle Sizer (APS), Model 3300, equipped with a dust dispersion system developed by Marple and Rubow (1984) will be used for determining total respirable dust size distributions for samples. The dust dispersion system is able to provide a steady flow of single particles through the APS. Results have not yet been received.

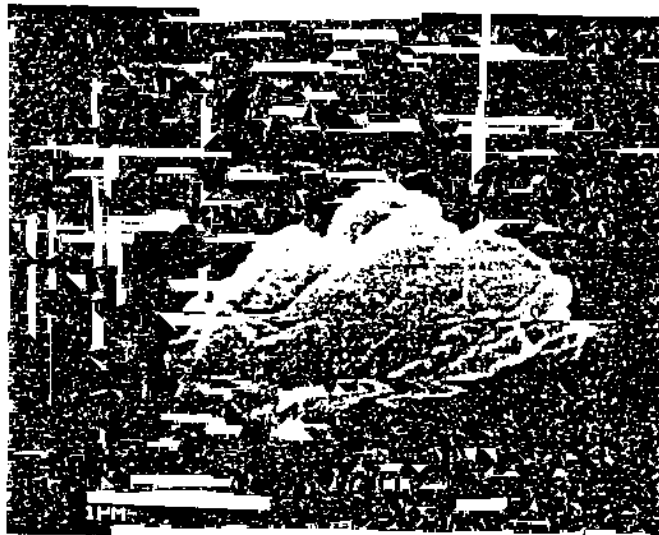
### RESULTS AND DISCUSSION

#### Respirable Mass Concentration

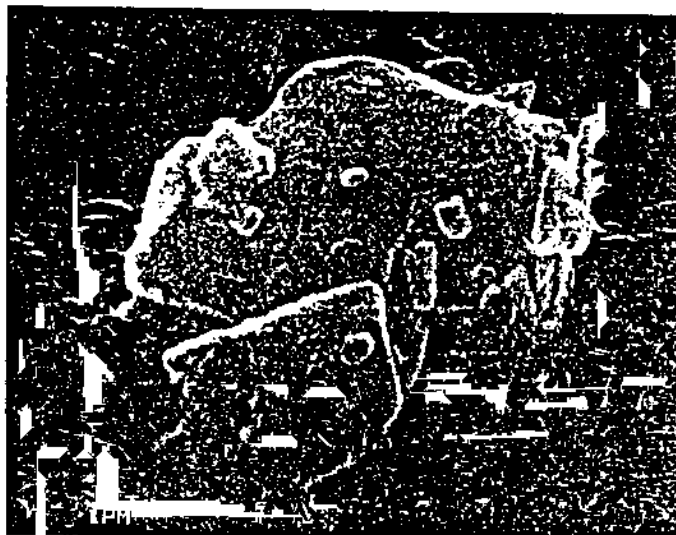
Table 1 shows the data used to build a regression model for the relationship



EQUIAXIAL

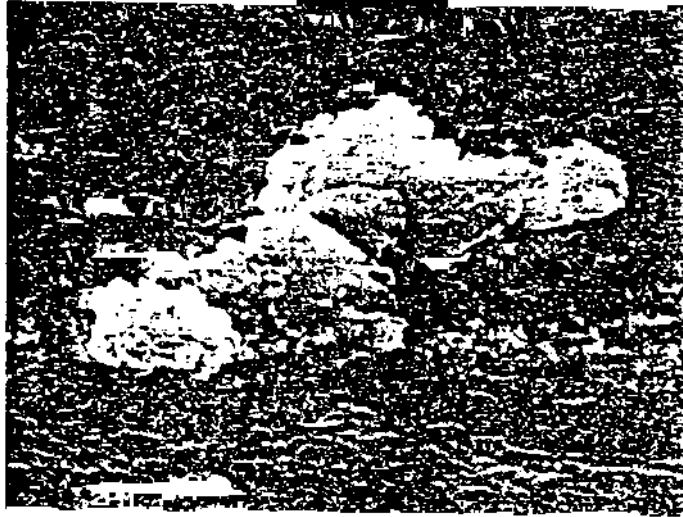


OBLATE

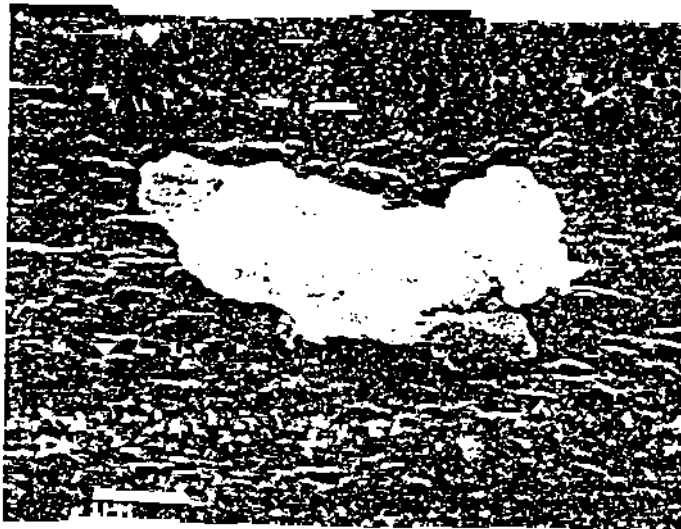


TABULAR

Figure 2. Particle Shape Ranking System.



IRREGULAR



PROLATE

Figure 2. Particle Shape Ranking System (Continued).

## THE RESPIRABLE DUST CENTER

between respirable mass concentration and location on the longwall panel. The sample number (SAMPNO), the date of sampling (DT), location on the longwall face (LOCN), and the normalized.

full-shift respirable mass concentration (CONC) are listed.

Location is coded proportional to the actual distance along the face:

Table 1. Respirable Dust Concentration Data.

OBS	SAMPNO	DT	LOCN	CONC
1	44526023	840517	0	0.45
2	44526469	840517	1	1.16
3	44526593	840517	4	3.02
4	44526920	840517	5	5.33
5	44683829	840524	0	0.00
6	44526442	840524	1	0.00
7	44526204	840524	3	0.73
8	44526076	840524	5	1.73
9	44682714	840525	0	0.00
10	44684021	840525	1	0.00
11	44684002	840525	3	1.01
12	44684010	840525	4	1.58
13	44684007	840525	5	3.02
14	44683370	840531	0	0.00
15	44682713	840531	1	0.72
16	44684008	840531	3	1.58
17	44684005	840531	4	1.15
18	44682718	840531	5	2.88
19	44684026	840607	0	0.00
20	44683845	840607	1	0.29
21	44683844	840607	3	1.01
22	44683825	840607	4	0.72
23	44683831	840607	5	2.76
24	44684003	840608	0	0.00
25	44684027	840608	1	1.01
26	44683830	840608	3	1.01
27	44683605	840608	4	1.01
28	44684014	840608	5	1.44
29	44683842	840614	0	0.00
30	44683827	840614	1	0.14
31	44682712	840614	3	0.29
32	44683584	840614	4	0.29
33	44683848	840614	5	2.30
34	44683590	840615	0	0.00
35	44684024	840615	1	0.29
36	44583586	840615	3	1.01
37	44683838	840615	5	3.31
38	44683608	840621	0	0.00
39	44683607	840621	1	0.00
40	44683589	840621	3	1.87
41	44683597	840621	4	2.44
42	44683596	840621	5	4.03

0 - Intake air,

1 - Headgate,

3 - Mid-face,

4 - 3/4-face, and

5- Tailgate.

The model could be expanded to include the worker positions at the lead and tail ends of the shearer, but coding of these locations would be contrived to fit the model (e.g., lead shearer = 6). Therefore, they were omitted.

## RESPIRABLE DUST ON A LONGWALL PANEL

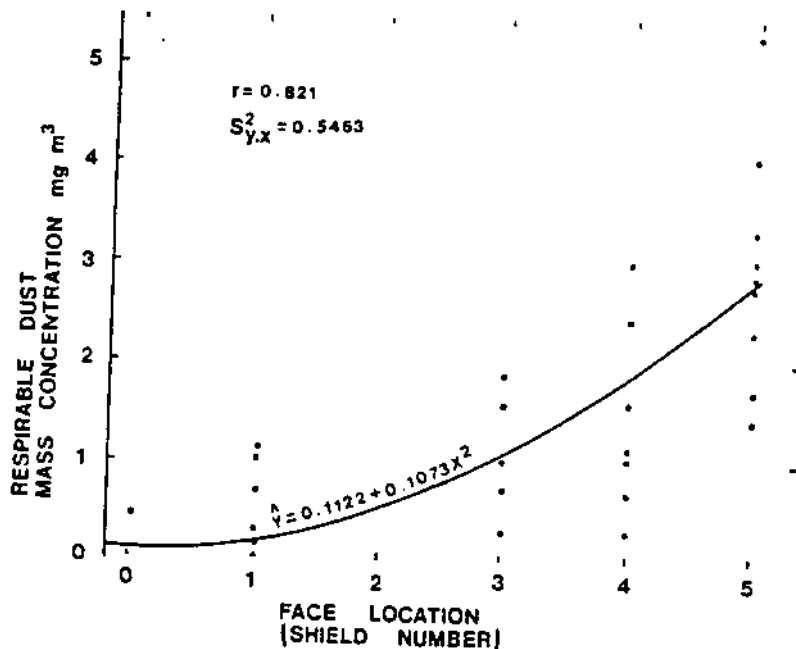


Figure 3. Relationship Between Respirable Mass Concentration and Face Location.

Figure 3 depicts the final model, reflecting a quadratic relationship between respirable mass concentration and location on this particular panel. The relationship is expressed by the formula:

$$(2) \quad \hat{Y} = 0.1122 + 0.1073X^2$$

where:

X is location on the face

$\hat{Y}$  is the estimated respirable mass concentration at X.

The linear term of the regression model proved insignificant. Pure error associated with the data amounted to 30.3% of the total variation, but the model fit was good. A high correlation coefficient ( $r=0.821$ ) was obtained. The estimated variance was 0.5463, which is not far from the 0.4 value associated with the sampling procedure (Jacobson, 1969). Of course, the variability with respect to different locations is lumped into this estimate of variance.

An examination of residuals shows a possible outlier at location 5 (tailgate, CONC=5.33). This is confirmed by using the following formula to test it:

$$(3) \quad \left| \frac{Y_1 - \bar{Y}}{s} \right| > 4 \text{ standard deviations}$$

However, it was not removed from the data set and the model was not rerun because other mass concentrations at corresponding face locations on the same date indicate that the value may be accurate.

### Mineral Composition

The mineral composition of each sample was determined by identifying the mineralogy of each of the particles. Quartz ( $\text{SiO}_2$ ), illite [ $(\text{OH})_4\text{K}_2(\text{Si}_4\text{-Al}_2)\text{Al}_4\text{O}_{12}$ ], calcite ( $\text{CaCO}_3$ ), and pyrite ( $\text{FeS}_2$ ) were the predominant minerals. Of the 1680 particles identified so far, 109 were quartz (6.5%), 926 were illite (55.1%), 361 were calcite (21.5%), and 137 were pyrite (8.2%). The remaining 147 particles were of many different types of mineralogy ( $\text{BaSO}_4$ ,  $\text{Ag}_2\text{S}$ ,  $\text{TiO}_2$ ,  $\text{CaSO}_4$ ), but they did not group to form another major mineral.

Figures 4, 5, 6, and 7 show a plot of the percentage of specific minerals by location on the panel. Modeling of the mineral count by location showed that a regression model, linear in LOCN, explains the relationship best for illite and calcite. No relationship was found significant between percentage of quartz and location or between pyrite and location. Table 2 gives the percentage composition by location.

# THE RESPIRABLE DUST CENTER

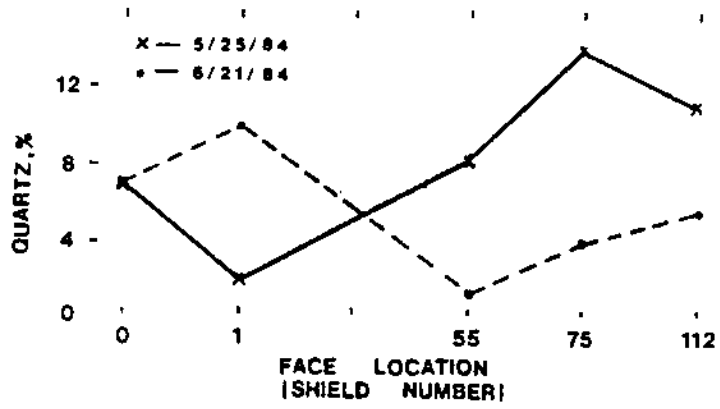


Figure 4. Percentage Quartz by Location.

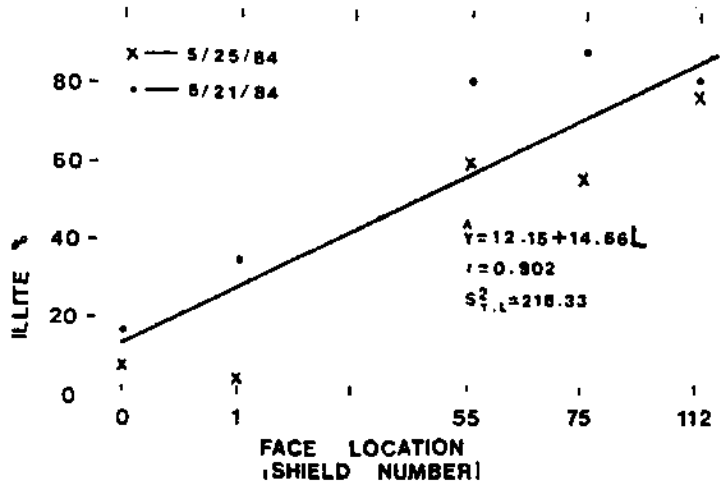


Figure 5. Percentage Illite by Location.

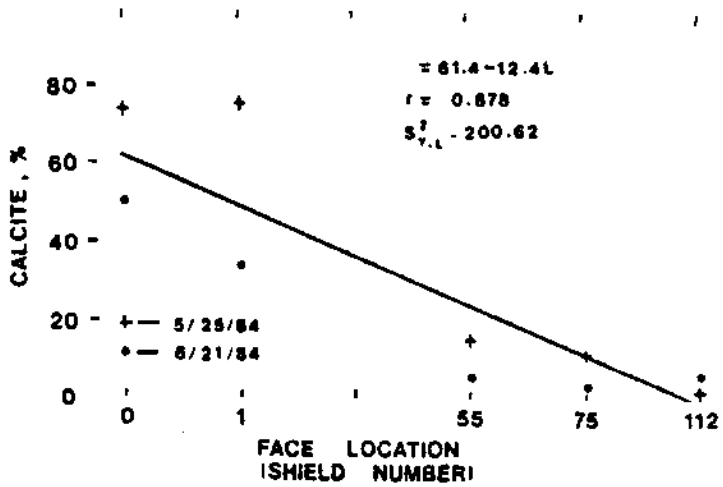


Figure 6. Percentage Calcite by Location.

## RESPIRABLE DUST ON A LONGWALL PANEL

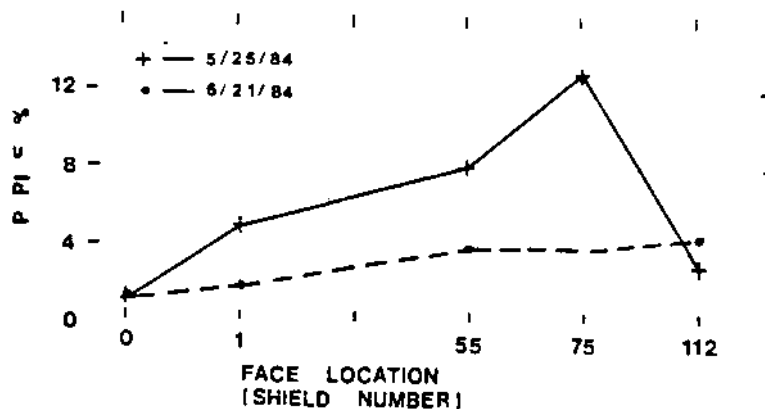


Figure 7. Percentage Pyrite by Location.

An increase in the percentage of pyrite was noted at the lead and tail shearer locations. This resulted from rollback of coal dust from the face to the operator location. Also, it was seen that the composition of mineral matter for the shield mover was split primarily between illite (43%) and calcite (31%), reflecting the amount of time spent in intake air during the shift. The generally reduced percentages of calcite for 6-21-84 can be attributed to the amount of shale which was falling from the roof and getting crushed at the headgate, yielding more illite.

### Mineral Size Distributions

Total size distributions for the different locations sampled are given in Table 3 by sample number. They follow the lognormal distribution in general. Geometric, count median Feret's diameters are listed. A plot of the geometric median diameters by location by date is shown in Figure 8. No low-order linear regression model fits the data (a quartic equation does but is not meaningful). No difference

was detected between the size distributions of different sampling dates. An analysis-of-variance (ANOVA) performed on the mineral means by location, however, indicates that the median particle size at the tailgate is smaller than those for all other locations. Results, using Fisher's least significant difference test following a significant F-test, were:

Location	Median Diameter (um)	Group
#112 Shield	1.171	A
#55 Shield	1.547	B
Lead Shearer	1.548	B
Tail Shearer	1.568	B
#75 Shield	1.658	B
#1 Shield	1.671	B
Shield Mover	1.749	B
Intake Air	1.816	B

It should be noted that only mineral means determined by more than five particles were used in the ANOVA. It is interesting to note that the mean particle size obtained for the shield mover reflects the fact that he spends much time in intake air, which had the largest mean particle size.

Mineral	Sample	Intake	#1	#55	#75	#112	Lead Shear	Tail Shear	Shield Mover
	Date								
Quartz	5-25	7.0	2.0	8.0	14.0	2.0	6.0	7.0	7.0
	6-21	7.0	10.0	1.0	4.0	9.0	3.2	3.0	-
Illite	5-25	8.0	3.0	60.0	56.0	79.0	42.0	33.0	43.0
	6-21	17.0	35.0	81.0	89.0	80.5	82.8	72.0	-
Calcite	5-25	74.0	76.0	16.0	12.0	2.0	0	23.0	31.0
	6-21	51.0	34.0	6.0	3.0	7.5	2.2	8.0	-
Pyrite	5-25	1.0	5.0	8.0	13.0	3.0	36.0	30.0	5.0
	6-21	1.0	2.0	4.0	4.0	4.5	5.4	12.0	-

Table 2. Mineral Composition by Location (in %).



**THE RESPIRABLE DUST CENTER**

For each sample, size distributions were also determined for quartz, illite calcite, and pyrite. The data is shown in Table 4. A plot of the data for face locations is given in Figure 9. Analysis-of-variance of the data in Table 4 reveals that the median diameters of quartz (1.44  $\mu\text{m}$ ) and pyrite (1.31  $\mu\text{m}$ ) are smaller than those of illite (1.74  $\mu\text{m}$ ) and calcite (1.79  $\mu\text{m}$ ). Cubic regression models containing linear and quadratic terms are required to accurately represent the data for quartz and illite, shown in Figure 9, but these relationships are not considered practical at this time with only two samples analyzed for each location. No meaningful relationship can be determined yet for pyrite or calcite either.

Sample Quartz Percentages

The percentages of quartz for samples, as determined by USBM method P7, are listed in Table 5. No significant difference exists among the mean quartz percentages for different dates. Likewise, there was no difference among means for different locations on the panel (intake air location being the only obvious exception). The average quartz percentage was very low for this panel (0.46%) when compared to many other operations. It is interesting to note that the highest (though not significantly so) mean quartz percentage was obtained on 6-14-84, when mining was maintained under coal top.

Sample Location (Number)	Geometric Median Diameter ( $\mu\text{m}$ )	Frequencies								
		Size Fraction Mid-point, $\mu\text{m}$ (Feret's Diameter)								
		0.5	1.0	1.5	2.0	2.5	3.0	4.0	5.0	>5.0
Intake (44682714)	1.496	1	31	25	21	15	1	5	0	0
#1 Shield (44684021)	1.865	1	13	19	29	13	17	7	0	0
#55 Shield (44684002)	1.499	9	30	12	20	12	7	3	4	1
#75 Shield (44684010)	1.773	1	22	24	26	7	11	5	3	0
#112 Shield (44684007)	1.179	12	41	28	17	1	1	0	0	0
Lead Shearer (44683847)	1.603	1	29	17	26	10	13	3	0	0
Mid-Shearer (44684023)	1.522	1	37	17	30	8	4	1	1	0
Tail Shearer (44684013)	1.578	2	29	23	18	15	7	4	1	0
Shield Mover (44683826)	1.951	3	17	18	21	15	12	9	1	3
Intake (44683608)	1.852	4	20	15	27	9	10	9	4	1
#1 Shield (44683607)	1.594	7	27	13	28	9	10	3	2	0
#55 Shield (44683589)	1.791	2	21	21	24	15	8	5	3	0
#75 Shield (44683597)	1.863	4	21	20	24	7	9	8	2	5
#112 Shield (44683596-1)	1.326	7	43	20	20	2	6	2	0	0
#112 Shield (44683596-2)	1.107	22	38	22	9	3	4	0	2	0
Lead Shearer (44683585)	1.355	10	32	18	20	4	7	2	0	0
Tail Shearer (44683602)	1.651	3	24	21	29	10	9	3	0	0
<b>Total</b>		<b>90</b>	<b>475</b>	<b>333</b>	<b>389</b>	<b>155</b>	<b>136</b>	<b>69</b>	<b>23</b>	<b>10</b>

Table 3. Total Particle Size Distributions for Different Locations on the Face.

# RESPIRABLE DUST ON A LONGWALL PANEL

## Particle Shape Characterization

As mentioned previously, the focus in shape characterization has been placed on detecting elongated particles. In particular, the percentage of particles classified as prolate (rod-shaped, aspect ratio  $\geq 3$  to 1) for each sample was determined. Table 6 indicates that only 3.45% of the 1680 particles characterized were classified as prolate (or acicular). It also shows that virtually identical results were

obtained for samples of 5-25-84 and 6-21-84 (3.59% and 3.30% respectively).

An analysis of particle shape by mineral type was done to detect differences. Table 7 shows the mean shape value of particles for the four major minerals, listed by location. ANOVA for this data revealed that the average shape value for illite is different from the other three minerals;

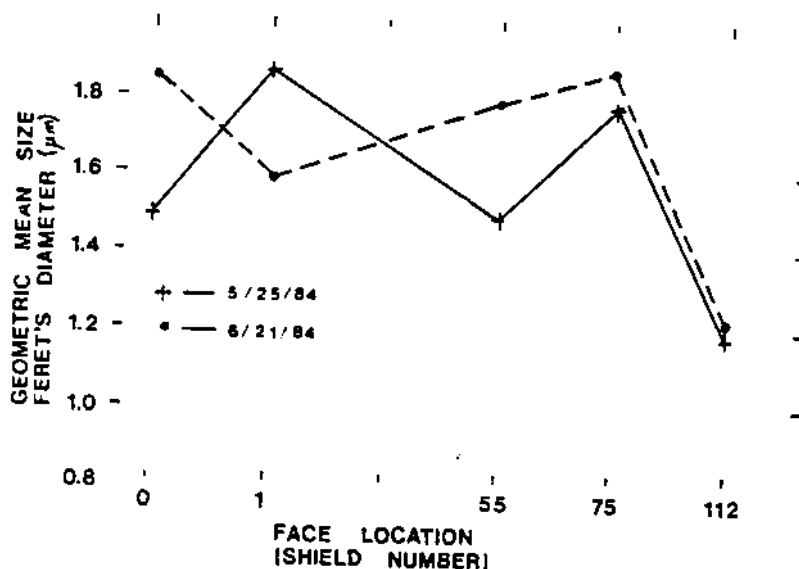


Figure 8. Sample Mean Particle Size by Location.

Table 4. Mean Feret's Diameter ( $\mu\text{m}$ ) for Minerals by Location.

Location	Mineral			
	Quartz	Illite	Calcite	Pyrite
Intake	1.667	2.170	1.610	-
#1 Shield	1.357	1.820	1.875	1.632
#55 Shield	1.408	1.663	1.882	1.235
#75 Shield	1.815	1.912	1.612	1.293
#112 Shield	0.967	1.219	1.527	0.970
Lead Shearer	1.657	1.438	-	1.548
Tail Shearer	1.339	1.750	1.997	1.184
Shield Mover	1.280	1.955	2.011	-

Note: Only mean sizes determined by more than five particles are listed.

## THE RESPIRABLE DUST CENTER

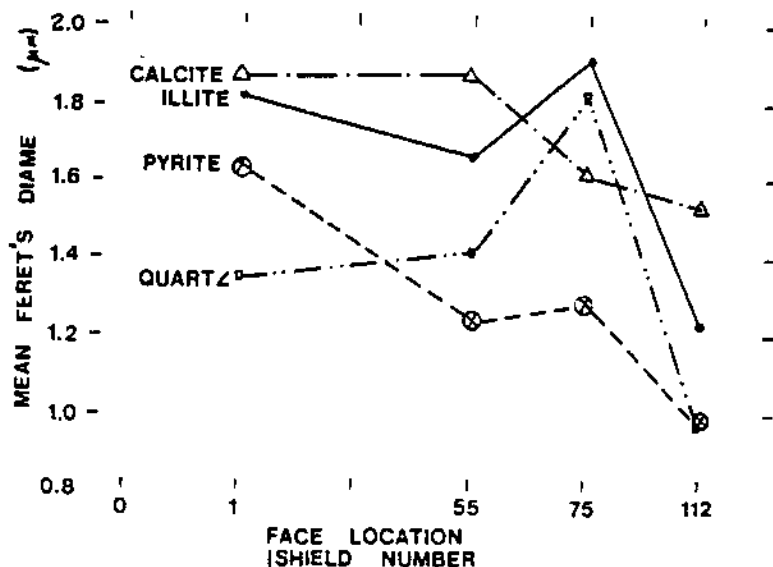


Figure 9. Mineral Mean Particle Size by Location.

both a Fisher's LSD and a Waller-Duncan K-ratio T-test were used. Illite was ranked consistently higher for all but one location. ANOVA of particle shape by location revealed no difference in shape among locations ( $F=0.93$ ). Therefore, no model was developed for particle shape by location. Information from the last set of samples may change the outcome, but it is unlikely. Figure 10 shows a plot of the mineral mean shape values by face location.

### Particle Angularity Characterization

The focus for the angularity analyses has been aimed at determining the percentage of particles classified as angular or very angular. Table 8 shows the percentage of particles classified as angular for samples analyzed thus far. Note that 23.93% of the 1680 particles were angular (on the average), but a difference of 10.65% exists between sampling dates. These results

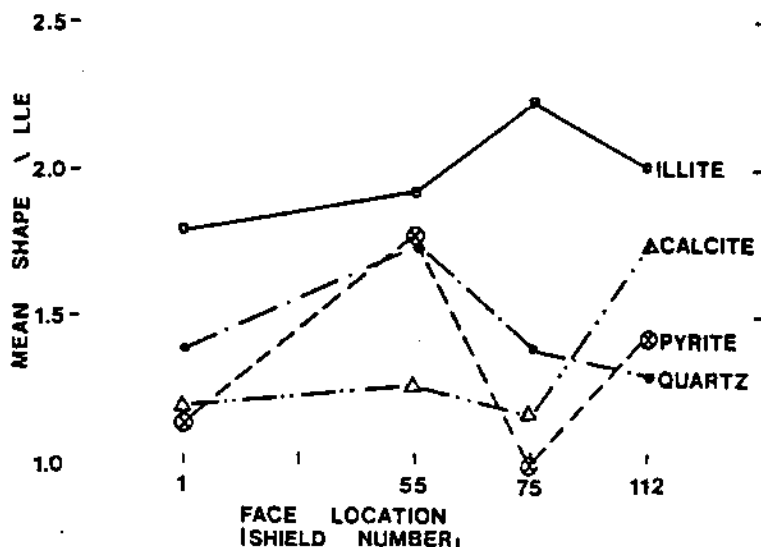


Figure 10. Mineral Mean Shape Values by Location.

## RESPIRABLE DUST ON A LONGWALL PANEL

suggest that a difference in angularity existed for varying conditions. Such a conclusion, however, is not warranted until all sample analyses are received, including fractal analyses on photographs from samples obtained under different roof conditions.

Angularity of particles by mineral and location was examined. Table 9 shows the mean angularity values for minerals by location. Analysis-of-variance on this data revealed that there is insufficient evidence to

conclude a difference exists among minerals but that particles at the tailgate are less angular than those at all other locations. This agrees with the findings reported by Stein and Corn (1976) that larger particles are less round than smaller ones. A conclusion, however, will be withheld at this time until fractal analyses on particles are made. It is possible that the ranking system employed and the resolution obtained by the SEM when examining smaller particles were inadequate to

Table 5. Percentage Quartz by Location.

Location	Sample Date			Mean Percentage
	5-31-84	6-14-84	6-15-84	
Intake	0	0	0	0
#1 Shield	0.45	0	0.75	0.40
#55 Shield	0.41	0.75	0.64	0.60
#75 Shield	0.66	1.88	-	-
#112 Shield	0.34	0.33	0.52	0.40
Lead Shearer	0.20	0.13	0.16	0.16
Tail Shearer	-	-	0.38	-
Shield Mover	0.54	0.75	0.75	0.68
Mean Percentage	0.37	0.55	0.46	0.46

Table 6. Percentage of Elongated Particles in Characterized Samples.

Date	Sample	Location	Number of Particles Classified as Prolate	Percentage
5-25-84	44683847	Lead Shearer	10	10.30
	44682714	Intake	6	6.00
	44684021	#1 Shield	4	4.04
	44684013	Tail Shearer	3	3.00
	44684002	#55 Shield	2	2.06
	44684010	#75 Shield	3	3.03
	44684007	#112 Shield	2	2.00
	44683826	Shield Mover	1	1.01
	44684023	Mid-Shearer	1	1.01
	6-21-84	44683608	Intake	2
44683607		#1 Shield	2	2.04
44683585		Lead Shearer	0	0.00
44683602		Tail Shearer	1	1.01
44683596		#112 Shield	6	6.00
44683596		#112 Shield	3	3.00
44683589		#55 Shield	4	4.04
44683597		#75 Shield	8	8.00
			58	3.45

**THE RESPIRABLE DUST CENTER**

Location	Mineral				Mean Value
	Quartz	Illite	Calcite	Pyrite	
#1 Shield	1.400	1.800	1.199	1.143	1.386
#55 Shield	1.750	1.933	1.269	1.773	1.681
#75 Shield	1.390	2.224	1.170	1.000	1.446
#112 Shield	1.295	2.003	1.730	1.415	1.611
Tail Shearer	1.860	1.778	1.100	1.227	1.491
Mean Value	1.539	1.948	1.294	1.312	

Table 7. Mean Shape Values for Minerals by Location.

Sample	Location	Number of Particles Classified as Angular	Percent Angular	Avg. for Date
Samples of 5-25-84				
44683847	Lead Shearer	30	30.30	
44682714	Intake	27	27.00	
44684021	#1 Shield	34	34.30	
44684013	Tail Shearer	21	21.00	
44684002	#55 Shield	20	20.62	
44684010	#75 Shield	23	23.23	
44684007	#112 Shield	21	21.00	
44683826	Shield Mover	46	46.46	
44684023	Mid-Shearer	36	36.36	28.92
Samples of 6-21-84				
44683608	Intake	32	32.32	
44683607	#1 Shield	19	19.39	
44683585	Lead Shearer	15	16.13	
44683602	Tail Shearer	24	24.24	
44683596	#112 Shield	10	10.00	
44683596	#112 Shield	8	8.00	
44683589	#55 Shield	18	18.18	
44683597	#75 Shield	18	18.00	18.27
		402	23.93	

Conditions: 5-25-84: no bad roof  
 6-21-84: bad roof #35 to #50 shields, all shift

Table 8. Percentage of Angular Particles in Characterized Samples.

## RESPIRABLE DUST ON A LONGWALL PANEL

Location	Mineral				Mean Value
	Quartz	Illite	Calcite	Pyrite	
#1 Shield	3.20	3.60	3.97	4.14	3.73
#55 Shield	4.13	3.87	4.04	3.64	3.92
#75 Shield	4.14	3.71	4.42	4.19	4.12
#112 Shield	2.91	3.47	3.47	3.25	3.28
Tail Shearer	3.85	3.96	4.00	4.00	3.95
Mean Value	3.65	3.72	3.98	3.84	

Table 9. Mean Angularity Values for Minerals by Location.

distinguish angularity. The particles at the tailgate averaged  $1.171 \mu\text{m}$  (Feret's diameter) whereas a range of  $1.547 \mu\text{m}$  to  $1.816 \mu\text{m}$  existed for the other locations. A manual fractal analysis is possible for a limited number of particles and may detect a real difference in angularity by location, but fractal analysis on a large number of particles is practical only with the aid of an image analyzer.

### Reproducibility of SEM Analyses

A dual analysis was made under the SEM of sample number 44683596, taken at the tailgate location on 6-21-84. Two separate and distinct analyses were made from a single mount to test reproducibility of results. Results from the analyses are given in Table 10. Both values obtained for Feret's mean diameter agree with the  $1.179 \mu\text{m}$  mean value obtained for the other tailgate sample. Likewise, the results for the shape and angularity analyses agree well within test limits.

T-tests, using

$$(4) \quad t = \frac{\log \bar{Y} - \log \mu_0}{\log(\text{GSD})/\sqrt{n}}$$

for the lognormal size distributions, and

$$(5) \quad t = \frac{\bar{Y} - \mu_0}{s/\sqrt{n}}$$

for the shape and angularity distributions

were performed to verify that all the means of Table 10 were in agreement within a 95% confidence interval. T-values of  $-1.778$ ,  $1.755$ ,  $-1.56$ ,  $1.44$ ,  $-0.81$ , and  $0.81$ , respectively, were obtained in the individual t-tests.

These were compared to a critical t-value of:

$$t(0.025, 100) = 1.99$$

### CONCLUSIONS

This study shows that respirable dust samples taken for compliance purposes can be useful in examining various physical characteristics of the dust. Many studies, including this one, have found a strong relationship between respirable mass concentration and worker location. Using scanning electron microscopy, the composition of mineral matter in dust can be estimated and meaningful correlations made with worker locations. It was seen that the percentage of illite particles increased at a constant rate and that the percentage of calcite particles decreased at a constant rate from the headgate to the tailgate of the first longwall panel. Pyrite particles were significantly more prevalent at the shearer operator locations. Mineral particle size analyses can reveal size differences among mineral types and among locations, which may prove useful in the study of long-term health effects. In this study, it was seen that smaller particles exist at the tailgate and that illite and calcite particles are larger than quartz and pyrite particles.

Examinations of particle shape and angularity (or periphery ruggedness) can also be made under the SEM. The use of an image analyzer would greatly enhance that capability, especially in studying angularity. But differences in particle shape among minerals and possibly among locations can be detected. In this study, it was determined that illite particles (generally of larger size) were more deviant from equiaxiality

## THE RESPIRABLE DUST CENTER

than the particles of other minerals. No differences in particle shape among locations, however, were detected. It was also seen that particles at the tailgate location are less angular than those at all other locations, but no differences in angularity were detected among minerals. It should be noted that using an image analyzer, which has superior capabilities in studying the profile ruggedness of particles, may discover differences which cannot be detected by the ranking system of this study. The ranking system is capable of detecting only gross differences.

### ACKNOWLEDGMENTS

This research was sponsored by the US Bureau of Mines through the Generic Technology Center for Respirable Dust. The authors gratefully acknowledge their support. USBM Grant No. G1135142

Very painstaking analytical work was accomplished by Eric Hopkins and Richard Ondrey through the US Geological Survey Laboratory under the direction of Dr. Jack Renton and by Thomas Simonyi and Marilyn Noah through the College of Mineral and Energy Resources Analytical Laboratory under the direction of Larry Nice. Their important contributions are sincerely appreciated.

### REFERENCES

Corn, M., et al., 1973, "Physical and Chemical Properties of Respirable

Coal Dust from Two United States Mines," American Industrial Hygiene Association Journal, Vol. 34, pp. 279-285.

Davis, J.M.G., Ottery, J., and Le Roux A., 1975, "The Effect of Quartz and Other Non-Coal Dusts in Coalworkers' Pneumoconiosis, Part II, Lung Autopsy Study," Inhaled Particles IV, Walton, W.H., ed., Unwin Bros., Old Woking, Surrey, pp. 691-702.

Hinds, W.C., 1982, Aerosol Technology: Properties, Behavior, and Measurement of Airborne Particles, John Wiley and Sons, New York.

Jacobsen, M., et al., 1971, "The Relationship Between Pneumoconiosis and Dust Exposure in British Coal Mines," Inhaled Particles III, Walton, W.H., ed., Unwin Bros., Old Woking, Surrey, pp. 903-917.

Jacobson, M., 1969, "Assessing Respirable Dust in United States Coal Mines," Proceedings, Symposium on Respirable Coal Mine Dust, Washington, pp. 42-54.

Kacsmar, P.M., and Tomb, T.F., 1984, "Comparison of Alpha Quartz Materials Used as Calibration Standards," Proceedings, Coal Mine Dust Conference, Pang, S.S., ed., West Virginia University, Morgantown, pp. 144-149.

Sub-sample Number	Ferret's Diameter ( $\mu\text{m}$ )		Shape Value (% Prolate)		Angularity (% angular)	
	Geometric Mean	GSD	Mean	SD	Mean	SD
1	1.326	1.58	2.00 (6%)	0.97	3.22 (10%)	0.57
2	1.107	1.727	1.73 (3%)	0.79	3.07 (8%)	1.00
Combined	1.211	1.667	1.87	0.90	3.15	0.99

100 particles from each sub-sample were analyzed.  
GSD = geometric standard deviation  
SD = standard deviation

Table 10. Reproducibility of SEM Analysis.

## RESPIRABLE DUST ON A LONGWALL PANEL

- Kaye, B.H., 1981, Direct Characterization of Fineparticles, John Wiley and Sons, New York.
- Leiteritz, H., Bauer, D., and Bruckman, E., 1971, "Mineralogical Characteristics of Airborne Dust in Coal Mines of Western Germany and Their Relations to Pulmonary Changes in Coal Hewers," Inhaled Particles III, Walton, W.H., ed., Unwin Bros., Old Woking, Surrey, pp. 729-743.
- Mandelbrot, B.P., 1977, Fractals, Form, Chance and Dimension, W.H. Freeman, San Francisco.
- Marple, V.A., and Rubow, K.L., 1984, "Instrumentation for the Measurement of Respirable Coal Mine Dust," Proceedings, Coal Mine Dust Conference, Peng, S.S., ed., West Virginia University, Morgantown, pp. 214-221.
- Morgan, W.K.C., 1971, "Coal Workers' Pneumoconiosis," American Industrial Hygiene Association Journal, Vol. 32, No. 1, January, pp. 29-34.
- Morgan, W.K.C., et al., 1973, "The Prevalence of Coal Workers' Pneumoconiosis in U.S. Coal Miners," Archives of Environmental Health, Vol. 27, No. 4, October, pp. 221-226.
- Powers, M.C., 1953, "A New Roundness Scale for Sedimentary Particles," Journal of Sedimentary Petrology, Vol. 23, No. 2, June, pp. 117-119.
- Raisner, M.T.R., and Robock, K., 1977, "Results of Epidemiological, Mineralogical, and Cytotoxicological Studies on the Pathogenicity of Coal-Mine Dusts," Inhaled Particles IV, Walton, W.H., ed., Unwin Bros., Old Woking, Surrey, pp. 703-715.
- Sharkey, A.G., Kessler, T., and Friedel, R.A., 1975, "Trace Elements in Coal Dust by Spark-Source Mass Spectrometry," Trace Elements in Fuel; Babu, S.B., ed., American Chemical Society, Washington, pp. 48-56.
- Shedd, K.B., Virta, R.L., and Wylie, A.G., 1982, "Size and Shape Characterization of Fibrous Zeolites by Electron Microscopy," USBM RI8674.
- Stein, F., and Corn, M., 1976, "Shape Factors of Narrow Size Range Samples of Respirable Coal Mine Dust," Powder Technology, Vol. 13, pp. 133-141.
- USBM, 1982, "Infrared Determination of Quartz in Respirable Coal Mine Dust," Chemical Method No. P7, Physical and Chemical Analysis Branch, revised March 12, 1982.
- Walton, W.H., Hadden, G.G., and Jacobsen, M., 1975, "The Effect of Quartz and Other Non-Coal Dusts in Coalworkers' Pneumoconiosis, Part I, Epidemiological Studies," Inhaled Particles IV, Walton, W.H., ed., Unwin Bros., Old Woking, Surrey, pp. 669-690.



# A Methodology for Determining the Mineral Content and Particle Size Distribution of Airborne Coal Mine Dust

T.J. Stobbe<sup>1</sup>, R. W. Plummer<sup>1</sup>, H. Kim<sup>1</sup> and W. G. Jones<sup>2</sup>

<sup>1</sup>Department of Industrial Engineering, West Virginia University

<sup>2</sup>Division of Respiratory Disease Studies, National Institute for Occupational Safety & Health

## Introduction

Disease-associated dusts in coal mine environments continue to afflict miners in today's modern mines. The relationship between exposure to coal mine dust and the development of various respiratory diseases has been well recognized; however, the reasons for variation in occurrence of these diseases among miners in different geographic areas,<sup>(1)</sup> rank of coal seams,<sup>(2,3)</sup> and jobs<sup>(4)</sup> remain uncertain. Several papers have reported on the causal agent in the development of these diseases. Davis<sup>(5)</sup> found that the percentage of the non-coal minerals present in the lungs of deceased miners increased as the level of pneumoconiosis became more severe. Reisner<sup>(6)</sup> reported that cell damage caused by coal mine dust increases with the mineral and quartz content of the dust and with the geological age and rank of the coals. Two studies, investigating the *in vitro* effects of mineral dusts, reported by Seemayer and Manojlovic<sup>(7)</sup> also obtained positive correlation between cytotoxicity and the mineral content of coal mine dust. Gormly<sup>(8)</sup> postulated that destruction of macrophages by certain mineral dusts is the first step in the development of pneumoconiosis. In 1980, Adamis and Timar<sup>(9)</sup> reported that quartz, sandstone, slate, respirable colliery dust, bentonite, illite, and some kaolins had

Exposure to airborne dust in coal mines has caused respiratory disease in coal miners. The causal agent in these diseases remains unknown, although the minerals found in and around the coal seam have been implicated. Toxicological studies designed to establish the effect of different mineral combinations and concentrations are lacking because the mineral content of coal mine dust has not been defined. This paper reports the initial results of a study done to characterize the mineral content of the coal mine dust found in a mine in the Upper Freeport seam in Northern West Virginia. Coal mine dust samples were collected using 4-stage cassette impactors at nine locations in the mine. The samples were analyzed by an x-ray microdiffraction film technique supplemented by energy dispersive scanning electron microscopy. Primary size modes of about 17 to 20 micrometers from the samples collected at the haulageway and the returnside of the continuous miner were found. From the returnside of the roof bolter samples, a primary size mode of 12 to 15 micrometers was measured. The minerals found in high percentages were illite, kaolinite, quartz, and calcite. The distribution of minerals in inter- and intra- location samples showed wide variations. Trends in these variations are presented. Stobbe, T. J.; Plummer, R. W.; Kim, H.; Jones, W.: Characterization of coal mine dust. *Appl. Ind. Hyg.* 2:95-100; 1986.

cytotoxic effects on rat peritoneal macrophages "*in vitro*." Walton,<sup>(10)</sup> however, reported that the presence of high clay, illite, and kaolin mineral exposures reversed the hazards associated with increasing quartz exposures. This finding was supported by Le Bouffant and coworkers.<sup>(11)</sup> They reported that illite present in coal mine dust strongly inhibited the pathogenic effects of quartz, while kaolin had a weaker inhibitory effect.

Previous studies on the role of minerals in the development of various miners' diseases demonstrate that the respiratory disease process in lung tissue induced by coal mine dust can be

more reliably assessed when the coal-mineral ratio, the types of minerals, and the mass and size distributions of the dust are characterized.

This paper develops the size-specific mineral data needed to study the toxicological effect of coal mine dust. Data are being collected only on continuous mining sections. Figure 1 illustrates the dust sources associated with this type of mining, as well as the dust sampling points used in the study.

## Experimental procedure

### Sampling

Dust samples were collected using 4-stage cassette impactors. They were

# SIZE DISTRIBUTION OF AIRBORNE DUST

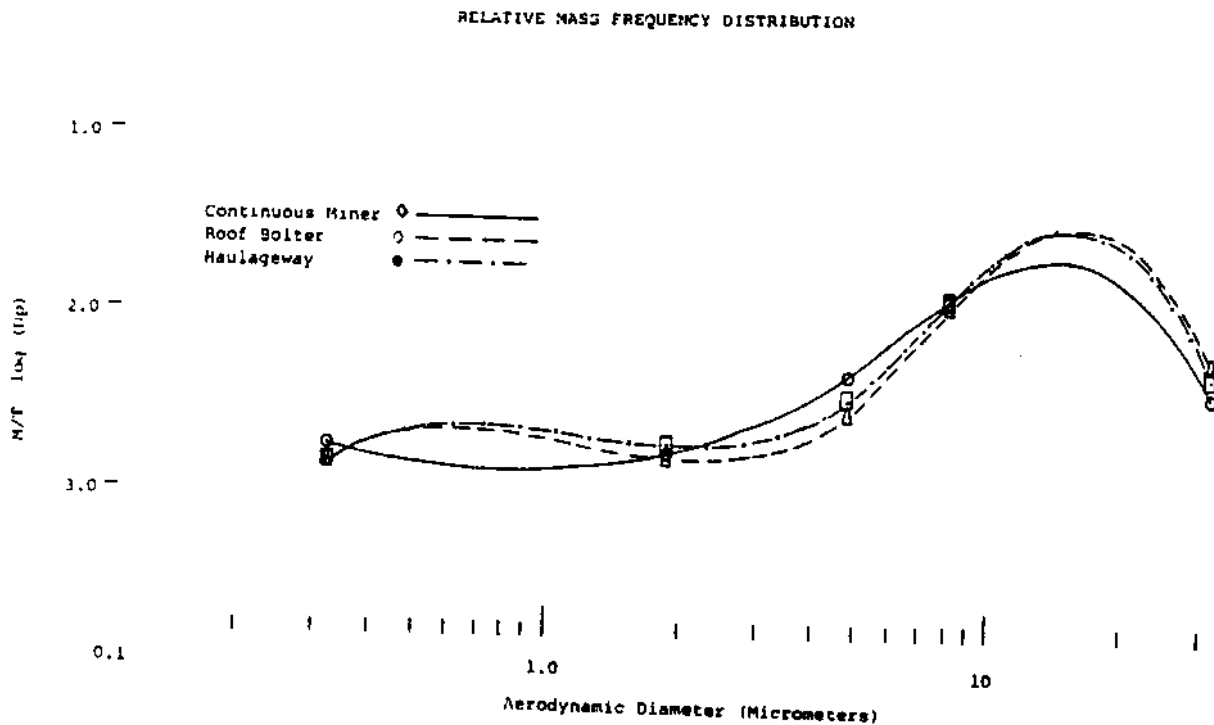


Figure 4—Coal mine dust size distributions.

be found in Knutson.<sup>(16)</sup> In the graphic presentation of these distributions, the upper cut-off diameter for the first stage and the lower cut-off diameter for the last stage were assumed to be 50 and 0.1 micrometers, respectively. The distribution curves were generated using the Lagrange polynomial curve smoothing technique.

An average mean particle diameter of 18 micrometers was found on the returnside continuous miner samples, which corresponds well with the samples from haulageway where a mean particle size of 17.5 micrometers was measured. The particle sizes measured in these locations correspond well to the "primary" size mode of 17 to 20 micrometers reported by Burkhart *et al.*<sup>(17)</sup> A smaller mean particle diameter of 12 micrometers was measured from the samples collected at the returnside roof bolter.

### Mineral content data

The mineral composition at the three sampling locations and in the individual impactor stages showed wide variations. The range of mineral composition as percentages for all size fractions at the three sampling locations is presented in Figure 5. The data in figures 5-8 are expressed as the percentage of

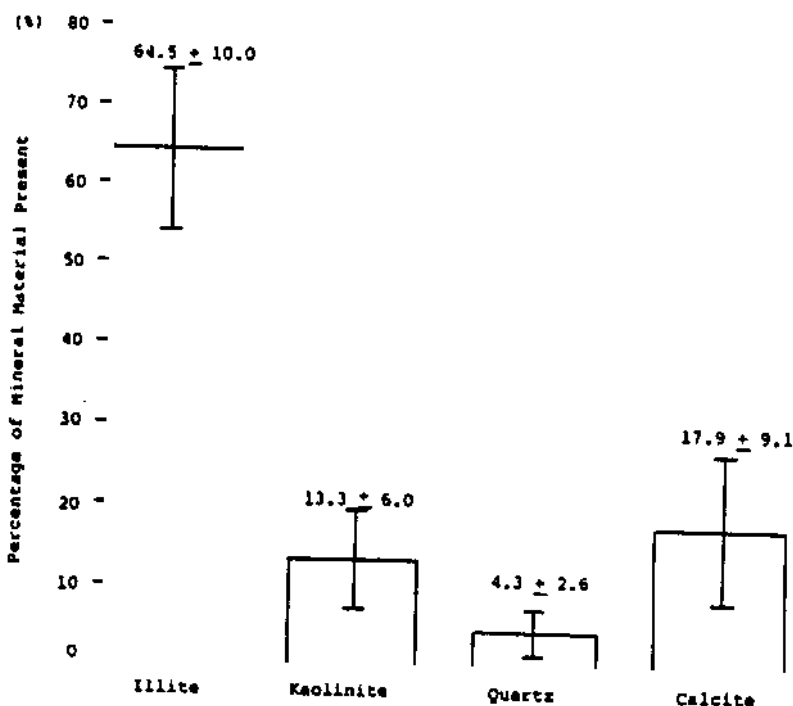


Figure 5—Range of mineral percentages, all size fractions.

the coal to the belt. The dust here is representative of the dust created by the coal dumping. Location 9 is in the area where the miners eat their lunch and take breaks. This sample is representative of the dust present in miners' rest areas.

**Analysis**

The analytical method used for the dust sample mineral content characterization was an x-ray microdiffraction film technique supplemented by energy dispersive scanning electron microscopy. The x-ray microdiffraction technique was selected because it does not require low temperature ashing to remove the organic constituents and is capable of obtaining a diffraction pattern from microgram quantities of dust samples. The x-ray camera is a Debye-Scherrer geometry camera with an inside circumference of 360 mm (a two radian camera). The samples were mounted on .05 mm diameter glass splines and were scanned using copper K $\alpha$  radiation with a filter monochromator. Exposure times of 3 to 10 hours were used to produce diffraction patterns identifying the minerals in the sample. Each mineral was identified from the location of its diffraction line by comparing the film spectrum with the spectral data reported in the ASTM (American Society of Testing Materials) Powder Data File. Quantitative estimation of the minerals present was accom-

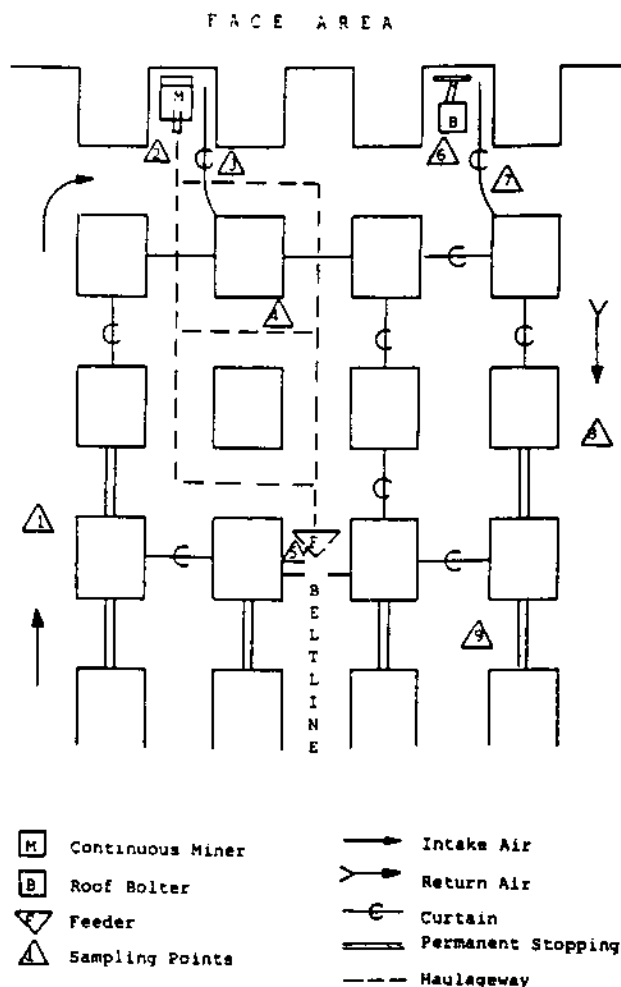


Figure 3—General section layout and sampling locations.

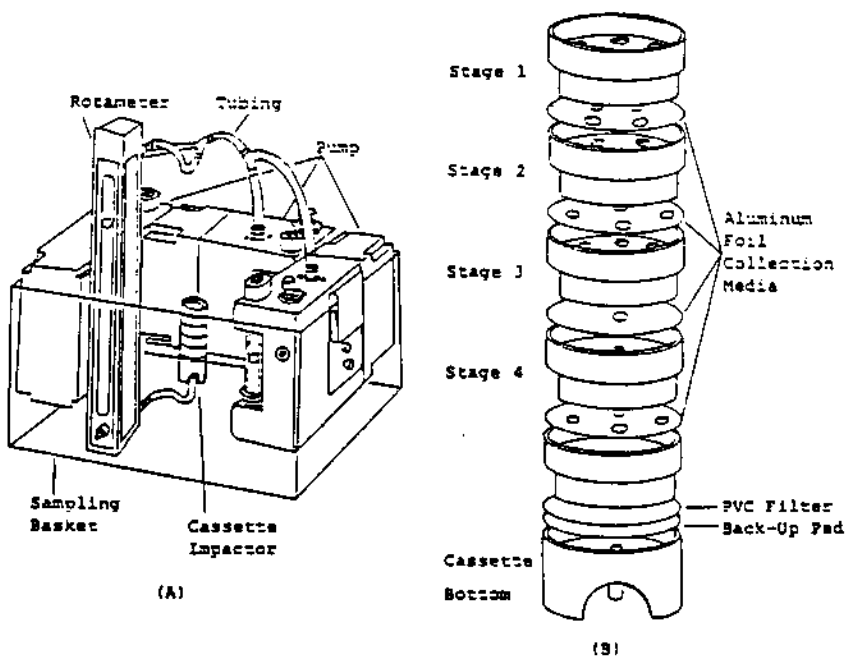


Figure 2—In-mine sampling arrangement with cassette impactor.

A—Three pumps, tubing and impactor.

B—Exploded view of cassette impactor assembly.

plished by measuring the intensity of diffraction lines and using weighting factors to compensate for the differences in diffraction intensity of individual minerals. The intensity of each mineral was measured from the developed x-ray films using a microphotodensitometer. The weighting factors were obtained using the method described by Renton.<sup>(15)</sup>

**Results and discussion**

*Particle size distributions*

The size distribution of the returnside continuous miner, haulageway, and returnside roof bolter samples (locations 3, 4, 7) are presented as continuous mass frequency distributions in Figure 4. The vertical axis of the distribution curve has been normalized by dividing the amount of mass in each size class by the width of that size class. The horizontal axis shows the particle aerodynamic diameter (micrometers). A general description of this method can

# SIZE DISTRIBUTION OF AIRBORNE DUST

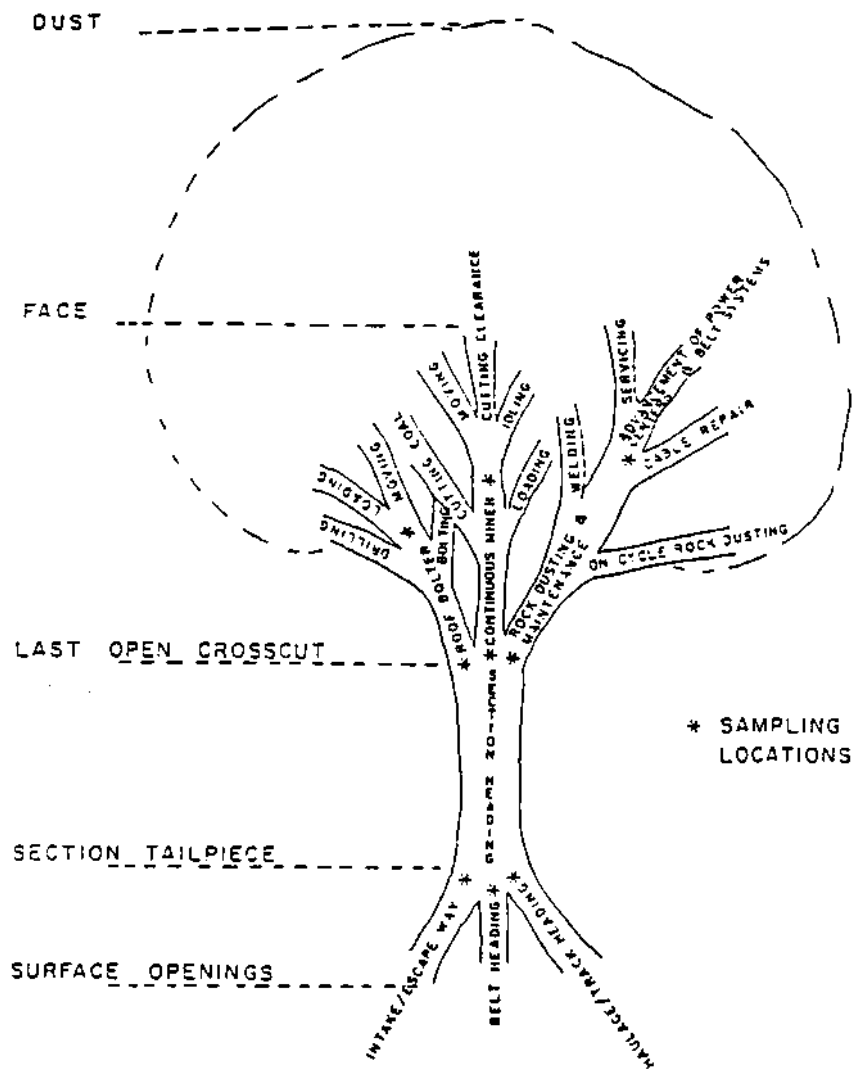


Figure 1—Dust generation source tree.

designed and constructed using a modification of an original design described by Jones.<sup>(12)</sup> Table I lists the stage number, number of holes, aerodynamic cut sizes, and coatings used for the impactors in the study. Greased aluminum foil was used as the collection substrate for stages 1 to 4 and a standard 37 mm, 5.0 um pore size, polyvinyl chloride (PVC) membrane filter was used for the last stage. The aluminum foil substrates were brush coated with a mixture of Apiezon L grease and toluene to reduce particle bounce. Sampling was done at a flow rate of 5 lpm to improve dust collection efficiency by increasing the Reynolds number (Re). An Re between 500 and 3000 improves the sharpness of the impactor cut.<sup>(13,14)</sup> With the 5 lpm flowrate, the impactor stages have Re's in the range of 450 to 4700. The flowrate was maintained with three MSA Model G air sampling pumps

connected with tubing and Y-connectors to a precalibrated rotameter. The tubing was then routed from the rotameter to the base of the impactor. Figure 2 shows the dust sampling equipment arrangement.

Dust samples were collected at nine different locations on a continuous mining section of a bituminous coal mine in West Virginia. The sampling locations are shown in Figure 3. The sampling locations were selected so that the researchers could monitor the

contributions of mining activities to the changes observed in the mineral content of the dust in the mine air as it moves from the intake side of the face to the return side. Location 1 is in the intake air a few hundred feet before the face area. The dust collected in this sample is representative of the dust in the outside air plus dust that is picked up in the mine as the intake air moves through the mine to the face. Location 2 is in the intake air in the face area, immediately before the continuous miner. The dust in this sample is representative of the intake air dust plus the dust stirred up in the face area by the movement of people and equipment—but not including dust generated by the continuous miner.

Location 3 is in the return air haulageway immediately beyond the continuous miner. The dust in this sample is representative of the dust at location 2 plus the dust generated by the continuous miner. Location 6 is in the return air haulageway immediately before the roof bolter. The dust at location 6 is representative of the dust at location 3, minus dust that has settled out of the air, plus dust generated by the movement of people and equipment in the face area. Location 7 is in the return air immediately beyond the roof bolter. The dust at location 7 is representative of the dust at location 6 plus the dust generated by roofbolting. Since roofbolting involves drilling into the overhead layers of rock, it is likely to produce a significant amount of mineral dust. Location 8 is in the return air, a few hundred feet past the last position of face activity. It is representative of the dust generated throughout the mine minus the dust that has settled out of the air.

Location 4 is along the main shuttle-car haulageway between the continuous miner and the feeder at the end of the bellline. The dust at location 4 is representative of the dust created by the shuttle cars as they move along the haulageway. Location 5 is alongside the feeder where the shuttle cars transfer

TABLE I  
Cassette impactor design specifications

Stage number	No. of holes	Cut sizes	Coating
1	4	>10 $\mu\text{m}$	Apiezon L
2	4	10-6.6	"
3	4	6.6-3.5	"
4	1	3.5-1.0	"
Backup filter	—	1.0-0	None

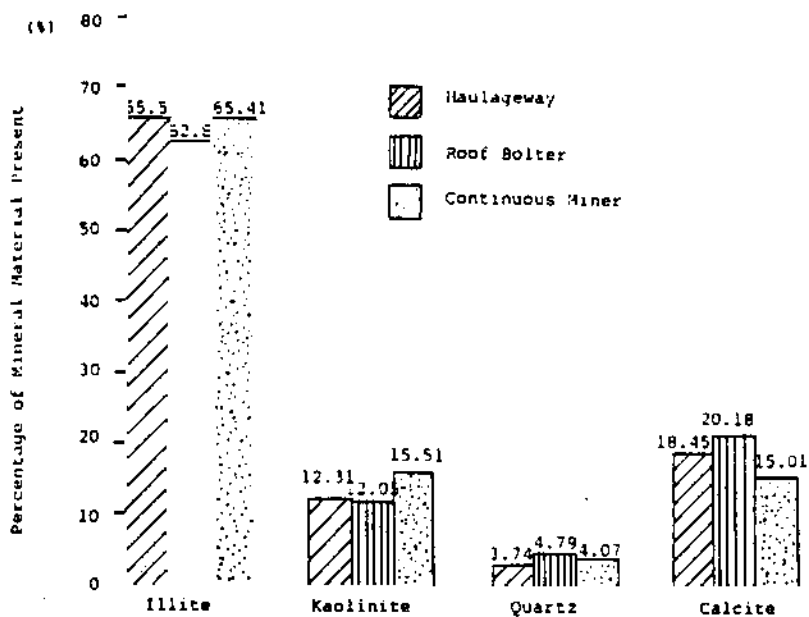


Figure 6—Comparison of mineral composition at different mine locations (size 1.0-3.5  $\mu$ m).

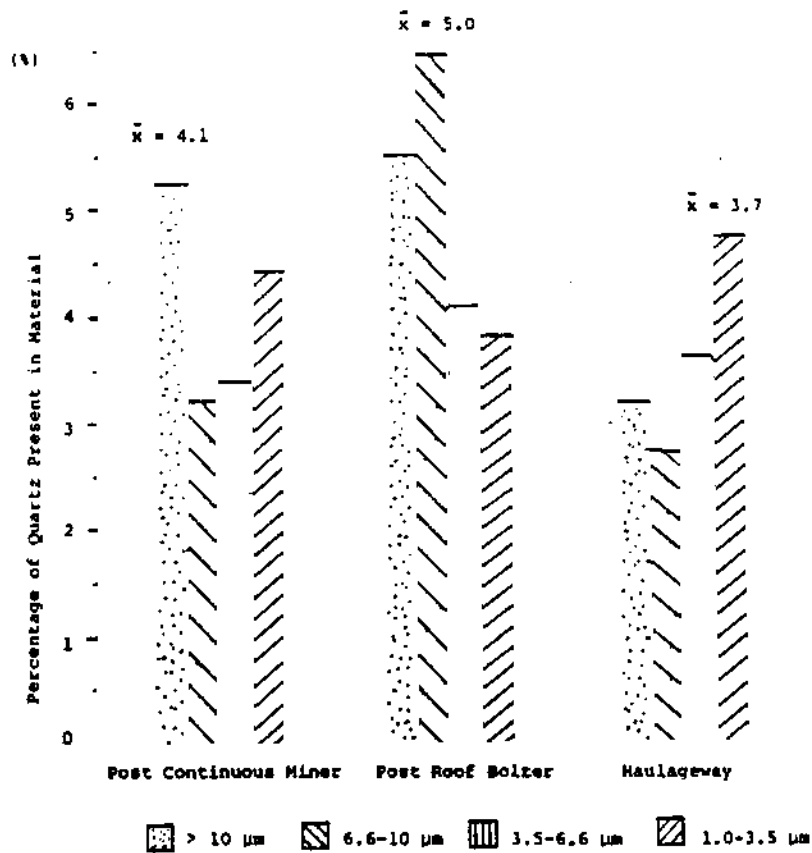


Figure 7—Size fractional quartz concentration per mining location.

mineral matter (coal excluded) present in the sample. The mean percentage of illite in all samples was found to be 64.5 percent with a standard deviation of 10.0. The mean percentages of kaolinite, quartz, and calcite were 13.3, 4.3, 17.9 percent with respective standard deviations of 6.0, 2.6, and 9.1. Figure 6 illustrates the mineralogical variability in three sampling locations for the 1.0 to 3.5 micrometer size fraction. The samples from the returnside continuous miner and the haulageway show no marked differences in mineral percentages for all major minerals measured. The samples from the returnside roof bolter, however, were different from the other area samples in mineral content. Illite and kaolinite percentages were at their lowest level while quartz and calcite levels were at their highest in this location. Figure 7 shows the quartz concentration of all size fractions at the three locations. The highest quartz level of 5.0 percent was measured from the returnside roof bolter samples. The returnside continuous miner and the haulageway samples show slightly lower quartz percentages than the returnside roof bolter samples with means of 4.1 and 3.7 percent, respectively. The returnside of the roof bolter samples were investigated further for changes in mineral level by size fractions. Figure 8 illustrates the mineralogical variability at the returnside roof bolter location. Kaolinite and quartz show no marked changes through the different size fractions; however, illite and calcite changed considerably across the size fractions. Illite levels increased 13 percent while the calcite levels decreased 34 percent as the dust size decreased.

### Recommendations

Respiratory disease in coal miners is an old problem still seeking understanding and solution. A number of authors have been cited who have described the effects of mineral content combinations on both human and animal respiratory systems. Some of these toxicological reports are in conflict with each other, perhaps because of variations in the size and mineral content of the dust used in the studies. These studies have been done with arbitrarily chosen dust size/mineral content combinations, but it seems clear that the

# SIZE DISTRIBUTION OF AIRBORNE DUST

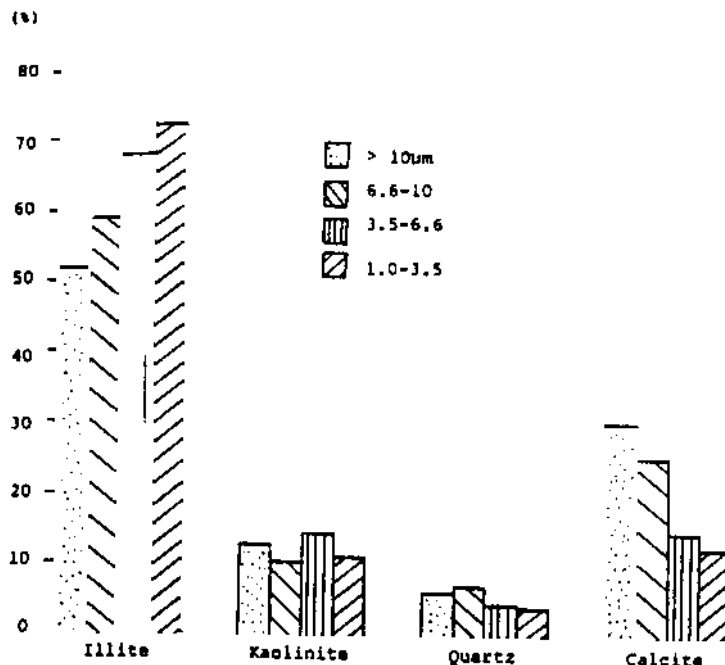


Figure 8—Size fractional mineral composition (post roof bolter).

more appropriate method of study is to use dust combinations representative of those actually found on the working sections of coal mines. Currently these studies cannot be done because the size/mineral content data is unavailable. This paper is part of an ongoing project of collecting data on continuous mining sections in West Virginia coal mines, while similar projects are collecting data on longwall sections in West Virginia and continuous mining sections in Pennsylvania coal mines. It is our recommendation that this and future data gathered by these projects be used by toxicologists to study the effects of dust size/mineral content on the respiratory system. The understanding of toxic effect gathered can then be used to set dust standards more specific to the toxic agents in coal mine dust. This in turn may lead to dust control techniques specific to the generation points of the toxic size/mineral combinations.

## Acknowledgements

The authors wish to thank Dr. John Renton of West Virginia Geological Survey and Dr. Arthur Pavlovic of the Department of Physics, WVU, for their assistance in developing the analytical method, and for analyzing these samples. We also wish to acknowledge the Bureau of Mines for its support of the

Generic Technology Center on Respirable Dust which is sponsoring this project. Grant No. G1135142

## References

- Morgan, W. K. C., D. B. Burgess, G. Jacobson, et al: The Prevalence of Coal Workers' Pneumoconiosis in U.S. Coal Mines. *Arch. Environ. Health* 27:221 (1973).
- Dessaer, P., E.J. Baier, G.M. Crawford and J.A. Beatty: Development of Patterns of Coal Workers' Pneumoconiosis in Pennsylvania and Its Association with Respiratory Impairment. *Ann. N. Y. Acad. Sci.* 200:220 (1972).
- McBride, W. E., E. P. Pendergrass and J. Lieben: Pneumoconiosis Study of Pennsylvania Anthracite Miners. *J. Occup. Med.* 8:366 (1966).
- Lainhart, W. S. and W. K. C. Morgan: Extent and Distribution of Respiratory Effects. *Pulmonary Reactions to Coal Dust*, pp. 29-56. Academic Press, New York (1971).
- Davis, J.M.G., J. Ottery and A. LeRoux: The Effect of Quartz and Other Non-Coal Dusts in Coalworkers' Pneumoconiosis, Part II. Lung Autopsy Study. In: *Inhaled Particles IV*, pp. 691-702. W. H. Walton, Ed. Unwin Bros. Old Waking (Surrey) (1971).
- Reisner, M.T.R. and K. Robock: Results of Epidemiological, Mineralogical and Cytotoxicological Studies on the Pathogenicity of Coal-Mine Dusts. In: *Inhaled Particles IV*, pp. 703-716. W. H. Walton, Ed. Unwin Bros. Old Waking (Surrey) (1971).
- Seemayer, N. H. and N. Manojlovic: Biological Effects of Coal Mine Dusts on Macrophages. *The In Vitro Effects of Mineral Dusts*, pp. 5-12. Academic Press, New York (1980).
- Gormly, I. P., G. M. Brown, P. L. Collings, et al: The Cytotoxicity of Respirable Dusts from Collieries. *The In Vitro Effects of Mineral Dusts*. Academic Press, New York (1980).
- Adams, Z. and M. Timar: Investigations of the Effects of Quartz, Aluminum Silicates, and Colliery Dusts on Peritoneal Macrophages 'In Vitro.' *The In Vitro Effects of Mineral Dusts*. Academic Press, New York (1980).
- Walton, W. H., J. Dodgson, G. G. Hedden and M. Jacobsen: The Effect of Quartz and Other Non-Coal Dusts in Coal Workers' Pneumoconiosis. In: *Inhaled Particles IV*, pp. 921-929. W. H. Walton, Ed., Unwin Bros. Old Waking (Surrey) (1971).
- Le Bouffant, L., H. Daniel and S.C. Martin: Quartz as a Causative Factor in Pneumoconiotic Lesions in Coal Miners. *Industrial Health and Medicine Series No. 19*. Commission of the European Communities (1977).
- Jones, W., J. Jankovic and P. Baron: Design, Construction, and Evaluation of a Multi-Stage "Cassette" Impactor. *Am. Ind. Hyg. Assoc. J.* 44(b):409 (1983).
- Marple, V. A. and B. Y. H. Liu: Characteristics of Laminar Jet Impactors. *Env. Sci. Technol.* 8:648 (1974).
- Newton, G. J., O. G. Raabe and B. V. Mokler: Cascade Impactor Design and Performance. *J. Aerosol Sci.* 8:339 (1977).
- Renton, J. J. Use of Weighted X-Ray Diffraction Data for Semi-Quantitative Estimation of Minerals in Low Temperature Ashes of Bituminous Coal and in Shales. U.S. Department of Energy, METC/CR-79/5 (1979).
- Knutson, E. O. and P. J. Lloy: Measurement and Presentation of Aerosol Size Distributions. *Air Sampling Instruments for Evaluation of Atmospheric Contaminants*, 6th Ed., Chap. G, pp. G1-G12. ACGIH, Cincinnati (1983).
- Burkhart, J. E., M. A. McCawley, and R. W. Wheeler: Particle Size Distributions in Underground Coal Mines. Presented at the *Am. Ind. Hyg. Conference*, Philadelphia, PA (May 28, 1983).

Received 11/12/85; review/decision 12/10/85; revision 1/21/86; accepted 2/11/86

# Characterization of Coal Mine Dust

Terrence J. Stobbe, Ralph W. Plummer, Hyunwook Kim and John M. Dower

Department of Industrial Engineering, West Virginia University

The relationship between exposure to coal mine dust and the development of various respiratory diseases is well recognized. The cause of these diseases, however, is still uncertain. To study this cause-effect relationship, it is necessary to characterize the coal mine dust in terms of the quantity of dust present, and mineral content of the dust. Dust samples were collected using a Portable Continuous Aerosol Monitor (PCAM) and 4-stage cassette impactors at various locations in an upper Freeport seam coal mine in West Virginia. The samples were analyzed using an X-ray microdiffraction film technique and energy dispersive scanning electron microscopy. This paper presents the results of the first phase of this characterization work, which includes determining the size distribution of the dust, and the mineral content of the size intervals.

## Introduction

Diseases associated with dusts in coal mine environments continue to afflict miners in today's modern mines. These diseases still persist because, as Olishifski points out, an employee rarely experiences exposures to a single environmental stress, but rather to an intricate interplay of multiple stresses.<sup>(1)</sup> In the case of coal mining, the multiple stresses are varying sizes of dust particles originating from coal imbedded minerals, immediate roof strata, bottom strata, incombustible rock and the coal itself. The site of this intricate interplay is the miner's lungs, and the resulting diseases are a function of the composite dust exposures.

The proper study of coal mine dust toxicity requires that the dusts used replicate existing coal and mineral dust compositions in their relevant size fractions. The purpose of this project is to develop the size and mineral content data necessary to support this ongoing toxicological effort.

Existing coal mining standards and regulations also address total and respirable dust exposures. These dust terms refer to both the quality and quantity of the dust segment in the mine atmosphere. Dust quality addresses its coal and mineral content, whereas dust quantity is described by mass per unit volume ( $\text{mg}/\text{m}^3$ ). The comprehen-

sive characterization of coal mine dust exposures will enable revision of these standards and regulations to address the specific minerals and size fractions found to be toxic to human lung tissue.

Only continuous miner sections are currently being addressed in this project. The minerals under study that are commonly associated with the coal are listed in Table I.

The constant changing nature of these mining sections necessitated the establishment of mineral content ranges in the size fractions specified in the Methods section.

Relevant data are also being collected on variables that may be factors in dust generation and movement. Examples include ventilation patterns, equipment types and usage, traffic flow patterns, coal seam characteristics. These factors are inherent mining activities that contribute to the total quantity of dust generated. An illustration of the mining activities and points of evaluation are presented in the dust generation source tree (Figure 1). This additional data will be used to model the contributions of these various mine activities to the total airborne dust in the mine atmosphere.





Davis study also found that the nodules containing more than 48.6% ash content dust were very similar to silicotic nodules, and that the lesion centers were often free of any dust particles. This study also reported differential retention of the mineral (non-coal) components of the dust in the lesions which was progressively more marked in men with the more serious grades of pneumoconiosis.

In 1980 Adamis and Timar reported that quartz, sandstone, slate, respirable colliery dust, bentonite, illite and some kaolins had cytotoxic effects on rat peritoneal macrophages *in vitro*.<sup>16)</sup> Two studies reported by Seemayer and Manojlovic obtained correlations between cytotoxicity and the mineral content of coal mine dust.<sup>17)</sup> Le Bouffant and co-workers, however, reported that illite present in coal mine dust strongly inhibited the pathogenic effects of quartz, while kaolin had a weaker inhibitory effect.<sup>18)</sup> Walton also reported that the presence of high clay, illite, and kaolin mineral exposures reversed the hazards associated with increasing quartz exposures.<sup>19)</sup>

These interactions demonstrate that the respiratory disease processes in lung tissue induced by coal dust can be more reliably determined when the coal-mineral ratio, the types of minerals,

the mass and size distributions of the dust are characterized.

### Experimental procedure

#### Sampling

The sampling equipment includes a direct reading instrument which allows the determination of the optimal sampling point at each sampling location, and 4-stage cassette impactors for sizing the collected dusts.

The direct reading instrument is a portable continuous aerosol monitor (PCAM) manufactured by PPM, Inc., which measures mass concentration and size distribution using an electro-optical method based on near-forward light scattering. This instrument and its theoretical background are described in more detail by Kreikebaum.<sup>110)</sup>

Four-stage cassette impactors using 37-mm cassette pieces were designed and constructed using a modification of an original design described by Jones.<sup>111)</sup> Table II lists the stage number, number of holes, aerodynamic cut sizes, and coatings used for the impactors in this study.

Greased aluminum foil was used as the collection substrate for stages 1 to 4 and a standard

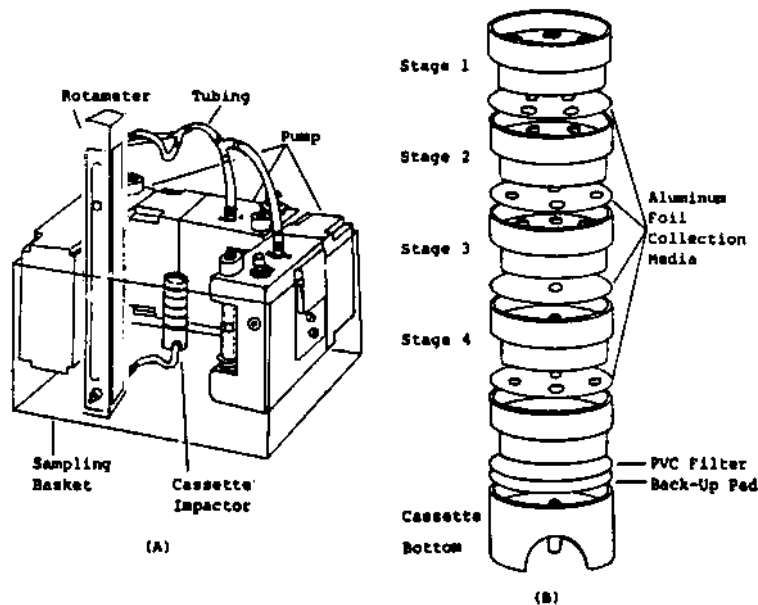


FIGURE 2 — Assembled in-mine sampling arrangement showing the three pumps, tubing, and impactor. Exploded view of the cassette impactor assembly.

# CHARACTERIZATION OF COAL MINE DUST

TABLE II  
Four-Stage Cassette Impactor Study

Stage Number	No. of Holes	Cut Sizes	Coating
1	4	> 10 $\mu\text{m}$	Apeizon L
2	4	10 - 6.6	"
3	4	6.6 - 3.5	"
4	1	3.5 - 1.0	"
Backup filter	--	1.0 - 0	None

37-mm, 5.0  $\mu\text{m}$  pore size, polyvinyl chloride (PVC) membrane filter was used for the last stage. The aluminum foil substrates were brush coated with a mixture of Apeizon L grease and toluene to reduce particle bounce.

A flow rate of 5 lpm was selected to enhance the dust collection efficiency by increasing the Reynolds number ( $R_e$ ). It has been recommended that the  $R_e$  be kept between 500 and 3000 to improve the sharpness of the impactors cut.<sup>(12,13)</sup> When the 5 lpm flowrate is used, the impactor stages have  $R_e$ 's in the range of 450 to 4700. To maintain the flowrate, three MSA Model G air sampling pumps were connected using commercially available tubing and Y-connectors to a precalibrated rotameter. The tubing was then routed from the rotameter to the base of the Impactor. Figure 2 shows the arrangement of the dust sampling assembly used in this study.

Dust samples were collected at nine different locations inside a bituminous coal mine in West Virginia where the continuous mining method was being used. Average sampling periods for the impactors ranged from 0.5 to 3 hours depending upon the dust load at the sampling point. The sampling locations are shown in Figure 3. To date, this study has focused on only one mine located in the Upper Freeport coal seam.

## Analysis

The analytical methods used for the characterization of mineral content of the dust samples include an X-ray microdiffraction film technique and scanning electron microscopy. The X-ray microdiffraction technique was selected because it does not require low temperature ashing to remove the organic constituents and is capable of obtaining a diffraction pattern from microgram quantities of dust samples. The X-ray camera employed is a 0.004 inch diameter X-ray beam collimator that produces a micro X-ray beam. The sample holder is a 0.75-inch square aluminum sheet with a 0.25-inch hole through the center. A portion of the dust impacted on the collection media is removed and mounted on a 0.0001-inch thick mylar film. The sample is then centered over the hole using a

microscope. Exposure times of 3 to 4 hours (up to 8 hours for some extremely small samples) were sufficient to produce a diffraction pattern that identifies the minerals in the sample. A general description of the method can be found in Willard.<sup>(14)</sup>

## Results and discussion

### Particle size distributions

The size distribution of the post continuous miner, haulageway, and post roof bolter samples collected in the working section are plotted in Figure 4. This illustrates that the particle size distribution was not a uniform log normal distribution. The largest mean particle diameter (18  $\mu\text{m}$ )

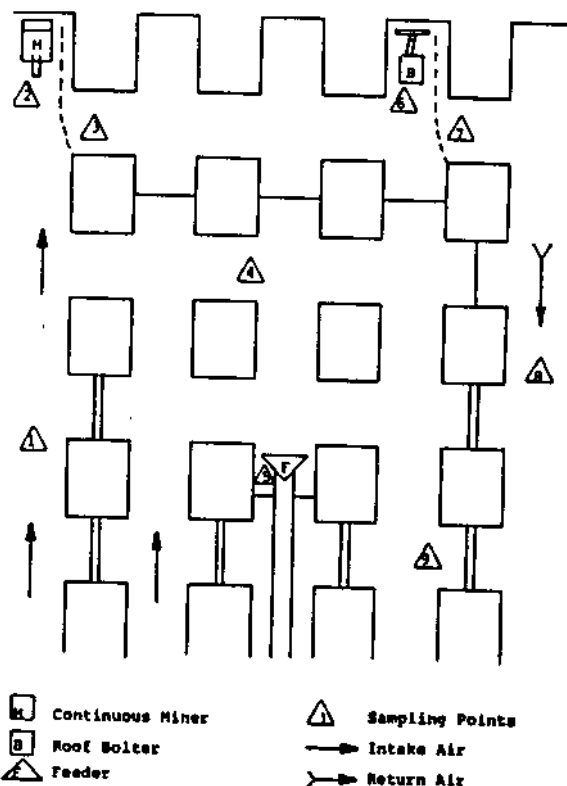


FIGURE 3 — General section layout and sampling locations.

was found in the post continuous miner samples, which corresponded very closely with the particle size distribution in the haulageway samples where a mean particle size of 17.5  $\mu\text{m}$  was found. Particle size distributions in these locations correspond well to the "primary" size mode of 17 to 20  $\mu\text{m}$  reported by McCawley.<sup>(15)</sup> A smaller mean particle diameter of 12  $\mu\text{m}$  was found from the post roof bolter samples.

## THE RESPIRABLE DUST CENTER

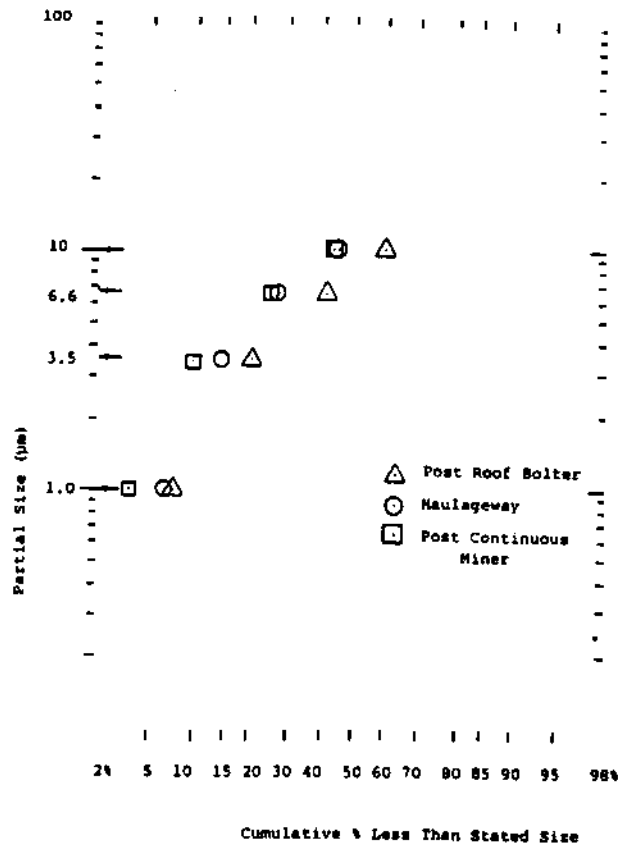


FIGURE 4 — Coal mine dust size distribution.

### Mineral content data

The mineral concentration at three sampling locations and in individual impactor stages showed wide variations. The range of mineral percentages for all size fractions at 3 sampling locations is shown in Figure 5. The mean percentage of illite in all samples was 64% with a standard deviation of 15.3. The mean percentages of kaolinite, quartz, and calcite were 8.5, 6.7, and 21% with respective standard deviations of 3.5, 3.6, and 13.9.

The following Figure 6 illustrates the mineralogical variability in three sampling locations for the 1.0 to 3.5 µm size fraction. Illite concentrations in the post roof bolter dust samples were greater than illite concentrations at the haulageway and post continuous miner sampling points that preceded this sampling point in the ventilation system. The concentrations of quartz and calcite in this size fraction was greater at the post continuous miner sampling location than at either the haulageway or post roof bolter sampling points that were before and after the continuous miner in the air stream. The concentration of kaolinite in this size fraction decreased from the haulageway sampling point to continuous miner and had increased again at the post roof bolter sampling locations.

The post roof bolter sampling point was therefore chosen to investigate the changes in size fractional mineral concentrations. As illustrated by

Figure 4, similar mineralogical variabilities existed by size fraction at the same sampling location.

The post roof bolter sampling point was chosen to further investigate the variability of size fractional mineral concentrations. Figure 7 illustrates the result of mineralogical variabilities in this location.

### Summary

This paper has summarized the development of a project designed to characterize the mineral content of selective size fractions of coal mine dusts. It has described the methodological and analytical techniques associated with the project. Some early results have also been reported, but no attempt to interpret these results have been made.

### Acknowledgements

The authors wish to thank Mr. William Jones of NIOSH-DRDS, Morgantown, for his assistance in the redesign of the impactors. We also wish to thank Dr. John Renton of the Department of Geology, West Virginia University, and Mr. Eric Hopkins of the West Virginia Geological Survey, for their assistance in the development of an analytical method for the samples, and for agreeing to analyze these and future samples.

Grant No.

G1135142.

# CHARACTERIZATION OF COAL MINE DUST

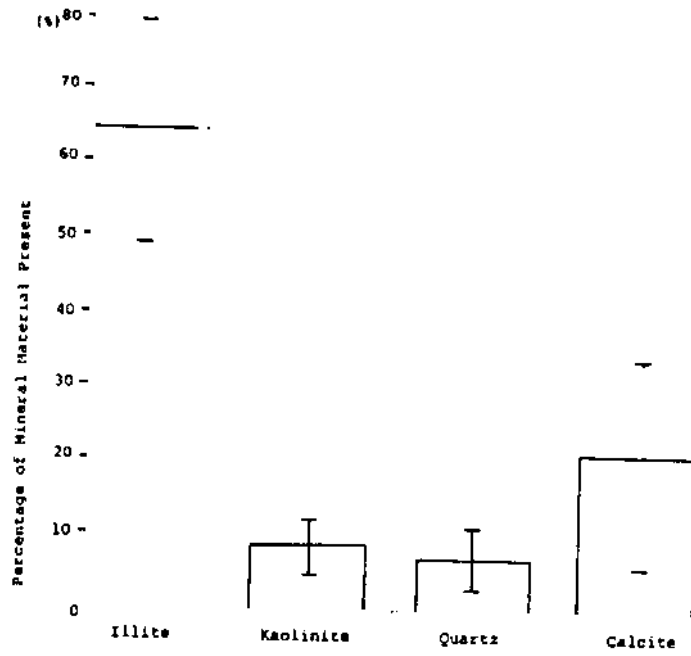


FIGURE 5 — Range of mineral percentages all size fractions.

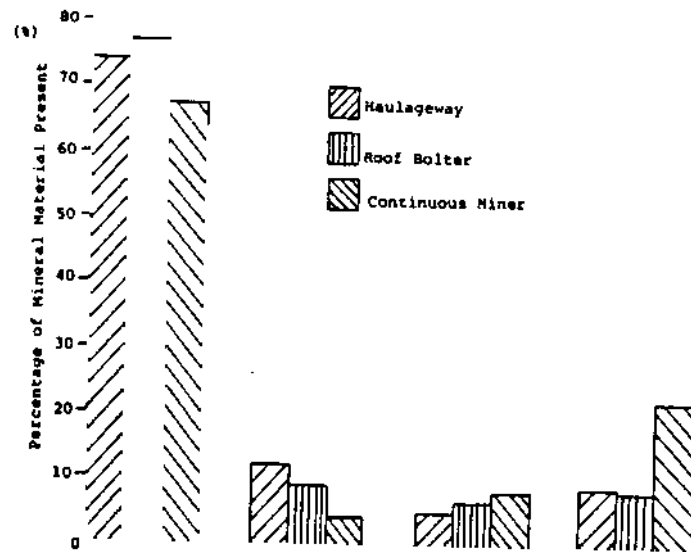


FIGURE 6 — Mineral concentrations at different mine locations (Size 1.0 - 3.5 μm).

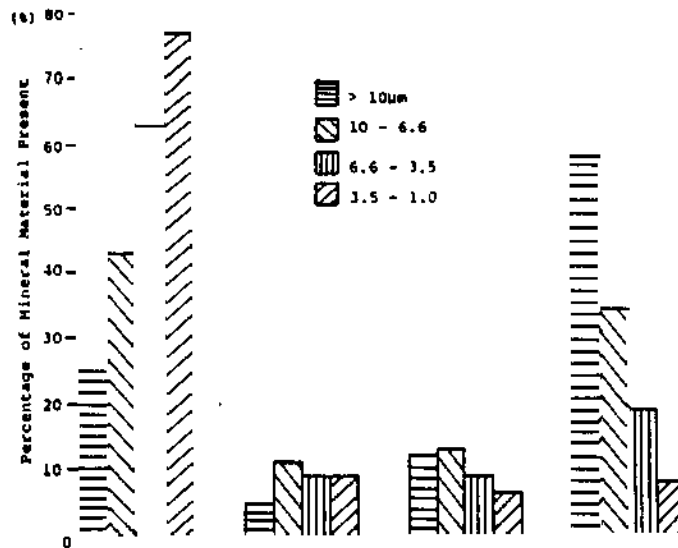
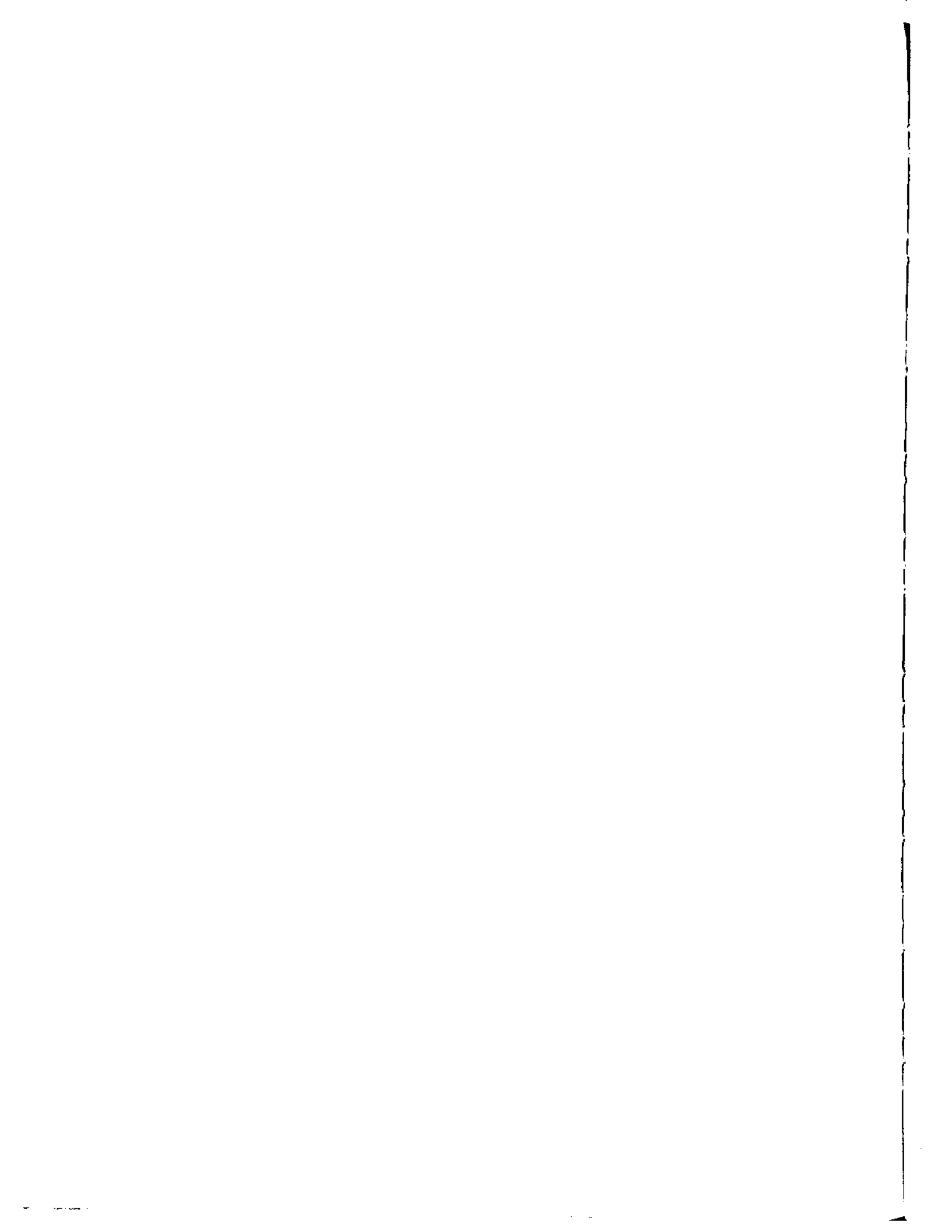


FIGURE 7 — Size fractional mineral concentration (post roof bolter).

## References

1. Olshifski, J.B., Ed.: *Fundamentals of Industrial Hygiene*, 2nd ed., p. 6 National Safety Council, Chicago, IL (1983)
2. King, Z.J. and G. Nagelschmidt: *Special Report Series No. 250B*, Medical Research Council, London (1945).
3. Davis, J.M.G.: The Relationship Between the Mass and Composition of Coal Mine Dust and the Development of Pneumoconiosis. *Health Implications of New Energy Technologies*, pp. 291.
4. Morgan, W.K.C., R. Reger, P.B. Burgess and E. Shoub: A Comparison of the Prevalence of Coal Workers' Pneumoconiosis and Respiratory Impairment in Pennsylvania Bituminous and Anthracite Miners. *Ann. N.Y. Acad. Sci.*, pp. 252-258.
5. Davis, J.M.G., J. Chapman, Paula Collings, et al: Variations in the Histological Patterns of the Lesions of Coal Worker's Pneumoconiosis in Britain and Their Relationship to Lung Dust Content. *Am Rev. Respir. Dis.* 128:118-124 (1984).
6. Adams, Z. and M. Timar: Investigations of the Effects of Quartz, Aluminum Silicates, and Colliery Dusts on Peritoneal Macrophages *in vitro*. *The In Vitro Effects of Mineral Dusts*, Academic Press (1980).
7. Seemayer, N.H. and N. Manojlovic: Biological Effects of Coal Mine Dusts on Macrophages. *Ibid.*, pp. 5-12.
8. Le Bouffant, L., H. Daniel and S.C. Martin: Quartz as a Causative Factor in Pneumoconiosis Lesions in Coal Miners. *Industrial Health and Medicine Series No. 19*, CEC, Luxembourg (1977).
9. Walton, W.H., J. Dodgson, G.G. Hadden and M. Jacobsen: The Effect of Quartz and Other Non-Coal Dusts in Coal Workers' Pneumoconiosis. In: *Inhaled Particles IV*, pp. 921-929. W.H. Walton, Ed. Urwin Bros., Old Woking, Surrey (1971).
10. Kreikebaum, G., A.C. Miller, Jr. and P.M. Shofner: Electrooptical Mass Concentration and Approximate Size Measurement. In: *Aerosols in the Mining and Industrial Work Environments*, Vol. 3, *Instrumentation*, pp. 719-732. V.A. Marple and B.Y. H. Liu, Eds. Ann Arbor Science (1983).
11. Jones, W., J. Jankovic and P. Baron: Design, Construction, and Evaluation of a Multi-stage "Cassette" Impactor. *Am. Ind. Hyg. Assoc. J.* 44(b):409-418, (1983).
12. Marple, V.A. and B.Y.H. Liu: Characteristics of Laminar Jet Impactors. *Env. Sci. Technol.* 8:648-654 (1984).
13. Newton, G.J., O.G. Raabe and B.V. Mokler: Cascade Impactor Design and Performance. *J. Aerosol Sci.* 8:339-347 (1977).
14. Willard, H.H., L.L. Merritt and J.A. Dean: *X-ray Diffraction Instrumental Methods of Analysis*, 5th ed., Chap. 10, pp. 258-301, D. Van Nostrand Co., New York (1974).
15. McCawley, M.A., J.E. Burkhart and R.W. Wheeler: Particle Size Distributions in Underground Coal Mines. Presented at the Am. Ind. Hyg. Assoc. Conference, Philadelphia, PA (May 28, 1983).



# A Review of the Programs and Activities of the Generic Mineral Technology Center for Respirable Dust

R. L. Frantz and R. V. Ramani

Department of Mineral Engineering, The  
Pennsylvania State University

**Abstract.** The U.S. Bureau of Mines (USBM) established on August 15, 1983, a Generic Mineral Technology Center (GTC) for Respirable Dust within the Mining and Mineral Resources Research Institutes (MRIs) at The Pennsylvania State University (PSU) and West Virginia University (WVU) in association with participating MRIs at Massachusetts Institute of Technology (MIT) and the University of Minnesota (UMN). The primary goal of the Center is to reduce the incidence and severity of respirable dust disease through researching and advancing the fundamental understanding of all aspects of respirable dust associated with mining and milling and the interaction of dust and lungs. Other Center activities include the training of engineers and scientists, graduate students and undergraduate students through their respective institutions, and the technology transfer to the industry. The Center also serves as the reference center for publications in the respirable dust area.

## Introduction

Exposure to respirable contaminants in mine atmospheres has long posed a serious hazard to miners. The control of these hazards, some of which can have sudden and catastrophic effects and some others, slow and long enduring consequences, has been a major concern for labor, management and government alike. This concern has manifested itself in four primary mechanisms of control -- (1) regulatory control through minimum standard setting by the passage of mine health and safety laws, (2) engineering control through design and operation of mines according to the best recommended practices, (3) interaction of dust and lung control through periodic physical examinations, wearing personal protection devices, etc., and (4) legal and social control through workmen's compensation laws for occupation related health deterioration.

The stated objective of the Federal Mine Safety and Health laws is to "... permit each miner the opportunity to work underground during

the period of his entire adult working life without incurring any disability from pneumoconiosis or any other occupation-related disease ...."

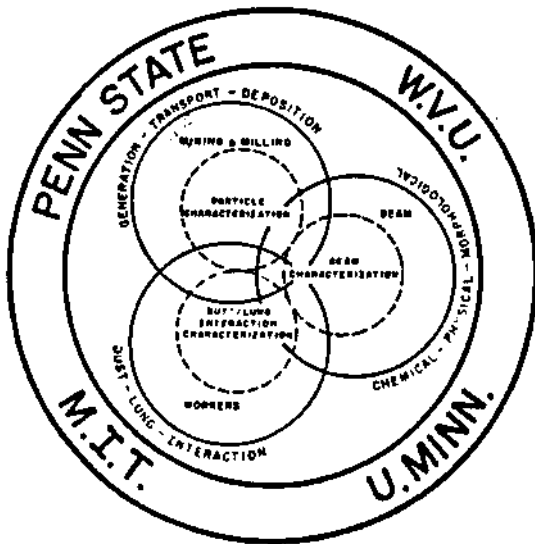
Significant progress has been made in lowering the dust levels in mines since the inception of the Bureau's respirable dust research program. It is generally agreed that mines are less dusty today than they were a decade ago. However, the most serious hazard for workers in the mining and minerals processing industries is still the exposure to respirable dust, and solutions to the problem of respirable dust disease remain to be found.

The National Academy of Sciences (NAS) Study, Measurement and Control of Respirable Dust in Mines, proposed a significant increase in research "for obtaining fundamental understanding of the origin, transport and characteristics of respirable coal mine dust." This recommendation considered the impact on society of mine workers' pneumoconiosis and the magnitude of the research and development effort needed to bridge the information gaps identified by the NAS study group. It is within this context that a comprehensive program designed to permit an accelerated attack on the fundamental research problems for the control of respirable dust in mines was initiated in the Center.

## Research Program

The Generic Technology Center's research program explores the health and safety concerns of respirable dust with the objective of refining existing strategies and developing new respirable dust control techniques that are consistent with the fundamental dust-lung interaction processes that lead to mine worker disability. The work concentrates on (1) control of dust generation; (2) dilution, dispersion and collection in mine airways; (3) characterization of dust particles; (4) interaction of dust and lungs; and (5) relationship of mine environment, geology, and seam characteristics to dust generation and mobility. The fundamental aspects of this work are applicable to the control of respirable dust problems in both hard rock mines and coal mines and to other dusts such as diesel-generated. The intertwined relationship of dust particle characterization, seam characterization and dust/lung

interaction characterization, which is the focus of the Center's activities, is shown in the figure.



At the present time, there are 25 principal investigators and an equal number of graduate students working on 26 projects in the five major areas of the Generic Technology Center. It will be difficult to describe all the activities of the Center in this paper. The bibliography at the end of this paper is a partial listing of the Center's publications in which more details on specific research activities can be found. A brief description of the scope of each of the five major areas and some of the current activities in each area is presented below.

#### Control of Dust Particle Generation

In any fragmentation process, particles will be produced in all size ranges below a top size. Fragmentation in underground mines occurs as a result of many processes: impact, crushing, grinding, blasting, etc. There has been a considerable body of literature developed that describes the results of research on respirable dust production by coal cutting machines (continuous miners/shearers, etc.). The influence of factors such as depth of cut, pick design, pick lacing, and cutting speed have been studied extensively both in the U.K. and the U.S. In reviewing these results, the NAS study found many disparities and recommended that studies on these factors be undertaken with the objective of understanding the fragmentation process and its relationship to respirable dust particle generation and characterization. Specific projects in this area include a fracture mechanics study of crack propagation in coal and experimental studies on the mechanism of dust generation and entrainment (4,5,12,13,14,15,16,32).

#### Dilution, Dispersion and Collection in Mine Airways

The U.S. Bureau of Mines research has shown that only a small fraction of the respirable dust

produced at the face becomes airborne. Experimental determinations have placed the amount of non-airborne respirable dust as ranging from 100 to 1,000 times that of airborne dust. There are several fundamental and applied studies needed in this area to understand more fully the role of mine ventilation and dust control practices in respirable dust control and its relationship to dust particle characteristics. The depositional characteristics of dust particles in mine airways and the velocities at which these deposited dusts may become airborne are variable with type of dust. Prediction of ambient dust concentrations using convective-diffusion equations and experimental studies of dispersion and transport of respirable dust in mine atmospheres are research projects in this area (1,2,3,8,24,28). Such studies are important for the design of equipment and the development of operating practices to remove dust from the worker zone or the worker from the dust zone and include theoretical, laboratory, and field components.

#### Characterization of Dust Particles

The importance of identifying the physical, chemical, mineralogical, size consist, shape and surface condition of respirable dust samples can hardly be over-emphasized. None of these characteristics will be single-valued quantities. In any given dust, there will be a distribution of sizes, shapes, etc. The characterization studies are aimed at evaluating these distributions. Characterization of the dust collected in the various areas of research identified earlier is essential. Thus, there is fundamental research aimed at developing better dust characterization methods. In this area, there are several projects dealing with such topics as wettability of coal mine dust particles; the theoretical and experimental determination of the aerodynamic diameter of coal dust particles; x-ray fluorescence analysis of dust particles on a one-by-one basis in an automated, computer-controlled scanning electron microscope (SEM); magnetic resonance spectroscopic characteristics of paramagnetic ions and free radicals in coal dust, black lung tissues and lung tissue under controlled exposures; shape and surface characterization of respirable mine dust particles; silica particle concentrations in the respirable size range; and investigation of gravity fractionation procedures for determining the specific gravity distribution of respirable dust (7,18,19,20,21,30,31).

#### Interaction of Dust and Lungs

The characterization of dust-lung interaction is critical for the development of effective engineering control measures in mines and milling operations. Research in this area is concentrating on developing an understanding of the basic processes that occur with the deposition of dust in the lungs and the interactions that occur between the dust and lungs. The objective of research in this area is to characterize dust-lung interrelationships necessary to relate dust control strategies in environments likely to create an occupational lung problem. The dust-lung interaction studies include, among others, characterization of mechanism of lung injury and morphometric study of the pulmonary inhalation toxicity of respirable coal mine dusts (9,10,26).



## REVIEW OF PROGRAMS AND ACTIVITIES

### Relationship of Mine Environment, Geology and Seam Characteristics to Dust Generation and Mobility

During the mining of a seam, dilution from the roof and floor and from partings and inclusions in the seam is a standard occurrence. In coal mining, since the roof and floor strata and inclusions and partings often have greater strength than coal, the mass of adverse dust generated can be much more than if only coal is cut, especially if quartz or other toxic material is present. The size distribution, chemical and mineralogical properties of the respirable dust can also be different from that obtained from cutting coal only. Therefore, the relationship between the coal and out-of-seam material characteristics and the characteristics of the mine respirable dust is being explored. Studies in this area have concentrated on establishment of standard procedures for characterization of coal seams for respirable dust generation potential; correlation of respirable dust characteristics of coal seams, worker locations and mining methods; and respirable dust testing procedures in metal, non-metal and metallurgical operations (6,11,17,22,23,29).

### Technology Transfer

The Center conducts research in the five specified areas with primary emphasis on the engineering control of dust in mines and the interaction of dust and lungs. The unique resources of the four institutions of higher education are being brought together to address these complex problems and to also foster industrial cooperation and technology transfer. Research results are being integrated into existing mining engineering education, short courses and seminar programs.

Graduate education is an integral part of the Center's research. Each project is designed not only to attack an important problem but to train at least one graduate student. Time is projected to allow for a full development of student involvement and to ensure that students fulfill the graduate program requirements. The scope of work and the time duration of each project for the Center have been developed taking into account the needs of the graduate research program and training.

Publication of papers in mining industry journals and reports on specific findings are presented at professional meetings. The Center sponsors conferences on respirable dust in mining. Proceedings of the first Coal Mine Dust Conference sponsored by the Generic Technology Center is available from West Virginia University. The next scheduled meeting is an International Conference titled "Respirable Dust in the Mineral Industries" to be held at Penn State on October 14-16, 1986. The major topics to be discussed at this conference include: generation, dissemination, control, measurement, characterization, legal and regulatory matters, clinical techniques and epidemiology, pathology and pathogenesis, biochemical aspects and complications.

### Reference Center

The Center also serves as the reference center for publications in the respirable dust area. A computer based reference search system is in place and functioning. The Respirable Dust

library is based on an IBM PC-XT system utilizing software designed to allow direct access and electronic mail services through a telephone line. Abstracts of Center generated publications are maintained in the Center. At each participating university a hard copy collection of the respirable dust research performed by that particular university's personnel is maintained, plus other relevant respirable dust publications. The Center encompasses two major medical schools and includes national and international experts in such diverse disciplines as geology, geomechanics, mining engineering, mineral processing, electrical engineering, industrial engineering, mechanical engineering, material sciences, physics, and the various fields of medicine. These authorities are constantly updating information regarding their special areas of expertise and serve as geographically dispersed resource references in the ten disciplines identified. If a more comprehensive literature search is desired, a researcher can utilize the on-line services of LIAS to search the Penn State library system.

The Reference Center also has access through the University Libraries and other institutional libraries to a large number of data bases such as MEDLINE at the National Library of Medicine, Lockheed Corporation, the energy data base of the U.S. Government, DIALOGUE Information Support System (comprised of over 100 data bases), ISI International Scientific Information System, and data bases of professional societies such as the Institute of Mining and Metallurgy (UK), and Information on Demand, Inc., a research service available to SME members and SPIRES, the Stanford University System. A one-time expenditure may be required to have a computer search performed on some of these data bases on key words such as black lung, respirable dust, silicosis, etc. Utilization can also be made of abstracting services such as Engineering Index and Coal Abstracts (EEC) as means of accessing specific information for researchers.

The most important goal of the Respirable Dust Reference Center is to identify what respirable dust related information is available at what location and provide the means of access for others to obtain the information. The second goal is to have both maximum input and retrieval capabilities to the broad team of experts in the reference center. Another goal is to ensure that the service provided to the inquiring public is complete, cost-effective, and the best professional service available.

The Center activities involve the training of engineers and scientists, graduate students and undergraduate students through their respective institutions, and the technology transfer to industry and government of scientific information regarding respirable dust.

### Summary

In summary, the Center presents a comprehensive program which accelerates the attack on the fundamental understanding of the origin, generation, transport, dust-lung interaction and particle characteristics in mines. Such a program is in the spirit of the NAS study and is complementary with existing and ongoing USBM respirable dust research activities. The comprehensive research program is believed to be economically justified in view of the gigantic \$1.7 billion annual cost and 500,000 person

severity (miners and dependents) of the respirable dust problem. Of greater importance, the control of dust-related diseases is supreme from the humane point of view. While significant progress has been made, and the prevalence of respirable dust illness has been reduced, the problem continues to exist and needs solution. Furthermore, as the nation's demand for coal and other minerals increases, both production and number of miners employed will also increase, demanding an accelerated effort to solve the problem.

Acknowledgments

This paper was supported under the Mineral Institutes Program by Grant No. G1135142 from the Bureau of Mines, U.S. Department of the Interior, as part of the Generic Mineral Technology Center for Respirable Dust.

Bibliography

1. Bhaskar, R. and R. V. Ramani, "Analyzing Dust Flows in Mine Workings: A Mathematical Model," Paper presented at the 15th Annual Meeting of the Fine Particle Society, Orlando, FL, July 30-August 1, 1984.
2. Bhaskar, R. and R. V. Ramani, "Behavior of Dust Clouds in Mine Airways," Paper presented at the Annual Meeting of the Society of Mining Engineers, New York, February 1985; accepted for publication in Transactions, Preprint #85-154.
3. Bhaskar, R. and R. V. Ramani, "Experimental Studies on Dust Dispersion in Mine Airways," Paper to be presented at the Annual Meeting of the Society of Mining Engineers, New Orleans, LA, March 2-6, 1986.
4. Bieniawski, Z. T. and C. Mark, "A Fracture Mechanics Study of Crack Propagation Mechanism in Coal," First Annual Report on Grant G1135142, Generic Mineral Technology Center for Respirable Dust, The Pennsylvania State University, University Park, PA, October 1, 1984, 70 pp.
5. Bieniawski, Z. T. and R. Karl Zipf, "A Fracture Mechanics Study of Crack Propagation Mechanism in Coal," Second Annual Report on Grant G1135142, Generic Mineral Technology Center for Respirable Dust, The Pennsylvania State University, University Park, PA, October 1, 1985, 116 pp.
6. Bise, C. J. and J. M. Mutmansky, "Coal Mine Respirable Dust," Earth and Mineral Sciences, The Pennsylvania State University, University Park, PA, pp. 43-45, Summer 1985.
7. Chander, S. and B. R. Mohal, "On the Mechanism of Imbibition of Particles in Liquids," Paper presented at the International Symposium-Workshop on Particulate and Multi-Phase Processes and 16th Annual Meeting of the Fine Particle Society, Miami Beach, FL, April 22-26, 1985.
8. Chiang, H. S., S. S. Peng, G. C. Sun, and Y. F. Zhao, "Some Factors Influencing the Airborne Dust Distribution in Longwall Face Area," Proceedings of Coal Mine Dust Conference, Morgantown, WV, October 8-10, 1984, pp. 206-213.
9. Dalal, N. S., M. M. S. Suryan, V. Vallyathan, F. H. Y. Green and R. Wheeler, "Detection of Reactive Free Radicals in Fresh Coal Mine Dust and Its Implications to Pneumoconiosis," Paper presented at the Sixth International Symposium on Inhaled Particles, Edinburgh, Scotland, September 1985.
10. DiGragorio, K. A., E. V. Cilento, R. C. Lantz, "The Development of an Electro-Optical Technique to Measure Superoxide Release from Pulmonary Alveolar Macrophages Exposed to Coal Dusts," Proceedings of Coal Mine Dust Conference, Morgantown, WV, October 8-10, 1984, pp. 222-227.
11. Grayson, R. L. and S. S. Peng, "Correlation of Respirable Dust Mass Concentration with Worker Positions," Proceedings of Coal Mine Dust Conference, Morgantown, WV, October 8-10, 1984, pp. 256-260.
12. Khair, A. Wahab, "Study of Fracture Mechanisms in Coal Subjected to Various Types of Surface Traction Using Holographic Interferometry," Paper presented at the 25th U.S. Symposium on Rock Mechanics, Northwestern University, Evanston, IL, June 25-27, 1984.
13. Khair, A. Wahab, "Design and Fabrication of a Rotary Coal Cutting Simulator," Proceedings of Coal Mine Dust Conference, Morgantown, WV, October 8-10, 1984, pp. 190-197.
14. Khair, A. Wahab and Nagendra P. Reddy, "The Effect of In-Situ and Operating Parameters on Fragmentation of Coal," Paper presented at the 26th U.S. Symposium on Rock Mechanics, South Dakota School of Mines and Technology, Rapid City, SD, June 26-28, 1985.
15. Khair, A. Wahab and Mark K. Quinn, "Mechanisms of Respirable Dust Generation by Continuous Miner," Paper presented at the SME-AIME Fall Meeting, Albuquerque, NM, October 16-18, 1985.
16. Khair, A. Wahab and Nagendra P. Reddy, "An Analysis of Respirable Dust Generation by Continuous Miner," Paper to be presented at the Annual Meeting of the Society of Mining Engineers, New Orleans, LA, March 2-6, 1986.
17. Lee, Changwoo and Jan M. Mutmansky, "A Strategy for Coal Mine Respirable Dust Sampling Using Multi-Stage Impactors for Characterization Purposes," Paper to be presented at the Annual Meeting of the Society of Mining Engineers, New Orleans, LA, March 2-6, 1986.
18. Marple, V. A. and K. L. Rubow, "An Instrument for Measuring Powder Particle Size Distributions Based on Aerodynamic Diameter," Paper presented at the 15th Annual Meeting of the Fine Particle Society, Orlando, FL, July 30-August 1, 1984.
19. Marple, V. A. and K. L. Rubow, "Instrumentation for the Measurement of Respirable Coal Mine Dust," Proceedings of Coal Mine Dust Conference, Morgantown, WV, October 8-10, 1984, pp. 214-221.
20. Mohal, B. R. and S. Chander, "A New Technique to Determine Wettability of Powders-Imbibition Time Measurements," Paper submitted for publication in a special issue of Colloids and Surfaces, Spring 1986.
21. Mohal, B. R., S. Chander and F. F. Aplan, "Wetting Behavior of Coal in the Presence of Some Nonionic Surfactants," Paper to be presented at the ACS Symposium, New York, April 6-11, 1986.
22. Moore, M. and C. J. Bise, "The Relationship Between the Hardgrove Grindability Index and the Potential for Respirable Dust Generation," Proceedings of Coal Mine Dust Confer-

## REVIEW OF PROGRAMS AND ACTIVITIES

- ence, Morgantown, WV, October 8-10, 1984, pp. 250-255.
23. Mutmansky, J. M. and C. Lee, "An Analysis of Coal and Geologic Variables Related to Coal Workers' Pneumoconiosis," Proceedings of Coal Mine Dust Conference, Morgantown, WV, October 8-10, 1984, pp. 236-249.
  24. Peng, S. S., "Airflow Distribution in Long-wall Faces," Paper presented at the SME-AIME Fall Meeting, Albuquerque, NM, October 16-18, 1985.
  25. Peng, S. S. (Editor), Coal Mine Dust Conference Proceedings, October 8-10, 1984, West Virginia University, Morgantown, 1984.
  26. Pisano, F., M. McCawley, D. Hinton, C. Stanley and R. C. Lantz, "Evaluation of the Size Distribution of Large Aerosols In An Animal Exposure Chamber," Proceedings of Coal Mine Dust Conference, Morgantown, WV, October 8-10, 1984, pp. 228-235.
  27. Ramani, R. V., "Generic Technology Center for Respirable Dust," Paper presented at the NIH and ACGIH Annual Meeting, Detroit, MI, May 24, 1984.
  28. Ramani, R. V. and R. Bhaskar, "Dust Transport in Mine Airways," Proceedings of Coal Mine Dust Conference, Morgantown, WV, October 8-10, 1984, pp. 198-205.
  29. Shen, A. T. and T. A. Ring, "Distinguishing Between Two Aerosol Size Distributions," to be published in J. Aerosol Sci., Vol. 6, No. 1.
  30. Stobbe, T. and R. Plummer, "Coal Mine Dust Characterization," Paper presented at the American Industrial Hygiene Association Conference, May 1985.
  31. Stobbe, Plummer, Kim and Dover, "Characterization of Coal Mine Dust," Paper presented at the International Conference on the Health of Miners, Pittsburgh, June 1985; To be published in the Annals of the ACGIH in 1986.
  32. Zipf, R. Karl and Z. T. Bieniawski, "Mixed Mode Testing for Fracture Toughness of Coal Based on Critical Energy Density," Proc. 27th U.S. Symposium on Rock Mechanics, AIME, New York, 1986 (in press).



# **INDEX**

## **THE CUMULATIVE AUTHOR INDEX**

Authors are sorted alphabetically. Papers by the same author are sorted in decreasing chronological order which puts the more recent papers first.

Authors' names appear in standardized form, that is, last names and initials. This is not necessarily the way the name appears on the paper.

## **THE CUMULATIVE SUBJECT INDEX**

Every entry in the CUMULATIVE SUBJECT INDEX contains the following information:

- 1) Last name of the first listed author with the number of authors in parenthesis if the article had multiple authors.
- 2) A short descriptive phrase, generally the title of the paper.
- 3) The year in which the paper was published or presented.
- 4) The location of the paper in The Respirable Dust Center publication volume.



GENERIC MINERAL TECHNOLOGY CENTER FOR RESPIRABLE DUST

CUMULATIVE AUTHORS INDEX  
1984-1986

- Ananth, G. Vol. 5, 244-248  
Andre, R. A. Vol. 5, 319-327  
Aplan, F. F. Vol. 5, 123-128; Vol. 5, 129-138
- Bartlett, G. L. Vol. 5, 274-281  
Bates, D. Vol. 5, 261-273  
Begley, R. D. Vol. 4, 9-55  
Bhaskar, R. Vol. 5, 55-60; Vol. 5, 61-71; Vol. 4, 109-118; Vol. 3, 25-31  
Bieniawski, Z. T. Vol. 5, 3-10; Vol. 5, 11-17  
Bise, C. J. Vol. 4, 155-157; Vol. 3, 85-90
- Castranova, V. Vol. 5, 261-273; Vol. 4, 121-139; Vol. 3, 53-60  
Chander, S. Vol. 5, 123-128  
Chiang, H. S. Vol. 5, 72-81; Vol. 5, 95-108; Vol. 5, 129-138; Vol. 5, 139-147; Vol. 3, 32-34  
Cilento, E. V. Vol. 5, 257-260; Vol. 3, 63-67
- Dalal, N. S. Vol. 5, 194-199; Vol. 5, 200-202  
Demers, L. M. Vol. 5, 282-288  
DeVilder, W. M. Vol. 4, 56-63  
DiGregorio, K. A. Vol. 5, 257-260; Vol. 3, 63-67  
Dower, J. M. Vol. 5, 352-358  
Dumm, T. F. Vol. 5, 148-154; Vol. 5, 155-185; Vol. 5, 186-193
- Edelson, R. E. Vol. 5, 282-288
- Fissan, H. J. Vol. 5, 244-248  
Frantz, R. L. Vol. 5, 361-365
- Grayson, R. L. Vol. 5, 319-327; Vol. 5, 328-345; Vol. 3, 35-42; Vol. 3, 91-94  
Greene, F. H. Y. Vol. 5, 200-202; Vol. 4, 121-139
- Hathaway, P. Vol. 4, 121-139  
Hering, S. Vol. 5, 224-243  
Hill, C. A. Vol. 5, 261-273  
Hinton, D. Vol. 5, 289-293; Vol. 4, 157-163  
Hogg, R. Vol. 5, 148-154; Vol. 5, 155-185; Vol. 5, 186-193
- Jafari, B. Vol. 5, 194-199; Vol. 5, 200-202  
Jones, W. G. Vol. 5, 346-351
- Keane, M. J. Vol. 5, 261-273; Vol. 4, 121-139; Vol. 4, 140-149; Vol. 3, 53-60  
Khair, A. W. Vol. 5, 18-41; Vol. 5, 42-52; Vol. 4, 3-8; Vol. 4, 9-55; Vol. 4, 56-63; Vol. 4, 64-91;  
Vol. 4, 92-106; Vol. 3, 3-10; Vol. 3, 11-22  
Kim, H. Vol. 5, 346-351; Vol. 5, 352-358

**THE RESPIRABLE DUST CENTER**

**Lantz, R. C.** Vol. 5, 257-260; Vol. 4, 157-163; Vol. 3, 63-67  
**Lee, C.** Vol. 5, 295-305; Vol. 5, 306-318; Vol. 3, 71-84  
**Lui, B. Y. H.** Vol. 5, 113-120  
**Luo, Y.** Vol. 5, 95-108

**Marple, V. A.** Vol. 5, 109-112; Vol. 5, 204-223; Vol. 5, 224-243; Vol. 5, 244-248;  
Vol. 3, 45-52

**McCawley, D.** Vol. 4, 157-163

**Meloy, T. P.** Vol. 5, 249-250; Vol. 5, 251-254

**Mohal, B. R.** Vol. 5, 123-128; Vol. 5, 129-138; Vol. 5, 139-147

**Moore, M. P.** Vol. 3, 85-90

**Mutmansky, J. M.** Vol. 5, 295-305; Vol. 5, 306-318; Vol. 4, 155-157; Vol. 3, 71-84

**Ong, T. M.** Vol. 3, 53-60

**Pederson, A. B.** Vol. 5, 274-281

**Peng, S. S.** Vol. 5, 72-81; Vol. 5, 95-108; Vol. 5, 328-345; Vol. 3, 32-34; Vol. 3, 35-42;  
Vol. 3, 91-94

**Pisano, F.** Vol. 4, 157-163

**Phummer, R. W.** Vol. 5, 346-351; Vol. 5, 352-358

**Ramani, R. V.** Vol. 5, 55-60; Vol. 5, 61-71; Vol. 5, 361-365; Vol. 4, 109-118; Vol. 3, 25-31

**Reddy, N. P.** Vol. 5, 18-41; Vol. 5, 42-52; Vol. 4, 64-91

**Regad, E. D.** Vol. 4, 121-139

**Robinson, V.** Vol. 4, 140-149

**Rose, M.** Vol. 5, 282-288

**Rubow, K. L.** Vol. 5, 109-112; Vol. 5, 204-223; Vol. 5, 244-248; Vol. 3, 45-52

**Saus, F.** Vol. 5, 261-273

**Shi, X.** Vol. 5, 194-199

**Simonyi, T.** Vol. 5, 319-327

**Stanley, C.** Vol. 5, 289-293; Vol. 4, 157-163

**Stobbe, T. J.** Vol. 5, 346-351; Vol. 5, 352-358

**Sun, G. C.** Vol. 3, 32-34

**Superdock, D. T.** Vol. 5, 282-288

**Suryan, B.** Vol. 5, 194-199

**Thompson, S. D.** Vol. 5, 82-94

**Ueng, T. H.** Vol. 5, 82-94

**Vallyathan, V.** Vol. 5, 200-202; Vol. 5, 261-273; Vol. 4, 121-139; Vol. 4, 140-149;  
Vol. 3, 53-60

**Wallace, W. E.** Vol. 5, 261-273; Vol. 4, 121-139; Vol. 4, 140-149; Vol. 3, 53-60

**Wang, Y. J.** Vol. 5, 82-94

**Zhiqun, Z.** Vol. 5, 113-120

**Zipf, Jr., R. K.** Vol. 5, 3-10; Vol. 5, 11-17



# GENERIC MINERAL TECHNOLOGY CENTER FOR RESPIRABLE DUST

## CUMULATIVE SUBJECT INDEX 1984-1986

### CONTROL OF DUST AND PARTICULATE MATTER GENERATION

- Begley, Richard D.** (2) Coal fracture analysis using two simultaneous wedge indentors and laser holographic interferometry, 1985, Vol. 4, 56-63.
- Khair, A. Wahab** (2) An analysis of respirable dust generation by continuous miner, 1986, Vol. 5, 18-41.
- Khair, A. Wahab** (2) Characterization of coal breakage as a function of operating parameters, 1986, Vol. 5, 42-52.
- Khair, A. Wahab** Characterizing fracture types in rock/coal subjected to quasi-static indentation using acoustic emission technique, 1985, Vol. 4, 3-8.
- Khair, A. Wahab** (2) Correlation of fragment size distribution and fracture surface in coal cutting under various conditions, 1985, Vol. 4, 9-57.
- Khair, A. Wahab** Design and fabrication of a rotary cutting simulator, 1984, Vol. 3, 3-10.
- Khair, A. Wahab** (2) Mechanisms of respirable dust generation by continuous miner, 1985, Vol. 4, 92-106.
- Khair, A. Wahab** Study of fracture mechanisms in coal subjected to various types of surface tractions using holographic interferometry, 1984, Vol. 3, 11-22.
- Zipf, Jr., R. Karl** (2) Fracture mode and loading rate influences on the formation of respirable size fragments on new fracture surfaces, 1986, Vol. 5, 11-17.
- Zipf, Jr., R. Karl** (2) Mixed mode testing for fracture toughness of coal based on critical - energy - density, 1986, Vol. 5, 3-10.

### DILUTION, DISPERSION, AND COLLECTION OF DUST

- Bhaskar, R.** (2) Behavior of dust clouds in mine airways, 1985, Vol. 4, 109-118.
- Bhaskar, R.** (2) Experimental studies of dust dispersion in mine airways, 1986, Vol. 5, 55-60.
- Chiang, H. S.** (3) Size distribution of the airborne dust in longwall coal faces, 1986, Vol. 5, 95-108.
- Chiang, H. S.** (4) Some factors influencing the airborne dust distribution in longwall face area, 1984, Vol. 3, 32-34.
- Grayson, Robert L.** (2) Analysis of an airborne dust study made for a southwestern Pennsylvania underground bituminous coal mine, 1984, Vol. 3, 35-42.

- Marple, V. A.** (3) Numerical technique for calculating the equivalent aerodynamic diameter of particles, 1986, Vol. 5, 113-120.
- Peng, S. S.** (2) Air velocity distribution measurements on four mechanized longwall coal faces, 1986, Vol. 5, 72-81.
- Ramani, R. V.** (2) Dust transport in mine airways, 1984, Vol. 3, 25-31.
- Ramani, R. V.** (2) Theoretical and experimental studies on dust transport in mine airways, 1986, Vol. 5, 61-71.
- Rubow, K. L.** (2) Application of a particle dispersion system for obtaining the size distribution of particles collected on filter samples, 1986, Vol. 5, 109-112.
- Ueng, T. H.** (3) Simulations on dust dispersion for a coal mine face using a scale model, 1986, Vol. 5, 82-94.

### CHARACTERIZATION OF DUST PARTICLES

- Chander, S.** (3) Wetting behavior of coal in the presence of some nonionic surfactants, 1986, Vol. 5, 129-138.
- Chander, S.** (3) Wetting characteristics of particles and their significance in dust abatement, 1986, Vol. 5, 123-128.
- Dalal, N. S.** (4) Electron spin resonance detection of reactive free radicals in fresh coal dust and quartz dust and its implications to pneumoconiosis and silicosis, 1986, Vol. 5, 194-199.
- Dumm, T. F.** (2) A procedure for extensive characterization of coal mine dust collected using a modified personal sampler, 1986, Vol. 5, 186-193.
- Dumm, T. F.** (2) Estimation of particle size distributions using pipet-withdrawal centrifuges, 1986, Vol. 5, 148-154.
- Dumm, T. F.** (2) Standard respirable dusts, 1986, Vol. 5, 155-185.
- Hering, Susanne** (2) Low-pressure and micro-orifice impactors for cascade impactor sampling and data analysis, 1986, Vol. 5, 224-243.
- Jafari, B.** (3) Detection of organozinc free radicals in coal-dust exposed lung tissue and correlations with their histopathological parameters, 1986, Vol. 5, 200-202.
- Marple, Virgil A.** (2) Instrumentation for the measurement of respirable coal mine dust, 1984, Vol. 3, 45-52.
- Marple, Virgil A.** (2) Low pressure and micro-orifice impactors, 1986, Vol. 5, 224-243.
- Marple, Virgil A.** (4) Micro-orifice uniform deposit impactor, 1986, Vol. 5, 244-248.
- Marple, Virgil A.** (2) Theory and design guidelines for cascade impactor sampling and data analysis, 1986, Vol. 5, 204-223.
- Meloy, Thomas P.** A hypothesis on the possible contribution of coal cleats to CWP, 1986, Vol. 5, 249-250.

## SUBJECT INDEX

- Meloy, Thomas P.** A working hypothesis on how silica and silica surface may cause silicosis and CWP, 1986, Vol. 5, 251-254.
- Mohal, B. R.** (2) A new technique to determine wettability of powders-inhibition time measurements, 1986, Vol. 5, 139-147.
- Wallace, Jr., W. E.** (4) In vitro biologic toxicity of native and surface-modified silica and kaolin, 1985, Vol. 4, 140-149.
- Wallace, Jr., W. E.** (5) Pulmonary surfactant interaction with respirable dust, 1984, Vol. 3, 53-60.
- Wallace, Jr., W. E.** (7) Suppression of inhaled particle cytotoxicity by pulmonary surfactants and re-toxication by phospholipase--distinguishing properties of quartz and kaolin, 1985, Vol. 4, 121-139.

### INTERACTION OF DUST AND LUNGS

- Bartlett, G. L.** (2) Effects of coal dusts and alveolar macrophages and growth of lung fibroblasts, 1986, Vol. 5, 274-281.
- Demers, Lawrence M.** (4) The effects of coal mine dust particles on the metabolism of arachidonic acid by pulmonary alveolar macrophages, 1986, Vol. 5, 282-288.
- DiGregorio, K. A.** (3) Superoxide release from single pulmonary alveolar macrophages, 1986, Vol. 5, 257-260.
- DiGregorio, K. A.** The development of an electro-optical technique to measure superoxide release from pulmonary alveolar macrophages exposed to coal dusts, 1984, Vol. 3, 63-67.
- Lantz, R. Clarke** (3) Development of alternations in the lung induced by inhaled silica: a morphometric study, 1986, Vol. 5, 289-292.
- Pisano, F.** (5) Evaluation of the size distribution of large aerosols in an animal exposure chamber, 1984, Vol. 4, 153-159.
- Wallace, W. E.** (7) The effect of lecithin surfactant and phospholipase enzyme treatment on some cytotoxic properties of respirable quartz and kaolin dusts, 1986, Vol. 5, 261-273.

### RELATIONSHIP OF MINE ENVIRONMENT, GEOLOGY AND SEAM CHARACTERISTICS TO DUST GENERATION AND MOBILITY

- Andre, R. A.** (3) Variation in mineral and elemental composition of respirable coal mine dusts by worker locations and coal seams, 1986, Vol. 5, 319-327.
- Bise, Christopher** (2) Coal mine respirable dust, 1985, Vol. 4, 163-165.
- Grayson, R. L.** (2) Characterization of respirable dust on a longwall panel, 1986, Vol. 5, 328-345.
- Grayson, R. L.** (2) Correlation of respirable dust mass concentration with worker positions, 1984, Vol. 3, 91-94.
- Lee, Changwoo** (2) A strategy for coal mine respirable dust sampling using multi-stage impactors for characterization purposes, 1986, Vol. 5, 295-305.

## THE RESPIRABLE DUST CENTER

- Lee, Changwoo** (2) Statistical analysis of the elemental characteristics of airborne coal mine dust, 1986, Vol. 5, 306-318.
- Moore, Michael P.** (2) The relationship between the hardgrove grindability index and the potential for respirable dust generation, 1984, Vol. 3, 85-90.
- Mutmansky, Jan M.** An analysis of coal and geological variables related to coal workers' pneumoconiosis, 1984, Vol. 3, 71-84.
- Stobbe, Terrence J.** (4) A methodology for determining the mineral content and particle size distribution of airborne coal mine dust, 1986, Vol. 5, 346-351.
- Stobbe, Terrence J.** (4) Characterization of coal mine dust, 1986, Vol. 5, 352-358.

### COORDINATION

- Frantz, Robert L.** (2) A review of the programs and activities of the Generic Mineral Technology Center for Respirable Dust, 1986, Vol. 5, 361-365.